

8-2015

Quantification of IMRT severity scores for improvement of FMEA results

Jacqueline T. Faught

Follow this and additional works at: https://digitalcommons.library.tmc.edu/utgsbs_dissertations



Part of the [Oncology Commons](#), and the [Other Physics Commons](#)

Recommended Citation

Faught, Jacqueline T., "Quantification of IMRT severity scores for improvement of FMEA results" (2015). *The University of Texas MD Anderson Cancer Center UTHealth Graduate School of Biomedical Sciences Dissertations and Theses (Open Access)*. 617.
https://digitalcommons.library.tmc.edu/utgsbs_dissertations/617

This Dissertation (PhD) is brought to you for free and open access by the The University of Texas MD Anderson Cancer Center UTHealth Graduate School of Biomedical Sciences at DigitalCommons@TMC. It has been accepted for inclusion in The University of Texas MD Anderson Cancer Center UTHealth Graduate School of Biomedical Sciences Dissertations and Theses (Open Access) by an authorized administrator of DigitalCommons@TMC. For more information, please contact digitalcommons@library.tmc.edu.

QUANTIFICATION OF IMRT SEVERITY SCORES FOR IMPROVEMENT OF FMEA RESULTS

by

Jacqueline Tonigan Faught, M.S.

APPROVED:

David S. Followill, Ph.D.
Advisory Professor

Peter A. Balter, Ph.D.

Laurence E. Court, Ph.D.

Jennifer L. Johnson, M.S., M.B.A.

Stephen F. Kry, Ph.D.

Francesco C. Stingo, Ph.D.

APPROVED:

Dean, The University of Texas
Graduate School of Biomedical Sciences at Houston

QUANTIFICATION OF IMRT SEVERITY SCORES FOR IMPROVEMENT OF FMEA RESULTS

A

DISSERTATION

Presented to the Faculty of
The University of Texas
Health Science Center at Houston
and
The University of Texas
MD Anderson Cancer Center
Graduate School of Biomedical Sciences
in Partial Fulfillment
of the Requirements
for the Degree of

DOCTOR OF PHILOSOPHY

by

Jacqueline Tonigan Faught, M.S.
Houston, Texas

August, 2015

Dedication

In dedication to the brilliant memory of

Richard F. Tonigan, Ph.D.

Acknowledgements

I first owe tremendous gratitude to my advisor, Dr. David Followill. He has ceaselessly supported and encouraged me every step of my graduate career and I would not be where I am today without him. He has been an outstanding example of a skilled medical physicist, an effective leader, and a thoughtful and genuine person for me and all of his students and colleagues. Thank you, Dr. Followill, especially for providing me with the environment I needed to learn and grow confidently and independently, for listening to and helping me work through my ideas, and assisting me in pursuing my aspired career path.

I would also like to sincerely thank each member of my supervisory committee for their contributions to this research and their aid in my professional growth. Thank you, Dr. Balter, especially for challenging me and teaching me in the clinic and for assisting with beam modeling. Thank you, Dr. Court, especially for helping me to improve my presentation skills and think through ideas. Thank you, Jennifer, especially for your guidance on conducting surveys, researching quality and safety, and for serving as a wonderful and encouraging role model. Thank you, Dr. Kry, especially for helping me talk through concepts and ideas and for always asking intriguing questions. And thank you, Dr. Stingo, for always taking the time to meet with me and discuss statistical approaches.

I would next like to acknowledge everyone at IROC Houston. The administrators, physicists, physics assistants, dosimetrists, and TLD/OSLD group have enriched my learning experience and have supported me throughout my graduate education. Thank you especially to Andrea Molineu, M.S. for help with the IMRT H&N phantom, Carrie Lujano for helping me with measurements, Nadia Hernandez for teaching me the ways of film analysis, Lynda McDonald for promptly reading my phantom TLD, and Huy Duong for his technical support.

My gratitude is extensively given to both Jared Ohrt, M.S. and Michael Kantor for their endless Pinnacle support including giving me numerous helpful scripts, guiding my beam modeling, and for always promptly addressing my problems. My gratitude is also extended to the MD Anderson Linac

Engineers, especially Chuck Smith and Tom Diel for teaching me so much about the machines and patiently assisting me with measurements, sometimes into the early morning hours. The MD Anderson Physics Assistants also were always willing to lend a hand with my measurements and have taught me so much. Thank you especially to Luke Whittlesey, Andrea Ohrt, and Scott LaNeave.

It has been a joy to collaborate and grow with my fellow students and friends throughout graduate school. Many of them supported me through my research and I would especially like to acknowledge and thank Adam Yock, Ph.D. for his thoughtful conversations and Pinnacle scripting help, Paige Taylor, M.S., for her help with measurements and endless encouragement, and Jessie Huang, Ph.D, for her support and company on the roller coaster that is dissertating.

My fellow student, best friend, and husband, Austin Faught, Ph.D., deserves a special thank you for supporting me both personally and professionally over the last six years. He has contributed to this research through insightful discussions, late night measurements at the linac, MATLAB scripting, and helpful editing, not to mention helping me to persevere through many challenges. This gratitude extends to all of my family for their support throughout my education. I especially thank my inspiring younger brother Andrew Tonigan, my personal cheerleader and aunt Debbie Contreras, my wise and sympathetic uncle J. Scott Tonigan, PhD., and my wonderful in-laws Mike, Lori, and Brianna Faught for their active support. Finally, even though they aren't physically here, I'd like to acknowledge and thank my parents Richard Eric and Diane Tonigan and my grandparents Richard (Dick) and June Tonigan for instilling me with confidence, encouraging me to pursue my goals, and setting me up for success.

QUANTIFICATION OF IMRT SEVERITY SCORES FOR IMPROVEMENT OF FMEA RESULTS

Jacqueline Tonigan Faught, M.S.

Supervisory Professor: David S. Followill, Ph.D.

Accurate delivery of intensity modulation radiation therapy (IMRT) requires perfect execution of a long, complicated chain of events; failure of any component of this process may contribute to dose delivery errors, compromising treatment quality and, more importantly, patient safety. Prospective, process-wide risk mitigation techniques are becoming more prevalent in radiotherapy to establish comprehensive quality management (QM) programs, such as failure modes and effects analysis (FMEA). The subjective nature of the ordinal scores used for FMEA leads questionable reliability and validity of the results. Additionally, physics components are commonly grouped together, leaving out valuable details important to physics QM. While the process of performing an FMEA is beneficial, it does not guarantee accurate assessment of failure modes. The objective of this project was to provide quantitative severity scores for IMRT delivery failure modes to decrease variability and increase the validity and applicability of FMEA results for improvement of physics QM. The hypothesis of this proposed work was that quantified IMRT physical failure mode severity scores were significantly more likely to describe the true severity compared to conventional qualitative scores. To test this hypothesis, physical failure modes were simulated in clinical IMRT patient treatment plans and the ability of qualitative subjective scores and quantitative scores to accurately describe the magnitude of the resultant dose discrepancies in clinical plans were compared. Qualitative subjective scores were obtained through an online survey of the medical physicist community. Quantitative scores were obtained through phantom treatment planning studies and measurements. Each set of severity data for the identified failure modes were compared to the true clinical severities in ten oropharyngeal patient treatment plans using Wilcoxon Signed Rank Tests. 8/11 failure mode true severity scores were predicted by quantitative approaches and 6/11 were predicted by qualitative approaches ($p < 0.05$). We concluded that the quantitative severity scores did better predict

the true severity scores for our failure modes. However, the qualitative severity scores provided useful information and the more important conclusion of this project was that while this process is very complicated the more information available to inform scoring decisions, the more reliable and accurate the severity scoring will be.

Table of Contents

Chapter 1: Introduction	1
1.1 Background	1
Failure Modes and Effects Analysis	8
Motivation	10
1.2 Objective	10
1.3 Hypothesis and Specific Aims	11
Chapter 2: Methods and Materials	13
2.1 Specific Aim 1: Identify qualitative and quantitative severity scores for IMRT delivery physical failure modes.....	13
2.1.1 Radiotherapy process focus and failure mode identification	13
2.1.2 Obtain qualitative severity scores by means of a traditional FMEA of the IMRT delivery process.....	16
2.1.3 Quantify the severity of head and neck IMRT delivery physical failure modes by means of computation and physical measurement.	22
Evaluation of Severity.....	22
Failure mode investigation.....	33
2.1.4 Compare qualitative and quantitative severity data.	68
2.2 Specific Aim 2: Evaluate and compare the ability of qualitative and quantitative severity scores to accurately describe the error magnitude induced in clinical cases by each physical failure mode.....	69
2.2.1 Evaluate the magnitude of error induced by each physical failure mode in clinical patient treatment plans to find the “true” severity.	69

2.2.2 Compare the validity of qualitative and quantitative severity scores.....	72
Chapter 3 Results and Discussion.....	74
3.1 Specific Aim 1	74
3.1.1 Qualitative severity scoring	74
3.1.2 Quantitative severity scoring	87
3.1.3 Comparison of qualitative and quantitative scores	176
3.2 Specific Aim 2	179
3.2.1 Patient treatment planning study results – true severity.....	179
3.2.2 Comparison of qualitative and quantitative severity scores ability to predict true severity scores	194
Chapter 4: Conclusions	203
4.1 Specific Aim 1 Conclusions.....	203
4.2 Specific Aim 2 Conclusions.....	203
4.3 Overall Conclusions.....	204
Appendix A: Surveys for qualitative severity scoring	207
A.1 Pilot Survey.....	207
Appendix B: Patient Failure Mode Dose Deviations	230
Patient 1	230
Patient 2	234
Patient 3	238
Patient 4	242
Patient 5	246

Patient 6	250
Patient 7	254
Patient 8	258
Patient 9	262
Patient 10	267
Appendix C: Failure Mode Patient DVH graphs	272
Bibliography	342
Vita.....	352

List of Figures

Figure 1: EBRT process map from used to evaluate the safety of the process in Ford, et. al (2009). 269 process nodes are shown and those highlighted in black indicate the top 15 most risky as defined by risk probability number (RPN) ⁷	3
Figure 2: EBRT process with potential errors, Radiation oncology personnel, and common barriers or checklists/timeouts to catch errors ⁸	4
Figure 3: General IMRT Process Tree	15
Figure 4: IROC-H's IMRT head and neck phantom (left), superior half of the phantom insert (right).	23
Figure 5: Treatment isocenter (left) and beam angles (right) for treatment plans using the IROC-H IMRT H&N phantom.....	24
Figure 6: Photon beam central axis percent depth dose curves of varying energies (Khan, pg 143). All beams have a field size of 10 x 10 cm with source to surface distance (SSD) of 100 cm except the 3.0 mm Cu HVL beam which has an SSD of 50 cm. ⁶¹	35
Figure 7: Schematic diagram of achromatic (270°) electron beam bending magnet with energy slit.	36
Figure 8: The percent difference in percent depth dose from the baseline beam (6 MV TrueBeam with no energy adjustments) of a beam with -10% energy. Curves were shifted 2.55 cm to the left for trend lines to intersect at approximately y=0. Data shown for field sizes of 30 x 30 cm ² , 10 x 10 cm ² , and 5 x 5 cm ² and respective trend line equations and coefficients of determination (R ²) are shown.	38
Figure 9: The percent difference in percent depth dose from the baseline beam (6 MV TrueBeam with no energy adjustments) of a beam with +10% energy. Curves were shifted 2.55 cm to the left for trend lines to intersect at approximately y=0. Data shown for field sizes of 30 x 30 cm ² , 10 x 10 cm ² , and 5 x 5 cm ² and respective trend line equations and coefficients of determination (R ²) are shown.	38
Figure 10: 30 x 30 cm ² dose profiles at a depth of 1.5 cm for the baseline beam (6 MV TrueBeam with no energy adjustments) in black and the beam with -10% energy in blue, as well as the percent difference	

between them in green. Linear trend lines, respective equations, and coefficients of determination (R^2) are shown with purple being the negative trend line and orange being the positive trend line.	39
Figure 11: 30 x 30 cm ² dose profiles at a depth of 10 cm for the baseline beam (6 MV TrueBeam with no energy adjustments) in black and the beam with -10% energy in blue, as well as the percent difference between them in green. Linear trend lines, respective equations, and coefficients of determination (R^2) are shown with purple being the negative trend line and orange being the positive trend line.	39
Figure 12: 30 x 30 cm ² dose profiles at a depth of 1.5 cm for the baseline beam (6 MV TrueBeam with no energy adjustments) in black and the beam with +10% energy in red, as well as the percent difference between them in green. Linear trend lines, respective equations, and coefficients of determination (R^2) are shown with purple being the negative trend line and orange being the positive trend line.	40
Figure 13: 30 x 30 cm ² dose profiles at a depth of 10 cm for the baseline beam (6 MV TrueBeam with no energy adjustments) in black and the beam with +10% energy in red, as well as the percent difference between them in green. Linear trend lines, respective equations, and coefficients of determination (R^2) are shown with purple being the negative trend line and orange being the positive trend line.	40
Figure 14: Depth dose curves for a 10 x 10 cm ² field defined by the MLC for the original MDACC TrueBeam model and the adjusted TrueBeam models with +10% energy and -10% energy.....	41
Figure 15: Dose profiles of a 10 x 10 cm ² field defined by the MLC at 1.5 cm depth (approximately d_{max}) for the original MDACC TrueBeam model and the adjusted TrueBeam models with +10% energy and -10% energy.	41
Figure 16: Dose profiles of a 10 x 10 cm ² field defined by the MLC at 10 cm depth for the original MDACC TrueBeam model and the adjusted TrueBeam models with +10% energy and -10% energy.	42
Figure 17: Computed and input altered (“measured”) depth dose data for 2 x 2 cm ² and 10 x 10 cm ² field sizes defined by the MLC for beam model of 6 MV – 10%.....	43
Figure 18: Computed and input altered (“measured”) depth dose data for 2 x 2 cm ² and 10 x 10 cm ² field sizes defined by the MLC for beam model of 6 MV + 10%.....	44

Figure 19: Computed and input altered (“measured”) dose profiles for 10 x 10 cm ² field size defined by the MLC at 1.5 cm (left) and 10 cm (right) depth for beam model of 6 MV -10%.	44
Figure 20: Computed and input altered (“measured”) dose profiles for 10 x 10 cm ² field size defined by the MLC at 1.5 cm (left) and 10 cm (right) depth for beam model of 6 MV +10%.	45
Figure 21: A dose profile example showing the central 80% of FWHM, where the minima and maxima would be used to compute field flatness and points at the edges, equidistant from the central axis, would be used to compute symmetry. Figure from Khan, 4 th ed.	48
Figure 22: Flattening filters are used to create flat photon dose distributions from forward peaked photon beam (a) but the flatness and symmetry of the photon beam are affected by the angle (b), position (c), and energy spectra (d) incident on the flattening filter.	49
Figure 23: Dose profiles for a 20 x 20 cm ² wedged field at depths of 1.5 cm, 6 cm, 12.5 cm, and 22 cm used to model a symmetry error of approximately 2% at a depth of 10 cm.	51
Figure 24: Dose profiles for a 20 x 20 cm ² wedged field at depths of 1.5 cm, 6 cm, 12.5 cm, and 22 cm used to model a symmetry error of approximately 3.5% at a depth of 10 cm.	51
Figure 25: Dose profiles for a 20 x 20 cm ² wedged field at depths of 1.5 cm, 6 cm, 12.5 cm, and 22 cm used to model a symmetry error of approximately 10% at a depth of 10 cm.	52
Figure 26: MU per segment for the nine beams in the standard phantom treatment plan used in treatment planning studies.	63
Figure 27: MU per segment for the nine beams in the complex phantom treatment plan used in treatment planning studies.	64
Figure 28: (a) Cross sectional view of Varian MLC leaves (looking from front) showing tongue-and-groove design. (b) Top view of MLC with the dashed line showing the tongue width.	65
Figure 29: Varian rounded MLC leaf end with radius of curvature of 8 cm.	66
Figure 30: CT tables used for treatment planning studies including the clinically used baseline MDACC CT Table #1, 2% high, and 2% low.	68

Figure 31: CT tables used for treatment planning studies: the clinically used baseline MDACC CT Table #1 and a CT table generate from a PET CT scanner.....	68
Figure 32: Demographics of the respondents for (left) years of experience and (right) time dedicated to clinical work.....	76
Figure 33: Demographics of the respondents for their current continent, certification, and familiarity with FMEA.	76
Figure 34: Distribution of linear accelerator manufacturer, treatment planning system, and IMRT technique listed as primarily used by respondents for head and neck cases.	77
Figure 35: Occurrence, lack of detectability, and severity scores for N=184 responses (including 3 groups) for eleven failure modes (as numbered on page 15). Box plots are shown with red representing the second quartile and blue representing the third quartile. Red circles represent the mean score, open circles represent outliers, and stars represent extreme outliers.	80
Figure 36: Risk Probability Number (RPN) calculated for N=184 responses (including 3 groups) for eleven failure modes (as numbered on page 15.). Box plots are shown with red representing the second quartile and blue representing the third quartile. Red circles represent the mean score, open circles represent outliers, and stars represent extreme outliers.	81
Figure 37: Ranking of failure modes in order of the risk they present using the RPN. The most risky failure mode would have the highest RPN and would be ranked “1”. The size of the bubbles in the chart indicate the frequency at which each failure mode was assigned each rank according to the RPNs calculated.	81
Figure 38: Estimated percent error assigned for N=184 responses (including 3 groups) for eleven failure modes (as numbered on page 15). Box plots are shown with red representing the second quartile and blue representing the third quartile. Red circles represent the mean score, open circles represent outliers, and stars represent extreme outliers. Purple crosses indicate that the maximum extreme outliers not shown. .	82
Figure 39: DVHs for baseline standard phantom treatment plan.....	88
Figure 40: DVHs for baseline complex phantom treatment plan.	89

Figure 41: Axial film dose distributions from the TPS (upper left), film from one irradiation (upper right), and the gamma maps (5%/3mm) from this film for the three irradiations of the phantom with the standard treatment plan (bottom).....	92
Figure 42: Sagittal film dose distributions from the TPS (upper left), film from one irradiation (upper right), and the gamma maps (5%/3mm) from this film for the three irradiations of the phantom with the standard treatment plan (bottom).	93
Figure 43: Axial film dose distributions from the TPS (upper left), film from one irradiation (upper right), and the gamma maps (5%/3mm) from this film for the three irradiations of the phantom with the complex treatment plan (bottom).....	93
Figure 44: Sagittal film dose distributions from the TPS (upper left), film from one irradiation (upper right), and the gamma maps (5%/3mm) from this film for the three irradiations of the phantom with the complex treatment plan (bottom).....	94
Figure 45: Axial film dose distributions from the TPS (upper left), film from one irradiation (upper right), and the gamma maps (5%/3mm) from this film for the three irradiations of the phantom with the baseline standard treatment plan for irradiation set #3 (bottom).	96
Figure 46: Sagittal film dose distributions from the TPS (upper left), film from one irradiation (upper right), and the gamma maps (5%/3mm) from this film for the three irradiations of the phantom with the baseline standard treatment plan for irradiation set #3 (bottom).	96
Figure 47: DVHs for phantom structures in the standard treatment plan with energy changes of 10%, with dashed lines showing baseline DVHs.	99
Figure 48: DVHs for phantom structures in the complex treatment plan with energy changes of 10%, with dashed lines showing baseline DVHs.	99
Figure 49: Axial film dose distributions from the TPS (upper left), film from one irradiation (upper right), and the gamma maps (5%/3mm) from this film for the three irradiations of the phantom with the standard treatment plan with decreased energy ($-0.8\% \text{ TMR}^{14}_5$) (bottom).	105

Figure 50: Sagittal film dose distributions from the TPS (upper left), film from one irradiation (upper right), and the gamma maps (5%/3mm) from this film for the three irradiations of the phantom with the standard treatment plan with decreased energy ($-0.8\% \text{ TMR}^{14}_5$) (bottom).	106
Figure 51: Axial film dose distributions from the TPS (upper left), film from one irradiation (upper right), and the gamma maps (5%/3mm) from this film for the three irradiations of the phantom with the standard treatment plan with increased energy ($+1.1\% \text{ TMR}^{14}_5$) (bottom).	106
Figure 52: Sagittal film dose distributions from the TPS (upper left), film from one irradiation (upper right), and the gamma maps (5%/3mm) from this film for the three irradiations of the phantom with the standard treatment plan with increased energy ($+1.1\% \text{ TMR}^{14}_5$) (bottom).	107
Figure 53: Axial film dose distributions from the TPS (upper left), film from one irradiation (upper right), and the gamma maps (5%/3mm) from this film for the three irradiations of the phantom with the complex treatment plan with decreased energy ($-0.8\% \text{ TMR}^{14}_5$) (bottom).	107
Figure 54: Sagittal film dose distributions from the TPS (upper left), film from one irradiation (upper right), and the gamma maps (5%/3mm) from this film for the three irradiations of the phantom with the complex treatment plan with decreased energy ($-0.8\% \text{ TMR}^{14}_5$).	108
Figure 55: Axial film dose distributions from the TPS (upper left), film from one irradiation (upper right), and the gamma maps (5%/3mm) from this film for the three irradiations of the phantom with the complex treatment plan with increased energy ($+1.1\% \text{ TMR}^{14}_5$) (bottom).	108
Figure 56: Sagittal film dose distributions from the TPS (upper left), film from one irradiation (upper right), and the gamma maps (5%/3mm) from this film for the three irradiations of the phantom with the complex treatment plan with increased energy ($+1.1\% \text{ TMR}^{14}_5$) (bottom).	109
Figure 57: DVHs for phantom structures in the standard treatment plan with beam symmetry changes of 2%, with dashed lines showing baseline DVHs.	113
Figure 58: DVHs for phantom structures in the standard treatment plan with beam symmetry changes of 3.5%, with dashed lines showing baseline DVHs.	114

Figure 59: DVHs for phantom structures in the standard treatment plan with beam symmetry changes of 10%, with dashed lines showing baseline DVHs.....	114
Figure 60: DVHs for phantom structures in the complex treatment plan with beam symmetry changes of 2%, with dashed lines showing baseline DVHs.....	115
Figure 61: DVHs for phantom structures in the complex treatment plan with beam symmetry changes of 3.5%, with dashed lines showing baseline DVHs.....	115
Figure 62: DVHs for phantom structures in the complex treatment plan with beam symmetry changes of 10%, with dashed lines showing baseline DVHs.....	116
Figure 63: Axial film dose distributions from the TPS (upper left), film from one irradiation (upper right), and the gamma maps (5%/3mm) from this film for the three irradiations of the phantom with the standard treatment plan with in plane symmetry angular adjustment of 3.6% (bottom).....	124
Figure 64 Sagittal film dose distributions from the TPS (upper left), film from one irradiation (upper right), and the gamma maps (5%/3mm) from this film for the three irradiations of the phantom with the standard treatment plan with in plane symmetry angular adjustment of 3.6% (bottom).	124
Figure 65: Axial film dose distributions from the TPS (upper left), film from one irradiation (upper right), and the gamma maps (5%/3mm) from this film for the three irradiations of the phantom with the standard treatment plan with in plane symmetry positional adjustment of 3.8% (bottom).	125
Figure 66: Sagittal film dose distributions from the TPS (upper left), film from one irradiation (upper right), and the gamma maps (5%/3mm) from this film for the three irradiations of the phantom with the standard treatment plan with in plane symmetry positional adjustment of 3.8% (bottom).....	125
Figure 67: Axial film dose distributions from the TPS (upper left), film from one irradiation (upper right), and the gamma maps (5%/3mm) from this film for the three irradiations of the phantom with the standard treatment plan with cross plane symmetry angular adjustment of 3.65% (bottom).....	126
Figure 68: Sagittal film dose distributions from the TPS (upper left), film from one irradiation (upper right), and the gamma maps (5%/3mm) from this film for the three irradiations of the phantom with the standard treatment plan with cross plane symmetry angular adjustment of 3.65% (bottom).	126

Figure 69: Axial film dose distributions from the TPS (upper left), film from one irradiation (upper right), and the gamma maps (5%/3mm) from this film for the three irradiations of the phantom with the complex treatment plan with in plane symmetry angular adjustment of 3.6% (bottom).....	127
Figure 70: Sagittal film dose distributions from the TPS (upper left), film from one irradiation (upper right), and the gamma maps (5%/3mm) from this film for the three irradiations of the phantom with the complex treatment plan with in plane symmetry angular adjustment of 3.6% (bottom).	127
Figure 71: Axial film dose distributions from the TPS (upper left), film from one irradiation (upper right), and the gamma maps (5%/3mm) from this film for the three irradiations of the phantom with the complex treatment plan with in plane symmetry positional adjustment of 3.8% (bottom).	128
Figure 72: Sagittal film dose distributions from the TPS (upper left), film from one irradiation (upper right), and the gamma maps (5%/3mm) from this film for the three irradiations of the phantom with the complex treatment plan with in plane symmetry positional adjustment of 3.8% (bottom).	128
Figure 73: Axial film dose distributions from the TPS (upper left), film from one irradiation (upper right), and the gamma maps (5%/3mm) from this film for the three irradiations of the phantom with the complex treatment plan with cross plane symmetry angular adjustment of 3.65% (bottom).....	129
Figure 74: Sagittal film dose distributions from the TPS (upper left), film from one irradiation (upper right), and the gamma maps (5%/3mm) from this film for the three irradiations of the phantom with the complex treatment plan with cross plane symmetry angular adjustment of 3.65% (bottom).	129
Figure 75: DVHs for phantom structures in the standard treatment plan with systematic MLC positional errors in one bank of 1 mm, with dashed lines showing baseline DVHs.....	134
Figure 76: DVHs for phantom structures in the standard treatment plan with systematic MLC positional errors in one bank of 2 mm, with dashed lines showing baseline DVHs.....	134
Figure 77: DVHs for phantom structures in the complex treatment plan with systematic MLC positional errors in one bank of 1 mm, with dashed lines showing baseline DVHs.....	135
Figure 78: DVHs for phantom structures in the complex treatment plan with systematic MLC positional errors in one bank of 2 mm, with dashed lines showing baseline DVHs.....	135

Figure 79: Axial image of phantom with complex treatment plan dose distributions: Baseline plan (left) and X2 MLC systematically shifted inward by 2 mm (right). Isodose values are shown in the upper left corner.	136
Figure 80: Axial film dose distributions from the TPS (upper left), film from one irradiation (upper right), and the gamma maps (5%/3mm) from this film for the three irradiations of the phantom with the standard treatment plan with the MLC shifted out 2 mm in one bank(bottom).	140
Figure 81: Sagittal film dose distributions from the TPS (upper left), film from one irradiation (upper right), and the gamma maps (5%/3mm) from this film for the three irradiations of the phantom with the standard treatment plan with the MLC shifted out 2 mm in one bank (bottom).	140
Figure 82: Axial film dose distributions from the TPS (upper left), film from one irradiation (upper right), and the gamma maps (5%/3mm) from this film for the three irradiations of the phantom with the complex treatment plan with the MLC shifted out 2 mm in one bank (bottom).	141
Figure 83: Sagittal film dose distributions from the TPS (upper left), film from one irradiation (upper right), and the gamma maps (5%/3mm) from this film for the three irradiations of the phantom with the complex treatment plan with the MLC shifted out 2 mm in one bank (bottom).	141
Figure 84: DVHs for phantom structures in the standard treatment plan with gantry angle errors of 2°, with dashed lines showing baseline DVHs.	144
Figure 85: DVHs for phantom structures in the complex treatment plan with gantry angle errors of 2°, with dashed lines showing baseline DVHs.	145
Figure 86: Axial image of phantom primary PTV (red) and spinal cord OAR (blue) with standard treatment plan dose distributions: Gantry angle -2° (left), baseline plan (center) and gantry angle +2° (right). Isodose values are shown in the upper left corner.	146
Figure 87: Axial film dose distributions from the TPS (upper left), film from one irradiation (upper right), and the gamma maps (5%/3mm) from this film for the three irradiations of the phantom with the standard treatment plan with the gantry rotated +2° (bottom).	147

Figure 88: Sagittal film dose distributions from the TPS (upper left), film from one irradiation (upper right), and the gamma maps (5%/3mm) from this film for the three irradiations of the phantom with the standard treatment plan with the gantry rotated $+2^\circ$ (bottom).	148
Figure 89: DVHs for phantom structures in the standard treatment plan with collimator angle errors of 2° , with dashed lines showing baseline DVHs.	151
Figure 90: DVHs for phantom structures in the complex treatment plan with collimator angle errors of 2° , with dashed lines showing baseline DVHs.	151
Figure 91: Axial film dose distributions from the TPS (upper left), film from one irradiation (upper right), and the gamma maps (5%/3mm) from this film for the three irradiations of the phantom with the standard treatment plan with the collimator rotated $+2^\circ$ (bottom).	154
Figure 92: Sagittal film dose distributions from the TPS (upper left), film from one irradiation (upper right), and the gamma maps (5%/3mm) from this film for the three irradiations of the phantom with the standard treatment plan with the collimator rotated $+2^\circ$ (bottom).	154
Figure 93: DVHs for phantom structures in the standard treatment plan with couch angle errors of 2° , with dashed lines showing baseline DVHs.	157
Figure 94: DVHs for phantom structures in the complex treatment plan with couch angle errors of 2° , with dashed lines showing baseline DVHs.	157
Figure 95: Axial images of the phantom with the complex treatment plan dose distribution: baseline (left) and with the couch rotated $+2^\circ$	158
Figure 96: Sagittal film dose distributions from the TPS (upper left), film from one irradiation (upper right), and the gamma maps (5%/3mm) from this film for the three irradiations of the phantom with the standard treatment plan with the couch rotated $+2^\circ$ (bottom).	160
Figure 97: Sagittal film dose distributions from the TPS (upper left), film from one irradiation (upper right), and the gamma maps (5%/3mm) from this film for the three irradiations of the phantom with the standard treatment plan with the collimator rotated $+2^\circ$ (bottom).	160

Figure 98: DVHs for phantom structures in the standard treatment plan with MU linearity errors, with dashed lines showing baseline DVHs.	163
Figure 99: DVHs for phantom structures in the complex treatment plan with MU linearity errors, with dashed lines showing baseline DVHs.	163
Figure 100: DVHs for phantom structures in the standard treatment plan with MLC leakage and transmission modeling errors, with dashed lines showing baseline DVHs.....	166
Figure 101: DVHs for phantom structures in the complex treatment plan with MLC leakage and transmission modeling errors, with dashed lines showing baseline DVHs.....	166
Figure 102: DVHs for phantom structures in the standard treatment plan with MLC tongue-and-groove modeling errors, with dashed lines showing baseline DVHs.....	169
Figure 103: DVHs for phantom structures in the complex treatment plan with MLC tongue-and-groove modeling errors, with dashed lines showing baseline DVHs.....	169
Figure 104: DVHs for phantom structures in the standard treatment plan with MLC leaf end modeling errors, with dashed lines showing baseline DVHs.....	172
Figure 105: DVHs for phantom structures in the complex treatment plan with MLC leaf end modeling errors, with dashed lines showing baseline DVHs.....	172
Figure 106: DVHs for phantom structures in the s treatment plan with CT Table errors, with dashed lines showing baseline DVHs.....	174
Figure 107: DVHs for phantom structures in the complex treatment plan with CT Table errors, with dashed lines showing baseline DVHs.	175
Figure 108: Summary of severity scores for survey (N=184) including the average scores, median scores (lines between 3 rd and 2 nd quartile boxes), and outliers and for standard and complex phantom treatment planning studies.	177
Figure 109: Summary of estimated percent dose errors for survey (N=184) including the averages, medians (lines between 3 rd and 2 nd quartile boxes), and outliers and maximum percent dose errors seen in phantom structures for standard and complex phantom treatment planning studies.	179

Figure 110: The distribution of segments with few MU which would be affected by MU linearity errors for each of our ten patients.....	188
Figure 111: Summary of severity scores obtained from survey, phantom treatment planning studies on standard and complex plans, and ten oropharyngeal clinical patients for our 11 IMRT physical failure modes.	200
Figure 112: Failure mode 1 DVHs for patient 1.	272
Figure 113: Failure mode 1 DVHs for patient 2.	273
Figure 114: Failure mode 1 DVHs for patient 3.	273
Figure 115: Failure mode 1 DVHs for patient 4.	274
Figure 116: Failure mode 1 DVHs for patient 5.	274
Figure 117: Failure mode 1 DVHs for patient 6.	275
Figure 118: Failure mode 1 DVHs for patient 7.	275
Figure 119: Failure mode 1 DVHs for patient 8.	276
Figure 120: Failure mode 1 DVHs for patient 9.	276
Figure 121: Failure mode 1 DVHs for patient 10.	277
Figure 122: Failure mode 2 (with 2% symmetry errors) DVHs for patient 1.	277
Figure 123: Failure mode 2 (with 3.5% symmetry errors) DVHs for patient 1.	278
Figure 124: Failure mode 2 (with 10% symmetry errors) DVHs for patient 1.	278
Figure 125: Failure mode 2 (with 2% symmetry errors) DVHs for patient 2.	279
Figure 126: Failure mode 2 (with 3.5% symmetry errors) DVHs for patient 2.	279
Figure 127: Failure mode 2 (with 10% symmetry errors) DVHs for patient 2.	280
Figure 128: Failure mode 2 (with 2% symmetry errors) DVHs for patient 3.	280
Figure 129: Failure mode 2 (with 3.5% symmetry errors) DVHs for patient 3.	281
Figure 130: Failure mode 2 (with 10% symmetry errors) DVHs for patient 3.	281
Figure 131: Failure mode 2 (with 2% symmetry errors) DVHs for patient 4.	282
Figure 132: Failure mode 2 (with 3.5% symmetry errors) DVHs for patient 4.	282

Figure 133: Failure mode 2 (with 10% symmetry errors) DVHs for patient 4.....	283
Figure 134: Failure mode 2 (with 2% symmetry errors) DVHs for patient 5.....	283
Figure 135: Failure mode 2 (with 3.5% symmetry errors) DVHs for patient 5.....	284
Figure 136: Failure mode 2 (with 10% symmetry errors) DVHs for patient 5.....	284
Figure 137: Failure mode 2 (with 2% symmetry errors) DVHs for patient 6.....	285
Figure 138: Failure mode 2 (with 3.5% symmetry errors) DVHs for patient 6.....	285
Figure 139: Failure mode 2 (with 10% symmetry errors) DVHs for patient 6.....	286
Figure 140: Failure mode 2 (with 2% symmetry errors) DVHs for patient 7.....	286
Figure 141: Failure mode 2 (with 3.5% symmetry errors) DVHs for patient 7.....	287
Figure 142: Failure mode 2 (with 10% symmetry errors) DVHs for patient 7.....	287
Figure 143: Failure mode 2 (with 2% symmetry errors) DVHs for patient 8.....	288
Figure 144: Failure mode 2 (with 3.5% symmetry errors) DVHs for patient 8.....	288
Figure 145: Failure mode 2 (with 10% symmetry errors) DVHs for patient 8.....	289
Figure 146: Failure mode 2 (with 2% symmetry errors) DVHs for patient 9.....	289
Figure 147: Failure mode 2 (with 3.5% symmetry errors) DVHs for patient 9.....	290
Figure 148: Failure mode 2 (with 10% symmetry errors) DVHs for patient 9.....	290
Figure 149: Failure mode 2 (with 2% symmetry errors) DVHs for patient 10.....	291
Figure 150: Failure mode 2 (with 3.5% symmetry errors) DVHs for patient 10.....	291
Figure 151: Failure mode 2 (with 10% symmetry errors) DVHs for patient 10.....	292
Figure 152: Failure mode 3 (with 1 mm errors) DVHs for patient 1.....	292
Figure 153: Failure mode 3 (with 2 mm errors) DVHs for patient 1.....	293
Figure 154: Failure mode 3 (with 1 mm errors) DVHs for patient 2.....	293
Figure 155: Failure mode 3 (with 2 mm errors) DVHs for patient 2.....	294
Figure 156: Failure mode 3 (with 1 mm errors) DVHs for patient 3.....	294
Figure 157: Failure mode 3 (with 2 mm errors) DVHs for patient 3.....	295
Figure 158: Failure mode 3 (with 1 mm errors) DVHs for patient 4.....	295

Figure 159: Failure mode 3 (with 2 mm errors) DVHs for patient 4.....	296
Figure 160: Failure mode 3 (with 1 mm errors) DVHs for patient 5.....	296
Figure 161: Failure mode 3 (with 2 mm errors) DVHs for patient 5.....	297
Figure 162: Failure mode 3 (with 1 mm errors) DVHs for patient 6.....	297
Figure 163: Failure mode 3 (with 2 mm errors) DVHs for patient 6.....	298
Figure 164: Failure mode 3 (with 1 mm errors) DVHs for patient 7.....	298
Figure 165: Failure mode 3 (with 2 mm errors) DVHs for patient 7.....	299
Figure 166: Failure mode 3 (with 1 mm errors) DVHs for patient 8.....	299
Figure 167: Failure mode 3 (with 2 mm errors) DVHs for patient 8.....	300
Figure 168: Failure mode 3 (with 1 mm errors) DVHs for patient 9.....	300
Figure 169: Failure mode 1 (with 2 mm errors) DVHs for patient 9.....	301
Figure 170: Failure mode 3 (with 1 mm errors) DVHs for patient 10.....	301
Figure 171: Failure mode 3 (with 2 mm errors) DVHs for patient 10.....	302
Figure 172: Failure mode 4 DVHs for patient 1.....	302
Figure 173: Failure mode 4 DVHs for patient 2.....	303
Figure 174: Failure mode 4 DVHs for patient 3.....	303
Figure 175: Failure mode 4 DVHs for patient 4.....	304
Figure 176: Failure mode 4 DVHs for patient 5.....	304
Figure 177: Failure mode 4 DVHs for patient 6.....	305
Figure 178: Failure mode 4 DVHs for patient 7.....	305
Figure 179: Failure mode 4 DVHs for patient 8.....	306
Figure 180: Failure mode 4 DVHs for patient 9.....	306
Figure 181: Failure mode 4 DVHs for patient 10.....	307
Figure 182: Failure mode 5 DVHs for patient 1.....	307
Figure 183: Failure mode 5 DVHs for patient 2.....	308
Figure 184: Failure mode 5 DVHs for patient 3.....	308

Figure 185: Failure mode 5 DVHs for patient 4.	309
Figure 186: Failure mode 5 DVHs for patient 5.	309
Figure 187: Failure mode 5 DVHs for patient 6.	310
Figure 188: Failure mode 5 DVHs for patient 7.	310
Figure 189: Failure mode 5 DVHs for patient 8.	311
Figure 190: Failure mode 5 DVHs for patient 9.	311
Figure 191: Failure mode 5 DVHs for patient 10.	312
Figure 192: Failure mode 6 DVHs for patient 1.	312
Figure 193: Failure mode 6 DVHs for patient 2.	313
Figure 194: Failure mode 6 DVHs for patient 3.	313
Figure 195: Failure mode 6 DVHs for patient 4.	314
Figure 196: Failure mode 6 DVHs for patient 5.	314
Figure 197: Failure mode 6 DVHs for patient 6.	315
Figure 198: Failure mode 6 DVHs for patient 7.	315
Figure 199: Failure mode 6 DVHs for patient 8.	316
Figure 200: Failure mode 6 DVHs for patient 9.	316
Figure 201: Failure mode 6 DVHs for patient 10.	317
Figure 202: Failure mode 7 DVHs for patient 1.	317
Figure 203: Failure mode 7 DVHs for patient 2.	318
Figure 204: Failure mode 7 DVHs for patient 3.	318
Figure 205: Failure mode 7 DVHs for patient 4.	319
Figure 206: Failure mode 7 DVHs for patient 5.	319
Figure 207: Failure mode 7 DVHs for patient 6.	320
Figure 208: Failure mode 7 DVHs for patient 7.	320
Figure 209: Failure mode 7 DVHs for patient 8.	321
Figure 210: Failure mode 7 DVHs for patient 9.	321

Figure 211: Failure mode 7 DVHs for patient 10.	322
Figure 212: Failure mode 8 DVHs for patient 1.	322
Figure 213: Failure mode 8 DVHs for patient 2.	323
Figure 214: Failure mode 8 DVHs for patient 3.	323
Figure 215: Failure mode 8 DVHs for patient 4.	324
Figure 216: Failure mode 8 DVHs for patient 5.	324
Figure 217: Failure mode 8 DVHs for patient 6.	325
Figure 218: Failure mode 8 DVHs for patient 7.	325
Figure 219: Failure mode 8 DVHs for patient 8.	326
Figure 220: Failure mode 8 DVHs for patient 9.	326
Figure 221: Failure mode 8 DVHs for patient 10.	327
Figure 222: Failure mode 9 DVHs for patient 1.	327
Figure 223: Failure mode 9 DVHs for patient 2.	328
Figure 224: Failure mode 9 DVHs for patient 3.	328
Figure 225: Failure mode 9 DVHs for patient 4.	329
Figure 226: Failure mode 9 DVHs for patient 5.	329
Figure 227: Failure mode 9 DVHs for patient 6.	330
Figure 228: Failure mode 9 DVHs for patient 7.	330
Figure 229: Failure mode 9 DVHs for patient 8.	331
Figure 230: Failure mode 9 DVHs for patient 9.	331
Figure 231: Failure mode 9 DVHs for patient 10.	332
Figure 232: Failure mode 10 DVHs for patient 1.	332
Figure 233: Failure mode 10 DVHs for patient 2.	333
Figure 234: Failure mode 10 DVHs for patient 3.	333
Figure 235: Failure mode 10 DVHs for patient 4.	334
Figure 236: Failure mode 10 DVHs for patient 5.	334

Figure 237: Failure mode 10 DVHs for patient 6.	335
Figure 238: Failure mode 10 DVHs for patient 7.	335
Figure 239: Failure mode 10 DVHs for patient 8.	336
Figure 240: Failure mode 10 DVHs for patient 9.	336
Figure 241: Failure mode 10 DVHs for patient 10.	337
Figure 242: Failure mode 11 DVHs for patient 1.	337
Figure 243: Failure mode 11 DVHs for patient 2.	338
Figure 244: Failure mode 11 DVHs for patient 3.	338
Figure 245: Failure mode 11 DVHs for patient 5.	339
Figure 246: Failure mode 11 DVHs for patient 6.	339
Figure 247: Failure mode 11 DVHs for patient 7.	340
Figure 248: Failure mode 11 DVHs for patient 8.	340
Figure 249: Failure mode 11 DVHs for patient 9.	341
Figure 250: Failure mode 11 DVHs for patient 10.	341

List of Tables

Table 1: Initiating events in 59 EBRT accidents for categorization. (E) indicates equipment failure ¹⁵	5
Table 2: Physics-specific failure modes evaluated in survey.....	19
Table 3: FMEA scoring scale used in survey.	20
Table 4: IROC-H's IMRT head and neck phantom dosimetric criteria for the planning target volumes (PTVs), organ at risk (OAR), and normal tissue.....	23
Table 5: Failure mode physical measurements made on machines going out of commission.....	26
Table 6: Treatment plan complexity metrics for plans used in second irradiation set.....	29
Table 7: Our unique quantitative severity scoring scale	33
Table 8: Summary of energy failure physical measurements made.....	47
Table 9: Symmetry of 20 x 20 cm ² wedged fields at depths of 1.5 cm, 6 cm, 12.5 cm, and 22 cm which were used to interpolate the symmetry at a depth of 10 cm, which is slightly larger than the desired symmetry for each model.....	50
Table 10: Physical wedge profiles for wedge models simulating symmetry errors of 2%, 3.5%, and 10%.	53
Table 11: Summary of symmetry failure physical measurements made.	55
Table 12: Summary of MLC positional failure physical measurements made.	58
Table 13: MU linearity error scenarios for treatment planning studies.	63
Table 14: Patient sites, planning target volume (PTV), and clinical target volume (CTV) levels.....	71
Table 15: Patient organs at risk used to evaluate severity.	71
Table 16: Evaluation parameters used for each structure to assign a severity score for each failure mode to patient treatment plans.	72

Table 17: Demographics for pilot survey. Subject of the question is listed in the left column, possible responses and corresponding number of responses out of 11 total reported.....	74
Table 18: Pilot survey results, failure mode (magnitude of the failure) are listed with the range and average of Severity scores assigned as well as the average percent dose error assigned (standard deviation).	74
Table 19: Percent dose errors estimated by survey respondents and corresponding severity scores that were assigned.	84
Table 20: Quantitative values assigned to severity scoring scale by groups (N=3).....	84
Table 21: Statistically significant relationships between demographics and FMEA scores or estimated percent dose errors for each failure mode. Rho value is given for Spearman's Rho correlations, Cramer's V (V) is given for Chi Squared Test for Association. Linac = linear accelerator.	85
Table 22: Qualitative severity scores obtained from online survey (N=184).	87
Table 23: Summary of structure doses for the standard phantom treatment plan.	88
Table 24: Summary of structure doses for the complex phantom treatment plan.....	88
Table 25: Baseline TLD results from the first irradiation set with a complex treatment plan.	90
Table 26: Baseline gamma analysis results for axial and sagittal films within the phantom for the first irradiation set.	90
Table 27: Baseline TLD results from the second irradiation set with the standard treatment plan.	91
Table 28: Baseline TLD results from the second irradiation set with the complex treatment plan.	92
Table 29: Baseline gamma analysis results for axial and sagittal films within the phantom for the second irradiation set.	92
Table 30: Baseline TLD results from the third irradiation set, with the measured dose reported as the average of three measurements.	95
Table 31: Baseline gamma analysis results for axial and sagittal films within the phantom for the third irradiation set.	95

Table 32: Color-coding used for severity scoring, corresponding to the scoring scale presented in Section.	97
Table 33: Dosimetric changes from baseline used for severity scoring for beam energy changes of +10% and -10% for the standard phantom treatment plan.	98
Table 34: Dosimetric changes from baseline used for severity scoring for beam energy changes of +10% and -10% for the complex phantom treatment plan.	98
Table 35: TLD differences from baseline from the first irradiation set with an energy adjustment of +1.6% TMR^{20}_{10} .	100
Table 36: Differences from baseline in gamma analysis results for axial and sagittal films within the phantom for the first irradiation set with an energy adjustment of +1.6% TMR^{20}_{10} .	101
Table 37: Average TLD differences from baseline from the second irradiation set with energy adjustments of +1.1% and -0.8% TMR^{14}_5 for the standard plan.	104
Table 38: Average differences from baseline in gamma analysis results for axial and sagittal films within the phantom for the second irradiation set with an energy adjustment of +1.1% and -0.8% TMR^{14}_5 for the standard plan.	104
Table 39: Average TLD differences from baseline from the second irradiation set with energy adjustments of +1.1% and -0.8% TMR^{14}_5 for the complex plan.	104
Table 40: Average differences from baseline in gamma analysis results for axial and sagittal films within the phantom for the second irradiation set with an energy adjustment of +1.1% and -0.8% TMR^{14}_5 for the complex plan.	105
Table 41: Dosimetric changes from baseline used for severity scoring for beam symmetry changes of 2% for the standard phantom treatment plan.	111
Table 42: Dosimetric changes from baseline used for severity scoring for beam symmetry changes of 3.5% for the standard phantom treatment plan.	111
Table 43: Dosimetric changes from baseline used for severity scoring for beam symmetry changes of 10% for the standard phantom treatment plan.	111

Table 44: Dosimetric changes from baseline used for severity scoring for beam symmetry changes of 2% for the complex phantom treatment plan.	112
Table 45: Dosimetric changes from baseline used for severity scoring for beam symmetry changes of 3.5% for the complex phantom treatment plan.	112
Table 46: Dosimetric changes from baseline used for severity scoring for beam symmetry changes of 10% for the complex phantom treatment plan.	112
Table 47: TLD differences from baseline from the first irradiation set with beam symmetry adjustments of 5% in-plane and 3% cross-plane (separately).	118
Table 48: Differences from baseline in gamma analysis results for axial and sagittal films within the phantom for the first irradiation set with beam symmetry adjustments of 5% in-plane and 3% cross-plane (separately).	118
Table 49: Average TLD differences from baseline from the second irradiation set with symmetry adjustments of 3.6% in-plane (angular steering), 3.8% in-plane (translational steering), and 3.65% cross-plane symmetry (angular steering) for the standard plan.	122
Table 50: Average Differences from baseline in gamma analysis results for axial and sagittal films within the phantom for the first irradiation set with symmetry adjustments of 3.6% in-plane (angular steering), 3.8% in-plane (translational steering), and 3.65% cross-plane symmetry (angular steering) for the standard plan.	122
Table 51: Average TLD differences from baseline from the second irradiation set with symmetry adjustments of 3.6% in-plane (angular steering), 3.8% in-plane (translational steering), and 3.65% cross-plane symmetry (angular steering) for the complex plan.	123
Table 52: Average differences from baseline in gamma analysis results for axial and sagittal films within the phantom for the first irradiation set with symmetry adjustments of 3.6% in-plane (angular steering), 3.8% in-plane (translational steering), and 3.65% cross-plane symmetry (angular steering) for the complex plan.	123

Table 53: Dosimetric changes from baseline used for severity scoring for systematic MLC positional errors of 1 mm in one bank of leaves (X1 or X2) for the standard phantom treatment plan.	132
Table 54: Dosimetric changes from baseline used for severity scoring for systematic MLC positional errors of 2 mm in one bank of leaves (X1 or X2) for the standard phantom treatment plan.	132
Table 55: Dosimetric changes from baseline used for severity scoring for systematic MLC positional errors of 1 mm in one bank of leaves (X1 or X2) for the complex phantom treatment plan.	133
Table 56: Dosimetric changes from baseline used for severity scoring for systematic MLC positional errors of 2mm in one bank of leaves (X1 or X2) for the complex phantom treatment plan.	133
Table 57: TLD differences from baseline from the first irradiation set with systematic MLC positional errors of 1 mm and 3 mm in both banks.	137
Table 58: Absolute differences from baseline in gamma analysis results for axial and sagittal films within the phantom for the first irradiation set with systematic MLC positional errors of 1 mm and 3 mm in both banks.	138
Table 59: Average TLD differences from baseline from the second irradiation set with systematic MLC positional errors of 2 mm in one bank for standard and complex plans.	139
Table 60: Average absolute differences from baseline in gamma analysis results for axial and sagittal films within the phantom for the second irradiation set with systematic MLC positional errors of 2 mm in one bank for standard and complex plans.	139
Table 61: Dosimetric changes from baseline used for severity scoring for gantry angle changes of +2° and -2° for the standard phantom treatment plan.	143
Table 62: Dosimetric changes from baseline used for severity scoring for gantry angle changes of +2° and -2° for the complex phantom treatment plan.	143
Table 63: Average TLD differences from baseline from the third irradiation set with gantry angle errors of +2°	147
Table 64: Average absolute differences from baseline in gamma analysis results for axial and sagittal films within the phantom for the third irradiation set with gantry angle errors of +2°	147

Table 65: Dosimetric changes from baseline used for severity scoring for collimator angle changes of +2° and -2° for the standard phantom treatment plan.	150
Table 66: Dosimetric changes from baseline used for severity scoring for collimator angle changes of +2° and -2° for the complex phantom treatment plan.	150
Table 67: Average TLD differences from baseline from the third irradiation set with collimator angle errors of +2°.	153
Table 68: Average absolute differences from baseline in gamma analysis results for axial and sagittal films within the phantom for the third irradiation set with collimator angle errors of +2°.	153
Table 69: Dosimetric changes from baseline used for severity scoring for couch angle changes of +2° and -2° for the standard phantom treatment plan.	156
Table 70: Dosimetric changes from baseline used for severity scoring for couch angle changes of +2° and -2° for the complex phantom treatment plan.	156
Table 71: Average TLD differences from baseline from the third irradiation set with couch angle errors of +2°.	159
Table 72: Average absolute differences from baseline in gamma analysis results for axial and sagittal films within the phantom for the third irradiation set with couch angle errors of +2°.	159
Table 73: Dosimetric changes from baseline used for severity scoring for six MU linearity error scenarios for the standard phantom treatment plan.	162
Table 74: Dosimetric changes from baseline used for severity scoring for six MU linearity error scenarios for the complex phantom treatment plan.	162
Table 75: Dosimetric changes from baseline used for severity scoring for MLC leakage and transmission modeling values of 0% and 10% for the standard phantom treatment plan.	165
Table 76: Dosimetric changes from baseline used for severity scoring for MLC leakage and transmission modeling values of 0% and 10% for the complex phantom treatment plan.	165
Table 77: Dosimetric changes from baseline used for MLC tongue-and-groove effect modeling with width values of 0.005 cm and 0.200 cm for the standard phantom treatment plan.	168

Table 78: Dosimetric changes from baseline used for MLC tongue-and-groove effect modeling with width values of 0.005 cm and 0.200 cm for the complex phantom treatment plan.	168
Table 79: Dosimetric changes from baseline used for severity scoring for MLC rounded leaf end modeling with radius values of 4 cm, 15 cm, and 20 cm for the standard phantom treatment plan.	171
Table 80: Dosimetric changes from baseline used for severity scoring for MLC rounded leaf end modeling with radius values of 4 cm, 15 cm, and 20 cm for the complex phantom treatment plan.	171
Table 81: Dosimetric changes from baseline used for severity scoring for differences in the CT table used for the standard phantom treatment plan.	173
Table 82: Dosimetric changes from baseline used for severity scoring for differences in the CT table used for the complex phantom treatment plan.	174
Table 83: Summary of the phantom severity scores based on structure evaluation criteria and our severity scoring scale for standard and complex treatment plans. The overall severity score assigned for each failure mode represents the maximum severity.	176
Table 84: For each failure mode: 95% confidence interval of the median of the qualitative severity scores, the quantitative severity scores and results of one-sample Wilcoxon Signed Rank Test, with significance level $p < 0.05$ indicated in red. P-values greater than significance level highlighted in green.	178
Table 85: Severity scores from PTVs, OARs, and overall for ten clinical oropharyngeal patients with - 10% and +10% beam energy adjustments.	181
Table 86: Severity scores from PTVs, OARs, and overall for ten clinical oropharyngeal patients with 2% beam symmetry errors.	182
Table 87: Severity scores from PTVs, OARs, and overall for ten clinical oropharyngeal patients with 3.5% beam symmetry errors.	182
Table 88: Severity scores from PTVs, OARs, and overall for ten clinical oropharyngeal patients with 10% beam symmetry errors.	183
Table 89: Severity scores from PTVs, OARs, and overall for ten clinical oropharyngeal patients with 1 mm systematic MLC shifts in one bank (X1 or X2).	184

Table 90: Severity scores from PTVs, OARs, and overall for ten clinical oropharyngeal patients with 2 mm systematic MLC shifts in one bank (X1 or X2).....	184
Table 91: Severity scores from PTVs, OARs, and overall for ten clinical oropharyngeal patients with -2° and +2° gantry angle errors.....	185
Table 92: Severity scores from PTVs, OARs, and overall for ten clinical oropharyngeal patients with -2° and +2° collimator angle errors.....	186
Table 93: Severity scores from PTVs, OARs, and overall for ten clinical oropharyngeal patients with -2° and +2° couch angle errors.	186
Table 94: Severity scores from PTVs, OARs, and overall for ten clinical oropharyngeal patients with MU linearity errors.....	187
Table 95: Severity scores from PTVs, OARs, and overall for ten clinical oropharyngeal patients with MLC leakage and transmission errors.	189
Table 96: Severity scores from PTVs, OARs, and overall for ten clinical oropharyngeal patients with MLC tongue-and-groove modeling errors.	190
Table 97: Severity scores from PTVs, OARs, and overall for ten clinical oropharyngeal patients with MLC leaf end modeling errors.....	191
Table 98: Severity scores from PTVs, OARs, and overall for ten clinical oropharyngeal patients with CT table errors.	192
Table 99: True severity scores based on PTV coverage ($D_{95\%}$) and QUANTEC criteria of OARs for ten clinical oropharyngeal patients for 11 IMRT physical failure modes near tolerance criteria levels.....	193
Table 100: True severity scores based on PTV coverage ($D_{95\%}$) and QUANTEC criteria of four common OARs for ten clinical oropharyngeal patients for 11 IMRT physical failure modes near tolerance criteria levels.	193
Table 101: A comparison of the overall true severity scores from 10 patients with two different OAR criteria evaluated.....	194

Table 102: Comparison of median qualitative severity scores from the survey (N=184) and the overall quantitative severity scores from standard and complex phantom treatment planning studies to the 95% confidence interval of the median true severity score based on the evaluation of PTVs and four common OARs in ten oropharyngeal patient treatment plans. Red indicates that the score does not lie within the 95% CI and green indicates it does.	201
Table 103: Comparison of median qualitative severity scores from the survey (N=184) and the overall quantitative severity scores from standard and complex phantom treatment planning studies to the 95% confidence interval of the median true severity score based on the evaluation of PTVs and all OARs in ten oropharyngeal patient treatment plans. Red indicates that the score does not lie within the 95% CI and green indicates it does.	201
Table 104: Comparison of maximum true severity scores from the evaluation of PTVs and four common OARs in ten oropharyngeal patient treatment plans to maximum quantitative severity scores from standard and complex phantom treatment planning studies and median and maximum qualitative severity scores from the survey (N=184). Green indicates matching exactly with maximum true severity, yellow indicates matching within 1 score.	202
Table 105: Comparison of maximum true severity scores from the evaluation of PTVs and all OARs in ten oropharyngeal patient treatment plans to maximum quantitative severity scores from standard and complex phantom treatment planning studies and median and maximum qualitative severity scores from the survey (N=184). Green indicates matching exactly with maximum true severity, yellow indicates matching within 1 score.	202
Table 106: Patient 1 dose differences from baseline at evaluation criteria for PTVs and OARs for each failure mode.	233
Table 107: Patient 2 dose differences from baseline at evaluation criteria for PTVs and OARs for each failure mode.	237
Table 108: Patient 3 dose differences from baseline at evaluation criteria for PTVs and OARs for each failure mode.	241

Table 109: Patient 4 dose differences from baseline at evaluation criteria for PTVs and OARs for each failure mode.	245
Table 110: Patient 5 dose differences from baseline at evaluation criteria for PTVs and OARs for each failure mode.	249
Table 111: Patient 6 dose differences from baseline at evaluation criteria for PTVs and OARs for each failure mode.	253
Table 112: Patient 7 dose differences from baseline at evaluation criteria for PTVs and OARs for each failure mode.	257
Table 113: Patient 8 dose differences from baseline at evaluation criteria for PTVs and OARs for each failure mode.	261
Table 114: Patient 9 dose differences from baseline at evaluation criteria for PTVs and OARs for each failure mode.	266
Table 115: Patient 10 dose differences from baseline at evaluation criteria for PTVs and OARs for each failure mode.	270

Chapter 1: Introduction

1.1 Background

Despite continuous improvements to the prevention, detection, and treatment of cancer, 25% of deaths in the United States can be attributed to cancer and over 1.6 million new cancer cases were diagnosed in 2014¹. There are a variety of treatment options available today, with the most elemental categories being surgery, chemotherapy, and radiation therapy. Currently, about two thirds of all cancers are treated with a form of radiation therapy either alone or in conjunction with another form of therapy². With our present level of knowledge, experience, and advanced technologies, a high level of safety, quality, and efficiency are expected of radiation treatments. However, as with any medical procedure, radiotherapy presents potentially very serious risks to the patient and errors have been known to occur.

Compounding with the inherent risks associated with radiotherapy, complicated advanced techniques such as various forms of intensity modulated radiation therapy (IMRT), precise delivery of Stereotactic Body Radiation Therapy (SBRT), and Image Guided Radiation Therapy (IGRT) present additional challenges in the clinic and may lead to increased risk if not implemented correctly and properly maintained. Recent advancements in imaging, targeting, and treatment techniques allow precise delivery of very high radiation doses to diseased tissue while sparing adjacent healthy tissue and critical organs using a variety of modalities. These advanced techniques have the potential for superior tumor control while maintaining minimal normal tissue complications or toxicities. With the advantages of advanced techniques, comes increased treatment complexity and risk of errors that requires an increase in the quality management of these techniques. Although reduced error rates have been reported with the implementation of advanced, automated treatment techniques over time³⁻⁵, increased treatment complexities have also been shown to significantly increase the rate of undetected errors⁶. The long chain of events making up the radiation therapy process relies upon complex machinery and software, highly trained staff, and various interfaces between these components. The extensive and complicated nature of

the external beam radiation therapy (EBRT) process is well demonstrated in the 269 node process map from Ford, *et. al.* shown in Figure 1⁷. Procedures, dose calculations, and delivery requirements are more complicated today than ever, leaving more potential for error. Figure 2 from Kalapurakal, *et al.* shows more simply a standard EBRT process demonstrating several of the potential failure points, personnel, and check points⁸. It is clear that from this figure that many potential points of failure exist, however this is not the whole picture. Behind many of the listed actions/errors lie several more steps, especially physics steps such as those required for proper dose calculations and dose delivery. In addition to the complicated advance treatment processes, the increased demand on staff, hardware, and software is a concern. With the challenges of busier clinics, advanced treatment techniques, and increased patient risk, the radiotherapy community is faced with complex challenges in safety and quality. Evidence of these challenges and the risks present in radiation therapy can be found in increasingly publicized error reports^{4,9-13}.

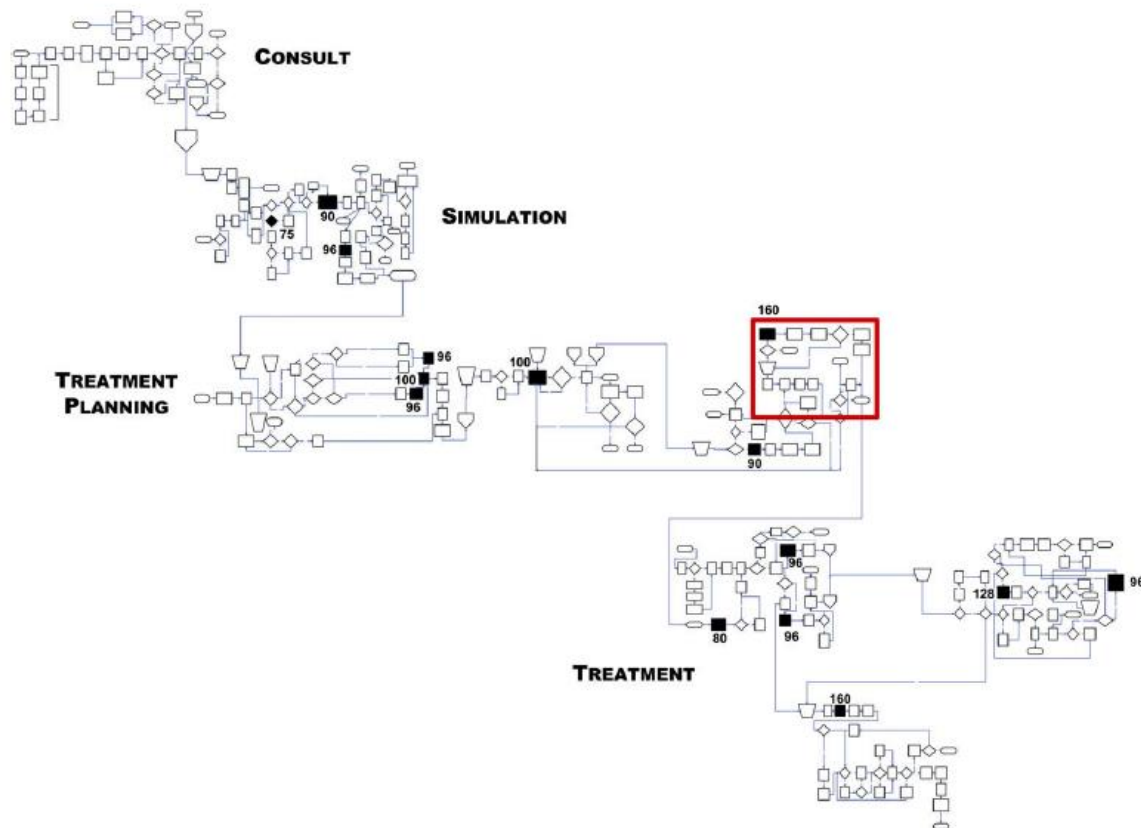


Figure 1: EBRT process map from used to evaluate the safety of the process in Ford, et. al (2009). 269 process nodes are shown and those highlighted in black indicate the top 15 most risky as defined by risk probability number (RPN)^{7, A}

^A Reprinted from Int. J of Rad Onc Bio Phys 74(3), Ford, E. C. , Gaudet, L. M., Vanderver, B., Engineer, L., Zellars, R., Song, D. Y., Wong, J., DeWeese, T. L., "Evaluation of safety in radiation oncology setting using failure mode and effects analysis." pp. 852-858. Copyright (2009), with permission from Elsevier.

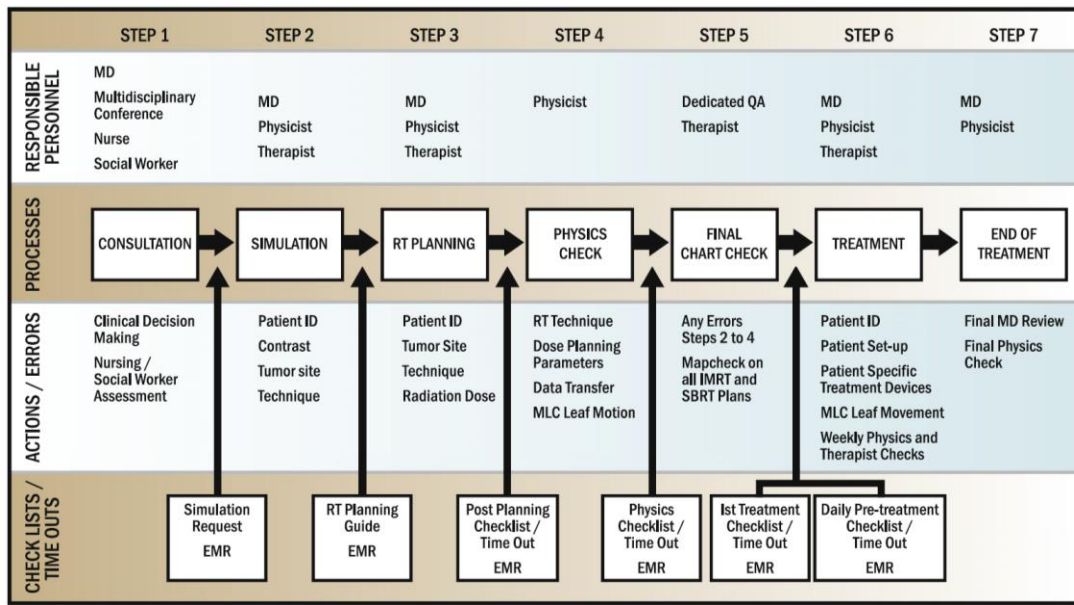


Figure 2: EBRT process with potential errors, Radiation oncology personnel, and common barriers or checklists/timeouts to catch errors^{8, B}

Although the true rate of errors in radiation therapy is unknown, several studies to date have reported on the error rates captured by incident reporting systems. Error rates reported by single institutions using incident reporting systems vary from 0.1% to approximately 5% per treatment course^{4,9-13}. Multi-institutional data is becoming available as national and international reporting databases gain popularity. Shafiq, *et al.* performed a review of all radiation therapy events published between 1976 and 2007, reporting 7741 incidents and near misses with 3125 of those resulting in some level of patient harm including 38 patient deaths due to overdose toxicities or under-dose failures¹⁴. These errors can originate from any point in the process and have a multitude of causes. One detailed example of this comes from a retrospective review and categorizations of 59 EBRT accidents which resulted in the compilation of initiating events and descriptions shown in Table 1.¹⁵ One consistent factor in error reporting is the prevalence of human errors, which lead to over 50% of incidents of potentially high severity reported by Terezakis, *et al*¹⁶. “One error is an error too many” is the common mentality amongst Radiation Oncology

^B Reprinted from Int. J of Rad Onc Bio Phys 86(2). Kalapurakal, J. A., Zafirovski, A., Smith, J., Fisher, P., Sathiaselalan, V., Barnard, C., Rademaker, A.W., Rave, N., Mittal, B.B. “A comprehensive quality assurance program for personnel and procedures in radiation oncology: value of voluntary error reporting and checklists.” pp. 241-248. Copyright (2013), with permission from Elsevier.

Stage (no. of cases)	Initiating events (no. of cases)	Description of initiating events	No. of cases of non-clear descriptions
Calibration (15)	Miscalibration of measuring instrument (5)	- Misinterpretation of calibration data, e.g., reference material in dose calculation, atmosphere pressure, etc. (3)	1
	Miscalibration of beam (10)	- Mislabeling the side of chamber by the previous physicist - Use of an inappropriate correction factor - Wrong conversion of units for the source strength from the installer to the hospital - Applying incorrect exposure time (30 seconds instead of 18 seconds [0.3 minutes]) - Incorrect positioning of detector - Incorrect calculation for the decay of source outputs (2) - Inconsistency of unit between physicist and oncologist - Use of inappropriate ionization chamber	2
Planning (18)	Applying incorrect reference data in dose calculation (8)	- Incorrect data use for dose calculation - Incorrect inclusion of wedge factors - Wrong basic data in a treatment planning system (TPS) different from measured data - Wrong measurement of depth dose data by manufacturer - Incorrect tables of treatment times - Misapplication of distance correction in TPS - The planning staff failed to use a computer program "wedge normalization factor in making initial dose calibrations"	1
	Dose calculation errors (10)	- Incorrect dose calculation using the inverse square law - Reversed treatment times for open and wedged beams - Misapplication of wedge factor in computer calculations - The physicist failed to record the wedges in the setup portion of the patient's chart and the wedges were not used during the treatment - The technologist make a mistake in the calculation of the treatment time - The dosimetrist calculated mistakenly the dose, i.e., for 3 Gy per each for two treatment instead of 1.5 Gy for each - Incorrect selection of wedge - Reversal of magnetic resonance images - Incorrect calculation of monitor units - (E) computer crash	0
Simulation (2)		- Incorrect labeling of a simulator film (right/left) - (E) electrical shock to the patient (mechanical failure)	0
Patient setup (12)	Misidentification of patients (3)	- Incorrect identification of patient (2) - The chart of another patient was picked up	0
	Incorrect setup for location (9)	- Technologist failed to recognize physician's verbal instruction about the different number of treatment fractions for the two sites - The technologist mistakenly continued treatment to the wrong region - The technologist setting up the treatment failed to review the patient's chart and used wrong tattoo - A technologist set up a new patient and marked the wrong beam position - The technologist mistakenly setup the treatment field - Incorrect positioning of patient (2) - Incorrect identification of location by misunderstanding of tattoos - The operator misunderstood (miscommunicated) the instruction about the field size from the physicist	0
Delivery (12)	Physical failure of equipment (5)	- (E) radiation leakage - (E) loosening wedge mounting - (E) the head of unit fell on the patient - (E) a lead block fell from a height of 0.5 m, striking the patient - (E) the cassette holder assembly detached and fell down to the patient	1
	Equipment malfunctioning (4)	- (E) failure of a microswitch required to select the scattering foil for electron beams or the beam flattening cone for photon beams - (E) wrong indication of beam energy - (E) software failure in selecting mode between electron and photon - (E) sudden drift of machine output	
	Setup errors by human (2)	- A plate left in the beam - Machine incorrectly set for rotation (check)	
Total (59)		Human (43), equipment (11)	5

Table 1: Initiating events in 59 EBRT accidents for categorization. (E) indicates equipment failure^{15, C}

^C Reprinted from Radiat Oncol J. 31(2), Kim, J. "Categorizing accident sequences in the external radiotherapy for risk analysis." pp. 88-96 Copyright (2013) under the Creative Commons Attribution Non-Commercial License (<http://creativecommons.org/licenses/by-nc/3.0/>).

professionals and so while these error rates indicate that radiation therapy is actually one of the safer areas of modern medicine, with these generally low probabilities of incident occurrence in comparison to the recently estimated 210,000 annual deaths due to preventable harm in hospitals, efforts to thoroughly understand and mitigate risks are critical^{17,18}.

Although reported radiation oncology error rates are dominated by small errors that are often not clinically significant, they still pose a threat to our uncertainty goals and open the door to potentially larger, more severe errors. Hunt *et al.* recently reported dose errors exceeding 5% per fraction in 52% of treatment events including one dose error exceeding 50% per fraction^{9-11,13}. Several more severe incidents were brought to the attention of the public with a series of New York Times articles published in 2010¹⁹⁻²¹. One article, for example, described an incident in 2005 in which a head and neck treatment plan did not save correctly, leaving out multi-leaf collimator (MLC) files. The resultant open field irradiations of the patient's head and neck persisted for three fractions before being caught. Overall the patient received over seven times the intended dose and ultimately suffered a painful and slow death²². While this is an extreme example, such detrimental consequences are not acceptable and we must question - are those expectations of efficiency, quality, and safety being fulfilled?

To address the risks in radiation therapy, extensive quality management efforts are made. Quality management aims to maintain that the intended dose is delivered to the intended location at the intended time for all patients. Goals of treatment uncertainty are discussed at length in the literature. Generally, the goal of $\pm 5\%$ uncertainty of the absolute dose delivered to the target required by ICRU Report 24 is considered the overall goal and this is based on the responses of tumor control probability and normal tissue complication probability^{23,24}. However, this takes into account a large number of variables and superior accuracy in each variable must be achieved in order to meet this goal. To aid in achieving this goal, routine quality assurance practices are commonly documented for technical aspects of radiation therapy techniques by national and international bodies such as the American Association of Physicists in Medicine (AAPM) and the International Atomic Energy Agency (IAEA). Secondary checks are another

essential tool for radiation therapy, where a simple oversight by a single individual can easily result in the mistreatment of a patient or worse yet, become a systematic error that affects many patients. An accepted method for detecting and assisting to correct errors is the use of external independent audits, which are widely encouraged and are required in many instances such as when clinics are participating in multi-institutional clinical trials or as a Department of Health regulation. In radiation therapy, the Imaging and Radiation Oncology Core in Houston (IROC-H) is one group that serves this purpose for radiotherapy institutions participating in the National Cancer Institute's funded clinical trials through mailed output checks, chart reviews, site visits, and end-to-end phantom assessments. The external audit of one widely used modality, intensity modulated radiation therapy (IMRT), using IROC-H's head and neck phantom initially had a 33% failure and even today, a decade later, still has nearly a 15% failure rate despite the generous pass criteria of 7% absolute dose agreement and 4 mm distance-to-agreement²⁵. It is evident that changes are needed if improvements to the safety and quality performance are going to be made in the rapidly-advancing and high pressure environment radiation therapy is in.

To more thoroughly, effectively, and efficiently address potential errors in radiation therapy and attempt to eliminate severe consequences from radiation therapy treatments, risk mitigation techniques, largely borrowed from other high risk industries, are being highlighted. The initiative for new approaches to quality management has led the Radiation Oncology community to include more process-wide risk mitigation techniques, recognizing that understanding the entire process is necessary when errors may propagate from any point in the system to eventually reach the patient. Retrospective approaches such as root cause analysis (RCA) have been in use formally and informally in response to errors that are caught and deemed sufficiently threatening to justify the investment. This approach is being encouraged as is the reactive approach of incident reporting and learning, as mentioned previously. With widespread implementation of these risk mitigation techniques, we can learn not only from our own mistakes, but experiences in other clinics, and potentially make large global improvements in the direction of more safe, high quality treatments. Additionally, several prospective risk analysis and mitigation tools are

being implemented for this cause including process mapping, fault tree analysis, and failure modes and effects analysis (FMEA)²⁶⁻²⁸. Each of these tools offer benefits to the radiotherapy process and may be implemented concurrently. FMEA in particular is gaining popularity in radiotherapy with studies published from several institutions and a soon to be published report by the American Association of Physicists in Medicine (AAPM) Task Group 100^{7,29-36}.

Failure Modes and Effects Analysis

The overall goal of an FMEA in radiation therapy is to identify potential points of weakness in the process and prioritize them in accordance to the risk they present to the process goal of safely and efficiently delivering a specific dose to a specific location at a specific time. An FMEA is conducted by a multi-disciplinary panel of personnel experienced in the process to be evaluated, starting with a detailed outline of the processes commonly in the form of a process map. The panel then identifies every failure mode possible for each step of each process and each of these failure modes is assigned three scores: likelihood of occurrence (O), likelihood it will go undetected (D), and the severity of the consequences (S). Each of these scores has a predetermined scale generally ranking from 1 (smallest risk) to 10 (largest risk). The product of the three scores for each failure mode results in the risk probability number (RPN), which is then used to rank the failure modes in order of their potential impact on the patient and the clinic. Generally, a threshold RPN value is assigned by the panel, and failure modes with an RPN score above the threshold require attention to reduce their potential impact. In addition, it is common to re-evaluate failure modes with high severity scores (≥ 8) because the perceived patient safety concerns are unacceptably large. After improvements to the process are implemented and the high severity scores are believed to have been reduced, an FMEA may be performed again to reevaluate the risks associated with potential failures. To date, FMEA has been performed on a number of radiation therapy processes. A commonly cited example is the FMEA of external beam radiation therapy (EBRT) at Johns Hopkins University by Ford, *et al*. In this study, they generated a process map of 269 nodes with 127 potential failure modes. RPNs ranged from 2 to 160, with process improvements implemented for the fifteen most

risky failure modes⁷. While this study is an excellent start to the implementation of a risk mitigation technique in radiation therapy, there are still no standards by which to judge at what level an RPN score requires attention.

FMEA of radiotherapy processes, while subjective, still provides many benefits to patients and the Radiation Oncology department participating in the processes being evaluated. Performing an FMEA of a process allows for a thorough understanding and recognition of the process as a whole and its component interactions. Also, this analysis clearly results in improvements to the overall treatment process and therefore reduced risk. Inter-disciplinary bonds and respect are achieved as the importance of each step of the process becomes evident and the challenges of each member's tasks can be further appreciated. This comprehensive analysis can be very time consuming, but in another EBRT study by Ford, *et al.* the time was significantly reduced by streamlining the process, obtaining a failure mode ranking with just four one-hour meetings (total of 55 hours staff time)³⁷. The resultant ranking was beneficial to the entire process team as they developed a better understanding of the process components, their interactions, and the potential risks.

In spite of the aforementioned benefits of FMEA, limitations and weaknesses of this tool may compromise its utility. The primary limitation of an FMEA is the subjective nature of the process and the use of ordinal scoring to obtain risk information. This results in large variability in failure mode identification, scoring, and prioritization which calls into question the reliability of the results of an FMEA. In one study by Shebl, *et al.* two independent teams each identified 50 failure modes for a common process, but only 17 were identified by both groups and none of the top five failure modes as ranked by RPN were shared³⁸. Another study showed that scoring by average versus consensus of team scores also yielded different results³⁹. The validity of FMEA results are also questionable as the assigned scores lack evidence of accuracy and are often biased. The mathematical principles behind FMEA have even been called into question with respect to the validity of results, primarily noting that ordinal numbers cannot be meaningfully multiplied and the relative values of RPNs lack quantitative meaning and may

lack consistency. For example, is a failure mode with an RPN of 180 twice as risky as one with an RPN of 90^{40,41}? In addition to the potential issues that arise due to the subjective, ordinal scoring of FMEA, process-wide radiotherapy and, specifically, IMRT FMEAs present potential for grouping together physics-specific components such as "Linac hardware," leaving out valuable information about the treatment planning and delivery stages and the associated necessary quality management. While the systematic aspect of this approach is desired in the implementation of FMEA, detailed information is required to make meaningful quality improvements and physics is a very active aspect of this.

Motivation

With the present identified deficiencies, the application of FMEA to physics-specific delivery processes and further investigation into the values of these scores is needed. As called for by the American Society for Radiation Oncology (ASTRO), several incident reporting systems are becoming available for the community including an international system known as the Radiation Oncology Safety Information System (ROSIS)⁴². Such systems will be one way to quantify the likelihood of occurrence. Lack of detectability will be slightly more challenging to quantify because of the vast array of safety barrier configurations and detection systems, with large variances between institutions. However, the effectiveness of detecting failures can be evaluated for specific safety barriers individually and a recent attempt to qualitatively analyze the effectiveness of several QA techniques has been published⁴³. The severity of failure modes, arguably the most important of the three scores, is theoretically directly measureable and was the focus of the present study.

1.2 Objective

The objective of this work was to compute and/or measure the severity for IMRT delivery physical failure modes, improving upon two current weaknesses of FMEA; reducing the subjectivity of the scoring and examining physics-related failure modes individually. The end goal was to provide key information to medical physicists and linac engineers for improvement of patient safety that to date has not been determined and can potentially be used in future FMEA for radiation therapy.

1.3 Hypothesis and Specific Aims

Failure modes and effects analysis (FMEA) provides a prospective end-to-end risk evaluation of radiotherapy processes by means of a subjective qualitative scoring system. The objective of this work was to reduce the subjectivity of IMRT delivery FMEA severity scores for physics components by providing quantitative data on the effects of these failures. The central hypothesis was that quantified IMRT dose delivery failure mode severity scores that are based on measurement were significantly more likely to describe the true clinical consequences than conventional subjective scores. The rationale for this research was that even though quantitative severity scores are called for in the literature, they are not currently available and their application will improve the results of an FMEA for physics applications to radiotherapy quality management. The hypothesis was tested with the following Specific Aims:

1. Identify qualitative and quantitative severity scores for IMRT delivery physical failure modes.

The working hypothesis of this specific aim was that subjective qualitative severity scores obtained through a conventional FMEA were significantly different than quantitative severity scores generated from computed and measured data. The IMRT delivery process was outlined and critical physical failure modes identified. Qualitative scores were obtained through conventional FMEA methods and on a larger scale through a survey. Quantitative scores were obtained through treatment planning studies and physical measurements using an anthropomorphic phantom. The hypothesis was tested by performing a one-sample Wilcoxon Signed Rank Test.

2. Evaluate and compare the ability of qualitative and quantitative severity scores to accurately describe the error magnitude induced in clinical cases by each physical failure mode.

The working hypothesis of this specific aim was that quantitative severity scores were significantly more likely to match true severity scores than qualitative scores. True severity scores for each of the physical failure modes were evaluated by modeling errors in the treatment planning system and calculating the resultant magnitude of error in ten clinical patient treatment plans. We then evaluated how well the qualitative and quantitative severity scores from specific aim 1 matched these true severity scores. The qualitative and quantitative severity data were each compared to the true clinical data with an independent sample and one-sample Wilcoxon Signed Rank Test, respectively.

Chapter 2: Methods and Materials

2.1 Specific Aim 1: Identify qualitative and quantitative severity scores for IMRT delivery physical failure modes.

The objective of this specific aim was to obtain and compare qualitative and quantitative FMEA severity scores for the identified critical physical failure modes. The working hypothesis of this specific aim was that subjective qualitative severity scores obtained through a conventional FMEA would be significantly different than quantitative severity scores generated from computed and measured data. The rationale of this specific aim was that completion of a traditional FMEA allowed us to obtain qualitative, subjective scores of the specific process we are analyzing. The subjective, qualitative scores found in a conventional radiotherapy FMEA have an unknown reliability, consistency and validity. To improve upon this risk analysis tool, computation and physical measurement of the magnitude of dose delivery errors induced by failure modes were used for more accurate assignment of severity scores as called for in the literature. The severity scores obtained allowed for comparison of the qualitative subjective severity scores to the quantitative severity scores. Additionally, examples of FMEA in radiotherapy available in the literature today analyze processes as a whole with the benefit of comprehensive understanding of the process and error propagation, but neglecting process details such as those applicable to physics quality management. Expansion of physics-based process components will provide a more detailed investigation of physical failure modes. Verified physical failure mode severity scores will allow for more confident risk-based ranking, but more importantly, knowing error magnitudes associated with physical failure modes will allow physicists to appropriately assess and implement their quality management programs.

2.1.1 Radiotherapy process focus and failure mode identification

This study focused on the process of step-and-shoot head and neck IMRT delivery and was based on the radiation therapy delivery process used at M. D. Anderson Cancer Center (MDACC)

utilizing. In order to follow AAPM TG-100 and compare directly to the outcomes of the task group report, we focused on the same process used in their example: IMRT. Step-and-shoot is a basic and widely familiar form of IMRT dose delivery and results generated for this process can be built upon for more advanced IMRT techniques. This project utilized measurement tools of the Imaging and Radiation Oncology Core in Houston (IROC-H), specifically an IMRT head and neck phantom⁴⁴. This phantom is well established in the measurement of step-and-shoot IMRT deliveries, with more than twice as many segmental irradiations than any other IMRT technique. It is reported that >85% of credentialing irradiations of this phantom that fail a generous 7%/4mm criteria are caused by true treatment delivery errors as opposed to one-time physicist errors²⁵. The ability of this phantom to detect the small failures subject to this project was of interest.

As at the beginning of any FMEA, the process we examined was outlined in detail to provide a comprehensive description and basis for identifying potential points of failure. A failure mode is defined as an error or shortcoming of any component, step or sub-step that compromises the goal of the process. In our case the process goal was to safely and efficiently deliver the correct radiation dose to the correct anatomic location at the intended time. Further, in our study a physical failure mode was a failure mode that involves a physics-based component of the radiation dose calculation or delivery and comprises of both hardware and software components. To identify failure modes, one must consider how the process could fail while examining the process tree. What could go wrong at each step that could result in an error in the dose delivery? The process tree and failure mode identification was completed by a small group of experienced physicists with review and confirmation by the Advisory Committee on this project.

The approach to creating this list was to include potential errors that are relatively common and could occur by a mechanical failure or by an incorrect calibration/commissioning. Based on experiences in the clinic, experiences of the IROC-H at other clinics, and the group's knowledge of the literature, the below general process tree (Figure 3) and list of failure modes was determined and are shown below.

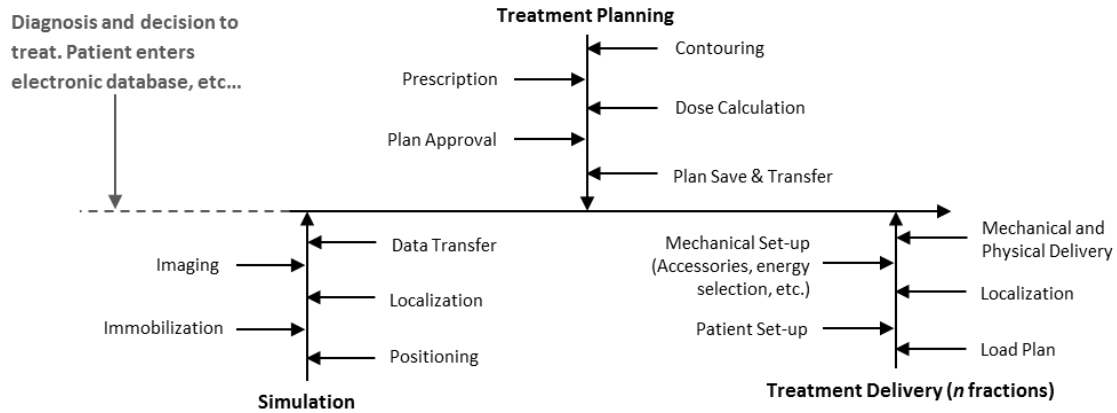


Figure 3: General IMRT Process Tree

IMRT physical delivery failure modes identified:

1. Beam quality
2. Beam Symmetry
3. MLC Position
4. Gantry angle
5. Collimator angle
6. Couch angle
7. MU linearity
8. MLC leakage and transmission modeling
9. MLC tongue-and-groove modeling
10. MLC leaf end modeling
11. CT number to electron density table in treatment planning system

Magnitude of Failure

The magnitude of the error induced (the magnitude of failure) was determined by the current criteria held in a common clinic which adheres to recommendations of the AAPM. We evaluated the severity at the tolerance level or just outside that level to simulate situations in which the clinic may or may not react to the failure. This approach to define the magnitude of failure differs from that of a

conventional FMEA, in which the worst effect is considered when evaluating severity⁴⁵. The reason for this departure was that, while rare catastrophic failures and their causes should be considered, the relatively small failures considered in this study are more clinically relevant. Failures of this magnitude occur with moderate frequency and are handled in different manners, depending on the clinic. Resultant data on failures of this magnitude will be useful for direct evaluation of the common quality assurance programs implemented in the clinic today and will serve to expand the functionality of an FMEA. The magnitude of failure evaluated in each situation will be described in the sections to follow.

2.1.2 Obtain qualitative severity scores by means of a traditional FMEA of the IMRT delivery process

Overview

Assignment of failure mode scores O, D, and S for an FMEA is conventionally completed by a multidisciplinary team of experts based on their opinions of the expected appropriate values. In order to obtain these qualitative scores, a survey of medical physicists was conducted. This served to evaluate the range of possible responses as well as the potential variability in interpretation. This survey also allowed us to gather the opinions of a wide range of physicists, with the target audience being therapy physicists that are active in the Radiation Oncology community.

Survey Design

Eleven different physical failure modes in step-and-shoot IMRT at or just outside commonly accepted tolerance criteria levels were briefly described and are listed in Table 2. Respondents were asked to estimate the worst case scenario percent dose error in a head and neck patient for each of the failure modes keeping in mind both target structures and organs at risk. Respondents were also asked to assign the three FMEA scores: Occurrence (O), Detectability (D), and Severity (S). The scales used in this survey for FMEA scores were based on conventional scales used in other radiotherapy FMEA studies and were color coordinated for ease of use as shown in Table 3. As described in the introduction, these

scales lack quantitative definitions for severity scores. The following demographic data was also collected: current IMRT clinical practices used including linear accelerator manufacturer, treatment planning system, and delivery technique, years of experience in medical physics, percent of time dedicated to clinical work, familiarity with FMEA, clinic location, and board certification.

Several factors were considered when designing this survey. Key components of the survey design were clarity and ease of completion. This topic of study presents challenges in meeting those goals. The identification of the process being evaluated with the survey, step-and-shoot head and neck IMRT, is very important to the scoring. However, description of the process could not be too specific or too broad so as to lead the respondent. The assignment of scores and percent dose errors can be confusing and had to be described clearly. FMEA is a new concept to most physicists and therefore could be intimidating or could discourage individuals from responding if they didn't feel qualified to answer. It was also important that the survey didn't take too long, was interesting, and felt worth the time to complete. Balancing these considerations with a complicated topic and the desire for the maximum amount of information possible was challenging. Some measures we took to address these challenges included the use of simple, concise language in the instructions. Color coding was used to help respondents quickly and easily use the scoring scale table. The scoring scale table was printed on each scoring sheet so respondents did not have to flip the pages back and forth. A pilot survey was conducted to assist with design and set up response expectations for our study.

The pilot survey was printed and handed out to colleagues at the 2013 AAPM Annual Meeting. An attempt was made to have individuals complete the survey at the IROC-H booth at this meeting, but this approach was not successful. A total of eleven responses were collected. Despite our efforts to make the survey easy to complete, many respondents complained that it took too long and this fact was considered heavily in the revision.

As a result of the pilot study, we decided to change the survey format in several ways to encourage participation. We used the tailored design survey method to guide our improvements to establish trust, increase the benefits of participation, and decrease the cost of participation⁴⁶. First, the survey was recreated for electronic completion on a web-based application called Survey Gizmo (<https://app.surveygizmo.com>). This allowed us to use simplified response formats such as drop down menus and check boxes which improve clarity. The order of the questions was changed to have the demographic questions at the end and scoring at the beginning. This was done to ensure that the participants focused on the specific process and scoring and to reduce distractions that may come from wondering what we are judging them on in the demographic questions. This also can help to make the survey feel legitimate and secure. Additionally, this enabled us to remove any mention of FMEA from the survey until the end when the respondent was asked about their familiarity with FMEA. Mention of FMEA was removed from the title and instructions with the intention of making the survey less intimidating and more familiar and appealing. Some of the language in the failure mode description was also clarified. Failure modes were presented one at a time so that respondents didn't feel distracted by how many questions were left or what was next. Since in-person efforts to distribute the survey had not proven effective, it was decided that this survey would be distributed by email and sent from the IROC-H office. This allowed for respondents to complete the survey on their own time. It also created a sense of being part of a larger study, which adds to the legitimacy and importance of the survey. In addition to the scoring described above, several groups completed the survey and before assigning scores as in the individual survey, they assigned quantitative error measures (percent dose error) to the severity scoring scale i.e., what does a severity score of "1" mean quantitatively? The remainder of the group survey was the same as the individual survey. Demographics collected from the groups were also the same, but were collected for the group overall. The full surveys can be found in Appendix A.

Failure Mode	Magnitude of Failure
1. Beam energy	1%
2. Beam symmetry	2%
3. MLC systematically in one bank	2 mm
4. Gantry angle systematically	2.0°
5. Collimator angle systematically	2.0°
6. Couch angle systematically	2.0°
7. MU linearity for < 5 MU systematically	6%
8. MLC transmission and leakage modeling	0.5%
9. MLC tongue-and-groove modeling	0.5%
10. MLC leaf end modeling	0.5%
11. CT number to electron density table systematically	2%

Table 2: Physics-specific failure modes evaluated in survey

Rank	Occurrence (O)		Detectability (D)		Severity (S)	
	Qualitative	Frequency	Qualitative	Estimated probability of failure going <u>undetected</u>	Qualitative	Categorization
1	Failure Unlikely	0.01%	Never undetected	0.01%	No effect	
2		0.02%	Very low likelihood undetected	0.2%	Inconvenience	Inconvenience
3	Relatively few failures	0.05%		0.5%		
4		0.1%	Low likelihood undetected	1%	Minor dosimetric error	Suboptimal plan or treatment
5		< 0.2%		2%	Limited toxicity or tumor underdose	Wrong dose, dose distribution, location or volume
6	Occasional failures	< 0.5%		5%		
7		< 1%	Moderate likelihood undetected	10%	Recordable event, Potentially serious toxicity or tumor underdose	
8	Repeated failures	< 2%		15%		
9		<5%	High likelihood undetected	20%	Reportable event, Possible very serious toxicity or tumor underdose	Very wrong dose, dose distribution, location or volume
10	Failures inevitable	> 5%	Always undetected	> 20%	Catastrophic	

Table 3: FMEA scoring scale used in survey.

Survey Distribution

The final survey for this study was distributed via email to approximately 2000 medical physicists worldwide that participate in quality assurance services provided by IROC-H. The survey was accessed online and was completed anonymously. Additionally, ten individuals were emailed the survey with the request to complete it using a group of experts at their clinic.

Analysis of survey results

Post survey collection analysis included RPN calculation and failure mode ranking according to RPN as well as each of the individual scores. This was done in order to assess the priority assigned to each failure mode in addition to magnitude of responses. In addition to visual inspection and direct comparisons, data was coded and statistically analyzed using IBM SPSS (International Business Machines Corp., New York). To investigate the relationship between percent dose error and severity scores, which in theory should be directly related, we used Spearman Rank Order Correlation (Spearman's rho) to look for a correlation between the two values over all the failure modes. The Chi-Squared Test was used to look for significant association between scoring and categorical demographic data (treatment planning system, linear accelerator manufacturer, familiarity with FMEA, etc.) with Bonferroni adjustments applied to the alpha levels. Spearman's rho was used to investigate the relationship between scoring and percent of time dedicated to clinical work or years of experience. Additionally, in the literature both consensus and averages have been used to evaluate FMEA scores, so both methodologies will be examined in this study using the Chi-Squared Test to look for differences between group and individual scoring³⁹. Extreme outliers (as conventionally defined on Tukey box-and-whisker plots, greater than 3 times the interquartile range from the bottom of the first quartile or top of the third) were excluded from statistical analysis.

2.1.3 Quantify the severity of head and neck IMRT delivery physical failure modes by means of computation and physical measurement.

In order to obtain quantitative severity scores for this specific process, all of the identified physical failure modes were simulated on a H&N phantom in the treatment planning system and the dose difference induced was calculated. Also when possible, these failure modes were physically induced and the resultant dose was measured in the same phantom used for treatment planning studies.

Evaluation of Severity

In both treatment planning studies and physical measurements, an anthropomorphic phantom was used to assess the effects of each failure mode on a head and neck step and shoot IMRT delivery. For physical measurements, two conditions were used to evaluate a baseline “correct” delivery and subsequent deliveries with failures. Open fields were used to assess the dose output and to evaluate the flatness and symmetry. Changes in beam output induced by failure modes were factored out of measurements to ensure isolation of each failure mode, as an output error should be a failure mode of its own.

The Phantom

The phantom used in this study is the IROC-H’s head and neck IMRT phantom which mimics an oropharyngeal primary tumor and lymph node along with the spinal cord (see Figure 4). This phantom is used for end-to-end evaluation of institutions participating in IMRT clinical trials and is representative of a complex clinical IMRT case.

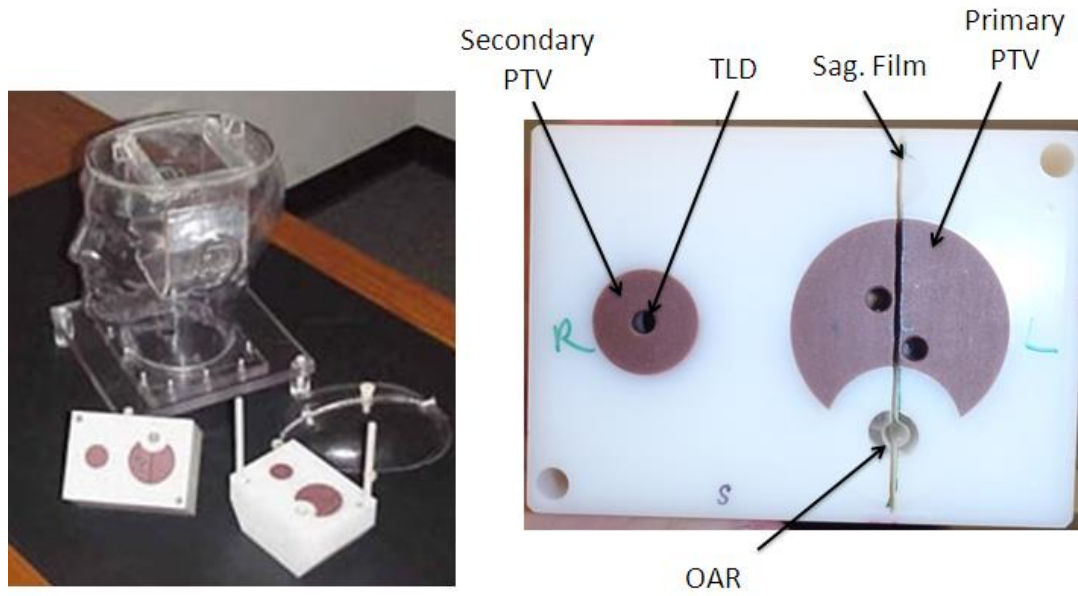


Figure 4: IROC-H's IMRT head and neck phantom (left), superior half of the phantom insert (right).

Structure	Dosimetric Criteria
Primary PTV	$D_{95\%} \geq 6.6 \text{ Gy}$
	$D_{99\%} \geq 6.14 \text{ Gy}$
Secondary PTV	$D_{95\%} \geq 5.4 \text{ Gy}$
	$D_{99\%} \geq 6.03 \text{ Gy}$
OAR (Spinal Cord)	Max Dose < 4.5 Gy
Normal Tissue	Max Dose $\leq 7.26 \text{ Gy}$

Table 4: IROC-H's IMRT head and neck phantom dosimetric criteria for the planning target volumes (PTVs), organ at risk (OAR), and normal tissue.

This phantom contains eight thermoluminescent dosimeters (TLD) and radiochromic film in the axial and sagittal planes. Treatment plans for this phantom followed the dosimetric criteria assigned by the IROC-H shown in the table in Table 5⁴⁴. Treatment plans followed MDACC protocol utilizing 6 MV photons and nine coplanar beam angles (0°, 40°, 80°, 120°, 160°, 200°, 240°, 280°, and 320°) which are shown along with the placement of isocenter in Figure 5. We used one treatment plan of average^D complexity and one of high complexity as defined by the number of monitor units (MU), segments, and modulation complexity score (MCS)⁴⁷. Increased treatment plan complexity has been the concern of several studies proposing resultant dose delivery errors⁴⁸⁻⁵⁰. A previous study with the IROC-H's IMRT head and neck phantom has indicated otherwise, with no significant errors caused by increased treatment

^D Based on previous irradiations of the IROC-H's head and neck IMRT phantom by various irradiations

plan complexity, but the question remains whether small errors caused by complexity could result in compounding effects when other errors are introduced⁵¹.

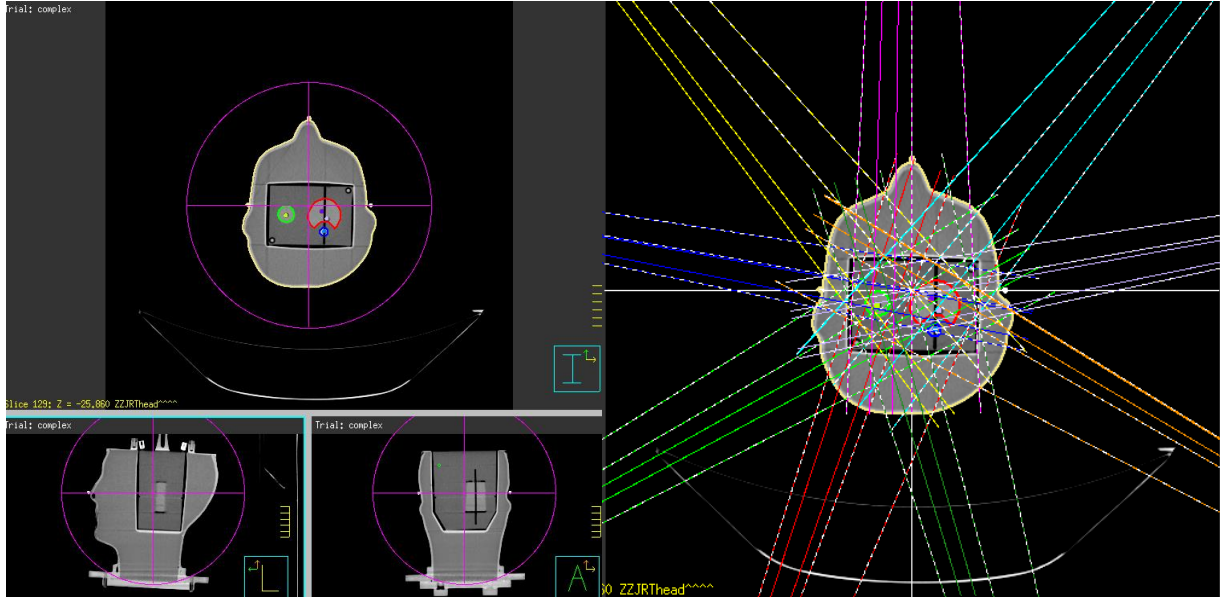


Figure 5: Treatment isocenter (left) and beam angles (right) for treatment plans using the IROC-H IMRT H&N phantom.

Quantifying the Severity

To assess the effects of each failure mode, we evaluated the difference in the dose distribution resultant from the induced failure mode compared to the unaltered baseline dose distribution (without any failures). For each failure mode, percent dose error to each of the primary structures (PTVs and OAR) was evaluated at using the prescription points as the evaluation criteria. The prescription points in the phantom are the PTVs prescribed to 95% of the volume and the OAR maximum point dose as a constraint. The error magnitude, or severity, of each failure mode was then assigned as the maximum of these dose errors. This means that out of the planning target volumes (PTV) and primary organs at risk (OAR), the largest deviation from the baseline dose as prescribed to that structure ($D_{x\%}$ or constraint level) was considered the magnitude of the error caused by that failure mode. This was chosen because each structure represents a critical component of the overall objective of the IMRT process and the dose volume prescriptions and constraints reflect those most important to the patient outcome. The maximum potential error in a treatment from the failure modes is our central concern. These values were obtained through our treatment planning studies.

Treatment Planning Studies

The Pinnacle treatment planning system (Philips Medical, Madison, WI) was used as our primary means to evaluate the effects of each of the physical failure modes on the phantom IMRT plan. A baseline plan was first established by calculating the phantom plan doses without any failure modes using a clinical MDACC beam model in order to provide a basis of comparison. This was the Varian TrueBeam1 model. Each of the physical failure modes was then simulated in the treatment planning system by means of altering the set up parameters or the beam modeling parameters. Utilizing our clinically implemented treatment planning system (TPS) as our means of dose calculation allowed for direct comparison with physical measurements as the beam model in the TPS corresponds to the beams used for irradiation. Most importantly, treatment planning studies allowed for evaluation of the volumetric dose distribution information through dose-volume histograms (DVH), enabling quantification of severity as described above.

All dose calculations used for treatment planning studies were performed with the Pinnacle CC Convolution algorithm. Treatment couches were removed from the planning CT image and a dose grid resolution of 2 mm x 2 mm x 2 mm was used.

Physical Measurement

Physical measurements were also made to further investigate the failure modes and with the intention of supporting our treatment planning studies. In many cases, physical measurement was dependent on altering a linear accelerator in a manner which would continue to affect the dose delivery after experiments, rendering it unable to appropriately deliver treatments clinically. Because of this, it was required that we were granted time on a clinical linear accelerator going out of commission. This measurement time was granted on three occasions and included four different Varian linear accelerators equipped with the Varian Millennium 120 MLC. These linear accelerators were in use clinically before our measurements were performed and were calibrated following the AAPM TG-51 protocol to 1.000

cGy/MU in muscle at d_{\max} under reference conditions of 100 cm SSD and 10 x 10 cm² field size. The basic information for these irradiation sets are listed in Table 5.

Irradiation Set	Date	Machine	Failure Modes
1	January 2012	Varian 2100	Energy, Symmetry, MLC Position
2	June 2012	Varian 2100	Energy, Symmetry, MLC Position
3	August 2013	Varian 6EX (2)	Gantry Angle, Collimator Angle, Couch Angle

Table 5: Failure mode physical measurements made on machines going out of commission.

For each irradiation set, the baseline condition of the machines and baseline phantom dose delivery with no failures were established in order to reference changes seen with the induced failure modes. To establish the baseline conditions of the machines, output measurements were performed in an open field using an ion chamber in a solid water phantom or water phantom. Ion chamber measurements at two or more different depths were used to characterize the beam energy. Also, the MatriXX ion chamber array (IBA Dosimetry, Schwarzenbruck, Germany) was used to measure open field photon beam flatness and symmetry. Basic warm up procedures for the ion chamber and MatriXX were followed including warm up irradiations of around 2000 MU before the start of each set of measurements. A baseline IMRT dose delivery to the head and neck phantom was performed for each irradiation set using the exact same phantom and beam configurations as subsequent failure irradiations. Failure mode conditions were established after each adjustment made to the beam, using the same methods as used to establish the baseline condition. These adjustments will be described in more detail in the following failure mode sections. Failure mode conditions were then used for IMRT dose delivery to the phantom. Resultant absolute doses measured with TLD and planar dose distributions measured with radiochromic film were used for comparison between baseline and failure mode delivery and between physically measured and computationally evaluated severities. The TLD and film were analyzed following the well-established protocol in practice at the IROC-H^{52,53}. TLD absolute doses in the PTVs for this IROC-H phantom are evaluated at the 7% agreement level. Planar dose distributions from the film are analyzed using a 3D gamma analysis with a 7%/4mm criteria, with 85% of pixels required to pass for IROC-H credentialing^{54,55}. Distance-to-agreement (DTA) between the primary PTV and OAR on the sagittal film

with a 4 mm criterion was previously used for this credentialing as well; however the gamma analysis is now the primary method for assessing the planar dose distributions²⁵. For this study, the TLD doses, DTA, and gamma analysis percent of pixels passing at both 7%/4mm and 5%/3mm criteria were compared directly between failure mode irradiations and baseline irradiations. When possible, irradiations were performed three times in order to account for the uncertainty in the measurements and account for potential set up errors. The TLD system has a precision of 3% and agrees with ion chamber measurements within $\pm 4\%$ at a 90% confidence level⁵². The film as read by the CCD100 Microdensitometer (Photoelectron Corporation, Lexington, MA) has a resolution of 0.3 mm and is registered within a 1 mm 2D and 3D RMS.

The time for each irradiation set was very limited, as was our ability to fully control all of the beam characteristics as desired. The baseline conditions and a summary of failure mode irradiations for each for each of the irradiation sets are described here. Failure mode irradiation details are described in each failure mode section.

Irradiation set #1

The first set of irradiations was performed on January 27, 2012 on the MDACC 2105 Varian Clinac 2100CD, which was set to be removed the following day. The IROC-H's head and neck IMRT phantom #21 was used with a complex treatment plan having 3533 MU, 216 segments, and a MCS of 0.181. A baseline irradiation of the phantom was performed. The TMR_{10}^{20} was measured in a water tank to establish the baseline energy. This measurement was performed using a 10 x 10 cm jaw-defined field with a source to axis distance (SAD) of 100 cm and 100 MU. The resultant TMR_{10}^{20} was 0.669. Next, the baseline flatness and symmetry were measured using the MatriXX at 100 cm source to surface distance (SSD), a 20 x 20 cm field, 50 MU, and 10 cm of solid water. The baseline symmetry was 0.04% cross plane and 0.2% in plane with flatness of 4.9% and 4.7%, respectively.

Following the baseline condition evaluation and phantom irradiation, the following failure mode irradiations were performed in the specified order:

1. In plane symmetry adjustment and phantom irradiation
2. Return to baseline
3. Cross plane symmetry adjustment and phantom irradiation
4. Return to baseline
5. Increase in energy and phantom irradiation
6. Return to baseline
7. Decrease in energy and phantom irradiation
8. Return to baseline
9. MLC positional error phantom irradiations

All TMR²⁰₁₀ and symmetry measurements were performed using the same methods as the baseline measurements and were all done in service mode. The phantom TLD and film was changed and it was realigned using the lasers between each irradiation, which were done in clinical mode.

Several lessons were learned from this set of irradiations. First, we gained an appreciation for the amount of time such measurements would take. Adjustment of the steering and bending magnet currents by hand adjusting the potentiometers is very sensitive and difficult to control; therefore it is challenging to precisely control the resultant symmetry and energy and requires several measurements along the way to reach the desired adjustments. We also noted that we did not account for changes in the output with adjustments, which could cause errors. This was useful in planning our next set of irradiations that needed to be much more complete.

Irradiation set #2

The second set of irradiations was performed on June 27th through the 29th of 2012, with establishment of the baseline conditions on day one following the last patient treatment. These

measurements were performed on the MDACC 2104 Varian Clinac 2100CD which was removed the day following the conclusion of our measurements. AAPM TG-51's protocol for photon beam output calibration was followed to establish the baseline beam output in the reference field of 10 x 10 cm at 100 cm SSD with 100 MU in a water tank. The resultant output was 1.013 cGy/MU. To ease the subsequent output measurements, the calibration factor was calculated for ion chamber measurement in polystyrene using a 10 x 10 cm field at 100 cm SSD and a depth of 5 cm with 100 MU and corrected for temperature and pressure. This calibration factor was calculated using Equation 1 and was determined to be 0.05719. This calibration factor was then used to assess future beam output using only the temperature and pressure corrected ion chamber reading at 5 cm polystyrene depth as done to find the calibration factor. The polystyrene phantom was used for TMR^{14}_5 measurements. This ratio was selected for ease of measurement with the specific configuration of polystyrene that was available at the time. At 100 cm SAD with a 10 x 10 cm² field and 100 MU, the TMR^{14}_5 was measured to be 0.612. Baseline flatness and symmetry were measured with the MatriXX using a 20 x 20 cm² field at 100 cm SSD and a depth of polystyrene of 10 cm with 100 MU. Flatness was measured as 2.4% and 1.1% and symmetry as 2.3% and 0.9% for the in plane and cross plane profile directions, respectively. Following these measurements, baseline phantom irradiations were performed with both standard and complex treatment plans. The IROC-H's head and neck IMRT phantom #21 was used with both a standard and a complex treatment plan with complexity metrics as described in Table 7. All phantom irradiations in this irradiation set were performed three times.

$$CF = \frac{Dose_{water}}{R_{5poly} \times k_{TPpoly}}$$

Equation 1: Calibration factor equation where $Dose_{water}$ is the output determined by TG-51, R_{5poly} is the ion chamber reading at 5 cm depth in polystyrene, and k_{TPpoly} is the temperature and pressure correction factor for the polystyrene measurement, all under baseline conditions.

Plan	MU	Number of segments	MCS
Standard	1948	90	0.482
Complex	3189	216	0.171

Table 6: Treatment plan complexity metrics for plans used in second irradiation set.

On day two, the baseline level was re-evaluated to ensure consistency. The output was calculated to be 1.019 cGy/MU. TMR^{14}_5 was measured to be 0.617. Flatness was 2.9% and 2.3% and symmetry was 1.6% and 1.2% for the in plane and cross plane directions, respectively. After the baseline conditions for the day were established, the following failure mode irradiations were performed in the specified order:

1. MLC positional error phantom irradiations
2. Re-establish to baseline
3. Increase in energy and phantom irradiations
4. Return to baseline
5. Decrease in energy and phantom irradiations

On the third and final day of this irradiation set, we began by returning the beam to baseline energy conditions. The TMR^{14}_5 we reached was 0.612. The beam was then altered for further failure mode irradiations and the conditions were evaluated as before for the following measurements:

1. Angular in plane symmetry adjustments and phantom irradiations
2. Return to baseline in plane
3. Angular cross plane symmetry adjustments and phantom irradiations
4. Return to baseline cross plane
5. Positional in plane symmetry adjustments and phantom irradiations

Once again, all output, TMR^{14}_5 , and symmetry measurements were performed using the same methods as the baseline measurements and were all done in service mode. The phantom TLD and film was changed and it was realigned using the lasers between each irradiation, which were done in clinical mode three times for each standard and complex treatment plans. Upon analysis, the output determined for each failure mode relative to the baseline output was factored out the TLD absolute dose results.

Irradiation set #3

The final set of irradiations was performed on August 21st through 23rd in 2013 on the MDACC 600 and 602 Varian Clinac 600 EX machines, which were removed from the clinic following our measurements. The original goal of this set of measurements was to take commissioning data for beams with energy or symmetry errors and irradiate the phantoms with the same altered beams. This commissioning data would then be used to create beam models for the treatment planning studies. However, we were not able to adjust the energy (PDD_{10}) of the machine by more than 0.5% from the baseline. We also were not able to adjust the symmetry on these machines because the symmetry and flatness are adjusted upon installation by physically adjusting the level of the flattening filter since there is no bending magnet. Adjusting the flattening filter would have required removal of the shielding which was too intensive and intrusive for us to perform. Therefore, this irradiation time was used to perform gantry, collimator, and couch angle failure mode irradiations using the 602 machine which had not been altered at all.

The MatriXX was used to establish the baseline conditions of this machine, which would not be altered for these irradiations. The PDD_{10}^5 was found to be 0.77 using solid water in a 10 x 10 cm² field with 100 cm SSD and 100 MU. In a 10 x 10 cm² field at 100 cm SSD and 10 cm depth of solid water, the flatness was 2.4% and 2.9% and the symmetry was 0.5% and 1.2% in the cross plane and in plane directions, respectively. The IROC-H's head and neck phantom #16 was used with the same standard treatment plan as the previous irradiation set having 1948 MU, 90 segments, and an MCS of 0.482. The baseline irradiation was performed three times. The phantom TLD and film were changed between each irradiation, which was performed in clinical mode three times for each failure mode. The phantom was aligned before each irradiation using the field crosshairs because the lasers were found to be several millimeters off. Failure mode irradiations were completed after baseline irradiations in the following order:

1. Gantry angle failure mode irradiation 1
2. Collimator angle failure mode irradiation 1

3. Gantry angle failure mode irradiation 2
4. Collimator angle failure mode irradiation 2
5. Another baseline phantom irradiation
6. Gantry angle failure mode irradiation 3
7. Collimator angle failure mode irradiation 3
8. Couch angle failure mode irradiations (3 total), performed the next day.

Assignment of Severity Scores

The error magnitude assigned to each of the failure modes was used to determine the severity score. These scores are important in two ways. As mentioned, severity scores are used to generate the RPN, but they are also evaluated independently to identify failure modes with extreme consequences that are unacceptable at any rate of occurrence and detectability. We used a unique severity score scale as described in the follow section.

Severity Score Scale

Currently, there is not a standardized scale for radiotherapy FMEA scores. Generally each score is assigned a scale from 1-5 or 1-10, with predetermined qualitative meaning assigned to the range of scores. Severity scales commonly assign a score of 1 to “no effect” and 10 to “death” or “catastrophic”^{7,34}. In order to achieve our goal of providing quantitative information for physics quality management on a clinically relevant scale, our severity score scale was be slightly different. We chose to maintain the commonplace 1-10 range and each score is assigned both qualitative meaning, more commonly seen in any FMEA, and a specific range of percent dose error, as required by the quantitative nature of our research. The qualitative definitions have been adapted from the upcoming AAPM TG-100 and an FMEA publication by Ford, *et al*⁷. The quantitative components were influenced by commonplace practices, regulations, and published radiation consequences. Our severity score scale is shown in Table 8. For a severity score of 2, deviation below the common clinical threshold for patient-specific IMRT QA measurements of 3% absolute dose agreement should be of minimal to no consequence, whereas if the

IMRT QA threshold is breached, at least a re-measurement would be made (an inconvenience)⁵⁶. A severity score of 4 indicates that the International Commission on Radiation Units and Measurements (IRCU) goal of 5% uncertainty has been surpassed, which is likely to result in a suboptimal plan and/or minor treatment consequences such as a few percent loss of tumor control probability⁵⁷. A dose deviation of 7% can cause observable biological consequences both with respect to tumor control and normal tissue complications, which has been assigned to the severity score of 5⁵⁸. Severity scores of 7-9 follow previous NRC regulations stating that a dose deviation of 10% is a “recordable event” and 20% is a reportable misadministration, which now fall under “medical event” criteria⁵⁹. The highest severity score of 10 quantitatively corresponds to a dose deviation of greater than or equal to 50%. This extreme level of failure has been reported in the past due to calibration errors at multiple institutions and while the consequences are not entirely clear, such an extreme deviation from expected dose has the potential for catastrophic consequences depending on the circumstances^{19,21}.

Severity Score (S)	Qualitative Definition	Quantitative Definition
1	No effect	0% - 2.9%
2	Inconvenience	3% - 3.9%
3		4% - 4.9%
4	Minor dosimetric error, suboptimal plan or treatment	5% - 6.9%
5	Limited toxicity or tumor under dose. Wrong dose, dose distribution, location, or volume.	7% - 8.9%
6		9% - 9.9%
7	Recordable event. Potentially serious toxicity or tumor under dose	10% - 14.9%
8		15% - 19.9%
9	Reportable event. Possible very serious toxicity or tumor under dose. Very wrong dose, dose distribution, location, or volume.	20%-49.9%
10	Catastrophic	≥50%

Table 7: Our unique quantitative severity scoring scale

Failure mode investigation

As described, treatment planning studies with the head and neck phantom were performed for each failure mode investigated in this study. Several failure modes were also investigated using physical

measurement of the dose delivered to the phantom. The failure modes and the specific methods to investigate each are described in detail in this section.

Failure mode 1: Beam energy

Overview

The energy of a photon beam produced by a linear accelerator for radiation therapy is fundamental to the calibration of the beam and the calculation of dose distributions in patients. The energy spectra and angular distribution of intensity of a photon beam is determined by the energy of the accelerated electrons striking the x-ray target. Penetrating ability and dose deposition increase with increasing photon beam energy, as demonstrated in Figure 6. These beams are commonly named for the nominal energy of the electrons at the accelerating structure window, which is approximately the maximum bremsstrahlung photon energy produced at the output of the linear accelerator. Measurement of the full energy spectra is challenging and not practical in the general radiation oncology setting, so the central axis depth dose information and specifically the ratio of doses at two depths are used to clinically characterize the beam energy. Commonly, this parameter is the ratio of the tissue maximum ratio (TMR) at 20 cm and 10 cm depth, denoted TMR_{10}^{20} , or the percent depth dose at 10 cm depth (PDD_{10}). These are both recommended to be kept within 1% of the baseline established upon commissioning and checked annually in the AAPM Task Group 142 report⁶⁰. As mentioned, only 6 MV photon beams were investigated in this study.

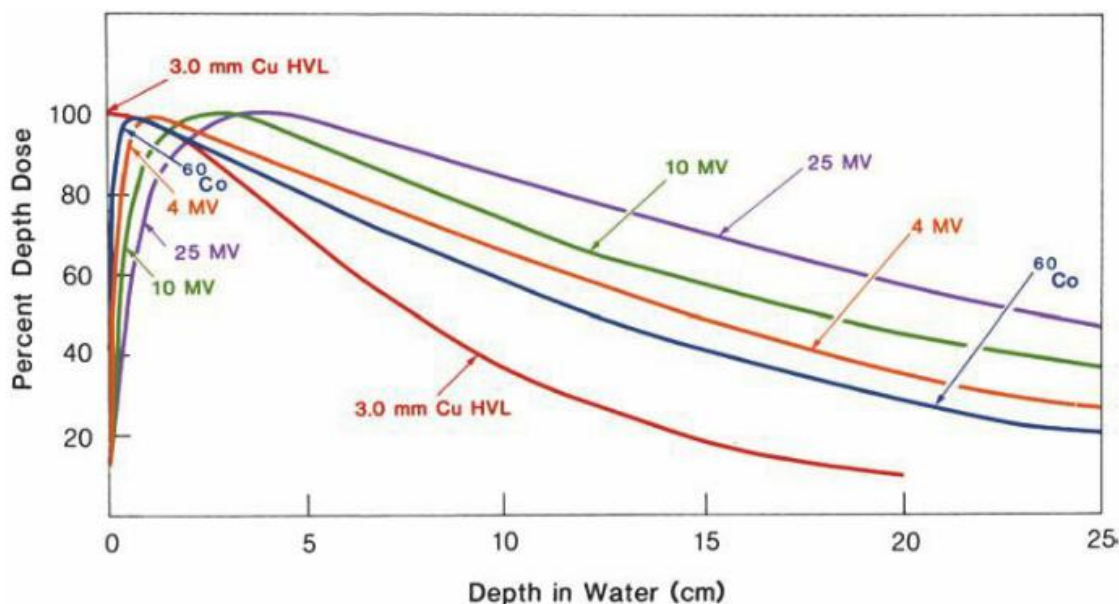


Figure 6: Photon beam central axis percent depth dose curves of varying energies (Khan, pg 143). All beams have a field size of 10 x 10 cm with source to surface distance (SSD) of 100 cm except the 3.0 mm Cu HVL beam which has an SSD of 50 cm.⁶¹

Practical adjustment of the photon beam energy on a medical linear accelerator is limited to small range around the nominal energies designated by the manufacturer. Clinical adjustments are made in high energy machines by altering the bending magnet current. This does not change the energy of the electrons in the accelerating structure, but rather changes the energy spectra and intensity distribution of the electrons that make it to the x-ray target. In Varian linear accelerators with photon energies greater than 6 MV, a 270 degree bending magnet steers and focuses the beam of electrons exiting the accelerating structure to be incident on the x-ray target. The energy spectra of the electrons that reach the x-ray target is bounded by a physical slit within the bending magnet, shown in Figure 7. This filters off the electrons on the low and high end of the energy spectrum. When the bending magnet current is altered, the spread of the electrons in the 270 degree turn shifts that is shown in the figure, becomes tighter or looser and therefore, either a higher energy or lower energy component of the electron beam is included in the spectrum that reaches the x-ray target. This change in the bending magnet current is approximately linearly proportional to the resultant change in the photon beam energy⁶². The magnitude of this adjustment is first limited by the energy spectrum that exists for a nominal x-ray energy, as set by the manufacturer. Further, the fluence of electrons is decreasing on the high and low ends of the energy

spectra and too large of an adjustment results in notable loss of x-ray fluence, such that the desired dose rate may not be achievable and the dose servo will halt the beam to prevent under dosing. This dose servo function can be overridden, however, insufficient dose rate may result in decreased output and under dosing.

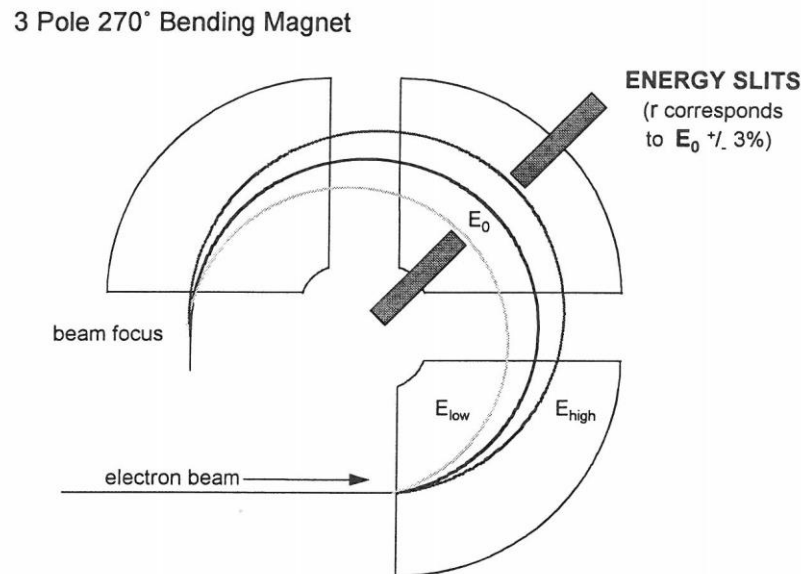


Figure 7: Schematic diagram of achromatic (270°) electron beam bending magnet with energy slit. ^E

Treatment planning studies

To simulate beam energy failures in the treatment planning system, it was necessary to create separate beam models with varied depth dose curves. To accomplish this, the depth dose and dose profile data from the established 6MV model for MDACC Varian TrueBeam linear accelerators was altered and used to generate new beam models. The alterations made to the depth dose and dose profile data was determined using data acquired at the Varian headquarters in Nevada by Dr. Peter Balter and Dr. Song Gao for research into characterizing beam energy changes⁶³. Using 5 x 5 cm², 10 x 10 cm², and 30 x 30

^E Image from Karzmark, C.J., Advances in linear accelerator design for radiotherapy, Med Phys (11): 105-128, 1984

cm² dose profiles and 30 x 30 cm² central axis percent depth dose data, patterns for changes from baseline beam data for 6 MV photon beams with $\pm 10\%$ bending magnet current adjustments were determined.

For percent depth dose curves, it was determined that the difference for both +10% and -10% beam energy models, the change from the baseline beam was approximately the same regardless of field size at depths shallower than 2.55 cm. Beyond 2.55 cm, linear trend lines originating at one point were fit to the change in percent depth dose from baseline for each field size. Larger field sizes changed less overall and had more constant amount of change with increasing depth. This is shown in Figure 8 for the -10% beam and Figure 9 for the +10% beam, where the curves have been shifted to the left by 2.55 cm so that each trend line could intersect at $y=0$, making the origination from the same point more simple. Small adjustments were made in the y intersection to maximize the coefficient of determination (R^2) for each trend line. To adjust the depth dose curves of field sizes that we did not have data for, we linearly interpolated between the shown trend lines. It can be seen that there is about a 2% difference in percent depth dose at depth of 10 cm from baseline for both energy adjustments.

For dose profiles, the differences within the field between baseline and energy adjusted beams were found to be approximately linear extending from central axis to either field edge, as shown in Figure 10 and Figure 11 for energy -10% and Figure 12 and Figure 13 for energy +10%. Linear trend lines were fit to the data within 97.5% of the full width half max and used for adjustment. The profiles were not exactly symmetric, so the larger difference of the negative and positive sides was used. We only had energy adjusted profiles for a 30 x 30 cm² field, so it was decided that these depth specific linear trends would be truncated and applied to smaller fields sizes. Changes in the penumbra and out of field dose were assumed to be negligible because the large differences beyond the field edge are largely due to the rapid falloff and appear artificially large out of field because of the small doses being dealt with. Additionally, only cross plane profiles (x) were modeled and in plane profiles are assumed to be the same.

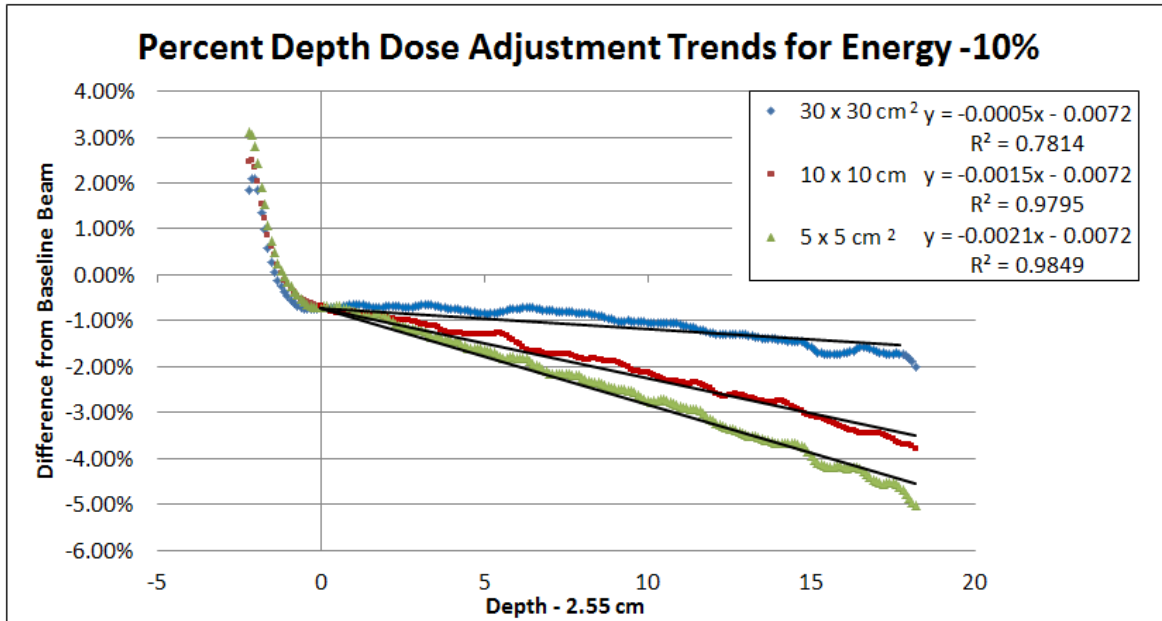


Figure 8: The percent difference in percent depth dose from the baseline beam (6 MV TrueBeam with no energy adjustments) of a beam with -10% energy. Curves were shifted 2.55 cm to the left for trend lines to intersect at approximately $y=0$. Data shown for field sizes of 30 x 30 cm², 10 x 10 cm², and 5 x 5 cm² and respective trend line equations and coefficients of determination (R^2) are shown.

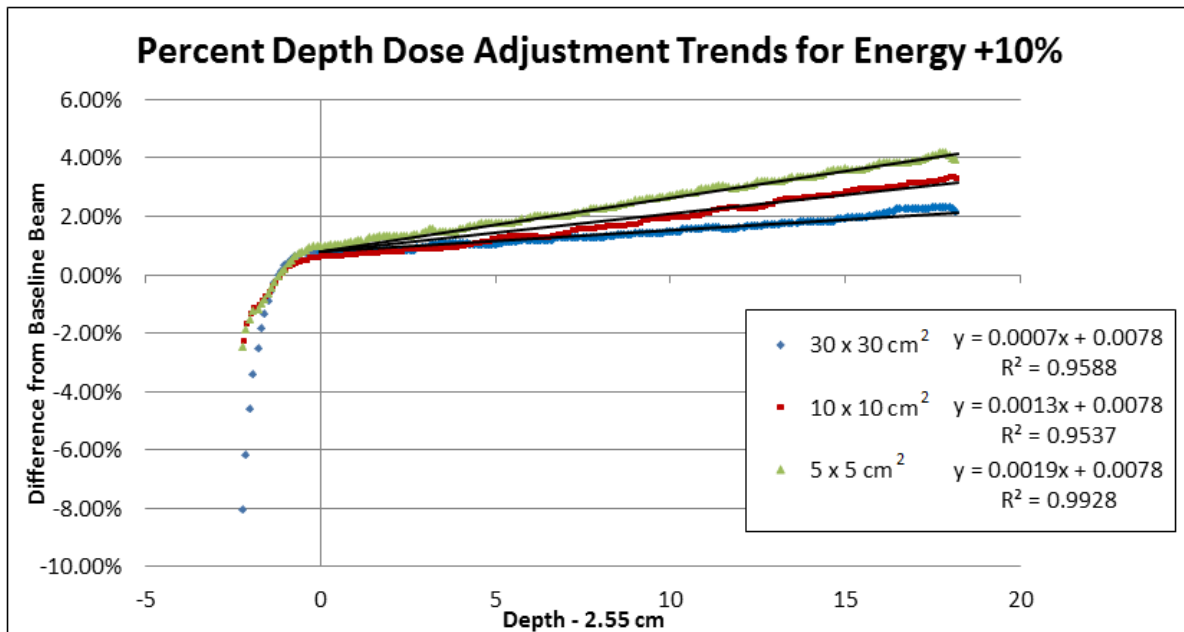


Figure 9: The percent difference in percent depth dose from the baseline beam (6 MV TrueBeam with no energy adjustments) of a beam with +10% energy. Curves were shifted 2.55 cm to the left for trend lines to intersect at approximately $y=0$. Data shown for field sizes of 30 x 30 cm², 10 x 10 cm², and 5 x 5 cm² and respective trend line equations and coefficients of determination (R^2) are shown.

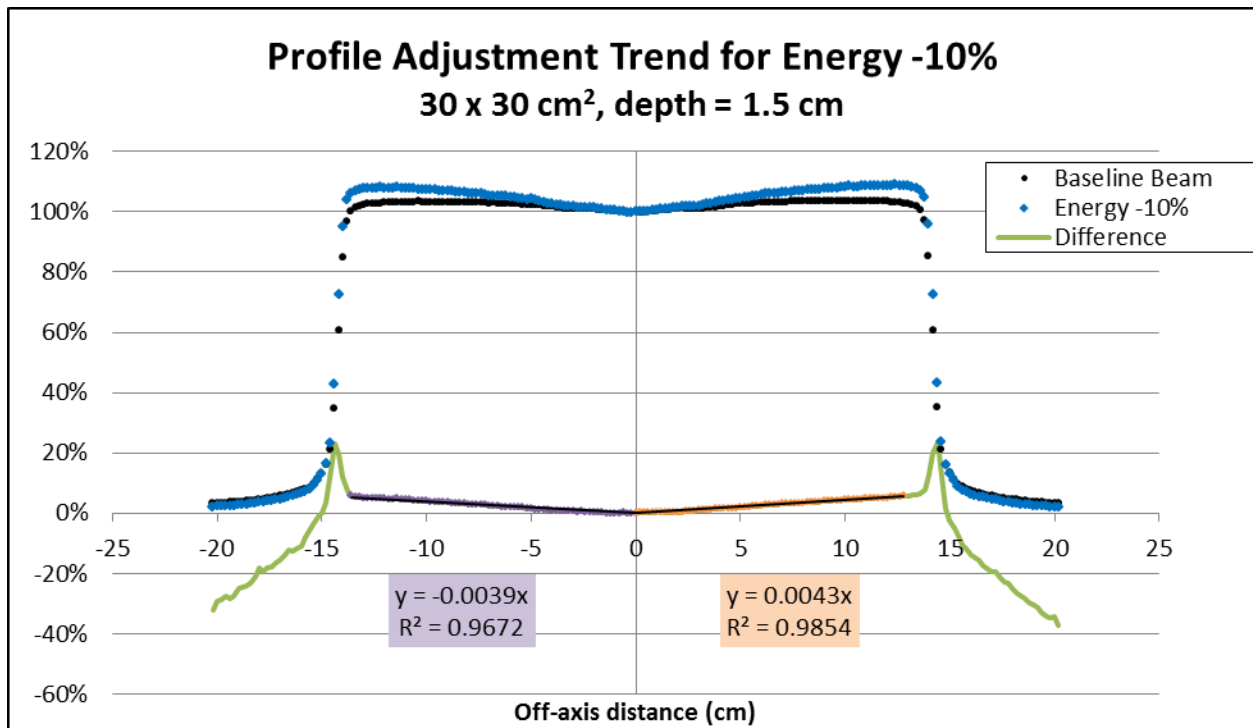


Figure 10: 30 x 30 cm² dose profiles at a depth of 1.5 cm for the baseline beam (6 MV TrueBeam with no energy adjustments) in black and the beam with -10% energy in blue, as well as the percent difference between them in green. Linear trend lines, respective equations, and coefficients of determination (R^2) are shown with purple being the negative trend line and orange being the positive trend line.

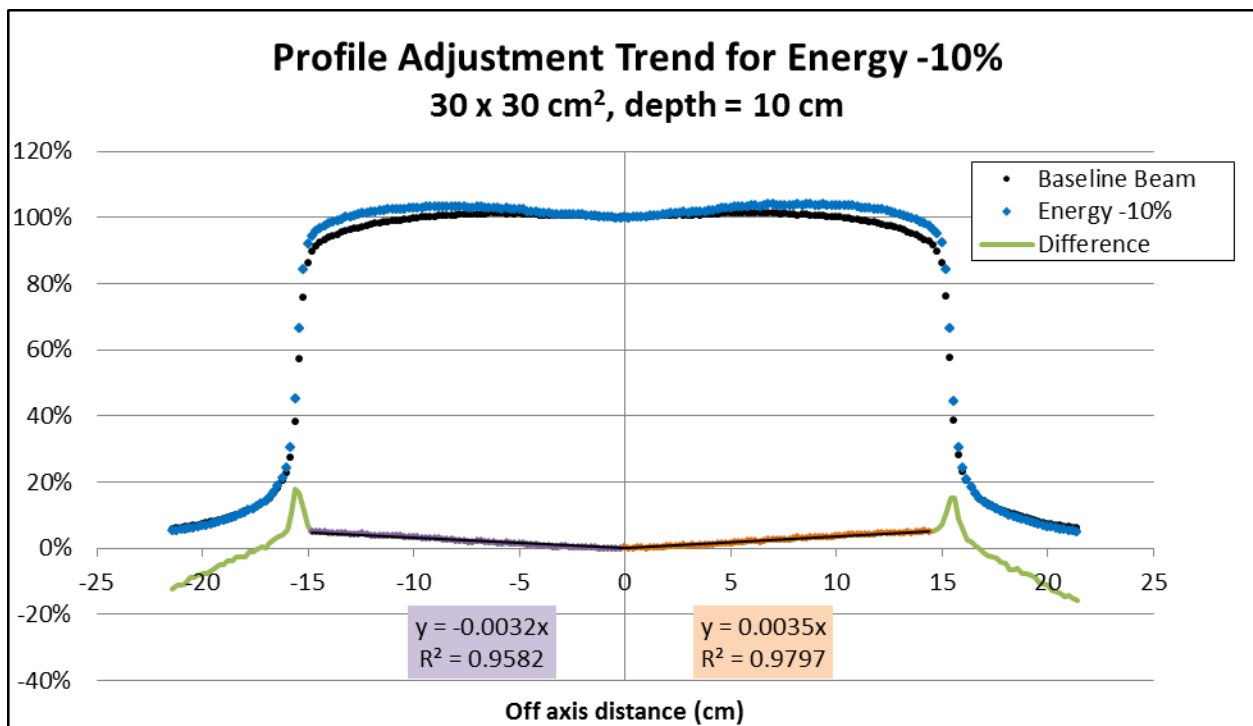


Figure 11: 30 x 30 cm² dose profiles at a depth of 10 cm for the baseline beam (6 MV TrueBeam with no energy adjustments) in black and the beam with -10% energy in blue, as well as the percent difference between them in green. Linear trend lines, respective equations, and coefficients of determination (R^2) are shown with purple being the negative trend line and orange being the positive trend line.

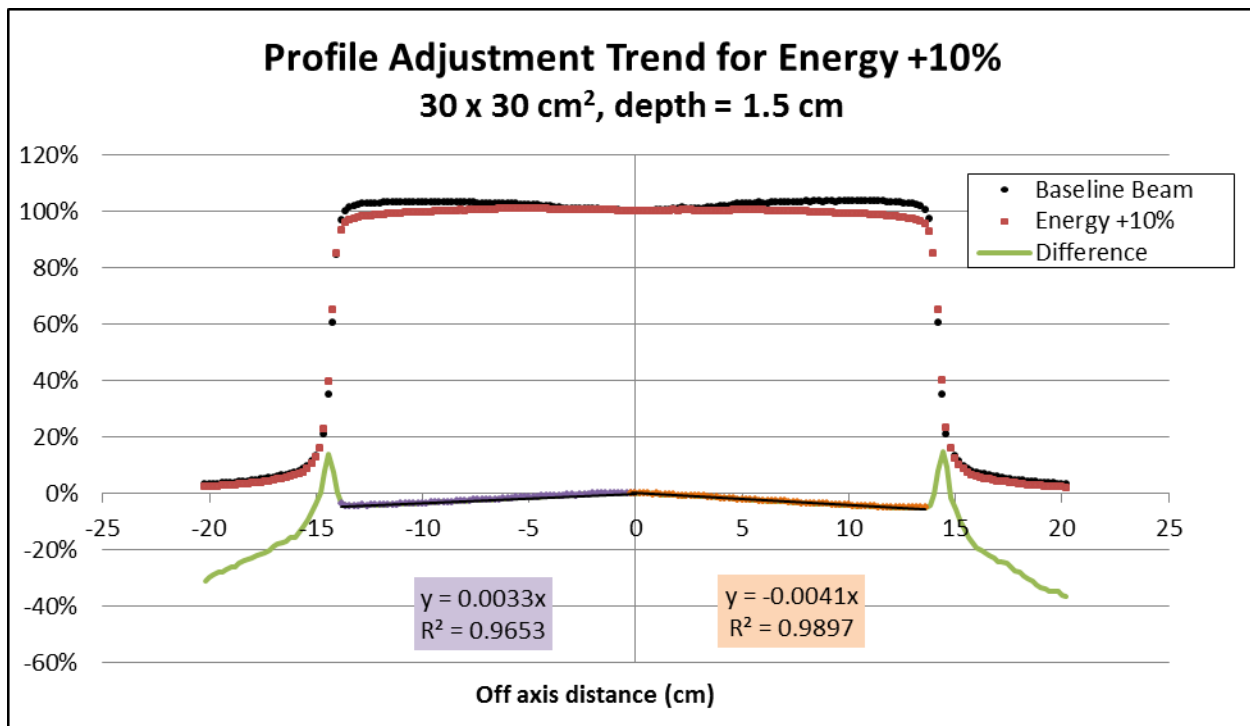


Figure 12: 30 x 30 cm² dose profiles at a depth of 1.5 cm for the baseline beam (6 MV TrueBeam with no energy adjustments) in black and the beam with +10% energy in red, as well as the percent difference between them in green. Linear trend lines, respective equations, and coefficients of determination (R²) are shown with purple being the negative trend line and orange being the positive trend line.

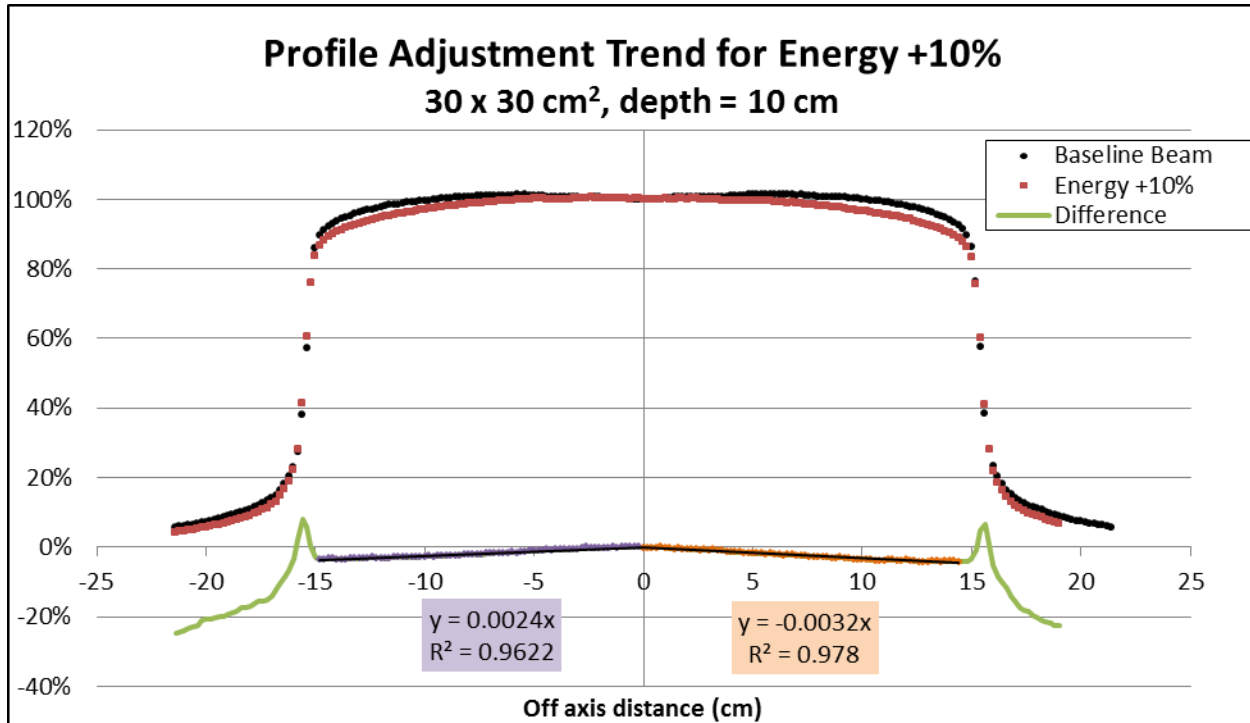


Figure 13: 30 x 30 cm² dose profiles at a depth of 10 cm for the baseline beam (6 MV TrueBeam with no energy adjustments) in black and the beam with +10% energy in red, as well as the percent difference between them in green. Linear trend lines, respective equations, and coefficients of determination (R²) are shown with purple being the negative trend line and orange being the positive trend line.

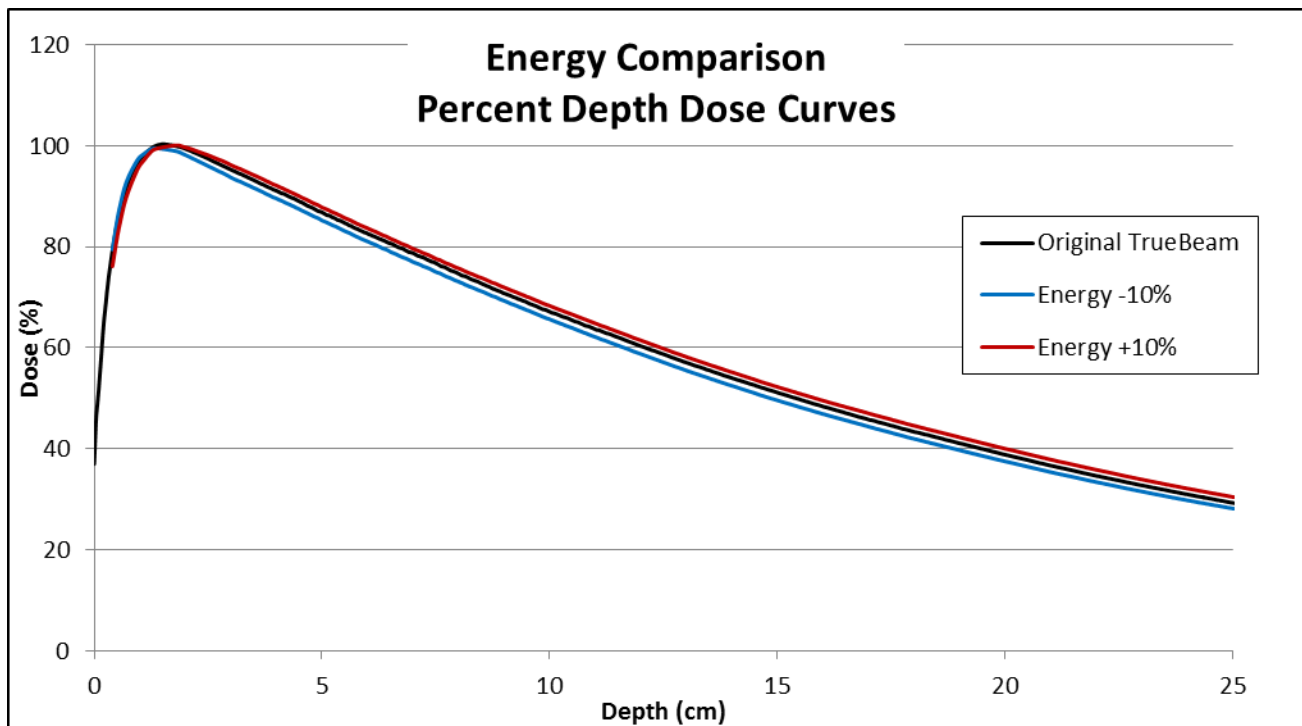


Figure 14: Depth dose curves for a 10 x 10 cm² field defined by the MLC for the original MDACC TrueBeam model and the adjusted TrueBeam models with +10% energy and -10% energy.

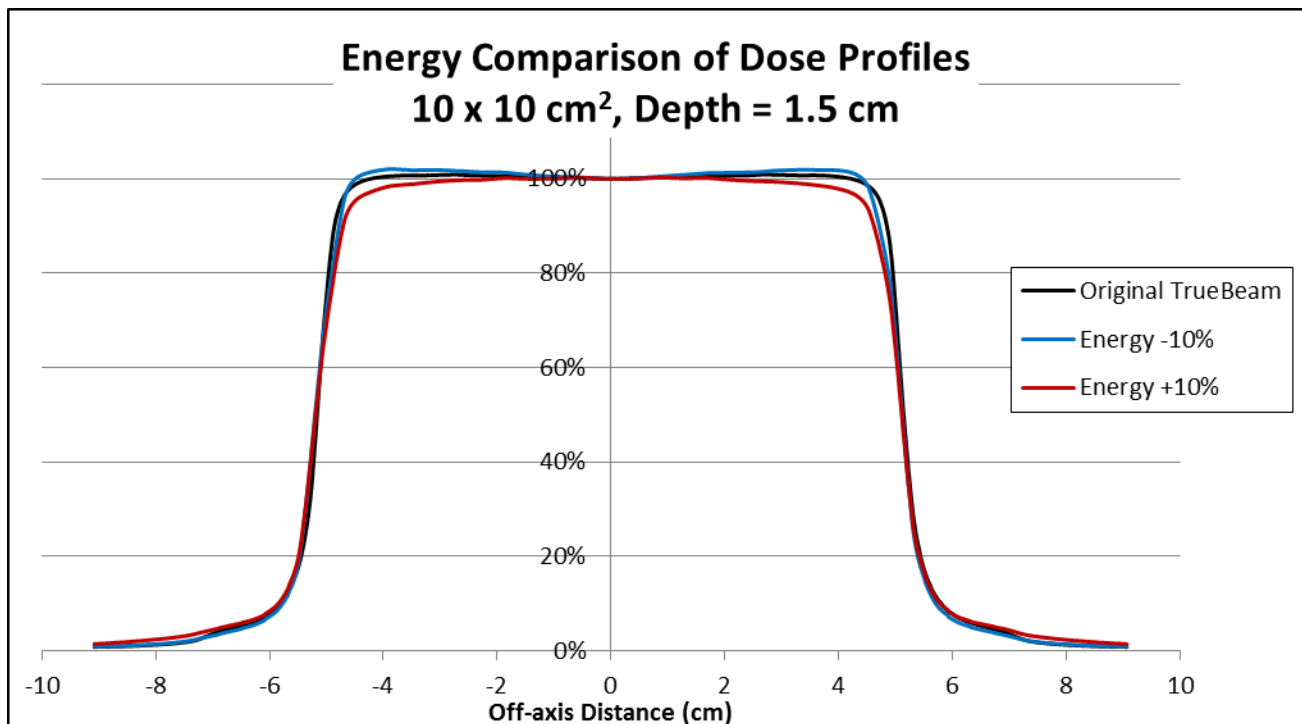


Figure 15: Dose profiles of a 10 x 10 cm² field defined by the MLC at 1.5 cm depth (approximately d_{max}) for the original MDACC TrueBeam model and the adjusted TrueBeam models with +10% energy and -10% energy.

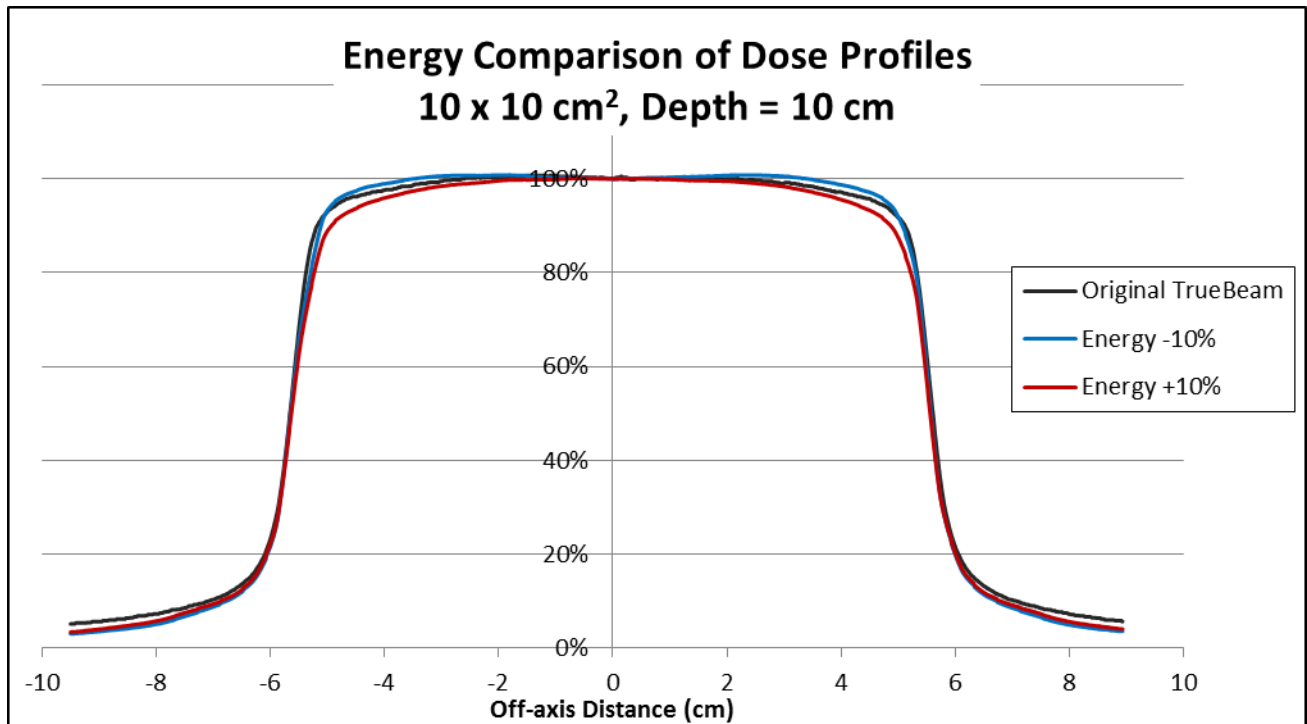


Figure 16: Dose profiles of a 10 x 10 cm² field defined by the MLC at 10 cm depth for the original MDACC TrueBeam model and the adjusted TrueBeam models with +10% energy and -10% energy.

Beam models using the altered depth dose and dose profile data were generated in Pinnacle by resetting the original TrueBeam model energy spectra to allow for up to 8 MV photons and then running the auto-model tool. When applied to the TrueBeam model, a -1.2% and 1.3% change in the PDD_{10}^{20} ratio that would be used to clinically characterize the beams was seen for the -10% and +10% energy changes, respectively. The depth dose curves computed by the Pinnacle models are shown for a 10 x 10 cm² field in Figure 14. Examples of the computed dose profiles for each of the models are shown in Figure 15 and Figure 16. When comparing computed beam characteristics using the newly generated models to the input altered data (the “measured” data), they qualitatively matched well and the accuracy was comparable to that of the original TrueBeam model. Computed depth doses qualitatively matched very well and were mostly within $\pm 1\%$ of the altered input depth dose data for depths greater than d_{max} . Computed profiles were mostly within $\pm 1\%$ of the input “measured” data within the field. The output factors from the original TrueBeam model were input to each of the energy altered models and the computed output factors agreed within 5%. These levels of accuracy are similar to those used for the clinical beam models and pushing beyond this had the potential for introducing unknown errors, so we kept the models as

similar as possible. This agreement can be seen in the examples of computed and altered input (“measured”) depth dose data that are shown in Figure 17 and Figure 18. Agreement between computed and altered input or “measured” dose profiles is demonstrated for the -10% energy model in Figure 19 and for the +10% energy model in Figure 20.

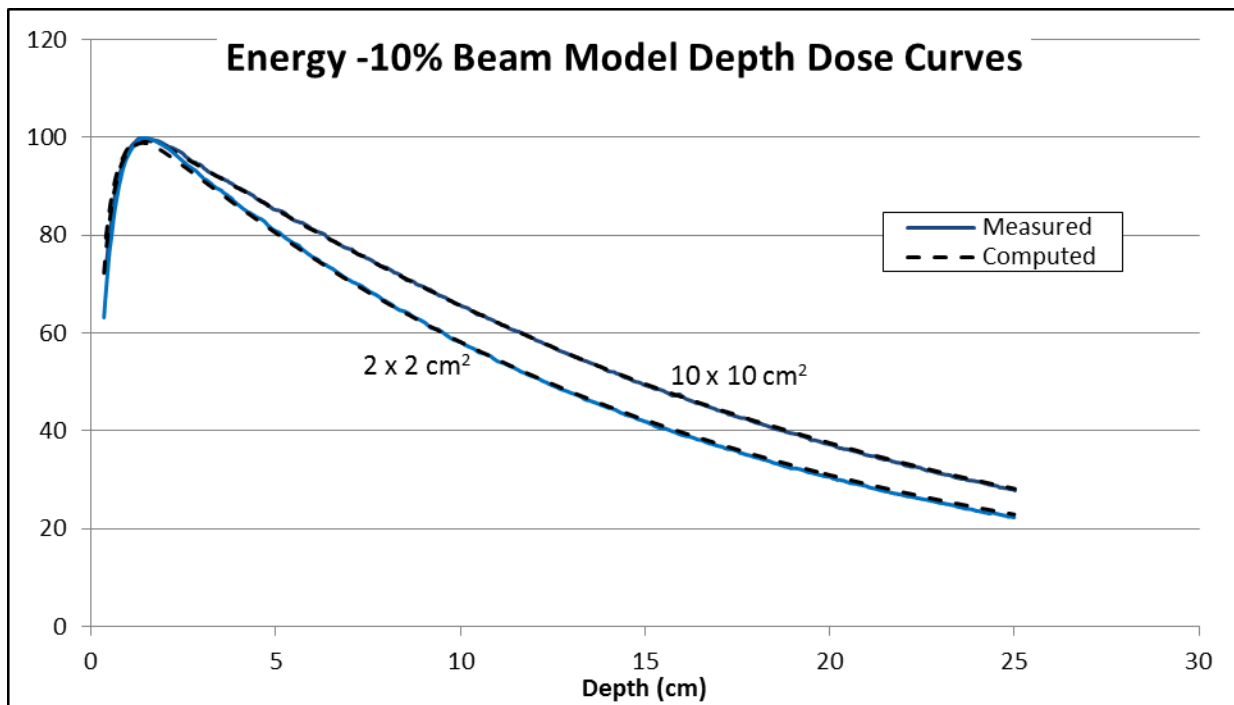


Figure 17: Computed and input altered (“measured”) depth dose data for $2 \times 2 \text{ cm}^2$ and $10 \times 10 \text{ cm}^2$ field sizes defined by the MLC for beam model of 6 MV – 10%.

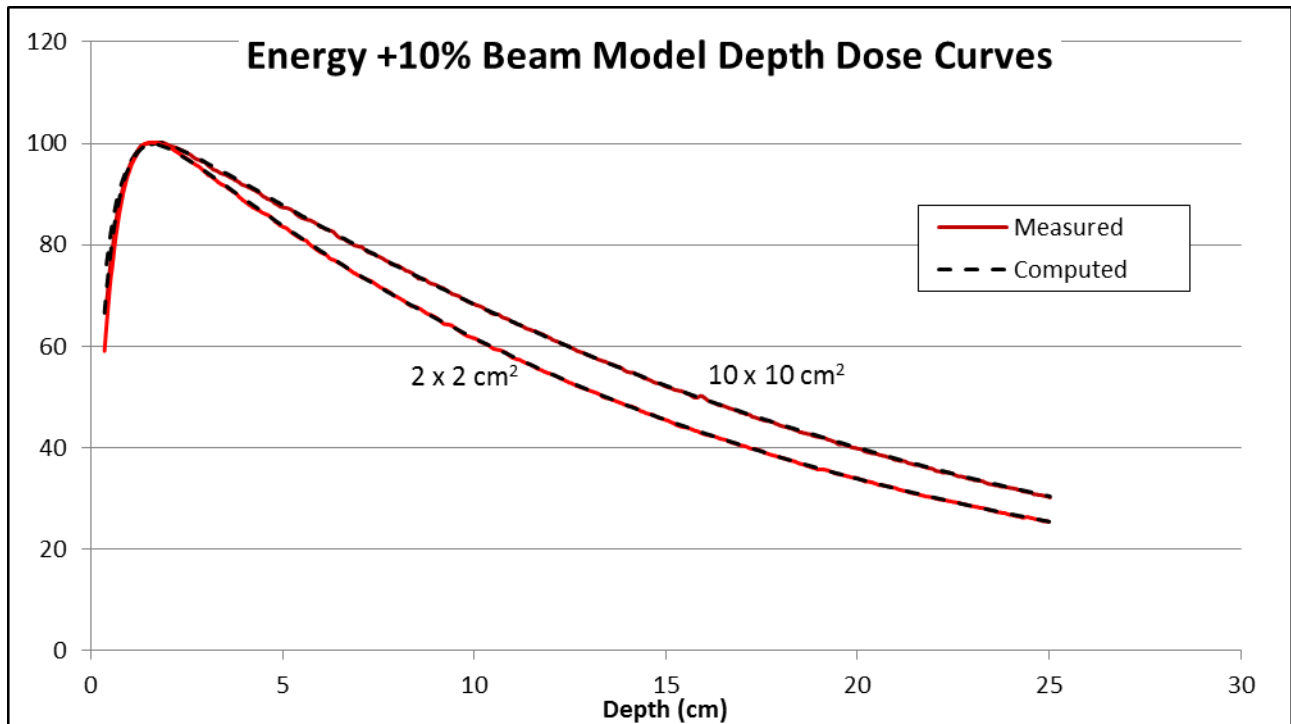


Figure 18: Computed and input altered (“measured”) depth dose data for $2 \times 2 \text{ cm}^2$ and $10 \times 10 \text{ cm}^2$ field sizes defined by the MLC for beam model of 6 MV + 10%.

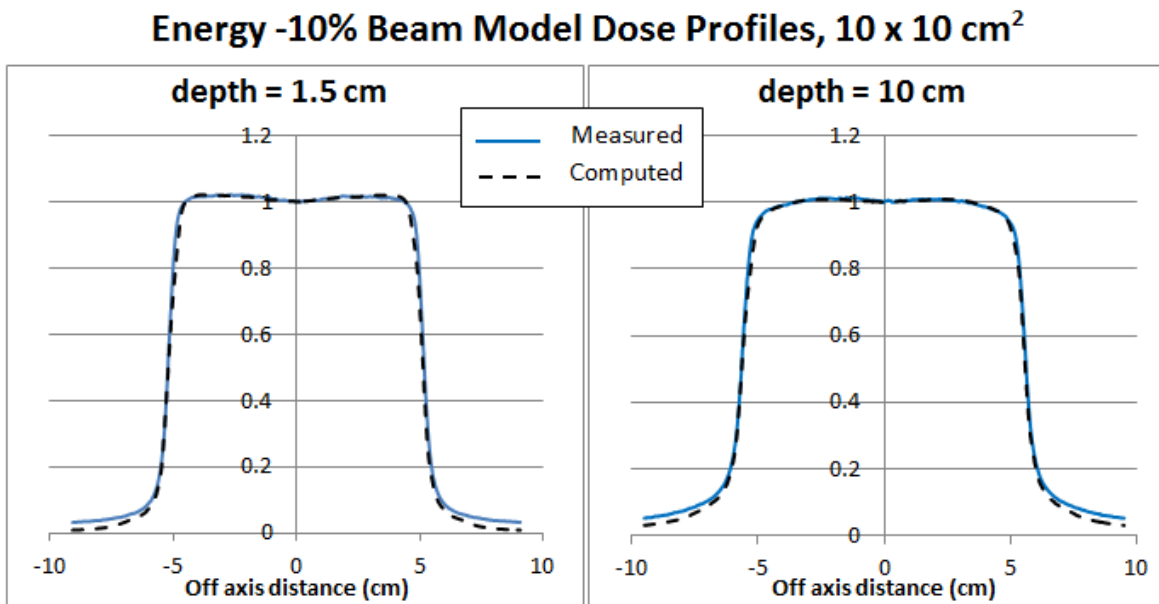


Figure 19: Computed and input altered (“measured”) dose profiles for $10 \times 10 \text{ cm}^2$ field size defined by the MLC at 1.5 cm (left) and 10 cm (right) depth for beam model of 6 MV -10%.

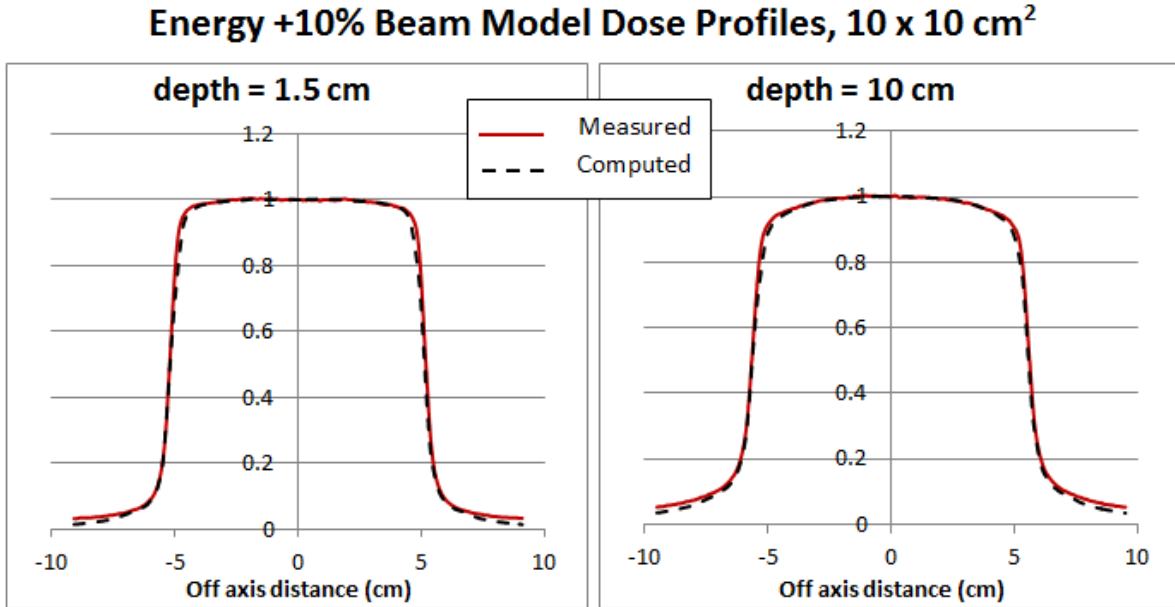


Figure 20: Computed and input altered (“measured”) dose profiles for 10 x 10 cm² field size defined by the MLC at 1.5 cm (left) and 10 cm (right) depth for beam model of 6 MV +10%.

Physical measurements

To induced changes in beam energy for physical measurements, the bending magnet current was adjusted with the assistance of the MDACC linear accelerator engineers. Phantom measurements under these conditions were performed on two occasions and the details of each are described.

Beam energy adjustment and measurements: Irradiation set #1

After establishing the baseline conditions and baseline phantom irradiation the energy of the beam was adjusted by altering the bending magnet current. This was done by physically adjusting the potentiometer in a slow, stepping fashion with measurements of TMR_{10}^{20} after each adjustment. It was our goal to first increase the TMR_{10}^{20} by 3%, however the linear accelerator interlocked several time due to low dose rate. The TMR_{10}^{20} after several adjustments was at maximum 0.68 which was a difference of about 1.6%. The beam was steered to reset the symmetry at the new energy, resulting in cross plane symmetry of 0.2% and in plane symmetry of 0.2%. The phantom was irradiated. Next the beam energy was adjusted with the goal of decreasing the TMR_{10}^{20} by 3%. A TMR_{10}^{20} of 0.652 was reached, which is a difference of about -2.5%. The symmetry was adjusted to be 0.6% cross plane and 0.5% in plane and an

irradiation of the phantom was attempted, however, the linac could not maintain the dose rate due to loss of fluence and so this phantom irradiation could not be completed.

Beam energy adjustment and measurements: Irradiation set #2

After the baseline conditions were re-established for this irradiation set engineers assisted in changing the bending magnet current by altering the shunt, with ion chamber readings at polystyrene depths of 5 and 14 cm after each adjustment. The original potentiometer reading was 13.7 mV for a baseline TMR^{14}_5 of 0.618. The goal was to adjust the energy as much as possible while maintaining the ability to operate the accelerator in clinical mode (up to a +2% TMR ratio). After adjusting a couple of times we only reached a 0.4% change in the TMR^{14}_5 with a 14.6 mV reading and TMR^{14}_5 of 0.62. Adjusting the bending magnet current potentiometer the next step to 15.05 mV, we ran into under-dosing interlocks shutting off the beam. After making several other adjustments including increasing the RF driver and reducing the dose rate from 600 MU/min to 300 MU/min, we were able to reach a TMR^{14}_5 of 0.624, which was about a 1.1% change from baseline TMR^{14}_5 that day. The flatness and symmetry were adjusted as well to account for the change in energy. The resultant flatness was 3.5% and 3.0% and symmetry was 0.7% and 1.1% in the cross plane and in plane directions, respectively. The output was determined to be 1.083 cGy/MU. Standard and complex treatment plans were delivered to the phantom three times each, with TLD and film changed between each irradiation.

The beam energy was then adjusted to be low by slowly adjusting the potentiometer to 12.4 mV, resulting in a TMR^{14}_5 of 0.609. Although we were able to tune the beam this low, the resultant dose rate was too low and caused interlocks that prevented irradiations in clinical mode. A slight adjustment was made to 12.9 mV which resulted in a TMR^{14}_5 of 0.612, an approximately -1% change from baseline and similar to the energy increase. MatriXX measurements determined that the flatness was 1.8% and 2.0% and symmetry was 1.3% and 1.1% in the cross plane and in plane directions, respectively. The output was determined to be 0.969 cGy/MU. Standard and complex treatment plans were delivered to the phantom three times each, with TLD and film changed between each irradiation.

Summary of beam energy physical measurements

Beam energy errors were induced on clinical linear accelerators going out of commission on two occasions. IROC-H IMRT head and neck phantoms were irradiated under these failure mode conditions with both standard and complex treatment plans. A summary of these adjustments and irradiations is summarized in Table 8.

Failure Mode	Magnitude	Phantom Plans
Energy High	1.6% TMR ²⁰ ₁₀	Complex x1
	1.1% TMR ¹⁴ ₅	Standard x3, Complex x3
Energy Low	-0.8% TMR ¹⁴ ₅	Standard x3, Complex x3

Table 8: Summary of energy failure physical measurements made.

Failure mode 2: Beam Symmetry

Overview

The characteristics of a photon beam field are commonly described by the dose profile flatness and symmetry. These characteristics are commonly assessed for the central 80% of the full width half maximum of the field, which is shown in Figure 21. Several different methods for computing beam symmetry are used and in our work we used Equation 2. Measurement and monitoring of the flatness and symmetry are key to ensuring that dose distributions are being delivered as intended. A photon beam coming directly from the x-ray target in a linear accelerator is forward peaked and for ease of planning treatments with uniform and/or conformal dose distributions, it is generally useful for the beam exiting the linear accelerator head to have a flat and symmetric shape. This is accomplished with a flattening filter which attenuates primarily in the center of the forward peaked photon beam. The photon beam flatness and symmetry are very sensitive and can be affected by a variety of things. For example, if the forward peaked beam is not properly incident on the flattening filter as it was designed to be, the flatness and symmetry will be off, as demonstrated in Figure 22. Even slight changes in the beam energy, as discussed in the previous section, will affect the beam flatness and symmetry. Often times, other objects are intentionally in the path of the beam and alter the flatness and symmetry, such as when wedges are used to create angled beam profiles to conform to the shape of the patient and/or target. However, slight

steering changes are commonly not intentional and it is possible that a photon beam may drift over time away from proper incidence on the x-ray target and/or flattening filter, resulting in a beam with less than optimal flatness and symmetry. It is recommended in the AAPM Task Group 142 report that a 1% tolerance on the photon beam flatness and symmetry be maintained with specific verification annually and profile constancy verified monthly.⁶⁰ It is common practice for the flatness and symmetry to be verified during daily output checks.

$$Symmetry = \frac{Dose_{neg80\%} - Dose_{pos80\%}}{Dose_{CAX}} \times 100\% \quad \text{Eq. 2}$$

Equation 2: Equation used to compute beam symmetry where $Dose_{neg80\%}$ is the dose value at the negative edge of the 80% FWHM, $Dose_{pos80\%}$ is the dose value at the positive end of the 80% FWHM, and $Dose_{CAX}$ is the dose value at the central axis (commonly 100 or 1.00).

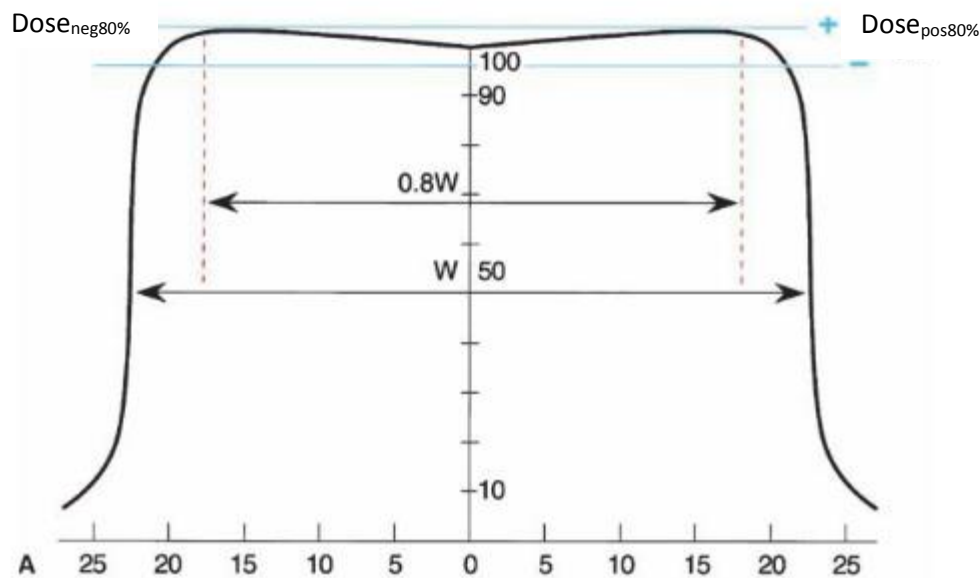


Figure 21: A dose profile example showing the central 80% of FWHM, where the minima and maxima would be used to compute field flatness and points at the edges, equidistant from the central axis, would be used to compute symmetry.^F

Treatment planning studies

To simulate beam symmetry errors in the treatment planning system, physical wedges were modeled and added to each beam in each plan. Currently, MDACC only utilizes electronic dynamic

^F Image from Khan, FM. The physics of radiation therapy, 4th ed. Lippincott Williams & Wilkins, 2010.

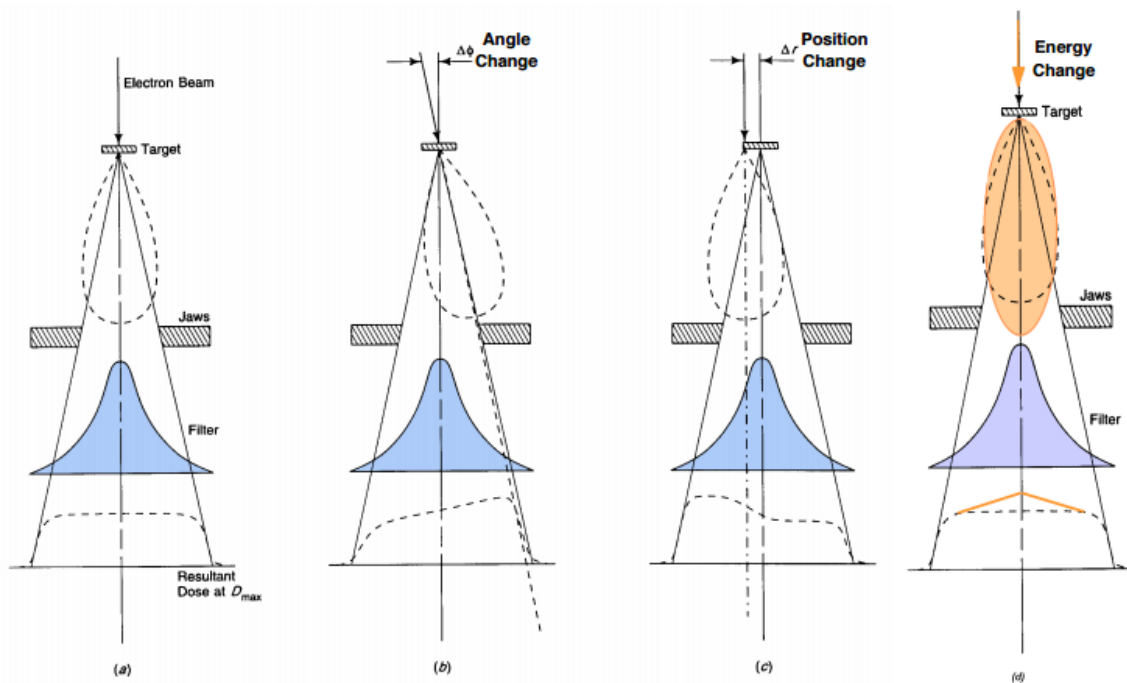


Figure 22: Flattening filters are used to create flat photon dose distributions from forward peaked photon beam (a) but the flatness and symmetry of the photon beam are affected by the angle (b), position (c), and energy spectra (d) incident on the flattening filter.^G

wedges (EDWs) on the Varian linear accelerators. EDWs work by closing one of the collimating jaws while the beam is on, creating a profile of varying dose along the axis of the moving jaw. The angle of this “wedge” is dependent upon the speed of the jaw and the dose rate. Although there is flexibility in the angle of the wedge created which is desirable for our study, EDWs would not work for our IMRT treatment planning studies because they would need to be applied to each field individually. With the number of individual fields in an IMRT treatment plan, this is highly impractical and would be challenging to implement in Pinnacle.

Instead, physical wedges were created in our copy of the existing Varian TrueBeam model. We chose to use this technique to model symmetry errors of 2% which is just outside of tolerance criteria, 3.5% which was what we were able to achieve for our more robust set of physical measurements, and 10% as an extreme case. First, the wedge angle required to create the desired symmetry errors was

^G Image from Salehpour, M. lecture , “Therapy electron linear accelerators explained”

approximated by interpolation using known wedge angles of 0°, 15°, 30°, and 45° and their respective symmetries of about 0%, 22%, 45%, and 70% in a 20 x 20 cm field at 10 cm depth. These wedge angles were determined to be 2°, 3°, and 7° for 2%, 3.5%, and 10% symmetry, respectively. Dose profiles from the MDACC TrueBeam model used for our baseline with no wedge and with a 15° EDW for field sizes of 5 x 5 cm², 10 x 10 cm², and 20 x 20 cm² at depths of 1.5 cm, 6 cm, 12.5 cm, and 22 cm were pulled into MATLAB (The Mathworks, Inc.). These profiles were added with weighting proportional to the wedge angle desired to create profiles for each of these field sizes and depths for the three wedges we wanted to model. For example, a 7.5° wedge would be created by adding the profiles with no wedge weighted by 50% and the profiles with a 15° wedge weighted by 50%. The symmetry of the resultant profiles was computed. The fact that wedged field dose profile data was not available at a depth of 10 cm where we would want to define the symmetry in the 20 x 20 cm² field made things slightly difficult. Ideally, the desired symmetry would lie between the symmetry at 6 cm and 12.5 cm depth. The symmetry for each model was slightly higher than intended. Since the beam modeling would not be exact and the wedges are so small and in the interest of time, these profiles were not further adjusted. A polynomial equation was fit to the symmetry according to depth for each wedge model and used to estimate the symmetry at 10 cm depth. These estimates as well as the symmetry for each of these 20 x 20 cm profiles are summarized in Table 9. The 20 x 20 cm² profiles for each of the wedges are shown in Figure 23, Figure 24, and Figure 25.

Approximate Wedge Angle	Symmetry Error Modeled (at d = 10 cm)	Symmetry				Interpolated Symmetry d = 10 cm
		d = 1.5 cm	d = 6 cm	d = 12.5 cm	d = 22 cm	
2°	2%	2.4%	2.31%	2.19%	1.94%	2.29%
3°	3.5%	4.01%	3.86%	3.66%	3.24%	3.79%
7°	10%	11.71%	11.09%	10.51%	9.31%	10.7%

Table 9: Symmetry of 20 x 20 cm² wedged fields at depths of 1.5 cm, 6 cm, 12.5 cm, and 22 cm which were used to interpolate the symmetry at a depth of 10 cm, which is slightly larger than the desired symmetry for each model.

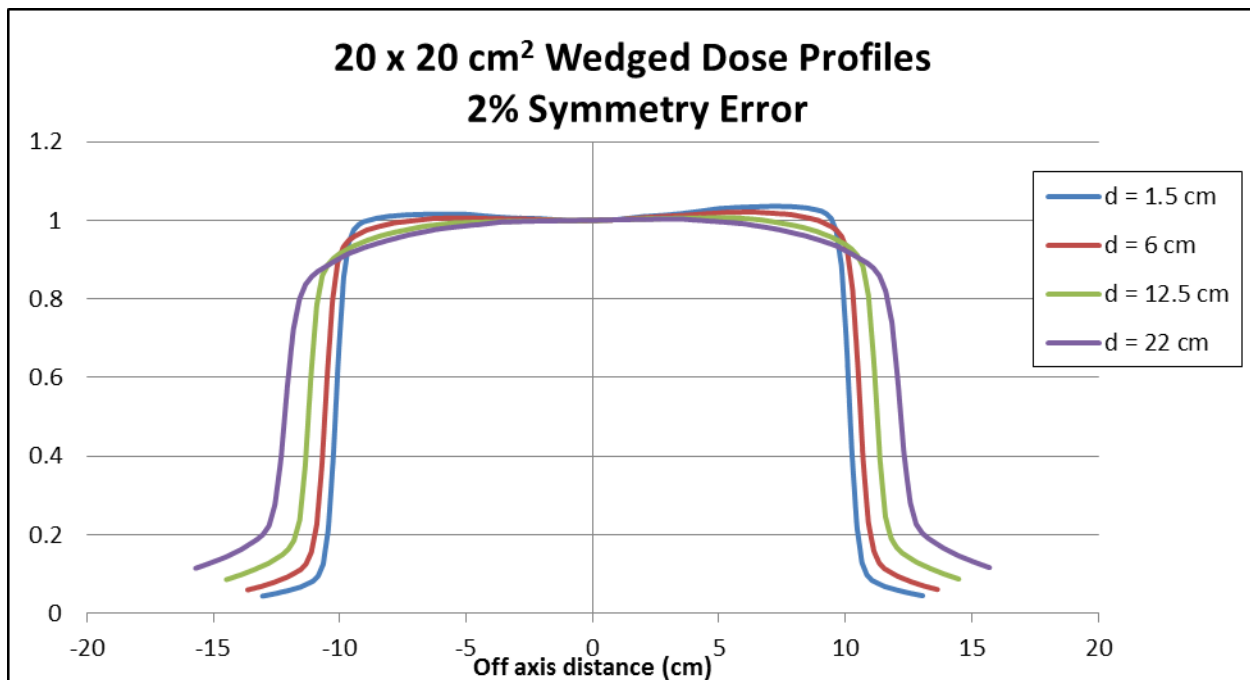


Figure 23: Dose profiles for a 20 x 20 cm² wedged field at depths of 1.5 cm, 6 cm, 12.5 cm, and 22 cm used to model a symmetry error of approximately 2% at a depth of 10 cm.

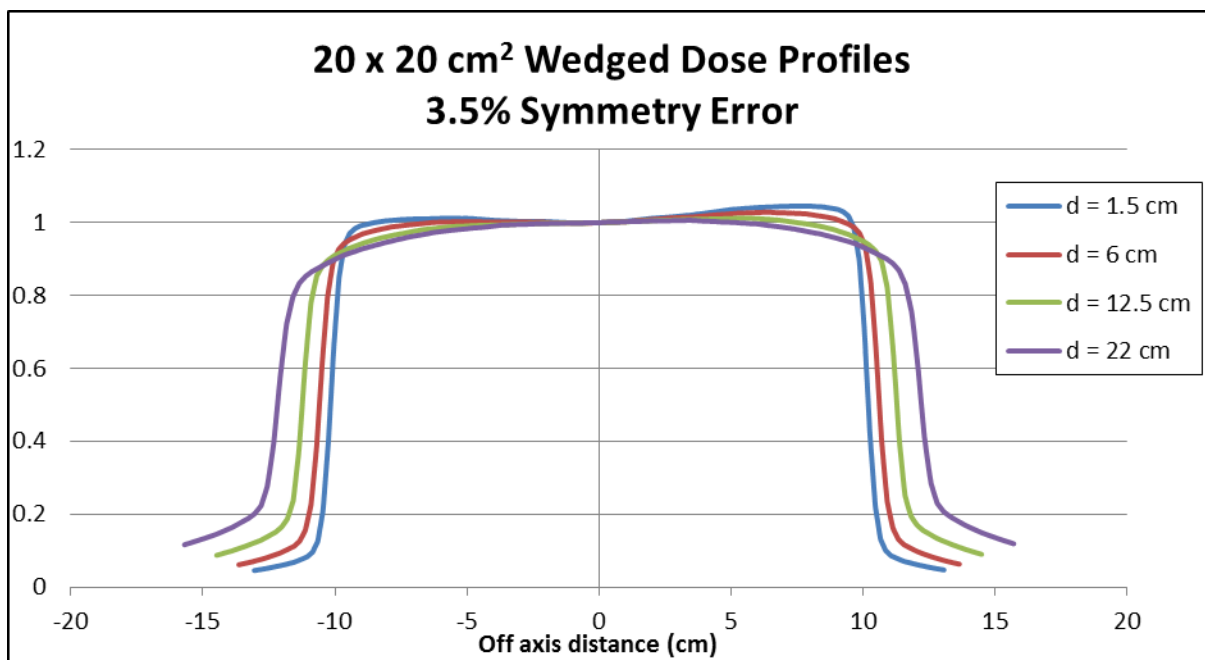


Figure 24: Dose profiles for a 20 x 20 cm² wedged field at depths of 1.5 cm, 6 cm, 12.5 cm, and 22 cm used to model a symmetry error of approximately 3.5% at a depth of 10 cm.

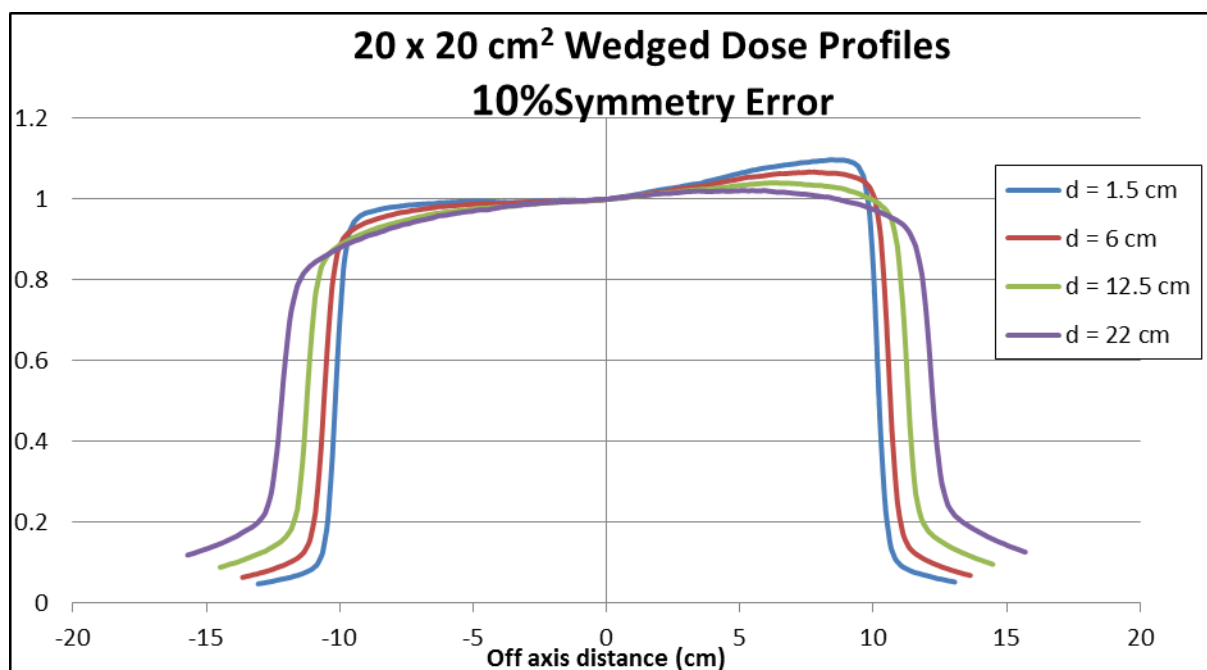


Figure 25: Dose profiles for a 20 x 20 cm² wedged field at depths of 1.5 cm, 6 cm, 12.5 cm, and 22 cm used to model a symmetry error of approximately 10% at a depth of 10 cm.

These wedge profiles were input for the three separate wedge models along with the percent depth dose curves for the same fields without a wedge. Wedge models were created with iron, which was not ideal, however we were unable to get the wedge model to produce good computed profiled when made of water. The density of iron used was 11.36 g/cc. It was determined that since the wedges are small, the beam hardening from the iron should be minimal. Each wedge used the typical Varian values for source to wedge (SWD) distance of 58.8 cm and length of 26 cm⁶⁴. The width of the wedges was assumed to be 18.2 cm, as listed for a Varian 15° wedge with maximum field size of 30 x 40 cm in Cheng *et al*⁶⁴. The physical thickness of the wedges had to be estimated for the models. We began by attempting to model the wedge resulting in 10% symmetry by estimating the thickness of lead required to attenuate the beam by 10% on the thick side. Using an attenuation coefficient for lead (6MeV) of 0.0305 cm²/g, we calculated the need for approximately 0.21 cm of lead using basic exponential attenuation. This was used as a starting point and then iteratively adjusted after running the wedge automodeling script (FineTuneAllForWedge) until the best computed profile fit was achieved. The final wedge physical profiles for each of the wedge models are shown in Table 10. The first row in each profile table with

positional offset of -9.10 cm must be 0.00 for the model to accept the wedge. Resulting modeled wedge profiles agreed with the input “measured” data within $\pm 1\%$ in the field. The typical wedge factor for Varian physical wedges of 0.5 was used. These wedges were then applied to each beam of each plan in each of the four directions: Top (Y2) to bottom (Y1) (“In plane 1”), bottom to top (“In plane 2”), left (X1) to right (X2) (“Cross plane 1”), and right to left (“Cross plane 2”), where X1 and X2 denote opposing set of jaws aligned with the MLC.

2% Symmetry Wedge Model		3.5% Symmetry Wedge Model		10% Symmetry Wedge Model	
Offset (cm)	Thickness(cm)	Offset (cm)	Thickness(cm)	Offset (cm)	Thickness(cm)
-9.10	0.00	-9.10	0.00	-9.10	0.00
-9.10	0.14	-9.10	0.17	-9.10	0.45
0.00	0.07	0.00	0.12	0.00	0.18
6.00	0.04	5.00	0.07	4.00	0.13
9.10	0.00	9.10	0.00	6.50	0.09
				9.10	0.09

Table 10: Physical wedge profiles for wedge models simulating symmetry errors of 2%, 3.5%, and 10%.

Physical measurements

To induced changes in beam symmetry for physical measurements, the steering magnets were adjusted with the assistance of the MDACC linear accelerator engineers. Phantom measurements under these conditions were performed on two occasions and the details of each are described.

Beam symmetry adjustment and measurements: Irradiation set #1

Following the establishment of baseline conditions and irradiation of the baseline phantom, the in plane symmetry was adjusted by altering the angular steering magnet current with the goal of adjusting it as much as possible. The symmetry was monitored real-time during the adjustment by using the movie mode in the OmniPro-I’^mRT software (IBA Dosimetry GmbH, Schwarzenbruck) with the MatriXX and was adjusted to 5.1%. The phantom was then set up and irradiated. The in plane symmetry was then returned to 0.2% and the cross plane symmetry was adjusted; however dosimetry interlocks prevented the steering from going beyond 3.3% symmetry. The phantom was irradiated again under these conditions.

Beam symmetry adjustment and measurements: Irradiation set #2

After establishing the baseline conditions on the third day of measurements for this irradiation set, the angular steering was adjusted with the goal of achieving 3% symmetry in plane. The symmetry was monitored real-time during the adjustment with the MatriXX in movie mode. With an adjustment of the potentiometer from 12.9 mV to 13.7 mV, an in plane symmetry of 3.5% was achieved with 0.9% cross plane symmetry. The flatness for this condition was 2.5% in plane and 3.6% cross plane. The output was 1.013 cGy/MU and TMR^{14}_5 was 0.616 which was about 0.7% higher than the baseline from that day. Standard and complex treatment plans were delivered to the phantom three times each, with TLD and film changed between each irradiation.

The angular steering was then adjusted to 3.7% cross plane and 1.1% in plane with 4.2% and 2.1% flatness for each plane, respectively. The potentiometer readings were not recorded. The output was measured to be 1.013 cGy/MU and TMR^{14}_5 was 0.618. Standard and complex treatment plans were delivered to the phantom three times each, with TLD and film changed between each irradiation.

Finally, the angular steering was adjusted back to baseline and steering was performed with the positional steering magnets. A symmetry of 3.8% in the in plane was achieved with 1.3% symmetry in the cross plane. Flatness was 3.7% in the in plane and 3.0% in the cross plane. The output was 1.059 cGy/mu and TMR^{14}_5 was 0.636, which is almost 4% higher than the day three baseline and about 3% higher than the overall baseline. This is likely caused by the change in the position on the x-ray target that the electron beam is incident upon, resulting in a changed energy spectra. Standard and complex treatment plans were delivered to the phantom three times each, with TLD and film changed between each irradiation.

Positional steering was not used to adjust the cross plane symmetry due to time constraints.

Summary of beam symmetry physical measurements

Beam symmetry errors were induced on clinical linear accelerators going out of commission on two occasions. IROC-H IMRT head and neck phantoms were irradiated under these failure mode

conditions with both standard and complex treatment plans. A summary of these adjustments and irradiations is summarized in Table 11.

Failure Mode	Steering	Magnitude	Phantom Plans
In plane symmetry	Angular	5.1%	Complex x1
	Angular	3.6%	Standard x3, Complex x3
	Positional	3.8%	Standard x3, Complex x3
Cross plane symmetry	Angular	3.3%	Complex x1
	Angular	3.7%	Standard x3, Complex x3

Table 11: Summary of symmetry failure physical measurements made.

Failure mode 3: MLC Position

Overview

IMRT utilizes multi-leaf collimators (MLCs) to modulate photon fluence by creating several complex field shapes for multiple beam angles. MLC positional accuracy, precision, and reproducibility are critical for proper IMRT dose delivery. Unlike conventional treatments, IMRT segment field edges not only block the borders of the targets, but often overlap targets and OARS. This compounds with the fact that IMRT commonly utilizes many segments with small areas and high MUs, increasing the importance of accurate MLC performance.

The dosimetric effects of MLC positional errors and the ability of routine QA practices to catch them have been studied in many cases. Luo *et al* found a 1% change in the prostate target dose for every error of 0.2 mm systematic leaf position in a Monte Carlo study⁶⁵. LoSasso *et al* found a similar magnitude of dose delivery error for dynamic-MLC IMRT with an average window width of 2 cm⁶⁶. With a 1 mm systematic leaf positional error, Rangel *et al* reported an average effect of 2.7% and 5.6% on the equivalent uniform dose (EUD) to CTVs in prostate and head and neck treatments, respectively⁶⁷. Mu *et al* also investigated the effects of 1 mm systematic errors on head and neck plans and saw a 4% average change in the target D_{95%} in simple treatment plans (with less than 50 segments) and 8% change in more complex plans (with more than 100 segments) as well as 9% and 13% dose changes in the parotid glands for simple and complex plans, respectively. It was also noted that these plans were unaffected by random

MLC errors⁴⁸. Using film measurements for step and shoot IMRT head and neck patient QA, Sastre-Padro *et al* measured a median dose difference of up 1.5% as a result of a 2 mm systematic leaf positional error⁶⁸.

While good MLC positional accuracy is generally expected of modern technology, miscalibration or drifting can occur. Bayouth, *et al* discovered up to 1.2 mm positional errors immediately following calibration due to a slight rotation of the MLC calibration tool⁶⁹. A drift of 1 mm static MLC gap width over 8 weeks was seen by Sasaki, *et al* after thorough weekly monitoring of their Siemens Primus linear accelerator⁷⁰.

These errors can be difficult to consistently detect with current patient specific IMRT QA practices. Yan *et al* found that gamma analysis performed with a 2%/2mm criteria on the MapCHECK® diode array (Sun Nuclear Corporation, Melbourne, FL) was more sensitive than the same analysis with radiochromic film, however neither system could detect random errors up to 2 mm or 1 mm systematic MLC positional error⁷¹. Rangel *et al* investigated the sensitivity of the MapCHECK® device and Varian's aS100 EPID with Portal Vision to 0.5 mm and 1 mm leaf offsets in both banks of leaves and 1 mm offsets in one bank in both prostate and head and neck patients. These QA devices were more sensitive to the changes in the more modulated head and neck plans than the prostate plans; however the authors concluded that neither approach was sufficiently sensitive as the smaller errors were not reliably detected and a tight criteria of 2%/2mm was required to detect the 1 mm offsets⁷². Finally, Moiseenko *et al* presented an interesting treatment planning study on the sensitivity of IMRT QA with ion chamber point doses and 3D gamma analysis to MLC systematic offsets of up to 2 mm and related this to the biological consequences of these errors. Similar to the study by Rangel *et al*, the increased modulation in head and neck treatment plans led to pronounced sensitivity MLC offsets over prostate plans. Although these QA methods were largely able to identify MLC offsets leading to 2% change in the generalized EUD (gEUD) in prostate and rectum, some plans with 3% changes were able to pass the 2% ion chamber criteria or the 3%/3mm with 95% of pixels passing. In head and neck patients, this QA was able to catch

MLC offsets resulting in 4% gEUD changes in the PTV and 5% changes in the maximum dose to the brainstem. It was noted that if the criteria was loosened to 3% for the ion chamber or 90% for the gamma analysis, up to 5% changes in the head and neck PTV and up to 8% changes in the brainstem maximum dose could pass QA⁷³.

Due to the heavy reliance of correct IMRT dose delivery upon the MLC positional accuracy, MLC QA has been specially recommended for linear accelerators performing IMRT. The AAPM Task Group 142 recommends weekly qualitative QA, for example using picket fence patterns, a monthly leaf positional accuracy tolerance of 1 mm at four cardinal gantry angles, and leaf position repeatability within 1 mm annually among other MLC tests⁶⁰.

Treatment planning studies

To simulate systematic MLC positional errors in the treatment planning system, a script was written to systematically shift all open MLC leaves in each segment by the specified distance in the specified direction. This script was used to apply ± 1 mm and ± 2 mm systematic shifts in each MLC bank, X1 and X2. A positive shift in the MLC indicates that the leaves are moving out, creating the segment area or window width larger, and a negative shift indicates the leaves are moving in. These systematic shifts were applied to both the baseline standard and complex plans, generating eight new plans for each, and the dose was computed with the new MLC positions just as for the baseline plans.

Physical measurements

To induced MLC positional errors for physical measurements, the script used for treatment planning studies was used to apply systematic MLC shifts to baseline plans. Phantom measurements were performed on two occasions with these altered treatment plans and the details of each are described.

MLC positional error measurements: Irradiation set #1

After energy and symmetry failures were investigated in this irradiation set, there was time remaining to perform irradiations so we decided to also do some MLC positional error measurements.

The energy was readjusted back to baseline to have a TMR^{20}_{10} of 0.669 and steering set the symmetry to 0.4% cross plane and 0.1% in plane. Phantom irradiations were performed using the same complex treatment plan, but with the MLC in both banks systematically moved out by 1 mm. This was also done with the MLC in both banks systematically moved out by 3 mm. TLD and film were changed and the phantom set up was verified between each irradiation.

MLC positional error measurements: Irradiation set #2

After the baseline conditions were established on day two (before any alterations were made to the beam), standard and complex plans with the X1 MLC shifted out by 2 mm were delivered to the phantom. TLD and film were changed and the phantom set up was verified between each irradiation.

Summary of MLC positional error physical measurements

Beam energy errors were induced on clinical linear accelerators going out of commission on two occasions. IROC-H IMRT head and neck phantoms were irradiated under these failure mode conditions with both standard and complex treatment plans. A summary of these adjustments and irradiations is summarized in Table 12.

Adjustment	Magnitude	Phantom Plans
MLC systematic shift	1 mm out (both banks)	Complex x1
	3 mm out (both banks)	Complex x1
	2 mm out (one bank)	Standard x3, Complex x3

Table 12: Summary of MLC positional failure physical measurements made.

Failure mode 4: Gantry Angle

Overview

IMRT utilizes multiple gantry angles to create conformal, heterogeneous dose distributions within patients. It is key that IMRT treatment plans are delivered as planned in order assure the desired dose distribution and resultant outcomes. Systematic angular misalignment of the gantry by 2° has been shown to cause up to 40% dose errors within a modulated field 10 cm away from isocenter in a pelvic

treatment⁷⁴. In a lumbar-vertebra patient, Xing *et al* demonstrated an almost 40% increase in the maximum spinal cord dose from a systematic error of 5° in the gantry angle. Even random errors such as a 5° gantry error in just one of the nine beam angles in the same lumbar-vertebra patient resulted in a 1.5% decrease in the minimum dose to the target and 5.1% change in the maximum dose to the cord⁷⁵. The AAPM Task Group 142 recommends gantry angle read out to be consistent within 1° at cardinal angles, checked on a monthly basis. The gantry rotation isocenter should be annually maintained within 1 mm of the baseline isocenter⁶⁰.

Treatment planning studies

To simulate systematic gantry angle errors in the treatment planning system, the angle for each beam in the standard and complex baseline plans was adjusted by +2° and doses were recomputed with no other changes. An increase in the gantry angle results in counterclockwise rotation of the gantry when looking at it from the isocenter. The same method was followed using a gantry angle adjustment of -2°.

Physical measurements

To induce gantry angle errors in physical measurements, the same methodology used in the treatment planning studies was used to generate a plan for delivery with a +2° gantry angle error. Phantom measurements under these conditions were performed during irradiation set #3. As described in Section, after baseline conditions were established on the second day, the standard treatment plan with +2° gantry angle errors were delivered to the phantom three times. TLD and film were changed and phantom alignment was verified between each irradiation.

Failure mode 5: Collimator Angle

Overview

Another degree of freedom present in IMRT plans is the collimator angle. Selection of the collimator angle determines the direction in which the MLC leaves may travel to modulate the field. The resultant dose distribution is sensitive to changes in this set up, with a study on collimator angle errors of

2° showing up to 20% dose errors in a modulated pelvic plan with the isocenter shifted from the central axis⁷⁴. As with the gantry angle, the AAPM Task Group 142 recommends collimator angle read out to be consistent within 1° at cardinal angles, checked on a monthly basis. The collimator rotation isocenter should be annually maintained within 1 mm of the baseline isocenter⁶⁰.

Treatment planning studies

To simulate systematic collimator angle errors in the treatment planning system, the collimator angle for each beam in the standard and complex baseline plans was adjusted by +2° and doses were recomputed with no other changes. An increase in the collimator angle results in counterclockwise rotation of the collimator when looking at it from the position of the source (beams eye view or BEV). The same method was followed using a collimator angle adjustment of -2°.

Physical measurements

To induce collimator angle errors in physical measurements, the same methodology used in the treatment planning studies was used to generate a plan for delivery with a +2° collimator angle error. Phantom measurements under these conditions were performed during irradiation set #3. As described in Section, after baseline conditions were established on the second day, the standard treatment plan with +2° collimator angle errors were delivered to the phantom three times, interspersed with the gantry angle error deliveries. TLD and film were changed and phantom alignment was verified between each irradiation.

Failure mode 6: Couch Angle

Overview

Yet another degree of freedom in the mechanical set up of IMRT treatments is the couch angle. The couch is commonly “kicked” to a different angle to allow non-coplanar beams to distribute dose through different angles in the patient. Our study is limited to the use of co-planar beams and the effects of couch angle errors from the single baseline position. Errors in the couch position directly result in

deviations from the desired patient set up as initialized in the simulation. Though it has been noted that angular misalignments of the couch may not result in as large of errors as translational couch displacements, angular errors have the potential to create dose errors similar in magnitude to gantry and collimator angle errors⁷⁵. Similar to gantry and collimator, the AAPM Task Group 142 recommends the couch rotation isocenter should be annually maintained within 1 mm of the baseline isocenter⁶⁰. We extended the monthly recommendations for gantry and collimator of 1° degree tolerance here to the couch and therefore chose to examine couch angle errors of 2°.

Treatment planning studies

To simulate systematic couch angle errors in the treatment planning system, the couch angle for each beam in the standard and complex baseline plans was adjusted by +2° and doses were recomputed with no other changes. An increase in the couch angle results in counterclockwise rotation of the couch when looking at it from the position of the collimator down when the gantry is straight up at 180°. The same method was followed using a collimator angle adjustment of -2°.

Physical measurements

To induce couch angle errors in physical measurements, the same methodology used in the treatment planning studies was used to generate a plan for delivery with a +2° couch angle error. Phantom measurements under these conditions were performed during irradiation set #3. As described in Section, the standard treatment plan with +2° couch angle errors were delivered to the phantom three times on day three. TLD and film were changed and phantom alignment was verified between each irradiation.

Failure mode 7: MU linearity

Overview

The stability and accuracy of the dose monitor unit system in a linear accelerator is another critical component required for accurate and safe treatment delivery. Since IMRT utilizes a large number of segments and commonly smaller number of MU per segment, i.e. commonly only 1 or 2 MU/segment,

dose linearity at these low MU levels is especially important. Step-and-shoot IMRT adds the challenge of starting and stopping the beam multiple times. Several studies have been published on the challenge of control of the output for small number of MU, particularly on older linear accelerators with separate MLC controllers that can exhibit an “overshoot” effect due to a communication time delay⁷⁶. Beams of less than 5 MU have been reported to have errors around 5%, with 1 MU beams having up to 32% error in the literature^{77,78}. These effects have been noted to increase with higher dose rates. In some cases, the overshoot effect is smeared out due to the nature of IMRT, however there is the potential for these small errors to accumulate and have a clinical impact⁷⁹. The AAPM Task Group 142 report recommends maintaining MU linearity on IMRT machines for 2-4 MU within 5% and ≥ 5 MU within 2%⁶⁰.

Treatment planning studies

To simulate MU linearity errors in the phantom treatment plans, the MU for each segment was adjusted according to three scenarios, each in the positive (A) and negative (B) directions. These scenarios are shown in Table 13. The MU weightings and MU values for all beam segments as well as total MU per beam for the baseline standard and complex phantom treatment plans were exported from the treatment planning system. These values were then run through a MATLAB script which reassigned the MU value for each segment according to the three scenarios and output a Pinnacle script to execute these reassignments within the treatment planning system. This Pinnacle script was then run on the treatment plans and beam MU adjusted appropriately, resulting in 6 new treatment plans with segment MU according to the described scenarios for the standard and complex plans. The distribution of segments with low MU in the standard and complex baseline treatment plans are shown in Figure 26 and Figure 27.

Scenario	MU/segment	Adjustment	
		A	B
1	1	+6%	-6%
	2	+5%	-5%
	3	+4%	-4%
	4	+3%	-3%
	5	+2%	-2%
2	1	+30%	-30%
	2	+15%	-15%
	3	+7.5%	-7.5%
	4	+3.25%	-3.25%
	5	+1.875%	-1.875%
3	1-5	+6%	-6%

Table 13: MU linearity error scenarios for treatment planning studies.

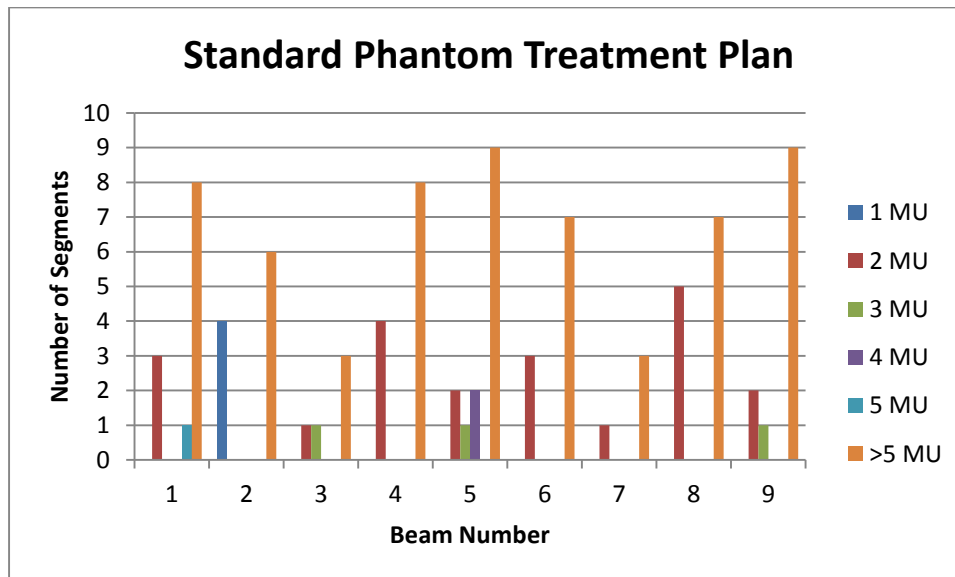


Figure 26: MU per segment for the nine beams in the standard phantom treatment plan used in treatment planning studies.

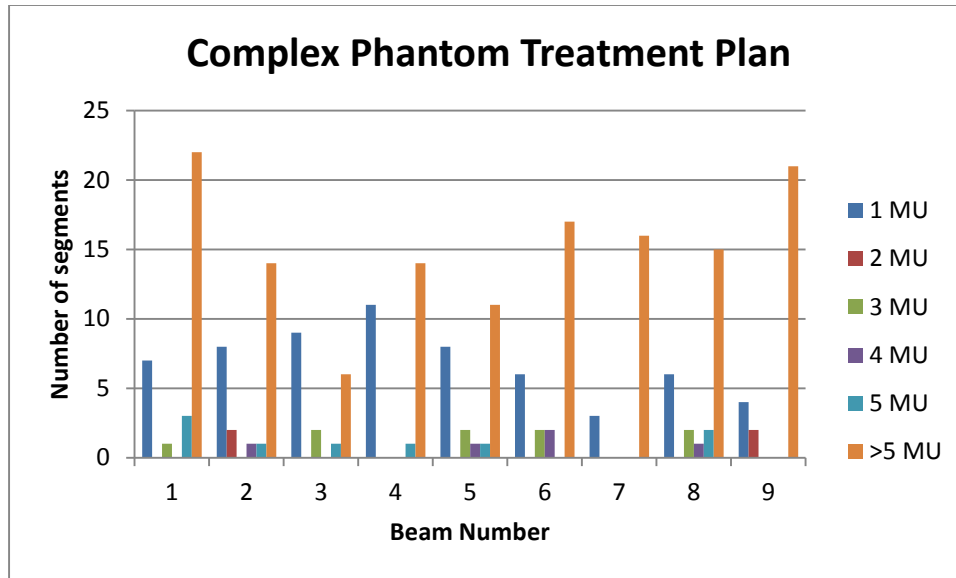


Figure 27: MU per segment for the nine beams in the complex phantom treatment plan used in treatment planning studies.

Failure mode 8: MLC transmission and leakage

Overview

Characterization of MLC transmission and leakage is important for accurate dose calculation, especially in heavily blocked fields with small segment sizes. Transmission and leakage doses can build up in complex IMRT treatments where the MLC are heavily utilized to block OARs. The average transmission and leakage (both mid-leaf and inter-leaf) is about 1.5% in Varian MLCs^{80,81}. Leakage between adjacent leaves (inter-leaf) has been reported between 1.8% and 2.7%^{66,82}. This additional leakage is modeled in the treatment planning system through the addition of a percentage transmission up to 10%, with a value of 1% recommended for a Varian MLC. The AAPM Task Group 142 report recommends annually maintaining that the MLC transmission (the average of leaf and interleaf) within $\pm 0.5\%$ of baseline⁶⁰.

Treatment planning studies

To simulate MLC transmission and leakage errors in the phantom treatment plans, two separate beam models were created with altered additional interleaf leakage transmission values. The baseline

value used for the MDACC TrueBeam model is 0.8%. Beam models were created with the extreme transmission values of 0% and 10% in order to assess the maximum effect of this specific parameter.

Failure mode 9: MLC tongue-and-groove effect

Overview

To reduce primary inter-leaf leakage, Varian leaves have overlapping side in the form of a tongue-and-groove cross sectional design, as shown in Figure 28. The width of the tongue affects the penumbra width of MLC-defined fields. This design also affects field edges that are defined by the stepped sides of the leaves, potentially resulting in a 10-25% under dose^{80,82,83}. When considering IMRT treatment plans with multiple beam angles, the tongue-and-groove effect is less severe. Even when the effect is smeared throughout the an IMRT dose distribution, Li *et al* showed up to about a 5% change in PTV dose^{83,84}.

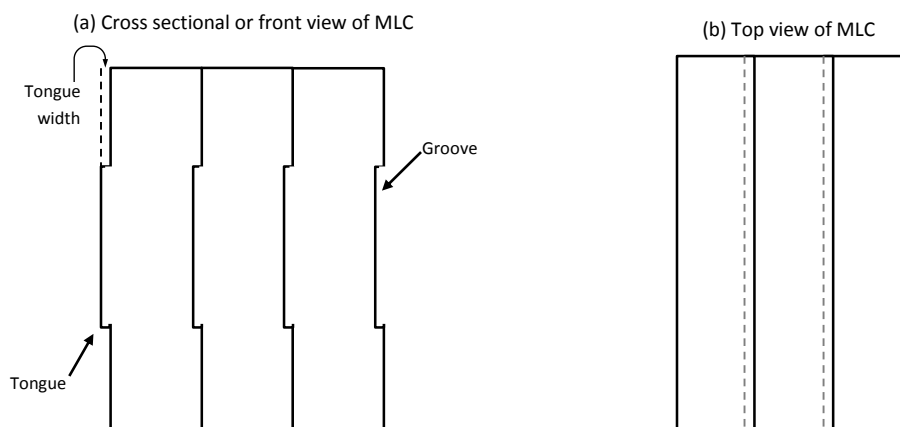


Figure 28: (a) Cross sectional view of Varian MLC leaves (looking from front) showing tongue-and-groove design. (b) Top view of MLC with the dashed line showing the tongue width.

Treatment planning studies

To simulate MLC tongue-and-groove effect errors in the phantom treatment plans, two separate beam models were created with altered MLC tongue-and-groove width values. The baseline width value used for the MDACC TrueBeam model is 0.04 cm. Beam models were created with the extreme width

values of 0.005 cm and 0.200 cm in order to assess the maximum effect of this specific parameter. An increase in the width increases the beam penumbra.

Failure mode 10: MLC leaf end effects

Overview

The Varian MLCs utilize a linear motion and rounded leaf end to match the divergence of the photon beam and maintain a relatively constant geometric penumbra as a function of leaf position. An example of the rounded leaf end is shown in Figure 29. The width of the penumbra depends on the curvature of the rounded end, which is approximated by the radius of a circle in the treatment planning system. Decreasing the leaf end radius increases the penumbra width^{66,85}.

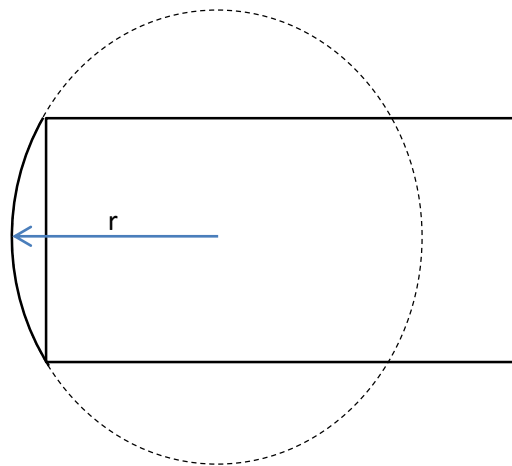


Figure 29: Varian rounded MLC leaf end with radius of curvature of 8 cm..

Treatment planning studies

To simulate MLC leaf end effect errors in the phantom treatment plans, three separate beam models were created with altered MLC rounded leaf end radius values. The baseline radius value used for the MDACC TrueBeam model is 8 cm. Beam models were created with the extreme width values of 4 and 20 cm in order to assess the maximum effect of this specific parameter. We also investigate the use of a radius value of 15 cm, which is commonly used for Elekta linear accelerators.

Failure mode 11: CT table

Overview

Computed tomography (CT) images are used to correct for tissue inhomogeneities by providing electron density information for treatment planning calculations. In order to achieve this, a conversion table from Hounsfield Unit (HU), which is the radiodensity read from the CT image, to electron density is applied within the treatment planning system. HU values can be scanner dependent, particularly those of high density materials, which can influence the calibration⁸⁷. Small changes in the dose of up to about 2% were demonstrated for tolerance level errors in CT tables for conformal radiation treatments⁸⁸.

Treatment planning studies

To simulate CT table errors in the phantom treatment plans, three alternate CT tables were used. Two of the alternate tables were based on the clinically used MDACC CT table which was systematically increased by 2% and decreased by 2%. The third alternate CT table was taken from a positron emission tomography (PET) CT scanner which exhibited larger differences at the low and high higher ends, representing non-uniform variations seen in scanners clinically. These CT tables are shown in Figure 30 and Figure 31.

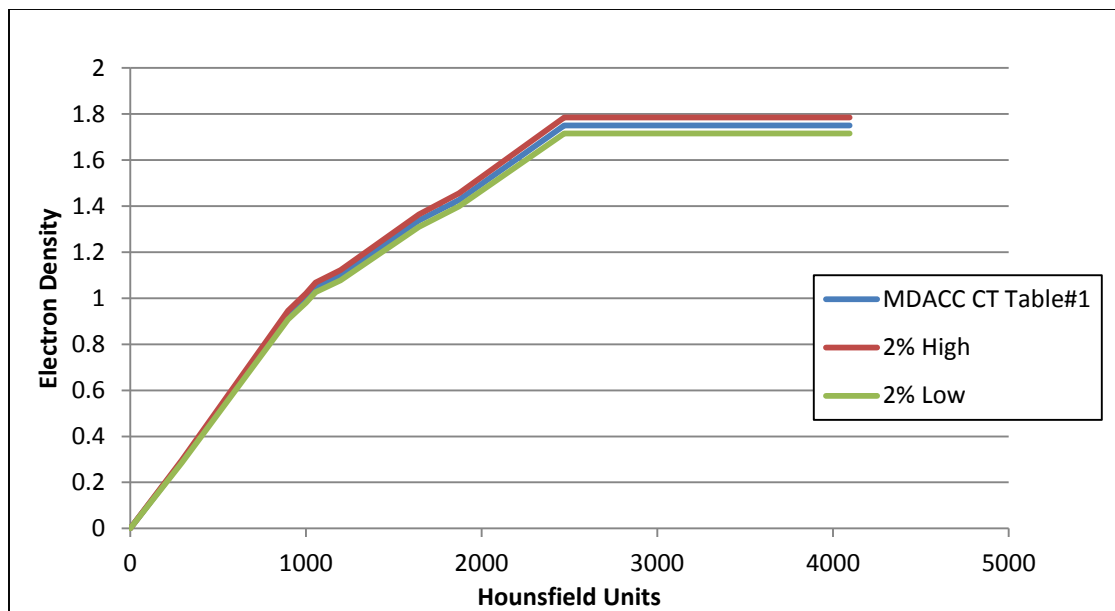


Figure 30: CT tables used for treatment planning studies including the clinically used baseline MDACC CT Table #1, 2% high, and 2% low.

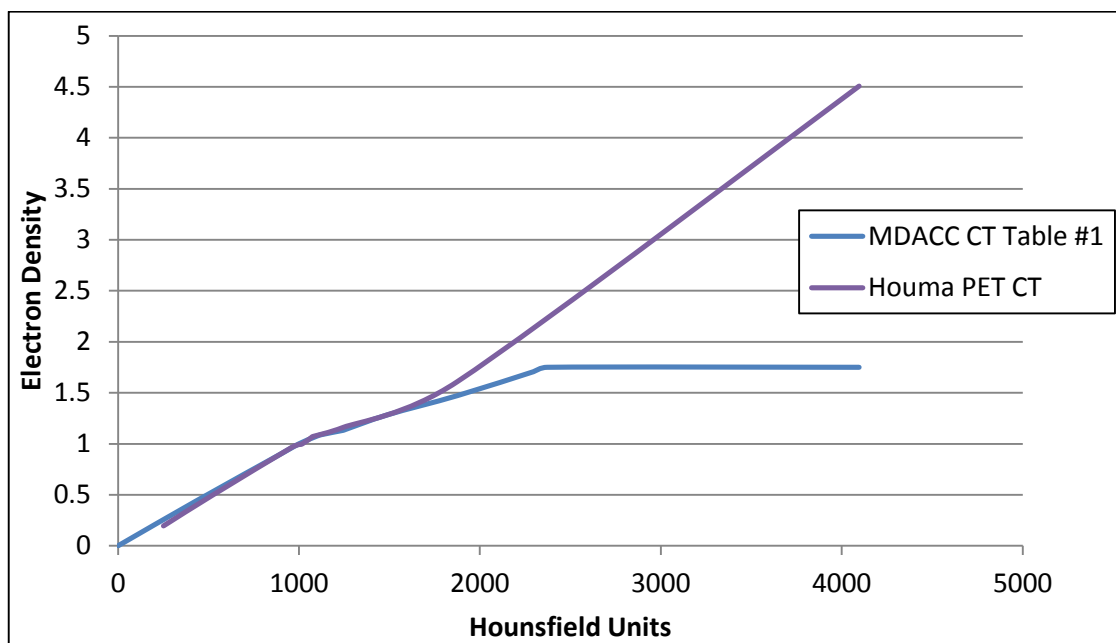


Figure 31: CT tables used for treatment planning studies: the clinically used baseline MDACC CT Table #1 and a CT table generate from a PET CT scanner.

2.1.4 Compare qualitative and quantitative severity data.

The qualitative and quantitative data were compared directly as well as statistically. In order to evaluate whether or not the severity data obtained by our two methods were statistically different, a one-

sample Wilcoxon Signed Rank Test was used, with the qualitatively assigned score as the test value, μ_0 . We also looked for exact matches and compared the 95% confidence interval of the median values from the survey severity scores to the values obtained through our treatment planning studies for each failure mode. T-tests were used to perform the same analysis with the percent dose errors estimated with in the survey and the maximum percent dose errors found in our phantom treatment planning studies.

2.2 Specific Aim 2: Evaluate and compare the ability of qualitative and quantitative severity scores to accurately describe the error magnitude induced in clinical cases by each physical failure mode.

The objective of this specific aim was to compare the validity of the quantitative and qualitative scores by evaluating the true severity for each failure mode in clinical H&N patients. The working hypothesis of this specific aim was that quantitative severity scores were significantly more likely than qualitative subjective scores to describe true clinical consequences. The rationale for this specific aim was that there is not a gold standard or a “correct” answer when it comes to severity scores. In order to assess whether the quantitative severity scores were an improvement upon the subjective qualitative scores, we first needed to determine what the goal or “correct” answer might be. We expected to see an improvement of the validity of these scores with quantification, meaning that they truly corresponded to the error that would be seen if each failure mode occurred in the clinic. This was done by evaluating ten actual clinical cases with each of the physical failure modes simulated in the treatment planning system and comparing the ability of each set of severity scores to accurately identify the magnitude of error induced by each.

2.2.1 Evaluate the magnitude of error induced by each physical failure mode in clinical patient treatment plans to find the “true” severity.

Overview

Each failure mode was simulated in the treatment planning system and these were applied to ten randomly selected step and shoot IMRT oropharyngeal patients previously treated at MDACC following

the same methodology described for the phantom treatment planning studies in Specific Aim 1. The PTVs and primary OARs were evaluated for max dose deviation and the severity score of each failure mode in each patient plan was assigned in the same manner as for the phantom. This resulted in ten true sets of severity data for each failure mode.

Patient descriptions

The ten patients randomly selected for this study consisted of six base of tongue (BOT) cases, two oropharynx cases, and two tonsil cases. These patients each had three to five PTVs and were prescribed 54-70 Gy over 22-33 fractions. Nine co-planar IMRT beams were used for each patient. Additional beams for supraclavicular nodes (SCV), midline block (MNB), and midneck boost (MNB) are included when done with 6 MV photons. Only beams using 6MV photons were used for this study. All patient doses were computed in Pinnacle using the CC Convolution algorithm and 0.2 cm x 0.2 cm x 0.2 cm dose grids. The couch was removed as was done in the clinical plan for each patient. Baseline plans for each patient were computed using the MDACC TrueBeam1 model. All patients had brainstem, spinal cord, and parotid gland organs at risk. Additional organs at risk considered on a patient-by-patient basis were determined by those with optimization constraints and those with DVH evaluation and these included cochlea, brain, mandible, larynx, esophagus, submandibular gland, orbit, lens, optic nerve, and chiasm. Normal tissue structures excluding the PTVs were also evaluated. The targets and organs at risk for each patient are shown in Table 14 and Table 15.

Patient	Site	PTV/CTV levels
1	Oropharynx	70 Gy, 66 Gy, 63 Gy, 57 Gy
2	BOT	70 Gy, 63 Gy, 57 Gy
3	Tonsil	66 Gy, 63 Gy, 60 Gy, 54 Gy
4	Right Oropharynx	66 Gy, 60 Gy, 54 Gy
5	Tonsil	69.96 Gy, 60 Gy, 54 Gy
6	Right BOT	66 Gy, 60 Gy, 54 Gy
7	BOT	70 Gy, 66 Gy, 63 Gy, 57 Gy
8	BOT	69.30 Gy, 66 Gy, 63 Gy, 60 Gy, 57 Gy
9	Left BOT	70 Gy, 66 Gy, 63 Gy, 57 Gy
10	BOT	66 Gy, 60 Gy, 54 Gy

Table 14: Patient sites, planning target volume (PTV), and clinical target volume (CTV) levels.

Patient	Organs at Risk Evaluated
1	Brainstem, Cord, L/R Parotid, L/R Cochlea, Brain, Mandible
2	Brainstem, Cord, L/R Parotid, L/R Cochlea, Brain, Mandible, Larynx, Esophagus
3	Brainstem, Cord, L/R Parotid, L/R Cochlea
4	Brainstem, Cord, L/R Parotid, L/R Cochlea
5	Brainstem, Cord, L/R Parotid, Mandible
6	Brainstem, Cord, L/R Parotid, Mandible, L Submandibular Gland
7	Brainstem, Cord, L/R Parotid, L/R Cochlea, L/R Submandibular Gland, L/R Orbit, L/R Lens
8	Brainstem, Cord, L/R Parotid, L/R Submandibular Gland
9	Brainstem, Cord, L/R Parotid, L/R Cochlea, L/R Submandibular Gland, Mandible, Larynx, Esophagus
10	Brainstem, Cord, L/R Parotid, Mandible, L/R Orbit, L/R Lens, L/R Optic Nerve, Chiasm

Table 15: Patient organs at risk used to evaluate severity.

For severity scoring, all PTVs and CTVs were evaluated at D_{95%}. Organs at risk were evaluated at the published Quantitative Analysis of Normal Tissue Effects in the Clinic (QUANTEC) normal tissue tolerance levels. These values are shown in Table 16. The difference from baseline in each of these values for each failure mode was computed. The severity scores corresponding to each of these differences for all structures were then determined for each failure mode. The maximum severity score of all structures in a given patient was used to assign a score for each failure for that patient.

Structures	Evaluation parameter(s)		
PTV	D _{95%}		
CTV	D _{95%}		
Brainstem	D _{100%}	Max to 1 cc	
Spinal Cord	Max		
Parotid Glands	Mean	D _{50%}	
Cochlea	Mean	D _{05%}	
Orbit	Mean	Max	
Lens	Max		
Optic Nerve	Max		
Chiasm	Max		
Mandible	Max	Max to 1 cc	
Brain	Max		
Submandibular Gland	Mean		
Esophagus	Mean	D _{33%}	D _{15%}
Larynx	Mean		D _{27%}

Table 16: Evaluation parameters used for each structure to assign a severity score for each failure mode to patient treatment plans.

2.2.2 Compare the validity of qualitative and quantitative severity scores.

The objective of this study was to compare the ability of each set of severity scores to accurately identify the true magnitude of error induced by each failure mode. The rationale for this specific aim was that current conventional methods of evaluating severity result in subjective scores of questionable validity. Our goal in this project was to improve FMEA by providing quantitative data on the effects of IMRT delivery physical failure modes to reduce the subjectivity of FMEA severity scores. To verify improvement, we had to compare the accuracy of qualitatively and quantitatively assigned severity scores.

For each physical failure mode individually, the percent dose difference assigned qualitatively and that found quantitatively were compared to the ten true differences. We first looked at them qualitatively by comparing the distributions of the scores as well as looking for exact matches in the scores. In order to determine if the qualitatively assigned severity scores were significantly different than

the true severity scores, a one-sample Wilcoxon Signed Rank Test was used, with the qualitatively assigned score as the test value, μ_0 . The same test was performed to compare the qualitatively assigned severity scores to the true scores. These results were used to compare the likelihood of each set of scores to describe the true clinical consequences. An alpha level of 0.05 was used for these tests.

Chapter 3 Results and Discussion

3.1 Specific Aim 1

3.1.1 Qualitative severity scoring

Pilot Survey Study Results

A total of 11 responses were collected for the pilot survey that was administered at the 2013 AAPM Annual Meeting, collecting the three FMEA scores for the listed failure modes as well as the perceived percent dose error and select demographic information. A summary of the demographics are shown in Table 17. The results for severity are tabulated below in Table 18.

Subject	Response (number respondents)		
Linac	Varian (9)	Siemens (1)	Other (1)
TPS	Pinnacle (7)	Eclipse (2)	Other (2)
Technique	Step and Shoot (8)	Sliding Window (2)	Other (1)
Familiarity with FMEA	Slightly (4)	Somewhat (5)	Very (2)

Table 17: Demographics for pilot survey. Subject of the question is listed in the left column, possible responses and corresponding number of responses out of 11 total reported.

Failure Mode (Magnitude of Failure)	Assigned Severity Score		Ave. % dose difference (σ)
	Range	Average	
Beam energy (1%)	1 - 6	2.9	1.94 (2.18)
Beam symmetry (2%)	2 - 5	3.4	1.82 (1.29)
MLC systematically in one bank (2 mm)	4 - 8	6	9.41 (9.42)
Gantry angle systematically (2.0°)	2 - 7	3.9	14.32 (27.76)
Collimator angle systematically (2.0°)	2 - 6	3.9	13.75 (26.36)
Couch angle systematically (2.0°)	2 - 6	3.8	12.57 (26.33)
MU linearity for < 5 MU systematically (6%)	3 - 7	4	2.67 (1.94)
MLC transmission and leakage modeling (0.5%)	2 - 7	3.9	2.93 (1.88)
MLC tongue-and-groove modeling (0.5%)	2 - 7	3.8	2.30 (0.91)
MLC leaf end modeling (0.5%)	2 - 8	4.7	4.50 (3.55)
CT number to electron density table systematically (2%)	1 - 7	2.9	1.11 (0.80)

Table 18: Pilot survey results, failure mode (magnitude of the failure) are listed with the range and average of Severity scores assigned as well as the average percent dose error assigned (standard deviation).

From the 11 responses gathered, 5 matched the specifics of the IMRT dose delivery process used in this study: Varian linear accelerator, Pinnacle treatment planning system (TPS), and Step-and-shoot IMRT technique. Overall, respondents most often used Varian machines (9/11) and with the Pinnacle

TPS (7/11). Step-and-shoot IMRT was the most used amongst respondents (8/11), supporting the notion that many are familiar with this fundamental form of IMRT. All respondents were at least slightly familiar with FMEA, as none responded with “Not familiar.” Ranges of severity scores assigned were large, as predicted. The standard deviation of the percent dose error reported for each failure mode is also large, indicating a large spread in opinions amongst the respondents. Average percent dose errors assigned were the largest for systematic angular displacements in gantry, collimator and couch.

Full FMEA Survey Results

A total of 184 complete responses were received for the individual FMEA survey. Three responses were discounted because respondent comments displayed lack of comprehension or lack of following instructions. Three medical physics groups also completed the group survey.

Demographics

The respondent demographic data collected are show in Figure 32, Figure 33, and Figure 34. Fourteen countries on four continents were represented in the responses, with 84% of all responses coming from North America and 95% of those from the United States. Most (76%) individual respondents dedicated at least 80% of their time to clinical work, with a large portion dedicated entirely to the clinic (36%). Almost all respondents (92%) were certified by a national organization, with the majority having American Board of Radiology certification (72%). Respondent experience in medical physics ranged from 2.5-45 years, with an average of 18 years. Just over half of individual respondents were at least somewhat familiar with FMEA (52%), while 17% were reportedly not familiar. Several IMRT techniques, linear accelerator models, and treatment planning systems were listed as those primarily used for head and neck IMRT treatments at respondent clinics as shown in Figure 34. Current practice of step-and-shoot and sliding window IMRT techniques were almost equally represented, with 41% and 47% of responses, respectively. Most respondents primarily used Varian linear accelerators (73%) and the most popular treatment planning system amongst respondents was the Varian Eclipse

(54%) system. The most represented IMRT technique/accelerator make/TPS combination amongst respondents was Sliding Window using Eclipse treatment planning on Varian linear accelerators (43%).

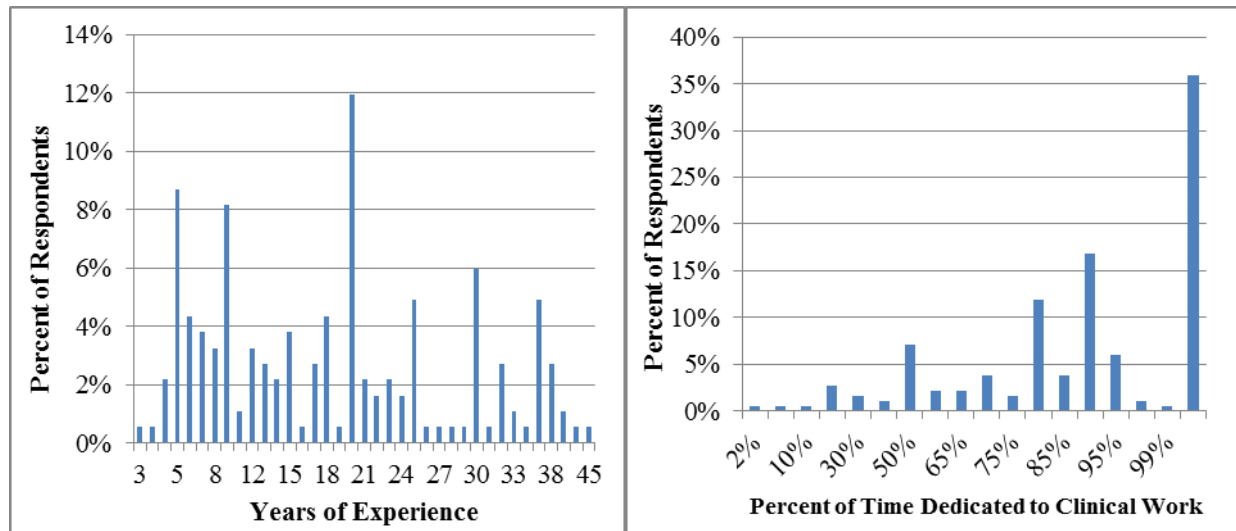


Figure 32: Demographics of the respondents for (left) years of experience and (right) time dedicated to clinical work.

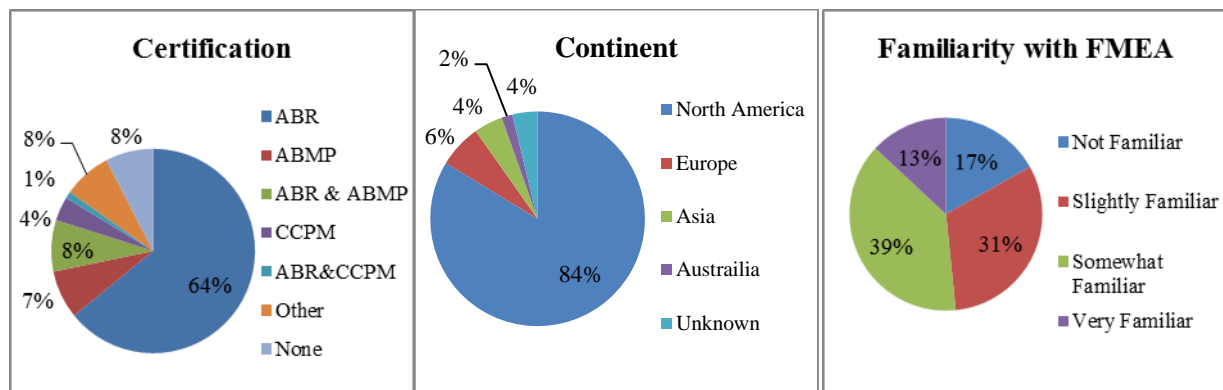


Figure 33: Demographics of the respondents for their current continent, certification, and familiarity with FMEA.

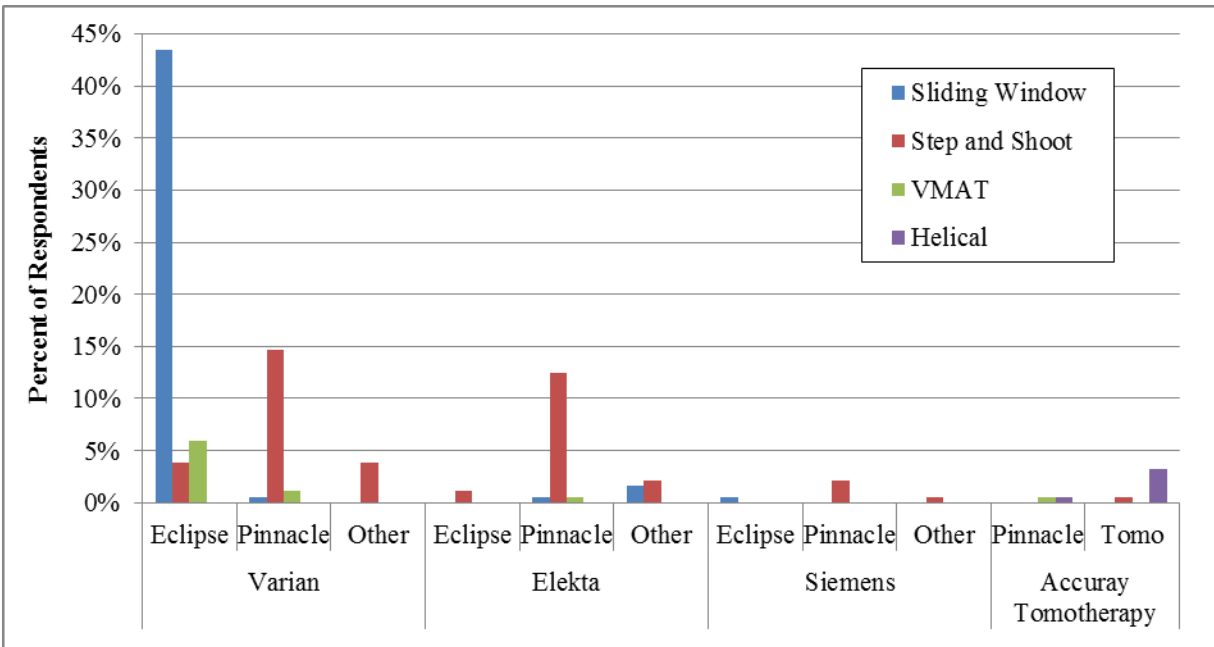


Figure 34: Distribution of linear accelerator manufacturer, treatment planning system, and IMRT technique listed as primarily used by respondents for head and neck cases.

Scores and Ranking

The details of values and variability in O, D, and S scores assigned for each failure mode and resultant RPNs are best presented in the box plots shown in Figure 35 and Figure 36, respectively. In these figures, it can be seen that all failure modes were scored in the mid- to low-risk ranges with median O, D, and S score values between 2 and 6 and median RPN values between 15 and 85. Interestingly, each of the eleven failure modes received scores ranging from 1-10 for occurrence, at least 1-9 for detectability, and at least 1-7 for severity. The largest mean severity score was 5 for failure mode 3 (MLC position shifted systematically in one bank by 2 mm), which also had the largest range in values excluding outliers. A large spread was also seen in the RPN scores, with the smallest spread in scores by different respondents for any one failure mode being 261 for failure mode 6 (couch angle offset of 2 degrees) and the largest spread being 575 for failure mode 7 (MU linearity error of 6% for <5 MU). These large spread in the data were indicative of the wide variation and subjectivity of assigning FMEA scores.

The ranking of failure modes according to RPN also resulted in large variability, with each failure mode being ranked both most risky (1st) and least risky (11th) by different respondents. Identical rankings

were given by only two respondents, in which case both respondents assigned scores of “1” across the board for O, D, and S, giving all failure modes equal ranking. The distribution of respondent RPN rankings is demonstrated in Figure 37. Based on the distribution of RPN scores, the respondents indicated more concern for failure modes 7-10 and less concern for failure modes 1, 4, 5, and 6. Failure modes 7-10 represent MU linearity and three MLC modeling parameters, respectively, tend to be ranked the highest in risk.

In addition to the FMEA scores and rankings, the respondent estimated percent dose error, keeping in mind both the target and OAR structures, for the worst case scenario of each failure mode was also collected. All failure modes had median estimated errors of 1-3% with the exception of failure mode 3 (MLC position shifted systematically in one bank by 2 mm) which had a median estimated error of 5%. The lowest mean percent dose errors are shown to be less than 2% for failure modes 1 and 11, corresponding to beam energy and CT number vs. electron density table, respectively. These values are shown in the box plots in Figure 38. Maximum extreme outliers, noted by purple crosses, are not displayed in the figure to preserve visibility of the data. These maximum extreme outliers included 50% errors for failure modes 3-6 and 8 assigned by various respondents. Maximum outliers, also included in failure modes 3-6, were assigned 100% error by a single respondent and failure mode 7 was assigned a maximum error of 105% by one other respondent. As observed with the FMEA O, D, S, and RPN scores, the variability in the estimated percent dose errors associated with the worst case failure modes was very large. Perceived severity is typically directly associated with estimates of dose error. The variability in this data from our survey shows the need for more accurate and consistent estimates of dose error associated with the failure modes. Having these better estimates would provide quantitative guidance for the medical physics community to estimate severity scores with less variability.

Overall, the eleven surveyed failure modes were evaluated to be low to medium risk as one would expect, with average RPNs under the commonly cited arbitrary threshold value of 125^{7,30,33-35}. Since the magnitude of these failures was just outside the currently established tolerance criteria levels which aim at

maintaining highly accurate dose deliver, it makes sense that the perception of their risk is not high; otherwise the tolerance levels would be different. Variability in the responses of the individuals assigning scores was expected, especially in this situation of a survey because of the large range of professional experiences possible in different clinics and individual career specialization. However, the variability demonstrated in the survey responses was extreme. This variability existed in both the scores themselves as well as the resultant ranking of the failure modes. The magnitude of the scores themselves was important, with respect to both predetermined thresholds that may be put in place as well as when assessing quantitative features of the scores and failures. There was no clear ranking of the failure modes agreed upon because of the very large variability in the rankings. This is especially important to note since the overall results of an FMEA rely primarily on the ranking of the failure modes, not just the magnitude of scores assigned. The fact that each failure mode was ranked both most risky and least risky by different respondents really underlines the fact that the FMEA process is extremely subjective and the results may be of questionable reliability. From our data, general groupings were made when examining Figure 37 such that failure modes 8-10 were ranked as high risk, 1, 4, and 5 were low risk but this clearly would not have been the conclusion drawn by all of the respondents if they were performing this process separately.

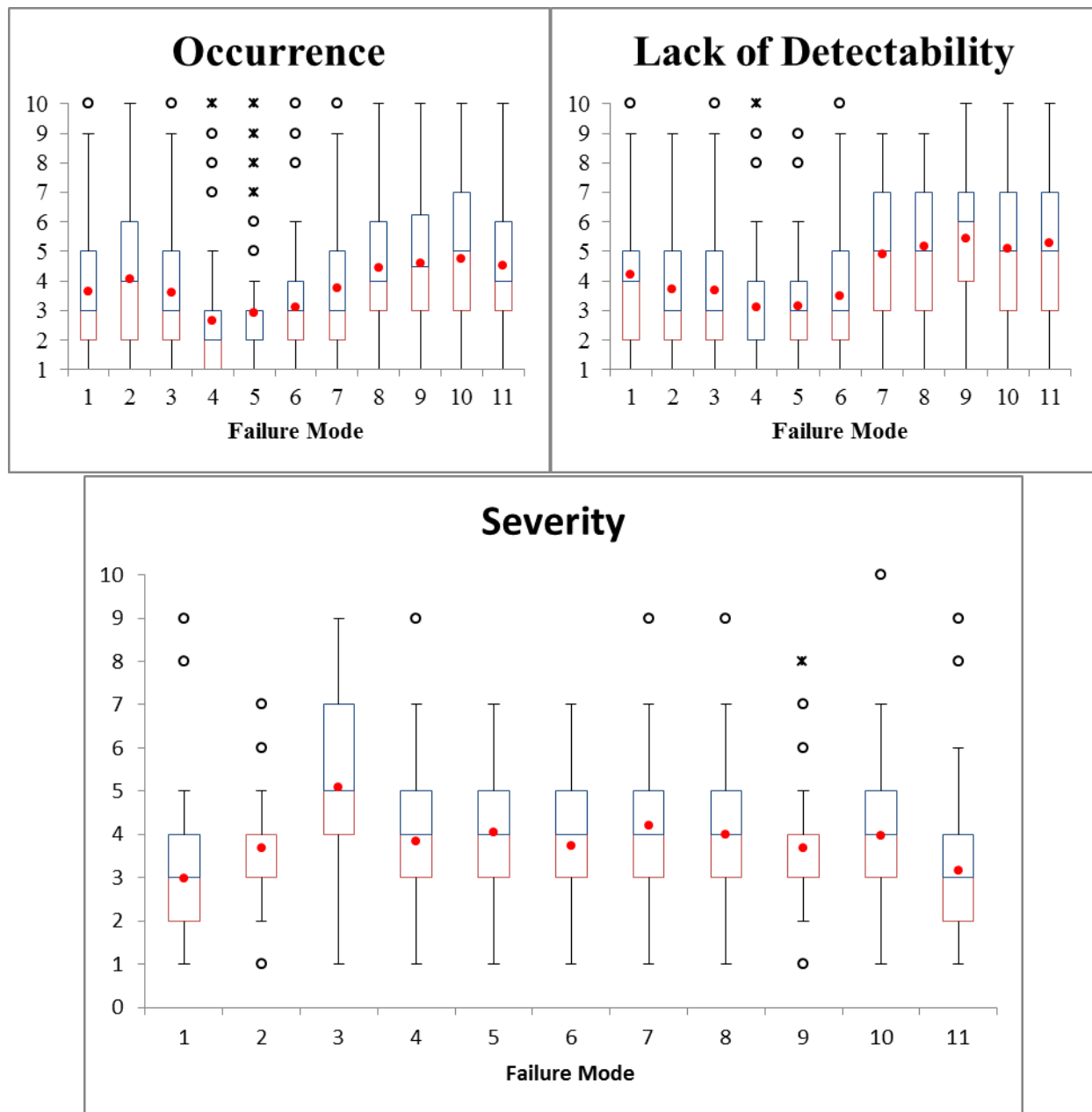


Figure 35: Occurrence, lack of detectability, and severity scores for N=184 responses (including 3 groups) for eleven failure modes (as numbered on page 15). Box plots are shown with red representing the second quartile and blue representing the third quartile. Red circles represent the mean score, open circles represent outliers, and stars represent extreme outliers.

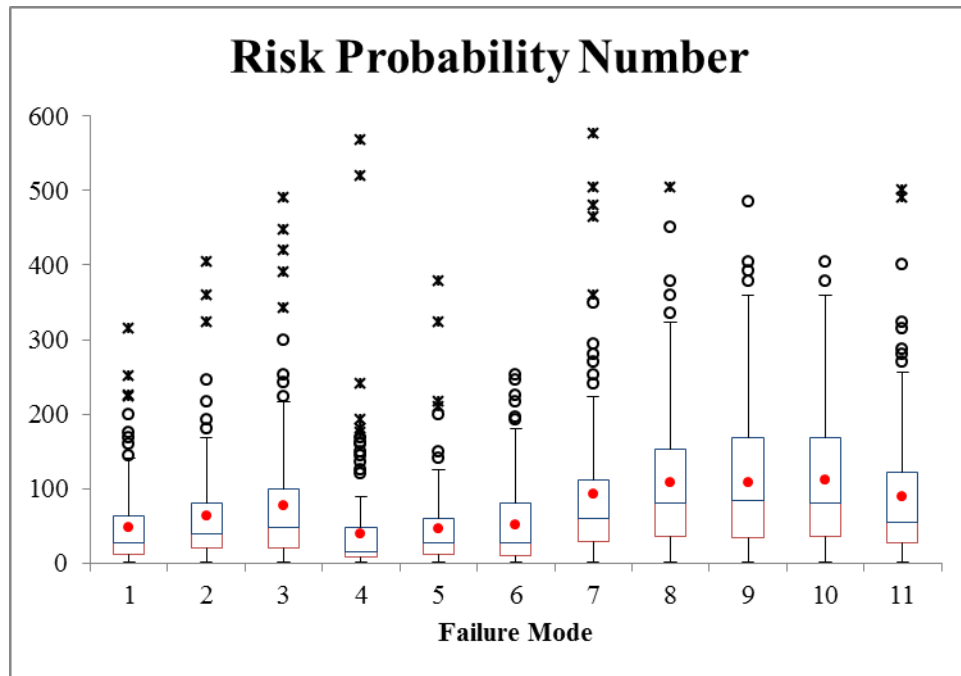


Figure 36: Risk Probability Number (RPN) calculated for N=184 responses (including 3 groups) for eleven failure modes (as numbered on page 15). Box plots are shown with red representing the second quartile and blue representing the third quartile. Red circles represent the mean score, open circles represent outliers, and stars represent extreme outliers.

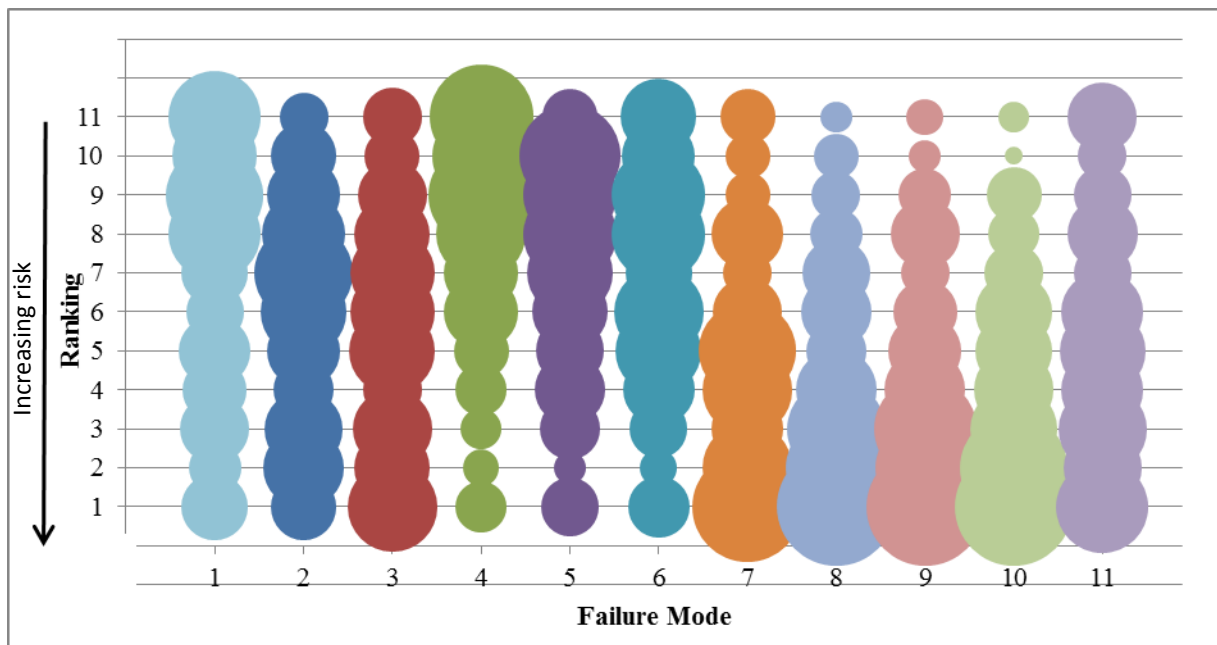


Figure 37: Ranking of failure modes in order of the risk they present using the RPN. The most risky failure mode would have the highest RPN and would be ranked "1". The size of the bubbles in the chart indicate the frequency at which each failure mode was assigned each rank according to the RPNs calculated.

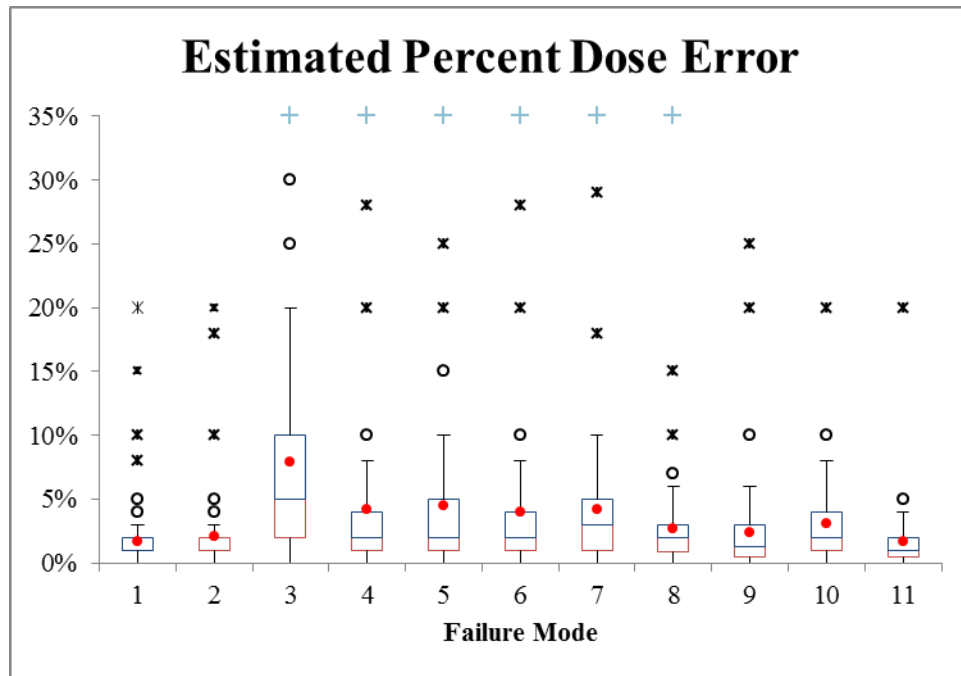


Figure 38: Estimated percent error assigned for N=184 responses (including 3 groups) for eleven failure modes (as numbered on page 15. Box plots are shown with red representing the second quartile and blue representing the third quartile. Red circles represent the mean score, open circles represent outliers, and stars represent extreme outliers. Purple crosses indicate that the maximum extreme outliers not shown.

Relationships

The severity score assigned to each failure mode in theory should increase with the estimated percent dose error resulting from each failure mode since they are both attempting to assess the outcome or consequences of the specific failure. As expected, a positive correlation of all respondent data was found between their estimated percent dose error and severity scores for each failure mode (data not shown). The strength of the correlation varied between failure modes, with the Spearman correlation coefficients falling between 0.3 and 0.6 and with each result being statistically significant at the $p < 0.01$ level. This correlation indicates that estimated percent dose error and severity scores monotonically increase together. Another way we assessed the relationship between percent dose error and severity scores was by evaluating the dose errors that were represented by each severity score as shown in Table 19, indirectly answering the question: what do the severity scores mean quantitatively? The three respondent groups directly assigned quantitative values to the severity scores and these are shown in Table 20. Although the ranges are not entirely consistent, the average percent dose error assigned for each

severity score flows nicely from least to greatest with the exception of S=10. This can be attributed to the fact that only one respondent assigned a catastrophic severity score of 10 for any failure mode and therefore the average does not represent the cohort distribution. The group-assigned quantitative meanings were fairly consistent across the three groups and had similar values to the average percent dose errors corresponding to severity scores from the individual responses. Despite the variability in the percent dose errors corresponding to severity scores, it seemed overall that quantitative definitions for severity scores could easily be agreed upon.

None of the various demographic data universally resulted in significant associations (Chi Squared) or correlations (Spearman' Rho) in any of the scores or estimated percent dose errors. Even though none of the demographics appeared to significantly relate to any score overall, several statistically significant differences and correlations were noted throughout the data. All of the significant results are presented in Table 21, according to demographic. The most interesting of these significant results include negative correlations between detectability scores (D) and percent of time dedicated to clinical work for the four failure modes regarding beam modeling (8-11). These negative correlations indicated that those physicists with more time dedicated to clinical work believed that such modeling errors would be more likely to be detected (lower detectability score). Although these correlations were significant, it is important to note that the strength of the relationships was very weak, with a rho of ± 1 indicative of a perfectly monotonous relationship. This was the case for all significant demographic correlations found, with the strongest correlation found between failure mode 1 (beam energy off by 1%) severity score and respondent years of experience with rho = -0.281. This relationship indicates that respondents with more experience tended to think that the consequences of a 1% beam energy error would be less severe than those with less experience, but again, although this relationship was statistically significant, the relationship was weak. It was also interesting to note that all correlations were negative, indicating those with more years of experience or those with more time dedicated to clinical work generally assigned lower scores for the failure modes and scores specified.

Severity Score	Estimated Percent Dose Error			
	Min	Max	Average	Median
1	0%	5%	0.62%	0.60%
2	0%	20%	1.08%	0.99%
3	0%	20%	1.74%	1.77%
4	0%	50%	2.77%	2.87%
5	0%	50%	4.00%	4.07%
6	0.01%	105%	6.13%	5.98%
7	0%	100%	12.06%	9.68%
8	1%	50%	16.80%	11.18%
9	3%	100%	20.22%	13.75%
10	15%	15%	15%	15%

Table 19: Percent dose errors estimated by survey respondents and corresponding severity scores that were assigned.

Severity Score	Quantitative Value	
	Min	Max
1	0%	3%
2	0%	4%
3	-	-
4	2%	5%
5	-	-
6	-	-
7	10%	>20%
8	-	-
9	20%	>30%
10	50%	>50%

Table 20: Quantitative values assigned to severity scoring scale by groups (N=3).

Demographic	Response	Statistical Relationship
Failure Mode 1: Energy		
Years of Experience	O	p=0.008, rho=-0.194
Years of Experience	S	p=0.000, rho=-0.281
Years of Experience	RPN	p=0.000, rho=-0.267
Failure Mode 2: Symmetry		
Years of Experience	S	p=0.018, rho=-0.175
Failure Mode 3: MLC Position		
Linac Manufacturer	% error	p=0.000, V=0.000
Failure Mode 4: Gantry Angle		
Years of Experience	S	p=0.049, rho=-0.149
Continent	RPN	p=0.000, V=0.000
Failure Mode 8: MLC tongue & groove modeling		
Clinical Time	D	p=0.011, rho=-0.187
Failure Mode 9: MLC leakage & transmission modeling		
Clinical Time	D	p=0.024, rho=-0.166
Linac Manufacturer	% error	p=0.000, V=0.000
Continent	D	p=0.000, V=0.000
Failure Mode 10: MLC leaf end modeling		
Clinical Time	D	p=0.006, rho=-0.201
Certification	D	p=0.000, V=0.000
Failure Mode 11: CT table		
Clinical Time	D	p=0.025, rho=-0.165

Table 21: Statistically significant relationships between demographics and FMEA scores or estimated percent dose errors for each failure mode. Rho value is given for Spearman's Rho correlations, Cramer's V (V) is given for Chi Squared Test for Association. Linac = linear accelerator.

Surprisingly, there were no strong universal correlations between any of the scores, rankings, or dose errors with any of the demographics. This indicates that the demographic information collected was not sufficient to categorize the individual experiences or interpretations, both of which would be expected causes of variability in the scoring. The negative correlations seen between time dedicated to clinical work and detectability for modeling errors (failure modes 8-11) could indicate a difference in understanding of the modeling parameters between those who practice mostly clinically and those who do not or it could be a reflection of one group having more or less experience with beam modeling. Since the relationships were very weak, these conclusions cannot be definitively drawn. The lack of strong relationships supports the notion that the scoring process is very complex and that individual clinics will need to assess their radiation oncology treatment processes on their own to find the scores that are most appropriate to their specific situation. However, it is of note that the FMEA findings between clinics most

likely will be very different if the variability observed with our survey is any indication of the opinions of the medical physics community.

Limitations and biases

This FMEA survey study provided insight into the variability present in opinions on basic IMRT dose delivery quality assurance failures at or just exceeding the AAPM's recommended tolerance limits. While the expectation for variability in opinions could be extended to FMEA scoring of all processes, the results of this survey were very specific. The process evaluated by an FMEA must be very specific, which limited this study in two ways. The first of these limitations was that the specific scores obtained apply only to step and shoot head and neck (H&N) IMRT. The second limitation was that although the process was described in detail to the respondents, the interpretation by each individual of the process, the failure modes, and the scoring could be different, and this likely influenced the results. Of course, these same limiting factors could also play a role in a conventional FMEA, but one would expect it to influence the results to a much lesser degree with an in-person team working in the same environment and discussing each failure mode in detail.

Another factor that may have added to the variability in the scoring could be that low level failures such as those near tolerance criteria levels may be more difficult to estimate the consequences and impact on a complex treatment such as IMRT than large scale, catastrophic failures. This was corroborated by the wide spread in estimated percent dose errors and severity scores from the survey respondents for each failure mode.

Summary of qualitative severity scores

The results of this survey provide valuable information with respect to the application of FMEA to physics-specific failure modes near tolerance criteria levels. More importantly for this project, the severity scores collected represented the subjective qualitative assessment approach to an FMEA of our

specific IMRT process. The percent dose estimates collected also allowed us to relate the qualitative scores to a quantitative definition. A summary of the qualitative severity scores is shown in Table 22.

Qualitative Severity Scores			
Failure Mode	Median	Average	Std Dev
1: Beam Energy	3	2.97	1.42
2: Beam Symmetry	4	3.68	1.21
3: MLC Position	5	5.09	1.77
4: Gantry Angle	4	3.85	1.51
5: Collimator Angle	4	4.06	1.47
6: Couch Angle	4	3.75	1.51
7: MU Linearity	4	4.20	1.48
8: MLC Leakage & Transmission Modeling	4	3.99	1.48
9: MLC Tongue & Groove Modeling	4	3.67	1.39
10: MLC Leaf End Modeling	4	3.96	1.39
11: CT Table	3	3.17	1.44

Table 22: Qualitative severity scores obtained from online survey (N=184).

3.1.2 Quantitative severity scoring

Baseline phantom

Treatment planning studies

Evaluation of DVH data for each of our eleven failure modes from treatment planning studies on the IROC-H H&N IMRT phantom was the primary means for quantitatively assessing severity in this study. Each of the failure modes was compared to baseline phantom plans, both standard and complex. The doses to the two targets, OAR, and normal tissue structures in the phantom for each plan type (i.e. basic and complex) are summarized in Table 23 and Table 24 and the DVHs are shown in Figure 39 and Figure 40. These plans did not quite meet the dosimetric criteria required by the IROC-H for credentialing, however this was acceptable since this was a comparative study.

Baseline Standard Phantom Treatment Plan Structure Doses							
Structure	Min. Dose	Max. Dose	Mean Dose	Std. Dev.	D _{95%}	D _{99%}	Max to 1 cc
	(cGy)						
Primary PTV	602.83	738.05	680.46	14.15	657.15	652.15	710.55
Secondary PTV	530.16	578.31	553.46	6.82	542.83	538.17	563.76
Spinal Cord	3.91	434.05	170.99	142.90	8.96	5.29	355.48
Normal Tissue	0.40	721.99	106.49	141.52	2.79	1.58	683.47

Table 23: Summary of structure doses for the standard phantom treatment plan.

Baseline Complex Phantom Treatment Plan Structure Doses							
Structure	Min. Dose	Max. Dose	Mean Dose	Std. Dev.	D _{95%}	D _{99%}	Max to 1 cc
	(cGy)						
Primary PTV	605.14	747.59	680.51	16.60	653.74	637.54	717.05
Secondary PTV	496.26	636.50	549.65	18.51	529.36	524.87	567.55
Spinal Cord	4.53	425.12	160.42	134.94	9.01	7.58	336.99
Normal Tissue	0.31	739.38	107.89	138.78	2.71	1.71	669.61

Table 24: Summary of structure doses for the complex phantom treatment plan.

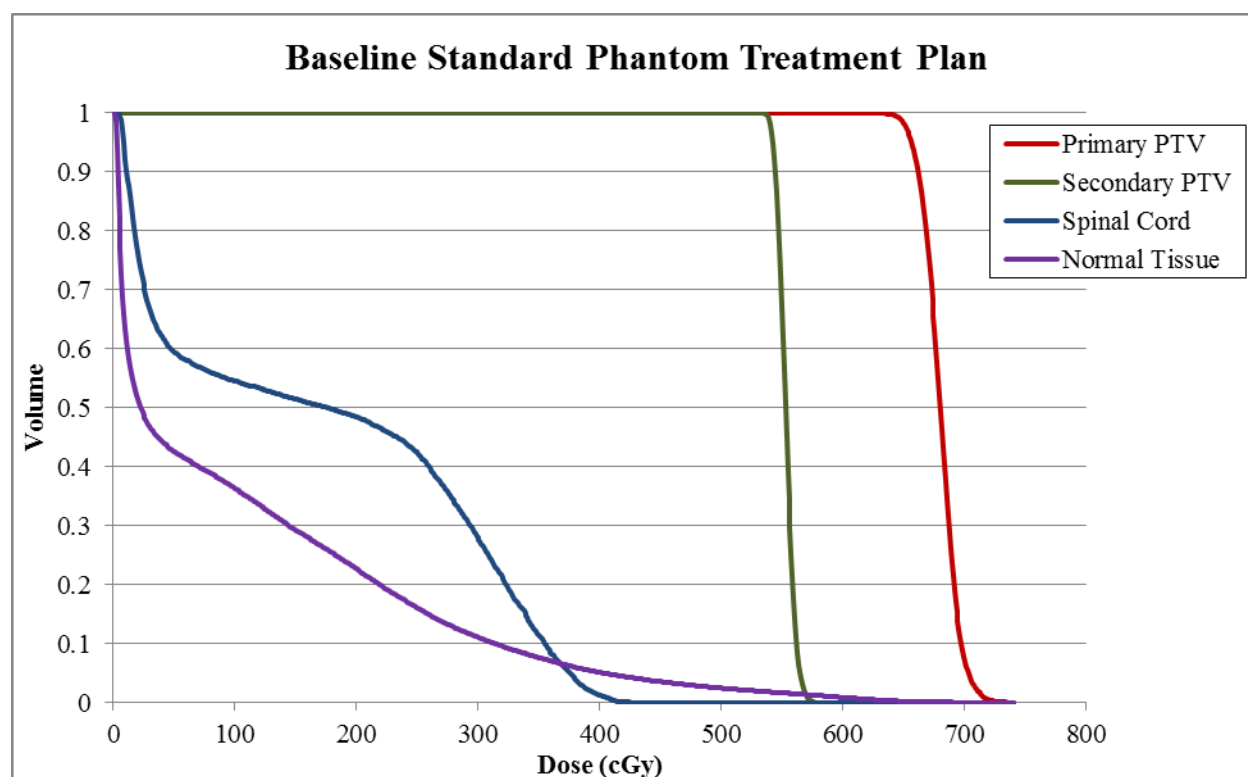


Figure 39: DVHs for baseline standard phantom treatment plan.

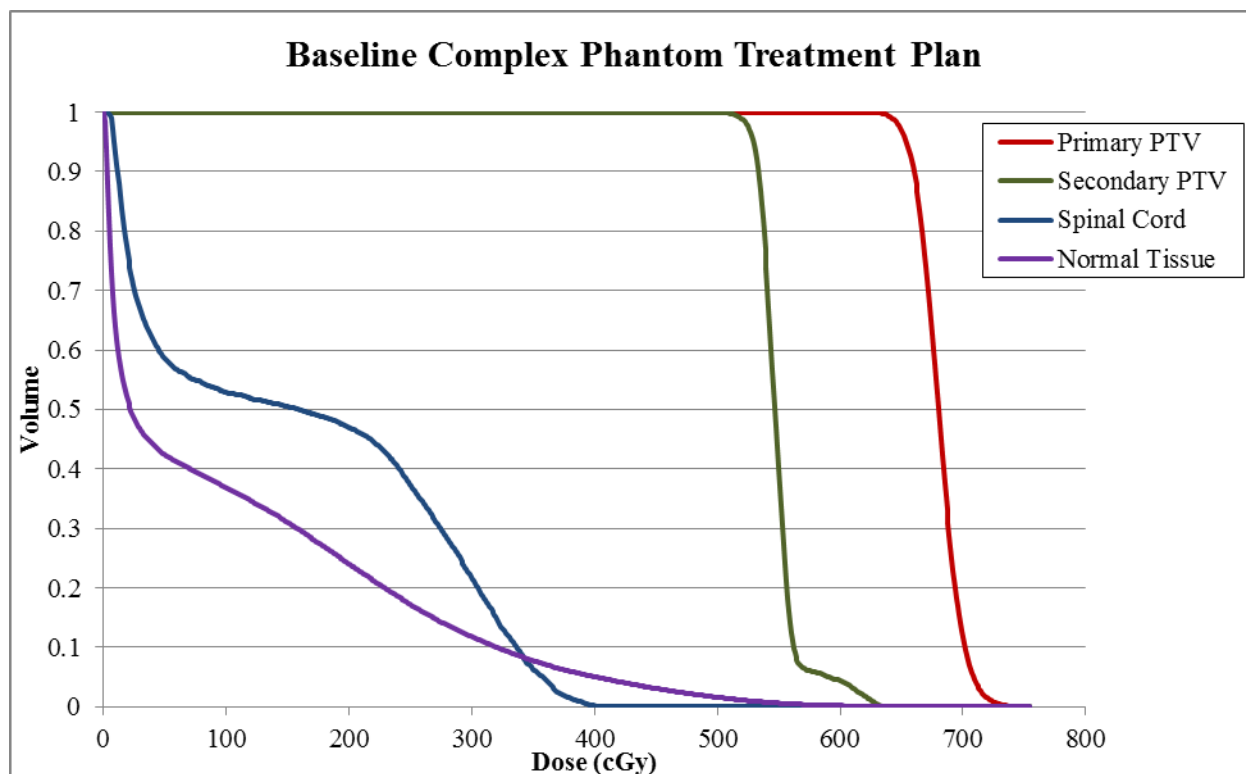


Figure 40: DVHs for baseline complex phantom treatment plan.

Physical Measurements

Irradiation Set #1

The baseline irradiation of the H&N phantom for this irradiation set was evaluated against the treatment planning system predicted doses as done for IROC-H credentialing. The absolute dose results from the eight TLD in the phantom insert are shown in Table 25. The calculated planned dose reported is the mean dose to a contour of the TLD. The distance-to-agreement (DTA) between the primary PTV and spinal cord OAR on the axial film was 1.7 mm. Gamma analysis assessing the agreement between computed planned dose distributions and those measured on the full axial and sagittal films was performed with criteria of 7%/4mm and 5%/3mm. The percent of pixels passing these analyses are shown in Table 26.

Structure	TLD position	Measured Dose (cGy)	Planned Dose (cGy)	% Difference
Primary PTV	Superior Anterior	650.3	690.9	-5.9%
Primary PTV	Inferior Anterior	654.5	693.1	-5.6%
Primary PTV	Superior Posterior	627.3	627.4	0.0%
Primary PTV	Inferior Posterior	676.1	662.5	2.1%
Secondary PTV	Superior	515.6	558.1	-7.6%
Secondary PTV	Inferior	524.5	574	-8.6%
Spinal Cord	Superior	196.5	249.4	-21.2%
Spinal Cord	Inferior	197.6	246.5	-19.8%

Table 25: Baseline TLD results from the first irradiation set with a complex treatment plan.

Film	Criterion	Pixels Passing
Axial	7%/4mm	71.6%
	5%/3mm	50.9%
Sagittal	7%/4mm	79.9%
	5%/3mm	54.6%

Table 26: Baseline gamma analysis results for axial and sagittal films within the phantom for the first irradiation set.

This baseline irradiation was not perfect, with TLD dose differences from the planned dose exceeding 7% in the secondary PTV. There were also large dose differences in the spinal cord TLD, but this was generally expected since the spinal cord was in a steep dose gradient region. The DTA in this steep dose gradient region showed acceptable agreement of the delivered dose with the planned dose. The gamma results were overall rather poor. The film was normalized to the PTV TLD and therefore the absolute dose differences seen in the TLD results were reflected in the gamma analysis results. The measured dose was largely lower than the planned dose. The output of the machine may have been low during these measurements and since this was more of a pilot study to examine the feasibility of performing measurements by altering the beam, we did not plan or have time to measure the output. This set of measurements also had increased uncertainty since phantom irradiations were only performed once for each scenario (baseline or induced failure mode). Regardless of how well the planned doses predicted the measured doses in this case, a comparison of the failure mode irradiations to this set of measured data still demonstrated the differences in delivery.

Irradiation Set #2

The baseline irradiations of the H&N phantom with the standard and complex treatment plans for the second irradiation set were also evaluated against the treatment planning system predicted doses. The absolute dose results are shown in Table 27 and

Complex Phantom Treatment Plan					
Structure	TLD position	Measured Dose (cGy)	Std Dev.	Planned Dose (cGy)	% Difference
Primary PTV	Superior Anterior	634.3	0.20%	682.2	-7.0%
Primary PTV	Inferior Anterior	623.0	0.09%	670.2	-7.0%
Primary PTV	Superior Posterior	649.3	1.83%	685.2	-5.2%
Primary PTV	Inferior Posterior	653.8	1.10%	687.2	-4.9%
Secondary PTV	Superior	522.6	0.47%	548.7	-4.8%
Secondary PTV	Inferior	521.6	0.58%	547.1	-4.7%
Spinal Cord	Superior	252.5	0.73%	276.4	-8.6%
Spinal Cord	Inferior	243.9	1.46%	270.9	-10.0%

Table 28 for the standard and complex plans, respectively. The measured dose reported for each TLD was the average over three irradiations. The average DTA between the primary PTV and spinal cord OAR on the axial film for three irradiations was 0.9 mm for the standard plan and 1.7 mm for the complex plan. The average gamma analysis results on the full axial and sagittal films for three irradiations of both the standard and complex plans are shown in Table 29. Gamma maps are also shown in Figure 41- Figure 44 for each of the three irradiations for this irradiation set.

Standard Phantom Treatment Plan					
Structure	TLD position	Measured Dose (cGy)	Std Dev.	Planned Dose (cGy)	% Difference
Primary PTV	Superior Anterior	640.2	0.78%	680.8	-6.0%
Primary PTV	Inferior Anterior	628.3	0.41%	675.0	-6.9%
Primary PTV	Superior Posterior	652.4	0.37%	691.2	-5.6%
Primary PTV	Inferior Posterior	645.2	0.45%	680.8	-5.2%
Secondary PTV	Superior	544.0	0.36%	555.5	-2.1%
Secondary PTV	Inferior	537.3	0.99%	561.0	-4.2%
Spinal Cord	Superior	291.2	1.11%	311.1	-6.4%
Spinal Cord	Inferior	288.8	0.27%	310.7	-7.0%

Table 27: Baseline TLD results from the second irradiation set with the standard treatment plan.

Complex Phantom Treatment Plan					
Structure	TLD position	Measured Dose (cGy)	Std Dev.	Planned Dose (cGy)	% Difference
Primary PTV	Superior Anterior	634.3	0.20%	682.2	-7.0%
Primary PTV	Inferior Anterior	623.0	0.09%	670.2	-7.0%
Primary PTV	Superior Posterior	649.3	1.83%	685.2	-5.2%
Primary PTV	Inferior Posterior	653.8	1.10%	687.2	-4.9%
Secondary PTV	Superior	522.6	0.47%	548.7	-4.8%
Secondary PTV	Inferior	521.6	0.58%	547.1	-4.7%
Spinal Cord	Superior	252.5	0.73%	276.4	-8.6%
Spinal Cord	Inferior	243.9	1.46%	270.9	-10.0%

Table 28: Baseline TLD results from the second irradiation set with the complex treatment plan.

Film	Criterion	Standard Plan		Complex Plan	
		Pixels Passing	Std Dev.	Pixels Passing	Std Dev.
Axial	7%/4mm	80.3%	12.66%	65.6%	2.70%
	5%/3mm	55.7%	12.39%	37.7%	2.50%
Sagittal	7%/4mm	81.5%	4.58%	69.6%	2.45%
	5%/3mm	66.9%	1.85%	55.7%	2.19%

Table 29: Baseline gamma analysis results for axial and sagittal films within the phantom for the second irradiation set.

Standard Phantom Treatment Plan: Baseline Axial Film, 5%/3mm

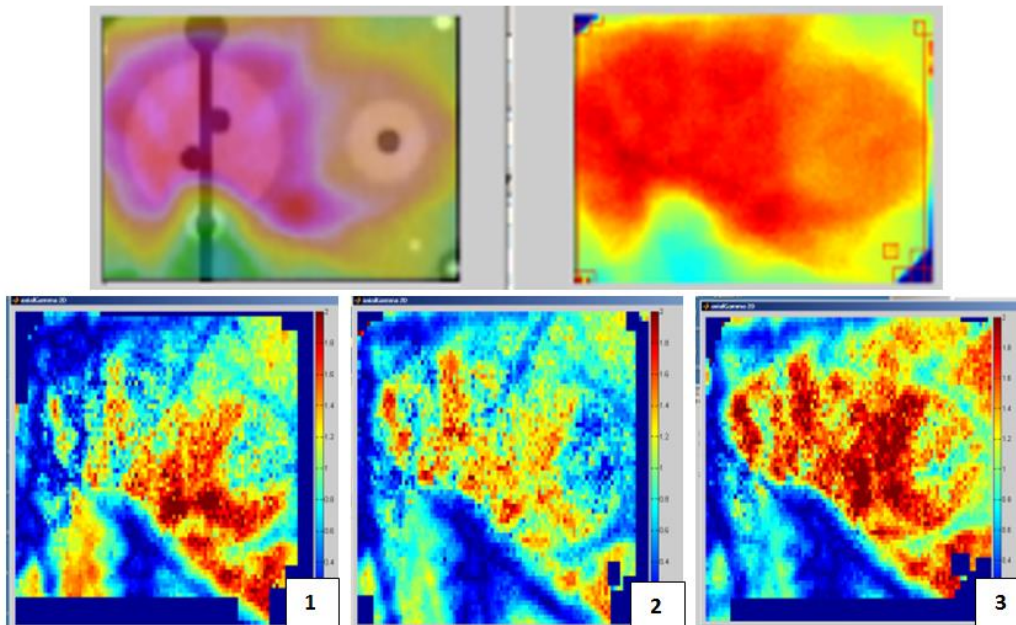


Figure 41: Axial film dose distributions from the TPS (upper left), film from one irradiation (upper right), and the gamma maps (5%/3mm) from this film for the three irradiations of the phantom with the standard treatment plan (bottom).

Standard Phantom Treatment Plan: Baseline Sagittal Film, 5%/3mm

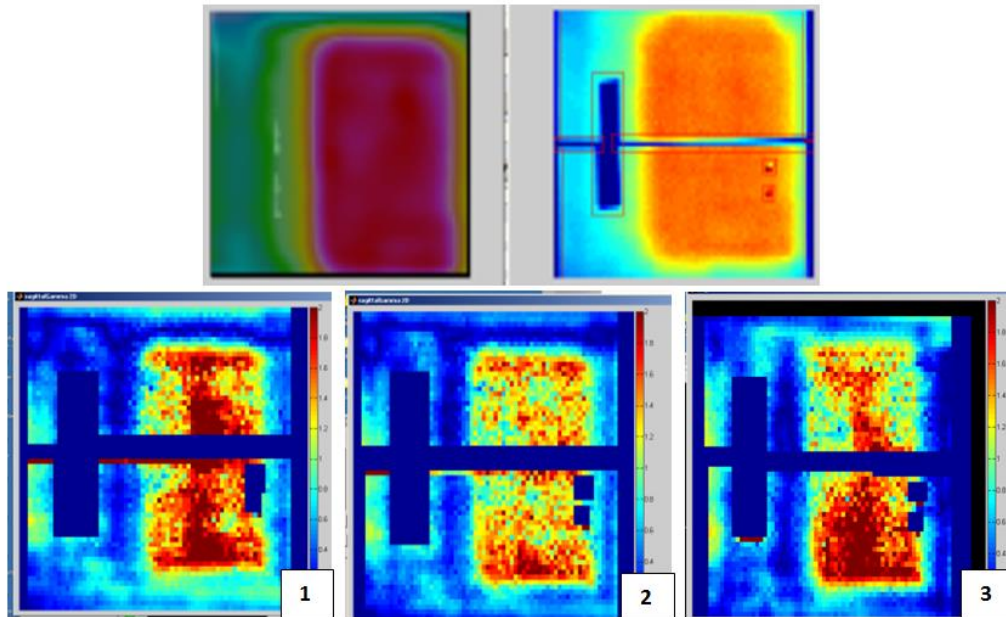


Figure 42: Sagittal film dose distributions from the TPS (upper left), film from one irradiation (upper right), and the gamma maps (5%/3mm) from this film for the three irradiations of the phantom with the standard treatment plan (bottom).

Complex Phantom Treatment Plan: Baseline Axial Film, 5%/3mm

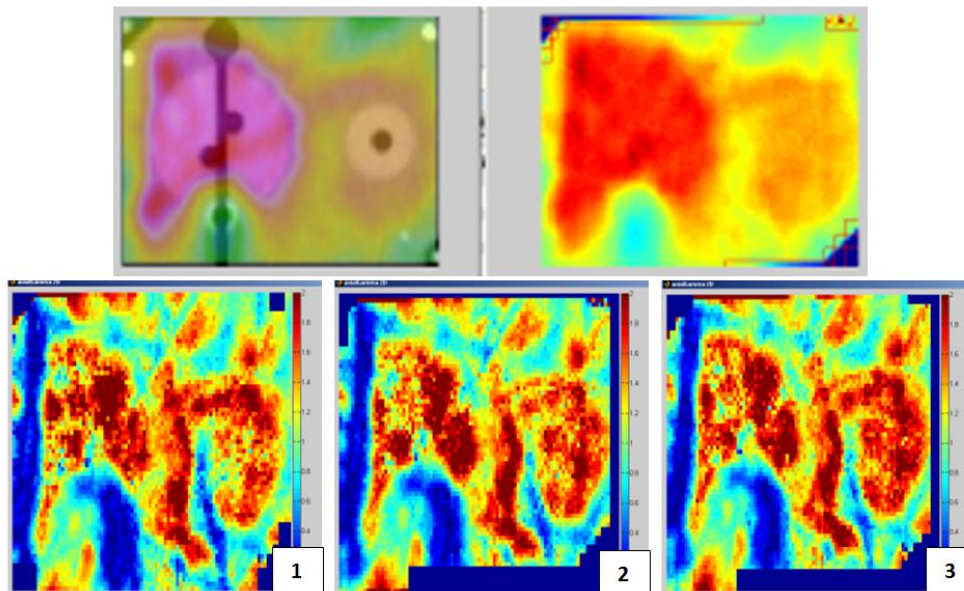


Figure 43: Axial film dose distributions from the TPS (upper left), film from one irradiation (upper right), and the gamma maps (5%/3mm) from this film for the three irradiations of the phantom with the complex treatment plan (bottom).

Complex Phantom Treatment Plan: Baseline Sagittal Film, 5%/3mm

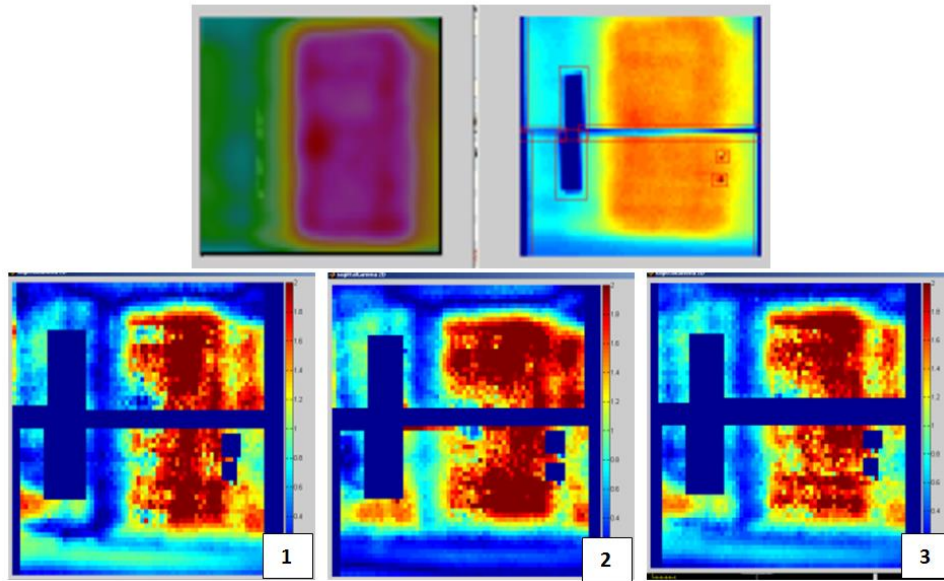


Figure 44: Sagittal film dose distributions from the TPS (upper left), film from one irradiation (upper right), and the gamma maps (5%/3mm) from this film for the three irradiations of the phantom with the complex treatment plan (bottom).

As with the first irradiation set, the baselines for this set of irradiations were not perfect. The average TLD in the PTVs and the DTA results would have passed the IROC-H criteria of 7% and 4 mm, respectively, however they were very close. The measured doses were again overall low, however this could not be explained by the output which was measured to be about 1% high (1.013 cGy/MU). The standard deviation of the TLD doses and gamma analysis percent of pixels passing were generally low, indicating that the irradiations were mostly consistent across the three irradiations. The gamma maps demonstrated where the failures occur and are shown with a 5%/3mm criterion to increase the visibility of the failure areas. The complex plan films failed in similar areas across the three irradiations, largely in the targets. This could have potentially been a result of a less homogenous dose in the targets due to the increased complexity. The simple plan films have larger differences in the gamma maps across the three irradiations. This could indicate that external factors such as small set up errors were responsible for these differences and the overall difference from the planned dose. It was also important to note that imperfect alignment of the two halves of the sagittal film was likely to play a role in decreased percent of pixels passing gamma analysis. Once again, the overall objective of this study was to compare the failure mode irradiations to the baseline irradiations. Although the baseline irradiations appear to have been imperfect

since they do not match the planned dose exactly, the set-up, measurement, and evaluation processes for this set of irradiations was controlled and consistent, enabling us to make meaningful comparisons.

Irradiation Set #3

The absolute dose results of the baseline irradiations for the third and final irradiation set are shown in Table 30. The planned dose reported was the mean dose to a contour of the TLD. The DTA between the primary PTV and spinal cord OAR on the axial film was 1.2 mm. The percent of pixels passing gamma analyses on the axial and sagittal films are shown in Table 31. The corresponding gamma maps for this baseline irradiation set are shown in Figure 45 and Figure 46.

Structure	TLD position	Measured Dose (cGy)	Std Dev.	Planned Dose (cGy)	% Difference
Primary PTV	Superior Anterior	673.7	0.60%	688.0	-2.1%
Primary PTV	Inferior Anterior	673.8	0.43%	687.0	-1.9%
Primary PTV	Superior Posterior	655.0	1.18%	659.3	-0.6%
Primary PTV	Inferior Posterior	664.2	0.82%	666.2	-0.3%
Secondary PTV	Superior	537.6	0.70%	556.2	-3.4%
Secondary PTV	Inferior	540.7	0.27%	558.9	-3.3%
Spinal Cord	Superior	347.7	0.22%	358.0	-2.9%
Spinal Cord	Inferior	349.4	0.35%	360.9	-3.2%

Table 30: Baseline TLD results from the third irradiation set, with the measured dose reported as the average of three measurements.

Film	Criterion	Pixels Passing	Film
Axial	7%/4mm	99.1%	0.34%
	5%/3mm	92.3%	1.86%
Sagittal	7%/4mm	99.2%	0.30%
	5%/3mm	94.3%	0.12%

Table 31: Baseline gamma analysis results for axial and sagittal films within the phantom for the third irradiation set.

Standard Phantom Treatment Plan: Baseline Axial Film, 5%/3mm

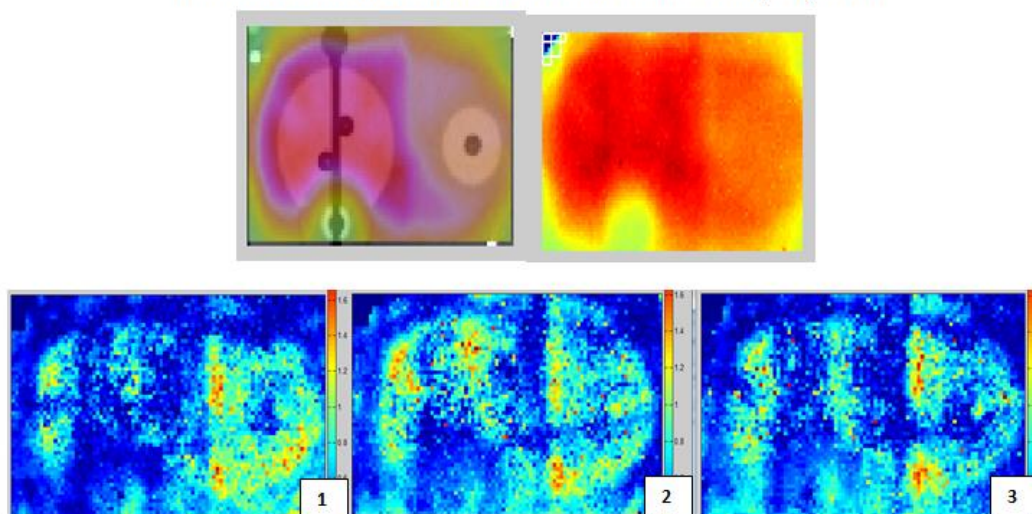


Figure 45: Axial film dose distributions from the TPS (upper left), film from one irradiation (upper right), and the gamma maps (5%/3mm) from this film for the three irradiations of the phantom with the baseline standard treatment plan for irradiation set #3 (bottom).

Standard Phantom Treatment Plan: Baseline Axial Film, 5%/3mm

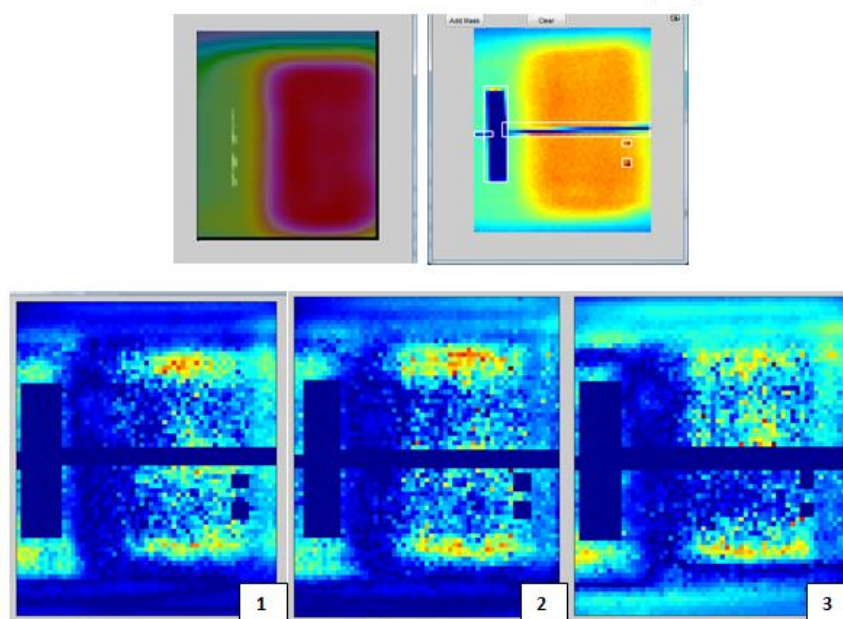


Figure 46: Sagittal film dose distributions from the TPS (upper left), film from one irradiation (upper right), and the gamma maps (5%/3mm) from this film for the three irradiations of the phantom with the baseline standard treatment plan for irradiation set #3 (bottom).

The agreement of this set of baseline irradiations with the planned dose was much better than the first two, with deviations between the average measured TLD dose and the planned TLD dose of up to 3.4% in the secondary PTV and 2.1% in the primary PTV. The gamma analysis results were also much

better with almost perfect agreement using 7%/4mm criterion and greater than 90% agreement using 5%/3mm criterion. The axial gamma maps showed that the small amount of failure was primarily in the PTVs and along the posterior edge of the film. On the sagittal film gamma maps, the small amount of failure was along the superior and inferior edges of the PTV, which was a region of relatively high dose gradient where the PTV dose dropped off and was collimated by the jaw. This baseline irradiation set may have been better than the other sets from increased experience with the process. The set up uncertainty may also have been decreased since the cross-hairs were used for each alignment instead of the lasers.

Failure mode evaluation

The severity scores for phantom treatment plans were evaluated at $D_{95\%}$ and $D_{99\%}$ for the PTVs and the maximum dose for the spinal cord OAR and normal tissue. The scoring scale determined was applied to the difference from baseline in the values and the scores were color coded as shown in Table 32. This color-coding system was applied for all severity scores for the remainder of this project.

Severity Score (S)	Quantitative Definition
1	0% - 2.9%
2	3% - 3.9%
3	4% - 4.9%
4	5% - 6.9%
5	7% - 8.9%
6	9% - 9.9%
7	10% - 14.9%
8	15% - 19.9%
9	20%-49.9%
10	$\geq 50\%$

Table 32: Color-coding used for severity scoring, corresponding to the scoring scale presented in Section.

Failure mode 1: Beam Energy

Treatment planning study results

The resultant changes in the phantom structure doses used for severity scoring for energy changes of +10% and -10% are summarized in Table 33 and Table 34 for both standard and phantom plans,

respectively. All structure dosimetry evaluation criteria had less than a 3% change from baseline with the exception of the dose to 99% of the primary PTV in the standard phantom treatment plan, which was under-dosed by 4% when the energy was decreased by 10%. As a result of this 4% under-dosing, this failure mode was assigned a severity score of 3 which is indicated in Table 33 and Table 34 by the color-coding described in Table 32.

Standard Phantom Treatment Plan			
Structure	Evaluation criteria	Energy +10%	Energy -10%
		Change from baseline	
Primary PTV	D _{95%}	0.13%	-1.49%
	D _{99%}	0.03%	-4.02%
Secondary PTV	D _{95%}	-0.02%	0.18%
	D _{99%}	-0.33%	0.16%
Spinal Cord	Max Dose	-1.29%	-2.71%
Normal Tissue	Max Dose	0.02%	0.71%

Table 33: Dosimetric changes from baseline used for severity scoring for beam energy changes of +10% and -10% for the standard phantom treatment plan.

Complex Phantom Treatment Plan			
Structure	Evaluation criteria	Energy +10%	Energy -10%
		Change from baseline	
Primary PTV	D _{95%}	0.24%	-0.14%
	D _{99%}	-0.01%	-0.80%
Secondary PTV	D _{95%}	0.66%	0.42%
	D _{99%}	0.22%	0.60%
Spinal Cord	Max Dose	-2.07%	-1.06%
Normal Tissue	Max Dose	0.22%	1.92%

Table 34: Dosimetric changes from baseline used for severity scoring for beam energy changes of +10% and -10% for the complex phantom treatment plan.

The DVHs for this failure mode are shown in Figure 47 and Figure 48. The loss of coverage in the primary PTV in the standard plan was evident, as was the slight decrease in spinal cord dose in the complex plan. Other differences in the DVHs from baseline were very small.

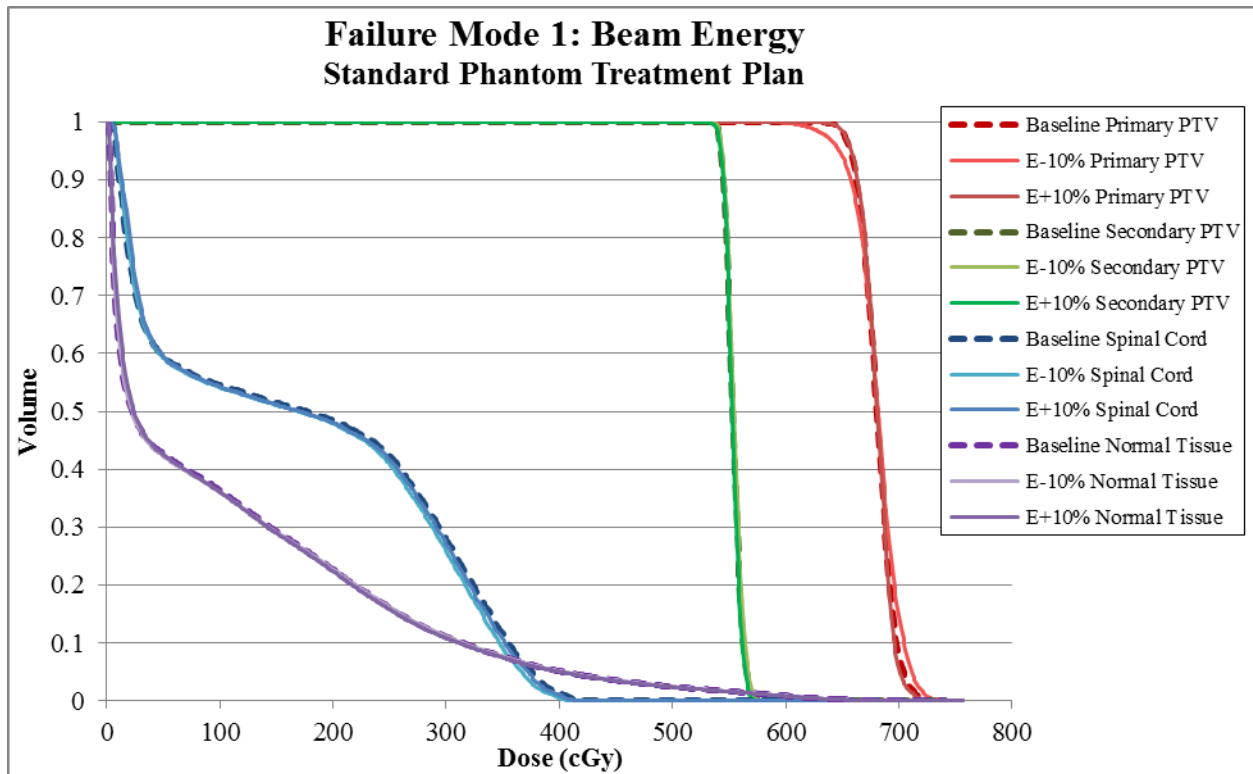


Figure 47: DVHs for phantom structures in the standard treatment plan with energy changes of 10%, with dashed lines showing baseline DVHs.

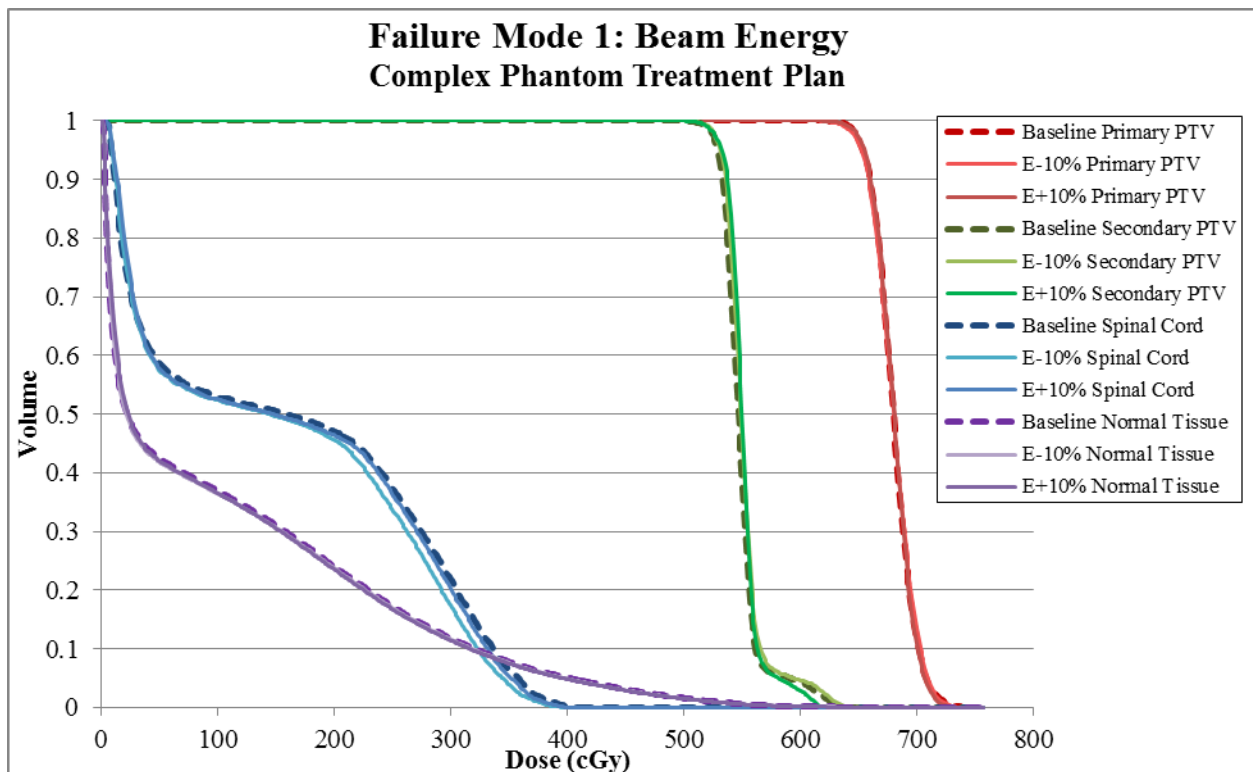


Figure 48: DVHs for phantom structures in the complex treatment plan with energy changes of 10%, with dashed lines showing baseline DVHs.

The differences in the energy altered dose distributions from baseline were mostly a result of the differences in the shape of the dose profiles off-axis. Since the isocenter is approximately in the center of the phantom insert (see Figure in methods), the far edge of the primary PTV was about 4 cm off axis where small changes in the profiles were evident. This compounded with the small change in depth dose and resulted in a slightly more heterogeneous dose distribution in the standard phantom plan and therefore a reduction in coverage.

Physical measurement results

Beam energy adjustment and measurements: Irradiation set #1

The differences in the doses measured to the phantom TLD for the irradiation with a beam energy adjustment of +1.6% TMR_{10}^{20} from the baseline irradiation for the first irradiation set are shown in Table 35 where a positive difference indicates that the failure mode dose was higher than the baseline dose. On average, the dose to the primary PTV was 5.5% higher than baseline and the secondary PTV dose was 5.8% higher than baseline. The dose to the spinal cord TLD was also higher than the baseline by an average of 6.9%. The DTA between the primary PTV and OAR on the axial field was 0.7 mm lower for the beam energy adjusted irradiation than the baseline irradiation. The absolute differences in the percent of pixels passing gamma analysis with 7%/4mm and 5%/3mm criteria are shown in Table 36, where a positive value indicates that the failure mode percent of pixels passing was higher than that for the baseline. The energy adjusted irradiation had almost 20% more pixels passing the 7%/4mm axial film gamma analysis and 16% more passing on the sagittal film.

Structure	TLD position	Difference in Dose from Baseline
Primary PTV	Superior Anterior	7.3%
Primary PTV	Inferior Anterior	5.1%
Primary PTV	Superior Posterior	4.7%
Primary PTV	Inferior Posterior	4.8%
Secondary PTV	Superior	6.3%
Secondary PTV	Inferior	5.2%
Spinal Cord	Superior	8.2%
Spinal Cord	Inferior	5.6%

Table 35: TLD differences from baseline from the first irradiation set with an energy adjustment of +1.6% TMR_{10}^{20} .

Film	Criterion	Absolute Difference in Pixels Passing from Baseline
Axial	7%/4mm	19.6%
	5%/3mm	25.3%
Sagittal	7%/4mm	16.1%
	5%/3mm	34.6%

Table 36: Differences from baseline in gamma analysis results for axial and sagittal films within the phantom for the first irradiation set with an energy adjustment of +1.6% TMR²⁰₁₀.

Beam energy adjustment and measurements: Irradiation set #2

The differences in the doses measured to the phantom TLD for the irradiations with a beam energy adjustments of +1.1% and -0.8% TMR¹⁴₅ from the baseline irradiation for the first irradiation set are shown in Table 37 and Table 39 where a positive difference indicates that the failure mode dose was higher than the baseline dose. For both the increase and decrease in energy in the standard plan, the average dose to the primary PTV TLD increased by around 1.5%. The dose to the secondary PTV also increased for both energy changes in the standard plan, on average 1% for the increased energy and 1.6% for the decreased energy. Finally, the spinal cord dose in the standard plan increased on average just over 5% for the increased energy irradiation, and was on average 0.6% high for the decreased energy irradiation. For the complex plan, we again saw increases in the primary PTV TLD doses, on average 2.4% for the increased energy irradiation and 1.7% for the decreased energy irradiation. The secondary PTV and spinal cord had increases in the average TLD dose for the increased energy irradiation of 1.4% and 3.9%, respectively. These two structures both had decreases in the average TL D dose for the decreased energy irradiation or -0.7% and -1.8%, respectively. The average DTA between the primary PTV and OAR on the axial field for the standard plan for the increased energy irradiation was 0.7 mm smaller than the baseline irradiation and 0.2 mm larger for the decreased energy irradiation. For the complex plan, the DTA for the increased energy irradiation was 0.1 mm larger for the increased energy irradiation with than the baseline irradiation and the average DTA for the decreased energy irradiation was 0.6 mm larger. The differences in the percent of pixels passing gamma analysis with 7%/4mm and 5%/3mm criteria are shown in Table 38 and Table 40, where a positive value indicates that the failure mode percent of pixels passing was higher than that for the baseline. The corresponding gamma maps for the increased and decreased energy changes with 5%/3mm criteria are shown in Figure 49 - Figure 52 for

the standard plan Figure 53 - Figure 56 for the complex plan. Smaller differences from baseline were seen in the percent of pixels passing the 7%/4mm gamma with the decreased energy irradiations on both the standard and complex plans, than the increased energy irradiations. For the increased energy irradiations, a 15.6% change from baseline on the axial film and 9.5% on the sagittal was seen for the standard plan and 19.5% change on the axial and 15.4% on the sagittal for the complex plan. In the axial film gamma maps for the standard plan, the failures followed a similar pattern to baseline but were obviously less prevalent. Similarly for the standard plan sagittal film gamma maps, the distribution of failures was not greatly different than the baseline with failure pretty evenly spread throughout the PTV. For the high energy complex plan films, there appear to be two foci of failure on the axial film: in the posterior left corner of the primary PTV and in the anterior right corner of the film. On the sagittal film, the failure is concentrated in the PTV again, with a denser failure region in the superior half. For the decreased energy, the 7%/4mm percent of pixels passing the standard plan was 5.4% higher than baseline on the axial film and 4.6% higher on the sagittal. The complex plan had 9.2% more pixels passing the 7%/4mm criteria on the axial film with the increased energy irradiation and 5.9% more on the sagittal film. On the standard plan axial gamma maps, the failures seems to be concentrated more in the secondary PTV and are slightly heavier on the anterior side of the film than on the baseline axial films, but the overall failure is decreased. Sagittal gamma map failures for the standard plan are concentrated mostly on the superior and inferior edges of the PTV, which is different than in the baseline plan. Failures on the low energy complex plan films are concentrated in the PTVs, particularly in the superior half of the sagittal film.

As we saw in the treatment planning studies, the changes in energy can result in a more heterogeneous dose distribution within the PTVs. TLD within the PTVs did not capture the volumetric effects that we saw in the treatment planning studies, such as the reduction in primary PTV coverage of 4%. However, the increases in dose to the TLD may have been coming from hot spots in the PTVs that were a result of the increased heterogeneity. It was also likely that the TLD did not capture the under-dosing due to their central location within the PTV since the change in the dose from baseline should

increase with increasing off-axis distance. The dose to the spinal cord TLD in the complex plan for the low energy irradiation decreased, which was in line with the low energy treatment planning studies. This was not the case for the standard treatment plan, which similar to the complex treatment plan, had a decrease in the maximum dose to the spinal cord in our treatment planning studies but the dose to the TLDs did not correspondingly decrease. This was likely due to the fact that while the maximum dose to the spinal cord increased in the standard plan, the dose to the volume as a whole was mostly unchanged as you can see in the DVHs. But the spinal cord DVHs for the complex plan reflect a decrease in the dose to the spinal cord volume overall. While these decreases in the spinal cord dose did not affect our severity scoring since we were solely concerned with increased OAR doses and decreased PTV doses, the treatment planning studies and measurements appear to have had consistent results within the spinal cord structure.

The distribution of failures on the gamma maps, especially on the decreased energy films, were different than those of the baseline plans, which also supports the notion that these dose distributions had increased heterogeneity. The foci of failure on increased energy axial film gamma maps may be a result of the rounder shoulder of the high energy profiles. Ideally, we could directly compare the TLD measurement results to the doses with the TLD structures on our treatment planning studies. But since our energy altered beam models were not based off of data from the same energy altered beams that the measurements were made with, we cannot assume that the dose distributions would be the same.

Standard Phantom Treatment Plan Irradiation – TLD Results			
Structure	TLD position	+1.1% TMR ¹⁴ ₅	-0.8% TMR ¹⁴ ₅
		Difference in Dose from Baseline	
Primary PTV	Superior Anterior	1.5%	1.9%
Primary PTV	Inferior Anterior	2.2%	1.8%
Primary PTV	Superior Posterior	1.2%	1.6%
Primary PTV	Inferior Posterior	1.0%	1.6%
Secondary PTV	Superior	1.0%	1.0%
Secondary PTV	Inferior	1.0%	2.2%
Spinal Cord	Superior	4.5%	0.8%
Spinal Cord	Inferior	5.6%	0.4%

Table 37: Average TLD differences from baseline from the second irradiation set with energy adjustments of +1.1% and -0.8% TMR¹⁴₅ for the standard plan.

Standard Phantom Treatment Plan Irradiation – Gamma Analysis Results			
Film	Criterion	+1.1% TMR ¹⁴ ₅	-0.8% TMR ¹⁴ ₅
		Absolute Difference in Average Pixels Passing from Baseline	
Axial	7%/4mm	15.6%	5.4%
	5%/3mm	0.9%	-21.3%
Sagittal	7%/4mm	9.5%	4.6%
	5%/3mm	-7.9%	-11.8%

Table 38: Average differences from baseline in gamma analysis results for axial and sagittal films within the phantom for the second irradiation set with an energy adjustment of +1.1% and -0.8% TMR¹⁴₅ for the standard plan.

Complex Phantom Treatment Plan Irradiation – TLD Results			
Structure	TLD position	+1.1% TMR ¹⁴ ₅	-0.8% TMR ¹⁴ ₅
		Difference in Dose from Baseline	
Primary PTV	Superior Anterior	3.6%	1.7%
Primary PTV	Inferior Anterior	3.3%	2.2%
Primary PTV	Superior Posterior	1.3%	2.2%
Primary PTV	Inferior Posterior	1.2%	0.8%
Secondary PTV	Superior	0.9%	-1.4%
Secondary PTV	Inferior	1.8%	0.1%
Spinal Cord	Superior	3.9%	-1.4%
Spinal Cord	Inferior	3.8%	-2.1%

Table 39: Average TLD differences from baseline from the second irradiation set with energy adjustments of +1.1% and -0.8% TMR¹⁴₅ for the complex plan.

Complex Phantom Treatment Plan Irradiation – Gamma Analysis Results			
Film	Criterion	+1.1% TMR ¹⁴ ₅	-0.8% TMR ¹⁴ ₅
		Absolute Difference in Pixels Passing from Baseline	
Axial	7%/4mm	19.5%	9.2%
	5%/3mm	-8.8%	-18.7%
Sagittal	7%/4mm	15.4%	5.9%
	5%/3mm	-3.8%	-11.9%

Table 40: Average differences from baseline in gamma analysis results for axial and sagittal films within the phantom for the second irradiation set with an energy adjustment of +1.1% and -0.8% TMR¹⁴₅ for the complex plan.

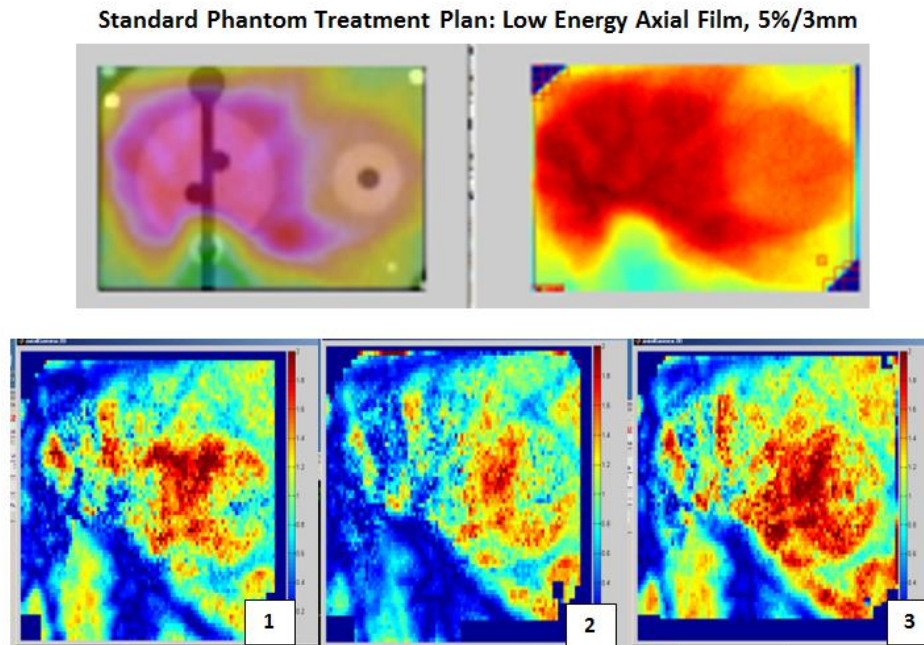


Figure 49: Axial film dose distributions from the TPS (upper left), film from one irradiation (upper right), and the gamma maps (5%/3mm) from this film for the three irradiations of the phantom with the standard treatment plan with decreased energy (-0.8% TMR¹⁴₅) (bottom).

Standard Phantom Treatment Plan: Low Energy Sagittal Film, 5%/3mm

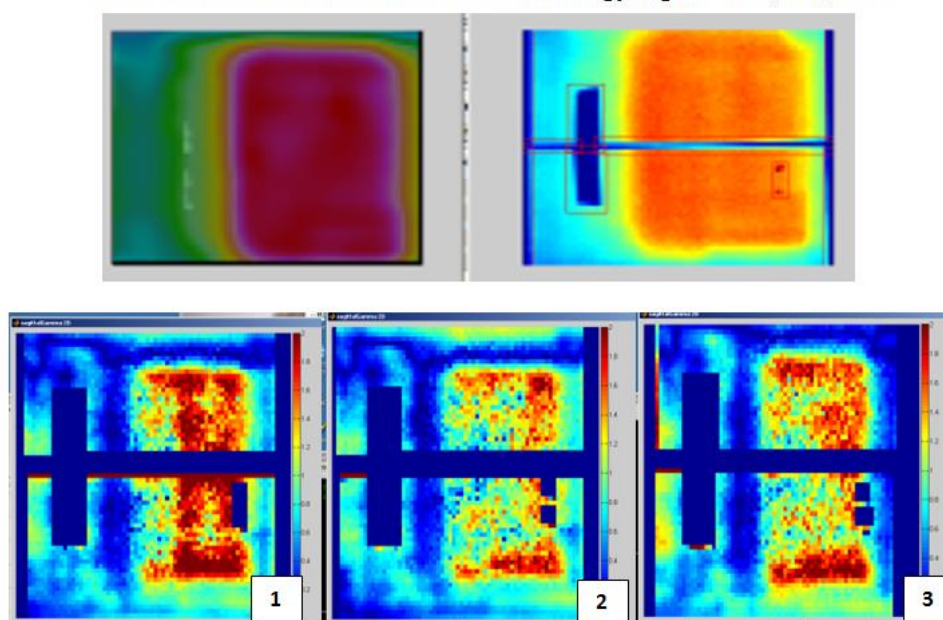


Figure 50: Sagittal film dose distributions from the TPS (upper left), film from one irradiation (upper right), and the gamma maps (5%/3mm) from this film for the three irradiations of the phantom with the standard treatment plan with decreased energy (-0.8% TMR^{14}_5) (bottom).

Standard Phantom Treatment Plan: High Energy Axial Film, 5%/3mm

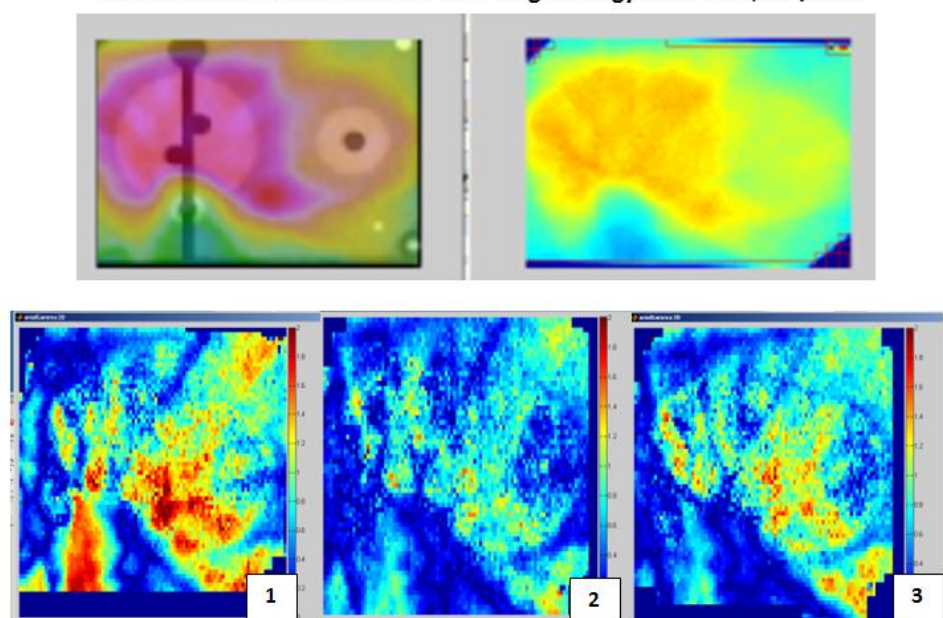


Figure 51: Axial film dose distributions from the TPS (upper left), film from one irradiation (upper right), and the gamma maps (5%/3mm) from this film for the three irradiations of the phantom with the standard treatment plan with increased energy ($+1.1\%$ TMR^{14}_5) (bottom).

Standard Phantom Treatment Plan: High Energy Sagittal Film, 5%/3mm

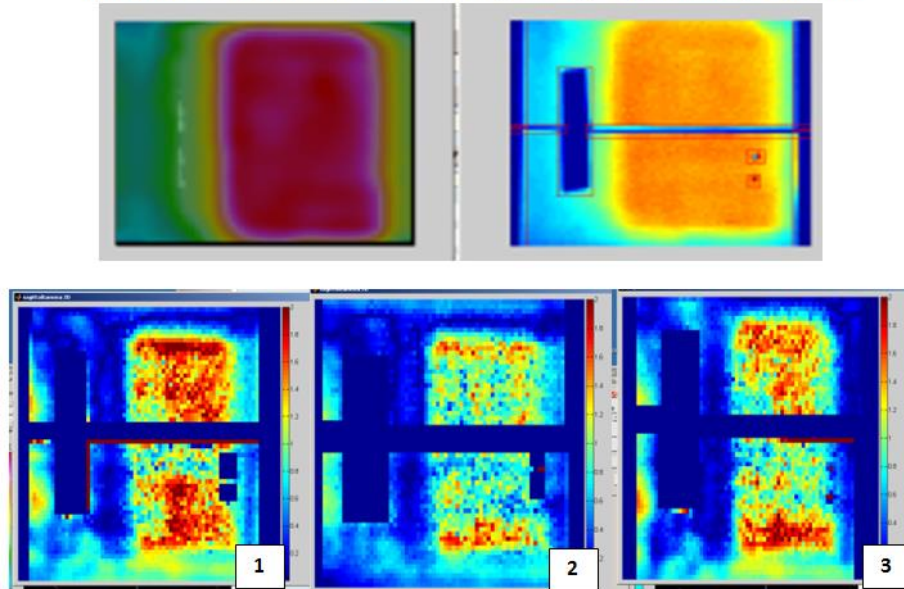


Figure 52: Sagittal film dose distributions from the TPS (upper left), film from one irradiation (upper right), and the gamma maps (5%/3mm) from this film for the three irradiations of the phantom with the standard treatment plan with increased energy (+1.1% TMR^{14s}) (bottom).

Complex Phantom Treatment Plan: Low Energy Axial Film, 5%/3mm

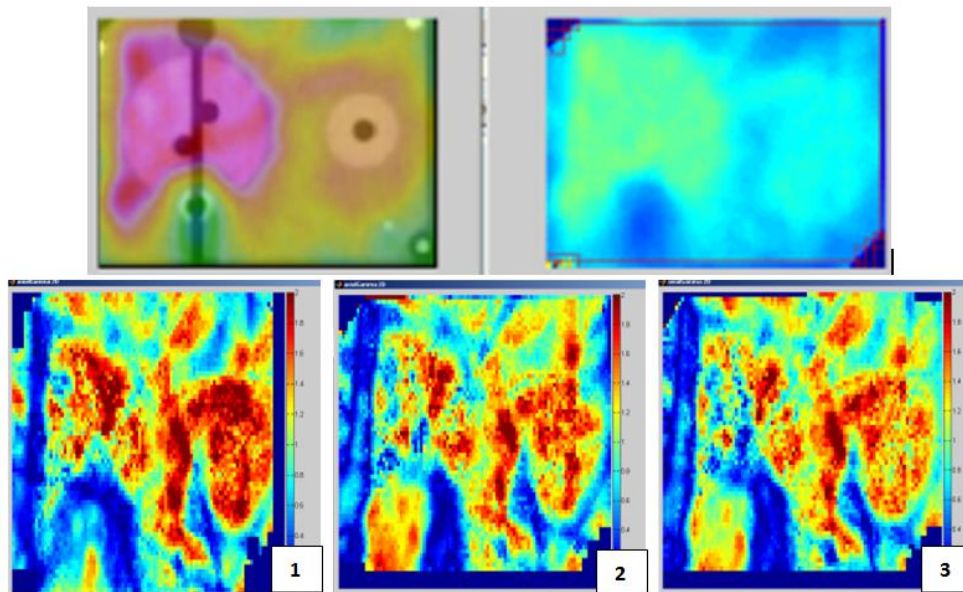


Figure 53: Axial film dose distributions from the TPS (upper left), film from one irradiation (upper right), and the gamma maps (5%/3mm) from this film for the three irradiations of the phantom with the complex treatment plan with decreased energy (-0.8% TMR^{14s}) (bottom).

Complex Phantom Treatment Plan: Low Energy Sagittal Film, 5%/3mm

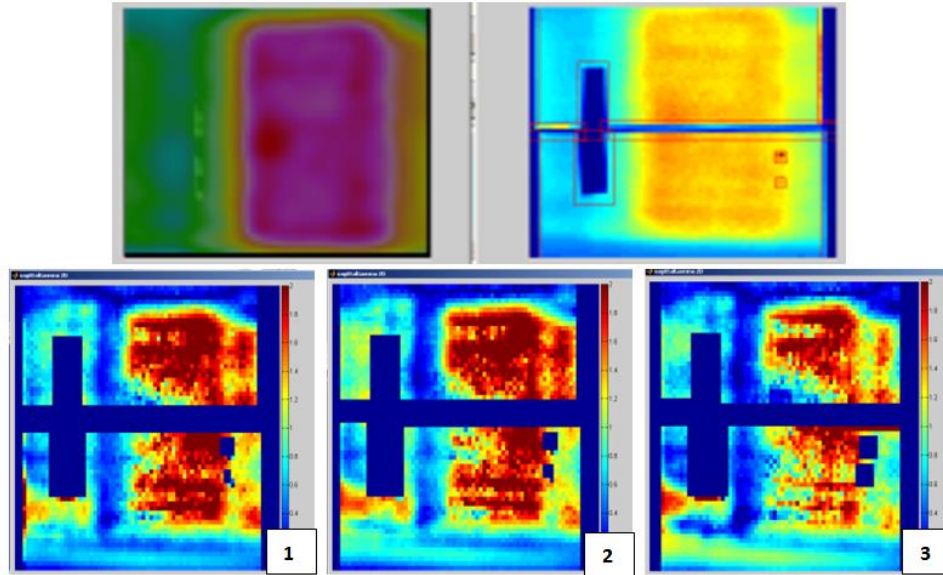


Figure 54: Sagittal film dose distributions from the TPS (upper left), film from one irradiation (upper right), and the gamma maps (5%/3mm) from this film for the three irradiations of the phantom with the complex treatment plan with decreased energy (-0.8% TMR¹⁴_s).

Complex Phantom Treatment Plan: High Energy Axial Film, 5%/3mm

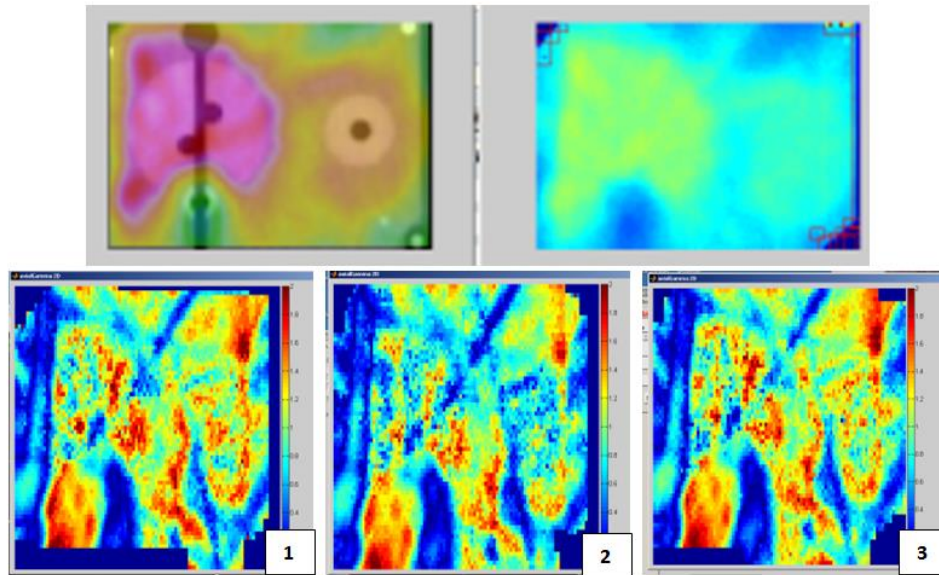


Figure 55: Axial film dose distributions from the TPS (upper left), film from one irradiation (upper right), and the gamma maps (5%/3mm) from this film for the three irradiations of the phantom with the complex treatment plan with increased energy (+1.1% TMR¹⁴_s) (bottom).

Complex Phantom Treatment Plan: High Energy Sagittal Film, 5%/3mm

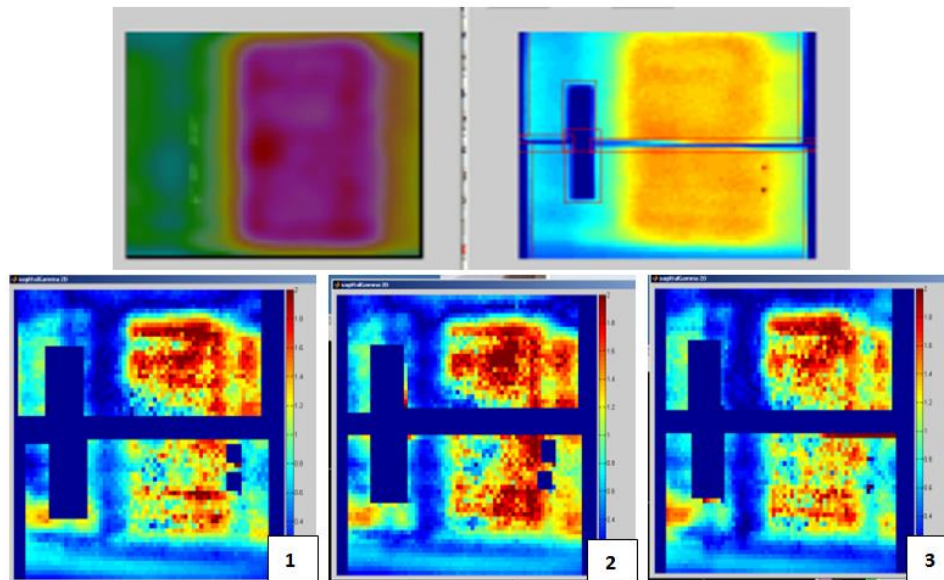


Figure 56: Sagittal film dose distributions from the TPS (upper left), film from one irradiation (upper right), and the gamma maps (5%/3mm) from this film for the three irradiations of the phantom with the complex treatment plan with increased energy (+1.1% TMR₁₄₅) (bottom).

Beam energy phantom studies summary

Changes in the beam energy in our treatment planning studies resulted in primarily small changes in the doses to the phantom structures, with some under-dosing of the primary PTV in the standard plan (up to 4%) and a decrease in the dose to the spinal cord. In our measurements, the doses measured by the TLD mostly increased from baseline. We did not measure an under-dosing in either PTV with the TLD as we saw in the treatment planning studies, however we suspect this was due to the TLD location and the increased heterogeneity within the PTVs. The dose to the spinal cord TLD decreased in the low energy irradiation to the complex plan, which was similar to what we saw in the treatment planning studies. Otherwise, increases in the dose to the spinal cord up to 8% were observed in our measurements, which was not consistent with the treatment planning studies. There was a larger uncertainty in the spinal cord TLD measurements, however. The severity score of 3, resultant of the treatment planning studies, overall was reasonable.

Failure mode 2: Beam symmetry

Treatment planning study results

The resultant changes in the phantom structure doses used for severity scoring for beam symmetry changes of approximately 2%, 3.5%, and 10% are summarized for standard phantom plans in Table 41 - Table 43 and complex phantom plans in Table 44 - Table 46. All structure evaluation criteria had below a 2% change from baseline (in the direction used for scoring, decrease in PTV or increase in OAR) for all three symmetry errors. These values ranged from 0% to -0.19% in the PTVs of the standard plan with 2% symmetry errors and 0.29% to 0.36% in the maximum dose to the normal tissue. All spinal cord doses decreased this is plan at 2% symmetry, up to -1.15%. The standard plan PTV dose differences from baseline ranged from -0.1% to -0.76% and 0.26% to 0.49% in the normal tissue maximum dose. Again, the spinal cord maximum doses only decreased, up to -0.95%. In the standard plan with 10% symmetry errors, PTV under-dosing ranged from -0.02 % to -1.18% and the normal tissue maximum dose increased up to 1.43% while the spinal cord maximum dose increased only with the bottom to top symmetry error, changing 0.54% from baseline. For the complex plan, PTV dose difference from baseline ranged from 0.06% to -0.63% with 2% symmetry errors and were at maximum 0.07% in the normal tissue. All spinal cord doses decreased this is plan at 2% symmetry, up to -1.63%. The complex plan PTV dose differences from baseline ranged from -0.04% to -0.81% and 0.22% in the normal tissue maximum dose. Again, the spinal cord maximum doses only decreased, up to -1.60% difference from baseline. In the complex plan with 10% symmetry errors, PTV under-dosing ranged from -0.01% to -1.62% and the normal tissue maximum dose increased up to 1.34% while the spinal cord maximum dose increased only with the top to bottom symmetry error, changing 0.03% from baseline. Otherwise, the spinal cord maximum dose decreased up to -3.0%. Overall, these small errors resulted in a severity score of 1 for this failure mode.

Standard Phantom Treatment Plan					
Structure	Evaluation criteria	2% Symmetry			
		Top to bottom	Bottom to top	Left to right	Right to left
		Change from baseline			
Primary PTV	D _{95%}	-0.09%	-0.06%	0.06%	0.01%
	D _{99%}	0.00%	-0.01%	0.15%	0.02%
Secondary PTV	D _{95%}	-0.30%	-0.43%	-0.29%	-0.07%
	D _{99%}	-0.38%	-0.49%	-0.39%	-0.16%
Spinal Cord	Max Dose	-1.15%	-0.55%	-0.81%	-0.98%
Normal Tissue	Max Dose	0.29%	0.36%	0.27%	0.24%

Table 41: Dosimetric changes from baseline used for severity scoring for beam symmetry changes of 2% for the standard phantom treatment plan.

Standard Phantom Treatment Plan					
Structure	Evaluation criteria	3.5% Symmetry			
		Top to bottom	Bottom to top	Left to right	Right to left
		Change from baseline			
Primary PTV	D _{95%}	0.09%	-0.15%	0.02%	-0.02%
	D _{99%}	0.15%	-0.18%	0.01%	-0.02%
Secondary PTV	D _{95%}	-0.01%	-0.58%	-0.29%	-0.17%
	D _{99%}	0.01%	-0.76%	-0.38%	-0.17%
Spinal Cord	Max Dose	-0.95%	-0.19%	-0.55%	-0.62%
Normal Tissue	Max Dose	0.43%	0.26%	0.29%	0.29%

Table 42: Dosimetric changes from baseline used for severity scoring for beam symmetry changes of 3.5% for the standard phantom treatment plan.

Standard Phantom Treatment Plan					
Structure	Evaluation criteria	10% Symmetry			
		Top to bottom	Bottom to top	Left to right	Right to left
		Change from baseline			
Primary PTV	D _{95%}	-0.17%	-0.38%	0.01%	-0.02%
	D _{99%}	-0.34%	-0.62%	0.16%	-0.03%
Secondary PTV	D _{95%}	-0.43%	-1.18%	-0.51%	-0.16%
	D _{99%}	-0.56%	-1.29%	-0.58%	-0.21%
Spinal Cord	Max Dose	-1.80%	0.54%	-0.93%	-1.17%
Normal Tissue	Max Dose	1.43%	0.34%	0.51%	0.43%

Table 43: Dosimetric changes from baseline used for severity scoring for beam symmetry changes of 10% for the standard phantom treatment plan.

Complex Phantom Treatment Plan					
Structure	Evaluation criteria	2% Symmetry			
		Top to bottom	Bottom to top	Left to right	Right to left
		Change from baseline			
Primary PTV	D _{95%}	-0.35%	-0.06%	-0.23%	-0.06%
	D _{99%}	-0.63%	-0.32%	-0.47%	-0.32%
Secondary PTV	D _{95%}	-0.07%	-0.34%	-0.17%	-0.34%
	D _{99%}	0.33%	-0.42%	0.03%	-0.42%
Spinal Cord	Max Dose	-0.76%	-1.63%	-1.31%	-1.63%
Normal Tissue	Max Dose	-0.43%	0.07%	-0.13%	0.07%

Table 44: Dosimetric changes from baseline used for severity scoring for beam symmetry changes of 2% for the complex phantom treatment plan.

Complex Phantom Treatment Plan					
Structure	Evaluation criteria	3.5% Symmetry			
		Top to bottom	Bottom to top	Left to right	Right to left
		Change from baseline			
Primary PTV	D _{95%}	-0.44%	-0.08%	-0.18%	-0.15%
	D _{99%}	-0.81%	-0.34%	-0.47%	-0.30%
Secondary PTV	D _{95%}	-0.04%	-0.38%	-0.24%	-0.22%
	D _{99%}	0.35%	-0.81%	-0.42%	-0.22%
Spinal Cord	Max Dose	-0.36%	-1.60%	-1.11%	-1.12%
Normal Tissue	Max Dose	-0.39%	0.22%	-0.20%	-0.43%

Table 45: Dosimetric changes from baseline used for severity scoring for beam symmetry changes of 3.5% for the complex phantom treatment plan.

Complex Phantom Treatment Plan					
Structure	Evaluation criteria	10% Symmetry			
		Top to bottom	Bottom to top	Left to right	Right to left
		Change from baseline			
Primary PTV	D _{95%}	-0.94%	0.01%	-0.31%	-0.28%
	D _{99%}	-1.28%	-0.01%	-0.61%	-0.67%
Secondary PTV	D _{95%}	-0.04%	-0.91%	-0.15%	-0.14%
	D _{99%}	0.40%	-1.62%	0.03%	0.41%
Spinal Cord	Max Dose	0.30%	-3.00%	-0.90%	-0.84%
Normal Tissue	Max Dose	0.48%	1.34%	0.07%	-0.45%

Table 46: Dosimetric changes from baseline used for severity scoring for beam symmetry changes of 10% for the complex phantom treatment plan.

The DVHs for this failure mode in the standard phantom treatment plan are shown in Figure 57- Figure 59. The DVHs for this failure mode in the complex phantom treatment plan are shown in Figure 60- Figure 62. It was observed that all changes from baseline were very small for both plans. The largest

differences appeared to be a decrease in the spinal cord dose for each case, though these changes were very small. This agreed with the severity scoring changes summarized above.

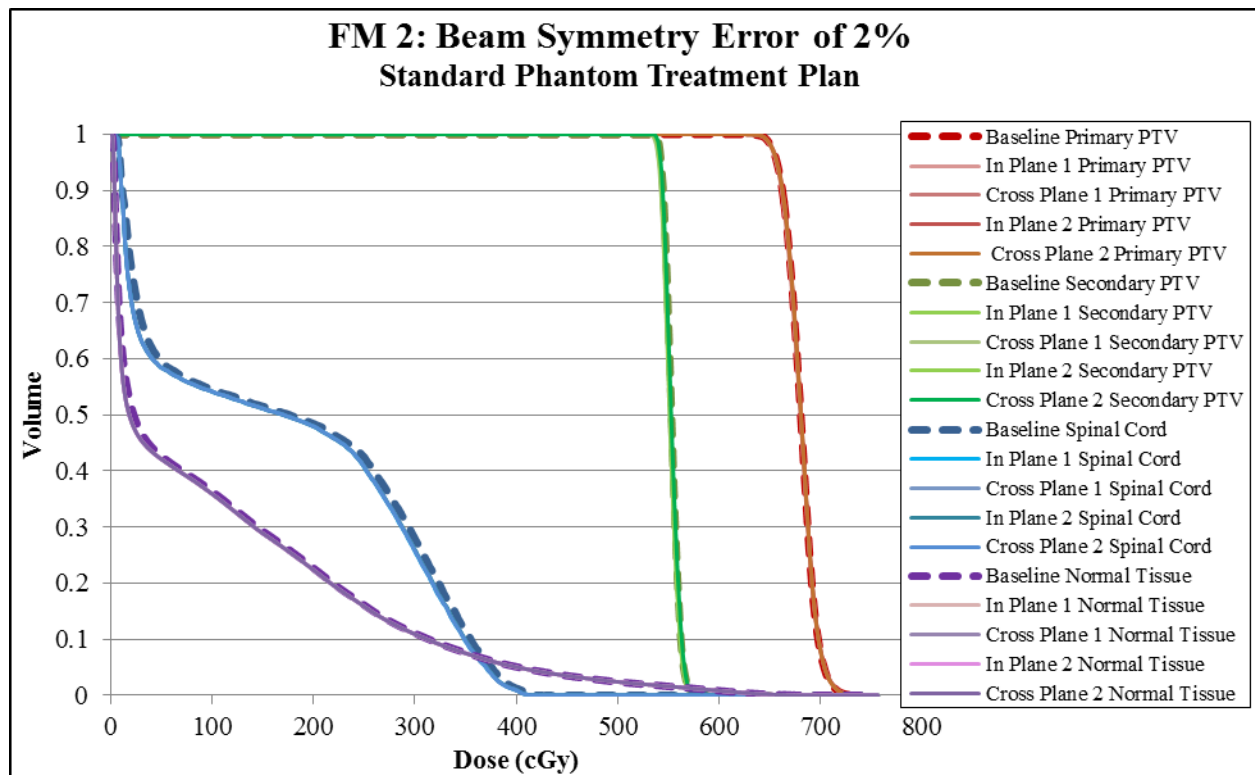


Figure 57: DVHs for phantom structures in the standard treatment plan with beam symmetry changes of 2%, with dashed lines showing baseline DVHs.

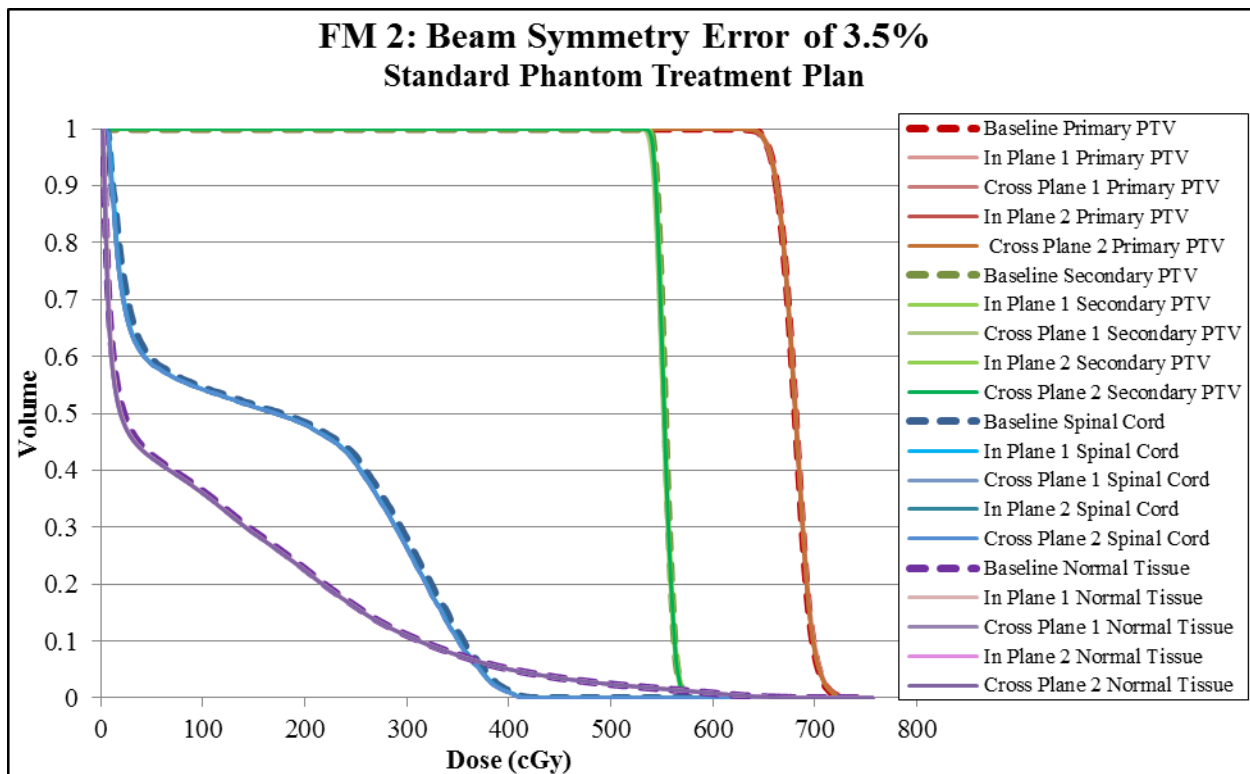


Figure 58: DVHs for phantom structures in the standard treatment plan with beam symmetry changes of 3.5%, with dashed lines showing baseline DVHs.

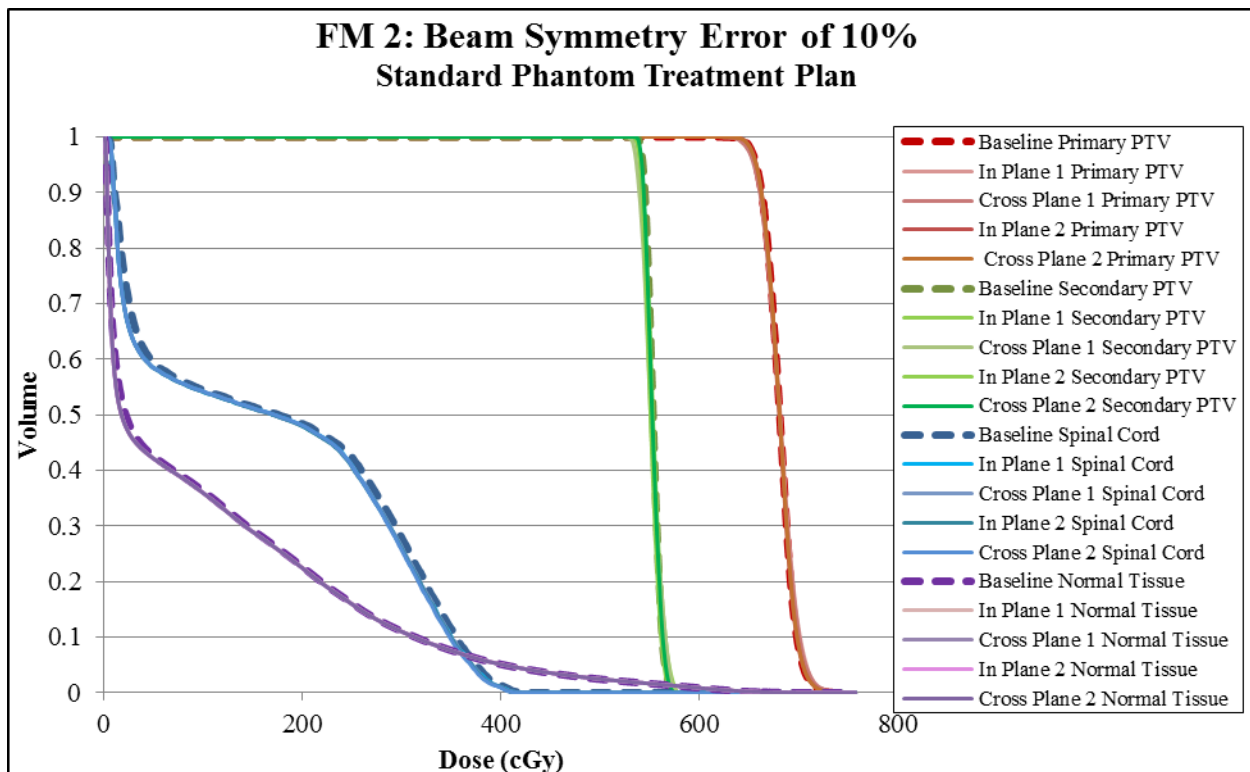


Figure 59: DVHs for phantom structures in the standard treatment plan with beam symmetry changes of 10%, with dashed lines showing baseline DVHs.

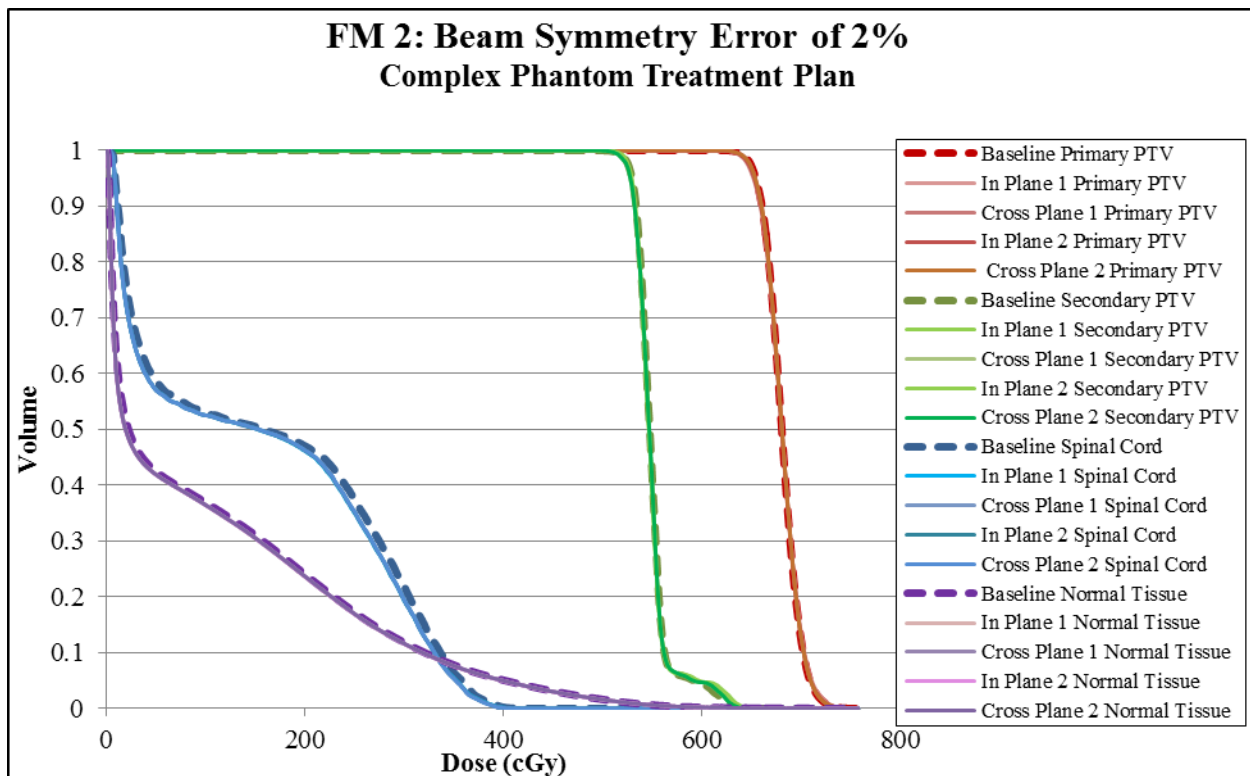


Figure 60: DVHs for phantom structures in the complex treatment plan with beam symmetry changes of 2%, with dashed lines showing baseline DVHs.

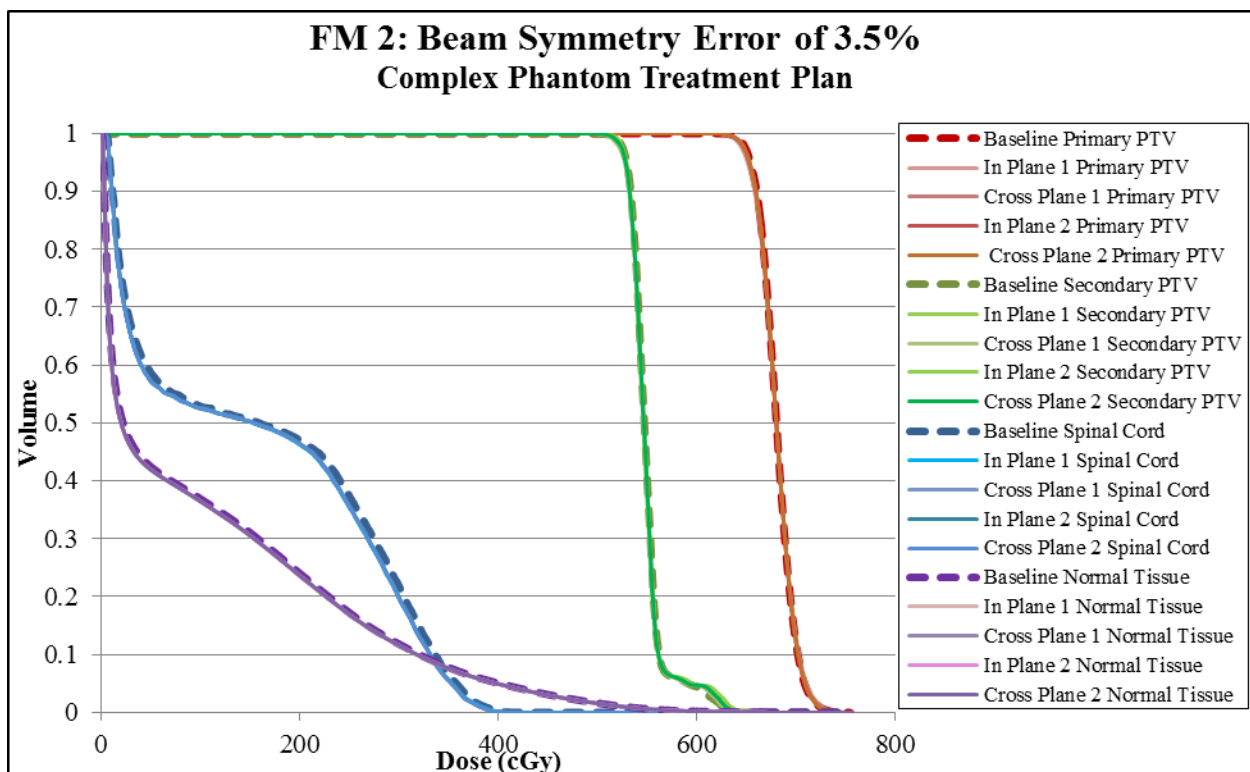


Figure 61: DVHs for phantom structures in the complex treatment plan with beam symmetry changes of 3.5%, with dashed lines showing baseline DVHs.

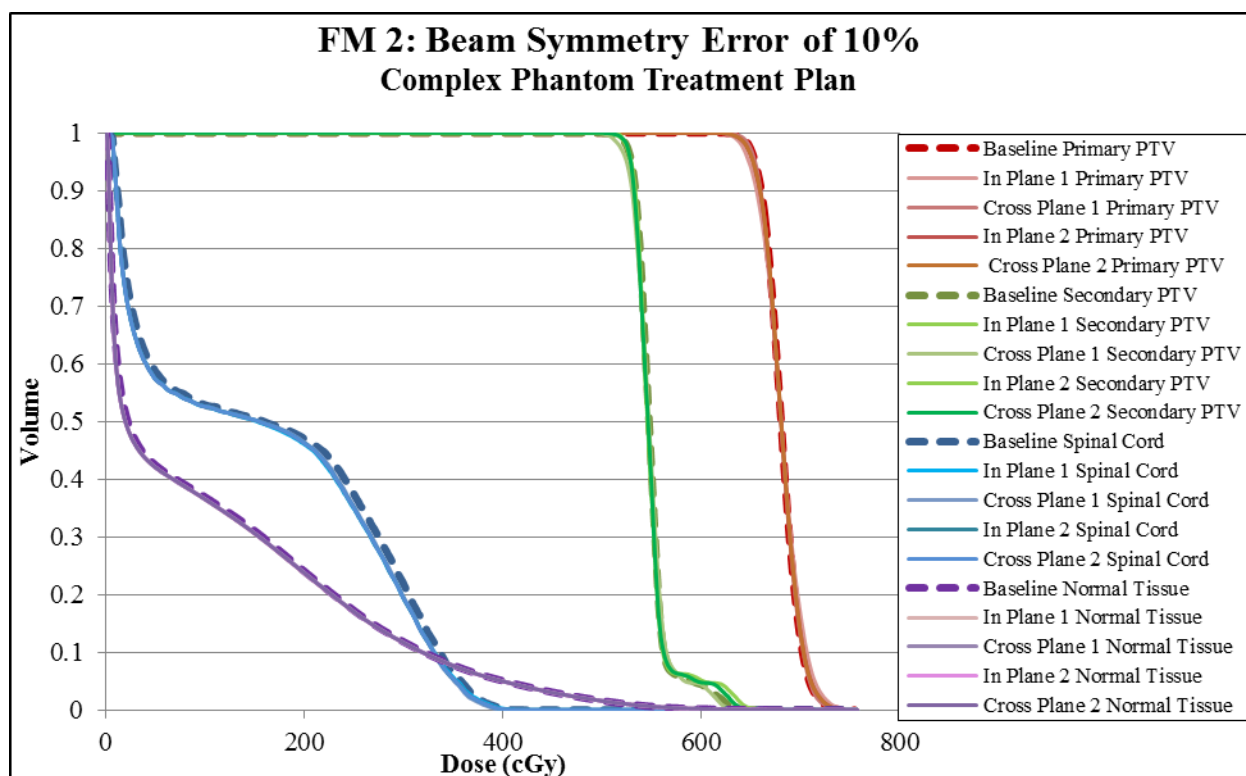


Figure 62: DVHs for phantom structures in the complex treatment plan with beam symmetry changes of 10%, with dashed lines showing baseline DVHs.

Considering the geometry of the phantom and delivery set up, we expected in plane symmetry (top to bottom or bottom to top) to affect all of the structures in the superior-inferior, increasing the dose to one side and decreasing the other. This effect would compound with beams coming from different gantry angles. These effects may not be evident in the mean doses, but would be volumetrically visible, changing the structure coverages. Cross plane symmetry (right to left or left to right) was expected to affect the outer edges of the structures most, but would likely be washed out with multiple beam angles. Overall, only very minimal changes were seen the doses to phantom structures with beam symmetry changes up to 10% in either direction, which was likely due to the central location of the structures within the phantom along with the central location of the isocenter. Additionally, the maximum jaw setting for these treatment plans was less than 10 x 10 cm², with the furthest jaw position off-axis being 5.4 cm in the X direction in the complex plan. Since symmetry errors were defined in a 20 x 20 cm² field, the symmetry errors in these smaller phantom fields were scaled down. The most prevalent changes were small decreases in the spinal cord doses, which likely were exaggerated because the cord structure extends

almost three times longer in the superior inferior direction than either of the PTVs. It also lies close to a steep dose gradient which increases the changes of small changes in the plan affecting the structure dose.

Physical measurement results

Beam symmetry adjustment and measurements: Irradiation set #1

The differences in the doses measured to the phantom TLD for the irradiation with beam symmetry adjustments of 5% in-plane and 3% cross-plane from the baseline irradiation for the first irradiation set are shown in Table 47, where a positive difference indicates that the failure mode dose was higher than the baseline dose. When the in plane symmetry was adjusted by 5%, TLD doses differed very little from the baseline irradiation on average. The primary PTV TLD dose differed from baseline on average by 0.4%, the secondary PTV TLD dose differed on average by 0.8%, and the spinal cord TLD on average by -0.5%. When the cross plane symmetry was adjusted by 3%, the anterior primary PTV TLD doses decreased on average by -1.5% and the posterior TLD doses increased on average by 3.2%. Overall, the primary PTV TLD average difference was 0.85%. Secondary PTV TLD doses differed on average by -1.2% and the spinal cord TLD dose increased from baseline by 2.5%.

The DTA between the primary PTV and OAR on the axial field was 0.2 mm higher and 0.9 mm lower for the irradiation with beam symmetry errors of 5% in-plane and 3% cross-plane, respectively. The absolute differences in the percent of pixels passing gamma analysis with 7%/4mm and 5%/3mm criteria are shown in Table 48, where a positive value indicates that the failure mode percent of pixels passing was higher than that for the baseline. For the in plane symmetry adjustment of 5%, the axial percent of pixels passing a 7%/4mm gamma analysis decreased from baseline 8.2% and on the sagittal film there was practically no change in the percent of pixels passing. When the cross plan symmetry was adjusted 3%, the percent of pixels passing a gamma analysis with 7%/4mm criteria decreased 4.6% on the axial film and increased 3.6% on the sagittal film.

Structure	TLD position	In-plane Symmetry 5%	Cross-plane Symmetry 3%
		Difference in Dose from Baseline	
Primary PTV	Superior Anterior	1.0%	-2.5%
Primary PTV	Inferior Anterior	0.1%	-0.5%
Primary PTV	Superior Posterior	-1.4%	4.1%
Primary PTV	Inferior Posterior	1.9%	2.3%
Secondary PTV	Superior	0.2%	-0.8%
Secondary PTV	Inferior	1.4%	-1.6%
Spinal Cord	Superior	-0.6%	2.3%
Spinal Cord	Inferior	-0.4%	2.7%

Table 47: TLD differences from baseline from the first irradiation set with beam symmetry adjustments of 5% in-plane and 3% cross-plane (separately).

Film	Criterion	In-plane Symmetry 5%	Cross-plane Symmetry 3%
		Absolute Difference in Pixels Passing from Baseline	
Axial	7%/4mm	-8.2%	-4.6%
	5%/3mm	-7.6%	-5.3%
Sagittal	7%/4mm	0.3%	3.6%
	5%/3mm	9.0%	15.6%

Table 48: Differences from baseline in gamma analysis results for axial and sagittal films within the phantom for the first irradiation set with beam symmetry adjustments of 5% in-plane and 3% cross-plane (separately).

Beam symmetry adjustment and measurements: Irradiation set #2

The differences in the doses measured to the phantom TLD for the three irradiations with a beam symmetry adjustments of 3.6% in-plane (angular steering), 3.8% in-plane (translational steering), and 3.65% cross-plane symmetry (angular steering) each from the baseline irradiation for the second irradiation set are shown in Table 49 and Table 51 for standard and complex plans, respectively. A positive difference indicates that the failure mode dose was higher than the baseline dose, which was the case for all TLD for all symmetry adjustments with both plans. These increases did not seem to follow exactly the same trends for standard and complex plans. With the angular in plane symmetry of 3.6%, with the average differences in TLD doses of 1.4% in the primary PTV, 3.1% in the secondary PTV, and 1.8% in the spinal cord. For the complex plan with this symmetry adjustment, the primary PTV TLD dose increased from baseline an average of 2.6%, the secondary PTV TLD increased by an average of 2.8%, and the spinal cord TLD doses increased an average of 3.4%. When the beam was steered translationally to adjust the in plane symmetry by 3.8%, the primary PTV TLD doses in the standard plan increased more than the angular in plane steering, on average 4.1%. The secondary PTV TLD doses increased on average

the same as the angular in plane steering, 3.1%, and the spinal cord TLD doses increased just slightly on average from baseline by 0.6%. In the complex plan, the primary PTV TLD dose increased from baseline an average of 3.4%, the secondary PTV TLD increased by an average of 2.7%, and the spinal cord TLD doses increased an average of 1.2%. When the cross plane symmetry was adjusted angularly by 3.65%, the standard plan primary PTV TLD doses increased on average by 2.6% from baseline and 4.2% in the secondary PTV. Spinal cord TLD doses increased an average of 1.9% from baseline for these irradiations. With the cross plan symmetry adjustment, the complex plan TLD doses increased on average by 3.1% in the primary PTV, 3.6% in the secondary PTV, and 2.6% in the spinal cord.

The average DTA between the primary PTV and OAR on the axial field for the standard plan for the 3.6% in-plane (angular steering) irradiation was 0.2 mm larger than the baseline irradiation, 0.2 mm larger for the 3.8% in-plane (translational steering) irradiation, and 0.3 mm smaller for the 3.65% cross-plane symmetry (angular steering) irradiation. For the complex plan, the DTA for the 3.6% in-plane (angular steering) irradiation was 0.5 mm smaller than the baseline irradiation, 0.2 mm smaller for the 3.8% in-plane (translational steering) irradiation, and 0.2 mm smaller for the 3.65% cross-plane symmetry (angular steering) irradiation.

The differences in the percent of pixels passing gamma analysis with 7%/4mm and 5%/3mm criteria are shown in Table 50 and Table 52 for standard and complex plans, respectively. A positive value indicates that the failure mode percent of pixels passing was higher than that for the baseline. The corresponding gamma maps are shown in Figure 63 - Figure 68 for the standard treatment plan and Figure 69 - Figure 74 for the complex plan. The in plane symmetry adjustments changed the percent of pixels passing the 7%/4mm gamma analysis on the standard plan axial film by 11.9% and -12.7% for angular and translational adjustments, respectively. Compared to the baseline axial film gamma maps, the angular in plane symmetry adjustment seemed to reduce failure on the anterior side of films 2 and 3 and slightly increased the failure on the posterior side. The positional in plane steering, on the other hand, increased failures on the axial films for the standard plan, particularly in the primary PTV and the right anterior

corner. The standard plan sagittal films had changes in percent of pixels passing for the in plane symmetry irradiations of 15.1% and -13.9%. The distribution of failures on the standard sagittal film with the angular in plane symmetry adjustment was very similar to the baseline, with reduced failures primarily on the superior half of the film. For the translational adjustment of the in plane symmetry, the sagittal film gamma map showed strong failure throughout the PTV, with slightly greater concentration of failure in the inferior half of the film, though the baseline standard sagittal film seemed to have that trend as well. The complex plan with in plane symmetry adjustments had 17.6% and -11.6% increases on the axial film and 14.3% and -9.6% on the sagittal film with angular and translational steering, respectively. On the axial film gamma map from irradiations with angular adjustment to the symmetry, the failures throughout the PTVs seen in the baseline gamma maps reduced overall and there was a concentration of failure in a high dose region outside the primary PTV in the left posterior corner as well as the other corner of the primary PTV. This angular in plane symmetry resulted in an overall reduction in the failures on the sagittal film, with not obvious pattern change compared to baseline. The translational steering of the in plane symmetry resulted in an overall increase in the failures on the complex plan axial film, which were distributed throughout the PTVs and in between them. There was not a change in the pattern of the failures from baseline. On the sagittal film, a similar overall increase in the failures was seen. For the cross symmetry angular adjustment of 3.65%, the standard plan had increases in percent of pixels passing the 7%/4mm gamma analysis of 17.4% on the axial film and 15.5% on the sagittal film. The failures on the standard plan axial film gamma map for the cross plane symmetry adjustment seemed to follow the same pattern as the baseline gamma map but had less failure overall and particularly in the left-anterior quadrant of the film. In the complex plan axial film, the failures were much less prevalent than in the baseline film but seemed to have increased in a concentrated spot where the primary PTV dose extended outside the structure in the left posterior corner. The sagittal film gamma map showed regions on failure along the superior and inferior edges of the PTV. The failures overall were less prevalent than the baseline irradiations, but it was difficult to determine whether the distribution of failures was very different since the distribution on the baseline films were rather dispersed throughout the PTV. In the

complex plan, the percent of pixels passing on the axial and sagittal films with a cross plane symmetry adjustment increased by 21.3% and 12.8%, respectively. On the axial film, the failures reduced throughout the PTVs and were concentrated in that higher dose region adjacent to the primary PTV in the left posterior corner as well as the other corner of the primary PTV and in a line along the outside of the secondary PTV. Similar to the standard plan sagittal film, the prevalence of failure was reduced on the film from the cross plane symmetry adjusted irradiations, but the pattern did not appear largely different than baseline with the exception of perhaps less failure in the inferior half of the film.

We saw larger differences in the doses to TLD and changes in the dose distributions from baseline with our measurements than were seen in our treatment planning studies. Part of this could be accounted for by the changes in beam flatness with physical beam steering which was likely not the same as that in the beam model. These differences in flatness would be difference since the physical measurements were made with an improper configuration of the beam (photon beam not properly incident on the flattening filter) versus the treatment planning study beams were made with proper beam configuration with an additional modifier (indecent properly on the flattening filter and on the physical wedge). The fact that differences were all positive could potentially be explained for in the in plane symmetry adjustments, which would be expected to cause changes in the superior-inferior direction, by the fact that the isocenter was just superior of the axial cut in the phantom insert, adjacent to which the TLD lie. For the angularly steered in plane symmetry measurements, the superior PTV TLD doses changed more than the inferior PTV TLD doses, which would support that notion. These changes were also slightly visible on the sagittal film gamma maps for the standard plan, with differences from the baseline gamma maps primarily in the superior half and more failures in the inferior half. The opposite was mostly true for the translationally steered in plane symmetry error, but the superior/inferior differences weren't as large. As mentioned, cross plane symmetry errors would be expected to approximately wash out when multiple beam angles are used, however this would depend on the beam weighting and the shapes created by the MLC segments. This would result in a decrease in the PTV dose

homogeneity may have been the cause of the measured changes that were seen with the cross plane symmetry adjusted.

Standard Phantom Treatment Plan Irradiation – TLD Results				
Structure	TLD position	3.6% In-plane	3.8% In-plane	3.65% Cross-plane
		Difference in Dose from Baseline		
Primary PTV	Superior Anterior	1.8%	3.7%	2.0%
Primary PTV	Inferior Anterior	0.8%	3.6%	2.1%
Primary PTV	Superior Posterior	2.0%	3.8%	3.6%
Primary PTV	Inferior Posterior	0.9%	5.1%	2.7%
Secondary PTV	Superior	3.4%	2.7%	4.3%
Secondary PTV	Inferior	2.8%	3.4%	4.1%
Spinal Cord	Superior	1.6%	0.7%	1.8%
Spinal Cord	Inferior	1.9%	0.4%	2.0%

Table 49: Average TLD differences from baseline from the second irradiation set with symmetry adjustments of 3.6% in-plane (angular steering), 3.8% in-plane (translational steering), and 3.65% cross-plane symmetry (angular steering) for the standard plan.

Standard Phantom Treatment Plan Irradiation – Gamma Analysis Results				
Film	Criterion	3.6% In-plane	3.8% In-plane	3.65% Cross-plane
		Difference in Pixels Passing from Baseline		
Axial	7%/4mm	11.9%	-12.7%	17.4%
	5%/3mm	-7.5%	-39.6%	5.6%
Sagittal	7%/4mm	15.1%	-13.9%	15.5%
	5%/3mm	2.3%	-25.8%	2.3%

Table 50: Average Differences from baseline in gamma analysis results for axial and sagittal films within the phantom for the first irradiation set with symmetry adjustments of 3.6% in-plane (angular steering), 3.8% in-plane (translational steering), and 3.65% cross-plane symmetry (angular steering) for the standard plan.

Complex Phantom Treatment Plan Irradiation – TLD Results				
Structure	TLD position	3.6% In-plane	3.8% In-plane	3.65% Cross-plane
		Difference in Dose from Baseline		
Primary PTV	Superior Anterior	2.1%	2.6%	2.7%
Primary PTV	Inferior Anterior	2.0%	2.9%	3.0%
Primary PTV	Superior Posterior	5.1%	3.7%	3.8%
Primary PTV	Inferior Posterior	1.3%	4.4%	2.7%
Secondary PTV	Superior	2.9%	2.5%	3.6%
Secondary PTV	Inferior	2.6%	2.8%	3.6%
Spinal Cord	Superior	1.9%	1.9%	2.8%
Spinal Cord	Inferior	4.9%	0.5%	2.4%

Table 51: Average TLD differences from baseline from the second irradiation set with symmetry adjustments of 3.6% in-plane (angular steering), 3.8% in-plane (translational steering), and 3.65% cross-plane symmetry (angular steering) for the complex plan.

Complex Phantom Treatment Plan Irradiation – Gamma Analysis Results				
Film	Criterion	3.6% In-plane	3.8% In-plane	3.65% Cross-plane
		Difference in Pixels Passing from Baseline		
Axial	7%/4mm	16.6%	-11.6%	21.3%
	5%/3mm	-10.1%	-37.2%	-3.4%
Sagittal	7%/4mm	14.3%	-9.6%	12.8%
	5%/3mm	-2.5%	-20.2%	-1.3%

Table 52: Average differences from baseline in gamma analysis results for axial and sagittal films within the phantom for the first irradiation set with symmetry adjustments of 3.6% in-plane (angular steering), 3.8% in-plane (translational steering), and 3.65% cross-plane symmetry (angular steering) for the complex plan.

Standard Phantom Treatment Plan: Angular In Plane Axial Film,

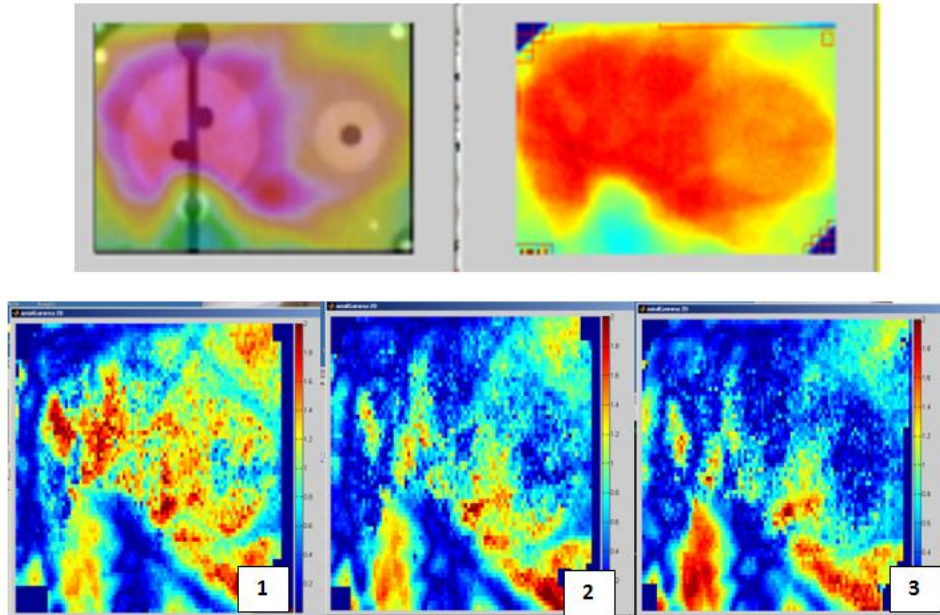


Figure 63: Axial film dose distributions from the TPS (upper left), film from one irradiation (upper right), and the gamma maps (5%/3mm) from this film for the three irradiations of the phantom with the standard treatment plan with in plane symmetry angular adjustment of 3.6% (bottom).

Standard Phantom Treatment Plan: Angular In Plane Sagittal Film, 5%/3mm

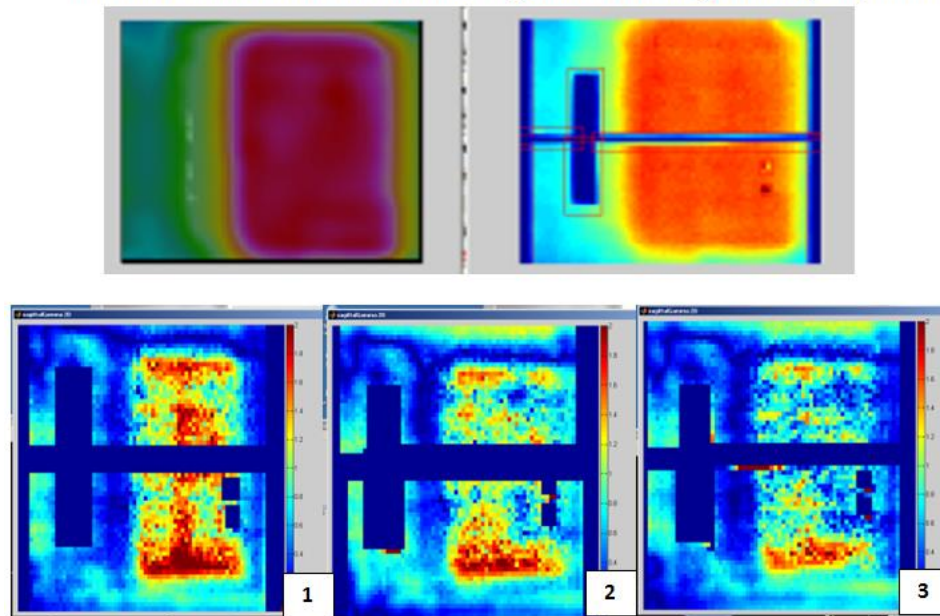


Figure 64 Sagittal film dose distributions from the TPS (upper left), film from one irradiation (upper right), and the gamma maps (5%/3mm) from this film for the three irradiations of the phantom with the standard treatment plan with in plane symmetry angular adjustment of 3.6% (bottom).

Standard Phantom Treatment Plan: Positional In Plane Axial Film, 5%/3mm

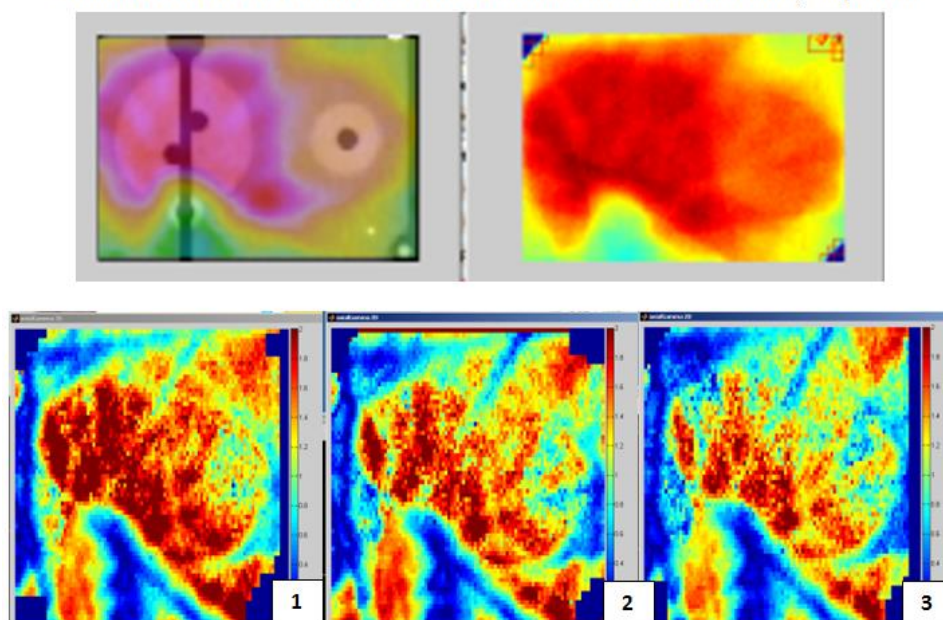


Figure 65: Axial film dose distributions from the TPS (upper left), film from one irradiation (upper right), and the gamma maps (5%/3mm) from this film for the three irradiations of the phantom with the standard treatment plan with in plane symmetry positional adjustment of 3.8% (bottom).

Standard Phantom Treatment Plan: Positional In Plane Sagittal Film, 5%/3mm

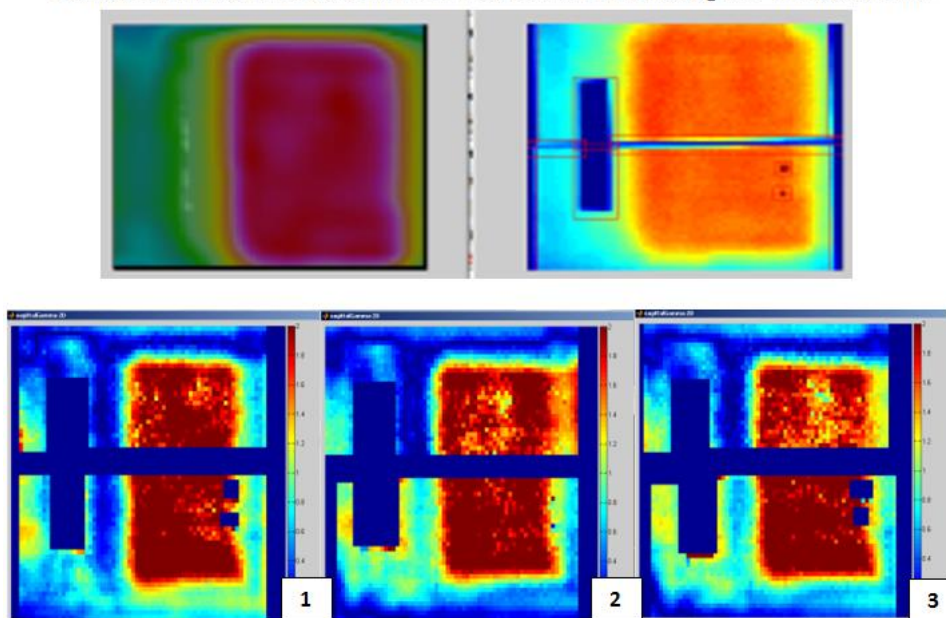


Figure 66: Sagittal film dose distributions from the TPS (upper left), film from one irradiation (upper right), and the gamma maps (5%/3mm) from this film for the three irradiations of the phantom with the standard treatment plan with in plane symmetry positional adjustment of 3.8% (bottom).

Standard Phantom Treatment Plan: Angular Cross Plane Axial Film, 5%/3mm

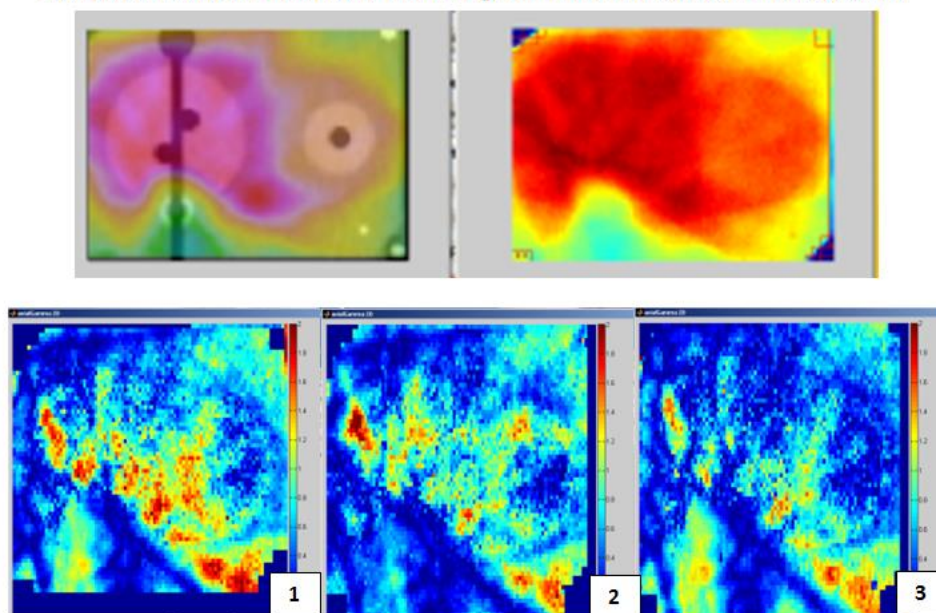


Figure 67: Axial film dose distributions from the TPS (upper left), film from one irradiation (upper right), and the gamma maps (5%/3mm) from this film for the three irradiations of the phantom with the standard treatment plan with cross plane symmetry angular adjustment of 3.65% (bottom).

Standard Phantom Treatment Plan: Angular Cross Plane Sagittal Film, 5%/3mm

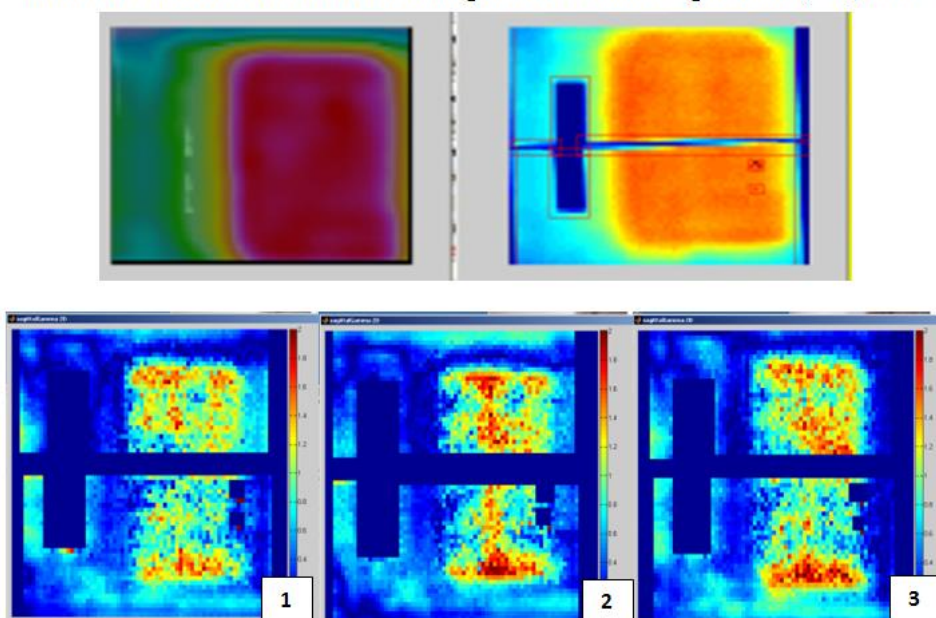


Figure 68: Sagittal film dose distributions from the TPS (upper left), film from one irradiation (upper right), and the gamma maps (5%/3mm) from this film for the three irradiations of the phantom with the standard treatment plan with cross plane symmetry angular adjustment of 3.65% (bottom).

Complex Phantom Treatment Plan: Angular In Plane Axial Film, 5%/3mm

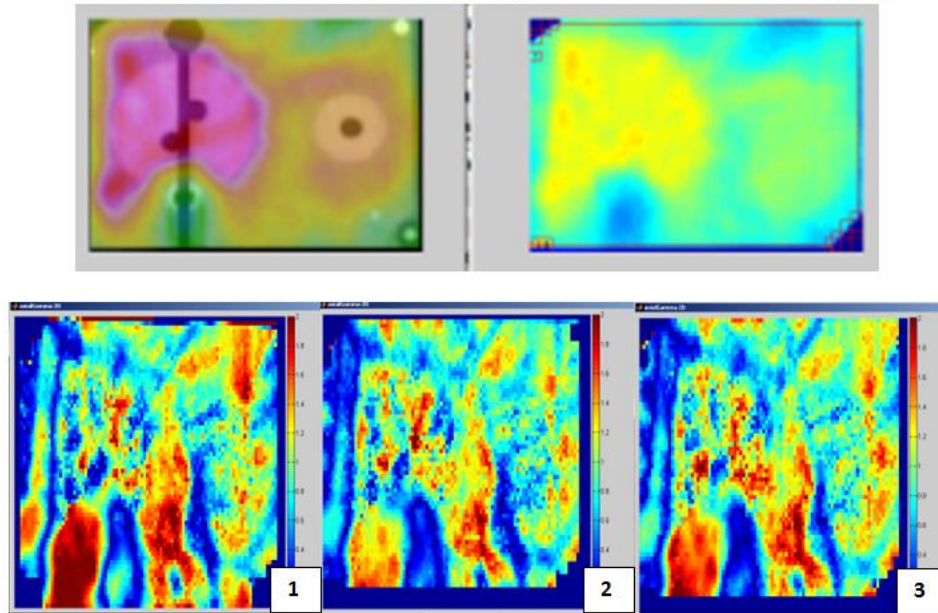


Figure 69: Axial film dose distributions from the TPS (upper left), film from one irradiation (upper right), and the gamma maps (5%/3mm) from this film for the three irradiations of the phantom with the complex treatment plan with in plane symmetry angular adjustment of 3.6% (bottom).

Complex Phantom Treatment Plan: Angular In Plane Sagittal Film, 5%/3mm

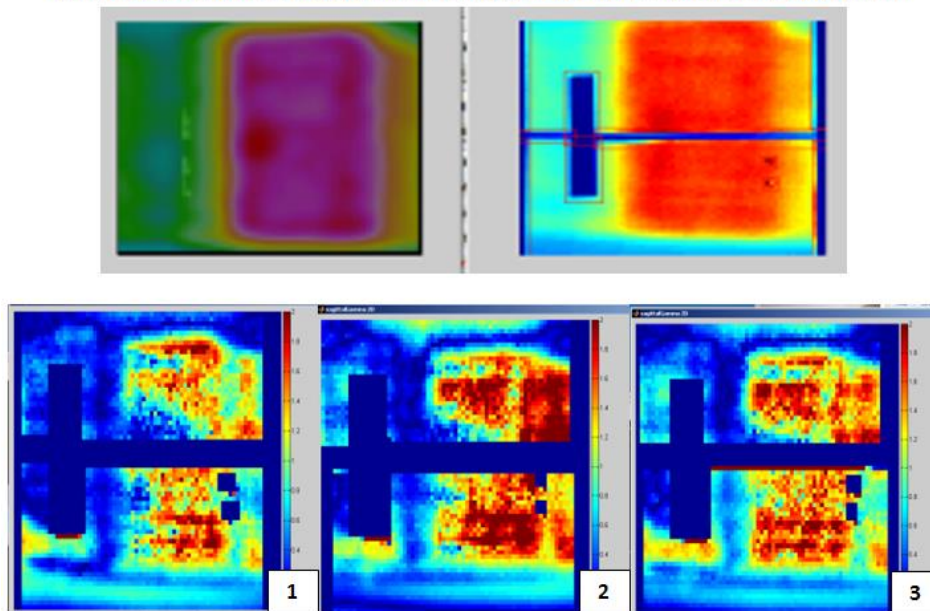


Figure 70: Sagittal film dose distributions from the TPS (upper left), film from one irradiation (upper right), and the gamma maps (5%/3mm) from this film for the three irradiations of the phantom with the complex treatment plan with in plane symmetry angular adjustment of 3.6% (bottom).

Complex Phantom Treatment Plan: Positional In Plane Axial Film, 5%/3mm

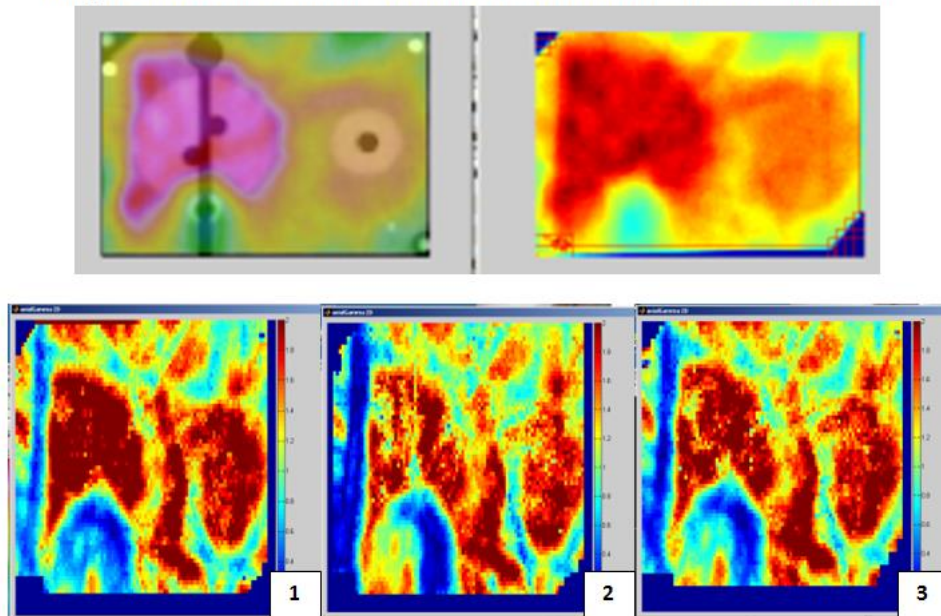


Figure 71: Axial film dose distributions from the TPS (upper left), film from one irradiation (upper right), and the gamma maps (5%/3mm) from this film for the three irradiations of the phantom with the complex treatment plan with in plane symmetry positional adjustment of 3.8% (bottom).

Complex Phantom Treatment Plan: Positional In Plane Sagittal Film, 5%/3mm

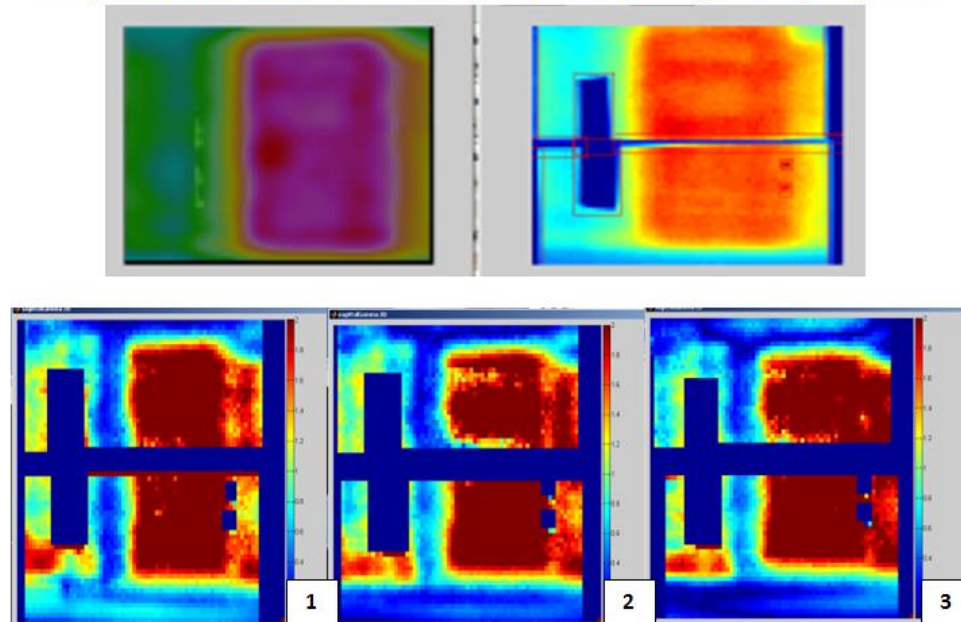


Figure 72: Sagittal film dose distributions from the TPS (upper left), film from one irradiation (upper right), and the gamma maps (5%/3mm) from this film for the three irradiations of the phantom with the complex treatment plan with in plane symmetry positional adjustment of 3.8% (bottom).

Complex Phantom Treatment Plan: Angular Cross Plane Axial Film, 5%/3mm

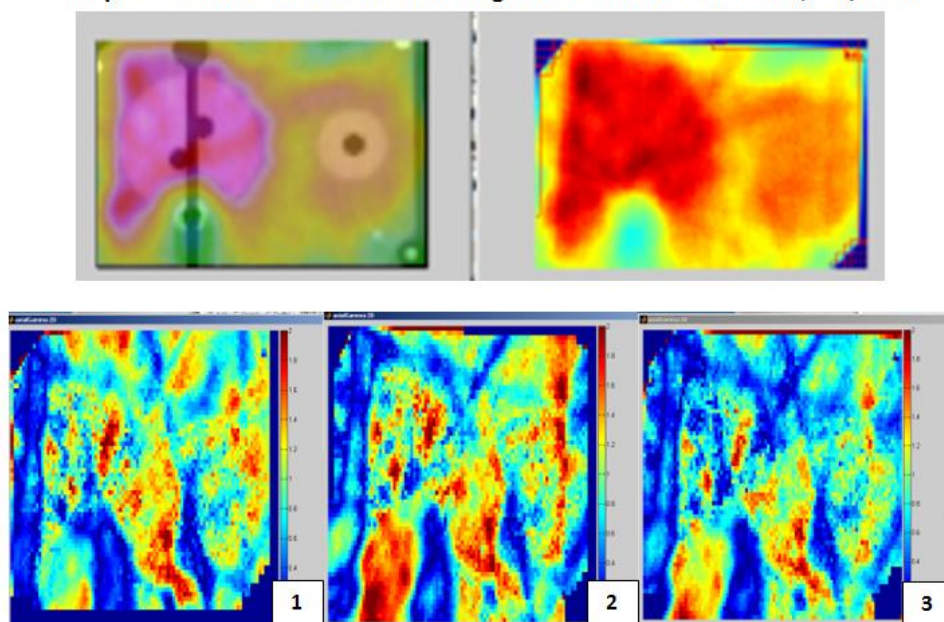


Figure 73: Axial film dose distributions from the TPS (upper left), film from one irradiation (upper right), and the gamma maps (5%/3mm) from this film for the three irradiations of the phantom with the complex treatment plan with cross plane symmetry angular adjustment of 3.65% (bottom).

Complex Phantom Treatment Plan: Angular Cross Plane Sagittal Film, 5%/3mm

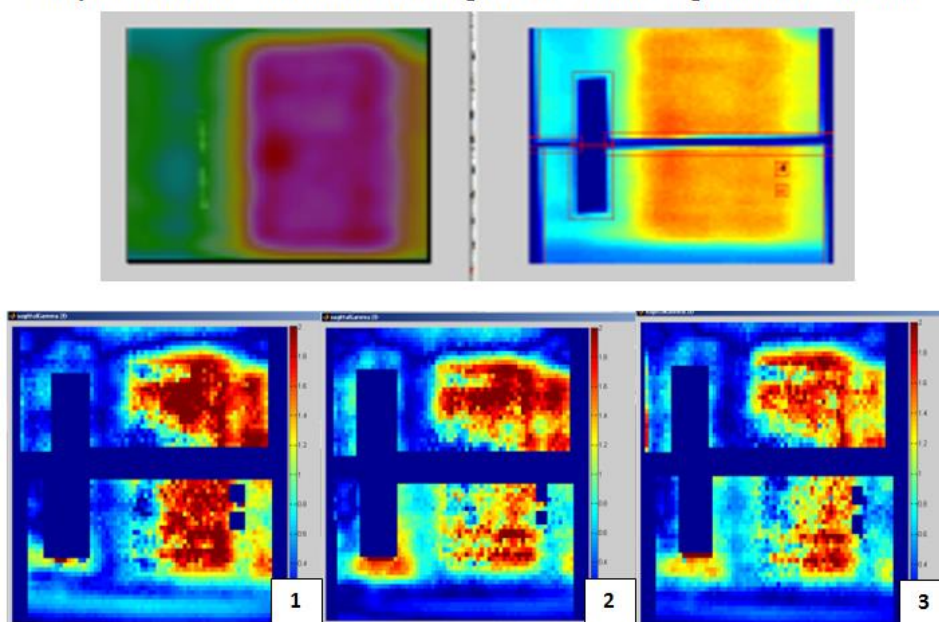


Figure 74: Sagittal film dose distributions from the TPS (upper left), film from one irradiation (upper right), and the gamma maps (5%/3mm) from this film for the three irradiations of the phantom with the complex treatment plan with cross plane symmetry angular adjustment of 3.65% (bottom).

Beam symmetry phantom studies summary

Changes in the beam symmetry in our treatment planning studies resulted in all small changes in the doses to the phantom structures, with the most prevalent difference from baseline being a small decrease in the dose to the spinal cord, especially with bottom-top (in plane) symmetry errors. In our measurements, the doses measured by the TLD all increased from baseline. We did not measure a decrease in the dose to the spinal cord but rather, an increase. The differences in treatment planning studies and measurements were likely due to both differences in the nature of the symmetry errors and the evaluations themselves, with TLD only capturing a small part of the full volumetric picture. The severity score of 1, resultant of the treatment planning studies, may be slightly low since differences were measured, however those differences were in the very sensitive spinal cord TLD or were increases in the PTV doses which are not considered for severity scoring according to our currently presented method.

Failure mode 3: MLC position

Treatment planning study results

The resultant changes in the phantom structure doses used for severity scoring for systematic MLC positional errors in one bank of leaves (X1 or X2) of both 1 mm and 2mm are summarized for standard phantom plans in Table 53 and Table 54. As in the first two failure modes, the dose differences are color-coded to demonstrate severity score levels. Dosimetric changes ranging from about 0% to 20% were seen in the standard phantom treatment plan structures at the evaluation criteria. Moving either MLC bank out by 1 mm resulted in increases to the maximum dose of the spinal cord, by 3.7% for the X1 bank and 5.7% for the X2 bank. This change in the X1 bank also resulted in small reductions in the PTV coverage. Moving the MLC in the X1 bank out by 2 mm did not result in substantial errors in any of the structures. However, moving this bank in by 2 mm resulted in under-dosing 99% of the primary PTV volume by over 9% and 95% of the primary PTV volume by about 7.5% as well as decreasing $D_{99\%}$ and $D_{95\%}$ for the secondary PTV by almost 4% and 5%, respectively. Shifts of 2 mm in the X2 MLC bank resulted in even larger changes. When the X2 leaves were shifted out by 2 mm, the dose to the primary

PTV was decreased by almost 3% and the spinal cord dose increased by over 8%. When the X2 leaves were shifted in by 2 mm on the standard phantom treatment plan, 95% of the primary PTV volume was under-dosed by 16% and 99% of the primary PTV volume was under-dosed by almost 20%. The secondary PTV was also under-dosed by about 8% for the $D_{99\%}$ and $D_{95\%}$. Based on these results from the standard phantom treatment plan, the severity scores for an MLC positional error of 1 mm was 4 and of 2 mm was 8. With the collimator at 0° , the X1 and X2 banks of leaves are used to modulate the dose to the left or right side of the field from the BEV, respectively. As the gantry rotates around the patient, the structures blocked by either bank change. The differences seen in shifting the X1 bank or the X2 bank likely has to do with the amount of modulation either bank is responsible for, the beam and segment weighting, and where the edges of the fields are. Based on the fact that larger changes were seen with the X2 bank, we would expect those leaves to move within the fields slightly more and therefore shifts have a greater impact on the dose distribution.

For complex plans, the resultant changes in the phantom structure doses used for severity scoring for systematic MLC positional errors in one bank of leaves (X1 or X2) of both 1 mm and 2mm are summarized in Table 55 and Table 56. All changes in the structure evaluation criteria for systematic MLC errors of 1 mm in the complex plan were under 2.5%, with the exception of moving the X2 bank out by 1 mm which resulted in slightly over a 3% increase in the maximum dose to the spinal cord. When the MLC banks were shifted 2 mm, dosimetric changes up to over 8% were seen in the complex phantom treatment plan structures at the evaluation criteria. Under-dosing of the primary PTV by about 4-8% resulted from moving either the X1 or X2 MLC bank in by 2 mm. Additionally when the X1 leaves were shifted in by 2 mm on the complex phantom treatment plan, the spinal cord maximum dose increased by almost 5%. When the X2 leaves were shifted in by 2 mm, the maximum dose to the normal tissue structure increased by about 5%. When the X2 leaves were shifted 2 mm out, only small changes were seen in the PTV doses, but the spinal cord maximum dose increased by over 8%. Discrepancies between the results from shifts in the X1 and X2 banks were a result of the complex modulation as in the standard

phantom treatment plan. The discrepancies weren't as large, which may indicate that since this plan was more complex, utilizing more segments and smaller segments, both banks were required to participate heavily in the modulation. Overall, the worst error in the complex treatment plan would result in a severity score of 2 for an error of 1 mm and severity score of 6 for an error of 2 mm. Since worse errors were seen with the standard phantom treatment plan, the severity score of 8 determined by those results was assigned to this failure mode.

Standard Phantom Treatment Plan					
Structure	Evaluation criteria	1 mm MLC positional errors			
		X1 + 1mm	X1 - 1mm	X2 +1mm	X2 - 1mm
		Change from baseline			
Primary PTV	D _{95%}	-1.08%	-0.01%	0.29%	-0.50%
	D _{99%}	-1.26%	-0.49%	0.42%	-0.92%
Secondary PTV	D _{95%}	-1.37%	0.89%	-0.42%	0.07%
	D _{99%}	-1.26%	0.55%	-0.50%	-0.36%
Spinal Cord	Max Dose	3.65%	-2.40%	5.74%	-5.06%
Normal Tissue	Max Dose	-0.29%	1.32%	0.00%	0.34%

Table 53: Dosimetric changes from baseline used for severity scoring for systematic MLC positional errors of 1 mm in one bank of leaves (X1 or X2) for the standard phantom treatment plan.

Standard Phantom Treatment Plan					
Structure	Evaluation criteria	2 mm MLC positional errors			
		X1 + 2mm	X1 - 2mm	X2 +2mm	X2 - 2mm
		Change from baseline			
Primary PTV	D _{95%}	0.46%	-7.45%	-2.46%	-16.08%
	D _{99%}	0.47%	-9.10%	-2.83%	-19.80%
Secondary PTV	D _{95%}	0.51%	-3.96%	-1.03%	-7.98%
	D _{99%}	0.59%	-4.80%	-1.91%	-8.63%
Spinal Cord	Max Dose	0.68%	-8.64%	8.17%	-24.17%
Normal Tissue	Max Dose	0.56%	-2.99%	0.92%	-7.95%

Table 54: Dosimetric changes from baseline used for severity scoring for systematic MLC positional errors of 2 mm in one bank of leaves (X1 or X2) for the standard phantom treatment plan.

Complex Phantom Treatment Plan					
Structure	Evaluation criteria	1 mm MLC positional errors			
		X1 + 1mm	X1 - 1mm	X2 +1mm	X2 - 1mm
		Change from baseline			
Primary PTV	D _{95%}	-1.26%	0.07%	0.61%	-1.24%
	D _{99%}	-1.25%	-0.16%	0.87%	-1.95%
Secondary PTV	D _{95%}	-2.26%	2.18%	0.24%	-0.64%
	D _{99%}	-1.62%	1.50%	0.41%	-0.55%
Spinal Cord	Max Dose	0.86%	0.69%	3.15%	-1.58%
Normal Tissue	Max Dose	-0.73%	1.32%	0.53%	1.10%

Table 55: Dosimetric changes from baseline used for severity scoring for systematic MLC positional errors of 1 mm in one bank of leaves (X1 or X2) for the complex phantom treatment plan.

Complex Phantom Treatment Plan					
Structure	Evaluation criteria	2 mm MLC positional errors			
		X1 + 2mm	X1 - 2mm	X2 +2mm	X2 - 2mm
		Change from baseline			
Primary PTV	D _{95%}	-0.02%	-5.64%	-2.01%	-4.39%
	D _{99%}	0.53%	-7.94%	-2.44%	-7.69%
Secondary PTV	D _{95%}	0.06%	6.14%	2.06%	3.84%
	D _{99%}	1.00%	4.77%	1.32%	3.35%
Spinal Cord	Max Dose	-0.05%	4.97%	8.35%	1.49%
Normal Tissue	Max Dose	0.36%	0.22%	1.77%	5.07%

Table 56: Dosimetric changes from baseline used for severity scoring for systematic MLC positional errors of 2mm in one bank of leaves (X1 or X2) for the complex phantom treatment plan.

The DVHs for MLC positional errors of 1 mm and 2 mm are shown in Figure 75 and Figure 77 and Figure 76 and Figure 78, respectively. Very small changes in the standard treatment plan PTV doses with a 1mm MLC positional error were seen, as was a spread in the dose to the spinal cord with moving the X2 bank out by 1 mm creating the largest increase. Changes in the complex plan spinal cord dose were similar and PTV dose changes were slightly larger than those in the standard plan.

Target under-dosing was seen very clearly when the MLC banks were shifted 2 mm in the standard phantom treatment plan (Figure 76). In the complex phantom treatment plan, however, the dose to the secondary PTV was clearly increased and the primary PTV lost coverage but gained hotspots (Figure 78). There was also a large spread in the dose to the spinal cord dose for both the standard and complex plans, with only a 2 mm shift out of the X2 bank causing an increase in the spinal cord DVH.

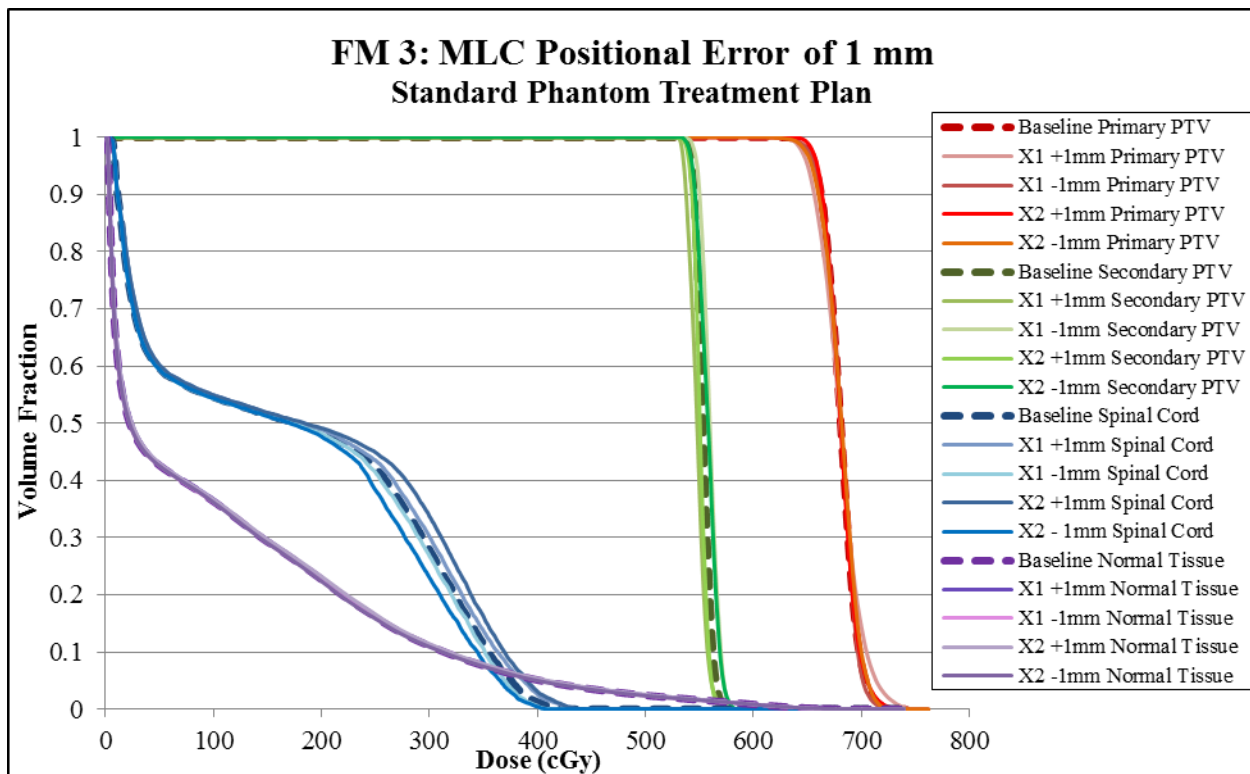


Figure 75: DVHs for phantom structures in the standard treatment plan with systematic MLC positional errors in one bank of 1 mm, with dashed lines showing baseline DVHs.

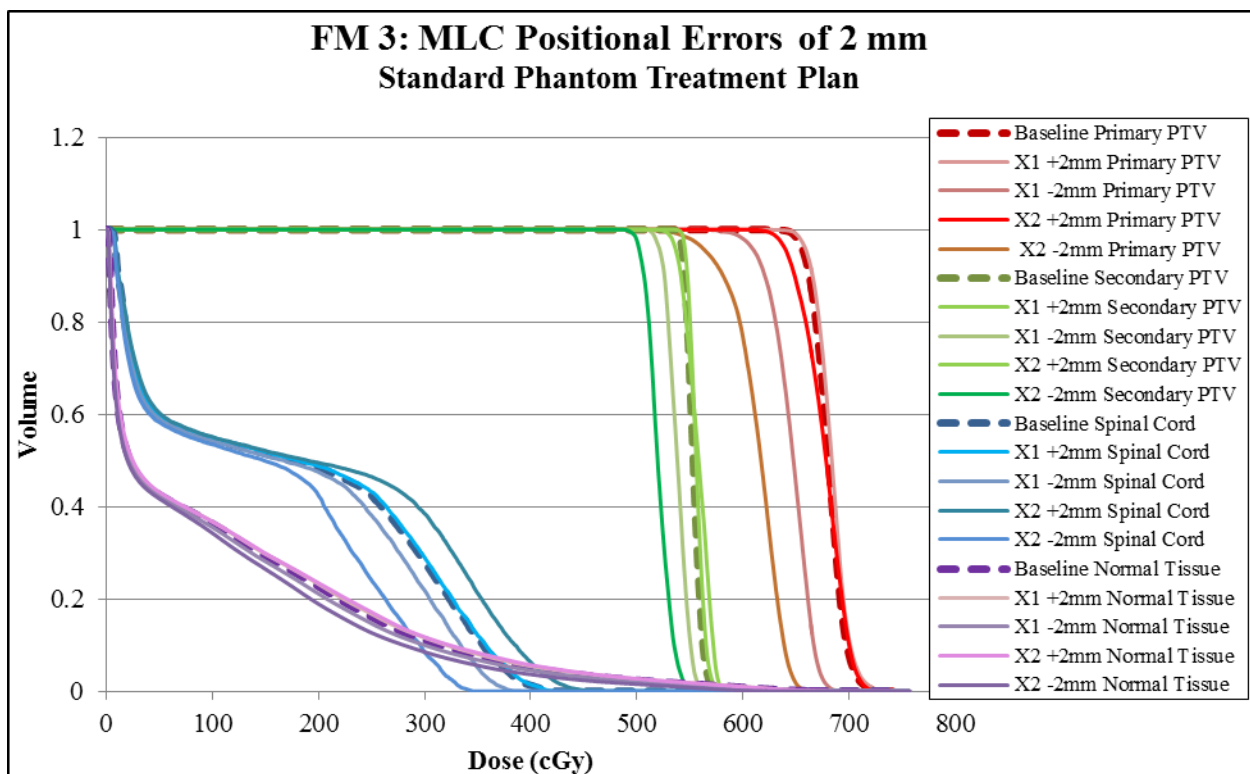


Figure 76: DVHs for phantom structures in the standard treatment plan with systematic MLC positional errors in one bank of 2 mm, with dashed lines showing baseline DVHs.

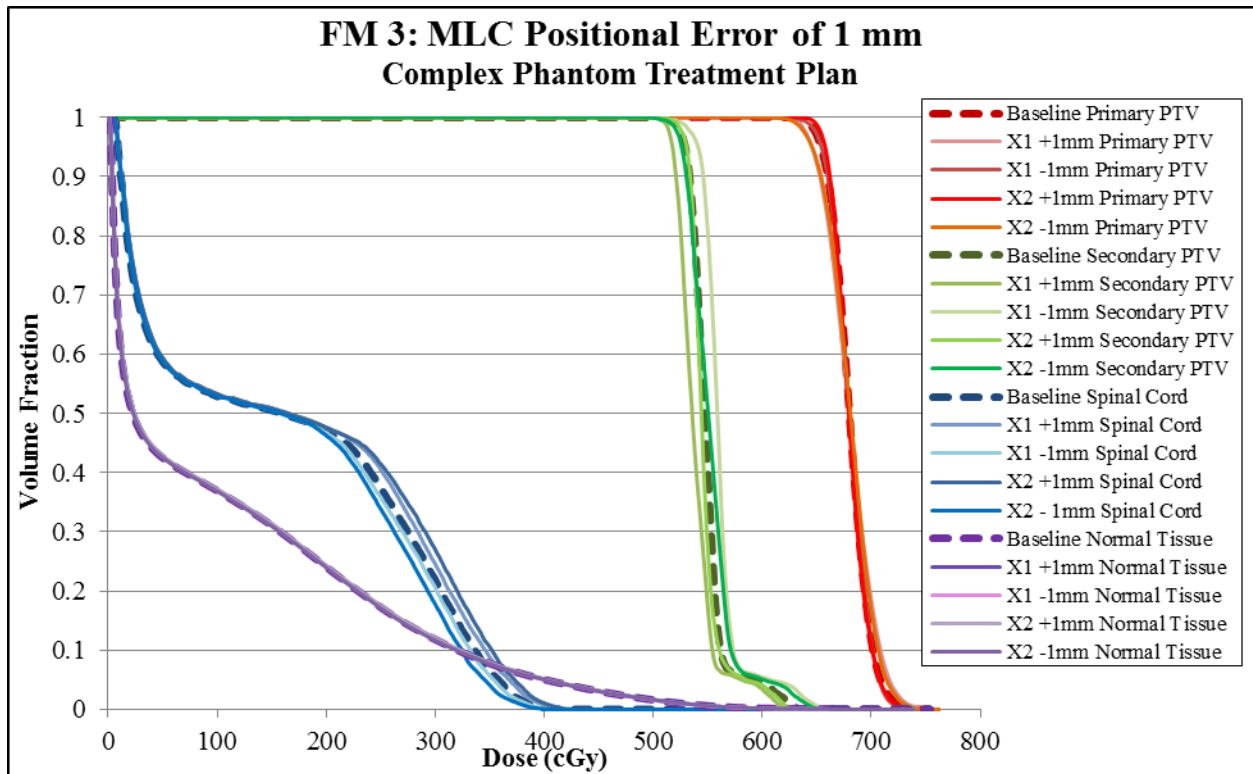


Figure 77: DVHs for phantom structures in the complex treatment plan with systematic MLC positional errors in one bank of 1 mm, with dashed lines showing baseline DVHs.

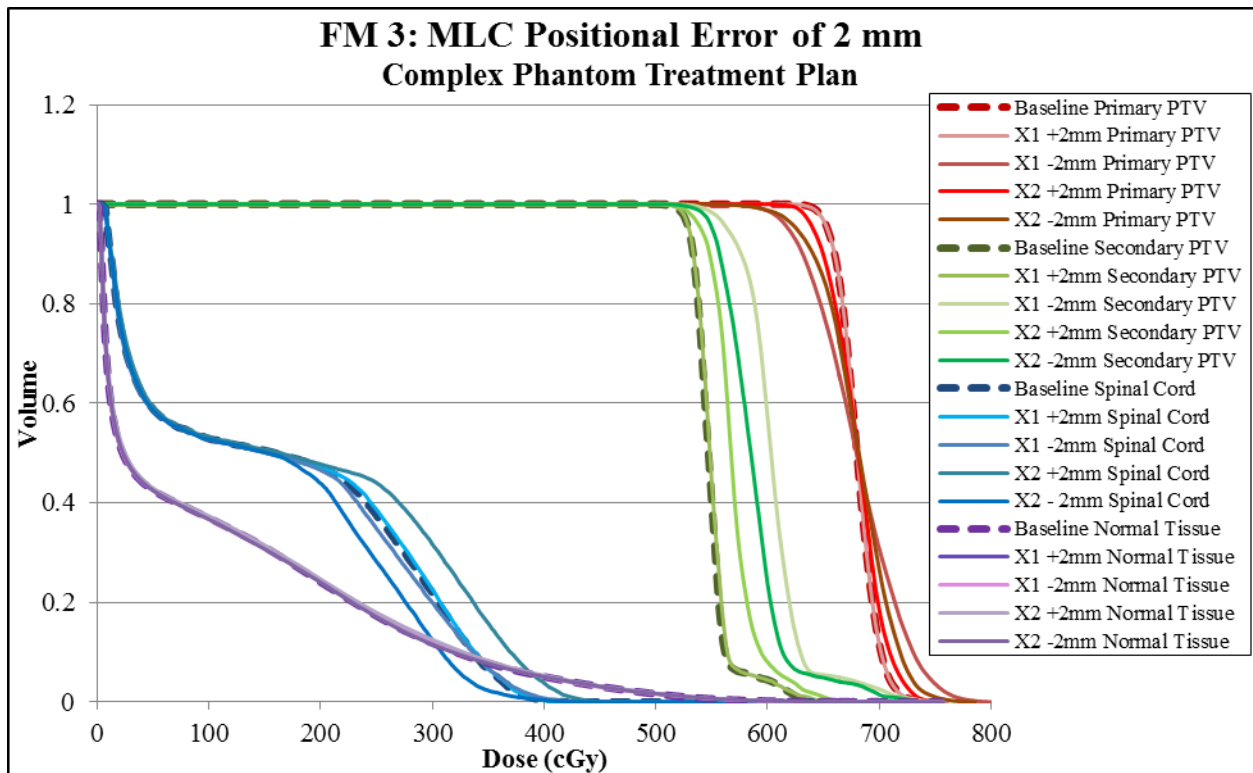


Figure 78: DVHs for phantom structures in the complex treatment plan with systematic MLC positional errors in one bank of 2 mm, with dashed lines showing baseline DVHs.

The increase in differences with larger MLC positional errors was obvious. As one would expect, when the MLC moved inward (-1 mm or -2 mm), the doses to structures generally decreased and the when the MLC moved outward (+1 mm or +2 mm), the doses to structures generally increased. The fact that the dose to the normal tissue was least effected reflects the role of the MLC in IMRT to not only block along the edges of the structures, but to modulate the dose within them. The relationship between MLC positional errors and structures doses was therefore rather complex. One surprising result was that the dose to the secondary PTV increased for 2 mm shifts inward in the complex plan which would be expected to universally reduce the doses since the fields were smaller. An axial image of the phantom and dose distribution is shown in Figure 79, with the baseline plan on the left and the plan with the X2 bank of MLC systematically shifted inward. The primary PTV clearly lost coverage, however the dose to the secondary PTV increased. This demonstrated the complexity of the role of modulation well.



Figure 79: Axial image of phantom with complex treatment plan dose distributions: Baseline plan (left) and X2 MLC systematically shifted inward by 2 mm (right). Isodose values are shown in the upper left corner.

Physical measurement results

MLC positional error measurements: Irradiation set #1

The differences in the doses measured to the phantom TLD for the irradiation with MLC positional errors of 1 mm out and 3 mm out in both banks from the baseline irradiation for the first irradiation set are shown in Table 57 where a positive difference indicates that the failure mode dose was higher than the baseline dose. On average, the dose to the primary PTV TLD increased from baseline by 14.2% with the MLC shifted out 1 mm. With this MLC shift, the dose to the secondary PTV and spinal cord TLD also increased, on average by 7.7% and 18.8%, respectively. With the MLC shifted out 3 mm, the dose to the primary PTV TLD increased from baseline by 36.6% on average. In the secondary PTV, the dose to the TLD increased on average by 22.3% and in the spinal cord the dose was close to doubling, increasing by 91.2% on average. The DTA between the primary PTV and OAR on the axial film was 0.7 mm lower than the baseline irradiation for the irradiation with a systematic MLC positional error of 1 mm out and 3 mm out, respectively. The absolute differences in the percent of pixels passing gamma analysis with 7%/4mm and 5%/3mm criteria are shown in Table 58.

Structure	TLD position	MLC 1 mm out	MLC 3 mm out
		Difference in Dose from Baseline	
Primary PTV	Superior Anterior	12.5%	35.3%
Primary PTV	Inferior Anterior	11.6%	38.5%
Primary PTV	Superior Posterior	17.6%	38.2%
Primary PTV	Inferior Posterior	15.0%	34.4%
Secondary PTV	Superior	8.9%	25.6%
Secondary PTV	Inferior	6.5%	19.0%
Spinal Cord	Superior	22.5%	92.7%
Spinal Cord	Inferior	15.1%	89.7%

Table 57: TLD differences from baseline from the first irradiation set with systematic MLC positional errors of 1 mm and 3 mm in both banks.

Film	Criterion	MLC 1 mm out	MLC 3 mm out
		Absolute Difference in Pixels Passing from Baseline	
Axial	7%/4mm	23.2%	-34.5%
	5%/3mm	35.9%	-15.9%
Sagittal	7%/4mm	7.7%	-34.5%
	5%/3mm	22.3%	-15.9%

Table 58: Absolute differences from baseline in gamma analysis results for axial and sagittal films within the phantom for the first irradiation set with systematic MLC positional errors of 1 mm and 3 mm in both banks.

MLC positional error measurements: Irradiation set #2

The differences in the doses measured to the phantom TLD for the irradiations with MLC positional errors of 2 mm out in one bank of leaves from the baseline irradiation for the second irradiation set are shown in Table 59 for standard and complex plans where a positive difference indicates that the failure mode dose was higher than the baseline dose. On average, the primary PTV TLD dose increased by 1.5% in the standard plan with the 2 mm shift outward. The secondary PTV and spinal cord TLD doses also increased from baseline, by 1.3% and 6.4% on average, respectively. In the complex plan, the primary PTV TLD dose increased by 2.3% on average, the secondary PTV TLD dose increased by 1.8% on average, and the spinal cord dose increased by 6.3% on average.

The DTA between the primary PTV and OAR on the axial field was 0.9 mm lower than the baseline irradiation for the irradiation for the standard plan and 0.9 mm lower for the complex plan. The differences in the percent of pixels passing gamma analysis with 7%/4mm and 5%/3mm criteria are shown in Table 60 for standard and complex plans. The corresponding gamma maps are shown in Figure 80 and Figure 81 for the standard plan and Figure 82 and Figure 83 for the complex plan. In the standard plan, the percent of pixels passing a 7%/4mm gamma analysis increased by 18% on the axial film and 11.3% on the sagittal film. On the axial films, there was a clear reduction in points failing compared to the baseline which was not expected with improper MLC positioning, however this must have been due to an error in the original baseline delivery. The distribution of failure was similar between the two sets of irradiations, though it appeared that there were fewer failures outside of the PTV regions. On the sagittal films, the failures were mostly along the superior and inferior edges of the PTV, as opposed to spread within the PTV like the baseline films. For the complex plan with 2 mm shifts outward, the axial film

gamma analysis with 7%/4mm criteria resulted in 17.9% more pixels passing than the baseline plan, while on the sagittal film the percent of pixels passing increased by 8.7%. These increases were similar in magnitude to those from the standard plan. On the axial films gamma maps, the failures within the PTVs decreased and on two of the three films there were concentrated spots of failure in the left posterior corner and the right anterior corner. On the sagittal film gamma maps, the distribution of failure was very similar to baseline just with an overall decrease in the amount of failure.

Structure	TLD position	Standard Plan Irradiation	Complex Plan Irradiation
		MLC 2 mm out, one bank	
		Difference in Dose from Baseline	
Primary PTV	Superior Anterior	1.7%	2.8%
Primary PTV	Inferior Anterior	2.0%	3.2%
Primary PTV	Superior Posterior	0.8%	2.2%
Primary PTV	Inferior Posterior	1.3%	1.0%
Secondary PTV	Superior	0.8%	2.3%
Secondary PTV	Inferior	1.7%	1.3%
Spinal Cord	Superior	6.8%	5.3%
Spinal Cord	Inferior	6.0%	7.2%

Table 59: Average TLD differences from baseline from the second irradiation set with systematic MLC positional errors of 2 mm in one bank for standard and complex plans.

Film	Criterion	Standard Plan Irradiation	Complex Plan Irradiation
		MLC 2 mm out, one bank	
		Differences in Pixels Passing from Baseline	
Axial	7%/4mm	18.0%	17.9%
	5%/3mm	-6.0%	-9.2%
Sagittal	7%/4mm	11.3%	8.7%
	5%/3mm	-4.1%	-6.9%

Table 60: Average absolute differences from baseline in gamma analysis results for axial and sagittal films within the phantom for the second irradiation set with systematic MLC positional errors of 2 mm in one bank for standard and complex plans.

Standard Phantom Treatment Plan: MLC Position Axial Film, 5%/3mm

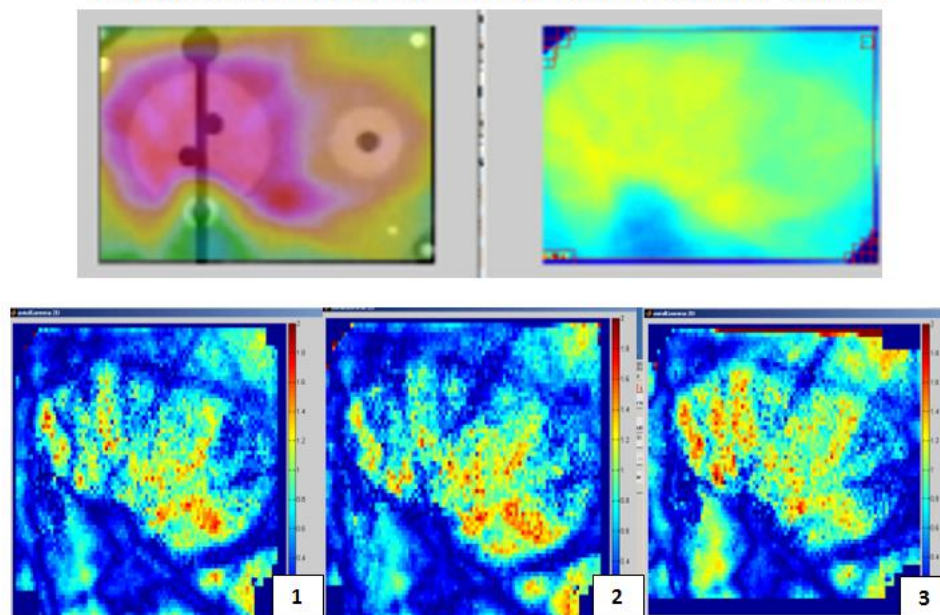


Figure 80: Axial film dose distributions from the TPS (upper left), film from one irradiation (upper right), and the gamma maps (5%/3mm) from this film for the three irradiations of the phantom with the standard treatment plan with the MLC shifted out 2 mm in one bank(bottom).

Standard Phantom Treatment Plan: MLC Position Sagittal Film, 5%/3mm

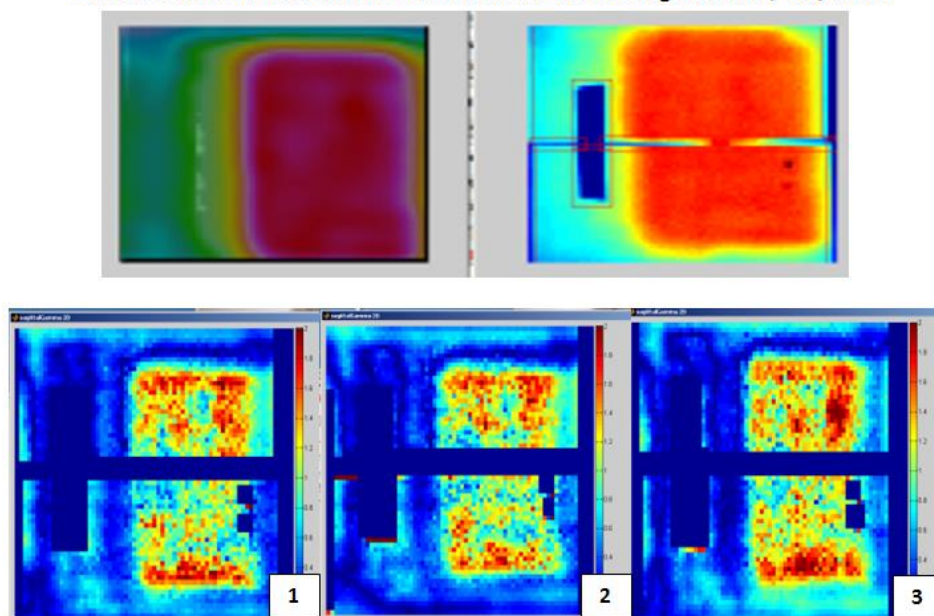


Figure 81: Sagittal film dose distributions from the TPS (upper left), film from one irradiation (upper right), and the gamma maps (5%/3mm) from this film for the three irradiations of the phantom with the standard treatment plan with the MLC shifted out 2 mm in one bank (bottom).

Complex Phantom Treatment Plan: MLC Position Axial Film, 5%/3mm

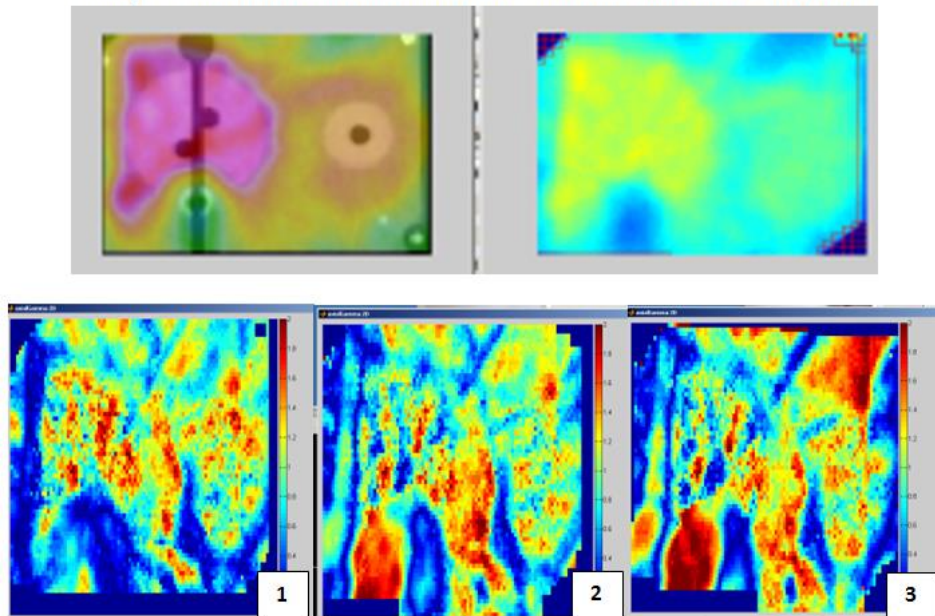


Figure 82: Axial film dose distributions from the TPS (upper left), film from one irradiation (upper right), and the gamma maps (5%/3mm) from this film for the three irradiations of the phantom with the complex treatment plan with the MLC shifted out 2 mm in one bank (bottom).

Complex Phantom Treatment Plan: MLC Position Sagittal Film, 5%/3mm

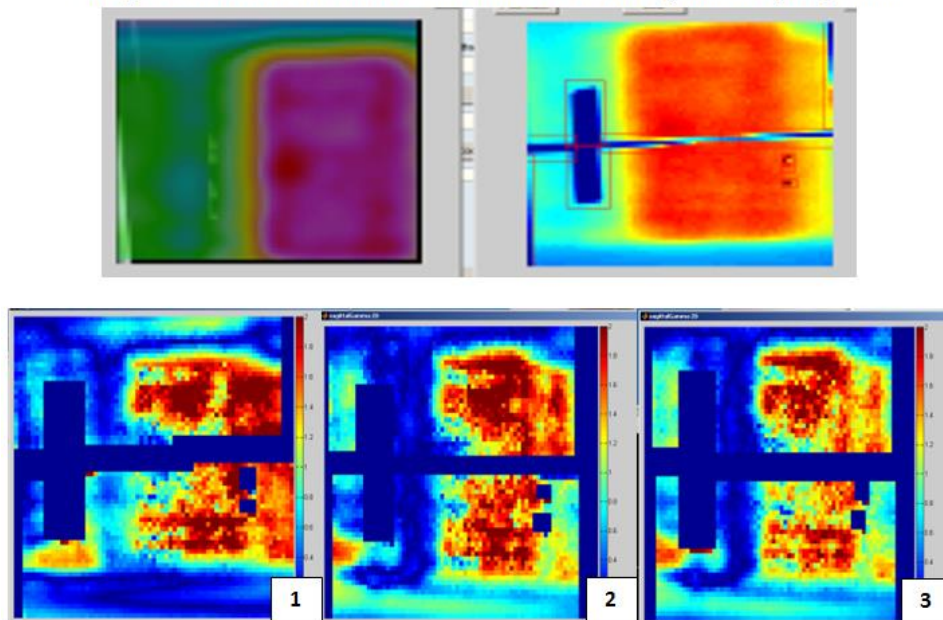


Figure 83: Sagittal film dose distributions from the TPS (upper left), film from one irradiation (upper right), and the gamma maps (5%/3mm) from this film for the three irradiations of the phantom with the complex treatment plan with the MLC shifted out 2 mm in one bank (bottom).

The differences seen in this second set of MLC positional error measurement should have corresponded well to the treatment planning studies since the treatment plan used was the same and the

errors simulated were the same. However, we did not see quite as large of differences in our measured doses as we did in the treatment planning studies, particularly in the PTVs. Outward motion of the leaves did not affect the PTVs as extremely as inward motion in the treatment planning studies, and so our ability to see those PTV changes were limited since we only performed measurements with outward motion. Differences between our treatment planning studies and measurements may also have been due to the fact that the TLD only measured the dose to a small volume and therefore were unable to capture the volumetric effects of this failure mode. The differences seen in the film were large, but the role of the MLC shift was not immediately obvious. That was likely due to the modulation effects discussed.

MLC position phantom studies summary

Systematic changes in the MLC positions in our treatment planning studies primarily showed changes in the dose to the spinal cord, with the maximum dose increasing with outward (positive) leaf displacement up to 8%. Inward displacement of one bank of leaves reduced structure doses as would be expected, with under-dosing of the PTVs up to 20% in the standard treatment plan. One may have expected the complex plan to have larger errors since there were more segments and therefore more MLC positions to change, but it may have been the case that there was more wash out of these errors with the more complex plan. Our measurements were limited to outward displacement of the leaves, and with 2 mm systematic shifts in one bank, the increased dose to the spinal cord as measured by the TLD was about 5-7%, which is comparable to what we saw in the treatment planning studies. The severity score of 8 is supported by both treatment planning studies and measurements with up to 2 mm systematic displacement in one bank of leaves.

Failure mode 4: Gantry Angle

Treatment planning study results

The resultant changes in the phantom structure doses used for severity scoring from 2° changes in the gantry angle are summarized in Table 61 and Table 62 for standard and complex phantom plans,

respectively. In the standard phantom treatment plan, a positive 2° change in the gantry angle only resulted in up almost 1% decrease PTV coverage, while a negative 2° change increased the maximum dose to the spinal cord by almost 12%. In the complex treatment plan, a positive 2° change in the gantry angle resulted in an increase in the spinal cord maximum dose of almost 8.5%, while a negative 2° change resulted in a decrease in D_{99%} for the primary PTV of about 2.5%. As a result of the increase in the maximum spinal cord dose in the standard treatment plan with a negative 2° change in gantry angle, the severity score for this failure mode is 7.

Standard Phantom Treatment Plan			
Structure	Evaluation criteria	+ 2 degrees	-2 degrees
		Change from baseline	
Primary PTV	D _{95%}	-0.27%	-0.04%
	D _{99%}	-0.93%	0.02%
Secondary PTV	D _{95%}	0.08%	-0.09%
	D _{99%}	0.02%	-0.19%
Spinal Cord	Max Dose	-5.91%	11.69%
Normal Tissue	Max Dose	0.11%	0.14%

Table 61: Dosimetric changes from baseline used for severity scoring for gantry angle changes of +2° and -2° for the standard phantom treatment plan.

Complex Phantom Treatment Plan			
Structure	Evaluation criteria	+ 2 degrees	-2 degrees
		Change from baseline	
Primary PTV	D _{95%}	-0.29%	-0.44%
	D _{99%}	-1.32%	-2.39%
Secondary PTV	D _{95%}	0.17%	0.18%
	D _{99%}	0.79%	0.78%
Spinal Cord	Max Dose	8.43%	-3.22%
Normal Tissue	Max Dose	-0.79%	0.00%

Table 62: Dosimetric changes from baseline used for severity scoring for gantry angle changes of +2° and -2° for the complex phantom treatment plan.

The DVHs for gantry angle errors of 2° are shown in Figure 84 and Figure 85 for standard and complex phantom treatment plans, respectively. The spinal cord dose is the primary structure affected by this failure mode, with increases in the overall dose then the gantry was rotated +2° in the standard plan and decreases in the overall dose when the gantry was rotated -2° in the standard plan. In the complex plan, the -2° rotation of the gantry had minimal effects on the spinal cord dose, but the +2° rotation

increased the overall cord dose. These spinal cord dose changes were supportive of the dosimetric changes seen at our evaluation criteria.

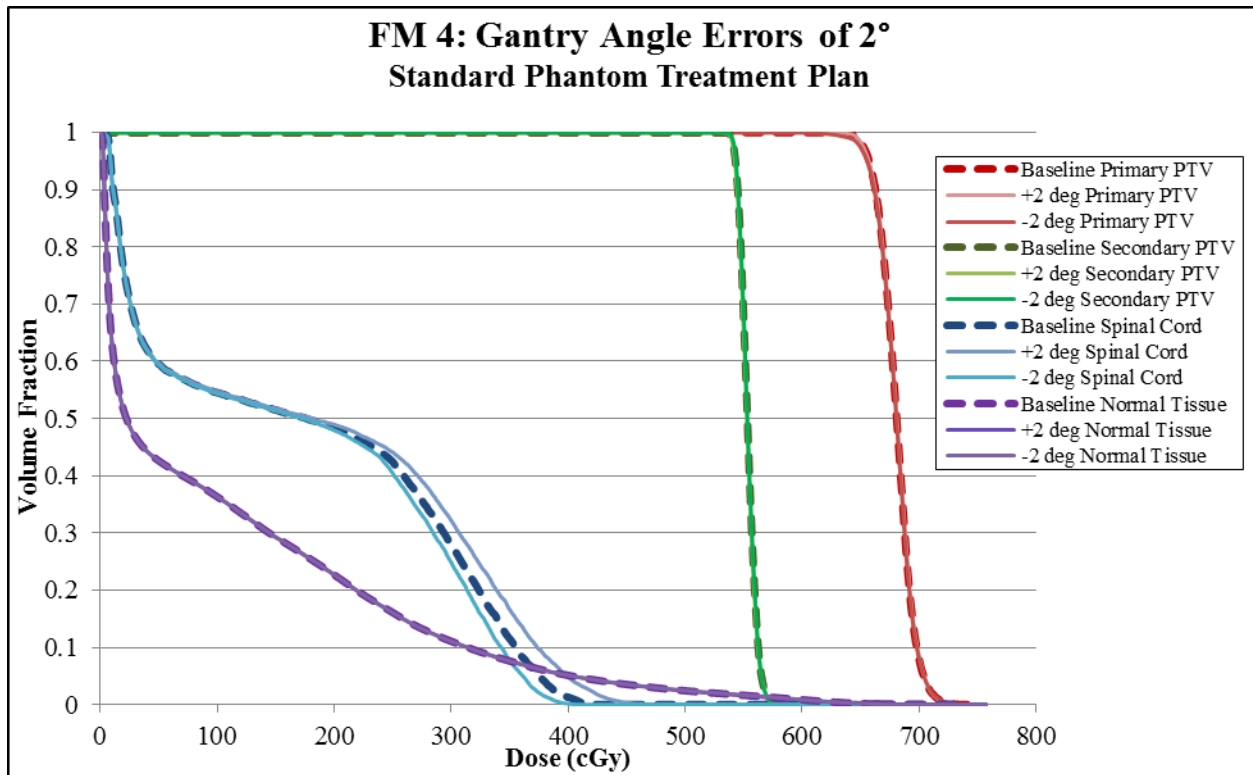


Figure 84: DVHs for phantom structures in the standard treatment plan with gantry angle errors of 2°, with dashed lines showing baseline DVHs.

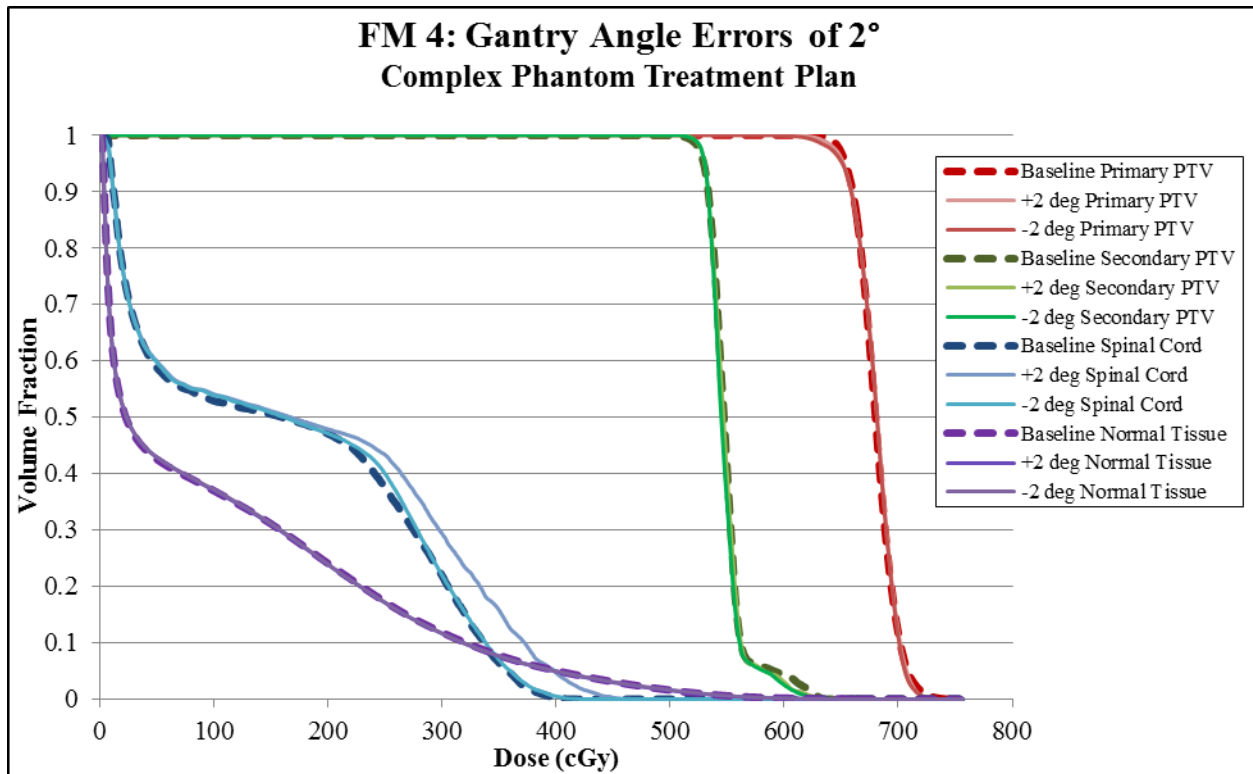


Figure 85: DVHs for phantom structures in the complex treatment plan with gantry angle errors of 2°, with dashed lines showing baseline DVHs.

Gantry angle changes slightly moved all of the structures we investigated, but since the spinal cord is located near a steep dose gradient, changes were most evident there. In the case of the standard plan, the shape of dose distribution around the spinal cord, gantry rotation in the positive direction resulted in the cord entering the steep dose gradient between it and the primary PTV. The other side of the spinal cord had more room to spare before entering the steep dose gradient, which was why the dose decreased with the negative gantry rotation. This is demonstrated in Figure 86. The complex plan had a similar effect with the positive gantry rotation, but due to the shape of the dose distribution in the sparing region, the negative rotation only managed to maintain the cord position within the sparing region and not move it away further from the gradient, therefore keeping the dose about the same.

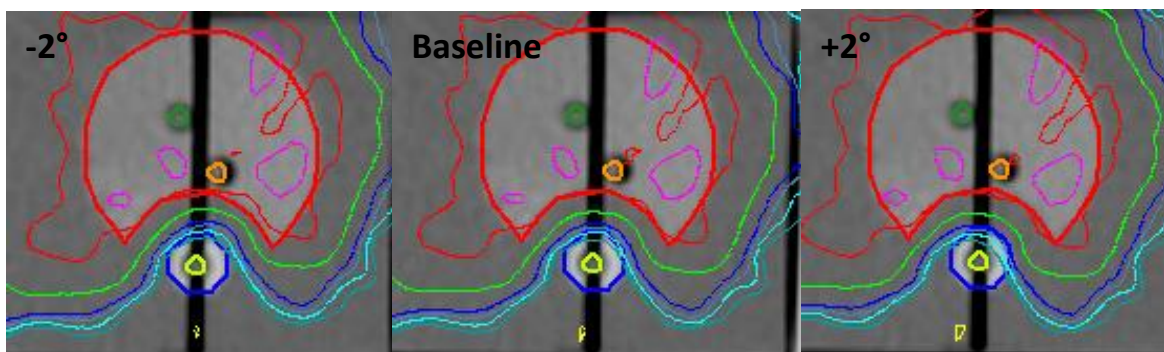


Figure 86: Axial image of phantom primary PTV (red) and spinal cord OAR (blue) with standard treatment plan dose distributions: Gantry angle -2° (left), baseline plan (center) and gantry angle $+2^\circ$ (right). Isodose values are shown in the upper left corner.

Physical measurement results

Gantry angle error measurements: Irradiation set #3

The average differences in the doses measured to the phantom TLD for the three irradiations with gantry errors of $+2^\circ$ for each beam from the baseline irradiation for the third irradiation set are shown in Table 63 where a positive difference indicates that the failure mode dose was higher than the baseline dose. On average, the primary PTV TLD doses decreased from baseline by -2.6% . The secondary PTV TLD did not change much from baseline, decreasing only -0.4% . Similarly, the spinal cord TLD dose barely changed from baseline, with an average of 0.1% .

There was no difference in the DTA between the primary PTV and OAR on the axial film. The differences in the percent of pixels passing gamma analysis with $7\%/4\text{mm}$ and $5\%/3\text{mm}$ criteria are shown in Table 64. The corresponding gamma maps are shown in Figure 87 and Figure 88 with the $5\%/3\text{mm}$ criteria to accentuate failure regions. The percent of pixels passing a $7\%/4\text{mm}$ gamma analysis on the axial film decreased -10.2% from baseline and on the sagittal film it decreased -8.7% . The failures on the gamma maps with gantry angle errors were most in the PTV regions and appeared to have a similar shape to the failures on the gamma maps of the baseline plan for this irradiation set which included a line of less failure where the dose to the primary PTV dropped off to the dose of the secondary PTV. The sagittal films showed increased failure focused in the PTV and distributed more throughout the PTV than

in the baseline sagittal films for this irradiation set, which had failures along the superior and inferior edges of the PTV.

Structure	TLD position	+2° Gantry Angle
		Difference in Dose from Baseline
Primary PTV	Superior Anterior	-2.2%
Primary PTV	Inferior Anterior	-1.8%
Primary PTV	Superior Posterior	-2.3%
Primary PTV	Inferior Posterior	-3.9%
Secondary PTV	Superior	-0.8%
Secondary PTV	Inferior	-0.0%
Spinal Cord	Superior	-0.3%
Spinal Cord	Inferior	0.4%

Table 63: Average TLD differences from baseline from the third irradiation set with gantry angle errors of +2°.

Film	Criterion	+2°
		Absolute Difference in Pixels Passing from Baseline
Axial	7%/4mm	-10.2%
	5%/3mm	-24.0%
Sagittal	7%/4mm	-8.7%
	5%/3mm	-19.6%

Table 64: Average absolute differences from baseline in gamma analysis results for axial and sagittal films within the phantom for the third irradiation set with gantry angle errors of +2°.

Standard Phantom Treatment Plan: Gantry Angle +2° Axial Film, 5%/3mm

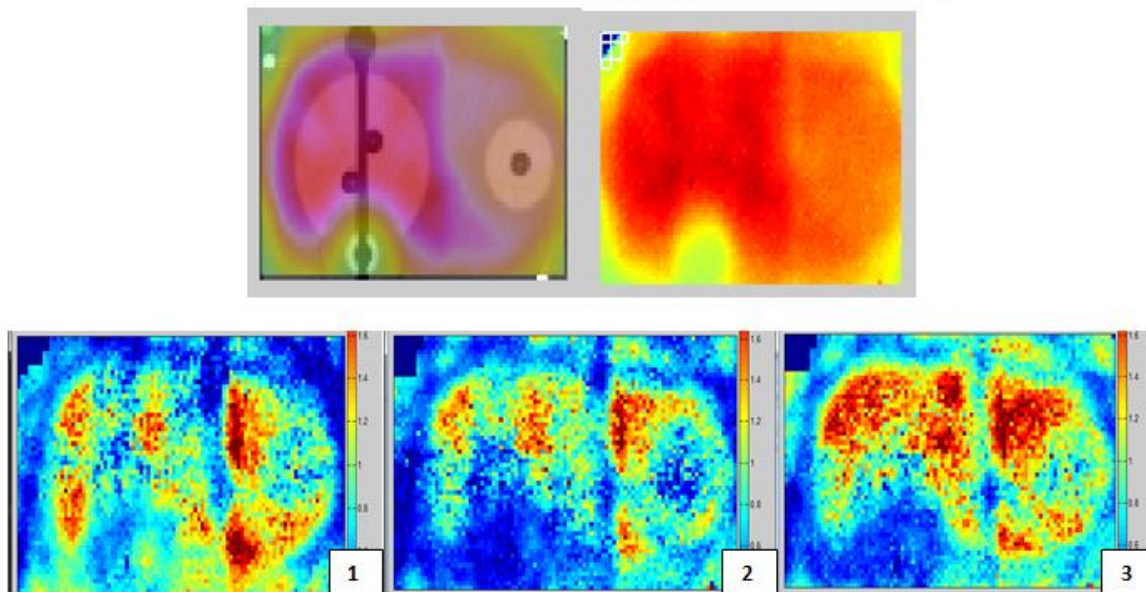


Figure 87: Axial film dose distributions from the TPS (upper left), film from one irradiation (upper right), and the gamma maps (5%/3mm) from this film for the three irradiations of the phantom with the standard treatment plan with the gantry rotated +2° (bottom).

Standard Phantom Treatment Plan: Gantry Angle +2° Sagittal Film, 5%/3mm

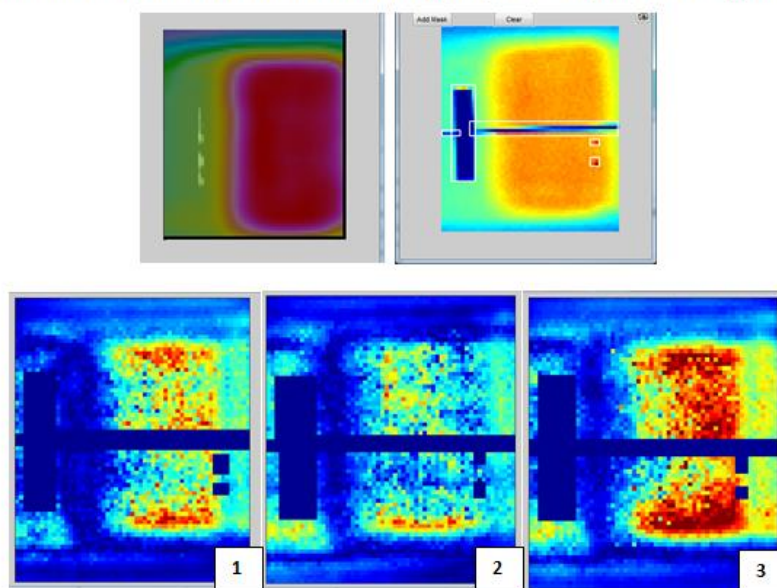


Figure 88: Sagittal film dose distributions from the TPS (upper left), film from one irradiation (upper right), and the gamma maps (5%/3mm) from this film for the three irradiations of the phantom with the standard treatment plan with the gantry rotated +2° (bottom).

Overall, the doses to the TLDs with +2° rotation of the gantry were decreased from baseline. Based on the treatment planning studies, we expected an increase in the spinal cord dose but this was not the case. This was likely due to the central location of the TLD within the spinal cord structure. The changes in dose to the spinal cord dose mostly occurred along the left edge when it entered the steep dose gradient or moved away from it in the treatment planning studies. The decrease in the primary PTV TLD doses was due to slight overall changes in the dose distribution from the gantry rotation and corresponded to very small losses in coverage of the targets in the treatment planning studies. These changes were well demonstrated on the axial film gamma maps, which showed failure concentrated in the PTVs. We would perhaps expect to see increasing failure with off-axis distance on the axial film since that would correspond to a larger displacement when the gantry was rotated. This was not evident on the axial film gamma maps, which captured such a small region that was dominated by high doses. The doses further off-axis rapidly fell off to more homogeneous low doses that were not as affected by the gantry rotation.

Gantry angle phantom studies summary

Systematic changes in the gantry angles in our treatment planning studies primarily showed changes to the spinal cord dose with an increase in the standard plan maximum cord dose of 12% with -2° gantry angle error and the complex plan maximum cord dose of 8% with $+2^\circ$ gantry angle error. There was also a slight reduction in primary PTV coverage with the $+2^\circ$ gantry angle error. Reduced dose to the primary PTV of up to 4% was the largest change observed in our measurements. Other TLD doses changed very little from baseline, including the spinal cord doses which the treatment planning studies showed to have large positive differences. The severity score of 7, resultant of the treatment planning studies, was higher than expected based on absolute dose measurements, however it was likely that the maximum spinal cord dose had a large change closer to the primary PTV where the dose is changing quickly as opposed to at the center of the cord where the TLD are located. This reflects the potential advantages of volumetric data when assessing these changes. Overall the treatment planning studies and measurements generally agree.

Failure mode 5: Collimator Angle

Treatment planning study results

The resultant changes in the phantom structure doses used for severity scoring from 2° changes in the collimator angle are summarized in Table 65 and Table 66 for standard and complex phantom plans, respectively. All structure evaluation criteria had below a 2% change from baseline for the standard phantom treatment plan, with all changes being negative with the exception of normal tissue maximum dose. The largest change in the standard plan with $+2^\circ$ collimator rotation was 1.46% increase in the maximum dose to the normal tissue. The largest change in the standard plan with -2° collimator rotation was 1.51% decrease in the dose to 99% of the secondary PTV. In the complex treatment plan, a positive 2° change in the collimator angle resulted in an increase in the spinal cord maximum dose of almost 7.5%. Other changes were all less than 2% for this collimator rotation in the complex plan with small decreases in the primary PTV coverage and increases in the secondary PTV coverage. A negative 2°

change in the collimator angle resulted in an under-dose to 99% of the secondary PTV of the complex plan of almost 3%. The coverage of the secondary PTV also decreased, up to -1.2%, and the dose to the spinal cord decreased over 3%. As a result of the increase in the maximum spinal cord dose in the complex plan with +2° collimator rotation, the severity score for this failure mode was 5.

Standard Phantom Treatment Plan			
Structure	Evaluation criteria	+ 2 degrees	- 2 degrees
		Change from baseline	
Primary PTV	D _{95%}	-0.33%	-0.22%
	D _{99%}	-0.32%	-0.64%
Secondary PTV	D _{95%}	-0.37%	-0.51%
	D _{99%}	-0.54%	-1.51%
Spinal Cord	Max Dose	-0.33%	-0.27%
Normal Tissue	Max Dose	1.46%	0.56%

Table 65: Dosimetric changes from baseline used for severity scoring for collimator angle changes of +2° and -2° for the standard phantom treatment plan.

Complex Phantom Treatment Plan			
Structure	Evaluation criteria	+ 2 degrees	- 2 degrees
		Change from baseline	
Primary PTV	D _{95%}	-0.59%	-0.91%
	D _{99%}	-1.13%	-2.87%
Secondary PTV	D _{95%}	0.81%	-1.15%
	D _{99%}	1.46%	-1.20%
Spinal Cord	Max Dose	7.44%	-3.33%
Normal Tissue	Max Dose	1.60%	1.26%

Table 66: Dosimetric changes from baseline used for severity scoring for collimator angle changes of +2° and -2° for the complex phantom treatment plan.

The DVHs for collimator angle errors of 2° are shown in Figure 89 and Figure 90 for standard and complex phantom treatment plans, respectively. DVHs for the standard phantom treatment showed little to no change from baseline. The spinal cord dose increase in the complex treatment plan with +2° collimator rotation was evident, as was some slight loss of coverage in the PTVs. There also appeared to be an increase in the spinal cord dose for the complex plan with -2° collimator rotation, which was not what we observed in our dosimetric evaluation criteria, however the DVH for the spinal cord with -2° collimator rotation is slightly more steep and therefore didn't result in an increase in the maximum spinal cord dose.

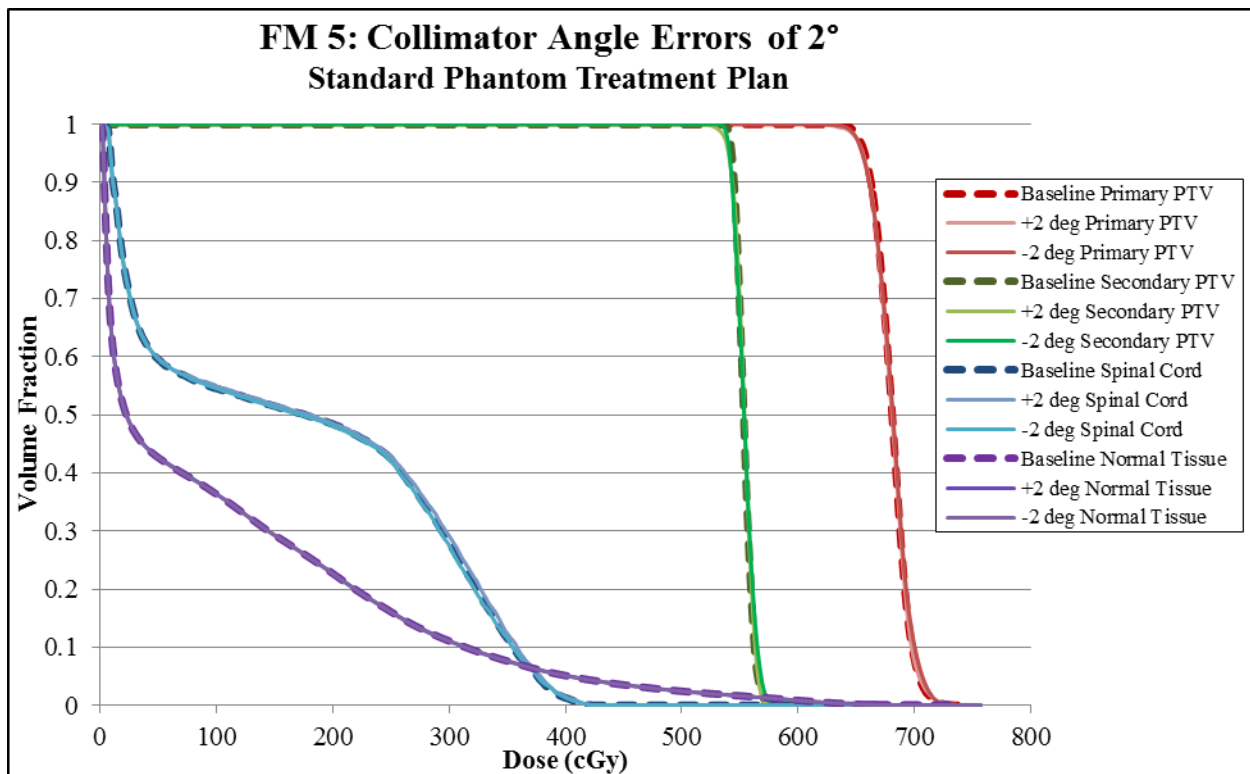


Figure 89: DVHs for phantom structures in the standard treatment plan with collimator angle errors of 2°, with dashed lines showing baseline DVHs.

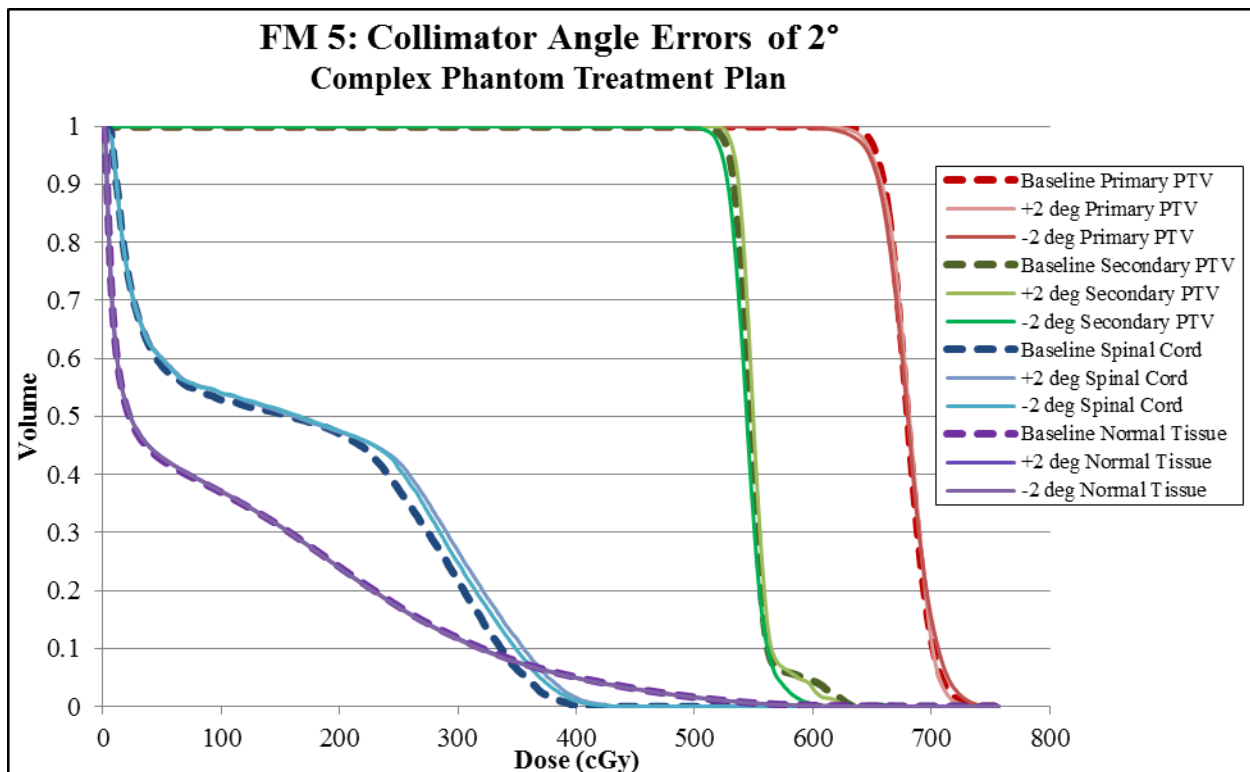


Figure 90: DVHs for phantom structures in the complex treatment plan with collimator angle errors of 2°, with dashed lines showing baseline DVHs.

Rotating the collimator by 2° did not result in very large changes in the dose to the phantom structures or the overall dose distribution. Small systematic rotational errors in the collimator would be expected to smear the dose distribution since opposing beams would have been rotated opposite each other. The maximum change of 7.4% increase in the maximum spinal cord dose in the complex plan was a result of the spinal cord coming just close enough to the steep dose gradient between it and the primary PTV that the maximum dose increased from around 425 cGy to almost 460 cGy, just outside of the tolerance criteria. This maximum dose was only over a very small volume and is difficult to see in the treatment plan. This emphasized that even very small changes that were not immediately obvious had the potential to threaten our goals, specifically critical structure sparing when they were immediately adjacent to our targets.

Physical measurement results

Collimator angle error measurements: Irradiation set #3

The average differences in the doses measured to the phantom TLD for the three irradiations with collimator angle errors of +2° for each beam from the baseline irradiation for the third irradiation set are shown in Table 63 where a positive difference indicates that the failure mode dose was higher than the baseline dose. Differences from the baseline were mostly negative, with a decrease in the primary PTV TLD of -1.4% on average. The dose to the TLD in the secondary PTV decreased by -0.3% on average and the dose to the spinal cord TLD decreased by -1.2% on average. The average DTA between the primary PTV and OAR on the axial film was 0.3 mm larger for the irradiations with the collimator angle adjusted by +2°.

The differences in the percent of pixels passing gamma analysis with 7%/4mm and 5%/3mm criteria are shown in Table 64. The corresponding gamma maps with are shown in Figure 91 and Figure 92, with 5%/3mm criteria to make failures more visible. The percent of pixels passing the gamma analysis changed very little from baseline, with a decrease of only -0.3% on the axial film and -1.8% on the

sagittal film, both with 7%/4mm criteria. Distribution of failure on the axial film gamma maps followed a similar pattern to the baseline measurements for this irradiation set, with failures mostly in the PTVs and along the posterior edge of the film. On the sagittal films, the failure was focused along the superior and inferior edges of the PTV as in the baseline, but were greater and more dense.

Structure	TLD position	+2° Collimator Angle
		Difference in Dose from Baseline
Primary PTV	Superior Anterior	-0.1%
Primary PTV	Inferior Anterior	0.3%
Primary PTV	Superior Posterior	-0.5%
Primary PTV	Inferior Posterior	-1.1%
Secondary PTV	Superior	-0.6%
Secondary PTV	Inferior	-0.0%
Spinal Cord	Superior	-1.1%
Spinal Cord	Inferior	-1.3%

Table 67: Average TLD differences from baseline from the third irradiation set with collimator angle errors of +2°.

Film	Criterion	+2° Collimator Angle
		Absolute Difference in Pixels Passing from Baseline
Axial	7%/4mm	-0.3%
	5%/3mm	-0.7%
Sagittal	7%/4mm	-1.8%
	5%/3mm	-4.7%

Table 68: Average absolute differences from baseline in gamma analysis results for axial and sagittal films within the phantom for the third irradiation set with collimator angle errors of +2°.

Standard Phantom Treatment Plan: Collimator Angle +2° Axial Film, 5%/3mm

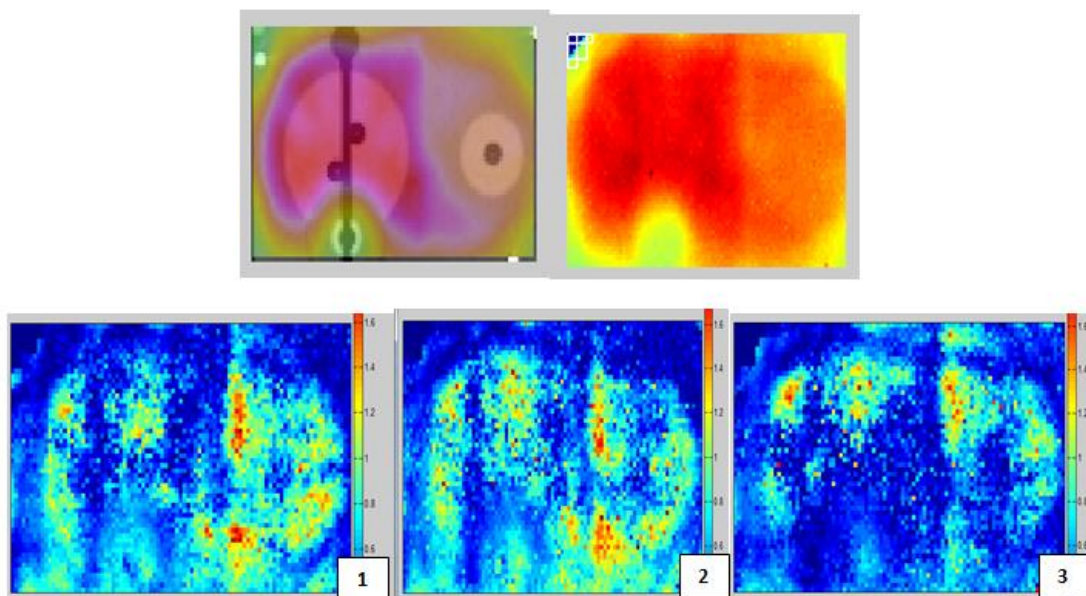


Figure 91: Axial film dose distributions from the TPS (upper left), film from one irradiation (upper right), and the gamma maps (5%/3mm) from this film for the three irradiations of the phantom with the standard treatment plan with the collimator rotated +2° (bottom).

Standard Phantom Treatment Plan: Collimator Angle +2° Sagittal Film, 5%/3mm

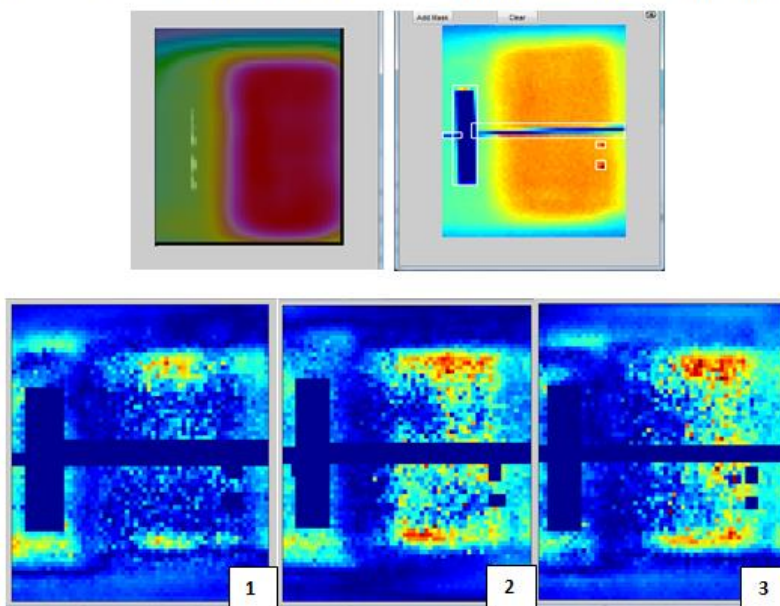


Figure 92: Sagittal film dose distributions from the TPS (upper left), film from one irradiation (upper right), and the gamma maps (5%/3mm) from this film for the three irradiations of the phantom with the standard treatment plan with the collimator rotated +2° (bottom).

We saw very small changes in the doses to the TLD for our measurements with systematic collimator angle rotations of +2°. This was consistent with our treatment planning studies for a standard

phantom treatment plan. As shown on the gamma maps, there were some changes to the doses within the PTVs on the axial films, but since this plane was very close to isocenter and is always perpendicular to the plane of the collimator, a small rotation of the collimator would not be expected to affect the dose much. Most notably we saw an increase in failure along the superior and inferior edges of the PTV on the sagittal films. These failures were caused by the collimator rotation because the sagittal plane was parallel to the collimator for some gantry angles and these edges were collimated by the jaw. Similar changes along the anterior and posterior edges of the PTV on this film were not seen because the MLC were responsible for the collimation and with modulation the dose errors were smeared.

Collimator angle phantom studies summary

Systematic changes in the collimator angles in our treatment planning studies primarily showed changes in the complex treatment plan, with an increase in the spinal cord maximum dose of almost 3% with -2° collimator angle error and over 7% with $+2^\circ$ gantry angle error. There was also a small reduction in PTV coverage, more so with the -2° gantry angle error. Small reductions in the primary PTV doses were observed in our measurements, as were small reductions in the dose to the spinal cord. The measurements were performed using a standard treatment plan and were consistent with the results of the treatment planning studies on the standard treatment plan. The changes to the dose distributions measured by the film were small but consistent with the effects expected of small collimator rotations. The severity score of 5 from the complex plan treatment planning study represented a more conservative estimate of failure mode consequences than we saw in the measurements which was appropriate since the treatment planning studies included different plans that were affected in different ways.

Failure mode 6: Couch Angle

Treatment planning study results

The resultant changes in the phantom structure doses used for severity scoring from 2° changes in the couch angle are summarized in Table 69 and Table 70 for standard and complex phantom plans,

respectively. All structure evaluation criteria had below a 2.5% change from baseline for the standard phantom treatment plan, with the largest changes being increases of 2.4% and 1.6% in the spinal cord maximum dose for couch rotations of +2° and -2°, respectively. Changes in the PTVs for the standard plan with couch angle errors were all less than 0.2%. In the complex treatment plan, a positive 2° change in the couch angle resulted in an under-dose to 99% of the secondary PTV of almost 6% and an increase in the spinal cord maximum dose of over 6%. A negative 2° change in the couch angle resulted in an under-dose to 99% of the primary PTV of almost 6%. Other changes in the complex plan were all less than 1.5%. As a result of these under-doses and the increase in spinal cord maximum dose, the severity score for this failure mode was 4.

Standard Phantom Treatment Plan			
Structure	Evaluation criteria	+ 2 degrees	- 2 degrees
		Change from baseline	
Primary PTV	D _{95%}	-0.06%	-0.06%
	D _{99%}	0.03%	-0.16%
Secondary PTV	D _{95%}	0.06%	-0.06%
	D _{99%}	0.04%	-0.17%
Spinal Cord	Max Dose	2.43%	1.56%
Normal Tissue	Max Dose	0.24%	-0.02%

Table 69: Dosimetric changes from baseline used for severity scoring for couch angle changes of +2° and -2° for the standard phantom treatment plan.

Complex Phantom Treatment Plan			
Structure	Evaluation criteria	+ 2 degrees	- 2 degrees
		Change from baseline	
Primary PTV	D _{95%}	0.11%	-0.54%
	D _{99%}	0.00%	-5.91%
Secondary PTV	D _{95%}	0.09%	0.26%
	D _{99%}	-5.94%	1.11%
Spinal Cord	Max Dose	6.35%	-1.36%
Normal Tissue	Max Dose	-0.07%	-0.03%

Table 70: Dosimetric changes from baseline used for severity scoring for couch angle changes of +2° and -2° for the complex phantom treatment plan.

The DVHs for couch angle errors of 2° are shown in Figure 93 and Figure 94 for standard and complex phantom treatment plans, respectively. There were very minimal changes in the structure doses in the standard phantom treatment plan. An increase in the dose to the spinal cord and small dips in the PTV coverage were evident in the complex plan DVHs.

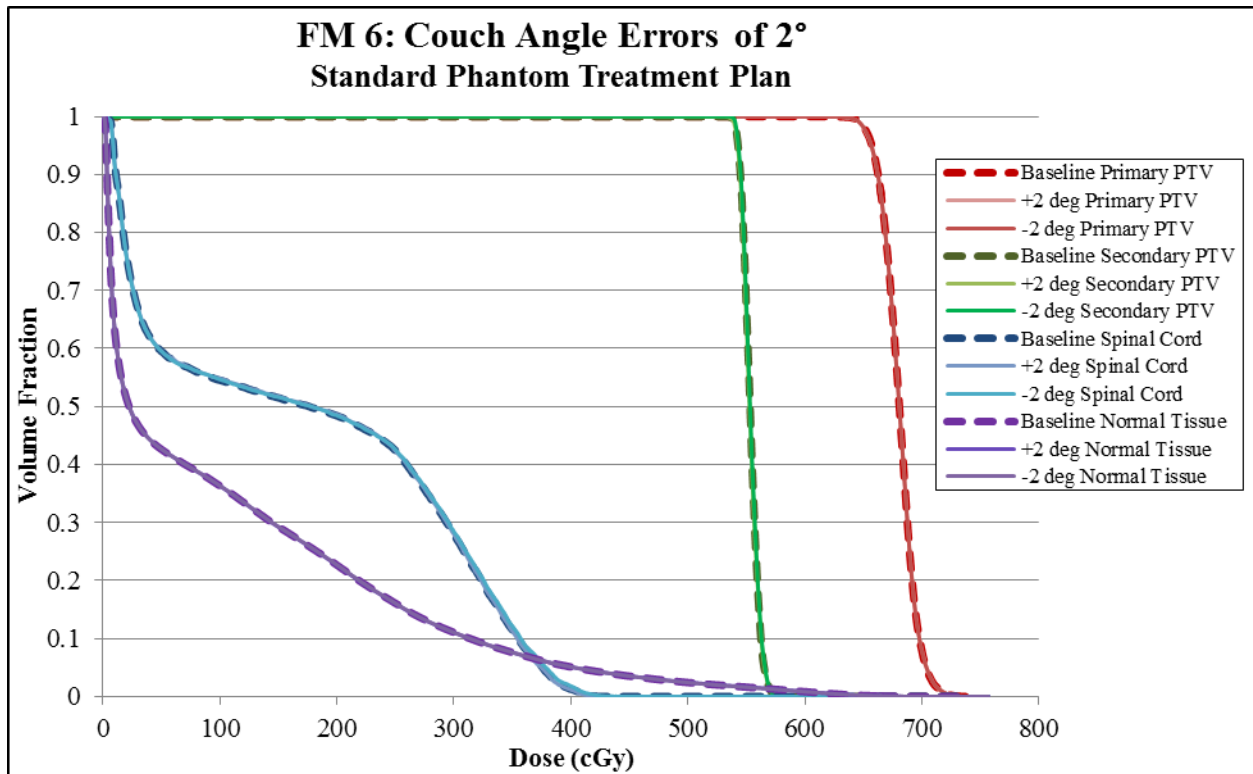


Figure 93: DVHs for phantom structures in the standard treatment plan with couch angle errors of 2°, with dashed lines showing baseline DVHs.

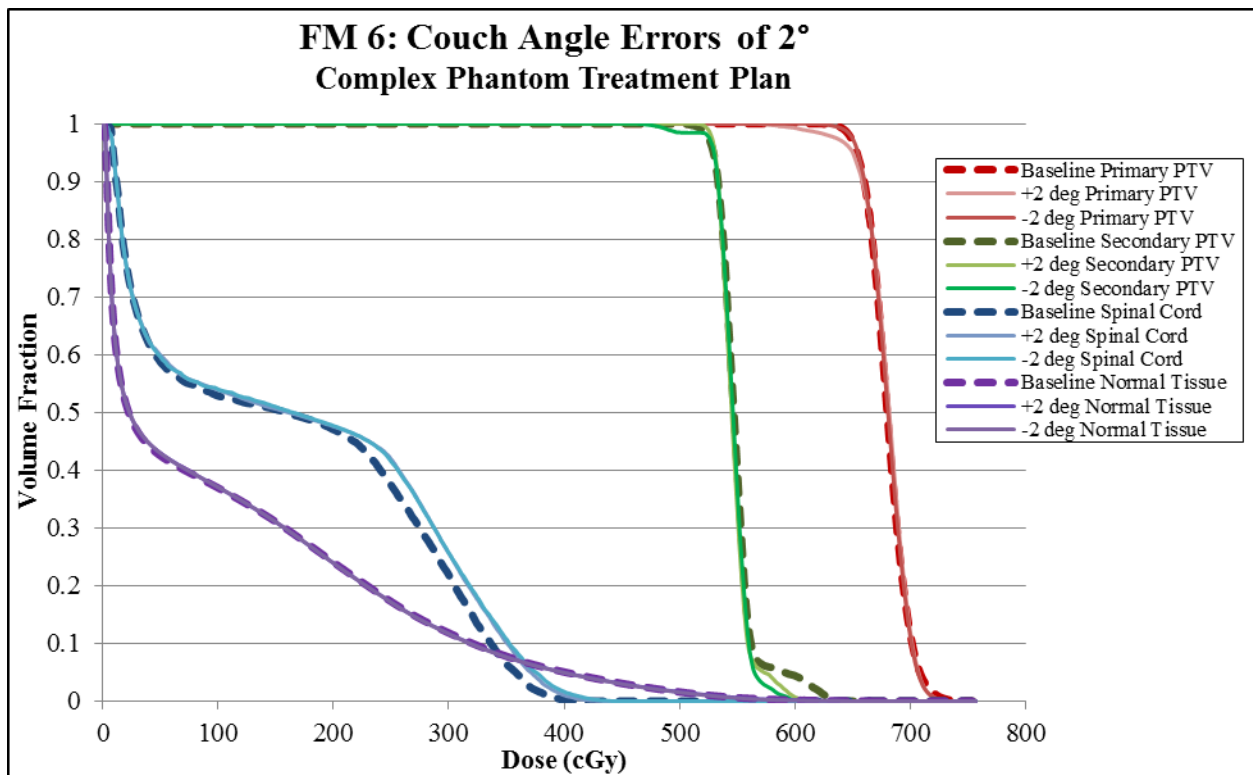


Figure 94: DVHs for phantom structures in the complex treatment plan with couch angle errors of 2°, with dashed lines showing baseline DVHs.

Overall, changing the couch angle by 2° primarily showed changes in the dose to the spinal cord. This was similar to the gantry angle and collimator angle failure modes, which all resulted in slight movement of the spinal cord with respect to the steep dose gradient required to spare it from the adjacent primary PTV dose. There was also some loss of coverage in the secondary PTV with the $+2^\circ$ rotation, which was a result of the orientation of dose distribution on the targets being just slightly different such as in Figure 95. Similarly with the -2° rotation, a slight decrease in primary PTV coverage occurred.

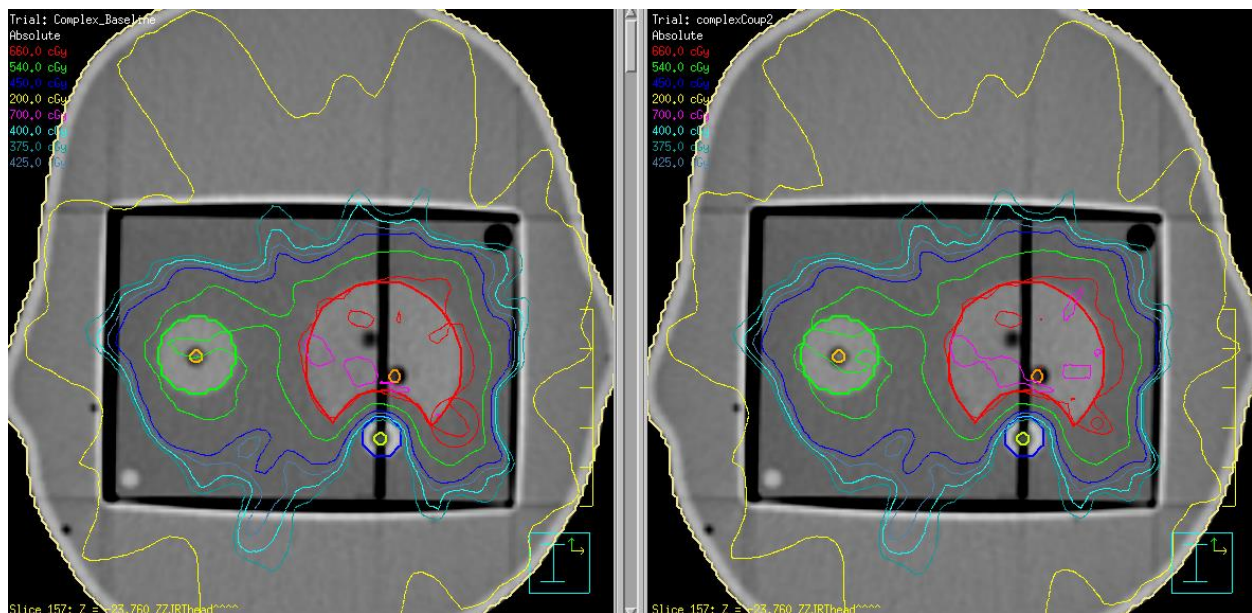


Figure 95: Axial images of the phantom with the complex treatment plan dose distribution: baseline (left) and with the couch rotated $+2^\circ$.

Physical measurement results

Couch angle error measurements: Irradiation set #3

The average differences in the doses measured to the phantom TLD for the three irradiations with couch angle errors of $+2^\circ$ for each beam from the baseline irradiation for the third irradiation set are shown in Table 71 where a positive difference indicates that the failure mode dose was higher than the baseline dose. On average, the dose to the primary PTV TLD changed from baseline by -0.35% . The secondary PTV TLD doses also had minimal changes, on average -0.3% . The dose to the spinal cord TLD decreased from baseline by -1.2% on average. There was no difference in the DTA between the primary

PTV and OAR on the axial film. The absolute differences in the percent of pixels passing gamma analysis with 7%/4mm and 5%/3mm criteria are shown in Table 72. The corresponding gamma maps are shown in Figure 96 and Figure 97. The percent of pixels passing gamma analysis with 7%/4mm criteria changed less than 1% on the axial film and reduced -3.4% from baseline on the sagittal film. The axial film gamma maps had failures mostly in the PTVs, though the distributions, especially on films 2 and 3, were different than those from the baseline gamma maps with less failure overall and more failure on the anterior side of the film. Failures on the sagittal films were distributed throughout the PTV and were more concentrated on the inferior edge of the PTV.

Structure	TLD position	+2° Couch Angle
		Difference in Dose from Baseline
Primary PTV	Superior Anterior	-0.1%
Primary PTV	Inferior Anterior	0.3%
Primary PTV	Superior Posterior	-0.5%
Primary PTV	Inferior Posterior	-1.1%
Secondary PTV	Superior	-0.6%
Secondary PTV	Inferior	-0.0%
Spinal Cord	Superior	-1.1%
Spinal Cord	Inferior	-1.3%

Table 71: Average TLD differences from baseline from the third irradiation set with couch angle errors of +2°.

Film	Criterion	+2° Couch Angle
		Absolute Difference in Pixels Passing from Baseline
Axial	7%/4mm	0.8%
	5%/3mm	3.9%
Sagittal	7%/4mm	-3.4%
	5%/3mm	-9.2%

Table 72: Average absolute differences from baseline in gamma analysis results for axial and sagittal films within the phantom for the third irradiation set with couch angle errors of +2°.

Standard Phantom Treatment Plan: Couch Angle +2° Axial Film, 5%/3mm

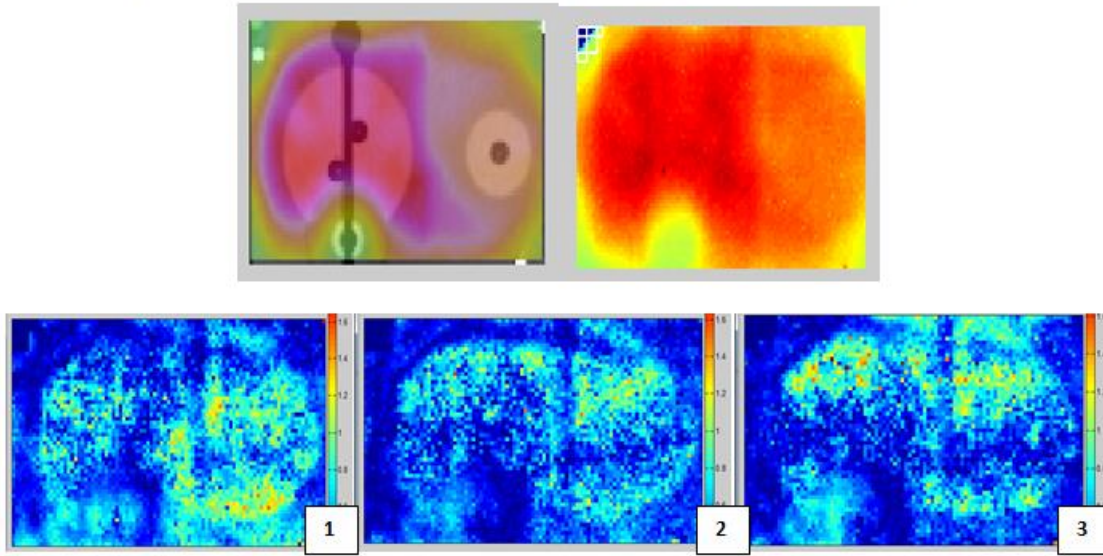


Figure 96: Sagittal film dose distributions from the TPS (upper left), film from one irradiation (upper right), and the gamma maps (5%/3mm) from this film for the three irradiations of the phantom with the standard treatment plan with the couch rotated +2° (bottom).

Standard Phantom Treatment Plan: Couch Angle +2° Sagittal Film, 5%/3mm

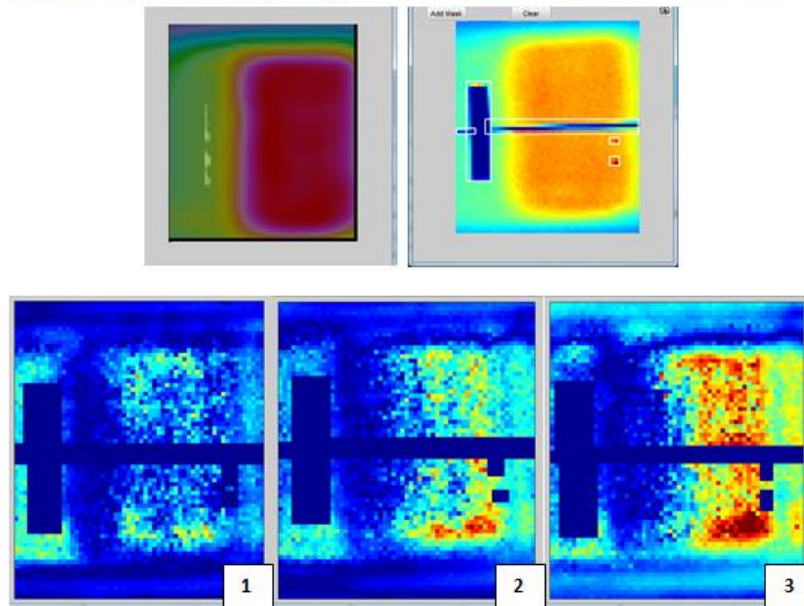


Figure 97: Sagittal film dose distributions from the TPS (upper left), film from one irradiation (upper right), and the gamma maps (5%/3mm) from this film for the three irradiations of the phantom with the standard treatment plan with the collimator rotated +2° (bottom).

The TLD dose differences from baseline did not reflect the changes we saw in the maximum dose to the spinal cord in our standard plan treatment planning studies. As with the other angular failure

modes, the lack of increase in the spinal cord was likely due to the central position of the TLD and the change in maximum spinal cord dose occurring on the edges near the steep dose gradient. The slight decreases in PTV coverage that we saw in the treatment planning studies were in the complex treatment plan and so they were not expected in the measurements and the changes we saw in the PTV TLD were very small. Similar to the collimator rotation, we expected small a rotation of the couch to effect the dose distribution on the axial films very little. Although there were slight changes to the distribution of the failures, this was likely within the uncertainty of the measurement. On the sagittal film, the change in the failures along the superior and inferior edge of the PTV was consistent with a small couch rotation.

Couch angle phantom studies summary

Systematic changes in the couch angles in our treatment planning studies primarily showed changes in the complex treatment plan, with a decrease in the secondary PTV coverage and an increase in the spinal cord maximum dose of almost 6% with $+2^\circ$ couch angle error and a decrease in primary PTV coverage of almost 6% with -2° couch angle error. The dose to the spinal cord in the standard plan increased slightly with either displacement of the couch angle. The measurements showed the opposite, with small decreases in the cord dose and primary PTV dose which was likely due to the location of the TLD. The changes seen in the standard treatment plan both through the treatment planning studies and the measurements were both comparably small overall, especially considering the uncertainty in the spinal cord TLD. The severity score of 4 from the complex plan treatment planning study was an appropriately conservative score considering the information we have.

Failure mode 7: MU linearity

Treatment planning study results

The resultant changes in the phantom structure doses used for severity scoring for the MU linearity error scenarios described in Table 13 are summarized in Table 73 and Table 74 for both standard and complex phantom plans, respectively. All structure evaluation criteria had below a 1% change from

baseline in the standard phantom treatment plan, with the maximum change from baseline of 0.56% occurring with the 3B scenario (-6% change in all MU ≤ 5) in the normal tissue maximum dose. That scenario had the largest changes in all dosimetric evaluation criteria of the 6 MU linearity scenarios. All structure evaluation criteria had below a 1.5% in the complex phantom treatment plan, with the largest difference from baseline being in the secondary PTV with the 3A scenario (+6% change in all MU ≤ 5). In the complex plan, this scenario had the largest changes from baseline for all dosimetric evaluation criteria. With these overall small errors, this failure mode was assigned a severity score of 1.

Standard Phantom Treatment Plan							
Structure	Evaluation criteria	1A	1B	2A	2B	3A	3B
		Change from baseline					
Primary PTV	D _{95%}	0.06%	0.00%	0.06%	0.00%	0.11%	0.33%
	D _{99%}	0.15%	0.00%	0.15%	0.00%	0.13%	0.32%
Secondary PTV	D _{95%}	0.11%	-0.01%	0.17%	-0.01%	0.27%	0.33%
	D _{99%}	0.06%	0.01%	0.21%	0.02%	0.20%	0.40%
Spinal Cord	Max Dose	0.15%	-0.01%	0.17%	-0.01%	0.40%	0.42%
Normal Tissue	Max Dose	0.09%	0.00%	0.13%	-0.01%	0.17%	0.56%

Table 73: Dosimetric changes from baseline used for severity scoring for six MU linearity error scenarios for the standard phantom treatment plan.

Complex Phantom Treatment Plan							
Structure	Evaluation criteria	1A	1B	2A	2B	3A	3B
		Change from baseline					
Primary PTV	D _{95%}	0.21%	-0.23%	0.17%	-0.19%	0.74%	0.03%
	D _{99%}	0.11%	-0.34%	0.14%	-0.15%	0.60%	-0.02%
Secondary PTV	D _{95%}	0.34%	-0.34%	0.36%	-0.31%	1.14%	-0.05%
	D _{99%}	0.35%	-0.17%	0.37%	-0.20%	1.11%	0.02%
Spinal Cord	Max Dose	0.26%	-0.29%	0.28%	-0.30%	0.79%	0.05%
Normal Tissue	Max Dose	0.15%	-0.17%	0.11%	-0.08%	0.60%	0.02%

Table 74: Dosimetric changes from baseline used for severity scoring for six MU linearity error scenarios for the complex phantom treatment plan.

The DVHs for the MU linearity errors are shown in Figure 98 and Figure 99 for standard and complex phantom treatment plans, respectively. Both sets of DVHs demonstrated that this failure mode only induced very small changes in the phantom plans by showing little to no changes from baseline.

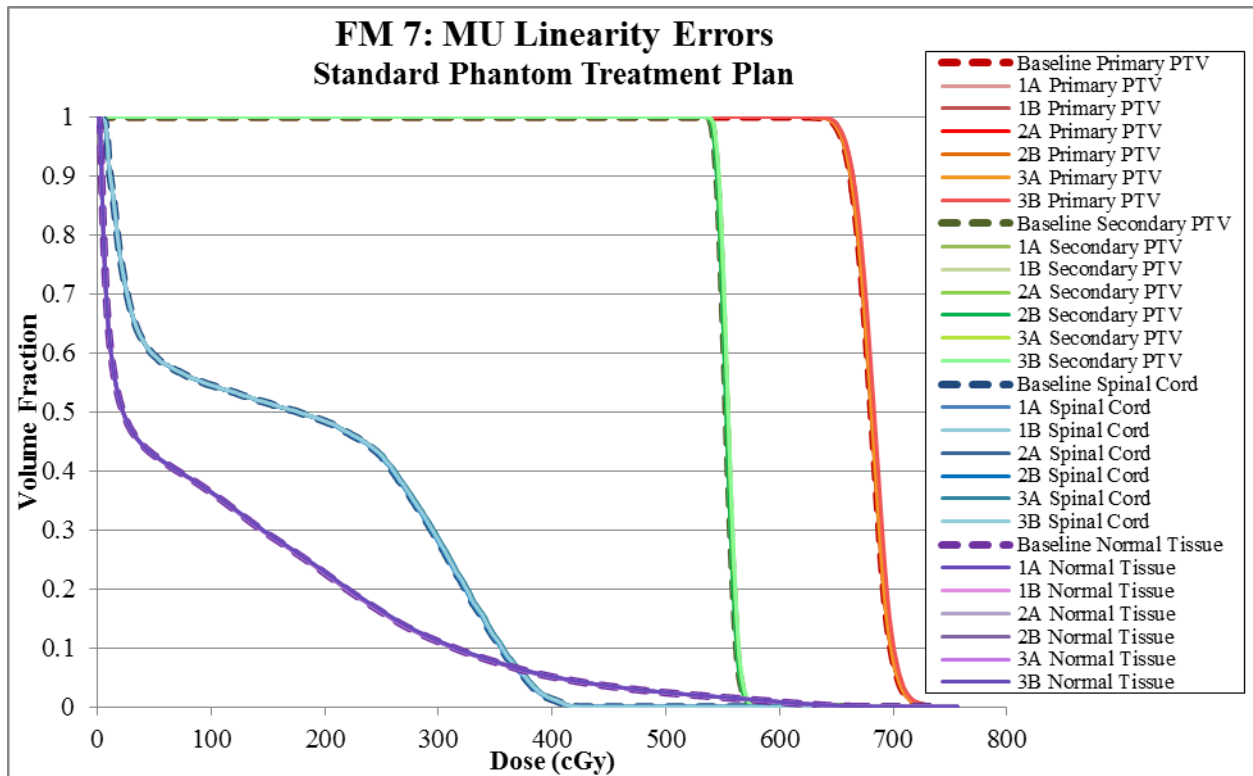


Figure 98: DVHs for phantom structures in the standard treatment plan with MU linearity errors, with dashed lines showing baseline DVHs.

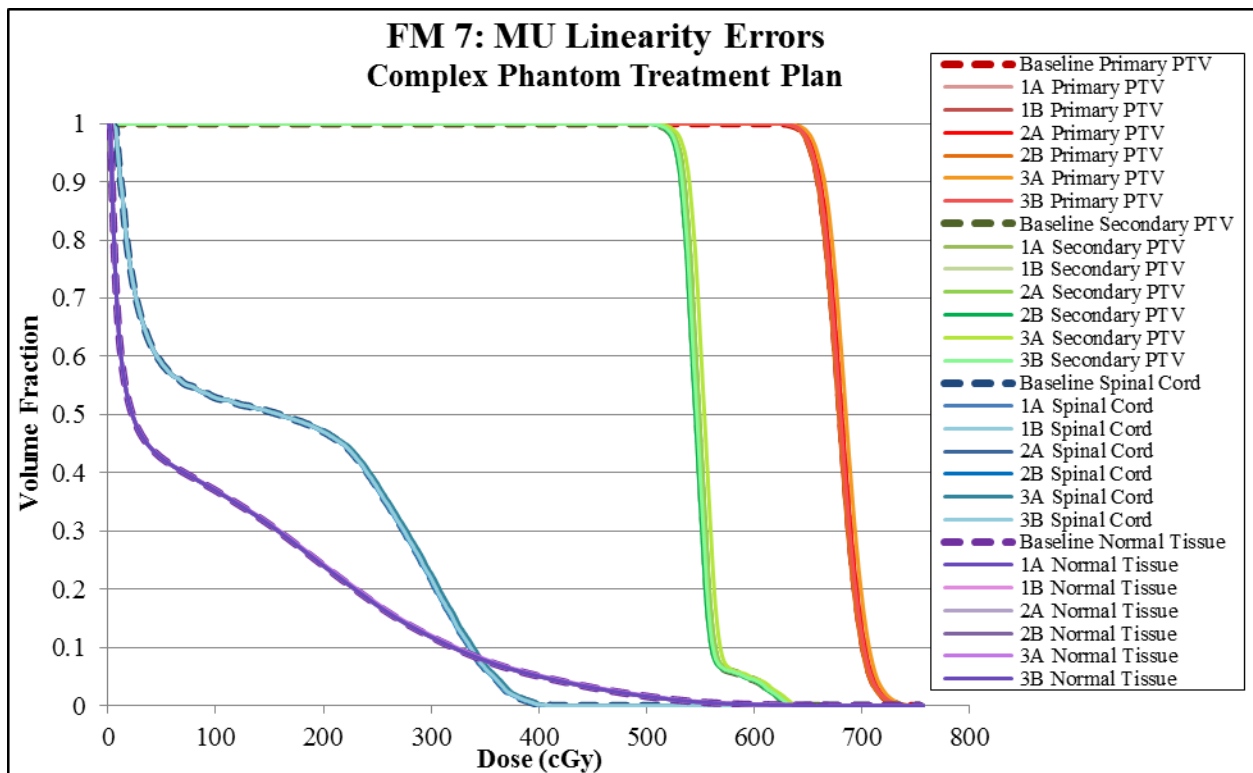


Figure 99: DVHs for phantom structures in the complex treatment plan with MU linearity errors, with dashed lines showing baseline DVHs.

Although 36% of the segments had less than or equal to 5 MU for the complex plan, which had just slightly larger changes than the standard plan, and were therefore either increased or decreased for this study, the largest change to the MU for any one segment was only 0.3 MU (Scenario 2, 1 or 2 MU segments, or Scenario 3, 5 MU). Even if all 36% of the segments with 5 MU or less were adjusted by 0.3 MU, that would only add up to 23.7 MU compared to the total MU of 3189 in the complex plan (an increase or decrease of 0.7% MU). The distribution of low MU segments throughout the beams had potential for creating errors, for example if one beam had all small MU segments with large adjustments, that beams's contribution to the overall dose distribution would change. Even so, the resultant changes in a complex IMRT plan wash out from these relatively small changes in MU. Overall, the severity score of 1 for this failure mode was reasonable.

Failure mode 8: MLC transmission and leakage

Treatment planning study results

The resultant changes in the phantom structure doses used for severity scoring for changes in beam modeling of the MLC transmission and leakage are summarized in Table 75 and Table 76 for both standard and complex phantom plans, respectively. The maximum change from baseline in all structure evaluation criteria for the standard phantom treatment plan was a 2% increase in the maximum spinal cord dose from baseline. All other changes in evaluation criteria for both the standard and complex phantom plan were less than 1%. PTV doses decreased very slightly with either an increase or decrease in interleaf leakage transmission, at maximum -0.48% in the standard plan and -0.84% in the complex plan. The maximum dose to the spinal cord with 0% interleaf leakage transmission decreased for both plans, and as mentioned, with 10% interleaf leakage transmission increased by 2% in the standard plan but only 0.48% in the complex plan. Overall, this failure mode was assigned a severity score of 1.

Standard Phantom Treatment Plan			
Structure	Evaluation criteria	Interleaf leakage transmission = 0	Interleaf leakage transmission = 0.1
		Change from baseline	
Primary PTV	D _{95%}	-0.07%	-0.23%
	D _{99%}	-0.04%	-0.48%
Secondary PTV	D _{95%}	-0.14%	-0.05%
	D _{99%}	-0.21%	-0.15%
Spinal Cord	Max Dose	-0.56%	2.04%
Normal Tissue	Max Dose	0.12%	-0.49%

Table 75: Dosimetric changes from baseline used for severity scoring for MLC leakage and transmission modeling values of 0% and 10% for the standard phantom treatment plan.

Complex Phantom Treatment Plan			
Structure	Evaluation criteria	Interleaf leakage transmission = 0	Interleaf leakage transmission = 0.1
		Change from baseline	
Primary PTV	D _{95%}	-0.10%	-0.46%
	D _{99%}	-0.45%	-0.67%
Secondary PTV	D _{95%}	-0.15%	-0.84%
	D _{99%}	0.19%	-0.60%
Spinal Cord	Max Dose	-0.40%	0.48%
Normal Tissue	Max Dose	-0.47%	0.53%

Table 76: Dosimetric changes from baseline used for severity scoring for MLC leakage and transmission modeling values of 0% and 10% for the complex phantom treatment plan.

The DVHs for the MLC leakage and transmission modeling errors are shown in Figure 100 and Figure 101 for standard and complex phantom treatment plans, respectively. Both sets of DVHs demonstrate that this failure mode induced mostly very small changes in the phantom plans. The figures show that in both plans the increase in leakage transmission from baseline to a value of 10% resulted in an increase in the dose to the spinal cord, which was minimally reflected in the spinal cord for the complex plan with an increase in the maximum dose increase of only 0.48%, but was more obviously reflected in the spinal cord for the standard plan with an increase of 2.04%.

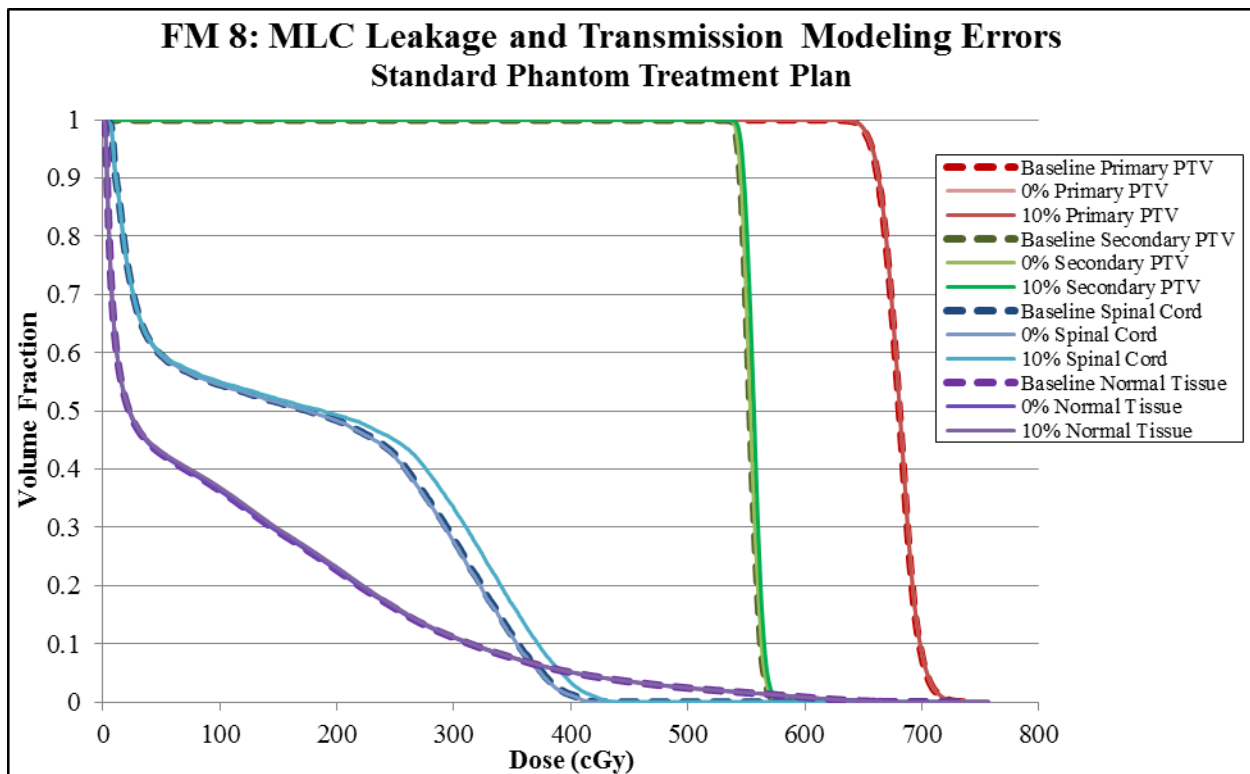


Figure 100: DVHs for phantom structures in the standard treatment plan with MLC leakage and transmission modeling errors, with dashed lines showing baseline DVHs.

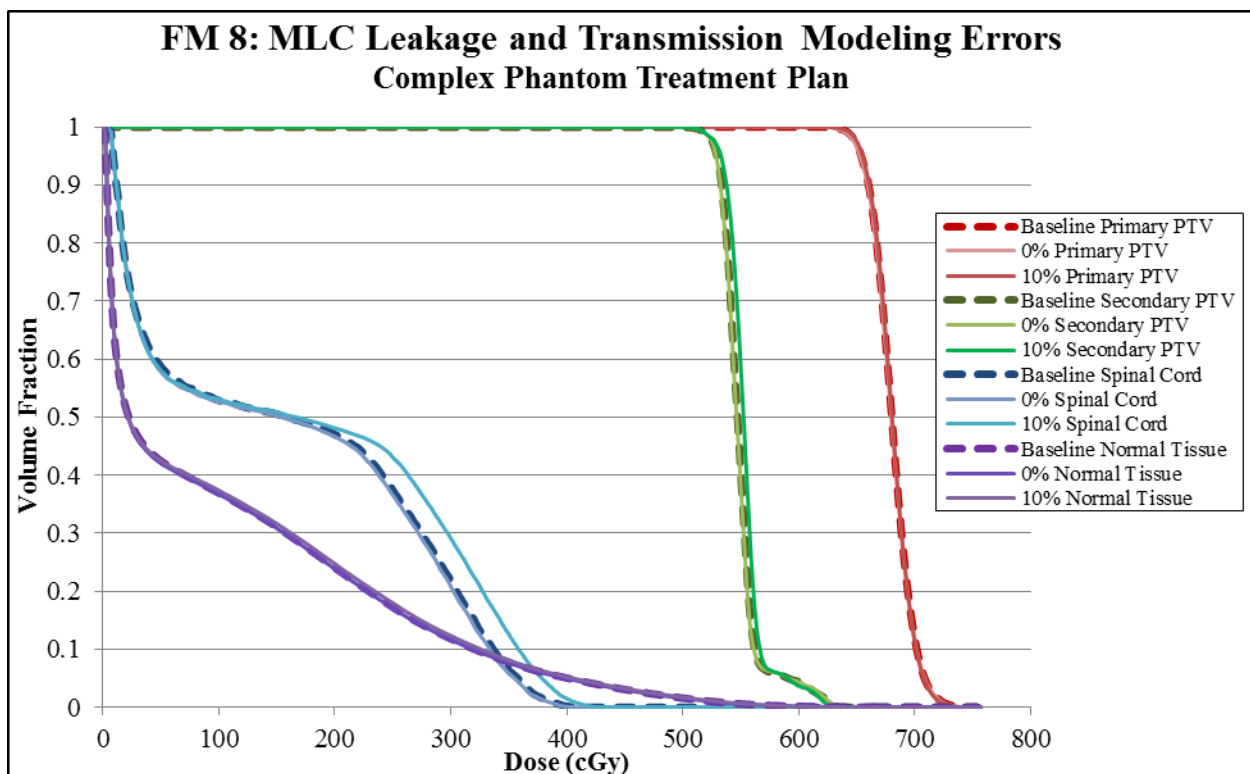


Figure 101: DVHs for phantom structures in the complex treatment plan with MLC leakage and transmission modeling errors, with dashed lines showing baseline DVHs.

The increased doses to the spinal cord seen in the DVHs for both the standard and complex treatment plans with increases in the interleaf leakage and transmission occurred because the MLC were used to block that structure and therefore it was subject to increased dose as a result of the increased leakage and transmission. Since greater changes occurred in the overall dose to the spinal cord volume as a whole than were captured by the increase in the maximum doses, this low severity score may have been an underestimation of the effects of changes in the MLC interleaf leakage and transmission on structures being blocked by the MLC, however we maintained our scoring system and this failure mode resulted in a severity score of 1.

Failure mode 9: MLC tongue-and-groove effect

Treatment planning study results

The resultant changes in the phantom structure doses used for severity scoring for changes in beam modeling of the MLC tongue-and-groove effect are summarized in Table 77 and Table 78 for both standard and complex phantom plans, respectively. All structure evaluation criteria in the standard treatment plan had below a 1% change from baseline with the exception of the maximum dose to the spinal cord, which was increased by 3.6% when the tongue-and-groove width of 0.200 cm was used. When the tongue-and-groove width was decreased, the maximum spinal cord dose decreased by -0.31%. All PTV doses increased a very small amount (under 0.20% with the decreased width and 0.65% with the increased) in the standard phantom plan with either change in the tongue-and-groove width, with the exception of the dose to 99% of the secondary PTV which decreased only -0.01%.. In the complex treatment plan, all evaluation criteria had below a 3% change. Similar to the standard phantom plan, the largest change in the complex plan was an increase of 2.97% in the maximum dose to the spinal cord with an increase of in the tongue-and-groove width. PTV coverage decreased less than 0.4% with the decreased tongue-and-groove width and overall increased with the increased width, up to 0.68%. The resulting severity score for this failure mode was 2.

Standard Phantom Treatment Plan			
Structure	Evaluation criteria	Tongue-and-groove width = 0.005 cm	Tongue-and-groove width = 0.200 cm
		<i>Change from baseline</i>	
Primary PTV	D _{95%}	0.05%	0.13%
	D _{99%}	0.16%	0.15%
Secondary PTV	D _{95%}	0.05%	0.58%
	D _{99%}	-0.01%	0.61%
Spinal Cord	Max Dose	-0.31%	3.62%
Normal Tissue	Max Dose	0.18%	-0.76%

Table 77: Dosimetric changes from baseline used for MLC tongue-and-groove effect modeling with width values of 0.005 cm and 0.200 cm for the standard phantom treatment plan.

Complex Phantom Treatment Plan			
Structure	Evaluation criteria	Tongue-and-groove width = 0.005 cm	Tongue-and-groove width = 0.200 cm
		<i>Change from baseline</i>	
Primary PTV	D _{95%}	-0.15%	0.17%
	D _{99%}	-0.32%	0.12%
Secondary PTV	D _{95%}	-0.15%	0.68%
	D _{99%}	-0.05%	-0.04%
Spinal Cord	Max Dose	-1.26%	2.97%
Normal Tissue	Max Dose	-0.56%	-0.76%

Table 78: Dosimetric changes from baseline used for MLC tongue-and-groove effect modeling with width values of 0.005 cm and 0.200 cm for the complex phantom treatment plan.

The DVHs for the MLC leakage and transmission modeling errors are shown in Figure 102 and Figure 103 for standard and complex phantom treatment plans, respectively. Very small changes in the dose to the spinal cord were visible in both sets of DVHs. There was also a change in the shape of the secondary PTV DVH in the complex treatment plan with increased tongue-and-groove width, indicating smaller or less severe hotspots. All other changes were very small in the DVHs.

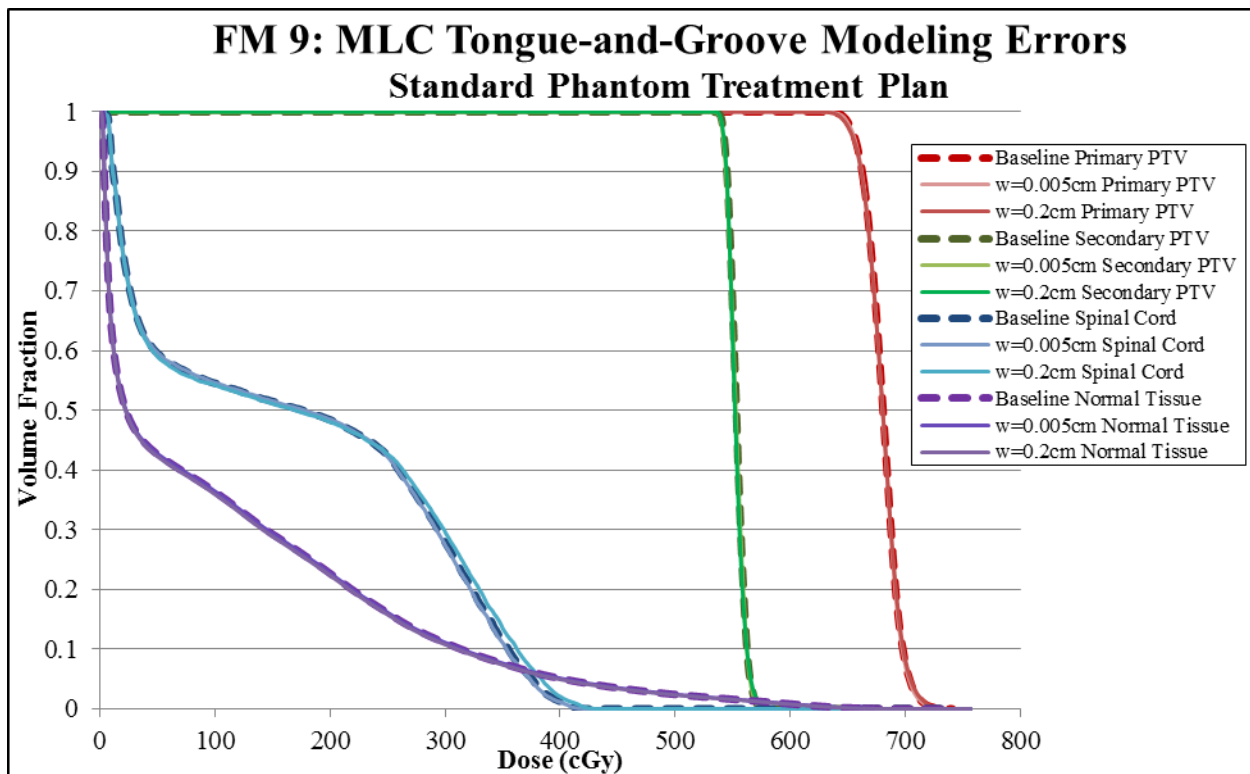


Figure 102: DVHs for phantom structures in the standard treatment plan with MLC tongue-and-groove modeling errors, with dashed lines showing baseline DVHs.

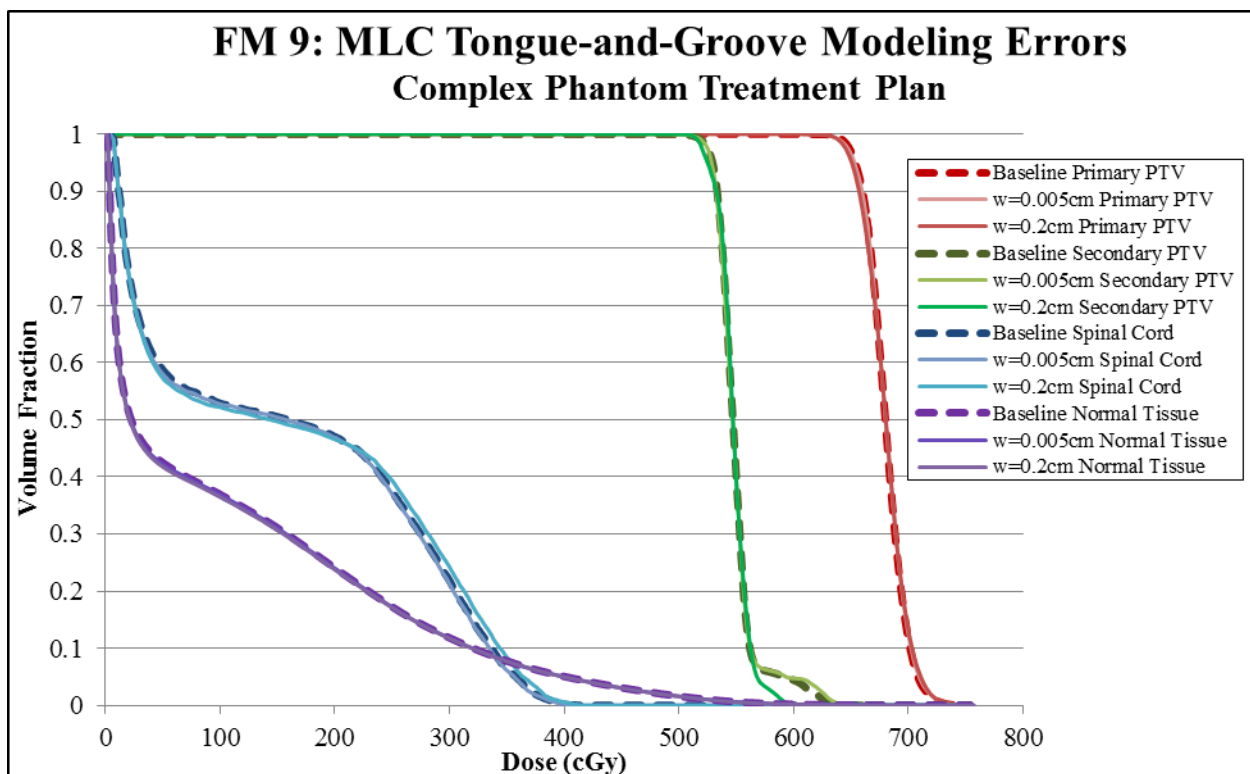


Figure 103: DVHs for phantom structures in the complex treatment plan with MLC tongue-and-groove modeling errors, with dashed lines showing baseline DVHs.

The tongue-and-groove design of the MLC reduces interleaf transmission, but can result in under dosing between leaves and affects the width of the penumbra. The small changes in the dose to the spinal cord for both the standard and complex treatment plans likely resulted from the MLC crossing over the spinal cord in the X direction to block it as well as to modulate the overall dose. The reduction in secondary PTV hotspots seen in the complex plan with the 0.2 cm wide tongue-and-groove was a result of decreased hotspots along the inferior edge of that PTV. This could have resulted from the under-dosing tongue-and-groove effect or it could have resulted from the widened penumbra. Overall, the effects were most prominent along field edges, but were mostly small.

Failure mode 10: MLC leaf end effects

Treatment planning study results

The resultant changes in the phantom structure doses used for severity scoring for changes in beam modeling of the MLC rounded leaf ends are summarized in Table 79 and Table 80 for both standard and complex phantom plans, respectively. An increase in the maximum dose to the spinal cord was seen in both the standard and complex plans when modeling the rounded MLC leaf ends using a 4 cm radius with magnitudes of over 7% and 6%, respectively. With this leaf end radius, changes in the PTVs were all under 1%, with the maximum decrease in the standard plan being -0.87% and in the complex plan -.81%. There was also some loss of coverage in the primary PTV for modeling radius values of 20 cm and 15 cm, up to -1.63% in the dose to 99% of the primary PTV in the complex plan. With these increased leaf end radii, the spinal cord maximum doses decreased, up to -6.45% in the standard plan and -4.93% in the complex plan. The largest error was the 7.4% increase in maximum spinal cord dose in the standard treatment plan, resulting in a severity score of 5.

Standard Phantom Treatment Plan				
Structure	Evaluation criteria	Leaf end radius = 4 cm	Leaf end radius = 20 cm	Leaf end radius = 15 cm
		Change from baseline		
Primary PTV	D _{95%}	-0.01%	-0.53%	-0.41%
	D _{99%}	0.34%	-0.81%	-0.61%
Secondary PTV	D _{95%}	-0.85%	0.40%	0.28%
	D _{99%}	-0.87%	0.43%	0.17%
Spinal Cord	Max Dose	7.39%	-6.45%	-4.77%
Normal Tissue	Max Dose	-2.18%	1.16%	0.86%

Table 79: Dosimetric changes from baseline used for severity scoring for MLC rounded leaf end modeling with radius values of 4 cm, 15 cm, and 20 cm for the standard phantom treatment plan.

Complex Phantom Treatment Plan				
Structure	Evaluation criteria	Leaf end radius = 4 cm	Leaf end radius = 20 cm	Leaf end radius = 15 cm
		Change from baseline		
Primary PTV	D _{95%}	0.27%	-0.83%	-0.60%
	D _{99%}	0.41%	-1.63%	-1.30%
Secondary PTV	D _{95%}	-0.81%	0.39%	0.28%
	D _{99%}	-0.22%	-0.22%	0.00%
Spinal Cord	Max Dose	6.38%	-4.93%	-3.85%
Normal Tissue	Max Dose	-2.83%	1.87%	1.25%

Table 80: Dosimetric changes from baseline used for severity scoring for MLC rounded leaf end modeling with radius values of 4 cm, 15 cm, and 20 cm for the complex phantom treatment plan.

The DVHs for the MLC leakage and transmission modeling errors are shown in Figure 104 and Figure 105 for standard and complex phantom treatment plans, respectively. An increase in the spinal cord dose for each case with a smaller rounded leaf end modeling radius of 4 cm was clear, as well as a decrease in the spinal cord doses with an increase in the radius. The dose to the secondary PTV also changed for both standard and complex plans, most visibly decreasing in the secondary PTV with the leaf end radius of 4 cm.

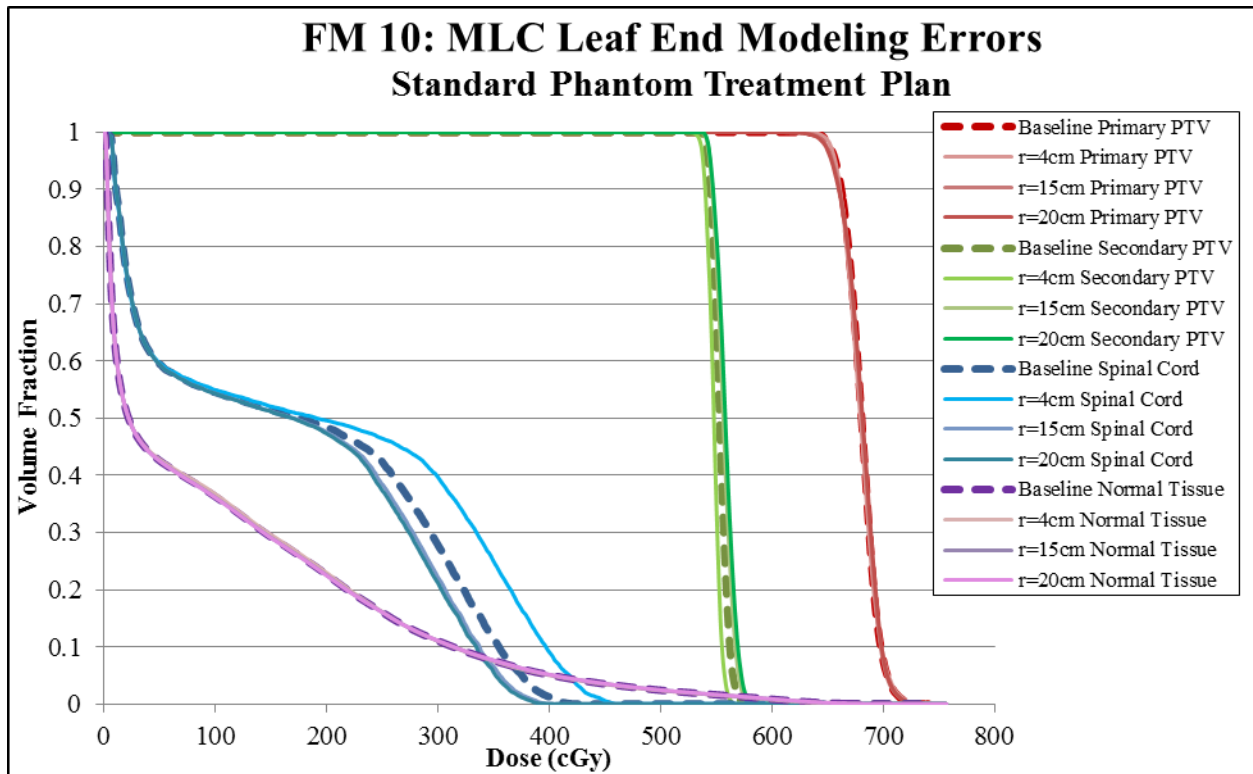


Figure 104: DVHs for phantom structures in the standard treatment plan with MLC leaf end modeling errors, with dashed lines showing baseline DVHs.

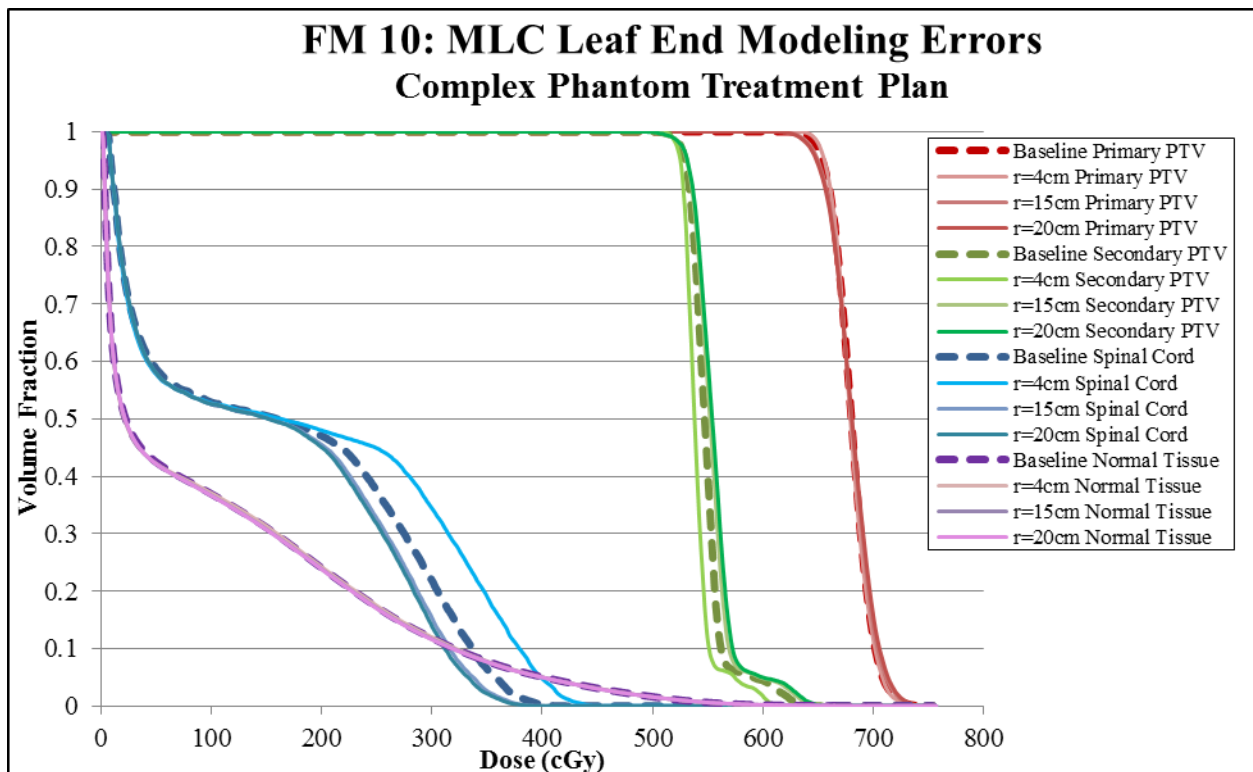


Figure 105: DVHs for phantom structures in the complex treatment plan with MLC leaf end modeling errors, with dashed lines showing baseline DVHs.

Decreasing the radius of the leaf end resulted in increased spinal cord doses, both the maximum and those seen on the DVHs. This was due to the increase in penumbra width along the end of the MLC that results from decreasing the leaf radius since the beam can then penetrate at greater angles through the leaf ends. Since the spinal cord is adjacent to a steep dose gradient and is blocked by the MLC, changes to the penumbra directly affect the dose. Decreases in the secondary PTV dose were also likely due to the increased penumbra width but were much smaller in magnitude. This would have depended on the way the field were modulated and how extensively the leaf ends stopped within the PTVs.

Failure mode 11: CT Table

Treatment planning study results

The resultant changes in the phantom structure doses used for severity scoring for changing the electron density to CT number table are summarized in Table 81 and Table 82 for both standard and complex phantom plans, respectively. All structure evaluation criteria in both the standard and complex phantom treatment plans had below a 0.50% change. Since the changes were so small, it was difficult to identify any trends. This failure mode was assigned a severity score of 1.

Standard Phantom Treatment Plan				
Structure	Evaluation criteria	+2%	-2%	PET CT
		<i>Change from baseline</i>		
Primary PTV	D _{95%}	-0.02%	0.03%	0.05%
	D _{99%}	0.01%	0.03%	0.18%
Secondary PTV	D _{95%}	0.02%	0.04%	-0.04%
	D _{99%}	-0.02%	0.00%	0.06%
Spinal Cord	Max Dose	0.11%	0.01%	0.03%
Normal Tissue	Max Dose	0.04%	0.05%	-0.05%

Table 81: Dosimetric changes from baseline used for severity scoring for differences in the CT table used for the standard phantom treatment plan.

Complex Phantom Treatment Plan				
Structure	Evaluation criteria	+2%	-2%	PET CT
		Change from baseline		
Primary PTV	D _{95%}	-0.18%	0.00%	-0.07%
	D _{99%}	-0.35%	0.01%	-0.18%
Secondary PTV	D _{95%}	0.01%	0.00%	-0.08%
	D _{99%}	0.15%	0.23%	0.00%
Spinal Cord	Max Dose	-0.26%	0.00%	-0.27%
Normal Tissue	Max Dose	0.09%	-0.07%	-0.33%

Table 82: Dosimetric changes from baseline used for severity scoring for differences in the CT table used for the complex phantom treatment plan.

The DVHs for the MLC leakage and transmission modeling errors are shown in Figure 106 and Figure 107 for standard and complex phantom treatment plans, respectively. There appeared to be no changes to the DVHs with changes in the CT table.

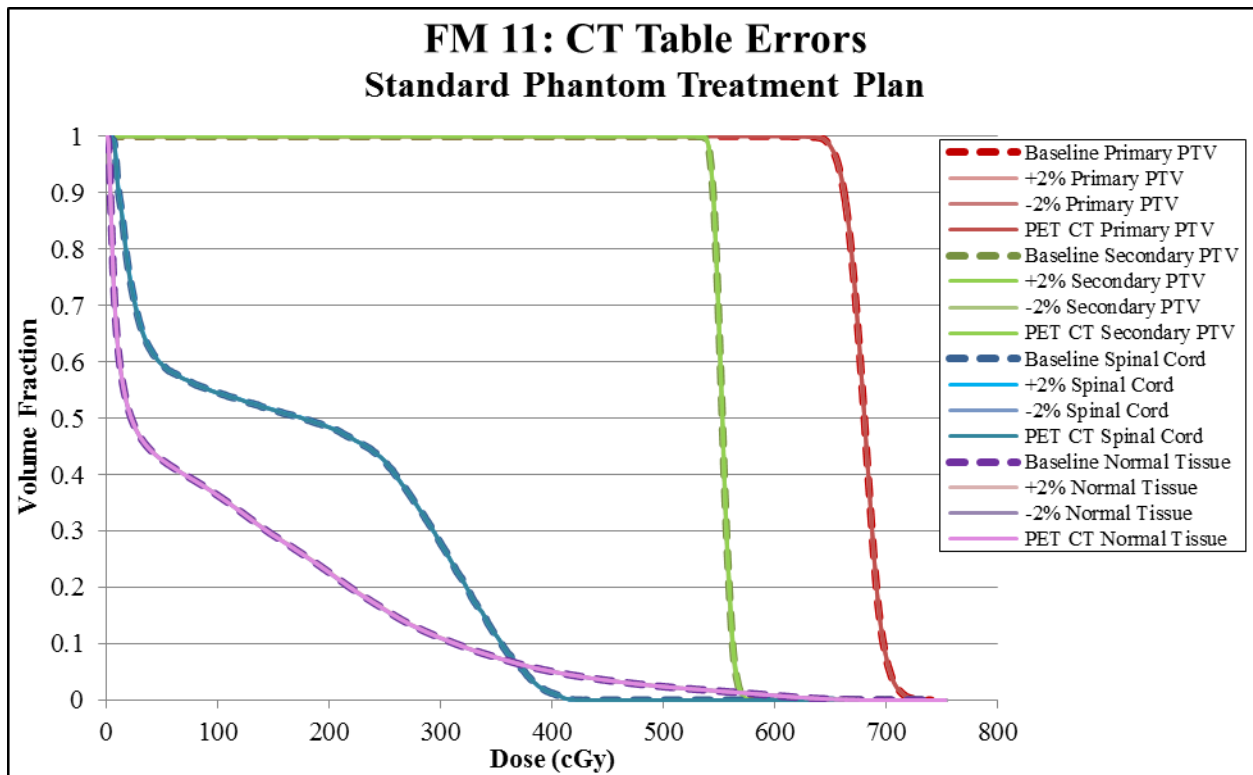


Figure 106: DVHs for phantom structures in the s treatment plan with CT Table errors, with dashed lines showing baseline DVHs.

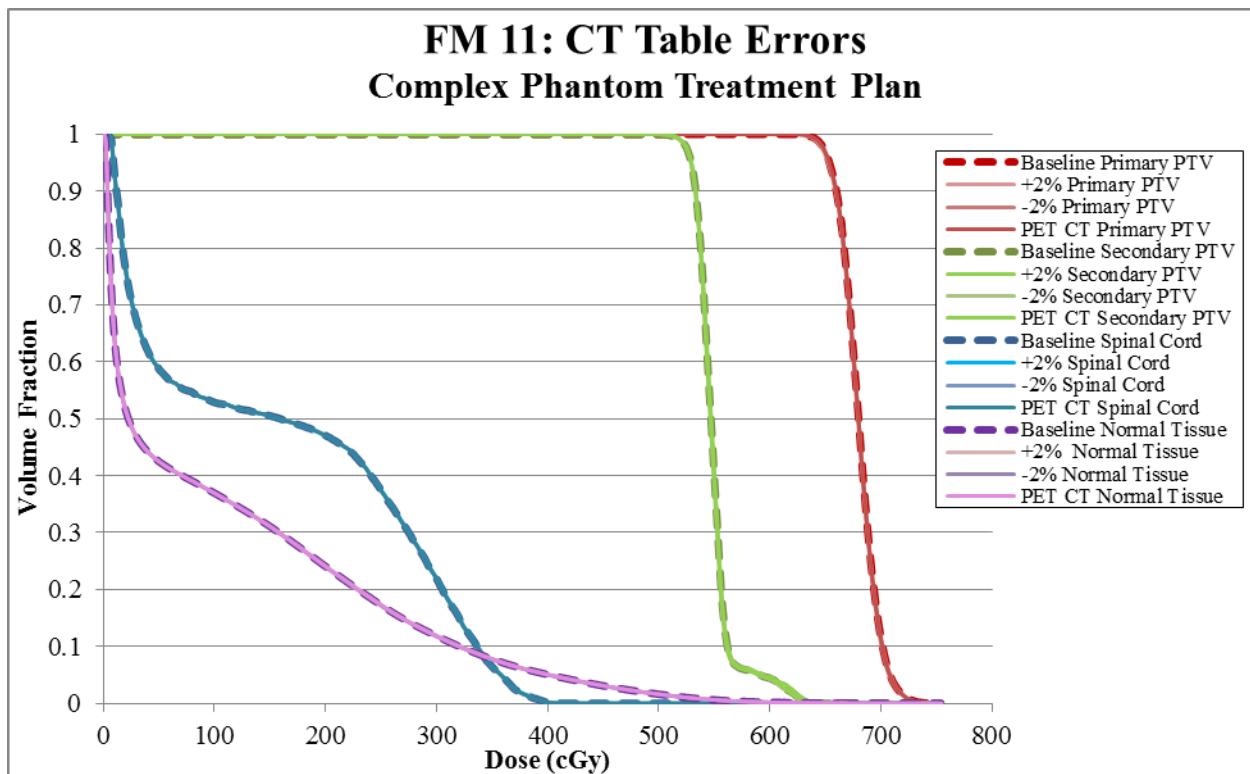


Figure 107: DVHs for phantom structures in the complex treatment plan with CT Table errors, with dashed lines showing baseline DVHs.

The phantom is overall rather homogeneous, containing no high-Z materials. The materials that would be changed the most by any of these CT table changes were not a part of the phantom, so it is therefore not surprising that this failure mode had minimal effect on the dose distribution. This may have resulted in an underestimate of the severity for this failure mode, since head and neck patients were likely to have high-Z materials within the field such as dental fillings, however the phantom did not enable us to further investigate these effects.

Phantom severity scoring summary

The severity scores resulting from the largest deviations from the baseline plans in our phantom structure evaluation criteria for the standard and complex plans are summarized in Table 83. Scores of 1-8 were assigned for our failure modes, with over half (6) of the failure modes having a severity score of 3 or lower. Beam symmetry, MU linearity, MLC leakage and transmission, and CT table failure modes resulted in a severity score of 1. Three of the failure modes, collimator angle, couch angle, and MLC leaf

end modeling, were of mid-range severity with scores of 4 and 5. Two failure modes, MLC position and gantry angle, had mid-high severity with scores of 8 and 7, respectively.

Failure Mode	Standard Plan Severity Score	Complex Plan Severity Score	Overall Severity Score
1. Beam Energy	3	1	3
2. Beam Symmetry	1	1	1
3. MLC Position (1 mm) (2 mm)	4 8	2 5	8
4. Gantry Angle	7	5	7
5. Collimator Angle	1	5	5
6. Couch Angle	1	4	4
7. MU Linearity	1	1	1
8. MLC Leakage & Transmission	1	1	1
9. MLC Tongue & Groove	2	1	2
10. MLC Leaf End	5	4	5
11. CT Table	1	1	1

Table 83: Summary of the phantom severity scores based on structure evaluation criteria and our severity scoring scale for standard and complex treatment plans. The overall severity score assigned for each failure mode represents the maximum severity.

3.1.3 Comparison of qualitative and quantitative scores

A comparison of the overall survey severity scores and those from our treatment planning studies is shown in Figure 108. Failure mode 1 (beam energy) is the only failure mode upon which the survey average and median agree with the more conservative of our phantom treatment planning study severity scores. The median survey severity score and more conservative phantom treatment planning study severity score also match for failure mode 6 (couch angle). For these two failure modes, the qualitative and quantitative severity scores were the same when compared directly. The severity scores from the complex phantom treatment planning studies also match the average and median survey severity scores for failure mode 3 and 10, however the severity scores for these failure modes resulting from the standard phantom treatment plan were more conservative and so in these cases the quantitative severity scores were higher than those from the qualitative assessment. Severity scores for failure modes 4 and 5 were

also higher for the quantitative assessment. For failure modes 2, 6, 7, 8, 9, and 11, the qualitative assessment predicted higher severity scores than the treatment planning studies quantitative scores.

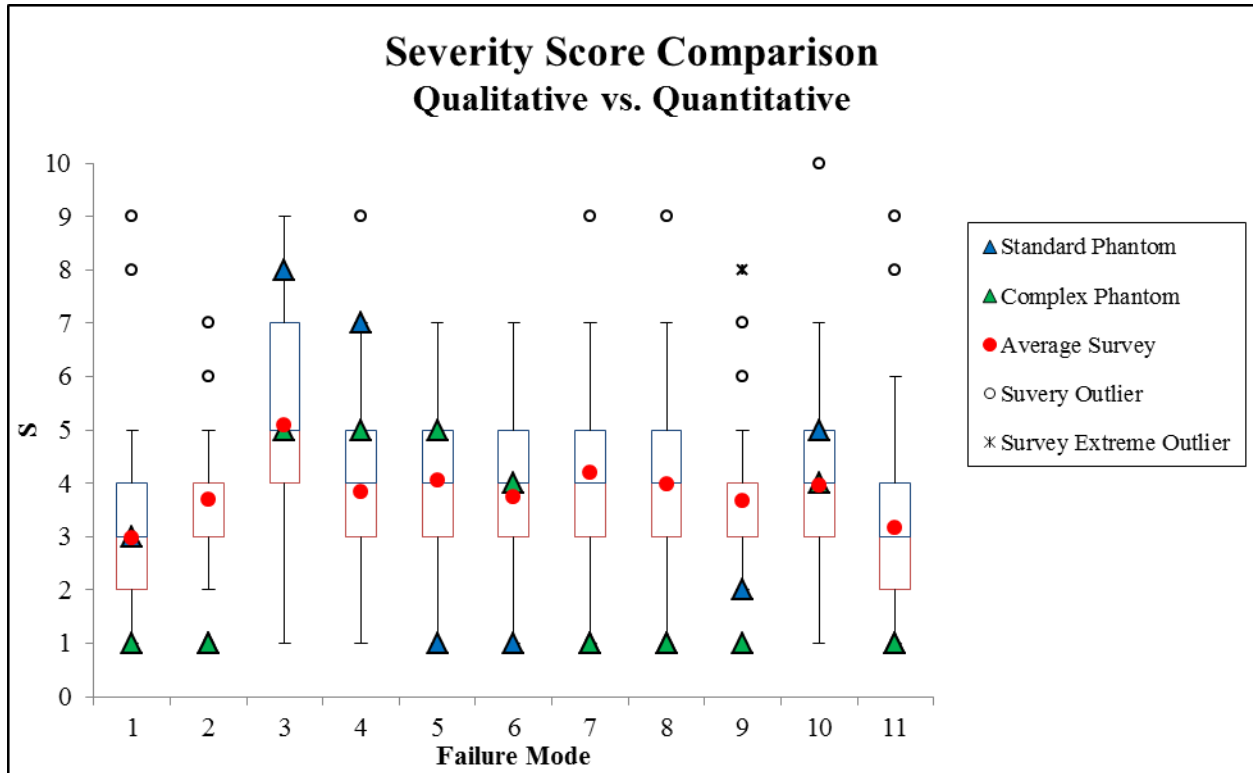


Figure 108: Summary of severity scores for survey (N=184) including the average scores, median scores (lines between 3rd and 2nd quartile boxes), and outliers and for standard and complex phantom treatment planning studies.

The results of one-sample Wilcoxon Signed Rank Tests used to more strictly compare the qualitative and quantitative severity scores for our IMRT H&N physical failure modes are presented in Table 84. This test evaluated whether the median qualitative severity score equaled the quantitative severity score for each failure mode, with the null hypothesis that they were equal. P-values under 0.05 indicated that the scores were significantly different and are highlighted in the table in red. P-values indicating that the severity scores were the same from qualitative and quantitative methods are highlighted in green. The median qualitative severity score and the 95% confidence interval of the median are shown for each failure mode. In this case, the 95% confidence intervals of the median severity scores only contained one possible severity score for each failure mode. The conclusions from this analysis were

that failure modes 1 and 6 were given the same severity score by both methods, while all others received different scores from each method, are the same as those we could draw from Figure 108.

Failure Mode	Qualitative Severity Score <i>95% Confidence Interval of the Median</i>			Quantitative Severity Score	Wilcoxon Signed Rank p-value
	Lower Bound	Median	Upper Bound		
1. Beam Energy	2.74	3	3.26	3	0.889
2. Beam Symmetry	3.78	4	4.22	1	0.000
3. MLC Position	4.67	5	5.33	8	0.000
4. Gantry Angle	3.72	4	4.28	7	0.000
5. Collimator Angle	3.73	4	4.27	5	0.000
6. Couch Angle	3.72	4	4.29	4	0.153
7. MU Linearity	3.72	4	4.28	1	0.000
8. MLC Leakage & Transmission	3.73	4	4.27	1	0.000
9. MLC Tongue & Groove	3.74	4	4.26	2	0.000
10. MLC Leaf End	3.75	4	4.26	5	0.000
11. CT Table	2.73	3	3.27	1	0.000

Table 84: For each failure mode: 95% confidence interval of the median of the qualitative severity scores, the quantitative severity scores and results of one-sample Wilcoxon Signed Rank Test, with significance level $p < 0.05$ indicated in red. P-values greater than significance level highlighted in green.

Overall, only two of the ten severity scores were the same following qualitative and quantitatively methods. In this analysis, qualitative and quantitative severity scores were considered significantly different if they were not exactly the same. Two of the ten failure modes, failure mode 5 (collimator angle) and failure mode 10 (MLC leaf end), had severity scores from qualitative and quantitative methods within one score. For every failure mode, the maximum severity score from the survey responses was greater than the severity score from either of the phantom treatment planning studies (as shown in Figure 108).

To better understand the effects of applying the scoring scale and the lack of a quantitative component in the severity scoring scale on the assessment of the consequences of these failure modes, we also looked at the distribution of the percent dose errors estimated in the survey compared to the maximum dose deviations from baseline seen in the standard and complex phantom treatment planning studies. A summary of this comparison can be seen in Figure 109. The range of estimated percent dose

errors when outliers were included far exceeded those resulting from our treatment planning studies. Only for failure mode 8 were the qualitative and quantitative percent dose errors approximately the same. The results of the two approaches tended to follow a similar trend, but the median survey estimate was up to a factor of four off from our maximum phantom treatment planning study results.

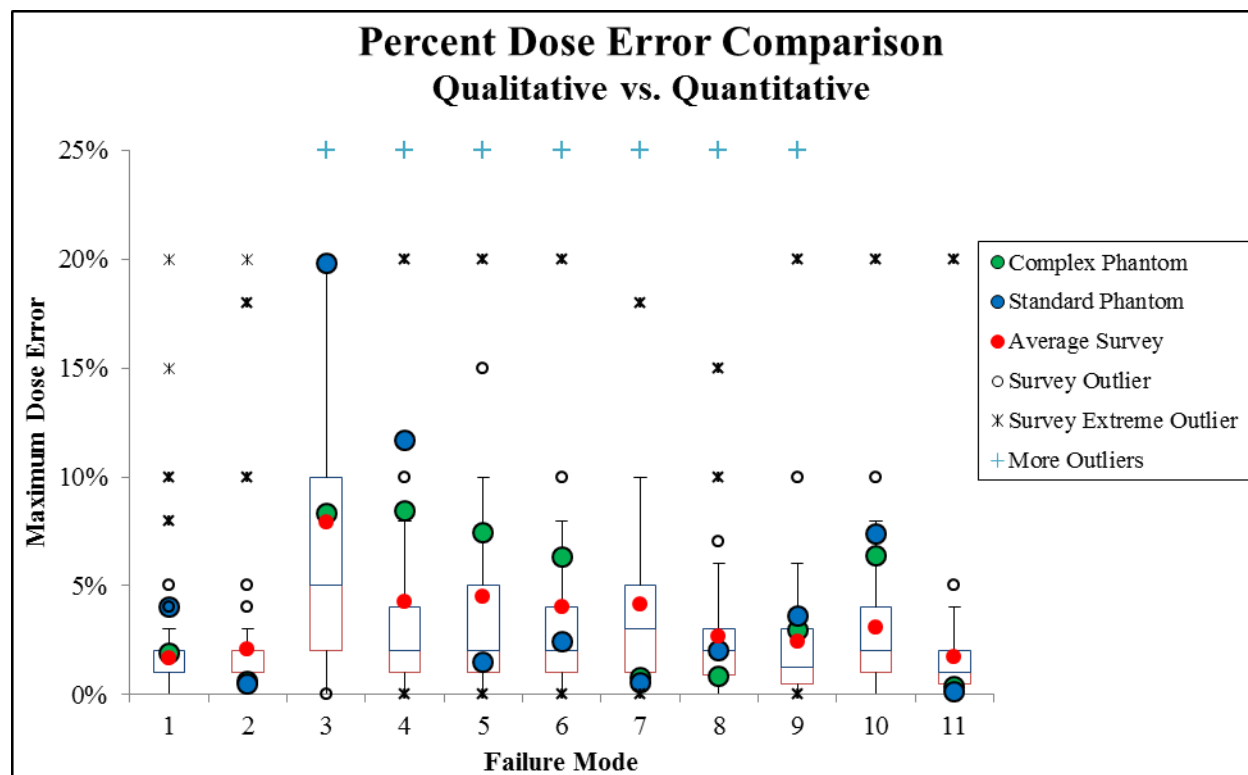


Figure 109: Summary of estimated percent dose errors for survey (N=184) including the averages, medians (lines between 3rd and 2nd quartile boxes), and outliers and maximum percent dose errors seen in phantom structures for standard and complex phantom treatment planning studies.

3.2 Specific Aim 2

3.2.1 Patient treatment planning study results – true severity

The results from our treatment planning studies on ten oropharyngeal patients are presented by failure mode. The dose differences from baseline for all structures evaluated and the evaluation criteria are tabulated for all ten patients for all eleven failure modes in Appendix B. Additionally, the DVHs corresponding to these structures for each of the patients are in Appendix C.

Failure mode 1: Beam energy true severity

As with the phantom treatment planning studies, our beam models with +10% and -10% energy were used to assess the true severity of this failure mode using clinical patient treatment plans. The resultant severity scores are shown in Table 85. The overall severity scores based on the maximum dose deviation from the baseline plan structure doses at the evaluation criteria ranged from 2 to 9, with patient 7 being the only one with a severity score less than 7 for this failure mode. All of the overall severity scores were based on the OARs and all patients except patient 2 had higher severity scores for the +10% energy adjustment.

In six of the ten patients, the dose to 100% of the brainstem increased largely and resulted in the high severity score. This effect could have been exaggerated because the dose to the 100% of the brainstem was only a couple hundred cGy over the course of the treatment, so an increase of only 20 cGy could result in a 10% dose difference from the baseline. In patients 2 and 3, the dose to 50% of the parotid glands increased enough to result in a severity score of 9. In both cases, the left parotid gland was right up against the primary PTV but this was not uncommon in this group of patients. In patients 7 and 10, the maximum doses to the orbits and lens increased substantially with the increase in the energy. These structures were very small and were out of the fields so they were receiving overall low doses. These factors were likely exaggerating the effect of beam energy changes on the dose. It was very likely that the changes in the shoulders of the dose profiles with changes in energy were the cause of these errors in structures out of the field and far from isocenter, since these patients all had isocenter on the neck, just inferior to the chin, which allowed for the upper IMRT fields to be matched to the supraclavicular fields.

Patient	Energy -10%			Energy +10%			Overall
	PTVs	OARs	Total	PTVs	OARs	Total	
1	5	3	5	6	7	7	7
2	4	9	9	4	9	9	9
3	4	7	7	4	8	8	8
4	1	1	1	1	7	7	7
5	1	1	1	1	8	8	8
6	1	4	4	1	9	9	9
7	1	1	1	1	2	2	2
8	1	3	3	1	8	8	8
9	1	3	3	1	9	9	9
10	1	4	4	1	9	9	9

Table 85: Severity scores from PTVs, OARs, and overall for ten clinical oropharyngeal patients with -10% and +10% beam energy adjustments.

Failure mode 2: Beam symmetry true severity

As with the phantom treatment planning studies, physical wedges with approximately 2%, 3.5%, and 10% symmetry were used to assess the true severity of this failure mode using clinical patient treatment plans. The resultant severity scores are shown in Table 86, Table 87, and Table 88. The severity scores for beam symmetry errors of 2% and 3.5% were 1 for all patients with the exception of patient 10, which had a severity score resulting from differences in the OAR dose, assigning a severity score of 9. A similar trend was seen with symmetry errors of 10%, however the severity scores ranged from 1 to 5 for patients 1-9. The severity scores of 9 for patient 10 all came from optic nerves and orbits, which had small volumes and low doses. This combined with the fact that the isocenter was far from these structures and therefore the differences in the dose caused by symmetry errors were larger resulted in an exaggeration of the severity similar to that seen in the beam energy true severity results. Without considering the optic nerves and orbits, the severity score for patient 10 would be 6 from the dose to 100% of the brainstem increasing. If we eliminated all of the mentioned low dose evaluations and small volume structures, the severity score for patient 10 would be 1. Other severity scores greater than 1 were largely, but not solely, the result of increases to the cochlear doses. While these doses were not as low in all cases, they were still relatively low and had a volume less than 1 cc, which may have contributed to the severity scores as in the other cases.

Patient	2% Beam Symmetry												Overall
	Top to bottom			Bottom to top			Left to right			Right to left			
	PTVs	OARs	Total	PTVs	OARs	Total	PTVs	OARs	Total	PTVs	OARs	Total	
1	1	1	1	1	1	1	1	1	1	1	1	1	1
2	1	1	1	1	1	1	1	1	1	1	1	1	1
3	1	1	1	1	1	1	1	1	1	1	1	1	1
4	1	1	1	1	1	1	1	1	1	1	1	1	1
5	1	1	1	1	1	1	1	1	1	1	1	1	1
6	1	1	1	1	1	1	1	1	1	1	1	1	1
7	1	1	1	1	1	1	1	1	1	1	1	1	1
8	1	1	1	1	1	1	1	1	1	1	1	1	1
9	1	1	1	1	1	1	1	1	1	1	1	1	1
10	1	9	9	1	9	9	1	9	9	1	9	9	9

Table 86: Severity scores from PTVs, OARs, and overall for ten clinical oropharyngeal patients with 2% beam symmetry errors.

Patient	3.5% Beam Symmetry												Overall
	Top to bottom			Bottom to top			Left to right			Right to left			
	PTVs	OARs	Total	PTVs	OARs	Total	PTVs	OARs	Total	PTVs	OARs	Total	
1	1	1	1	1	1	1	1	1	1	1	1	1	1
2	1	1	1	1	1	1	1	1	1	1	1	1	1
3	1	1	1	1	1	1	1	1	1	1	1	1	1
4	1	1	1	1	1	1	1	1	1	1	1	1	1
5	1	1	1	1	1	1	1	1	1	1	1	1	1
6	1	1	1	1	1	1	1	1	1	1	1	1	1
7	1	1	1	1	1	1	1	1	1	1	1	1	1
8	1	1	1	1	1	1	1	1	1	1	1	1	1
9	1	1	1	1	1	1	1	1	1	1	1	1	1
10	1	9	9	1	9	9	1	9	9	1	9	9	9

Table 87: Severity scores from PTVs, OARs, and overall for ten clinical oropharyngeal patients with 3.5% beam symmetry errors.

Patient	10% Beam Symmetry												Overall
	Top to bottom			Bottom to top			Left to right			Right to left			
	PTVs	OARs	Total	PTVs	OARs	Total	PTVs	OARs	Total	PTVs	OARs	Total	
1	1	1	1	1	1	1	1	2	2	1	1	1	2
2	1	1	1	1	1	1	1	3	3	1	1	1	3
3	1	1	1	1	1	1	2	2	2	1	1	1	2
4	1	2	2	1	2	2	1	4	4	1	1	1	4
5	1	4	4	1	3	3	1	2	2	1	2	2	4
6	1	1	1	1	1	1	1	1	1	1	1	1	1
7	1	1	1	1	1	1	1	1	1	1	2	2	2
8	1	1	1	1	1	1	1	2	2	1	1	1	2
9	1	2	2	1	2	2	2	5	5	1	1	1	5
10	1	9	9	1	9	9	1	9	9	1	9	9	9

Table 88: Severity scores from PTVs, OARs, and overall for ten clinical oropharyngeal patients with 10% beam symmetry errors.

Failure mode 3: MLC position true severity

Systematic MLC shifts of 1 mm and 2 mm in one bank were applied to our ten clinical patients as in the phantom treatment planning studies. The resultant severity scores are shown in Table 89 and Table 90 for 1 mm and 2 mm shifts, respectively. For 1 mm errors, the overall severity scores ranged from 3 to 10. For 2 mm errors, they ranged from 7 to 10. The causes of these severity scores were all OAR dose increases, though PTV coverage was decreased in several cases. The severity scores of 10 in patient 9 were from an increase in the dose to the larynx with shifts of the X1 MLC out, which also resulted in severity scores of 9 from an increase in the dose to the parotid glands. The highest severity scores were seen in patient 10 for this failure mode, which had a severity score of 9 and 10 for all of the eye-related structures. There were also severity scores of 9 from increases to the left parotid gland dose, increases in the brainstem and cord doses (S=4-8) and loss of coverage of the tertiary PTV (PTV3 with 54 Gy) for all of the different MLC positional errors.

Patient	1 mm MLC Positional Errors												Overall
	X1 -1mm			X1 +1mm			X2 -1mm			X2 +1mm			
	PTVs	OARs	Total	PTVs	OARs	Total	PTVs	OARs	Total	PTVs	OARs	Total	
1	1	1	1	1	1	1	1	1	1	1	7	7	7
2	1	1	1	1	1	1	1	1	1	1	2	2	2
3	1	1	1	1	1	1	1	1	1	1	5	5	5
4	1	1	1	1	1	1	1	1	1	1	5	5	5
5	1	3	3	1	9	9	1	9	9	1	9	9	9
6	1	1	1	1	9	9	1	9	9	1	9	9	9
7	1	1	1	1	4	4	1	1	1	1	4	4	4
8	1	1	1	1	1	1	1	1	1	1	7	7	7
9	1	9	9	1	10	10	1	1	1	1	6	6	10
10	3	10	10	2	10	10	3	10	10	3	10	10	10

Table 89: Severity scores from PTVs, OARs, and overall for ten clinical oropharyngeal patients with 1 mm systematic MLC shifts in one bank (X1 or X2).

Patient	2 mm MLC Positional Errors												Overall
	X1 -2mm			X1 +2mm			X2 -2mm			X2 +2mm			
	PTVs	OARs	Total	PTVs	OARs	Total	PTVs	OARs	Total	PTVs	OARs	Total	
1	6	1	6	1	2	2	1	1	1	1	9	9	9
2	1	1	1	1	5	5	1	1	1	1	5	5	5
3	1	1	1	1	5	5	1	1	1	1	7	7	7
4	3	1	3	1	1	1	3	1	3	1	8	8	8
5	4	3	4	1	9	9	3	3	3	1	9	9	9
6	1	1	1	1	9	9	2	9	9	1	9	9	9
7	1	1	1	1	7	7	7	1	7	1	7	7	7
8	4	1	4	1	1	1	2	1	2	1	9	9	9
9	3	9	9	1	10	10	1	1	1	1	9	9	10
10	4	10	10	2	10	10	3	10	10	3	10	10	10

Table 90: Severity scores from PTVs, OARs, and overall for ten clinical oropharyngeal patients with 2 mm systematic MLC shifts in one bank (X1 or X2).

Failure mode 4: Gantry angle true severity

Systematic gantry angle errors of -2° and $+2^\circ$ were introduced into our ten patient plans as done with the phantom treatment planning studies. The resultant severity scores are shown in Table 91. The overall severity scores for this failure mode ranged from 1 to 7, with most being either 4 or 5. The maximum overall severity score of 7 in patient 5 came from the gantry angle changing -2° , resulting in an

increase in the dose to the left parotid gland. Moving the gantry the opposite direction for this patient resulted in a lesser increase in the right parotid gland dose. The parotid glands were affected in this same orientation in most patients, which made sense since they all utilize the same gantry angle protocol.

Patient	Gantry Angle Errors						Overall
	-2°			+2°			
	PTVs	OARs	Total	PTVs	OARs	Total	
1	1	4	4	1	1	1	4
2	1	4	4	1	4	4	4
3	1	1	1	1	1	1	1
4	1	4	4	1	1	1	4
5	1	7	7	1	5	5	7
6	1	5	5	1	4	4	5
7	1	1	1	1	5	5	5
8	1	2	2	1	2	2	2
9	1	3	3	1	4	4	4
10	1	4	4	1	5	5	5

Table 91: Severity scores from PTVs, OARs, and overall for ten clinical oropharyngeal patients with -2° and +2° gantry angle errors.

Failure mode 5: Collimator angle true severity

Systematic collimator angle errors of -2° and +2° were introduced into our ten patient plans as done with the phantom treatment planning studies. The resultant severity scores are shown in Table 92. The overall severity scores for collimator angle errors ranged from 4 to 9 for this set of patients. As with most of the other failure modes, the severity scores were largely from increases in OAR doses. The severity scores of 9 all came from cochlear dose increases, with patient 8 also having a severity score of 9 from the right parotid gland dose increasing with a +2° error.

Patient	Collimator Angle Errors						
	-2°			-2°			Overall
	PTVs	OARs	Total	PTVs	OARs	Total	
1	1	9	9	2	9	9	9
2	2	4	7	1	5	5	7
3	1	5	7	4	7	7	7
4	1	4	9	2	8	8	9
5	1	4	7	1	7	7	7
6	1	7	3	4	4	4	4
7	2	9	7	4	9	9	9
8	1	4	7	5	9	9	9
9	3	7	7	4	5	5	7
10	1	4	2	1	9	9	9

Table 92: Severity scores from PTVs, OARs, and overall for ten clinical oropharyngeal patients with -2° and +2° collimator angle errors.

Failure mode 6: Couch angle true severity

Systematic couch angle errors of -2° and +2° were introduced into our ten patient plans as done with the phantom treatment planning studies. The resultant severity scores are shown in Table 93. The overall severity scores for couch angle errors ranged from 2 to 9, with half of the patients having a score of 7. All of the severity scores were a result of increases in the OAR doses. Similar to the collimator angle errors, the severity scores of 9 came from cochlea dose increase and, in patient 8, an increase in the dose to the right parotid gland.

Patient	Couch Angle Errors						
	-2°			-2°			Overall
	PTVs	OARs	Total	PTVs	OARs	Total	
1	1	9	9	1	2	2	9
2	1	7	7	1	5	5	7
3	1	7	7	1	1	1	7
4	1	9	9	1	4	4	9
5	1	7	7	1	5	5	7
6	1	3	3	1	2	2	3
7	1	7	7	1	7	7	7
8	4	7	7	1	9	9	9
9	1	7	7	1	7	7	7
10	1	2	2	1	2	2	2

Table 93: Severity scores from PTVs, OARs, and overall for ten clinical oropharyngeal patients with -2° and +2° couch angle errors.

Failure mode 7: MU linearity true severity

As in the phantom treatment planning studies, three MU linearity error scenarios were applied to ten clinical patient treatment plans. The resultant severity scores are shown in Table 94. All patients had an overall severity score of 1. These results were interesting in the same manner as the phantom results since there are a large number of segments with few MU in the patient plans which would be affected by these linearity errors. The distribution of the MU/segment for the ten patients is shown in Figure 110. However, these changes were so small overall that they did not substantially affect the dose to any of the structures.

Patient	MU Linearity Errors																		Overall
	1A			1B			2A			2B			3A			3B			
	PTVs	OARs	Total	PTVs	OARs	Total	PTVs	OARs	Total	PTVs	OARs	Total	PTVs	OARs	Total	PTVs	OARs	Total	
1	1	1	1	1	1	1	1	1	1	1	1	1	1	1	1	1	1	1	1
2	1	1	1	1	1	1	1	1	1	1	1	1	1	1	1	1	1	1	1
3	1	1	1	1	1	1	1	1	1	1	1	1	1	1	1	1	1	1	1
4	1	1	1	1	1	1	1	1	1	1	1	1	1	1	1	1	1	1	1
5	1	1	1	1	1	1	1	1	1	1	1	1	1	1	1	1	1	1	1
6	1	1	1	1	1	1	1	1	1	1	1	1	1	1	1	1	1	1	1
7	1	1	1	1	1	1	1	1	1	1	1	1	1	1	1	1	1	1	1
8	1	1	1	1	1	1	1	1	1	1	1	1	1	1	1	1	1	1	1
9	1	1	1	1	1	1	1	1	1	1	1	1	1	1	1	1	1	1	1
10	1	1	1	1	1	1	1	1	1	1	1	1	1	1	1	1	1	1	1

Table 94: Severity scores from PTVs, OARs, and overall for ten clinical oropharyngeal patients with MU linearity errors.

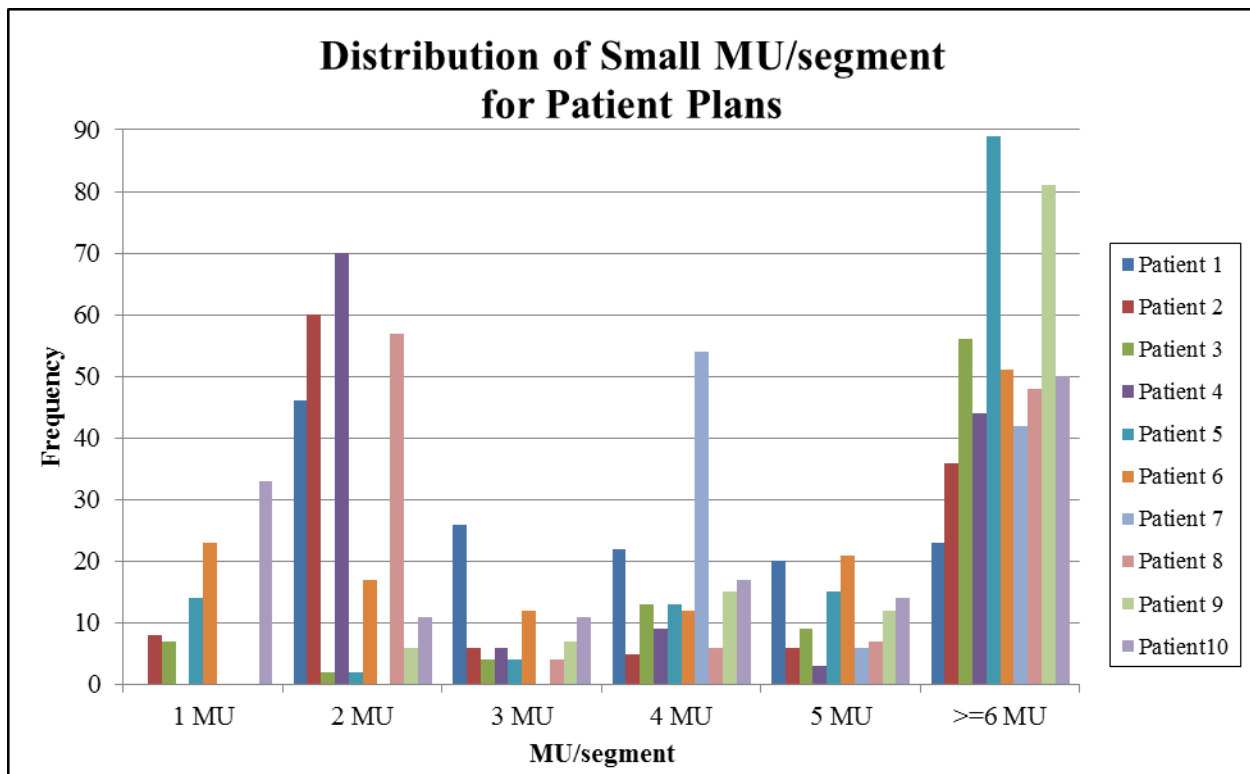


Figure 110: The distribution of segments with few MU which would be affected by MU linearity errors for each of our ten patients.

Failure mode 8: MLC leakage and transmission modeling true severity

As in the phantom treatment planning studies, beam models with errors in the interleaf leakage transmission were applied to ten clinical patient treatment plans to assess the severity of this failure mode. The resultant severity scores are shown in Table 95 resulting from an increase in the MLC interleaf leakage transmission. Overall severity scores all resulted from cochlea and parotid gland increased doses. There were also some small increases in brainstem and spinal cord doses for some patients, but the errors with this failure mode were dominated by the cochlear and parotids. This was likely due to the small volume and lower doses associated with the cochlea and the large amount of MLC blocking required for parotid glands immediately adjacent to targets.

Patient	MLC Leakage and Transmission Modeling Errors						
	Interleaf leakage transmission = 0%			Interleaf leakage transmission = 10%			Overall
	PTVs	OARs	Total	PTVs	OARs	Total	
1	1	1	1	1	7	7	7
2	1	1	1	1	7	7	7
3	1	1	1	1	5	5	5
4	1	1	1	1	8	8	8
5	1	3	3	1	7	7	7
6	1	1	1	1	6	6	6
7	1	1	1	1	7	7	7
8	1	1	1	1	5	5	5
9	1	1	1	1	8	8	8
10	1	1	1	1	7	7	7

Table 95: Severity scores from PTVs, OARs, and overall for ten clinical oropharyngeal patients with MLC leakage and transmission errors.

Failure mode 9: MLC tongue-and-groove modeling true severity

As in the phantom treatment planning studies, beam models with errors in MLC tongue-and-groove width were applied to ten clinical patient treatment plans to assess the severity of this failure mode. The resultant severity scores are shown in

Patient	MLC Tongue-and-Groove Modeling Errors						
	Tongue-and-groove width = 0.005 cm			Tongue-and-groove width = 0.200 cm			Overall
	PTVs	OARs	Total	PTVs	OARs	Total	
1	1	1	1	1	2	2	2
2	1	1	1	1	2	2	2
3	1	1	1	1	1	1	1
4	1	1	1	1	4	4	4
5	1	4	4	1	3	3	4
6	1	1	1	1	1	1	1
7	1	1	1	1	2	2	2
8	1	1	1	1	2	2	2
9	1	1	1	1	4	4	4
10	1	1	1	1	3	3	3

Table 96. The overall severity scores for this failure mode ranged from 1 to 4. Only for patient 5

did a decrease in the tongue width result in a higher severity score than an increase which was a result of an increase in the dose to the spinal cord with either tongue width.

Patient	MLC Tongue-and-Groove Modeling Errors						
	Tongue-and-groove width = 0.005 cm			Tongue-and-groove width = 0.200 cm			Overall
	PTVs	OARs	Total	PTVs	OARs	Total	
1	1	1	1	1	2	2	2
2	1	1	1	1	2	2	2
3	1	1	1	1	1	1	1
4	1	1	1	1	4	4	4
5	1	4	4	1	3	3	4
6	1	1	1	1	1	1	1
7	1	1	1	1	2	2	2
8	1	1	1	1	2	2	2
9	1	1	1	1	4	4	4
10	1	1	1	1	3	3	3

Table 96: Severity scores from PTVs, OARs, and overall for ten clinical oropharyngeal patients with MLC tongue-and-groove modeling errors.

Failure mode 10: MLC leaf end modeling true severity

As in the phantom treatment planning studies, beam models with errors in MLC leaf end modeling radius were applied to ten clinical patient treatment plans to assess the severity of this failure mode. The resultant severity scores are shown in Table 97. Overall severity scores for changes in the rounded leaf end modeling radius ranged from 5 to 9 and were all a result of decreasing this radius to 4 cm, making the ends more round. Again, parotid gland dose increases were largely the cause of these severity scores, as well as increases in the cochlear doses.

Patient	MLC Leaf End Modeling Errors									Overall
	Leaf end radius = 4 cm			Leaf end radius = 20 cm			Leaf end radius = 15 cm			
	PTVs	OARs	Total	PTVs	OARs	Total	PTVs	OARs	Total	
1	1	8	8	1	1	1	1	1	1	8
2	1	8	8	1	1	1	1	1	1	8
3	1	5	5	1	1	1	1	1	1	5
4	1	9	9	1	1	1	1	1	1	9
5	1	7	7	3	1	3	2	2	2	7
6	1	5	5	1	1	1	1	1	1	5
7	1	9	9	1	1	1	1	1	1	9
8	1	7	7	1	1	1	1	1	1	7
9	1	8	8	1	1	1	1	1	1	8
10	1	7	7	1	1	1	1	1	1	7

Table 97: Severity scores from PTVs, OARs, and overall for ten clinical oropharyngeal patients with MLC leaf end modeling errors.

Failure mode 11: CT table true severity

As in the phantom treatment planning studies, beam models with errors in the CT table used for heterogeneity corrections in the treatment planning system were applied to ten clinical patient treatment plans to assess the severity of this failure mode. The resultant severity scores are shown in Table 98. The overall severity scores for this failure mode ranged from 1 to 3. Patient 2 had changes in the dose to the spinal cord with when the PET CT table was used, which had large differences in the more dense materials. Patient 5 had increases to the spinal cord maximum dose for all three CT tables evaluated. It seemed that the spinal cord of patient 5 was in a particularly steep dose gradient so that any little change could result in a substantial change in the maximum dose to the cord, because it had increases in dose of some magnitude resulting in a severity score greater than one for all failure modes except failure mode 1. Other patients' spinal cords weren't necessarily this sensitive, for example patient one only had substantial increases in spinal cord maximum doses in 5/11 failure modes.

Patient	CT Table Errors									Overall
	2% high			PET CT			2% low			
	PTVs	OARs	Total	PTVs	OARs	Total	PTVs	OARs	Total	
1	1	1	1	1	1	1	1	1	1	1
2	1	1	1	1	2	2	1	1	1	2
3	1	1	1	1	1	1	1	1	1	1
4	1	1	1	1	1	1	1	1	1	1
5	1	3	3	1	3	3	1	3	3	3
6	1	1	1	1	1	1	1	1	1	1
7	1	1	1	1	1	1	1	1	1	1
8	1	1	1	1	1	1	1	1	1	1
9	1	1	1	1	1	1	1	1	1	1
10	1	1	1	1	1	1	1	1	1	1

Table 98: Severity scores from PTVs, OARs, and overall for ten clinical oropharyngeal patients with CT table errors.

Summary of true severity scores

A summary of the overall severity scores for all failure modes for each patient is tabulated in Table 99, which includes symmetry errors of 2% and MLC positional errors of 2 mm. Several factors may have played a role in exaggerating the severity of some failure modes including structures or constraints with low doses or small volumes. Not all patients had these structures, such as cochlea, orbits, lenses, and optic nerves, so we reassessed the severity scores for all failure modes using only the four OARs that each patient had, which were: brainstem, spinal cord, and left and right parotid glands. We used the difference from baseline in the maximum dose to the brainstem and cord and the mean dose to the parotid glands. The results of this reevaluation are shown in Table 100. This resulted in generally lower severity scores, but not in every case. Patients 1, 4, 8, and 10 were especially affected by this since those challenging structures were a part of the evaluation of these patients. A side-by-side comparison of the overall true severity scores from these to OAR evaluation criteria is shown in Table 101.

True Severity Scores <i>PTVs and All OARs</i>										
Failure Mode	Patient Number									
	1	2	3	4	5	6	7	8	9	10
1	7	9	8	7	8	9	2	8	9	9
2	1	1	1	1	1	1	1	1	1	9
3	9	5	7	8	9	9	7	9	10	10
4	4	4	1	4	7	5	5	2	4	5
5	9	7	7	9	7	4	9	9	7	9
6	9	7	7	9	7	3	7	9	7	2
7	1	1	1	1	1	1	1	1	1	1
8	7	7	5	8	7	6	7	5	8	7
9	2	2	1	4	4	1	2	2	4	3
10	8	8	5	9	7	5	9	7	8	7
11	1	2	1	1	3	1	1	1	1	1

Table 99: True severity scores based on PTV coverage ($D_{95\%}$) and QUANTEC criteria of OARs for ten clinical oropharyngeal patients for 11 IMRT physical failure modes near tolerance criteria levels.

True Severity Scores <i>PTVs and 4 Common OARs</i>										
Failure Mode	Patient Number									
	1	2	3	4	5	6	7	8	9	10
1	7	9	8	7	8	9	2	8	9	3
2	1	1	1	1	1	1	1	1	1	2
3	5	5	7	6	9	9	7	5	4	9
4	4	4	1	4	7	5	5	1	4	5
5	7	5	7	2	7	7	5	5	7	7
6	5	7	7	4	7	3	4	8	7	2
7	1	1	1	1	1	1	1	1	1	1
8	7	7	5	5	7	6	7	5	8	7
9	1	2	1	1	4	1	1	1	4	3
10	4	8	4	3	7	5	4	1	4	7
11	1	2	1	1	3	1	1	1	1	1

Table 100: True severity scores based on PTV coverage ($D_{95\%}$) and QUANTEC criteria of four common OARs for ten clinical oropharyngeal patients for 11 IMRT physical failure modes near tolerance criteria levels.

Failure Mode	True Severity Score Comparison					
	PTVs & All OARs			PTVs & 4 Common OARs		
	Median	Average	Std Dev	Median	Average	Std Dev
1	8	7.6	2.12	8	7	2.49
2	1	1.8	2.53	1	1.1	0.32
3	9	8.8	1.14	7	7.1	2.08
4	4	4.1	1.66	4	4	1.83
5	8	7.7	1.64	7	5.9	1.66
6	7	6.7	2.41	6	5.4	2.07
7	1	1	0	1	1	0
8	7	6.7	1.06	7	6.4	1.07
9	2	2.5	1.18	1	1.9	1.29
10	7.5	7.3	1.42	4	4.7	2.11
11	1	1.3	0.67	1	1.3	0.67

Table 101: A comparison of the overall true severity scores from 10 patients with two different OAR criteria evaluated.

The set of severity scores found using the four common OARs was less conservative, but may have been more reasonable. This problem highlighted the limitation of using our straight-forward and simplified quantitative approach to assigning severity scores. The simple approach allowed us to assess severity in a straight forward manner which was easily relatable to physics measurements, goals, and tolerances. However, the complicated nature of tissue response and the balancing act of achieving coverage while sparing normal tissues was over-simplified with this approach. The true severity was extremely challenging to identify for any given patient, none the less an entire patient population. Our approach simplified this problem and enabled us to still provide meaningful information with respect to the severity of the consequences of these failure modes and make comparisons.

3.2.2 Comparison of qualitative and quantitative severity scores ability to predict true severity scores

An overall comparison of the survey results (qualitative severity scores), phantom treatment planning studies on standard and complex plans (quantitative severity scores), and treatment planning studies using ten clinical oropharyngeal patients (true severity scores) using the evaluation of the PTVs and four common OARs is shown in Figure 111. The spread in the true severities seemed to exceed that in both our qualitative and quantitative severity scores for many of the eleven failure modes.

For failure mode 1 (beam energy), eight of the ten true severity scores were larger than both the qualitative and quantitative severity scores we predicted. Qualitative and quantitative severity scores for this failure mode agreed only with patient 10. The lack of agreement between quantitative and true severity here is likely due to the fact that in the phantom isocenter was at the center of the patient, between PTVs, and all structures were fairly central, while in the patient plans isocenter was below the chin, with field edges further off axis covering PTVs and OARs. This meant that the changes in the off axis dose due to energy changes that were more pronounced further off-axis had a greater effect on the patient plans.

For failure mode 2 (beam symmetry 2%), the true severity scores were all lower than the survey predicted and agreed well with the quantitative phantom scores. Patient 10 had a higher severity for failure mode 2 than the quantitative phantom scores predicted, indicating that the quantitative scores may not have been sufficiently conservative for all oropharyngeal patients with this failure mode. This made sense since we would expect the effects of symmetry errors to affect the patients with larger field sizes and non-central isocenters more than the phantom.

For failure mode 3 (MLC position 2 mm), the true severity scores were high, up to 10 for one patient. The qualitative severity scores underestimated this as did the quantitative scores, however the overall quantitative score of 8 appeared to be a better estimate than the median qualitative score of 5. In the literature the reported severity of this failure mode was lower, with Mu *et al.* showing up to 13% changes in parotid dose for a H&N patient with 1 mm systematic errors which would correspond to a severity score of 7 on our scale⁴⁸. Our high true severity score for this failure mode resulted from parotid and eye-related structure dose increases in patient 10 for both 1 mm and 2 mm shifts. With a comparable set up to the study by Mu, *et al.* we saw up to a 33% increase in the mean dose to the left parotid gland with 1 mm systematic shifts (S=9). This difference first demonstrated that it was difficult to fully capture patient variability with just one severity score. This comparison also demonstrated that our quantitative severity score provided a better estimate of the severity in our study and the literature.

For failure mode 4 (gantry angle 2°), the phantom and patient plans both fell within the whiskers of the survey. The overall quantitative severity score matched the highest true severity score of this failure mode ($S=7$) while the median qualitative score was low ($S=4$). The steep dose gradient in the phantom near a critical structure, which was cause of the phantom severity score, conservatively represented the potential failures in true clinical patients. Severity of gantry angle errors were reported to be high in the literature, up to 40% dose errors 10 cm from isocenter in a pelvic IMRT case with 2° systematic rotation⁷⁴. Our patient plans included doses delivered up to 13.4 cm from the isocenter, but the patient structures at the evaluation criteria did not capture errors that large. This comparison again highlighted the complexity of comparing patient-specific dose distributions as well as the challenge of capturing the magnitude of errors in a clinically meaningful manner.

For failure mode 5 (collimator angle 2°), quantitative and true severity scores again fell within the whiskers of the survey results, but both the median qualitative and overall quantitative severity scores, $S=4$ and $S=5$ respectively, were low compared to the maximum true severity score of 7. Unlike for failure mode 4, the phantom for this failure mode did not provide a conservative representation of true clinical patients, likely due to the patients OARs further off-axis than those in the phantom that experienced a greater displacement in the dose as a result of the collimator rotation. An IMRT pelvic plan in the literature reported up to 20% dose errors with 2° collimator rotation, which was slightly higher than the errors we saw in our H&N patient population⁷⁴.

For failure mode 6 (couch angle 2°), qualitative and quantitative severity scores were again lower than the true severity score, though there was a relatively large spread in the patient results. The highest true severity score of 8 was completely outside of the range of survey responses, while both quantitative and qualitative severity scores predicted $S=4$. The sensitivity of off-axis OARs to couch angle rotations was much greater in the large field patients than in our smaller field phantom. As reported in the literature, errors in the couch angle had the potential to cause errors comparable in magnitude to collimator and gantry angular misalignments⁷⁵.

For failure mode 7 (MU linearity), the quantitative severity scores matched all true severity scores at $S = 1$, but the qualitative severity scores were high. This was not surprising since MU linearity at low MU has been published on extensively, one would expect this failure mode to have an effect on the true severity. This, however, was not the case in our study.

For failure mode 8 (MLC leakage and transmission modeling), the qualitative ($S=4$) and especially quantitative ($S=1$) severity scores underestimated the true severity scores, the maximum of which was 7. The fields in the patient treatment plans were larger than those in the phantom treatment plans because the targets were much larger and extended to include many more nodes. As a result, the MLC were used more extensively for blocking and therefore the effects of interleaf leakage and transmission were greater.

For failure mode 9 (MLC tongue-and-groove modeling) the median qualitative severity score predicted the highest true severity score of 4, while the overall quantitative score was within the spread of the true severity scores but low ($S=2$). The larger patient fields would also be affected more greatly by tongue-and-groove effects than the smaller phantom fields, which may explain this discrepancy. The magnitude of errors seen in our patient studies was comparable to the 5% dose error reported in the literature⁸⁴.

For failure mode 10 (MLC leaf end modeling), there was a relatively large spread in the true severity scores and both median qualitative and overall quantitative underestimated the maximum true severity ($S=8$), but lay around the average true severity score ($S=4.7$). This phantom has been known to respond to errors in rounded leaf end modeling as demonstrated by Cadman, *et al.* an increase in the spinal cord TLD doses and DTA in the high dose gradient region were seen when the leaf offset used to account for transmission were not accounted for. Although this was a different component of MLC leaf end modeling, the effects on the phantom results were seen in similar regions in the phantom⁸⁹. Most

likely, the changes in penumbra resultant from changes in the leaf end modeling effected patient treatment plans more than phantom plans since there were larger fields in which more MLC leaf ends were exposed.

Finally, for failure mode 11 (CT table), the median qualitative severity score predicted the maximum true score, while the quantitative score agreed with most of the true scores at $S=1$. The phantom was made of a rather homogenous medium and therefore was not affected by the change in CT table, while there were some small changes in some of the patient treatment plans. Small changes that would not have increased the severity score from 1 were reported in the literature for conformal radiation treatments with errors in the CT table comparable to our study⁸⁸. Patient-specific anatomy played a large role in the severity of this failure mode.

As was done to compare the qualitative and quantitative severity scores, we performed Wilcoxon Signed Rank tests to compare the quantitative (one-sample) and qualitative severity scores (independent samples) to the true severity scores. The results of this comparison are shown in Table 102 and in addition to the significance values for these tests, this table includes the 95% confidence intervals of the median true severity scores, the overall quantitative severity scores, and the median qualitative severity scores. Based on this assessment, neither method perfectly predicted the true severity scores but the quantitative assessment performed better than the qualitative with eight of the eleven failure mode severity scores not having significant differences from the median true severity score for the quantitative scores compared to six of the eight of the qualitative scores. If we performed this same analysis with the true severity scores from all of the OARs instead of just the four common OARs, the ability of both the quantitative and qualitative severity scores to predict the true severity scores were reduced, with five of the eleven failure mode quantitative severity scores not significantly different than the true median severity score and three of the eleven qualitative severity scores. This analysis is shown in Table 103. In either case, the quantitative severity scores matched the median true severity scores better, technically proving our hypothesis to be true. In addition to this analysis, we compared the maximum severity scores for each the qualitative, quantitative, and true, since we were most concerned with the maximum

consequences of our IMRT H&N physical failure modes. This comparison is shown in Table 104. Based on the maximum true severity scores, the maximum qualitative severity scores better predicted the true severity, with two of the qualitative severity scores matching perfectly and 3 matching within one score. The maximum quantitative severity scores (used as the overall quantitative severity score), median qualitative, and maximum qualitative severity scores all directly matched two of the failure mode maximum true severity scores. In each case, these two matches were for different failure modes. Additionally, the quantitative severity score was within one score for one failure mode and the maximum qualitative severity score was within one score for two failure modes. This told us that when considering the overall maximum severity scores, the qualitative approach performed slightly better, by predicting two additional failure mode severity scores within one score than the quantitative, though both approaches matched the same number of severity scores directly.

In the end, neither the qualitative or quantitative approach to providing severity scores for our step and shoot IMRT H&N physical failure modes fully captured the true severities that we observed in ten clinical patients. These true severity scores were highly variable amongst patients for many of the failure modes, indicating that patient-specific components play a large role in the severity of consequences from a particular failure mode. This was well-reflected in the variability of severity scoring amongst survey responses from members of the medical physics community however the qualitative scores obtained did not always reflect the true severity. The IROC-H IMRT H&N phantom designed to mimic an oropharyngeal patient and assess an institution's ability to properly deliver a complex IMRT treatment, represented the effects of many of the failure modes in a true patient moderately well. The phantom was limited in its representation of true patients, particularly in the field sizes used and the presence of structures far off-axis, and therefore did not always capture the maximum true severity. When considering maximum true severity scores, each approach to scoring matched the true severity for different failure modes, demonstrating that overall, these methods are imperfect along but have the potential to provide complementary information.

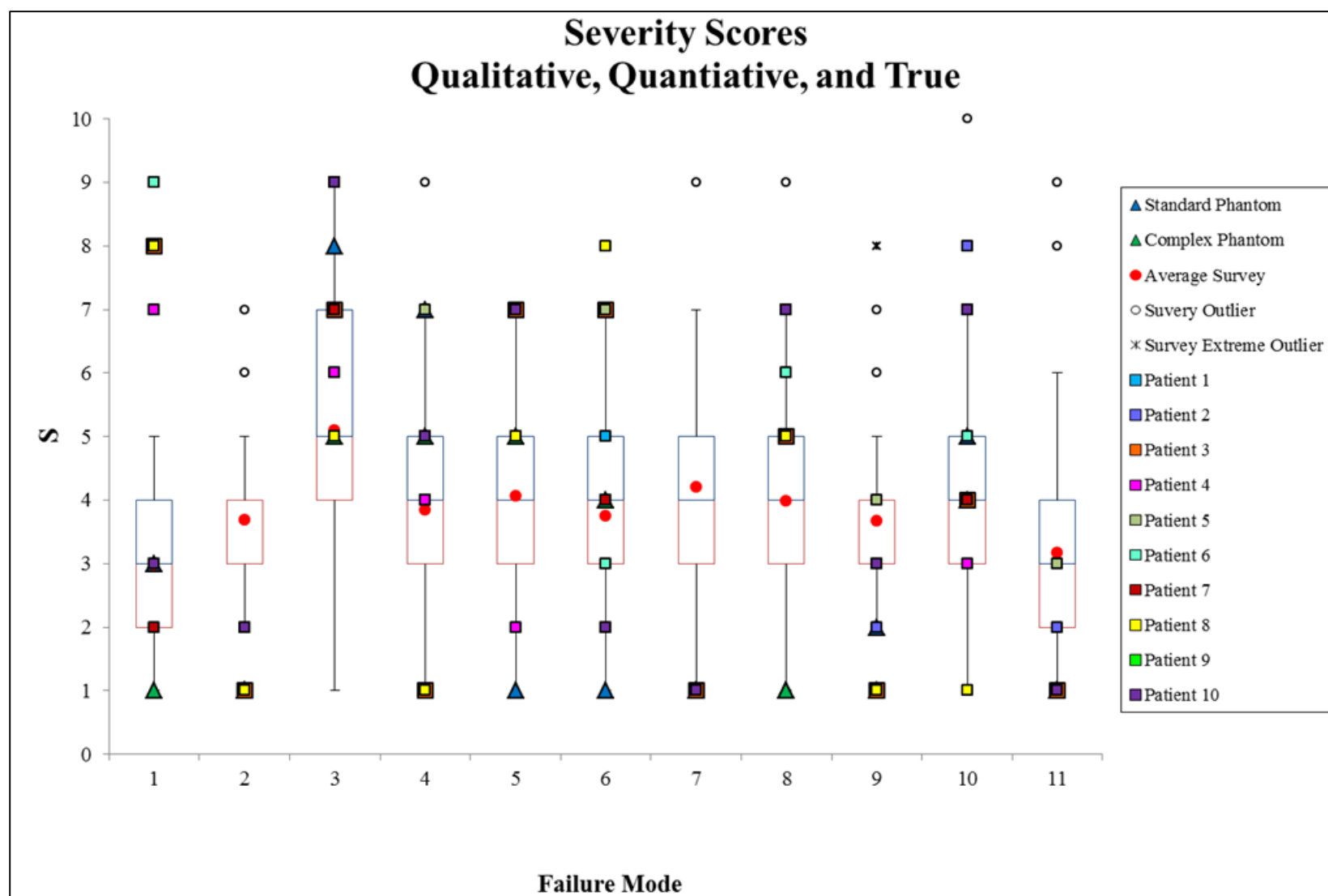


Figure 111: Summary of severity scores obtained from survey, phantom treatment planning studies on standard and complex plans, and ten oropharyngeal clinical patients for our 11 IMRT physical failure modes.

Failure Mode	True Severity Score <i>95% Confidence Interval of the Median</i>			Quantitative Severity Score	Sig.	Qualitative Severity Score	Sig.
	Lower Bound	Median	Upper Bound				
1. Beam Energy	6.02	8	9.98	3	0.010	3	0.026
2. Beam Symmetry	0.75	1	1.25	1	0.317	4	0.233
3. MLC Position	5.35	7	8.65	8	0.215	5	0.061
4. Gantry Angle	2.55	4	5.45	7	0.007	4	0.746
5. Collimator Angle	5.68	7	8.32	5	0.206	4	0.001
6. Couch Angle	4.36	6	7.64	4	0.055	4	0.068
7. MU Linearity	1.0	1	1.0	1	1.000	4	0.020
8. MLC Leakage & Transmission	6.15	7	7.85	1	0.004	4	0.000
9. MLC Tongue & Groove	0	1	2.02	2	0.851	4	0.168
10. MLC Leaf End	2.33	4	5.67	5	0.764	4	0.890
11. CT Table	0.46	1	1.54	1	0.180	3	0.017

Table 102: Comparison of median qualitative severity scores from the survey (N=184) and the overall quantitative severity scores from standard and complex phantom treatment planning studies to the 95% confidence interval of the median true severity score based on the evaluation of PTVs and four common OARs in ten oropharyngeal patient treatment plans. Red indicates that the score does not lie within the 95% CI and green indicates it does.

Failure Mode	True Severity Score <i>95% Confidence Interval of the Median</i>			Quantitative Severity Score	Sig.	Qualitative Severity Score	Sig.
	Lower Bound	Median	Upper Bound				
1. Beam Energy	6.32	8	9.68	3	0.006	3	0.004
2. Beam Symmetry	0	1	3.01	1	0.317	4	0.679
3. MLC Position	8.10	9	9.90	8	0.057	5	0.000
4. Gantry Angle	2.68	4	5.32	7	0.007	4	0.746
5. Collimator Angle	6.70	8	9.30	5	0.006	4	0.001
6. Couch Angle	5.09	7	8.91	4	0.011	4	0.002
7. MU Linearity	1.0	1	1.0	1	1.000	4	0.020
8. MLC Leakage & Transmission	6.16	7	7.84	1	0.004	4	0.000
9. MLC Tongue & Groove	1.7	2	2.93	2	0.163	4	0.168
10. MLC Leaf End	6.38	7.5	8.62	5	0.011	4	0.000
11. CT Table	0.46	1	1.54	1	0.180	3	0.017

Table 103: Comparison of median qualitative severity scores from the survey (N=184) and the overall quantitative severity scores from standard and complex phantom treatment planning studies to the 95% confidence interval of the median true severity score based on the evaluation of PTVs and all OARs in ten oropharyngeal patient treatment plans. Red indicates that the score does not lie within the 95% CI and green indicates it does.

Failure Mode	Severity Scores			
	True	Quantitative	Qualitative	
	Maximum	Maximum	Median	Maximum
1	9	3	3	9
2	2	1	4	7
3	10	8	5	9
4	7	7	4	9
5	7	5	4	8
6	8	4	4	8
7	1	1	4	9
8	8	1	4	9
9	4	2	4	8
10	8	5	4	10
11	3	1	3	9

Table 104: Comparison of maximum true severity scores from the evaluation of PTVs and four common OARs in ten oropharyngeal patient treatment plans to maximum quantitative severity scores from standard and complex phantom treatment planning studies and median and maximum qualitative severity scores from the survey (N=184). Green indicates matching exactly with maximum true severity, yellow indicates matching within 1 score.

Failure Mode	Severity Scores			
	True	Quantitative	Qualitative	
	Maximum	Maximum	Median	Maximum
1	9	3	3	9
2	9	1	4	7
3	10	8	5	9
4	7	7	4	9
5	9	5	4	8
6	9	4	4	8
7	1	1	4	9
8	8	1	4	9
9	4	2	4	8
10	9	5	4	10
11	3	1	3	9

Table 105: Comparison of maximum true severity scores from the evaluation of PTVs and all OARs in ten oropharyngeal patient treatment plans to maximum quantitative severity scores from standard and complex phantom treatment planning studies and median and maximum qualitative severity scores from the survey (N=184). Green indicates matching exactly with maximum true severity, yellow indicates matching within 1 score.

Chapter 4: Conclusions

4.1 Specific Aim 1 Conclusions

The objective of this specific aim was to obtain and compare qualitative and quantitative FMEA severity scores for the identified critical IMRT H&N physical dose delivery failure modes. The working hypothesis of this specific aim was that subjective qualitative severity scores obtained through a conventional FMEA were significantly different than quantitative severity scores generated from computed and measured data. Based on our comparison using the one-sample Wilcoxon Signed Rank Test, our hypothesis was true for nine of the eleven failure modes. Large variability was observed in the qualitative severity scores for our failure modes obtained through an online survey of medical physicists, though no universal trends in the scores with demographics were identified. Treatment planning studies with the IROC-H IMRT H&N phantom using standard and complex treatment plans often resulted in different severity scores, providing insight to the potential variability amongst patients. Physical measurements with the phantom generally demonstrated agreement with the treatment planning studies, though the sensitivity of the phantom to the failure modes was lower, particularly the absolute dose measurements with TLD because of the higher uncertainty associated with the TLD compared to ion chamber measurements.

4.2 Specific Aim 2 Conclusions

The objective of this specific aim was to compare the validity of the quantitative and qualitative scores by evaluating the true severity for each failure mode in clinical H&N patients. The working hypothesis of this specific aim was that quantitative severity scores were significantly more likely than qualitative subjective scores to describe true clinical consequences. Based on our comparison of the median qualitative and maximum quantitative severity scores to the true severity scores from patient plans using independent sample and one sample Wilcoxon Signed Rank Tests, respectively, our hypothesis was true with quantitative severity scores matching the median true severity for eight of the eleven failure modes and median qualitative severity scores matching the median true severity for six of the eleven

failure modes. Patient treatment plans demonstrated sensitivity to failure modes primarily in OARs and overall severity scores for each failure mode had large variability amongst patients. OAR structures with small volumes and relatively small doses proved to be extremely sensitive in some cases when using our severity scoring scale (Table 7).

4.3 Overall Conclusions

FMEA has been gaining popularity in radiation therapy in response to both 1) catastrophic errors which highlight our need for comprehensive process quality management and 2) the ever-increasing work load required to keep up with the advancing technologies and techniques in today's busy clinics. Many advantages and disadvantages of the application of FMEA to radiation therapy processes have been discussed^{7,37-41}. Our goal was to draw on some of the disadvantages to expand the utility of FMEA for radiation therapy and improve the results of these analyses. Based on our comparison of qualitative and quantitative severity scores to true clinical severity scores, we concluded that quantitative severity scores better predicted true severity scores for our step and shoot IMRT H&N physical failure modes, indicating that using a quantitative approach to severity scoring is a valuable and needed improvement over the subjective traditional qualitative approach for physics specific components of radiation therapy processes.

From this work, a few observations on step and shoot H&N IMRT QA procedures for specific failure modes can be made. First, beam energy had a greater potential for inducing high severity errors in patient plans than expected in our survey or phantom studies. These errors appeared to be primarily a result of the off-axis changes caused by energy changes as opposed to the commonly measured PDD changes. Gao, *et al.* has recommended measuring diagonal profiles to monitor beam energy and our results support that idea⁶³. What was also observed during the phantom measurements using clinically decommissioned linacs, was that the safeguards currently in place with modern linacs do not allow for any significant energy changes that would exceed current AAPM TG-40's QA 2% acceptability criteria and possibly the TG-142's criteria of 1% from baseline^{60,90}. Second, the MLC tolerance recommended for IMRT by AAPM TG-142 of ± 1 mm is critical. We saw the potential for severe consequences in our

studies with systematic MLC offsets of 2 mm and even offsets of 1 mm had the potential for introducing dose delivery errors to normal tissues. These failure modes were determined to be the most critical in our analysis. Our study also indicated that angular misalignments and MLC modeling failures can be serious, but not to the same degree as the energy and MLC offset failures. Alternatively, we saw that MU linearity errors for segments with less than 5 MU did not have a substantial impact on H&N patient treatment plans. More recent machines are not as susceptible to the over-shoot effect and it is becoming more common to set lower limits on the number of MU/segment allowed in the TPS, which both serve to eliminate this failure mode. We do not have sufficient data to recommend completely removing this QA test, however these factors along with our results indicate that this failure mode is of low priority.

Regarding FMEA in radiation therapy, we can conclude that quantitative data can provide insight into the effects of tolerance criteria level failures that can be underestimated within the perception the medical physics community. However, the qualitative severity scores provided useful information as well and the more important conclusion of this project was that while this process is very complicated the more information available to inform scoring decisions, the more reliable and accurate the severity scoring will be. The benefit of generating a more comprehensive understanding of the entire process by the full participating team is clear and can only improved by utilizing quantitative data that solidify the understanding of the risks these failure modes present. Moving forward, FMEA and other risk-based prospective quality improvement methods will continue to become more widely implemented due to the publication of AAPM TG-100, the progression of radiation therapy advancements and required quality management, and the continued mentality of “one error is an error too many.” Based on the results of this study, we recommend further quantitative investigation into the severity of physical failure modes in additional treatment sites to fully utilize the FMEA process for the improvement of physics-specific components to the radiation therapy process. An FMEA as conventionally proposed already requires a significant allocation of time and resources, so adding a quantitative component to the analysis for each clinic is not necessarily feasible. A robust yet generalized investigation of failure mode effects on various

treatment sites such as that performed in this study and expanded to include other common treatment equipment and techniques would be valuable for guiding individual clinics attempting to improve their physics quality management through FMEA. Since we have shown that the effect of these failure modes are very patient specific, a study of the impacts on different treatment sites would allow for the identification of the most conservative severity estimates for certain radiation therapy processes as whole enabling clinics treating multiple sites to maintain a conservative approach. In order to integrate this quantitative approach, we also recommend the formulation of a severity scoring scale and method that includes a quantitative component as ours did. This scoring scale and method should be physician driven to ensure that our clinical objectives remain forefront in these efforts. Following these steps, the FMEA process, particularly for the improvement of physics quality management, has the potential for being extremely useful in not only increasing our appreciation for radiation therapy processes as a whole but in allowing us to understand and effectively mitigate risks.

Appendix A: Surveys for qualitative severity scoring

A.1 Pilot Survey

2013 IMRT FMEA Survey

Failure Modes and Effects Analysis (FMEA) is a risk analysis tool recommended in the upcoming AAPM TG-100 report. FMEA provides a prospective end-to-end risk evaluation of radiotherapy processes by means of a subjective qualitative scoring system. Several institutions are already beginning to implement FMEA, though its proper place in radiotherapy quality management is currently unclear.

Objective: This survey is being conducted to evaluate the subjective nature of FMEA in radiotherapy. We are examining dose calculation and linac delivery failures near tolerance criteria levels. Data will be used for a dissertation project.

Instructions: Please answer the questions to the best of your ability based on your knowledge and experience. Please only complete this survey once. If you have any questions or comments, please fill in the blank comment section at the end and feel free to contact Jackie Tonigan at JRTonigan@mdanderson.org.

General Information:

1. How many years of clinical physics experience do you have?

2. Are you currently ABR certified? Check one.

☐ Yes

☐ No

3. Approximately what percentage of your time is dedicated to clinical work?

Consider a head and neck IMRT treatment delivery (not VMAT).
For this type of treatment in your current practice:

4. What linear accelerator manufacturer do you primarily use? Check one.

☐ Varian

☐ Elekta

- ☐ Siemens
☐ Other _____

5. What treatment planning system do you primarily use? Check one.

- ☐ Eclipse
☐ Pinnacle
☐ Other _____

6. What technique do you primarily use? Check one.

- ☐ Step and shoot/Segmental MLC
☐ Sliding window/Dynamic MLC
☐ Other _____

Failure Mode Scoring

Failure Modes and Effects Analysis (FMEA) is a prospective quality tool. It is used to rank potential failures of a process (failure modes) in order of the risk they present. To rank the failures, three scores are assigned for each failure mode by a team of experts: the likelihood of occurrence (O), severity (S), and lack of detectability (D).^{7,45}

7. How familiar are you with Failure Modes and Effects Analysis? Circle one.

- ☐ Very familiar
☐ Somewhat familiar
☐ Slightly familiar
☐ Not familiar

Consider a head and neck IMRT treatment delivery (not VMAT) in your current practice. For each of the 12 planning and delivery failures in Table 1*, think about the failure propagating through the treatment process to the patient for the whole treatment course. You will evaluate the risk associated with each failure.

Estimating Percent Dose Error

In Table 1*, column 2, fill in your best estimate of the percent dose error for patient target structures for each failure. Imagine the worst case scenario. Consider each failure independently.

Estimating Failure Mode Scores

In columns 3-5 of Table 1*, use Table A (provided on each of the following sheets) to fill in your best estimate of the following scores:

O = Occurrence. The likelihood the failure would occur. (1-10)

D = Detectability. The likelihood the failure would go undetected. (1-10)

S = Severity. The severity of the consequences of the failure. (1-10)

Note that risk increases for each score from 1 to 10, with 10 being the most risky.

Again, imagine the worst case scenario. Consider each failure independently.

*Table 1 is on pages 3 and 4

Rank	Occurrence (O)		Detectability (D)		Severity (S)	
	Qualitative	Frequency	Qualitative	Estimated probability of failure going <u>undetected</u>	Qualitative	Categorization
1	Failure Unlikely	0.01%	Never undetected	0.01%	No effect	
2		0.02%	Very low likelihood undetected	0.2%	Inconvenience	Inconvenience
3	Relatively few failures	0.05%		0.5%		
4		0.1%	Low likelihood undetected	1%	Minor dosimetric error	Suboptimal plan or treatment
5		< 0.2%		2%	Limited toxicity or tumor underdose	Wrong dose, dose distribution, location or volume
6	Occasional failures	< 0.5%		5%		
7		< 1%	Moderate likelihood undetected	10%	Recordable event, Potentially serious toxicity or tumor underdose	
8	Repeated failures	< 2%		15%		
9		<5%	High likelihood undetected	20%	Reportable event, Possible very serious toxicity or tumor underdose	Very wrong dose, dose distribution, location or volume
10	Failures inevitable	> 5%	Always undetected	> 20%	Catastrophic	

Table A: FMEA Score Scales

Table 1: Failure Mode Scoring

Please **fill in this table** using Table A above for columns 3-5 as instructed.

Failure		% dose error	O Occurrence (1-10)	D Detectability (1-10)	S Severity (1-10)
Delivery Failures					
1	Beam energy differs from baseline by 1% (TMR or PDD ratio)				
2	Beam symmetry differs from baseline by 2%				
3	MLC systematically differs in one bank by 2 mm				
4	Gantry angle systematically differs from baseline by 2.0°				
5	Collimator angle systematically differs from baseline by 2.0°				
6	Couch angle systematically differs from baseline by 2.0°				

Table A: FMEA Score Scales

Table 1: Failure Mode Scoring Continued...

Rank	Occurrence (O)		Detectability (D)		Severity (S)	
	Qualitative	Frequency	Qualitative	Estimated probability of failure going <u>undetected</u>	Qualitative	Categorization
1	Failure Unlikely	0.01%	Never undetected	0.01%	No effect	
2		0.02%	Very low likelihood undetected	0.2%	Inconvenience	Inconvenience
3	Relatively few failures	0.05%		0.5%		
4		0.1%	Low likelihood undetected	1%	Minor dosimetric error	Suboptimal plan or treatment
5		< 0.2%		2%	Limited toxicity or tumor underdose	Wrong dose, dose distribution, location or volume
6	Occasional failures	< 0.5%		5%		
7		< 1%	Moderate likelihood undetected	10%	Recordable event, Potentially serious toxicity or tumor underdose	
8	Repeated failures	< 2%		15%		
9		<5%	High likelihood undetected	20%	Reportable event, Possible very serious toxicity or tumor underdose	Very wrong dose, dose distribution, location or volume
10	Failures inevitable	> 5%	Always undetected	> 20%	Catastrophic	

Please fill in this table using Table A above for columns 3-5 as instructed.

Failure		% dose error	O Occurrence (1-10)	D Detectability (1-10)	S Severity (1-10)
7	Patient setup systematically differs from baseline by 3 mm in one direction				
8	MU linearity for < 5 MU systematically differs from baseline by 6%				
Dose Calculation Failures					
9	MLC transmission and leakage modeling is off by 0.5%				
10	MLC tongue-and-groove modeling is off by 0.5%				
11	MLC leaf end modeling is off by 0.5%				
12	CT number to electron density table systematically is off by 2%				

Questions or Comments:

-
-
-
-
1. Ford EC, Gaudette R, Myers L, et al. Evaluation of safety in a radiation oncology setting using failure mode and effects analysis. *Int J Radiat Oncol Biol Phys*. Jul 1 2009;74(3):852-858.
 2. Stamatis DH. *Failure mode and effect analysis : FMEA from theory to execution*. 2nd ed. Milwaukee, Wisc.: ASQ Quality Press; 2003.

Thank you for your time!

A.2 Full Survey

2014 IMRT Error Survey (Groups)

Objective and Instructions

Objective: This survey is being conducted to evaluate the perception of linac delivery and dose calculation errors near tolerance criteria levels. Data collected will be used for a doctoral dissertation and responses will remain anonymous.

Instructions

Please answer the questions as a group by means of consensus.

There are three parts to this survey:

1. Scoring Scale: You will be asked to fill in the quantitative component of a scoring scale.
2. Risk Assessment: You will be asked to evaluate the risk associated with 11 different failure modes near tolerance criteria levels.
3. Tell Us About You: Finally, you will give us some general information about your group.

Thank you very much for your time and input!

Scoring Scale

Part 1 Instructions

Table A below shows a scoring scale for assessing the risk associated with radiotherapy process failure modes (ways in which treatment can fail). The three scores range from 1 to 10, with 10 being the most risky.

Occurrence = The likelihood the error would occur. (1-10)

Lack of Detectability = The likelihood the error would go undetected. (1-10)

Severity = The severity of the consequences of the error. (1-10)

Score	Occurrence		Lack of Detectability		Severity	
	Qualitative	Frequency	Qualitative	Estimated probability of error going undetected	Qualitative	Categorization
1	Errors Unlikely	0.01%	Never undetected	0.01%	No effect	
2		0.02%	Very low likelihood undetected	0.2%	Inconvenience	Inconvenience
3	Relatively few errors	0.05%		0.5%		
4		0.1%	Low likelihood undetected	1%	Minor dosimetric error	Suboptimal plan or treatment
5		< 0.2%		2%	Limited toxicity or tumor underdose	Wrong dose, dose distribution, location or volume
6	Occasional errors	< 0.5%		5%		
7		< 1%	Moderate likelihood undetected	10%	Recordable event, Potentially serious toxicity or tumor underdose	
8	Repeated errors	< 2%		15%		
9		< 5%	High likelihood undetected	20%	Reportable event, Possible very serious toxicity or tumor underdose	Very wrong dose, dose distribution, location or volume
10	Errors inevitable	> 5%	Always undetected	> 20%	Catastrophic	

Both Occurrence and Lack of Detectability have quantitative components.

For Severity: Fill in the blanks to the right with your best estimate of the percent dose error corresponding to the severity scores 1-10.

Quantitative Severity - Percent dose error

- 1: _____
- 2: _____
- 3: _____
- 4: _____
- 5: _____
- 6: _____
- 7: _____
- 8: _____
- 9: _____
- 10: _____

Rank	Severity (S)		
	Qualitative	Categorization	Quantitative
1	No effect		
2	Inconvenience	Inconvenience	
3			
4	Minor dosimetric error	Suboptimal plan or treatment	
5	Limited toxicity or tumor underdose	Wrong dose, dose distribution, location or volume	
6			
7	Recordable event, Potentially serious toxicity or tumor underdose		
8			
9	Reportable event, Possible very serious toxicity or tumor underdose	Very wrong dose, dose distribution, location or volume	
10	Catastrophic		

Risk Assessment

Part 2 Instructions

Remember, please answer the questions as a group by means of consensus.

- Consider a head and neck (ex: Oropharyngeal) IMRT treatment delivery (not VMAT) in your current practice.
- For each of the 11 linac delivery and dose calculation failure modes in the questions, think about the error propagating through the treatment process to the patient for the entire treatment course.
- Evaluate the risk associated with each failure mode by estimating the percent dose error and assigning scores to them as described below.

Estimating Percent Dose Error

Fill in your best estimate of the percent dose error caused by each of the linac delivery and dose calculation errors on the following pages. Keep both patient target and critical structures in mind. Imagine the worst-case scenario. Consider each error independently.

Assigning Scores

From Table A, use the drop down menus to select your best estimate of each of the following scores:

Occurrence = The likelihood the error would occur. (1-10)

Lack of Detectability = The likelihood the error would go undetected. (1-10)

Severity = The severity of the consequences of the error. (1-10)

Remember that risk increases for each score from 1 to 10, with 10 being the most risky. Again, imagine the worst-case scenario for critical structures. Consider each error independently.

Linac Delivery Error 1

1) Beam energy differs from baseline by 1% (TMR or PDD ratio)

Percent Dose Error: _____

Occurrence

- () 1 - Errors Unlikely
- () 2
- () 3
- () 4
- () 5
- () 6
- () 7
- () 8
- () 9
- () 10 - Errors Inevitable

Lack of Detectability

- () 1 - Never Undetected
- () 2
- () 3
- () 4
- () 5
- () 6
- () 7
- () 8
- () 9
- () 10 - Always Undetected

Severity

- () 1 - No Effect
- () 2
- () 3
- () 4
- () 5
- () 6
- () 7
- () 8
- () 9
- () 10 - Catastrophic

Score	Occurrence		Lack of Detectability		Severity	
	Qualitative	Frequency	Qualitative	Estimated probability of error going undetected	Qualitative	Categorization
1	Errors Unlikely	0.01%	Never undetected	0.01%	No effect	
2		0.02%	Very low likelihood undetected	0.2%	Inconvenience	Inconvenience
3	Relatively few errors	0.05%		0.5%		
4		0.1%	Low likelihood undetected	1%	Minor dosimetric error	Suboptimal plan or treatment
5		< 0.2%		2%	Limited toxicity or tumor underdose	Wrong dose, dose distribution, location or volume
6	Occasional errors	< 0.5%		5%		
7		< 1%	Moderate likelihood undetected	10%	Recordable event, Potentially serious toxicity or tumor underdose	
8	Repeated errors	< 2%		15%		
9		< 5%	High likelihood undetected	20%	Reportable event, Possible very serious toxicity or tumor underdose	Very wrong dose, dose distribution, location or volume
10	Errors inevitable	> 5%	Always undetected	> 20%	Catastrophic	

Linac Delivery Error 2

2) Beam symmetry differs from baseline by 2%

Percent Dose Error: _____

Occurrence

- () 1 - Errors Unlikely
- () 2
- () 3
- () 4
- () 5
- () 6
- () 7
- () 8
- () 9
- () 10 - Errors Inevitable

Lack of Detectability

- () 1 - Never Undetected
- () 2
- () 3
- () 4
- () 5
- () 6
- () 7
- () 8
- () 9
- () 10 - Always Undetected

Severity

- () 1 - No Effect
- () 2
- () 3
- () 4
- () 5
- () 6
- () 7
- () 8
- () 9
- () 10 - Catastrophic

Score	Occurrence		Lack of Detectability		Severity	
	Qualitative	Frequency	Qualitative	Estimated probability of error going undetected	Qualitative	Categorization
1	Errors Unlikely	0.01%	Never undetected	0.01%	No effect	
2		0.02%	Very low likelihood undetected	0.2%	Inconvenience	Inconvenience
3	Relatively few errors	0.05%		0.5%		
4		0.1%	Low likelihood undetected	1%	Minor dosimetric error	Suboptimal plan or treatment
5		< 0.2%		2%	Limited toxicity or tumor underdose	Wrong dose, dose distribution, location or volume
6	Occasional errors	< 0.5%		5%		
7		< 1%	Moderate likelihood undetected	10%	Recordable event, Potentially serious toxicity or tumor underdose	
8	Repeated errors	< 2%		15%		
9		< 5%	High likelihood undetected	20%	Reportable event, Possible very serious toxicity or tumor underdose	Very wrong dose, dose distribution, location or volume
10	Errors inevitable	> 5%	Always undetected	> 20%	Catastrophic	

Linac Delivery Error 3

3) MLC position systematically differs in one bank by 2 mm.

Percent Dose Error: _____

Occurrence

- () 1 - Errors Unlikely
- () 2
- () 3
- () 4
- () 5
- () 6
- () 7
- () 8
- () 9
- () 10 - Errors Inevitable

Lack of Detectability

- () 1 - Never Undetected
- () 2
- () 3
- () 4
- () 5
- () 6
- () 7
- () 8
- () 9
- () 10 - Always Undetected

Severity

- () 1 - No Effect
- () 2
- () 3
- () 4
- () 5
- () 6
- () 7
- () 8
- () 9
- () 10 - Catastrophic

Score	Occurrence		Lack of Detectability		Severity	
	Qualitative	Frequency	Qualitative	Estimated probability of error going undetected	Qualitative	Categorization
1	Errors Unlikely	0.01%	Never undetected	0.01%	No effect	
2		0.02%	Very low likelihood undetected	0.2%	Inconvenience	Inconvenience
3	Relatively few errors	0.05%		0.5%		
4		0.1%	Low likelihood undetected	1%	Minor dosimetric error	Suboptimal plan or treatment
5		< 0.2%		2%	Limited toxicity or tumor underdose	Wrong dose, dose distribution, location or volume
6	Occasional errors	< 0.5%		5%		
7		< 1%	Moderate likelihood undetected	10%	Recordable event, Potentially serious toxicity or tumor underdose	
8	Repeated errors	< 2%		15%		
9		< 5%	High likelihood undetected	20%	Reportable event, Possible very serious toxicity or tumor underdose	Very wrong dose, dose distribution, location or volume
10	Errors inevitable	> 5%	Always undetected	> 20%	Catastrophic	

Linac Delivery Error 4

4) Gantry angle systematically differs from baseline by 2.0°.

Percent Dose Error: _____

Occurrence

- () 1 - Errors Unlikely
- () 2
- () 3
- () 4
- () 5
- () 6
- () 7
- () 8
- () 9
- () 10 - Errors Inevitable

Lack of Detectability

- () 1 - Never Undetected
- () 2
- () 3
- () 4
- () 5
- () 6
- () 7
- () 8
- () 9
- () 10 - Always Undetected

Severity

- () 1 - No Effect
- () 2
- () 3
- () 4
- () 5
- () 6
- () 7
- () 8
- () 9
- () 10 - Catastrophic

Score	Occurrence		Lack of Detectability		Severity	
	Qualitative	Frequency	Qualitative	Estimated probability of error going undetected	Qualitative	Categorization
1	Errors Unlikely	0.01%	Never undetected	0.01%	No effect	
2		0.02%	Very low likelihood undetected	0.2%	Inconvenience	Inconvenience
3	Relatively few errors	0.05%		0.5%		
4		0.1%	Low likelihood undetected	1%	Minor dosimetric error	Suboptimal plan or treatment
5		< 0.2%		2%	Limited toxicity or tumor underdose	Wrong dose, dose distribution, location or volume
6	Occasional errors	< 0.5%		5%		
7		< 1%	Moderate likelihood undetected	10%	Recordable event, Potentially serious toxicity or tumor underdose	
8	Repeated errors	< 2%		15%		
9		< 5%	High likelihood undetected	20%	Reportable event, Possible very serious toxicity or tumor underdose	Very wrong dose, dose distribution, location or volume
10	Errors inevitable	> 5%	Always undetected	> 20%	Catastrophic	

Linac Delivery Error 5

5) Collimator angle systematically differs from baseline by 2.0°.

Percent Dose Error: _____

Occurrence

- () 1 - Errors Unlikely
- () 2
- () 3
- () 4
- () 5
- () 6
- () 7
- () 8
- () 9
- () 10 - Errors Inevitable

Lack of Detectability

- () 1 - Never Undetected
- () 2
- () 3
- () 4
- () 5
- () 6
- () 7
- () 8
- () 9
- () 10 - Always Undetected

Severity

- () 1 - No Effect
- () 2
- () 3
- () 4
- () 5
- () 6
- () 7
- () 8
- () 9
- () 10 - Catastrophic

Score	Occurrence		Lack of Detectability		Severity	
	Qualitative	Frequency	Qualitative	Estimated probability of error going undetected	Qualitative	Categorization
1	Errors Unlikely	0.01%	Never undetected	0.01%	No effect	
2		0.02%	Very low likelihood undetected	0.2%	Inconvenience	Inconvenience
3	Relatively few errors	0.05%		0.5%		
4		0.1%	Low likelihood undetected	1%	Minor dosimetric error	Suboptimal plan or treatment
5		< 0.2%		2%	Limited toxicity or tumor underdose	Wrong dose, dose distribution, location or volume
6	Occasional errors	< 0.5%		5%		
7		< 1%	Moderate likelihood undetected	10%	Recordable event, Potentially serious toxicity or tumor underdose	
8	Repeated errors	< 2%		15%		
9		< 5%	High likelihood undetected	20%	Reportable event, Possible very serious toxicity or tumor underdose	Very wrong dose, dose distribution, location or volume
10	Errors inevitable	> 5%	Always undetected	> 20%	Catastrophic	

Linac Delivery Error 6

6) Couch angle systematically differs from baseline by 2.0°.

Percent Dose Error: _____

Occurrence

- ☐ 1 - Errors Unlikely
- ☐ 2
- ☐ 3
- ☐ 4
- ☐ 5
- ☐ 6
- ☐ 7
- ☐ 8
- ☐ 9
- ☐ 10 - Errors Inevitable

Lack of Detectability

- ☐ 1 - Never Undetected
- ☐ 2
- ☐ 3
- ☐ 4
- ☐ 5
- ☐ 6
- ☐ 7
- ☐ 8
- ☐ 9
- ☐ 10 - Always Undetected

Severity

- ☐ 1 - No Effect
- ☐ 2
- ☐ 3
- ☐ 4
- ☐ 5
- ☐ 6
- ☐ 7
- ☐ 8
- ☐ 9
- ☐ 10 - Catastrophic

Score	Occurrence		Lack of Detectability		Severity	
	Qualitative	Frequency	Qualitative	Estimated probability of error going undetected	Qualitative	Categorization
1	Errors Unlikely	0.01%	Never undetected	0.01%	No effect	
2		0.02%	Very low likelihood undetected	0.2%	Inconvenience	Inconvenience
3	Relatively few errors	0.05%		0.5%		
4		0.1%	Low likelihood undetected	1%	Minor dosimetric error	Suboptimal plan or treatment
5		< 0.2%		2%	Limited toxicity or tumor underdose	Wrong dose, dose distribution, location or volume
6	Occasional errors	< 0.5%		5%		
7		< 1%	Moderate likelihood undetected	10%	Recordable event, Potentially serious toxicity or tumor underdose	
8	Repeated errors	< 2%		15%		
9		< 5%	High likelihood undetected	20%	Reportable event, Possible very serious toxicity or tumor underdose	Very wrong dose, dose distribution, location or volume
10	Errors Inevitable	> 5%	Always undetected	> 20%	Catastrophic	

Linac Delivery Error 7

7) MU linearity for < 5 MU systematically differs from baseline by 6%.

Percent Dose Error: _____

Occurrence

- ☐ 1 - Errors Unlikely
- ☐ 2
- ☐ 3
- ☐ 4
- ☐ 5
- ☐ 6
- ☐ 7
- ☐ 8
- ☐ 9
- ☐ 10 - Errors Inevitable

Lack of Detectability

- ☐ 1 - Never Undetected
- ☐ 2
- ☐ 3
- ☐ 4
- ☐ 5
- ☐ 6
- ☐ 7
- ☐ 8
- ☐ 9
- ☐ 10 - Always Undetected

Severity

- ☐ 1 - No Effect
- ☐ 2
- ☐ 3
- ☐ 4
- ☐ 5
- ☐ 6
- ☐ 7
- ☐ 8
- ☐ 9
- ☐ 10 - Catastrophic

Score	Occurrence		Lack of Detectability		Severity	
	Qualitative	Frequency	Qualitative	Estimated probability of error going undetected	Qualitative	Categorization
1	Errors Unlikely	0.01%	Never undetected	0.01%	No effect	
2		0.02%	Very low likelihood undetected	0.2%	Inconvenience	Inconvenience
3	Relatively few errors	0.05%		0.5%		
4		0.1%	Low likelihood undetected	1%	Minor dosimetric error	Suboptimal plan or treatment
5		< 0.2%		2%	Limited toxicity or tumor underdose	Wrong dose, dose distribution, location or volume
6	Occasional errors	< 0.5%		5%		
7		< 1%	Moderate likelihood undetected	10%	Recordable event, Potentially serious toxicity or tumor underdose	
8	Repeated errors	< 2%		15%		
9		< 5%	High likelihood undetected	20%	Reportable event, Possible very serious toxicity or tumor underdose	Very wrong dose, dose distribution, location or volume
10	Errors inevitable	> 5%	Always undetected	> 20%	Catastrophic	

Dose Calculation Error 1

8) MLC transmission and leakage modeling is off by 0.5%.

Percent Dose Error: _____

Occurrence

- () 1 - Errors Unlikely
- () 2
- () 3
- () 4
- () 5
- () 6
- () 7
- () 8
- () 9
- () 10 - Errors Inevitable

Lack of Detectability

- () 1 - Never Undetected
- () 2
- () 3
- () 4
- () 5
- () 6
- () 7
- () 8
- () 9
- () 10 - Always Undetected

Severity

- () 1 - No Effect
- () 2
- () 3
- () 4
- () 5
- () 6
- () 7
- () 8
- () 9
- () 10 - Catastrophic

Score	Occurrence		Lack of Detectability		Severity	
	Qualitative	Frequency	Qualitative	Estimated probability of error going undetected	Qualitative	Categorization
1	Errors Unlikely	0.01%	Never undetected	0.01%	No effect	
2		0.02%	Very low likelihood undetected	0.2%	Inconvenience	Inconvenience
3	Relatively few errors	0.05%		0.5%		
4		0.1%	Low likelihood undetected	1%	Minor dosimetric error	Suboptimal plan or treatment
5		< 0.2%		2%	Limited toxicity or tumor <u>underdose</u>	Wrong dose, dose distribution, location or volume
6	Occasional errors	< 0.5%		5%		
7		< 1%	Moderate likelihood undetected	10%	Recordable event, Potentially serious toxicity or tumor <u>underdose</u>	
8	Repeated errors	< 2%		15%		
9		< 5%	High likelihood undetected	20%	Reportable event, Possible very serious toxicity or tumor <u>underdose</u>	Very wrong dose, dose distribution, location or volume
10	Errors inevitable	> 5%	Always undetected	> 20%	Catastrophic	

Dose Calculation Error 2

9) MLC tongue-and-groove modeling is off by 0.5%.

Percent Dose Error: _____

Occurrence

- () 1 - Errors Unlikely
- () 2
- () 3
- () 4
- () 5
- () 6
- () 7
- () 8
- () 9
- () 10 - Errors Inevitable

Lack of Detectability

- () 1 - Never Undetected
- () 2
- () 3
- () 4
- () 5
- () 6
- () 7
- () 8
- () 9
- () 10 - Always Undetected

Severity

- () 1 - No Effect
- () 2
- () 3
- () 4
- () 5
- () 6
- () 7
- () 8
- () 9
- () 10 - Catastrophic

Score	Occurrence		Lack of Detectability		Severity	
	Qualitative	Frequency	Qualitative	Estimated probability of error going undetected	Qualitative	Categorization
1	Errors Unlikely	0.01%	Never undetected	0.01%	No effect	
2		0.02%	Very low likelihood undetected	0.2%	Inconvenience	Inconvenience
3	Relatively few errors	0.05%		0.5%		
4		0.1%	Low likelihood undetected	1%	Minor dosimetric error	Suboptimal plan or treatment
5		< 0.2%		2%	Limited toxicity or tumor underdose	Wrong dose, dose distribution, location or volume
6	Occasional errors	< 0.5%		5%		
7		< 1%	Moderate likelihood undetected	10%	Recordable event, Potentially serious toxicity or tumor underdose	
8	Repeated errors	< 2%		15%		
9		< 5%	High likelihood undetected	20%	Reportable event, Possible very serious toxicity or tumor underdose	Very wrong dose, dose distribution, location or volume
10	Errors Inevitable	> 5%	Always undetected	> 20%	Catastrophic	

Dose Calculation Error 3

10) MLC leaf end modeling is off by 0.5%.

Percent Dose Error: _____

Occurrence

- () 1 - Errors Unlikely
- () 2
- () 3
- () 4
- () 5
- () 6
- () 7
- () 8
- () 9
- () 10 - Errors Inevitable

Lack of Detectability

- () 1 - Never Undetected
- () 2
- () 3
- () 4
- () 5
- () 6
- () 7
- () 8
- () 9
- () 10 - Always Undetected

Severity

- () 1 - No Effect
- () 2
- () 3
- () 4
- () 5
- () 6
- () 7
- () 8
- () 9
- () 10 - Catastrophic

Score	Occurrence		Lack of Detectability		Severity	
	Qualitative	Frequency	Qualitative	Estimated probability of error going undetected	Qualitative	Categorization
1	Errors Unlikely	0.01%	Never undetected	0.01%	No effect	
2		0.02%	Very low likelihood undetected	0.2%	Inconvenience	Inconvenience
3	Relatively few errors	0.05%		0.5%		
4		0.1%	Low likelihood undetected	1%	Minor dosimetric error	Suboptimal plan or treatment
5		< 0.2%		2%	Limited toxicity or tumor underdose	Wrong dose, dose distribution, location or volume
6	Occasional errors	< 0.5%		5%		
7		< 1%	Moderate likelihood undetected	10%	Recordable event, Potentially serious toxicity or tumor underdose	
8	Repeated errors	< 2%		15%		
9		< 5%	High likelihood undetected	20%	Reportable event, Possible very serious toxicity or tumor underdose	Very wrong dose, dose distribution, location or volume
10	Errors inevitable	> 5%	Always undetected	> 20%	Catastrophic	

Dose Calculation Error 4

11) CT number to electron density table systematically is off by 2%.

Percent Dose Error: _____

Occurrence

- () 1 - Errors Unlikely
- () 2
- () 3
- () 4
- () 5
- () 6
- () 7
- () 8
- () 9
- () 10 - Errors Inevitable

Lack of Detectability

- () 1 - Never Undetected
- () 2
- () 3
- () 4
- () 5
- () 6
- () 7
- () 8
- () 9
- () 10 - Always Undetected

Severity

- () 1 - No Effect
- () 2
- () 3
- () 4
- () 5
- () 6
- () 7
- () 8
- () 9
- () 10 - Catastrophic

Score	Occurrence		Lack of Detectability		Severity	
	Qualitative	Frequency	Qualitative	Estimated probability of error going undetected	Qualitative	Categorization
1	Errors Unlikely	0.01%	Never undetected	0.01%	No effect	
2		0.02%	Very low likelihood undetected	0.2%	Inconvenience	Inconvenience
3	Relatively few errors	0.05%		0.5%		
4		0.1%	Low likelihood undetected	1%	Minor dosimetric error	Suboptimal plan or treatment
5		< 0.2%		2%	Limited toxicity or tumor underdose	Wrong dose, dose distribution, location or volume
6	Occasional errors	< 0.5%		5%		
7		< 1%	Moderate likelihood undetected	10%	Recordable event, Potentially serious toxicity or tumor underdose	
8	Repeated errors	< 2%		15%		
9		< 5%	High likelihood undetected	20%	Reportable event, Possible very serious toxicity or tumor underdose	Very wrong dose, dose distribution, location or volume
10	Errors inevitable	> 5%	Always undetected	> 20%	Catastrophic	

Revisit: Scoring Scale

12) Now that you have used the scoring scale in Table A to assign scores for each of the 11 failure modes, would you make any changes to the quantitative component of the severity scale you assigned?

(Note: Your scale and Table A will be shown at this time.)

General Information

Part 3

Tell us about your group:

13) How many participants are in your group?

14) What is the maximum number of years of clinical physics experience an individual on your team has?

15) What is the minimum number of years?

16) What is the approximate average percent of time dedicated to clinical work among your group?

17) What certifications are held among your group?

☐ ABR

☐ ABMP

☐ Other: _____

Failure Modes and Effects Analysis (FMEA) is a risk analysis tool recommended in the upcoming AAPM TG-100 report. The scoring scale used in this survey reflects that used in an FMEA.

18) Overall, how familiar is your group with Failure Modes and Effects Analysis?

☐ Very Familiar

☐ Somewhat Familiar

☐ Slightly Familiar

☐ Not Familiar

For head and neck IMRT treatment delivery (not VMAT) currently at your institution:

19) What linear accelerator manufacturer do you primarily use?

☐ Varian

☐ Elekta

☐ Siemens

☐ Other: _____

20) What treatment planning system do you primarily use?

☐ Eclipse

☐ Pinnacle

☐ Other: _____

21) What technique do you primarily use?

☐ Step-and-shoot/Segmental MLC

☐ Sliding window/Dynamic MLC

☐ Other: _____

22) We recognize this is a challenging process and we appreciate your time. Please feel free to leave any questions or comments below. (If a response to your question/comment is desired, please leave your name and email address).

Thank You!

Thank you for your time, we appreciate your input!

Appendix B: Patient Failure Mode Dose Deviations

Patient 1

Structures	Evaluation Criteria	Baseline Dose (cGy))	Failure Mode 1: Beam Energy		Failure Mode 2: Beam Symmetry							
			+10%	-10%	2 degrees						3.5 degrees	
					Top to bottom	Bottom to top	Left to right	Right to left	Top to bottom	Bottom to top	Left to right	Right to left
PTVs												
PTV 66	D95%	6813.93	-3.08%	-2.96%	0.05%	0.16%	0.27%	0.06%	0.16%	0.21%	0.12%	-0.08%
PTV 63	D95%	6555.78	-9.82%	-8.56%	-0.08%	-0.03%	0.08%	-0.30%	0.10%	0.06%	-0.28%	-0.44%
PTV 60	D95%	6227.13	-8.58%	-7.45%	-0.19%	-0.07%	0.19%	-0.47%	-0.01%	-0.01%	-0.05%	-0.54%
PTV 54	D95%	5592.63	-8.32%	-7.37%	-0.05%	0.10%	0.30%	-0.22%	0.10%	0.25%	0.06%	-0.28%
OARs												
Brainstem	Max to 1 cc	3574.97	-3.20%	-2.96%	-1.42%	-1.34%	-0.28%	-2.31%	-1.24%	-1.15%	0.63%	-2.03%
	D100%	232.00	10.34%	-3.88%	-13.36%	-13.36%	-12.93%	-13.79%	-10.34%	-10.34%	-9.48%	-11.21%
Cord	Max	3616.88	5.59%	4.26%	-0.97%	-0.83%	-0.25%	-1.41%	-0.85%	-0.59%	0.35%	-1.44%
	Max to 0.3 cc	3562.91	4.93%	3.61%	-0.71%	-0.63%	-0.04%	-1.05%	-0.49%	-0.21%	0.47%	-1.08%
L parotid	Mean	1603.28	-0.87%	-5.59%	-3.62%	-3.40%	-2.86%	-3.98%	-2.81%	-2.45%	-2.01%	-3.43%
	D50%	1064.86	0.26%	-9.08%	-7.02%	-6.95%	-6.18%	-7.72%	-5.67%	-5.49%	-4.38%	-6.51%
R parotid	Mean	3097.12	-3.05%	-3.46%	-2.24%	-2.06%	-1.50%	-2.68%	-1.71%	-1.57%	-0.94%	-2.30%
	D50%	5876.52	-0.27%	-0.77%	0.07%	0.19%	0.28%	0.30%	0.23%	0.42%	0.02%	0.12%
L cochlea	Mean	1245.11	-18.43%	-19.85%	-3.44%	-3.47%	-2.12%	-4.67%	-3.26%	-3.32%	-1.04%	-4.62%
	D05%	1763.35	-15.26%	-15.44%	-2.15%	-2.21%	-0.74%	-3.40%	-1.76%	-1.88%	0.45%	-3.18%
R cochlea	Mean	2045.89	-11.42%	-10.88%	-3.20%	-2.91%	-1.50%	-4.24%	-2.63%	-2.44%	-0.22%	-3.81%
	D05%	2851.25	-7.19%	-5.54%	-1.99%	-1.99%	-0.55%	-3.29%	-1.60%	-1.78%	0.68%	-2.94%

Structures	Evaluation Criteria	Baseline Dose (cGy)	Failure Mode 2: Beam Symmetry					Failure Mode 3: MLC Position						
			10 degrees					1 mm Errors				2 mm Errors		
			Top to bottom	Bottom to top	Left to right	Right to left	X1 + 1mm	X1 - 1mm	X2 +1mm	X2 - 1mm	X1 + 2mm	X1 - 2mm	X2 +2mm	X2 - 2mm
PTVs														
PTV 66	D95%	6813.93	0.07%	0.00%	-0.33%	-0.24%	0.11%	0.03%	0.08%	-0.02%	0.80%	-0.47%	0.70%	-0.69%
PTV 63	D95%	6555.78	-0.65%	-0.65%	-1.90%	-1.19%	-0.24%	-1.18%	0.02%	-0.32%	0.05%	-8.86%	0.57%	-1.54%
PTV 60	D95%	6227.13	-0.03%	-0.10%	-0.90%	-1.67%	-0.23%	-0.42%	0.28%	-0.39%	0.10%	-6.49%	1.03%	-1.44%
PTV 54	D95%	5592.63	-0.11%	0.02%	-0.57%	-1.08%	0.22%	-0.17%	0.59%	-0.54%	0.63%	-2.13%	1.34%	-1.80%
OARs														
Brainstem	Max to 1 cc	3574.97	0.52%	0.86%	2.73%	-4.07%	0.96%	-0.46%	1.06%	-0.86%	2.37%	-1.53%	2.54%	-2.28%
	D100%	232.00	-10.78%	-10.78%	-9.48%	-13.36%	0.43%	0.43%	3.88%	-3.02%	0.86%	0.00%	7.76%	-7.33%
Cord	Max	3616.88	0.20%	0.84%	1.51%	-2.63%	1.07%	0.24%	0.34%	0.23%	3.56%	-0.41%	1.20%	-0.21%
	Max to 0.3 cc	3562.91	0.24%	0.85%	1.35%	-2.31%	1.42%	0.35%	0.70%	0.66%	3.97%	-0.54%	-3.05%	-0.03%
L parotid	Mean	1603.28	-2.50%	-1.81%	-0.99%	-4.01%	0.61%	-0.02%	4.38%	-3.81%	1.52%	-0.73%	9.27%	-8.02%
	D50%	1064.86	-5.40%	-5.13%	-3.55%	-8.33%	1.36%	-0.96%	1.87%	-1.60%	3.17%	-2.41%	4.42%	-3.74%
R parotid	Mean	3097.12	-0.72%	-0.62%	1.00%	-50.31%	-0.29%	0.26%	3.42%	-50.21%	0.23%	0.17%	7.77%	-7.14%
	D50%	5876.52	-0.27%	0.05%	-0.31%	0.34%	0.26%	0.22%	0.33%	0.16%	0.76%	-0.15%	0.91%	-0.31%
L cochlea	Mean	1245.11	0.99%	0.82%	3.77%	-4.57%	-0.11%	0.12%	11.84%	-10.26%	0.33%	-0.30%	27.09%	-18.80%
	D05%	1763.35	1.70%	1.30%	4.47%	-4.03%	0.22%	0.56%	12.45%	-11.34%	0.83%	0.28%	29.10%	-21.54%
R cochlea	Mean	2045.89	-0.14%	0.40%	3.42%	-5.27%	-0.31%	0.42%	10.26%	-9.14%	-0.08%	0.02%	21.86%	-17.38%
	D05%	2851.25	1.03%	0.46%	4.01%	-4.66%	0.32%	-0.31%	12.41%	-11.70%	0.86%	-0.72%	26.98%	-21.55%

Structures	Evaluation Criteria	Baseline Dose (cGy)	Failure Mode 4: Gantry Angle		Failure Mode 5: Collimator Angle		Failure Mode 6: Couch Angle		Failure Mode 7: MU Linearity					
			+ 2°	-2°	+ 2°	-2°	+ 2°	-2°	1A	1B	2A	2B	3A	3B
PTVs														
PTV 66	D95%	6813.93	-0.30%	-0.25%	-0.56%	-1.30%	-0.60%	-0.32%	0.01%	0.00%	0.06%	-0.03%	0.06%	-0.13%
PTV 63	D95%	6555.78	-0.34%	-0.10%	-2.62%	-3.94%	-1.61%	-0.78%	0.01%	0.00%	0.05%	-0.03%	0.00%	-0.08%
PTV 60	D95%	6227.13	0.21%	-0.47%	-0.61%	-3.74%	-2.22%	-0.84%	0.07%	0.00%	0.14%	-0.03%	0.08%	-0.07%
PTV 54	D95%	5592.63	-0.31%	-0.12%	-1.98%	-1.08%	0.11%	-1.39%	0.11%	-0.01%	0.19%	-0.03%	0.29%	-0.14%
OARs														
Brainstem	Max to 1 cc	3574.97	0.00%	-0.07%	6.10%	-0.59%	1.50%	0.71%	0.05%	-0.01%	-0.18%	-0.03%	0.20%	-0.11%
	D100%	232.00	0.43%	0.43%	-0.43%	-2.59%	-0.43%	0.00%	0.00%	0.00%	0.00%	0.00%	0.43%	0.00%
Cord	Max	3616.88	1.29%	-0.68%	13.54%	9.81%	7.36%	-0.27%	0.20%	-0.02%	0.06%	-0.04%	0.79%	-0.27%
	Max to 0.3 cc	3562.91	1.16%	-0.22%	10.96%	3.74%	5.45%	-0.71%	0.59%	0.37%	0.47%	0.31%	1.15%	0.06%
L parotid	Mean	1603.28	6.56%	-3.94%	-5.16%	13.58%	3.98%	1.09%	-0.09%	0.00%	0.00%	-0.02%	0.15%	-0.24%
	D50%	1064.86	0.20%	1.54%	-0.97%	13.74%	8.77%	-4.53%	0.06%	-0.01%	0.06%	-0.02%	0.76%	-0.35%
R parotid	Mean	3097.12	-0.41%	1.86%	6.26%	-0.73%	0.01%	3.62%	-0.20%	0.00%	-0.19%	-0.01%	-0.29%	-0.14%
	D50%	5876.52	-0.14%	0.10%	-0.29%	0.74%	0.38%	-0.35%	0.08%	-0.01%	0.18%	-0.03%	0.30%	-0.18%
L cochlea	Mean	1245.11	1.40%	-0.34%	20.78%	-10.44%	7.19%	-0.31%	0.13%	-0.01%	-0.02%	-0.02%	0.55%	-0.17%
	D05%	1763.35	1.89%	1.03%	35.83%	-6.87%	9.21%	11.66%	0.12%	0.00%	0.00%	0.00%	0.51%	-0.12%
R cochlea	Mean	2045.89	3.81%	-2.98%	1.95%	28.05%	23.22%	-3.63%	0.13%	-0.01%	0.24%	-0.03%	0.15%	-0.05%
	D05%	2851.25	2.99%	-1.23%	-28.83%	35.79%	20.06%	11.05%	0.18%	0.00%	0.42%	-0.04%	0.25%	-0.07%

Structures	Evaluation Criteria	Baseline Dose (cGy)	MLC Modeling							Failure Mode 11: CT Table		
			Failure Mode 8: Leakage & Transmission		Failure Mode 9: Tongue-and-groove		Failure Mode 10: Leaf End					
			0%	10%	width = 0.005 cm	width = 0.200 cm	radius = 4 cm	radius = 15 cm	radius = 20 cm	+2%	-2%	PET CT
PTVs												
PTV 66	D95%	6813.93	-0.10%	0.06%	-0.13%	0.14%	0.49%	-0.34%	-0.48%	0.34%	0.09%	0.09%
PTV 63	D95%	6555.78	-0.14%	0.17%	-0.09%	0.08%	0.27%	-0.15%	-0.14%	0.31%	0.11%	0.11%
PTV 60	D95%	6227.13	-0.14%	0.40%	-0.07%	0.20%	1.17%	-0.42%	-0.32%	0.31%	0.14%	0.14%
PTV 54	D95%	5592.63	-0.07%	0.84%	-0.13%	0.09%	0.96%	-0.75%	-0.93%	0.52%	0.07%	0.07%
OARs												
Brainstem	Max to 1 cc	3574.97	-0.39%	2.71%	-0.34%	1.43%	2.07%	-1.65%	-0.76%	0.35%	0.28%	0.28%
	D100%	232.00	0.00%	0.86%	0.00%	1.29%	0.86%	-0.43%	0.00%	1.72%	-0.86%	-0.86%
Cord	Max	3616.88	-0.43%	2.67%	-0.32%	0.99%	1.83%	-0.31%	-0.32%	0.45%	-0.68%	0.06%
	Max to 0.3 cc	3562.91	-0.05%	2.07%	0.07%	0.02%	1.94%	-0.11%	-0.32%	0.92%	0.52%	0.52%
L parotid	Mean	1603.28	-0.96%	10.61%	-0.67%	1.99%	6.04%	-3.37%	-4.26%	0.94%	0.11%	-0.25%
	D50%	1064.86	-1.66%	17.99%	-1.32%	5.32%	5.57%	-2.25%	-2.27%	0.83%	-0.27%	-0.27%
R parotid	Mean	3097.12	-0.59%	4.42%	-0.28%	0.21%	4.65%	-2.74%	-3.77%	0.53%	-0.18%	-0.25%
	D50%	5876.52	-0.03%	0.69%	-0.18%	0.39%	0.55%	-0.04%	0.02%	0.65%	0.03%	0.03%
L cochlea	Mean	1245.11	-0.86%	7.75%	-0.69%	3.32%	16.18%	-9.10%	-8.03%	0.33%	-2.41%	0.22%
	D05%	1763.35	-0.79%	6.82%	-0.52%	2.78%	16.31%	-9.70%	-8.55%	0.33%	0.39%	0.39%
R cochlea	Mean	2045.89	-0.70%	5.76%	-0.74%	3.50%	11.52%	-6.62%	-5.55%	0.40%	-2.46%	0.46%
	D05%	2851.25	-0.67%	5.66%	-0.98%	4.63%	14.39%	-8.21%	-6.87%	0.17%	0.53%	0.53%

Table 106: Patient 1 dose differences from baseline at evaluation criteria for PTVs and OARs for each failure mode.

Patient 2

Structures	Evaluation Criteria	Baseline Dose (cGy)	Failure Mode 1: Beam Energy		Failure Mode 2: Beam Symmetry							
					2 degrees				3.5 degrees			
			+10%	-10%	Top to bottom	Bottom to top	Left to right	Right to left	Top to bottom	Bottom to top	Left to right	Right to left
PTVs												
PTV 70	D95%	6854.12	-3.42%	-3.25%	-0.45%	-0.57%	-0.03%	-0.76%	-0.45%	-0.22%	-0.22%	-0.72%
PTV 63	D95%	6163.19	-4.62%	-5.76%	-0.27%	-0.59%	-0.63%	-0.36%	-0.27%	-0.72%	-0.72%	-0.40%
PTV 57	D95%	5545.40	-5.68%	-4.88%	-0.34%	-0.55%	-0.32%	-0.54%	-0.34%	-0.46%	-0.46%	-0.43%
OARs												
Brainstem	Max to 1 cc	3863.71	-1.58%	-0.59%	-1.15%	-1.02%	0.96%	-2.14%	-1.15%	0.33%	0.33%	-1.77%
	D100%	1167.00	6.43%	4.88%	-3.17%	-3.68%	0.51%	-4.71%	-3.17%	-1.29%	-1.29%	-4.37%
Cord	Max	4082.86	21.30%	22.05%	-1.16%	-1.09%	-0.56%	-1.23%	-0.87%	-0.57%	-0.57%	-0.96%
	Max to 0.3 cc	4038.64	18.35%	18.86%	-3.35%	-1.41%	-0.66%	-4.21%	-3.35%	-1.74%	-1.74%	-1.85%
L Parotid	Mean	2026.93	6.04%	3.63%	-3.88%	-3.48%	-3.09%	-3.67%	-3.03%	-2.37%	-2.37%	-3.26%
	D50%	1392.89	35.43%	29.83%	-5.18%	-6.44%	-4.42%	-6.44%	-5.18%	-4.69%	-4.69%	-5.83%
R Parotid	Mean	1544.70	9.12%	5.70%	-3.70%	-3.76%	-2.89%	-3.73%	-2.67%	-2.35%	-2.35%	-3.18%
	D50%	1021.88	26.60%	19.72%	-5.62%	-7.25%	-4.97%	-7.25%	-5.62%	-4.88%	-4.88%	-6.29%
L Cochlea	Mean	2689.28	1.82%	4.14%	-2.09%	-2.29%	-1.07%	-3.60%	-1.82%	-0.11%	-0.11%	-3.06%
	D05%	3192.78	2.43%	5.32%	-1.44%	-1.69%	0.88%	-3.01%	-16.98%	0.50%	0.50%	-2.66%
Mandible	Max	7220.01	4.00%	4.66%	-0.69%	-0.58%	0.10%	-0.21%	-0.48%	-0.25%	-0.25%	-0.34%
Brain	Max	5007.83	-3.34%	-0.79%	0.06%	-0.05%	1.32%	-0.85%	-0.01%	1.36%	1.36%	-0.61%

Structure s	Evaluation Criteria	Baseline Dose (cGy)	Failure Mode 2: Beam Symmetry					Failure Mode 3: MLC Position						
			10 degrees					1 mm Errors				2 mm Errors		
			Top to bottom	Bottom to top	Left to right	Right to left	X1 + 1mm	X1 - 1mm	X2 +1mm	X2 - 1mm	X1 + 2mm	X1 - 2mm	X2 +2mm	X2 - 2mm
PTVs														
PTV 70	D95%	6854.12	-0.03%	0.15%	-0.41%	-1.31%	-0.02%	-0.79%	0.02%	-0.79%	-0.10%	-1.81%	0.01%	-0.83%
PTV 63	D95%	6163.19	-0.63%	-0.54%	-1.50%	-0.74%	0.00%	-0.80%	0.33%	-1.29%	0.15%	-2.86%	0.65%	-1.91%
PTV 57	D95%	5545.40	-0.32%	-0.07%	-0.55%	-0.96%	0.10%	-0.91%	0.45%	-1.33%	0.14%	-2.74%	0.79%	-1.96%
OARs														
Brainstem	Max to 1 cc	3863.71	0.96%	1.18%	2.70%	-3.47%	1.56%	-1.69%	1.31%	-1.71%	2.69%	-2.68%	2.23%	-2.44%
	D100%	1167.00	0.51%	-0.77%	2.49%	-5.48%	0.00%	-8.51%	-2.77%	-8.13%	8.11%	-9.97%	-0.99%	3.70%
Cord	Max	4082.86	-0.35%	-0.28%	-0.43%	-1.80%	0.88%	-0.55%	0.64%	-0.51%	1.74%	-0.49%	2.15%	-0.39%
	Max to 0.3 cc	4038.64	-0.66%	-0.55%	-0.61%	-1.75%	-0.51%	-3.09%	-0.59%	-2.95%	0.82%	-3.40%	0.50%	-0.15%
L Parotid	Mean	2026.93	-2.75%	-1.40%	-1.28%	-3.18%	-0.64%	-0.14%	1.03%	-1.70%	-0.75%	0.09%	2.69%	-2.87%
	D50%	1392.89	-4.42%	-4.07%	-3.45%	-5.72%	-0.62%	0.02%	0.48%	-0.94%	-0.57%	0.21%	1.69%	-1.45%
R Parotid	Mean	1544.70	-1.72%	-1.95%	-0.70%	-3.60%	-0.20%	-0.05%	3.84%	-3.89%	-0.39%	0.18%	7.81%	-7.28%
	D50%	1021.88	-4.97%	-4.69%	-3.64%	-7.06%	-0.15%	-0.09%	1.65%	-1.77%	0.08%	-0.08%	3.64%	-2.13%
L Cochlea	Mean	2689.28	0.65%	0.11%	2.83%	-4.60%	0.78%	-1.14%	1.18%	-1.87%	1.93%	-1.04%	2.77%	-2.77%
	D05%	3192.78	0.88%	0.81%	3.29%	-3.95%	1.48%	-0.85%	1.87%	-1.50%	2.70%	-0.65%	2.76%	-1.44%
Mandible	Max	7220.01	-0.03%	0.30%	0.68%	-0.28%	0.13%	-0.28%	-0.01%	-0.12%	-0.10%	0.06%	-0.25%	0.40%
Brain	Max	5007.83	2.72%	2.31%	4.57%	-2.40%	0.92%	-0.25%	2.68%	-1.27%	1.71%	-0.17%	3.85%	-1.26%

Structures	Evaluation Criteria	Baseline Dose (cGy)	Failure Mode 4: Gantry Angle				Failure Mode 5: Collimator Angle			Failure Mode 6: Couch Angle			Failure Mode 7: MU Linearity		
			+ 2°	-2°	+ 2°	-2°	+ 2°	-2°	1A	1B	2A	2B	3A	3B	
PTVs															
PTV 70	D95%	6854.12	-0.22%	-0.35%	-0.38%	0.00%	-0.49%	-1.08%	-0.02%	0.00%	0.04%	0.00%	-0.08%	0.04%	
PTV 63	D95%	6163.19	0.02%	-0.88%	-3.12%	0.00%	-1.28%	-0.17%	0.04%	0.00%	0.15%	-0.01%	0.11%	0.01%	
PTV 57	D95%	5545.40	-0.49%	-0.71%	-1.51%	0.00%	-1.26%	-0.45%	-0.02%	0.00%	0.07%	-0.01%	-0.07%	0.05%	
OARs															
Brainstem	Max to 1 cc	3863.71	-0.05%	0.01%	3.07%	0.00%	-0.92%	2.41%	0.07%	0.00%	0.26%	-0.01%	0.15%	0.06%	
	D100%	1167.00	0.09%	0.43%	3.34%	0.00%	0.26%	1.37%	0.00%	0.00%	-0.09%	0.00%	-0.09%	0.09%	
Cord	Max	4082.86	0.75%	0.69%	1.98%	0.23%	0.95%	1.16%	0.15%	-0.01%	0.38%	-0.02%	0.22%	0.03%	
	Max to 0.3 cc	4038.64	0.16%	0.63%	1.27%	-0.28%	-1.09%	1.10%	0.09%	-0.03%	0.13%	-0.03%	0.25%	0.01%	
L Parotid	Mean	2026.93	5.16%	-4.01%	-4.38%	7.76%	11.96%	-9.43%	0.23%	-0.01%	0.20%	-0.01%	0.85%	-0.14%	
	D50%	1392.89	3.79%	-2.09%	-1.26%	0.00%	8.34%	-6.02%	0.58%	-0.24%	0.47%	-0.24%	0.91%	-0.43%	
R Parotid	Mean	1544.70	-4.10%	5.96%	5.16%	-0.99%	-4.13%	7.36%	0.04%	-0.01%	0.04%	-0.01%	0.42%	-0.05%	
	D50%	1021.88	-0.50%	2.13%	3.28%	0.00%	-2.48%	4.64%	0.37%	-0.02%	0.41%	-0.02%	1.35%	-0.21%	
L Cochlea	Mean	2689.28	-2.27%	3.44%	6.15%	6.00%	10.55%	-2.79%	-0.05%	0.01%	-0.03%	0.01%	0.05%	0.03%	
	D05%	3192.78	-2.25%	5.11%	7.41%	0.00%	6.83%	1.96%	-0.03%	0.00%	-0.03%	0.00%	0.25%	0.00%	
Mandible	Max	7220.01	-0.67%	0.01%	1.75%	1.05%	0.06%	-0.03%	-0.11%	0.01%	-0.15%	0.01%	-0.24%	0.08%	
Brain	Max	5007.83	0.67%	0.08%	6.62%	5.18%	4.29%	0.52%	-0.13%	0.01%	-0.08%	0.00%	-0.17%	0.10%	

Structures	Evaluation Criteria	Baseline Dose (cGy)	MLC Modeling								Failure Mode 11: CT Table	
			Failure Mode 8: Leakage & Transmission		Failure Mode 9: Tongue-and-groove			Failure Mode 10: Leaf End				
			0%	10%	width = 0.005 cm	width = 0.200 cm	radius = 4 cm	radius = 15 cm	radius = 20 cm	+2%	-2%	PET CT
PTVs												
PTV 70	D95%	6854.12	-0.10%	0.02%	-0.10%	-0.18%	0.45%	-0.70%	-0.63%	-0.64%	-0.77%	-0.17%
PTV 63	D95%	6163.19	-0.10%	0.49%	-0.11%	-0.18%	0.69%	-0.89%	-0.84%	-0.67%	-0.97%	-0.28%
PTV 57	D95%	5545.40	-0.11%	0.92%	-0.14%	-0.10%	0.91%	-1.24%	-1.04%	-1.04%	-1.08%	-0.28%
OARs												
Brainstem	Max to 1 cc	3863.71	-0.13%	2.44%	-0.12%	-0.11%	3.51%	-2.11%	-2.93%	-0.52%	-0.45%	0.32%
	D100%	1167.00	-0.86%	7.46%	-0.69%	3.17%	19.79%	-7.88%	-7.54%	1.46%	2.06%	0.26%
Cord	Max	4082.86	-0.11%	2.45%	-0.21%	0.86%	0.86%	-0.12%	-0.11%	-1.50%	-1.00%	0.13%
	Max to 0.3 cc	4038.64	-0.37%	2.13%	-0.17%	0.20%	1.13%	-0.59%	-0.43%	-2.13%	-1.14%	-0.10%
L Parotid	Mean	2026.93	-0.77%	6.82%	-0.07%	-0.66%	1.99%	-1.10%	-0.88%	2.42%	3.02%	-0.79%
	D50%	1392.89	-1.51%	9.76%	-1.00%	3.02%	2.00%	-3.94%	-1.32%	-9.04%	3.81%	-1.75%
R Parotid	Mean	1544.70	-0.93%	10.75%	-0.68%	2.95%	5.74%	-3.69%	-2.74%	-1.89%	-1.50%	-0.46%
	D50%	1021.88	-1.57%	18.03%	-1.14%	6.04%	5.57%	-1.36%	-1.15%	-0.06%	0.54%	-0.76%
L Cochlea	Mean	2689.28	-0.41%	4.52%	-0.25%	1.10%	9.67%	-1.90%	-2.55%	1.47%	-1.96%	0.39%
	D05%	3192.78	-0.22%	3.32%	-0.15%	1.51%	8.21%	-1.25%	-1.94%	1.46%	-2.04%	0.50%
Mandible	Max	7220.01	-0.11%	-0.15%	0.17%	-0.31%	-0.10%	0.39%	0.47%	-1.26%	-1.54%	-0.11%
Brain	Max	5007.83	0.09%	1.21%	-0.17%	1.33%	1.55%	-0.99%	-1.77%	-2.71%	-3.57%	0.19%

Table 107: Patient 2 dose differences from baseline at evaluation criteria for PTVs and OARs for each failure mode.

Patient 3

Structures	Evaluation Criteria	Baseline Dose (cGy)	Failure Mode 1: Beam Energy		Failure Mode 2: Beam Symmetry							
					2 degrees				3.5 degrees			
			+10%	-10%	Top to bottom	Bottom to top	Left to right	Right to left	Top to bottom	Bottom to top	Left to right	Right to left
PTVs												
PTV 66	D95%	6484.89	-3.34%	-3.64%	-0.08%	-0.03%	0.15%	-0.85%	-0.20%	-0.13%	0.08%	-0.51%
PTV 63	D95%	6308.66	-2.96%	-6.56%	0.38%	0.36%	-0.27%	1.25%	0.57%	0.54%	-0.79%	1.35%
PTV 60	D95%	5927.20	-5.43%	-5.58%	-0.08%	0.07%	0.03%	-0.50%	-0.03%	0.09%	-0.14%	-0.21%
PTV 54	D95%	5231.74	-4.89%	-5.56%	-0.12%	-0.08%	0.14%	-0.95%	-0.29%	-0.24%	0.20%	-0.58%
OARs												
Brainstem	Max	4687.22	3.01%	3.80%	-0.10%	-0.07%	0.33%	-1.25%	-0.58%	-0.53%	0.75%	-0.86%
	D100%	306.00	15.36%	6.21%	-15.36%	-15.36%	-14.38%	-16.34%	-12.42%	-12.09%	-10.46%	-12.75%
Spinal Cord	Max	4408.54	10.25%	10.84%	0.09%	0.11%	0.40%	-0.83%	-0.37%	-0.35%	0.32%	-0.62%
	Max to 0.3 cc	4250.74	10.22%	10.52%	-1.53%	-1.48%	-1.18%	-2.42%	-1.90%	-1.86%	-1.22%	-2.16%
L Parotid	Mean	2457.69	5.92%	4.76%	-2.66%	-2.68%	-2.30%	-3.29%	-2.09%	-2.16%	-1.53%	-2.53%
	D50%	1493.25	21.94%	17.74%	-5.61%	-5.76%	-5.13%	-6.61%	-4.83%	-5.05%	-3.77%	-5.43%
R Parotid	Mean	2202.19	7.19%	5.96%	-1.81%	-1.75%	-1.51%	-2.16%	-1.45%	-1.36%	-1.18%	-1.45%
	D50%	1149.00	43.29%	37.90%	-5.57%	-5.37%	-5.13%	-6.18%	-5.21%	-4.96%	-4.43%	-5.28%
L Cochlea	Mean	3054.16	2.51%	5.78%	-1.45%	-1.73%	-0.06%	-3.32%	-1.44%	-1.81%	0.98%	-2.73%
	D05%	4375.51	-1.73%	2.18%	-3.53%	-3.92%	-2.25%	-5.54%	-3.71%	-4.13%	-1.27%	-4.97%
Mandible	Max	7128.23	-0.41%	2.29%	-0.16%	-0.19%	0.58%	-1.02%	-0.22%	-0.48%	0.60%	-0.82%

Structures	Evaluation Criteria	Baseline Dose (cGy)	Failure Mode 2: Beam Symmetry				Failure Mode 3: MLC Position							
			10 degrees				1 mm Errors				2 mm Errors			
			Top to bottom	Bottom to top	Left to right	Right to left	X1 + 1mm	X1 - 1mm	X2 +1mm	X2 - 1mm	X1 + 2mm	X1 - 2mm	X2 +2mm	X2 - 2mm
PTVs														
PTV 66	D95%	6484.89	-0.14%	-0.09%	-1.08%	-1.76%	0.12%	-0.23%	0.62%	-0.28%	-0.11%	-0.77%	-0.10%	-1.39%
PTV 63	D95%	6308.66	-1.22%	-1.32%	-3.14%	2.40%	0.04%	0.07%	0.07%	0.51%	-0.67%	-0.42%	-0.96%	0.43%
PTV 60	D95%	5927.20	-0.51%	-0.27%	-1.47%	-1.22%	0.03%	0.08%	0.69%	-0.75%	-0.81%	0.07%	-0.18%	-2.29%
PTV 54	D95%	5231.74	0.08%	0.18%	-0.78%	-2.28%	0.16%	-0.25%	0.96%	-0.47%	0.20%	-0.83%	0.57%	-1.72%
OARs														
Brainstem	Max	4687.22	1.19%	1.46%	2.28%	-2.66%	0.93%	-0.18%	0.92%	0.36%	1.13%	-0.82%	0.44%	-0.39%
	D100%	306.00	-12.42%	-12.09%	-10.13%	-15.69%	0.98%	-1.96%	7.19%	-5.56%	7.19%	-2.61%	12.09%	-9.80%
Spinal Cord	Max	4408.54	1.33%	1.53%	1.79%	-1.67%	0.13%	0.05%	0.28%	0.74%	0.25%	-0.69%	-0.63%	0.63%
	Max to 0.3 cc	4250.74	-0.35%	0.06%	0.88%	-3.12%	-1.74%	-3.83%	-1.15%	-1.16%	-3.22%	-6.88%	-1.68%	-3.15%
L Parotid	Mean	2457.69	-1.41%	-1.51%	-0.22%	-2.91%	0.10%	0.18%	4.25%	-3.54%	-0.48%	0.32%	7.49%	-7.48%
	D50%	1493.25	-3.63%	-1.82%	-5.66%	-8.27%	0.12%	0.08%	7.81%	-5.60%	0.09%	0.06%	15.80%	-11.17%
R Parotid	Mean	2202.19	-0.94%	-0.73%	-0.37%	-1.49%	0.03%	0.21%	4.63%	-3.48%	0.20%	-0.20%	7.98%	-7.58%
	D50%	1149.00	0.99%	0.44%	0.65%	1.03%	0.04%	-0.19%	5.72%	-3.57%	1.24%	-0.52%	11.54%	-6.78%
L Cochlea	Mean	3054.16	0.26%	-0.68%	3.56%	-5.54%	0.07%	-0.18%	2.65%	-2.18%	0.21%	-0.64%	4.88%	-4.97%
	D05%	4375.51	-1.87%	-2.95%	2.40%	-8.74%	-3.43%	-3.86%	-0.40%	-5.10%	-1.69%	-4.23%	1.04%	-8.20%
Mandible	Max	7128.23	0.99%	0.49%	2.32%	-0.85%	0.03%	-0.67%	0.32%	0.22%	0.20%	-0.78%	-0.46%	0.04%

Structures	Evaluation Criteria	Baseline Dose (cGy)	Failure Mode 4: Gantry Angle		Failure Mode 5: Collimator Angle		Failure Mode 6: Couch Angle		Failure Mode 7: MU Linearity					
			+ 2 degrees	-2 degrees	+ 2 degrees	-2 degrees	+ 2 degrees	-2 degrees	1A	1B	2A	2B	3A	3B
PTVs														
PTV 66	D95	6484.89	-0.37%	-0.33%	-1.37%	-2.93%	-0.51%	-0.33%	-0.27%	0.00%	-0.22%	-0.01%	-0.25%	0.02%
PTV 63	D95	6308.66	-0.15%	0.15%	-0.90%	0.68%	-0.22%	0.15%	-0.11%	-0.01%	0.12%	-0.03%	-0.06%	0.01%
PTV 60	D95	5927.20	-0.93%	0.76%	-0.52%	-1.34%	-1.46%	0.76%	-0.29%	-0.01%	-0.16%	-0.02%	-0.21%	0.00%
PTV 54	D95	5231.74	-0.06%	-0.96%	-2.08%	-5.55%	-0.18%	-0.96%	-0.17%	-0.01%	-0.09%	-0.01%	-0.12%	0.00%
OARs														
Brainstem	Max	4687.22	0.33%	-0.81%	0.10%	5.89%	3.35%	-0.81%	-0.07%	-0.01%	0.07%	-0.02%	0.02%	-0.01%
	D100	306.00	0.00%	1.31%	-3.27%	2.94%	-0.65%	1.31%	-0.33%	0.00%	-0.33%	0.00%	-0.33%	0.00%
Spinal Cord	Max	4408.54	0.46%	-0.93%	-4.28%	10.48%	1.25%	-0.93%	-0.06%	-0.01%	0.10%	-0.02%	0.05%	-0.01%
	Max to 0.3 cc	4250.74	0.51%	0.04%	-3.83%	11.52%	1.35%	0.04%	-2.16%	-1.90%	-2.02%	-1.93%	-2.01%	-1.93%
L Parotid	Mean	2457.69	0.50%	-5.77%	2.03%	6.64%	11.08%	-5.77%	-0.29%	0.00%	-0.22%	-0.01%	-0.30%	0.03%
	D50%	1493.25	1.88%	-9.63%	28.71%	-9.63%	14.96%	19.45%	-0.23%	0.00%	-0.14%	0.00%	-0.01%	0.00%
R Parotid	Mean	2202.19	-1.81%	2.02%	2.74%	2.22%	0.56%	2.02%	-0.04%	-0.01%	0.01%	-0.01%	0.07%	0.00%
	D50%	1149.00	-0.54%	9.67%	-0.58%	9.67%	5.44%	16.56%	0.02%	-0.06%	0.15%	-0.06%	0.31%	-0.09%
L Cochlea	Mean	3054.16	-2.09%	-12.84%	8.00%	-4.03%	12.67%	-12.84%	-0.43%	0.00%	-0.53%	0.01%	-0.32%	-0.02%
	D05%	4375.51	-6.58%	-21.99%	6.20%	-14.38%	14.68%	-21.99%	-4.38%	-3.86%	-4.51%	-3.86%	-4.30%	-3.89%
Mandible	Max	7128.23	0.32%	-1.22%	0.15%	2.49%	0.89%	-1.22%	-0.39%	0.00%	-0.38%	0.00%	-0.44%	0.03%

Structures	Evaluation Criteria	Baseline Dose (cGy)	MLC Modeling							Failure Mode 11: CT Table		
			Failure Mode 8: Leakage & Transmission		Failure Mode 9: Tongue-and-groove		Failure Mode 10: Leaf End					
			0%	10%	width = 0.005 cm	width = 0.200 cm	radius = 4 cm	radius = 15 cm	radius = 20 cm	+2%	-2%	PET CT
PTVs												
PTV 66	D95	6484.89	-0.04%	0.42%	-0.08%	-0.19%	0.39%	-0.81%	-0.87%	0.00%	0.00%	0.00%
PTV 63	D95	6308.66	-0.05%	0.58%	-0.19%	0.41%	-0.52%	0.59%	0.64%	0.00%	0.00%	0.00%
PTV 60	D95	5927.20	-0.04%	0.81%	-0.11%	-0.23%	0.02%	-0.39%	-0.48%	0.00%	0.00%	0.00%
PTV 54	D95	5231.74	-0.06%	1.25%	-0.01%	-0.25%	1.16%	-0.96%	-0.98%	0.00%	0.00%	0.00%
OARs												
Brainstem	Max	4687.22	-0.16%	1.70%	-0.08%	0.66%	1.17%	-0.18%	-0.57%	0.00%	0.00%	0.00%
	D100	306.00	0.00%	1.96%	0.00%	1.31%	4.90%	-0.33%	-0.98%	0.00%	0.00%	0.00%
Spinal Cord	Max	4408.54	-0.23%	1.96%	-0.09%	0.59%	1.01%	-0.08%	-0.18%	0.00%	0.00%	0.00%
	Max to 0.3 cc	4250.74	-2.16%	-1.32%	-1.90%	-3.86%	-1.48%	-5.77%	-6.14%	-1.90%	-1.90%	-1.90%
L Parotid	Mean	2457.69	-0.65%	6.45%	-0.33%	0.57%	5.50%	-3.67%	-3.25%	0.00%	0.00%	0.00%
	D50%	1493.25	-1.28%	13.48%	-0.44%	3.01%	14.38%	-6.40%	-6.27%	0.00%	0.00%	0.00%
R Parotid	Mean	2202.19	-0.60%	7.82%	-0.66%	2.75%	5.76%	-3.86%	-2.98%	0.00%	0.00%	0.00%
	D50%	1149.00	-1.56%	18.73%	-1.42%	6.79%	16.56%	-5.21%	-4.83%	0.00%	0.00%	0.00%
L Cochlea	Mean	3054.16	-0.45%	3.47%	-0.44%	0.69%	8.60%	-1.34%	-1.93%	0.00%	0.00%	0.00%
	D05%	4375.51	-4.09%	-2.45%	-4.32%	-4.87%	2.74%	-5.51%	-5.78%	-3.86%	-3.86%	-3.86%
Mandible	Max	7128.23	0.01%	0.15%	-0.05%	-0.48%	0.31%	-0.45%	-0.72%	0.00%	0.00%	0.00%

Table 108: Patient 3 dose differences from baseline at evaluation criteria for PTVs and OARs for each failure mode.

Patient 4

Structures	Evaluation Criteria	Baseline Dose (cGy)	Failure Mode 1: Beam Energy		Failure Mode 2: Beam Symmetry							
					2 degrees				3.5 degrees			
			+10%	-10%	Top to bottom	Bottom to top	Left to right	Right to left	Top to bottom	Bottom to top	Left to right	Right to left
PTVs												
PTV 66	D95%	6503.93	-0.21%	-0.07%	0.08%	0.02%	0.05%	-0.17%	0.16%	0.10%	-0.17%	0.08%
PTV 60	D95%	5825.80	-0.15%	-0.77%	-0.02%	-0.13%	0.18%	-0.70%	-0.05%	-0.17%	0.19%	-0.41%
PTV 54	D95%	5233.56	-0.14%	-1.82%	0.16%	0.09%	0.47%	-0.86%	0.04%	-0.04%	0.65%	-0.69%
OARs												
Brainstem	Max	3531.81	-1.21%	-1.90%	-0.84%	-0.86%	-0.26%	-2.12%	-0.75%	-0.77%	0.55%	-1.61%
	Max to 1 cc	2945.23	-0.68%	-1.40%	-1.47%	-1.47%	-0.71%	-2.88%	-1.33%	-1.30%	0.33%	-2.25%
Spinal Cord	Max	3331.31	0.43%	0.64%	-0.23%	-1.88%	-1.79%	-1.33%	0.05%	-1.57%	-0.72%	0.54%
	Max to 0.03 cc	3291.92	0.44%	0.47%	-0.18%	-1.82%	-1.73%	-1.24%	0.15%	-1.52%	-0.67%	0.58%
L Parotid	Mean	2090.86	-2.81%	-1.26%	-2.30%	-2.34%	-1.85%	-3.21%	-1.74%	-1.80%	-1.30%	-2.53%
	D50%	1489.64	-5.19%	-1.68%	-4.35%	-4.48%	-3.63%	-5.56%	-3.43%	-3.57%	-2.86%	-4.40%
R Parotid	Mean	3805.94	-1.21%	-2.63%	-1.29%	-1.36%	-0.63%	-2.01%	-0.98%	-1.02%	-0.26%	-1.55%
	D50%	3210.12	-2.57%	-3.94%	-1.21%	-1.06%	-0.31%	-2.57%	-1.27%	-1.14%	-1.31%	-1.90%
L Cochlea	Mean	1044.82	-8.57%	-6.90%	-1.38%	-1.70%	-0.43%	-3.26%	-2.23%	-2.52%	-0.54%	-3.50%
	D05%	1322.08	-7.17%	-6.35%	-0.76%	-1.19%	0.15%	-2.70%	-1.72%	-1.97%	0.08%	-2.87%
R Cochlea	Mean	1639.80	-3.33%	-4.74%	-2.42%	-2.45%	-1.09%	-4.05%	-2.30%	-2.33%	0.14%	-3.22%
	D05%	2074.80	-3.28%	-3.96%	-1.83%	-1.91%	-0.53%	-3.50%	-1.71%	-1.83%	0.66%	-2.75%

Structures	Evaluation Criteria	Baseline Dose (cGy)	Failure Mode 2: Beam Symmetry				Failure Mode 3: MLC Position							
			10 degrees				1 mm Errors				2 mm Errors			
			Top to bottom	Bottom to top	Left to right	Right to left	X1 + 1mm	X1 - 1mm	X2 +1mm	X2 - 1mm	X1 + 2mm	X1 - 2mm	X2 +2mm	X2 - 2mm
PTVs														
PTV 66	D95%	6503.93	-0.36%	-0.24%	-0.80%	-0.32%	-0.13%	0.10%	-0.42%	0.34%	-0.76%	0.05%	-1.25%	0.45%
PTV 60	D95%	5825.80	0.26%	0.16%	0.39%	-1.19%	-0.42%	0.23%	-1.10%	0.99%	-4.15%	0.36%	-2.86%	1.74%
PTV 54	D95%	5233.56	0.85%	0.95%	1.39%	-1.67%	-0.48%	0.62%	-1.64%	1.36%	-3.76%	0.98%	-4.35%	2.19%
OARs														
Brainstem	Max	3531.81	0.68%	0.90%	2.49%	-3.32%	-2.68%	2.82%	-2.50%	2.01%	-6.07%	4.81%	-5.96%	4.31%
	Max to 1 cc	2945.23	0.09%	0.62%	2.46%	-4.39%	-2.16%	2.53%	-2.64%	2.76%	-4.76%	4.88%	-5.62%	5.21%
Spinal Cord	Max	3331.31	2.14%	-2.92%	-4.01%	-0.42%	-1.52%	0.01%	-2.37%	4.18%	-2.48%	0.78%	-2.91%	6.51%
	Max to 0.03 cc	3291.92	2.28%	-2.97%	-3.93%	-0.30%	-1.38%	0.11%	-3.60%	4.30%	-3.80%	-58.21%	-5.11%	6.73%
L Parotid	Mean	2090.86	-1.43%	-1.28%	-0.32%	-3.29%	-0.05%	0.64%	-2.08%	2.71%	-0.55%	1.02%	-4.24%	5.37%
	D50%	1489.64	-2.99%	-3.12%	-1.66%	-5.63%	-0.51%	0.95%	-1.68%	2.08%	-1.54%	1.81%	-3.45%	4.16%
R Parotid	Mean	3805.94	0.04%	0.06%	1.52%	-2.23%	0.07%	0.25%	-1.93%	2.11%	-0.49%	0.46%	-4.14%	4.21%
	D50%	3210.12	-1.72%	-0.12%	2.20%	-2.45%	-1.61%	-0.25%	-2.94%	2.32%	-1.40%	-1.09%	-7.17%	7.54%
L Cochlea	Mean	1044.82	3.69%	3.42%	6.25%	-1.91%	-0.81%	0.26%	-6.87%	7.82%	-2.81%	0.50%	-13.37%	17.99%
	D05%	1322.08	6.27%	5.74%	6.28%	0.33%	-1.02%	0.39%	-6.49%	9.26%	-4.35%	0.85%	-13.24%	21.09%
R Cochlea	Mean	1639.80	1.73%	1.79%	4.87%	-4.07%	0.74%	-0.14%	-9.94%	8.45%	0.51%	-0.60%	-20.77%	18.63%
	D05%	2074.80	1.86%	1.47%	4.82%	-4.09%	0.94%	-0.10%	-9.00%	8.55%	0.72%	-0.63%	-17.71%	21.47%

Structures	Evaluation Criteria	Baseline Dose (cGy)	Failure Mode 4: Gantry Angle		Failure Mode 5: Collimator Angle		Failure Mode 6: Couch Angle		Failure Mode 7: MU Linearity					
			+ 2 degrees	-2 degrees	+ 2 degrees	-2 degrees	+ 2 degrees	-2 degrees	1A	1B	2A	2B	3A	3B
PTVs														
PTV 66	D95%	6503.93	-0.13%	-0.11%	-0.23%	-0.43%	-0.89%	-1.35%	-0.16%	-0.02%	-0.08%	-0.03%	-0.10%	0.05%
PTV 60	D95%	5825.80	-0.80%	0.16%	-0.06%	-1.61%	-0.09%	-3.68%	-0.30%	-0.02%	-0.28%	-0.03%	-0.45%	0.08%
PTV 54	D95%	5233.56	-0.28%	-0.48%	-1.49%	-1.64%	-2.56%	-3.41%	-0.19%	-0.02%	-0.24%	-0.02%	-0.34%	0.20%
OARs														
Brainstem	Max	3531.81	-2.61%	3.03%	6.31%	5.35%	3.90%	-4.44%	-0.45%	-0.01%	-0.53%	0.00%	-0.98%	0.31%
	Max to 1 cc	2945.23	-0.21%	0.43%	1.59%	0.10%	8.77%	-3.99%	-0.27%	0.00%	-0.19%	0.00%	-0.72%	0.31%
Spinal Cord	Max	3331.31	3.54%	1.14%	2.07%	0.29%	0.07%	0.36%	-0.01%	0.00%	-0.01%	0.00%	-0.01%	0.00%
	Max to 0.03 cc	3291.92	0.30%	0.58%	0.77%	-0.03%	-0.11%	0.07%	-0.03%	0.00%	-0.03%	0.00%	0.06%	0.00%
L Parotid	Mean	2090.86	5.64%	-4.53%	6.59%	-3.92%	-0.11%	3.15%	0.11%	-0.03%	0.10%	-0.04%	0.46%	0.13%
	D50%	1489.64	4.85%	-2.87%	7.78%	-5.06%	-2.60%	6.87%	0.39%	-0.06%	0.47%	-0.07%	1.22%	-0.22%
R Parotid	Mean	3805.94	-2.22%	2.49%	-3.74%	5.59%	3.33%	-1.34%	-0.30%	-0.02%	-0.22%	-0.03%	-0.34%	-0.02%
	D50%	3210.12	-4.02%	9.89%	-6.62%	14.85%	12.79%	-3.71%	-0.05%	-0.02%	-0.05%	-0.05%	-0.52%	0.30%
L Cochlea	Mean	1044.82	-0.69%	1.22%	-0.88%	1.96%	5.50%	-4.56%	-0.44%	-0.02%	-0.34%	-0.03%	-0.39%	0.16%
	D05%	1322.08	-0.41%	2.49%	2.54%	1.59%	6.05%	-4.39%	-0.45%	0.00%	-0.19%	0.00%	-0.74%	0.23%
R Cochlea	Mean	1639.80	3.66%	-3.46%	23.88%	-8.44%	-2.56%	17.09%	-0.18%	-0.02%	-0.26%	-0.01%	-0.35%	-0.06%
	D05%	2074.80	4.90%	-4.40%	29.46%	1.58%	7.44%	23.74%	-0.38%	0.00%	-0.47%	0.00%	-0.88%	-0.05%

Structures	Evaluation Criteria	Baseline Dose (cGy)	MLC Modeling							Failure Mode 11: CT Table		
			Failure Mode 8: Leakage & Transmission		Failure Mode 9: Tongue-and-groove		Failure Mode 10: Leaf End					
			0%	10%	width = 0.005 cm	width = 0.200 cm	radius = 4 cm	radius = 15 cm	radius = 20 cm	+2%	-2%	PET CT
PTVs												
PTV 66	D95%	6503.93	0.03%	-0.26%	-0.04%	0.27%	0.60%	-0.79%	-0.29%	0.00%	0.00%	0.00%
PTV 60	D95%	5825.80	0.12%	-1.02%	-0.11%	0.63%	1.53%	-1.86%	-1.06%	0.00%	0.00%	0.00%
PTV 54	D95%	5233.56	0.08%	-0.95%	-0.02%	1.19%	1.78%	-2.40%	-1.87%	0.00%	0.00%	0.00%
OARs												
Brainstem	Max	3531.81	-0.01%	-0.20%	-0.23%	3.30%	3.17%	-5.60%	-3.97%	0.00%	0.00%	0.00%
	Max to 1 cc	2945.23	-0.32%	1.38%	-0.34%	4.84%	3.94%	-4.70%	-4.46%	0.00%	0.00%	0.00%
Spinal Cord	Max	3331.31	-0.12%	0.24%	-0.14%	1.58%	1.54%	-1.76%	-1.28%	0.00%	0.00%	0.00%
	Max to 0.03 cc	3291.92	-0.15%	0.24%	-0.15%	1.49%	1.64%	-1.75%	-1.23%	0.00%	0.00%	0.00%
L Parotid	Mean	2090.86	-0.02%	0.27%	-0.50%	7.31%	4.25%	-2.82%	-1.87%	0.00%	0.00%	0.00%
	D50%	1489.64	-0.46%	2.14%	-1.10%	11.80%	4.84%	-2.93%	-2.12%	0.00%	0.00%	0.00%
R Parotid	Mean	3805.94	-0.14%	0.40%	-0.42%	3.06%	2.67%	-2.67%	-1.68%	0.00%	0.00%	0.00%
	D50%	3210.12	-0.17%	0.00%	-0.28%	4.45%	5.05%	-3.86%	-2.75%	0.00%	0.00%	-3.11%
L Cochlea	Mean	1044.82	-1.29%	6.32%	-1.49%	16.00%	21.51%	-7.45%	-8.40%	0.00%	0.00%	0.00%
	D05%	1322.08	0.38%	7.43%	-1.49%	15.11%	23.44%	-8.74%	-10.06%	0.00%	0.00%	0.00%
R Cochlea	Mean	1639.80	-0.89%	4.04%	-0.99%	8.64%	12.48%	-7.28%	-7.93%	0.00%	0.00%	0.00%
	D05%	2074.80	-1.00%	4.77%	-0.94%	6.09%	11.98%	-8.39%	-9.23%	0.00%	0.00%	0.00%

Table 109: Patient 4 dose differences from baseline at evaluation criteria for PTVs and OARs for each failure mode.

Patient 5

Structures	Evaluation Criteria	Baseline Dose (cGy)	Failure Mode 1: Beam Energy		Failure Mode 2: Beam Symmetry							
					2 degrees				3.5 degrees			
			+10%	-10%	Top to bottom	Bottom to top	Left to right	Right to left	Top to bottom	Bottom to top	Left to right	Right to left
PTVs												
PTV 70	D95%	6750.39	-0.40%	-0.51%	0.03%	0.09%	0.15%	0.17%	-0.03%	0.22%	-0.16%	-0.11%
PTV 60	D95%	6021.80	-0.38%	-1.89%	-0.11%	0.33%	0.29%	0.19%	-0.17%	0.45%	0.07%	-0.04%
PTV 56	D95%	5670.80	-1.50%	-1.94%	-0.39%	0.06%	0.15%	0.10%	-0.46%	0.21%	-0.19%	-0.25%
OARs												
Brainstem	Max	4732.41	-0.30%	-2.28%	-1.36%	0.09%	-0.39%	-0.43%	-1.18%	0.76%	-0.63%	-0.77%
	Max to 1 cc	4278.49	0.48%	-1.86%	-1.48%	-0.18%	-0.26%	-0.41%	-1.25%	1.02%	-0.42%	-0.60%
Spinal Cord	Max	3982.58	-0.08%	2.04%	-0.62%	-0.38%	-0.24%	-0.26%	-0.41%	0.17%	-0.28%	-0.43%
	Max to 0.3 cc	3864.34	0.17%	2.27%	-9.27%	-28.66%	0.20%	-0.80%	0.12%	0.15%	0.43%	0.35%
L Parotid	Mean	1803.35	-9.04%	-6.09%	-2.40%	-1.95%	-2.10%	-1.93%	-2.11%	-1.24%	-1.99%	-1.73%
	D50%	1232.46	-11.20%	-5.17%	-2.48%	-1.91%	-2.13%	-1.96%	-1.69%	-0.59%	-1.50%	-1.32%
R Parotid	Mean	2371.41	-3.71%	-2.22%	-1.88%	-1.45%	-1.52%	-1.67%	-1.67%	-0.90%	-1.37%	-1.55%
	D50%	1686.91	-3.44%	0.54%	-0.45%	0.25%	0.02%	0.06%	-0.03%	1.24%	0.32%	0.39%
Mandible	Max	7408.85	1.64%	-1.20%	-0.29%	0.87%	0.50%	0.35%	-0.42%	0.77%	0.23%	0.01%

Structures	Evaluation Criteria	Baseline Dose (cGy)	Failure Mode 2: Beam Symmetry				Failure Mode 3: MLC Position							
			10 degrees				1 mm Errors				2 mm Errors			
			Top to bottom	Bottom to top	Left to right	Right to left	X1 + 1mm	X1 - 1mm	X2 +1mm	X2 - 1mm	X1 + 2mm	X1 - 2mm	X2 +2mm	X2 - 2mm
PTVs														
PTV 70	D95%	6750.39	-0.57%	-0.08%	-0.06%	0.06%	-1.00%	0.73%	3.19%	0.26%	-2.36%	0.93%	-1.40%	3.54%
PTV 60	D95%	6021.80	-1.17%	0.14%	0.11%	0.07%	-1.53%	0.83%	2.93%	0.46%	-3.82%	1.03%	-2.85%	4.10%
PTV 56	D95%	5670.80	-2.58%	-1.60%	-1.12%	-1.30%	-2.53%	-0.44%	-2.14%	-0.80%	-5.68%	-0.52%	-4.02%	-0.23%
OARs														
Brainstem	Max	4732.41	-2.53%	2.81%	1.20%	1.22%	-1.45%	1.62%	1.75%	1.62%	-2.21%	2.71%	0.33%	2.94%
	Max to 1 cc	4278.49	-2.52%	3.51%	1.89%	1.34%	1.11%	0.12%	2.29%	0.53%	1.48%	-0.32%	1.10%	1.99%
Spinal Cord	Max	3982.58	6.55%	2.55%	2.85%	3.46%	4.42%	7.66%	6.16%	7.92%	4.65%	10.11%	4.92%	11.19%
	Max to 0.3 cc	3864.34	0.09%	0.12%	8.10%	3.77%	5.74%	8.18%	7.38%	7.35%	5.30%	9.77%	5.60%	11.17%
L Parotid	Mean	1803.35	-8.12%	-6.52%	-7.49%	-6.89%	-11.86%	2.12%	-6.86%	-3.09%	-17.80%	9.71%	-8.49%	-0.46%
	D50%	1232.46	-10.55%	-8.69%	-9.56%	-9.52%	-11.06%	1.78%	-6.60%	-3.81%	-15.58%	10.23%	-8.20%	0.35%
R Parotid	Mean	2371.41	-1.02%	0.78%	-0.10%	-0.67%	-1.90%	4.27%	23.72%	7.03%	-4.35%	7.51%	-9.40%	13.69%
	D50%	1686.91	-1.14%	1.73%	0.18%	0.16%	-0.69%	6.84%	46.68%	10.04%	-2.86%	12.23%	-8.19%	68.67%
Mandible	Max	7408.85	1.56%	4.31%	3.27%	2.96%	2.18%	1.61%	13.57%	3.23%	1.73%	0.90%	0.28%	4.05%

Structures	Evaluation Criteria	Baseline Dose (cGy)	Failure Mode 4: Gantry Angle		Failure Mode 5: Collimator Angle		Failure Mode 6: Couch Angle		Failure Mode 7: MU Linearity					
			+ 2 degrees	-2 degrees	+ 2 degrees	-2 degrees	+ 2 degrees	-2 degrees	1A	1B	2A	2B	3A	3B
PTVs														
PTV 70	D95%	6750.39	0.06%	-0.75%	0.36%	-0.75%	-1.17%	-0.29%	-0.06%	0.00%	-0.22%	-0.01%	-0.11%	-0.05%
PTV 60	D95%	6021.80	-2.23%	-0.55%	-0.42%	-0.55%	-1.48%	-1.87%	-0.07%	0.00%	-0.35%	-0.01%	-0.19%	-0.01%
PTV 56	D95%	5670.80	-0.15%	-0.81%	0.85%	-0.81%	-2.77%	-1.22%	-0.06%	0.00%	-0.25%	-0.01%	-0.05%	-0.08%
OARs														
Brainstem	Max	4732.41	0.41%	1.68%	3.63%	1.68%	2.16%	1.06%	0.00%	0.00%	-0.22%	-0.01%	-0.17%	0.04%
	Max to 1 cc	4278.49	-0.10%	0.14%	0.59%	0.14%	3.14%	-2.47%	0.00%	0.00%	-0.29%	-0.02%	-0.03%	-0.05%
Spinal Cord	Max	3982.58	1.68%	3.46%	1.00%	3.46%	5.06%	0.61%	0.10%	-0.01%	0.25%	-0.03%	0.17%	-0.06%
	Max to 0.3 cc	3864.34	1.26%	3.47%	1.32%	3.47%	4.99%	0.95%	0.13%	0.00%	0.27%	-0.02%	0.20%	-0.08%
L Parotid	Mean	1803.35	14.31%	-7.17%	11.16%	-7.17%	-8.04%	12.92%	-0.03%	-0.01%	-0.26%	-0.01%	0.44%	-0.27%
	D50%	1232.46	18.70%	-5.39%	15.54%	-5.39%	-6.28%	21.63%	0.07%	-0.02%	-0.13%	-0.04%	0.77%	-0.44%
R Parotid	Mean	2371.41	-8.50%	8.70%	-4.84%	8.70%	6.49%	-2.21%	-0.08%	0.00%	-0.36%	-0.01%	0.14%	-0.17%
	D50%	1686.91	-2.85%	16.44%	-3.07%	16.44%	14.50%	3.41%	-0.13%	-0.02%	-0.43%	-0.04%	0.15%	-0.28%
Mandible	Max	7408.85	0.54%	0.78%	-0.13%	0.78%	1.06%	-1.24%	0.01%	0.00%	-0.20%	-0.01%	0.11%	-0.07%

Structures	Evaluation Criteria	Baseline Dose (cGy)	MLC Modeling							Failure Mode 11: CT Table		
			Failure Mode 8: Leakage & Transmission		Failure Mode 9: Tongue-and-groove		Failure Mode 10: Leaf End					
			0%	10%	width = 0.005 cm	width = 0.200 cm	radius = 4 cm	radius = 15 cm	radius = 20 cm	+2%	-2%	PET CT
PTVs												
PTV 70	D95%	6750.39	-0.19%	0.34%	0.00%	0.06%	0.73%	-1.27%	-0.84%	0.04%	0.04%	0.04%
PTV 60	D95%	6021.80	-0.29%	1.04%	-0.14%	0.34%	1.92%	-2.99%	-2.16%	0.08%	0.08%	0.08%
PTV 56	D95%	5670.80	-1.32%	0.29%	-1.17%	-0.49%	0.78%	-4.42%	-3.16%	-1.06%	-1.06%	-1.06%
OARs												
Brainstem	Max	4732.41	-0.12%	1.93%	0.24%	0.25%	3.05%	-1.63%	-1.29%	0.24%	0.24%	0.24%
	Max to 1 cc	4278.49	0.27%	2.93%	0.73%	0.27%	2.08%	0.61%	0.50%	0.64%	0.64%	0.64%
Spinal Cord	Max	3982.58	4.40%	6.70%	5.65%	3.08%	9.42%	2.95%	3.38%	4.78%	4.78%	4.78%
	Max to 0.3 cc	3864.34	4.92%	5.27%	6.00%	8.48%	-4.15%	-18.16%	10.32%	7.25%	3.54%	6.37%
L Parotid	Mean	1803.35	-6.45%	6.03%	-6.04%	-1.39%	6.31%	-12.60%	-10.72%	-5.25%	-5.25%	-5.25%
	D50%	1232.46	-7.38%	13.48%	-6.83%	1.27%	12.08%	-12.67%	-11.27%	-5.41%	-5.41%	-5.41%
R Parotid	Mean	2371.41	-0.23%	11.21%	0.15%	4.53%	13.16%	-7.09%	-5.03%	1.07%	1.07%	1.07%
	D50%	1686.91	0.62%	20.71%	1.31%	8.90%	24.83%	-7.27%	-5.22%	2.79%	2.79%	2.79%
Mandible	Max	7408.85	1.74%	1.51%	1.90%	2.34%	1.76%	1.13%	1.85%	1.86%	1.86%	1.86%

Table 110: Patient 5 dose differences from baseline at evaluation criteria for PTVs and OARs for each failure mode.

Patient 6

Structures	Evaluation Criteria	Baseline Dose (cGy)	Failure Mode 1: Beam Energy		Failure Mode 2: Beam Symmetry							
					2 degrees				3.5 degrees			
			+10%	-10%	Top to bottom	Bottom to top	Left to right	Right to left	Top to bottom	Bottom to top	Left to right	Right to left
PTVs												
PTV 66	D95%	6555.71	0.27%	0.03%	-0.09%	-0.05%	0.07%	0.12%	0.03%	0.21%	0.18%	0.25%
PTV 60	D95%	5770.01	0.68%	-0.61%	-0.39%	0.06%	-0.08%	0.00%	-0.29%	0.38%	0.01%	0.12%
PTV 54	D95%	5269.47	-0.06%	-1.70%	-0.81%	-0.45%	-0.18%	-0.27%	-0.64%	-0.24%	-0.18%	-0.21%
OARs												
Brainstem	Max	3788.73	-0.25%	-3.36%	-2.41%	-0.05%	-0.72%	-0.88%	-2.08%	0.79%	-1.02%	-1.25%
	Max to 1 cc	3462.73	0.03%	-2.60%	-2.26%	-0.17%	-0.75%	-0.84%	-2.10%	0.72%	-1.05%	-1.11%
Spinal Cord	Max	4313.56	-0.37%	0.16%	-0.88%	-0.69%	-0.56%	-0.47%	-0.34%	-0.13%	-0.21%	-0.18%
	Max to 0.3 cc	4210.19	-0.35%	0.50%	-0.78%	-0.59%	-0.43%	-0.36%	-0.28%	-0.24%	-0.17%	-0.05%
L Parotid	Mean	1820.60	-4.22%	-3.81%	-3.05%	-1.93%	-2.39%	-2.35%	-2.65%	-1.31%	-2.13%	-2.05%
	D50%	1023.41	-9.05%	-5.30%	-5.71%	-4.27%	-4.77%	-4.95%	-5.06%	-2.86%	-4.29%	-4.59%
R Parotid	Mean	2244.12	-3.41%	-4.31%	-3.36%	-2.04%	-2.77%	-2.40%	-3.05%	-1.24%	-2.36%	-1.94%
	D50%	1230.34	-11.62%	-7.02%	-7.31%	-5.99%	-6.59%	-6.39%	-6.70%	-4.65%	-6.07%	-5.82%
Mandible	Max	6759.36	0.14%	-1.93%	-0.72%	0.44%	0.10%	0.12%	-0.54%	0.61%	0.05%	0.10%
L Submandibular	Max	5956.60	1.14%	1.84%	-0.06%	0.02%	0.06%	0.08%	0.36%	0.29%	0.26%	0.21%
	Mean	5130.42	-0.21%	1.19%	-0.07%	-0.21%	-0.29%	-0.18%	0.18%	0.01%	-0.06%	0.08%

Structures	Evaluation Criteria	Baseline Dose (cGy)	Failure Mode 2: Beam Symmetry					Failure Mode 3: MLC Position						
			10 degrees					1 mm Errors				2 mm Errors		
			Top to bottom	Bottom to top	Left to right	Right to left	X1 + 1mm	X1 - 1mm	X2 +1mm	X2 - 1mm	X1 + 2mm	X1 - 2mm	X2 +2mm	X2 - 2mm
PTVs														
PTV 66	D95%	6555.71	-0.19%	-0.19%	0.02%	-0.09%	-0.46%	0.37%	-0.44%	0.78%	-1.12%	0.83%	-1.52%	1.11%
PTV 60	D95%	5770.01	-0.64%	0.30%	0.19%	0.14%	-0.38%	0.41%	-0.99%	1.42%	-1.06%	0.84%	-2.72%	2.12%
PTV 54	D95%	5269.47	-1.48%	-0.95%	-0.14%	-0.77%	-0.74%	0.44%	-0.99%	0.68%	-2.01%	0.47%	-3.09%	0.67%
OARs														
Brainstem	Max	3788.73	-3.70%	3.82%	1.78%	1.02%	-0.49%	1.33%	-0.71%	2.49%	-1.04%	1.45%	-1.86%	4.35%
	Max to 1 cc	3462.73	-3.43%	3.56%	1.33%	1.04%	-0.15%	1.81%	-0.04%	2.50%	-0.56%	2.17%	-0.77%	3.43%
Spinal Cord	Max	4313.56	-0.80%	-0.06%	-0.52%	-0.50%	-0.36%	0.05%	-0.44%	1.49%	-1.07%	1.32%	-1.21%	3.24%
	Max to 0.3 cc	4210.19	-1.29%	-0.15%	-0.52%	-0.50%	-1.12%	0.47%	-0.85%	1.31%	-1.21%	1.80%	-1.71%	2.64%
L Parotid	Mean	1820.60	-2.90%	0.47%	-1.15%	-1.01%	-3.04%	3.57%	-1.57%	2.39%	-6.03%	7.88%	-3.52%	4.65%
	D50%	1023.41	-6.30%	-0.28%	-1.99%	-3.07%	-5.55%	3.85%	-1.08%	2.32%	-5.32%	9.69%	-2.93%	4.85%
R Parotid	Mean	2244.12	-3.44%	0.88%	-1.50%	-0.70%	-1.46%	3.08%	-1.93%	4.63%	-2.78%	5.71%	-4.43%	8.40%
	D50%	1230.34	-8.45%	-1.62%	-3.90%	-3.55%	-4.07%	6.69%	-1.17%	7.02%	-6.18%	12.51%	-3.89%	12.81%
Mandible	Max	6759.36	-1.07%	1.78%	0.83%	0.71%	-0.82%	1.81%	-1.10%	1.31%	-1.04%	3.35%	-2.59%	1.94%
L Submandibular	Max	5956.60	-0.02%	0.05%	-0.14%	-0.19%	-0.29%	-0.14%	-0.75%	0.74%	-0.93%	0.70%	-1.06%	2.53%
	Mean	5130.42	0.10%	-0.38%	-0.52%	-0.34%	-0.87%	0.85%	-0.57%	0.91%	-2.05%	2.33%	-1.69%	2.08%

Structures	Evaluation Criteria	Baseline Dose (cGy)	Failure Mode 4: Gantry Angle		Failure Mode 5: Collimator Angle		Failure Mode 6: Couch Angle		Failure Mode 7: MU Linearity					
			+ 2 degree s	-2 degree s	+ 2 degree s	-2 degree s	+ 2 degree s	-2 degrees	1A	1B	2A	2B	3A	3B
PTVs														
PTV 66	D95%	6555.71	-0.05%	-0.23%	0.34%	-0.99%	1.33%	0.42%	-0.09%	0.00%	-0.05%	-0.01%	0.12%	0.15%
PTV 60	D95%	5770.01	-0.33%	-0.22%	1.24%	-1.44%	0.38%	-1.29%	-0.05%	0.00%	-0.07%	-0.01%	0.27%	0.09%
PTV 54	D95%	5269.47	-0.38%	-0.17%	-0.08%	-0.79%	-2.90%	-5.11%	-0.17%	-0.01%	-0.31%	0.00%	0.16%	0.07%
OARs														
Brainstem	Max	3788.73	0.09%	-0.15%	3.33%	-0.96%	17.26%	12.84%	-0.39%	0.00%	-0.44%	0.01%	-0.71%	0.36%
	Max to 1 cc	3462.73	1.09%	-0.89%	2.94%	-2.92%	11.77%	7.88%	-0.12%	0.00%	-0.09%	-0.02%	-0.33%	0.36%
Spinal Cord	Max	4313.56	0.54%	0.00%	0.74%	-0.54%	11.27%	6.43%	-0.28%	0.00%	-0.47%	0.01%	0.19%	0.05%
	Max to 0.3 cc	4210.19	0.63%	0.48%	0.64%	0.12%	9.41%	6.10%	-0.33%	0.00%	-0.50%	0.02%	0.31%	0.02%
L Parotid	Mean	1820.60	7.08%	-5.46%	3.59%	-2.38%	-2.21%	2.31%	0.34%	-0.03%	0.25%	-0.03%	1.91%	-0.31%
	D50%	1023.41	5.19%	-3.25%	1.15%	-0.87%	-0.55%	0.75%	0.25%	-0.04%	0.01%	-0.04%	1.67%	-0.32%
R Parotid	Mean	2244.12	-3.88%	5.57%	1.73%	3.06%	11.01%	1.48%	0.06%	0.00%	0.21%	-0.02%	0.29%	0.12%
	D50%	1230.34	-3.50%	7.90%	2.83%	1.68%	22.26%	8.57%	-0.06%	0.00%	0.04%	0.00%	-0.37%	0.00%
Mandible	Max	6759.36	-1.48%	1.30%	-1.55%	2.32%	1.57%	2.65%	-0.31%	0.00%	-0.37%	0.01%	-0.39%	0.27%
L Submandibular	Max	5956.60	-0.03%	0.53%	1.86%	-1.28%	3.04%	-1.87%	-0.12%	-0.01%	-0.26%	0.01%	0.39%	-0.04%
	Mean	5130.42	0.66%	-0.50%	2.05%	-1.66%	-0.11%	-0.40%	-0.02%	-0.01%	-0.13%	0.00%	0.75%	-0.14%

Structures	Evaluation Criteria	Baseline Dose (cGy)	MLC Modeling							Failure Mode 11: CT Table		
			Failure Mode 8: Leakage & Transmission		Failure Mode 9: Tongue-and-groove		Failure Mode 10: Leaf End					
			0%	10%	width = 0.005 cm	width = 0.200 cm	radius = 4 cm	radius = 15 cm	radius = 20 cm	+2%	-2%	PET CT
PTVs												
PTV 66	D95%	6555.71	0.20%	0.67%	0.18%	0.11%	0.71%	-0.38%	0.13%	0.00%	0.00%	0.00%
PTV 60	D95%	5770.01	0.16%	1.23%	0.16%	0.01%	1.59%	-0.96%	-0.36%	0.00%	0.00%	0.00%
PTV 54	D95%	5269.47	0.02%	1.40%	0.15%	-0.20%	0.80%	-1.28%	-0.63%	0.00%	0.00%	0.00%
OARs												
Brainstem	Max	3788.73	-0.09%	2.91%	0.23%	0.24%	2.89%	-1.05%	-0.63%	0.00%	0.00%	0.00%
	Max to 1 cc	3462.73	-0.11%	3.75%	0.37%	0.25%	2.83%	-0.83%	-0.46%	0.00%	0.00%	0.00%
Spinal Cord	Max	4313.56	0.00%	2.62%	0.11%	0.27%	2.63%	-0.84%	-0.32%	0.00%	0.00%	0.00%
	Max to 0.3 cc	4210.19	0.02%	2.78%	0.26%	-0.26%	3.09%	-1.14%	-0.50%	0.00%	0.00%	0.00%
L Parotid	Mean	1820.60	-0.83%	9.76%	-0.34%	2.27%	8.39%	-4.37%	-3.22%	0.00%	0.00%	0.00%
	D50%	1023.41	-1.80%	20.81%	-1.01%	6.00%	17.53%	-5.99%	-4.67%	0.00%	0.00%	0.00%
R Parotid	Mean	2244.12	-0.43%	8.39%	-0.14%	1.58%	8.01%	-4.24%	-2.85%	0.00%	0.00%	0.00%
	D50%	1230.34	-1.54%	19.51%	-1.05%	5.45%	21.86%	-8.13%	-6.54%	0.00%	0.00%	0.00%
Mandible	Max	6759.36	0.22%	0.36%	0.06%	0.35%	1.46%	-0.71%	-0.32%	0.00%	0.00%	0.00%
L Submandibular	Max	5956.60	0.06%	0.96%	0.19%	-0.44%	1.13%	-0.13%	0.14%	0.00%	0.00%	0.00%
	Mean	5130.42	-0.08%	1.87%	0.01%	0.33%	2.35%	-1.44%	-0.85%	0.00%	0.00%	0.00%

Table 111: Patient 6 dose differences from baseline at evaluation criteria for PTVs and OARs for each failure mode.

Patient 7

Structures	Evaluation Criteria	Baseline Dose (cGy)	Failure Mode 1: Beam Energy		Failure Mode 2: Beam Symmetry							
					2 degrees				3.5 degrees			
			+10%	-10%	Top to bottom	Bottom to top	Left to right	Right to left	Top to bottom	Bottom to top	Left to right	Right to left
PTVs												
PTV 66	D95	6555.71	-0.06%	-0.73%	-0.15%	-0.16%	-0.50%	-0.06%	-0.04%	-0.05%	-0.29%	0.12%
PTV 60	D95	5770.01	-0.34%	-0.16%	-0.03%	-0.02%	0.16%	-0.07%	0.17%	0.18%	0.46%	0.17%
PTV 54	D95	5269.47	-0.27%	-0.93%	-0.25%	-0.07%	0.22%	-0.31%	0.09%	0.32%	0.37%	-0.31%
OARs												
Brainstem	Max	3839.33	0.81%	-1.40%	-1.38%	-1.33%	-2.72%	-0.27%	-1.43%	-1.46%	-2.19%	1.25%
	Max to 1 cc	3666.80	0.47%	-1.00%	-1.55%	-1.50%	-2.76%	-0.57%	-1.49%	-1.47%	-2.09%	0.99%
Cord	Max	4326.81	-0.48%	-0.04%	-0.05%	-0.26%	-0.26%	0.13%	0.02%	-0.23%	0.20%	0.67%
	Max to 0.3 cc	4242.28	-0.60%	0.03%	-0.24%	-0.39%	-0.59%	0.03%	-0.18%	-0.42%	-0.37%	0.63%
L Parotid	Mean	3550.33	-2.19%	-1.65%	-2.01%	-2.07%	-2.43%	-1.53%	-1.70%	-1.77%	-2.14%	-0.88%
	D50	2526.12	-6.15%	-3.20%	-3.18%	-3.21%	-3.80%	-2.56%	-3.21%	-3.33%	-4.82%	-2.06%
R Parotid	Mean	1969.74	-5.43%	-2.00%	-3.02%	-2.78%	-3.26%	-2.43%	-2.66%	-2.37%	-2.72%	-1.78%
	D50	1139.00	-11.59%	-1.67%	-6.50%	-6.41%	-6.94%	-5.97%	-5.79%	-5.62%	-10.97%	-4.74%
L Cochlea	Mean	2418.05	-4.03%	-5.23%	-2.56%	-2.66%	-4.25%	-1.22%	-2.61%	-2.75%	-3.85%	-0.24%
	D05	2743.95	-2.95%	-4.77%	-2.37%	-2.19%	-3.94%	-0.84%	-2.48%	-2.33%	-3.66%	0.07%
R Cochlea	Mean	1579.52	-3.70%	-3.66%	-3.75%	-3.75%	-5.37%	-2.42%	-3.97%	-3.94%	-4.77%	-1.22%
	D05	2087.93	-1.94%	-2.71%	-2.35%	-2.25%	-3.93%	-1.01%	-2.44%	-2.44%	-3.39%	0.38%
L Submandibular	Mean	7176.21	-0.41%	0.97%	0.01%	-0.08%	0.70%	-0.29%	0.31%	0.21%	0.84%	-0.41%
	Max to 1 cc	7348.09	-0.43%	1.19%	0.03%	-0.04%	0.81%	-0.27%	0.35%	0.24%	0.94%	-0.41%
R Submandibular	Mean	5955.18	-0.78%	0.27%	0.02%	0.18%	0.68%	-0.25%	0.25%	0.47%	0.98%	-0.32%
	Max to 1 cc	6755.93	-0.35%	0.79%	0.15%	0.23%	0.93%	-0.10%	0.45%	0.55%	1.16%	-0.17%
L Eye	Max	251.57	-1.94%	12.26%	-14.51%	-14.61%	-15.49%	-13.74%	-12.61%	-12.71%	-13.14%	-10.96%
R Eye	Max	219.09	-0.21%	13.57%	-12.30%	-12.47%	-13.19%	-11.65%	-10.68%	-10.85%	-11.32%	-9.25%
L Lens	Max	151.82	2.98%	19.46%	-11.99%	-12.14%	-12.82%	-11.55%	-9.45%	-9.61%	-9.85%	-8.21%
R Lens	Max	136.56	3.49%	18.00%	-9.68%	-9.83%	-10.39%	-9.21%	-7.79%	-7.97%	-8.32%	-6.71%

Structures	Evaluation Criteria	Baseline Dose (cGy)	Failure Mode 2: Beam Symmetry					Failure Mode 3: MLC Position						
			10 degrees					1 mm Errors				2 mm Errors		
			Top to bottom	Bottom to top	Left to right	Right to left	X1 + 1mm	X1 - 1mm	X2 +1mm	X2 - 1mm	X1 + 2mm	X1 - 2mm	X2 +2mm	X2 - 2mm
PTVs														
PTV 66	D95	6555.71	0.08%	0.13%	-1.74%	-0.76%	-0.31%	0.28%	-0.25%	0.14%	-1.29%	0.45%	-0.76%	0.36%
PTV 60	D95	5770.01	0.05%	0.04%	-0.23%	-0.60%	-0.03%	0.15%	0.22%	-0.01%	-0.34%	0.24%	0.16%	0.16%
PTV 54	D95	5269.47	-0.43%	0.13%	0.50%	-0.88%	-0.75%	0.32%	-2.77%	0.05%	-2.25%	0.48%	-12.17%	0.19%
OARs														
Brainstem	Max	3839.33	0.51%	0.61%	-5.35%	3.38%	-0.34%	0.88%	-0.30%	0.85%	-0.46%	1.43%	-0.75%	1.89%
	Max to 1 cc	3666.80	0.39%	0.50%	-5.11%	3.03%	-0.13%	0.43%	-0.32%	0.33%	-0.61%	0.92%	-0.65%	1.07%
Cord	Max	4326.81	1.33%	0.49%	-1.35%	1.12%	0.20%	0.33%	-0.66%	1.10%	0.00%	0.53%	-1.88%	2.13%
	Max to 0.3 cc	4242.28	1.19%	0.47%	-1.54%	1.28%	-0.23%	0.52%	-0.84%	0.81%	-0.72%	1.19%	-1.67%	1.73%
L Parotid	Mean	3550.33	-0.46%	-0.68%	-2.97%	0.88%	-3.36%	3.56%	-0.12%	0.21%	-6.88%	7.21%	-0.34%	0.54%
	D50	2526.12	-0.99%	-1.11%	-4.34%	0.70%	-7.79%	9.02%	0.40%	-0.22%	-15.10%	18.77%	0.46%	-0.25%
R Parotid	Mean	1969.74	-1.94%	-1.13%	-3.44%	-0.28%	-3.90%	4.34%	-0.05%	0.26%	-7.94%	8.77%	-0.27%	0.59%
	D50	1139.00	-4.13%	-3.78%	-6.41%	-2.46%	-2.90%	3.51%	-0.61%	0.79%	-5.79%	7.81%	-0.97%	1.67%
L Cochlea	Mean	2418.05	0.46%	-0.02%	-5.79%	3.82%	-1.61%	2.25%	-0.13%	0.13%	-3.42%	5.19%	0.24%	0.60%
	D05	2743.95	0.29%	0.66%	-5.65%	4.07%	-1.06%	2.11%	-0.14%	0.26%	-2.24%	5.25%	0.33%	0.86%
R Cochlea	Mean	1579.52	-1.21%	-1.15%	-7.16%	2.42%	-5.67%	4.24%	-0.85%	1.10%	-11.15%	9.67%	-1.70%	2.44%
	D05	2087.93	-0.10%	-0.05%	-6.13%	3.50%	-3.60%	5.68%	-1.87%	1.68%	-8.40%	13.02%	-3.78%	2.68%
L Submandibular	Mean	7176.21	-0.46%	-0.72%	1.26%	-1.50%	0.45%	-0.05%	0.31%	-0.03%	0.52%	-0.05%	0.33%	0.11%
	Max to 1 cc	7348.09	-0.58%	-0.76%	1.45%	-1.60%	0.56%	-0.15%	0.42%	-0.10%	0.77%	-0.22%	0.59%	-0.05%
R Submandibular	Mean	5955.18	-0.59%	-0.03%	1.30%	-1.18%	0.36%	0.22%	0.18%	0.34%	0.25%	0.32%	-0.12%	0.76%
	Max to 1 cc	6755.93	-0.56%	-0.21%	1.48%	-1.30%	0.66%	-0.09%	0.35%	0.16%	0.93%	-0.24%	0.27%	0.44%
L Eye	Max	251.57	-9.97%	-10.34%	-13.95%	-7.71%	-6.72%	8.59%	-3.74%	7.23%	-10.72%	16.21%	-4.29%	14.83%
R Eye	Max	219.09	-8.05%	-8.69%	-11.96%	-6.23%	-7.04%	10.17%	-4.13%	7.91%	-10.78%	19.60%	-4.58%	16.24%
L Lens	Max	151.82	-9.86%	-10.35%	-12.99%	-8.47%	-7.37%	12.53%	-5.65%	9.92%	-10.22%	25.46%	-6.19%	19.61%
R Lens	Max	136.56	-7.02%	-7.57%	-10.08%	-5.79%	-7.74%	13.91%	-6.08%	11.32%	-10.29%	27.23%	-6.63%	21.96%

Structures	Evaluation Criteria	Baseline Dose (cGy)	Failure Mode 4: Gantry Angle		Failure Mode 5: Collimator Angle		Failure Mode 6: Couch Angle		Failure Mode 7: MU Linearity					
			+ 2 degrees	-2 degrees	+ 2 degrees	-2 degrees	+ 2 degrees	-2 degrees	1A	1B	2A	2B	3A	3B
PTVs														
PTV 66	D95	6555.71	-0.05%	-0.03%	-0.57%	-0.17%	-3.19%	-1.20%	-0.05%	0.11%	0.13%	0.10%	0.00%	0.11%
PTV 60	D95	5770.01	0.49%	-0.40%	-1.28%	1.24%	0.26%	-1.43%	-0.01%	0.15%	0.19%	0.12%	0.03%	0.14%
PTV 54	D95	5269.47	-0.85%	0.52%	-1.16%	-0.70%	-2.06%	-1.65%	0.03%	0.11%	0.25%	0.09%	0.07%	0.11%
OARs														
Brainstem	Max	3839.33	1.06%	-0.29%	1.49%	10.09%	14.22%	0.97%	0.05%	0.20%	0.38%	0.17%	0.14%	0.19%
	Max to 1 cc	3666.80	0.14%	0.31%	-1.79%	2.85%	0.63%	-0.73%	0.05%	0.21%	0.39%	0.19%	0.12%	0.21%
Cord	Max	4326.81	1.06%	-0.26%	2.18%	2.76%	2.41%	1.23%	0.06%	0.18%	0.17%	0.17%	0.09%	0.18%
	Max to 0.3 cc	4242.28	0.80%	-0.06%	1.50%	1.37%	2.41%	1.47%	-0.08%	0.17%	0.12%	0.17%	-0.01%	0.17%
L Parotid	Mean	3550.33	0.11%	0.79%	0.14%	2.38%	0.97%	2.21%	-0.17%	0.09%	-0.06%	0.08%	-0.15%	0.09%
	D50	2526.12	-0.43%	3.40%	2.79%	4.17%	5.61%	5.02%	-0.49%	0.15%	-0.09%	0.14%	-0.25%	0.15%
R Parotid	Mean	1969.74	-6.13%	7.85%	-1.47%	5.03%	8.52%	-4.03%	-0.05%	0.09%	0.07%	0.08%	-0.02%	0.09%
	D50	1139.00	-1.58%	3.95%	-0.88%	6.50%	12.99%	-2.46%	-0.70%	0.18%	0.18%	0.18%	-0.44%	0.18%
L Cochlea	Mean	2418.05	1.97%	0.14%	12.85%	-6.16%	23.04%	-13.27%	0.00%	0.22%	0.10%	0.21%	0.05%	0.22%
	D05	2743.95	0.57%	1.12%	6.62%	-4.96%	23.14%	-16.62%	-0.16%	0.20%	-0.29%	0.20%	-0.12%	0.20%
R Cochlea	Mean	1579.52	-1.23%	2.60%	-3.67%	10.83%	-16.49%	29.34%	-0.03%	0.08%	0.24%	0.06%	0.02%	0.08%
	D05	2087.93	0.12%	1.14%	-4.41%	9.55%	-14.94%	30.65%	-0.12%	0.10%	0.19%	0.05%	-0.07%	0.10%
L Submandibular	Mean	7176.21	0.34%	-0.20%	0.25%	-0.20%	0.99%	-0.36%	0.06%	0.08%	0.34%	0.06%	0.11%	0.08%
	Max to 1 cc	7348.09	0.02%	0.24%	0.30%	0.09%	1.30%	-0.41%	0.05%	0.08%	0.33%	0.05%	0.10%	0.08%
R Submandibular	Mean	5955.18	0.63%	-0.30%	-2.46%	3.01%	1.65%	-0.86%	0.01%	0.18%	0.24%	0.16%	0.05%	0.18%
	Max to 1 cc	6755.93	0.60%	-0.33%	-1.26%	2.11%	0.38%	0.19%	0.09%	0.19%	0.39%	0.16%	0.13%	0.18%
L Eye	Max	251.57	1.09%	-0.90%	-4.04%	2.61%	-2.35%	0.03%	-0.07%	0.06%	0.04%	0.05%	-0.02%	0.06%
R Eye	Max	219.09	-0.14%	0.78%	-0.12%	-1.11%	0.27%	-3.88%	-0.17%	0.10%	0.05%	0.08%	-0.11%	0.09%
L Lens	Max	151.82	0.94%	-0.79%	-2.17%	1.33%	-0.76%	-2.15%	-0.13%	0.08%	-0.01%	0.06%	-0.08%	0.07%
R Lens	Max	136.56	-0.52%	1.72%	0.90%	-0.22%	-0.41%	-2.77%	-0.20%	0.06%	-0.06%	0.05%	-0.16%	0.06%

Structures	Evaluation Criteria	Baseline Dose (cGy)	MLC Modeling							Failure Mode 11: CT Table		
			Failure Mode 8: Leakage & Transmission		Failure Mode 9: Tongue-and-groove		Failure Mode 10: Leaf End					
			0%	10%	width = 0.005 cm	width = 0.200 cm	radius = 4 cm	radius = 15 cm	radius = 20 cm	+2%	-2%	PET CT
PTVs												
PTV 66	D95	6555.71	0.24%	-0.22%	0.05%	0.43%	0.58%	-0.88%	-0.90%	0.00%	0.00%	0.00%
PTV 60	D95	5770.01	0.24%	-0.30%	-0.03%	0.60%	0.37%	-0.15%	-0.04%	0.00%	0.00%	0.00%
PTV 54	D95	5269.47	0.29%	-0.17%	0.03%	0.99%	0.44%	-0.50%	-0.07%	0.00%	0.00%	0.00%
OARs												
Brainstem	Max	3839.33	0.27%	0.16%	-0.22%	3.56%	4.15%	0.01%	-0.40%	0.00%	0.00%	0.00%
	Max to 1 cc	3666.80	0.11%	0.48%	-0.32%	4.07%	3.34%	-0.07%	-0.42%	0.00%	0.00%	0.00%
Cord	Max	4326.81	0.53%	-0.36%	-0.05%	2.97%	1.41%	-1.43%	-1.21%	0.00%	0.00%	0.00%
	Max to 0.3 cc	4242.28	0.29%	-0.04%	-0.11%	3.02%	1.54%	-1.56%	-1.20%	0.00%	0.00%	0.00%
L Parotid	Mean	3550.33	-0.17%	1.43%	-0.43%	5.17%	5.52%	-3.62%	-3.04%	0.00%	0.00%	0.00%
	D50	2526.12	-0.25%	0.96%	-0.90%	9.70%	13.93%	-8.95%	-8.83%	0.00%	0.00%	0.00%
R Parotid	Mean	1969.74	-0.50%	2.48%	-1.01%	11.30%	6.38%	-4.31%	-3.68%	0.00%	0.00%	0.00%
	D50	1139.00	-1.32%	-0.61%	-2.28%	22.65%	11.94%	-4.92%	-5.79%	0.00%	0.00%	0.00%
L Cochlea	Mean	2418.05	-0.39%	2.06%	-0.57%	8.01%	14.01%	-1.94%	-1.96%	0.00%	0.00%	0.00%
	D05	2743.95	-0.22%	1.48%	-0.48%	6.52%	11.90%	-1.63%	-1.62%	0.00%	0.00%	0.00%
R Cochlea	Mean	1579.52	-0.93%	3.62%	-1.15%	12.33%	23.87%	-5.13%	-6.16%	0.00%	0.00%	0.00%
	D05	2087.93	-0.96%	2.37%	-1.06%	10.73%	21.74%	-6.05%	-6.53%	0.00%	0.00%	0.00%
L Submandibular	Mean	7176.21	0.21%	0.38%	0.09%	0.40%	-0.01%	0.50%	0.60%	0.00%	0.00%	0.00%
	Max to 1 cc	7348.09	0.21%	0.49%	0.11%	0.30%	-0.20%	0.75%	0.79%	0.00%	0.00%	0.00%
R Submandibular	Mean	5955.18	0.39%	-0.50%	0.02%	1.15%	0.55%	0.18%	0.32%	0.00%	0.00%	0.00%
	Max to 1 cc	6755.93	0.28%	0.15%	0.08%	0.63%	0.12%	0.62%	0.59%	0.00%	0.00%	0.00%
L Eye	Max	251.57	0.06%	0.10%	-0.19%	1.23%	3.12%	-0.32%	-0.69%	0.00%	0.00%	0.00%
R Eye	Max	219.09	-0.05%	0.40%	-0.24%	1.68%	3.73%	-0.82%	-0.98%	0.00%	0.00%	0.00%
L Lens	Max	151.82	0.01%	0.03%	-0.23%	1.30%	3.12%	-0.70%	-1.02%	0.00%	0.00%	0.00%
R Lens	Max	136.56	-0.13%	0.41%	-0.31%	1.93%	3.98%	-1.24%	-1.32%	0.00%	0.00%	0.00%

Table 112: Patient 7 dose differences from baseline at evaluation criteria for PTVs and OARs for each failure mode.

Patient 8

Structures	Evaluation Criteria	Baseline Dose (cGy)	Failure Mode 1: Beam Energy		Failure Mode 2: Beam Symmetry							
					2 degrees				3.5 degrees			
			+10%	-10%	Top to bottom	Bottom to top	Left to right	Right to left	Top to bottom	Bottom to top	Left to right	Right to left
PTVs												
PTV 70	D95	6742.59	-0.27%	-0.05%	0.23%	0.24%	0.29%	0.17%	0.20%	0.13%	0.24%	0.18%
PTV 66	D95	6373.08	-0.76%	-0.13%	0.43%	0.53%	0.28%	0.68%	0.46%	0.44%	-0.06%	0.65%
PTV 63	D95	6141.76	-1.39%	0.80%	0.56%	0.50%	0.03%	1.04%	0.62%	0.43%	-0.20%	1.12%
PTV 60	D95	6134.02	-0.11%	-1.80%	-0.84%	0.16%	0.90%	-0.59%	-0.10%	-0.10%	1.42%	-0.68%
PTV 57	D95	5339.39	-0.50%	-1.38%	0.32%	0.27%	0.50%	0.02%	0.35%	0.08%	0.73%	0.04%
OARs												
Brainstem	Max	4138.24	-0.61%	-0.11%	-0.15%	-0.34%	0.10%	-0.85%	-0.14%	-0.57%	0.85%	-0.71%
	Max to 1 cc	3716.32	-0.66%	-0.55%	-0.79%	-0.84%	-0.18%	-1.71%	-0.99%	-1.20%	0.56%	-1.40%
Spinal cord	Max	3966.48	-1.31%	1.20%	-0.30%	-0.53%	-0.16%	-0.55%	-0.06%	-0.52%	0.18%	-0.11%
	Max to 0.3 cc	3730.08	0.14%	1.23%	0.00%	-0.21%	0.38%	0.31%	0.38%	-0.31%	3.36%	1.33%
L parotid	Mean	2544.98	-3.64%	-0.96%	-2.07%	-1.90%	-1.97%	-2.17%	-1.64%	-1.64%	-1.36%	-1.69%
	D50	2228.97	-5.51%	-6.27%	-3.27%	-2.52%	0.73%	1.00%	-2.15%	0.31%	2.83%	-0.20%
R parotid	Mean	2518.84	-5.11%	-2.06%	-2.43%	-2.59%	-2.36%	-2.57%	-1.80%	-2.08%	-1.63%	-2.11%
	D05	1754.00	-4.45%	-3.25%	-2.74%	-2.91%	-1.82%	0.97%	-1.60%	-2.68%	8.72%	1.82%
L cochlea	Mean	1506.44	-5.74%	-5.34%	-2.65%	-3.06%	-2.20%	-3.92%	-2.32%	-2.93%	-0.64%	-3.23%
	D05	1715.00	-0.93%	-6.53%	-0.06%	-0.35%	1.28%	2.62%	0.76%	-0.76%	12.77%	3.67%
R cochlea	Mean	3269.92	-2.25%	-4.29%	-1.02%	-0.66%	-0.15%	-2.19%	-1.34%	-1.04%	1.04%	-1.73%
	D05	3507.80	-1.07%	-4.99%	-0.11%	0.25%	1.09%	0.26%	-0.35%	-0.43%	6.00%	0.73%
L submandibular	Max	7475.57	-0.51%	1.63%	0.90%	0.80%	-0.01%	1.89%	0.93%	0.83%	-0.41%	1.89%
	Mean	6982.24	-0.70%	1.10%	0.54%	0.50%	0.14%	1.28%	0.65%	0.50%	-0.29%	1.21%
R. submandibular	Max	7354.29	-0.62%	1.09%	0.25%	0.51%	0.09%	0.80%	0.34%	0.63%	-0.12%	0.96%
	Mean	6915.01	-0.87%	1.46%	0.37%	0.50%	-0.02%	1.20%	0.46%	0.59%	-0.32%	1.17%

Structures	Evaluation Criteria	Baseline Dose (cGy)	Failure Mode 2: Beam Symmetry				Failure Mode 3: MLC Position							
			10 degrees				1 mm Errors				2 mm Errors			
			Top to bottom	Bottom to top	Left to right	Right to left	X1 + 1mm	X1 - 1mm	X2 +1mm	X2 - 1mm	X1 + 2mm	X1 - 2mm	X2 +2mm	X2 - 2mm
PTVs														
PTV 70	D95	6742.59	0.30%	0.07%	-0.14%	-0.55%	0.07%	0.55%	-0.04%	0.61%	-0.04%	0.20%	-0.37%	0.29%
PTV 66	D95	6373.08	0.01%	-0.03%	-1.21%	-0.06%	-1.82%	0.30%	-0.35%	0.75%	-6.69%	-0.22%	-1.32%	0.73%
PTV 63	D95	6141.76	-0.23%	-0.66%	-1.78%	1.04%	-0.34%	0.63%	-0.50%	0.88%	-1.33%	0.32%	-1.39%	0.64%
PTV 60	D95	6134.02	1.27%	1.73%	3.37%	-2.22%	0.00%	-0.53%	-1.99%	1.07%	0.20%	-0.96%	-3.54%	1.85%
PTV 57	D95	5339.39	0.93%	0.51%	1.06%	-0.94%	-0.04%	0.49%	-0.61%	1.00%	-2.53%	0.28%	-1.76%	1.20%
OARs														
Brainstem	Max	4138.24	1.66%	0.64%	1.87%	-2.16%	-0.08%	0.50%	-0.27%	0.59%	-0.35%	0.23%	-0.99%	0.96%
	Max to 1 cc	3716.32	1.20%	0.58%	2.00%	-3.41%	-0.38%	0.77%	-0.20%	0.58%	-0.80%	1.17%	-0.66%	0.91%
Spinal cord	Max	3966.48	0.33%	-0.67%	-0.41%	-1.54%	0.13%	0.58%	-0.36%	0.72%	0.01%	0.71%	-1.29%	0.70%
	Max to 0.3 cc	3730.08	4.72%	2.51%	2.63%	2.86%	2.39%	3.29%	0.00%	3.50%	2.01%	2.41%	0.02%	1.57%
L parotid	Mean	2544.98	-1.56%	-1.03%	-0.27%	-2.14%	0.08%	0.74%	-0.72%	1.61%	0.01%	0.54%	-1.55%	2.33%
	D50	2228.97	-0.27%	1.02%	2.02%	1.75%	1.36%	3.04%	1.93%	5.33%	-1.73%	2.06%	1.68%	5.83%
R parotid	Mean	2518.84	-1.46%	-2.16%	-1.05%	-2.67%	-0.21%	0.91%	-0.84%	1.59%	-0.43%	1.24%	-1.65%	2.60%
	D05	1754.00	3.71%	5.02%	3.93%	7.13%	0.40%	2.17%	-1.08%	4.16%	1.03%	4.68%	-2.11%	6.39%
L cochlea	Mean	1506.44	1.35%	-0.07%	3.11%	-3.85%	0.74%	0.06%	-14.53%	12.48%	1.31%	-0.73%	-26.90%	25.80%
	D05	1715.00	8.98%	9.50%	10.61%	8.45%	1.69%	0.82%	-10.26%	19.45%	10.09%	1.98%	-30.26%	28.98%
R cochlea	Mean	3269.92	0.77%	1.72%	3.47%	-3.83%	-0.85%	1.17%	-5.21%	4.13%	-2.07%	1.24%	-12.02%	7.77%
	D05	3507.80	3.61%	5.22%	6.20%	0.92%	-0.64%	1.00%	-4.22%	4.80%	-1.08%	1.44%	-8.94%	8.83%
L submandibular	Max	7475.57	-0.24%	-0.38%	-1.59%	3.67%	-0.31%	1.17%	-0.30%	1.93%	-0.55%	1.44%	-0.15%	2.82%
	Mean	6982.24	-0.28%	-0.43%	-1.13%	2.09%	-0.01%	0.83%	0.12%	0.72%	-0.28%	0.63%	-0.01%	0.42%
R. submandibular	Max	7354.29	-0.63%	-0.12%	-0.71%	2.21%	-0.33%	1.02%	-0.01%	0.78%	-0.11%	1.03%	0.08%	0.82%
	Mean	6915.01	-0.73%	-0.56%	-1.70%	1.74%	0.04%	0.64%	0.39%	0.31%	0.01%	0.47%	0.74%	-0.22%

Structures	Evaluation Criteria	Baseline Dose (cGy)	Failure Mode 4: Gantry Angle		Failure Mode 5: Collimator Angle		Failure Mode 6: Couch Angle		Failure Mode 7: MU Linearity					
			+ 2 degree s	-2 degree s	+ 2 degrees	-2 degree s	+ 2 degree s	-2 degree s	1A	1B	2A	2B	3A	3B
PTVs														
PTV 70	D95	6742.59	-0.42%	0.01%	-0.54%	-1.66%	0.01%	-0.36%	0.13%	-0.01%	0.15%	-0.01%	0.07%	-0.07%
PTV 66	D95	6373.08	0.63%	-2.08%	-2.47%	-2.88%	-4.32%	0.26%	0.18%	-0.01%	0.24%	-0.01%	0.16%	-0.07%
PTV 63	D95	6141.76	0.12%	-0.19%	-1.03%	0.33%	-0.19%	0.00%	0.15%	0.00%	0.27%	-0.01%	0.02%	-0.05%
PTV 60	D95	6134.02	0.80%	-0.99%	-0.99%	-7.64%	-6.81%	-0.38%	0.15%	-0.01%	0.22%	-0.01%	-0.08%	-0.02%
PTV 57	D95	5339.39	-1.08%	0.50%	-1.98%	-3.60%	-0.27%	-2.23%	0.12%	-0.01%	0.17%	-0.01%	-0.11%	-0.05%
OARs														
Brainstem	Max	4138.24	1.29%	-0.26%	3.50%	6.14%	0.59%	7.03%	-0.12%	0.00%	-0.27%	0.02%	-0.71%	0.03%
	Max to 1 cc	3716.32	1.03%	-1.02%	0.69%	3.00%	0.51%	2.05%	0.00%	0.00%	-0.06%	0.00%	-0.52%	-0.01%
Spinal cord	Max	3966.48	-0.07%	0.90%	5.77%	1.06%	-2.03%	2.85%	-0.17%	0.01%	-0.34%	0.02%	-0.78%	0.04%
	Max to 0.3 cc	3730.08	1.40%	3.80%	6.84%	2.93%	-2.64%	3.68%	1.38%	0.00%	1.14%	0.03%	1.97%	0.04%
L parotid	Mean	2544.98	2.61%	-0.33%	0.07%	5.71%	13.01%	-8.01%	0.10%	0.00%	0.18%	-0.01%	-0.12%	-0.03%
	D50	2228.97	5.99%	0.32%	-6.19%	19.28%	12.73%	13.92%	-2.24%	-1.41%	4.36%	-2.67%	-4.62%	3.57%
R parotid	Mean	2518.84	2.42%	-0.12%	6.90%	0.75%	-12.18%	18.27%	0.50%	-0.03%	0.59%	-0.04%	1.20%	-0.21%
	D05	1754.00	7.92%	7.01%	23.83%	6.84%	-18.07%	33.75%	0.51%	-0.06%	0.11%	-0.06%	0.80%	-0.29%
L cochlea	Mean	1506.44	-3.38%	3.16%	-1.53%	12.62%	-24.56%	37.01%	-0.17%	0.01%	-0.30%	0.02%	-0.77%	0.06%
	D05	1715.00	6.85%	9.21%	7.32%	15.71%	-25.51%	39.48%	-0.41%	0.00%	-1.05%	0.00%	-1.92%	0.00%
R cochlea	Mean	3269.92	3.69%	-3.01%	-6.34%	21.09%	8.97%	1.47%	0.28%	-0.02%	0.25%	-0.02%	0.43%	-0.14%
	D05	3507.80	6.25%	-0.48%	-8.14%	22.75%	9.60%	6.92%	-0.37%	0.00%	-0.04%	0.00%	-0.11%	-0.17%
L submandibular	Max	7475.57	1.09%	-0.67%	-0.32%	1.33%	-0.51%	1.91%	0.19%	-0.01%	0.24%	-0.01%	0.32%	-0.10%
	Mean	6982.24	-0.95%	1.14%	0.99%	-0.30%	0.80%	-0.30%	0.23%	-0.01%	0.31%	-0.02%	0.34%	-0.11%
R. submandibular	Max	7354.29	1.36%	-0.46%	-0.67%	2.99%	-0.18%	1.14%	0.21%	-0.01%	0.19%	-0.01%	0.47%	-0.12%
	Mean	6915.01	1.33%	-0.88%	-0.71%	1.32%	-0.61%	1.15%	0.32%	-0.02%	0.37%	-0.02%	0.72%	-0.15%

Structures	Evaluation Criteria	Baseline Dose (cGy)	MLC Modeling							Failure Mode 11: CT Table		
			Failure Mode 8: Leakage & Transmission		Failure Mode 9: Tongue-and-groove		Failure Mode 10: Leaf End					
			0%	10%	width = 0.005 cm	width = 0.200 cm	radius = 4 cm	radius = 15 cm	radius = 20 cm	+2%	-2%	PET CT
PTVs												
PTV 70	D95	6742.59	0.31%	0.70%	-0.05%	0.16%	0.36%	-0.44%	-0.04%	0.00%	0.00%	0.00%
PTV 66	D95	6373.08	0.25%	0.80%	-0.08%	-0.02%	1.25%	-0.59%	-0.28%	0.00%	0.00%	0.00%
PTV 63	D95	6141.76	0.28%	1.15%	-0.06%	0.15%	1.11%	-0.63%	-0.10%	0.00%	0.00%	0.00%
PTV 60	D95	6134.02	0.26%	0.69%	-0.20%	-0.46%	0.99%	-1.37%	-1.58%	0.00%	0.00%	0.00%
PTV 57	D95	5339.39	0.31%	1.67%	0.03%	-0.35%	0.93%	-1.04%	-0.62%	0.00%	0.00%	0.00%
OARs												
Brainstem	Max	4138.24	-0.01%	2.68%	0.07%	0.38%	0.53%	-0.64%	-0.41%	0.00%	0.00%	0.00%
	Max to 1 cc	3716.32	-0.20%	3.43%	-0.49%	1.45%	1.00%	-0.82%	-0.93%	0.00%	0.00%	0.00%
Spinal cord	Max	3966.48	0.08%	3.13%	-0.07%	0.89%	0.37%	-0.04%	0.40%	0.00%	0.00%	0.00%
	Max to 0.3 cc	3730.08	3.31%	6.80%	2.88%	4.58%	4.23%	2.51%	3.00%	3.17%	3.17%	3.17%
L parotid	Mean	2544.98	-0.23%	6.77%	-0.25%	0.43%	2.23%	-1.53%	-0.94%	0.00%	0.00%	0.00%
	D50	2228.97	4.36%	13.34%	4.48%	4.75%	6.64%	3.45%	3.92%	4.53%	4.53%	4.53%
R parotid	Mean	2518.84	-0.38%	7.05%	-0.19%	-0.31%	2.19%	-1.76%	-1.09%	0.00%	0.00%	0.00%
	D05	1754.00	11.12%	23.72%	11.46%	12.09%	15.56%	9.29%	10.03%	11.57%	11.57%	11.57%
L cochlea	Mean	1506.44	-1.17%	6.91%	-2.07%	3.47%	11.23%	-8.85%	-11.74%	0.00%	0.00%	0.00%
	D05	1715.00	11.55%	19.59%	10.44%	16.01%	22.58%	3.56%	1.71%	11.84%	11.84%	11.84%
R cochlea	Mean	3269.92	-0.45%	2.84%	-1.04%	1.15%	5.43%	-4.43%	-5.13%	0.00%	0.00%	0.00%
	D05	3507.80	4.26%	7.68%	3.46%	5.20%	9.82%	-1.10%	-1.24%	4.63%	4.63%	4.63%
L submandibular	Max	7475.57	0.17%	0.28%	-0.21%	0.41%	0.84%	0.06%	0.26%	0.00%	0.00%	0.00%
	Mean	6982.24	0.32%	0.75%	0.02%	0.35%	0.64%	-0.08%	0.31%	0.00%	0.00%	0.00%
R. submandibular	Max	7354.29	0.36%	0.54%	-0.11%	0.68%	0.30%	-0.20%	0.18%	0.00%	0.00%	0.00%
	Mean	6915.01	0.35%	0.73%	-0.17%	1.07%	0.15%	0.25%	0.57%	0.00%	0.00%	0.00%

Table 113: Patient 8 dose differences from baseline at evaluation criteria for PTVs and OARs for each failure mode.

Patient 9

Structures	Evaluation Criteria	Baseline Dose (cGy)	Failure Mode 1: Beam Energy		Failure Mode 2: Beam Symmetry							
					2 degrees				3.5 degrees			
			+10%	-10%	Top to bottom	Bottom to top	Left to right	Right to left	Top to bottom	Bottom to top	Left to right	Right to left
PTVs												
PTV 70	D95	7007.01	-0.88%	-0.54%	-0.14%	-0.14%	-0.42%	-0.37%	-0.25%	-0.24%	-0.37%	-0.05%
PTV66	D95	6512.64	-1.83%	2.13%	0.10%	-0.05%	-0.81%	0.86%	0.16%	0.00%	-0.94%	1.16%
PTV63	D95	6123.06	-0.28%	-0.86%	-0.19%	-0.38%	-0.37%	-0.35%	-0.10%	-0.35%	-0.32%	-0.12%
PTV57	D95	5466.70	-0.28%	-1.89%	-0.46%	-0.39%	-0.38%	-0.95%	-0.45%	-0.42%	-0.22%	-0.57%
OARs												
Brainstem	Max	3804.72	0.72%	-1.72%	-1.44%	-1.42%	-0.42%	-3.26%	-1.73%	-1.71%	1.12%	-2.59%
	Max to 1 cc	3491.02	0.44%	-1.29%	-1.09%	-1.08%	-0.01%	-2.76%	-1.39%	-1.38%	1.36%	-2.18%
spinal cord	Max	3473.37	-1.74%	-0.27%	-1.44%	-1.51%	-1.28%	-2.14%	-1.37%	-1.44%	-0.34%	-1.43%
	Max to 0.3 cc	3254.01	1.36%	4.79%	1.13%	2.02%	1.23%	1.22%	0.88%	2.18%	2.19%	1.99%
L Parotid	Mean	3179.66	-1.79%	-1.83%	-2.02%	-1.88%	-1.46%	-2.70%	-1.73%	-1.58%	-0.73%	-2.09%
	D05	2354.24	-2.48%	-0.77%	-1.55%	-1.25%	-0.64%	-2.44%	-1.27%	-0.93%	0.30%	-1.76%
R Parotid	Mean	1439.25	-8.99%	-1.23%	-4.60%	-4.62%	-4.16%	-5.46%	-3.86%	-3.91%	-2.68%	-4.26%
	D50	1014.42	-10.83%	2.34%	-5.45%	-5.45%	-4.88%	-6.44%	-4.11%	-4.15%	-2.77%	-4.61%
L Cochlea	Mean	859.37	-9.11%	-7.22%	-4.68%	-4.55%	-3.18%	-6.51%	-5.18%	-4.98%	-2.05%	-6.09%
	D05	1182.70	-4.60%	-2.57%	-1.04%	-0.88%	0.56%	-2.90%	-0.96%	-0.71%	2.34%	-1.97%
R Cochlea	Mean	804.55	-7.56%	-8.13%	-3.01%	-3.08%	-1.66%	-4.93%	-3.90%	-3.98%	-0.79%	-4.85%
	D05	1020.60	-4.14%	-4.51%	2.64%	2.62%	4.11%	0.58%	2.25%	2.22%	5.65%	1.24%
L submandibular	Max	7338.10	0.07%	0.61%	-0.79%	-0.78%	-0.67%	-0.33%	-0.69%	-0.68%	-0.34%	-0.28%
	Mean	7109.58	-0.65%	0.65%	-0.40%	-0.32%	-0.70%	-0.06%	-0.36%	-0.25%	-0.70%	0.17%
R submandibular	Max	7352.05	-1.07%	-0.42%	-0.29%	-0.35%	-0.60%	-0.20%	-0.36%	-0.32%	-0.38%	0.17%
	Mean	6344.45	-1.57%	-0.63%	-0.33%	-0.34%	-0.59%	-0.20%	-0.37%	-0.38%	-0.51%	0.06%
esophagus	D15	3855.20	-0.35%	1.82%	-1.31%	-0.07%	-1.50%	-0.60%	-1.77%	0.18%	-1.01%	0.33%
	D33	3716.70	-0.24%	0.76%	-1.45%	-0.32%	-1.96%	-0.55%	-1.96%	-0.04%	-1.49%	0.48%
larynx	Max	7112.80	-1.13%	1.81%	0.16%	0.15%	-0.78%	1.03%	-0.06%	-0.10%	-1.16%	1.05%
	Mean	2384.19	-3.53%	6.04%	-4.41%	-4.14%	-4.98%	-3.70%	-3.84%	-3.42%	-4.34%	-2.71%
	D27	2940.24	-5.48%	2.28%	-3.81%	-3.06%	-3.40%	-3.40%	-3.33%	-2.14%	-2.41%	-2.28%

Structures	Evaluation Criteria	Baseline Dose (cGy)	Failure Mode 2: Beam Symmetry					Failure Mode 3: MLC Position						
			10 degrees				1 mm Errors				2 mm Errors			
			Top to bottom	Bottom to top	Left to right	Right to left	X1 + 1mm	X1 - 1mm	X2 +1mm	X2 - 1mm	X1 + 2mm	X1 - 2mm	X2 +2mm	X2 - 2mm
PTVs														
PTV 70	D95	7007.01	-0.76%	-0.67%	-1.45%	-0.44%	-0.42%	-0.46%	-0.57%	-0.28%	-0.70%	-0.85%	-1.18%	-0.62%
PTV66	D95	6512.64	-1.21%	-1.59%	-3.03%	2.11%	-0.38%	-0.68%	-0.18%	-0.53%	-1.53%	-1.22%	0.07%	-1.00%
PTV63	D95	6123.06	-0.07%	-0.67%	-0.59%	0.08%	-0.89%	-0.01%	-1.23%	0.41%	-2.17%	-0.32%	-2.41%	0.52%
PTV57	D95	5466.70	-0.44%	0.00%	-0.22%	-1.47%	-1.21%	0.03%	-1.37%	0.65%	-4.97%	-0.08%	-2.90%	1.05%
OARs														
Brainstem	Max	3804.72	0.64%	0.81%	3.38%	-5.42%	-1.03%	0.89%	-1.01%	0.52%	-2.44%	1.54%	-2.27%	1.18%
	Max to 1 cc	3491.02	1.11%	1.15%	3.72%	-4.78%	-0.78%	1.00%	-0.74%	0.55%	-1.63%	1.62%	-1.69%	1.46%
spinal cord	Max	3473.37	-0.38%	-0.62%	0.31%	-2.98%	-1.42%	1.28%	-0.73%	1.38%	-2.68%	2.23%	-1.56%	2.28%
	Max to 0.3 cc	3254.01	2.15%	4.16%	3.44%	1.09%	1.81%	3.55%	1.29%	3.67%	1.28%	4.76%	0.73%	4.51%
L Parotid	Mean	3179.66	-0.55%	-0.08%	1.38%	-2.54%	-0.32%	-0.08%	-3.73%	3.35%	-0.33%	-0.15%	-7.09%	6.71%
	D05	2354.24	1.05%	1.74%	3.72%	-1.74%	1.58%	1.53%	-7.15%	10.88%	1.71%	1.30%	-14.84%	20.42%
R Parotid	Mean	1439.25	-2.87%	-2.96%	-1.20%	-5.41%	-0.39%	0.09%	-3.53%	3.37%	-0.53%	0.22%	-6.65%	6.89%
	D50	1014.42	-3.45%	-3.46%	-1.52%	-6.51%	1.86%	2.74%	0.06%	4.64%	1.60%	3.01%	-1.74%	6.82%
L Cochlea	Mean	859.37	1.00%	1.44%	5.34%	-5.27%	-0.04%	-0.11%	-7.18%	9.09%	-0.02%	-0.28%	-12.80%	21.60%
	D05	1182.70	3.69%	4.11%	8.17%	-2.90%	3.10%	2.68%	-8.06%	18.23%	3.27%	2.34%	-16.26%	41.91%
R Cochlea	Mean	804.55	3.45%	3.18%	7.41%	-3.44%	0.70%	0.72%	-6.02%	7.29%	0.72%	0.47%	-12.11%	15.47%
	D05	1020.60	8.42%	8.20%	12.63%	1.07%	6.14%	5.85%	-3.07%	15.89%	6.34%	5.48%	-10.02%	31.23%
L submandibular	Max	7338.10	-0.39%	-0.74%	0.04%	1.05%	-0.42%	0.02%	-0.20%	-0.34%	0.05%	0.34%	0.21%	-0.18%
	Mean	7109.58	-1.23%	-0.98%	-1.52%	0.79%	-0.08%	-0.52%	-0.02%	-0.58%	0.36%	-0.86%	0.50%	-1.01%
R submandibular	Max	7352.05	-0.95%	-0.88%	-0.87%	0.86%	-0.15%	0.07%	-0.04%	-0.57%	0.01%	0.78%	0.66%	0.12%
	Mean	6344.45	-0.88%	-0.86%	-1.06%	0.62%	-0.53%	-0.09%	-0.43%	-0.19%	-0.53%	0.07%	-0.33%	-0.15%
esophagus	D15	3855.20	-2.30%	2.25%	-3.33%	0.21%	0.32%	1.05%	-0.34%	0.10%	0.15%	1.10%	-0.67%	0.62%
	D33	3716.70	-2.06%	2.56%	-3.90%	0.72%	0.14%	0.69%	-0.26%	-0.17%	-0.01%	0.60%	-0.78%	0.37%
larynx	Max	7112.80	-1.36%	-1.30%	-2.86%	2.71%	0.64%	1.63%	0.18%	-0.03%	-0.88%	10.19%	0.94%	6.63%
	Mean	2384.19	-6.28%	-5.23%	-7.26%	-3.10%	21.63%	52.38%	-2.37%	2.38%	12.38%	70.36%	-3.33%	6.39%
	D27	2940.24	-5.75%	-2.45%	-4.39%	-4.32%	30.35%	89.86%	-3.67%	4.64%	22.34%	110.21%	-5.22%	12.05%

Structures	Evaluation Criteria	Baseline Dose (cGy)	Failure Mode 4: Gantry Angle		Failure Mode 5: Collimator Angle		Failure Mode 6: Couch Angle		Failure Mode 7: MU Linearity					
			+ 2°	-2°	+ 2°	-2°	+ 2°	-2°	1A	1B	2A	2B	3A	3B
PTVs														
PTV 70	D95	7007.01	0.00%	-0.25%	-0.37%	-0.47%	-2.87%	-1.40%	0.02%	0.00%	-0.25%	-0.01%	-0.11%	0.03%
PTV66	D95	6512.64	-0.06%	0.15%	0.49%	-0.58%	-0.77%	0.54%	0.07%	0.00%	-0.22%	-0.01%	-0.04%	0.02%
PTV63	D95	6123.06	-0.82%	0.41%	-1.44%	-0.66%	-1.92%	-1.27%	0.07%	0.00%	-0.16%	-0.01%	0.03%	0.01%
PTV57	D95	5466.70	-0.79%	-0.30%	-2.74%	-1.55%	-4.92%	-6.88%	0.06%	0.00%	-0.06%	-0.01%	0.03%	0.01%
OARs														
Brainstem	Max	3804.72	-0.22%	-0.14%	-0.45%	-0.37%	5.19%	15.20%	-0.03%	0.00%	-0.14%	0.00%	0.01%	-0.01%
	Max to 1 cc	3491.02	0.13%	-0.08%	-0.17%	-0.54%	-3.22%	5.45%	-0.05%	0.00%	-0.16%	0.01%	-0.07%	0.01%
spinal cord	Max	3473.37	1.09%	-1.02%	3.53%	1.12%	-1.40%	4.02%	0.17%	0.00%	0.13%	-0.03%	0.13%	0.00%
	Max to 0.3 cc	3254.01	3.53%	1.73%	7.35%	3.60%	2.51%	7.89%	0.34%	0.01%	-5.96%	-0.07%	-5.77%	-0.03%
L Parotid	Mean	3179.66	4.67%	-3.58%	4.64%	-2.30%	-4.09%	8.23%	-0.06%	0.00%	-0.39%	0.01%	-0.10%	0.01%
	D05	2354.24	15.67%	-6.62%	13.18%	-4.42%	-3.42%	22.26%	0.95%	0.03%	-0.32%	-0.03%	1.14%	0.03%
R Parotid	Mean	1439.25	-2.60%	5.35%	-6.07%	11.60%	10.32%	-0.36%	-0.01%	0.00%	-0.34%	0.00%	0.03%	-0.01%
	D50	1014.42	3.20%	2.87%	-2.20%	12.27%	13.97%	4.80%	-2.96%	0.04%	-0.75%	-0.04%	1.28%	-0.58%
L Cochlea	Mean	859.37	-1.42%	1.15%	-3.56%	13.32%	9.07%	2.72%	0.20%	-0.01%	0.03%	-0.01%	0.59%	-0.09%
	D05	1182.70	0.39%	7.24%	4.99%	27.45%	29.23%	13.11%	0.31%	0.05%	-0.14%	-0.05%	0.54%	-0.03%
R Cochlea	Mean	804.55	1.00%	-1.37%	10.75%	-6.49%	-1.07%	4.02%	0.12%	-0.01%	-0.31%	0.00%	0.51%	-0.09%
	D05	1020.60	5.60%	2.13%	19.30%	2.45%	0.26%	20.47%	0.17%	0.07%	-0.67%	-0.07%	0.22%	-0.03%
L submandibular	Max	7338.10	-0.14%	0.25%	0.23%	-0.31%	0.47%	3.42%	-0.02%	0.00%	-0.27%	-0.01%	-0.18%	0.03%
	Mean	7109.58	-0.11%	0.07%	0.25%	-0.44%	0.13%	-0.21%	0.01%	0.00%	-0.31%	-0.01%	-0.16%	0.04%
R submandibular	Max	7352.05	0.23%	-0.26%	-0.49%	0.37%	0.36%	0.00%	0.00%	0.00%	-0.23%	-0.01%	-0.19%	0.04%
	Mean	6344.45	1.99%	-1.99%	-2.32%	2.30%	-2.48%	2.44%	0.01%	0.00%	-0.25%	-0.01%	-0.19%	0.04%
esophagus	D15	3855.20	0.15%	0.21%	1.59%	-0.85%	1.62%	-0.89%	0.00%	0.00%	0.00%	0.00%	0.00%	0.00%
	D33	3716.70	-0.14%	0.22%	1.58%	-1.17%	1.59%	-1.23%	0.00%	0.00%	0.00%	0.00%	0.00%	0.00%
larynx	Max	7112.80	-0.42%	0.12%	0.85%	-1.12%	-0.08%	-0.15%	0.09%	0.00%	-0.14%	-0.02%	-0.05%	0.03%
	Mean	2384.19	0.51%	-0.54%	0.83%	-0.75%	0.09%	0.08%	0.04%	0.00%	-0.17%	-0.01%	-0.06%	0.02%
	D27	2940.24	1.77%	-1.36%	0.99%	-4.29%	4.79%	-3.69%	0.03%	0.00%	0.00%	0.00%	0.00%	0.00%

Structures	Evaluation Criteria	Baseline Dose (cGy)	MLC Modeling							Failure Mode 11: CT Table		
			Failure Mode 8: Leakage & Transmission		Failure Mode 9: Tongue-and-groove		Failure Mode 10: Leaf End					
			0%	10%	width = 0.005 cm	width = 0.200 cm	radius = 4 cm	radius = 15 cm	radius = 20 cm	+2%	-2%	PET CT
PTVs												
PTV 70	D95	7007.01	-0.08%	-0.67%	-0.34%	-0.29%	-0.34%	-0.69%	-0.90%	0.00%	0.00%	0.00%
PTV66	D95	6512.64	0.01%	-0.61%	-0.32%	-0.21%	1.92%	0.98%	0.09%	0.00%	0.00%	0.00%
PTV63	D95	6123.06	-0.05%	-0.60%	-0.41%	0.48%	1.16%	-0.76%	-1.03%	0.00%	0.00%	0.00%
PTV57	D95	5466.70	-0.13%	-0.53%	-0.47%	1.24%	1.44%	-1.12%	-1.62%	0.00%	0.00%	0.00%
OARs												
Brainstem	Max	3804.72	-0.28%	0.02%	-0.68%	3.55%	1.36%	-0.54%	-2.07%	0.00%	0.00%	0.00%
	Max to 1 cc	3491.02	-0.29%	0.75%	-0.72%	4.21%	1.28%	-0.26%	-1.80%	0.00%	0.00%	0.00%
spinal cord	Max	3473.37	0.00%	-0.42%	-0.77%	4.50%	1.64%	-2.29%	-1.69%	0.00%	0.00%	0.00%
	Max to 0.3 cc	3254.01	-6.12%	1.61%	-0.67%	-1.61%	-3.61%	-8.03%	0.51%	0.00%	0.00%	0.00%
L Parotid	Mean	3179.66	-0.50%	1.17%	-0.93%	6.05%	4.33%	-3.76%	-3.62%	0.00%	0.00%	0.00%
	D05	2354.24	1.08%	-0.22%	-2.56%	10.16%	13.81%	-8.57%	-7.87%	0.00%	0.00%	0.00%
R Parotid	Mean	1439.25	-1.31%	5.15%	-2.08%	18.86%	5.12%	-3.45%	-3.54%	0.00%	0.00%	0.00%
	D50	1014.42	-0.70%	7.99%	-4.83%	28.35%	7.10%	-4.78%	-6.33%	0.00%	0.00%	0.00%
L Cochlea	Mean	859.37	-1.43%	6.13%	-1.85%	15.49%	16.11%	-6.33%	-7.65%	0.00%	0.00%	0.00%
	D05	1182.70	-1.28%	5.28%	-3.24%	16.85%	30.27%	-11.17%	-15.11%	0.00%	0.00%	0.00%
R Cochlea	Mean	804.55	-0.96%	3.88%	-1.24%	9.25%	8.99%	-2.53%	-4.19%	0.00%	0.00%	0.00%
	D05	1020.60	-0.36%	6.27%	-2.98%	12.87%	17.74%	-5.31%	-11.82%	0.00%	0.00%	0.00%
L submandibular	Max	7338.10	-0.07%	-0.12%	-0.32%	-0.43%	-0.52%	0.47%	-0.39%	0.00%	0.00%	0.00%
	Mean	7109.58	-0.13%	0.03%	-0.34%	-0.28%	-0.87%	0.74%	-0.03%	0.00%	0.00%	0.00%
R submandibular	Max	7352.05	0.27%	-1.25%	-0.32%	-0.41%	-0.24%	0.70%	-0.07%	0.00%	0.00%	0.00%
	Mean	6344.45	-0.03%	-0.75%	-0.39%	0.28%	-0.15%	0.01%	-0.59%	0.00%	0.00%	0.00%
esophagus	D15	3855.20	-0.03%	-0.30%	-0.11%	0.33%	0.20%	-0.24%	-0.23%	0.00%	0.00%	0.00%
	D33	3716.70	0.02%	-0.36%	-0.09%	0.22%	0.02%	-0.15%	-0.14%	0.00%	0.00%	0.00%

larynx	Max	7112.80	-0.09%	0.21%	-0.31%	-0.40%	1.67%	1.33%	0.36%	0.00%	0.00%	0.00%
	Mean	2384.19	-0.11%	-0.08%	-0.51%	2.15%	6.46%	-1.56%	-1.83%	0.00%	0.00%	0.00%
	D27	2940.24	1.36%	-4.05%	-0.07%	0.17%	5.44%	-3.78%	-2.39%	0.00%	0.00%	0.00%

Table 114: Patient 9 dose differences from baseline at evaluation criteria for PTVs and OARs for each failure mode.

Patient 10

Structures	Evaluation n Criteria	Baseline Dose (cGy)	Failure Mode 1: Beam Energy		Failure Mode 2: Beam Symmetry							
					2 degrees				3.5 degrees			
			+10%	-10%	Top to bottom	Bottom to top	Left to right	Right to left	Top to bottom	Bottom to top	Left to right	Right to left
PTVs												
PTV 66	D95	6391.40	0.07%	-0.83%	-0.71%	-0.10%	-0.25%	-0.21%	-0.54%	0.04%	-0.16%	-0.45%
PTV 60	D95	5820.33	-0.39%	-1.79%	-1.01%	-0.07%	-0.40%	-0.43%	-0.84%	0.12%	-0.32%	-0.63%
PTV 54	D95	5277.46	-0.19%	-2.37%	-1.14%	-0.03%	-0.47%	-0.45%	-1.02%	0.15%	-0.33%	-0.56%
OARs												
Brainstem	D100	246.00	-3.25%	4.88%	1.22%	3.66%	2.03%	2.03%	2.44%	5.28%	3.66%	3.25%
	Max to 1 cc	3898.80	-0.28%	-1.96%	-2.35%	-0.41%	-1.39%	-1.48%	-1.91%	0.19%	-1.19%	-1.34%
Spinal Cord	Max	4236.31	-0.90%	-0.28%	-1.12%	-0.87%	-0.66%	-0.79%	-0.91%	-0.23%	-0.36%	-0.86%
L Parotid	Mean	1846.32	-5.54%	-3.80%	-4.08%	-3.03%	-3.50%	-3.39%	-3.52%	-2.31%	-2.78%	-3.11%
	D50	932.71	-10.09%	-2.70%	-8.38%	-6.95%	-7.24%	-7.31%	-6.49%	-4.69%	-5.66%	-6.11%
R parotid	Mean	1364.51	-7.46%	-3.54%	-5.23%	-4.15%	-4.46%	-4.57%	-4.41%	-3.06%	-3.61%	-4.00%
	D50	932.71	-10.09%	-2.70%	-8.38%	-6.95%	-7.24%	-7.31%	-6.49%	-4.69%	-5.66%	-6.11%
L Eye	Max	149.05	1.58%	24.62%	7.38%	9.81%	8.67%	8.81%	11.23%	14.47%	12.48%	12.38%
R Eye	Max	154.87	0.41%	20.37%	14.13%	16.57%	15.49%	15.28%	16.06%	19.36%	17.50%	16.88%
L lens	Max	89.39	5.06%	23.41%	-1.89%	-0.48%	-1.05%	-1.08%	2.27%	4.28%	3.21%	2.94%
R lens	Max	85.15	4.42%	21.50%	1.79%	3.35%	2.71%	2.63%	5.55%	7.69%	6.57%	6.09%
L Optic Nerve	Max	201.67	-0.35%	17.97%	24.40%	27.80%	26.17%	26.20%	26.06%	30.42%	27.71%	27.35%
R Optic Nerve	Max	195.40	-0.49%	17.84%	23.16%	26.55%	24.90%	24.92%	25.57%	29.89%	27.17%	26.85%
Chiasm	Max	299.29	-2.36%	7.17%	16.81%	20.04%	18.54%	18.52%	16.89%	20.85%	18.32%	17.99%

Structures	Evaluation Criteria	Baseline Dose (cGy)	Failure Mode 2: Beam Symmetry				Failure Mode 3: MLC Position							
			10 degrees				1 mm Errors				2 mm Errors			
			Top to botto m	Botto m to top	Left to right	Right to left	X1 + 1mm	X1 - 1mm	X2 +1mm	X2 - 1mm	X1 + 2mm	X1 - 2mm	X2 +2mm	X2 - 2mm
PTVs														
PTV 66	D95	6391.40	0.21%	0.21%	0.21%	0.21%	-0.32%	0.18%	-0.23%	-0.06%	-0.58%	0.38%	-0.71%	-0.37%
PTV 60	D95	5820.33	0.55%	0.55%	0.55%	0.55%	-1.30%	-0.08%	-1.13%	-0.28%	-2.26%	0.66%	-2.37%	-0.45%
PTV 54	D95	5277.46	0.60%	0.60%	0.60%	0.60%	-4.45%	-3.98%	-4.14%	-4.18%	-5.42%	-3.73%	-4.88%	-4.39%
OARs														
Brainstem	D100	246.00	9.35%	9.35%	9.35%	9.35%	11.79%	15.45%	11.79%	15.04%	11.38%	16.67%	11.38%	16.26%
	Max to 1 cc	3898.80	1.02%	1.02%	1.02%	1.02%	7.80%	7.21%	7.64%	6.82%	8.38%	7.21%	7.98%	6.62%
Spinal Cord	Max	4236.31	-0.30%	-0.30%	-0.30%	-0.30%	10.76%	12.58%	10.66%	12.40%	8.90%	13.91%	9.37%	13.19%
L Parotid	Mean	1846.32	-2.11%	-2.11%	-2.11%	-2.11%	29.61%	33.42%	30.94%	32.41%	27.84%	36.71%	30.09%	34.48%
	D50	932.71	-5.53%	-5.53%	-5.53%	-5.53%	-1.97%	1.91%	-2.39%	2.30%	-3.13%	4.50%	-4.47%	4.72%
R parotid	Mean	1364.51	-2.91%	-2.91%	-2.91%	-2.91%	-3.71%	0.78%	-4.98%	2.31%	-5.48%	3.71%	-8.02%	6.74%
	D50	932.71	-5.53%	-5.53%	-5.53%	-5.53%	-1.97%	1.91%	-2.39%	2.30%	-3.13%	4.50%	-4.47%	4.72%
L Eye	Max	149.05	15.21%	15.21%	15.21%	15.21%	46.45%	57.11%	46.16%	58.50%	46.31%	57.99%	45.28%	60.71%
R Eye	Max	154.87	24.80%	24.80%	24.80%	24.80%	35.32%	44.84%	35.15%	44.08%	34.24%	47.49%	33.40%	45.45%
L lens	Max	89.39	1.16%	1.16%	1.16%	1.16%	33.90%	38.72%	34.46%	41.91%	33.45%	39.69%	33.45%	45.26%
R lens	Max	85.15	6.00%	6.00%	6.00%	6.00%	25.26%	30.15%	24.49%	30.38%	24.58%	31.95%	22.70%	32.35%
L Optic Nerve	Max	201.67	38.10%	38.10%	38.10%	38.10%	51.28%	59.12%	50.90%	58.88%	50.88%	60.56%	50.01%	59.80%
R Optic Nerve	Max	195.40	36.24%	36.24%	36.24%	36.24%	44.44%	52.34%	44.57%	51.80%	43.20%	54.30%	43.42%	52.98%
Chiasm	Max	299.29	30.25%	30.25%	30.25%	30.25%	31.96%	36.29%	31.55%	36.22%	32.08%	37.10%	31.18%	36.64%

Structures	Evaluation Criteria	Baseline Dose (cGy)	Failure Mode 4: Gantry Angle		Failure Mode 5: Collimator Angle		Failure Mode 6: Couch Angle		Failure Mode 7: MU Linearity					
			+ 2 degrees	-2 degrees	+ 2 degrees	-2 degrees	+ 2 degrees	-2 degrees	1A	1B	2A	2B	3A	3B
PTVs														
PTV 66	D95	6391.40	-0.02%	-0.20%	-0.70%	-1.57%	-0.51%	-0.63%	-0.17%	0.01%	-0.13%	0.01%	-0.12%	-0.01%
PTV 60	D95	5820.33	0.24%	-0.39%	-2.35%	0.93%	-1.08%	0.11%	-0.20%	0.01%	-0.18%	0.01%	-0.07%	-0.08%
PTV 54	D95	5277.46	-1.01%	-0.48%	-2.42%	2.16%	-1.48%	-0.18%	-0.04%	0.00%	0.08%	-0.01%	0.17%	-0.13%
OARs														
Brainstem	D100	246.00	0.00%	-1.22%	-2.03%	2.85%	-0.81%	-0.41%	0.00%	0.00%	0.00%	0.00%	0.00%	-0.41%
	Max to 1 cc	3898.80	0.10%	-0.19%	0.80%	13.09%	0.22%	0.42%	0.16%	0.00%	0.44%	-0.03%	0.33%	-0.32%
Spinal Cord	Max	4236.31	-0.30%	0.53%	1.01%	12.71%	-0.23%	-0.26%	0.03%	0.00%	0.22%	-0.01%	0.36%	-0.09%
L Parotid	Mean	1846.32	6.70%	-4.99%	-1.22%	9.41%	0.85%	3.24%	0.04%	0.00%	0.13%	-0.01%	0.70%	-0.08%
	D50	932.71	-0.62%	1.60%	3.53%	12.72%	-2.74%	4.41%	-0.16%	0.00%	-0.26%	0.01%	0.44%	-0.09%
R parotid	Mean	1364.51	-5.99%	8.55%	5.88%	13.98%	1.16%	2.90%	-0.11%	0.01%	-0.11%	0.01%	0.30%	-0.15%
	D50	932.71	-0.62%	1.60%	3.53%	12.72%	-2.74%	4.41%	-0.16%	0.00%	-0.26%	0.01%	0.44%	-0.09%
L Eye	Max	149.05	0.91%	-0.33%	-0.75%	20.28%	-0.82%	3.00%	-0.01%	0.01%	0.13%	-0.01%	0.01%	-0.04%
R Eye	Max	154.87	-0.45%	-0.27%	1.53%	13.26%	3.56%	-2.26%	-0.05%	0.01%	0.07%	0.00%	0.15%	0.00%
L lens	Max	89.39	2.81%	-0.25%	0.05%	26.89%	-0.07%	-2.11%	0.03%	0.00%	0.21%	-0.01%	0.22%	0.04%
R lens	Max	85.15	1.30%	1.02%	4.64%	12.96%	2.59%	-1.48%	-0.03%	0.01%	0.09%	-0.01%	0.23%	0.05%
L Optic Nerve	Max	201.67	-1.32%	-1.10%	-3.02%	13.85%	0.53%	-3.59%	-0.07%	0.01%	0.01%	0.00%	-0.01%	-0.11%
R Optic Nerve	Max	195.40	0.04%	-0.67%	-2.09%	8.23%	-1.63%	3.64%	-0.13%	0.01%	-0.09%	0.01%	-0.06%	-0.08%
Chiasm	Max	299.29	0.16%	-0.34%	-0.91%	8.77%	-0.54%	-1.17%	-0.11%	0.01%	-0.06%	0.00%	-0.07%	-0.14%

Structures	Evaluation n Criteria	Baseline Dose (cGy)	MLC Modeling							Failure Mode 11: CT Table		
			Failure Mode 8: Leakage & Transmission		Failure Mode 9: Tongue-and-groove		Failure Mode 10: Leaf End					
			0%	10%	width = 0.005 cm	width = 0.200 cm	radius = 4 cm	radius = 15 cm	radius = 20 cm	+2%	-2%	PET CT
PTVs												
PTV 66	D95	6391.40	-0.30%	-0.18%	-0.09%	-0.23%	0.74%	-0.47%	-0.52%	0.00%	0.00%	0.00%
PTV 60	D95	5820.33	-0.37%	0.25%	-0.06%	-0.43%	1.86%	-1.41%	-1.22%	0.00%	0.00%	0.00%
PTV 54	D95	5277.46	-0.40%	0.79%	-0.17%	0.14%	1.76%	-1.73%	-1.43%	0.00%	0.00%	0.00%
OARs												
Brainstem	D100	246.00	-0.41%	0.41%	0.00%	-0.41%	0.81%	0.00%	-0.41%	0.00%	0.00%	0.00%
	Max to 1 cc	3898.80	-0.49%	1.88%	0.05%	-0.35%	1.60%	0.23%	-0.16%	0.00%	0.00%	0.00%
Spinal Cord	Max	4236.31	-0.50%	1.85%	-0.42%	0.66%	3.00%	-1.39%	-1.28%	0.00%	0.00%	0.00%
L Parotid	Mean	1846.32	-1.28%	10.44%	-0.64%	2.48%	10.14%	-4.93%	-3.99%	0.00%	0.00%	0.00%
	D50	932.71	-2.36%	22.21%	-1.78%	8.17%	15.46%	-3.51%	-3.25%	0.00%	0.00%	0.00%
R parotid	Mean	1364.51	-1.68%	14.60%	-1.14%	4.72%	12.43%	-5.75%	-4.73%	0.00%	0.00%	0.00%
	D50	932.71	-2.36%	22.21%	-1.78%	8.17%	15.46%	-3.51%	-3.25%	0.00%	0.00%	0.00%
L Eye	Max	149.05	-0.37%	0.68%	-0.16%	0.34%	1.54%	-0.97%	-0.92%	0.00%	0.00%	0.00%
R Eye	Max	154.87	-0.36%	0.79%	-0.15%	0.50%	2.26%	-1.46%	-1.26%	0.00%	0.00%	0.00%
L lens	Max	89.39	-0.38%	0.95%	-0.19%	0.49%	2.50%	-1.77%	-1.54%	0.00%	0.00%	0.00%
R lens	Max	85.15	-0.43%	1.57%	-0.25%	0.63%	3.64%	-2.25%	-1.88%	0.00%	0.00%	0.00%
L Optic Nerve	Max	201.67	-0.31%	0.12%	-0.07%	0.08%	1.49%	-0.85%	-0.82%	0.00%	0.00%	0.00%
R Optic Nerve	Max	195.40	-0.32%	0.18%	-0.13%	0.25%	1.69%	-1.07%	-0.97%	0.00%	0.00%	0.00%
Chiasm	Max	299.29	-0.24%	-0.70%	0.02%	-0.51%	0.40%	-0.08%	-0.29%	0.00%	0.00%	0.00%

Table 115: Patient 10 dose differences from baseline at evaluation criteria for PTVs and OARs for each failure mode.

Appendix C: Failure Mode Patient DVH graphs

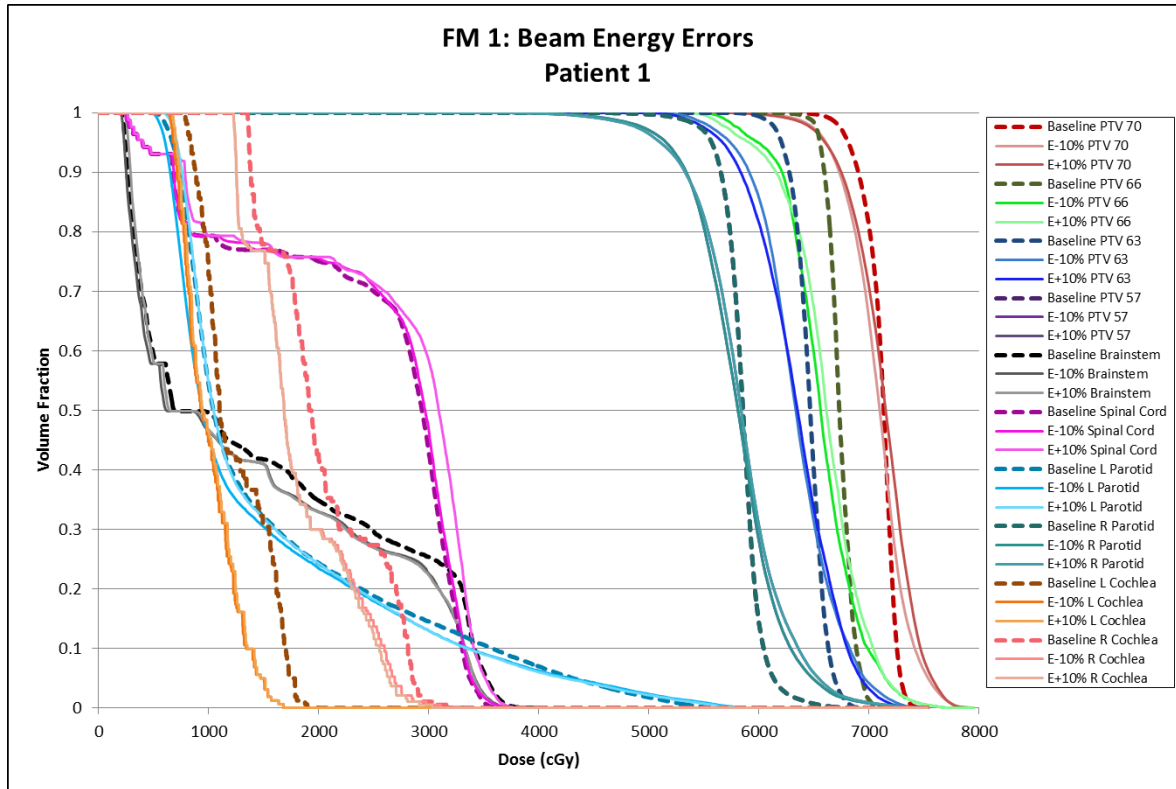


Figure 112: Failure mode 1 DVHs for patient 1.

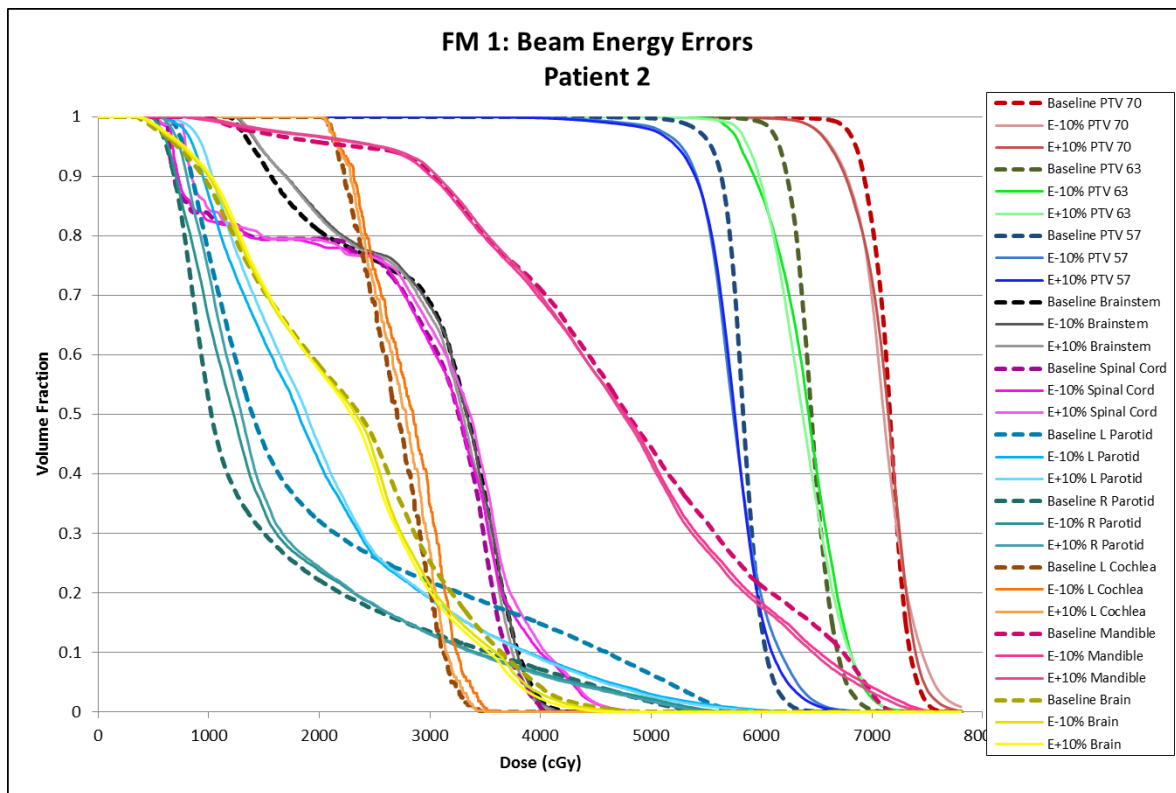


Figure 113: Failure mode 1 DVHs for patient 2.

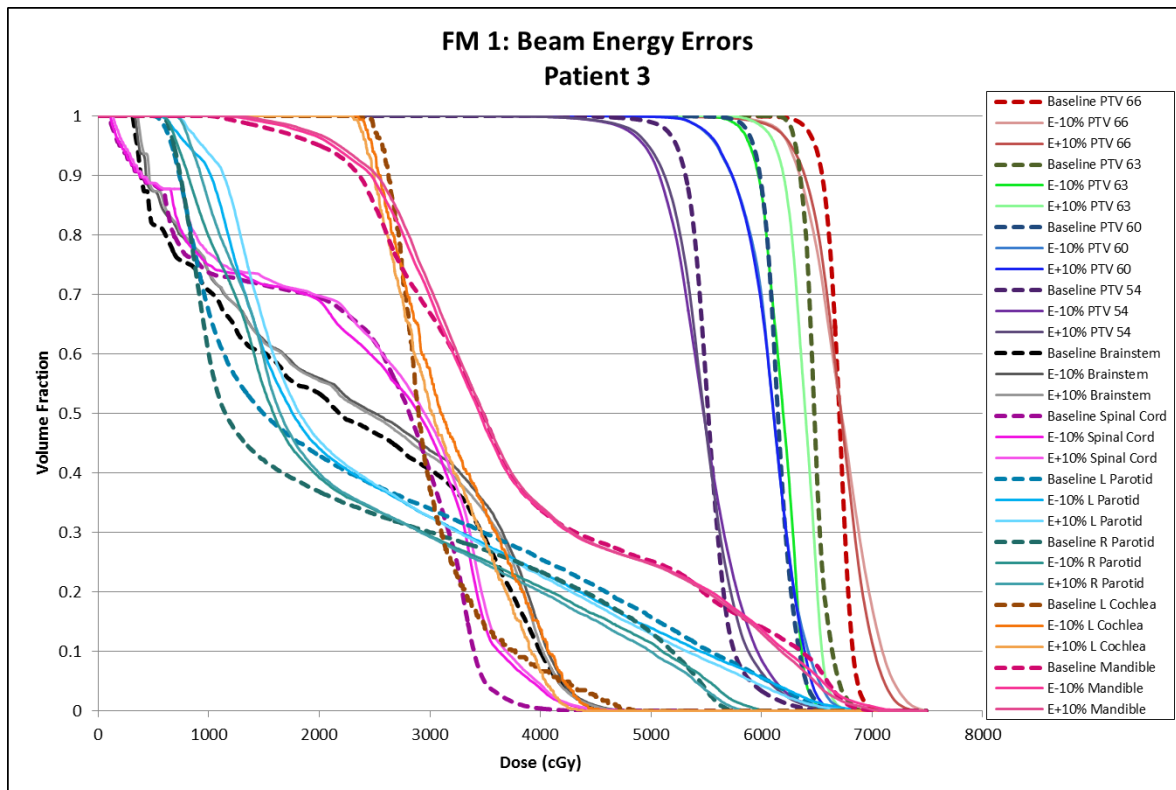


Figure 114: Failure mode 1 DVHs for patient 3.

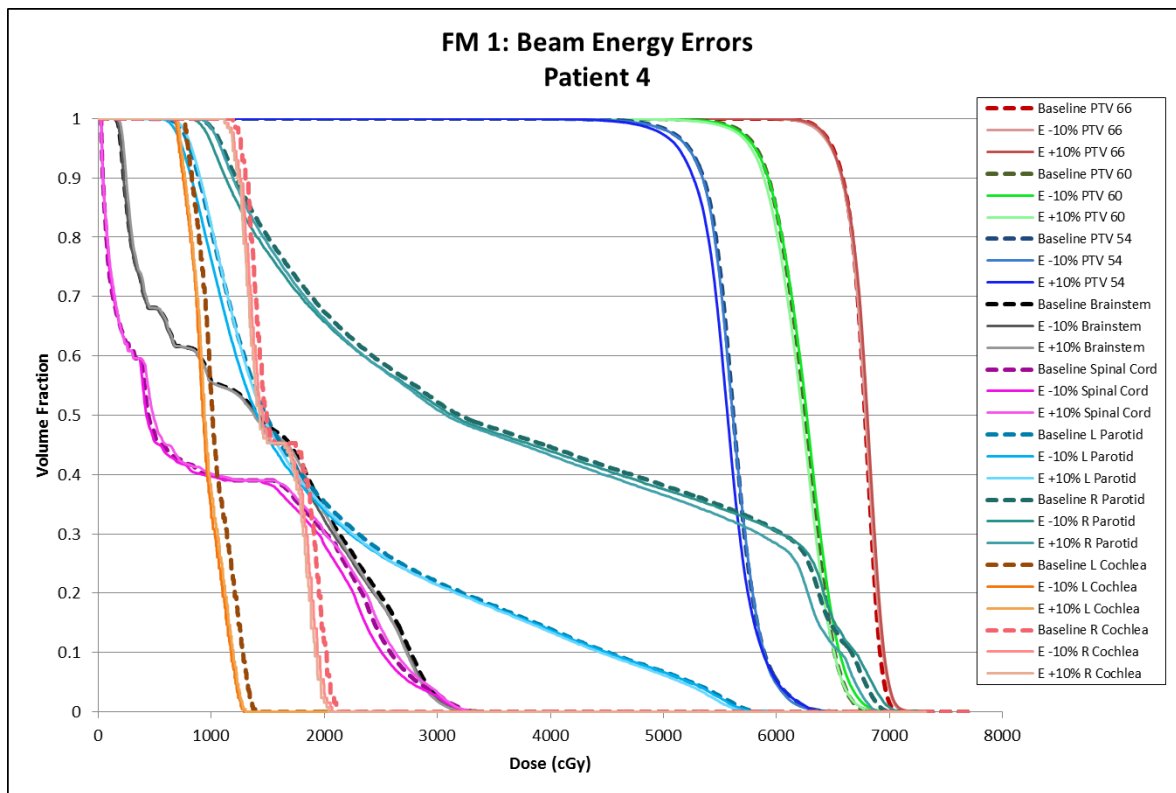


Figure 115: Failure mode 1 DVHs for patient 4.

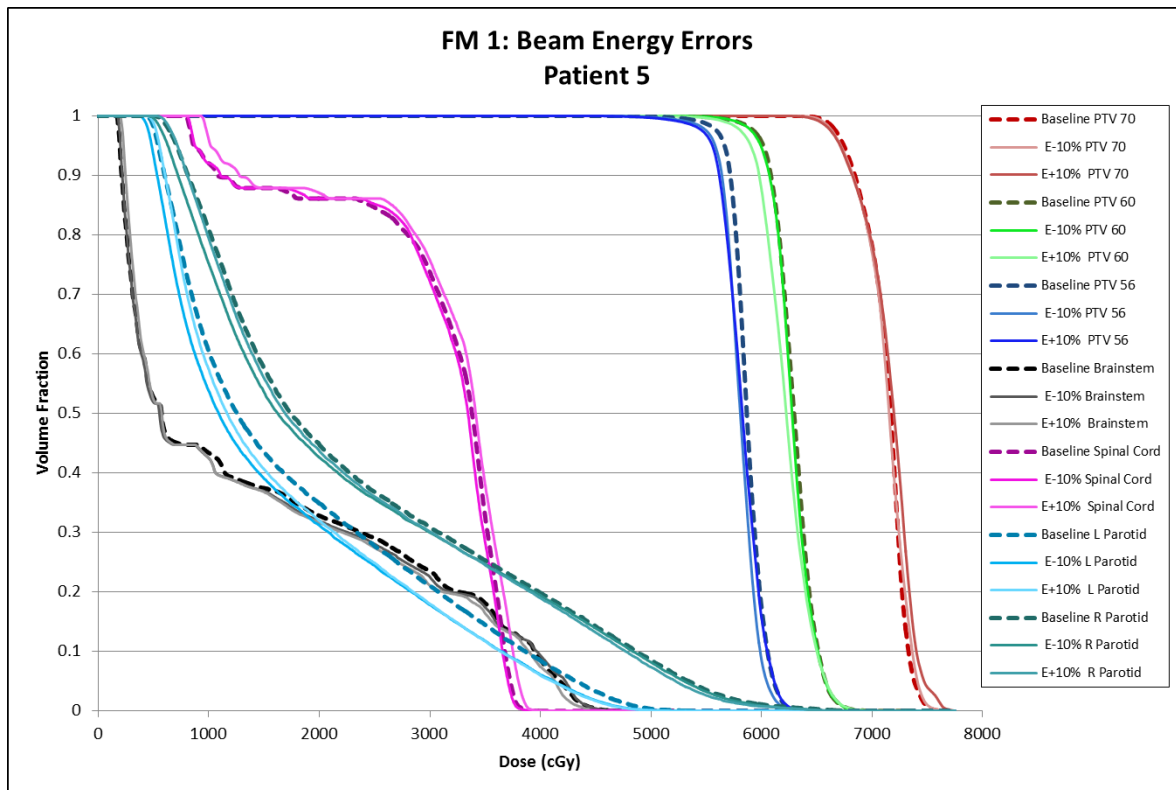


Figure 116: Failure mode 1 DVHs for patient 5.

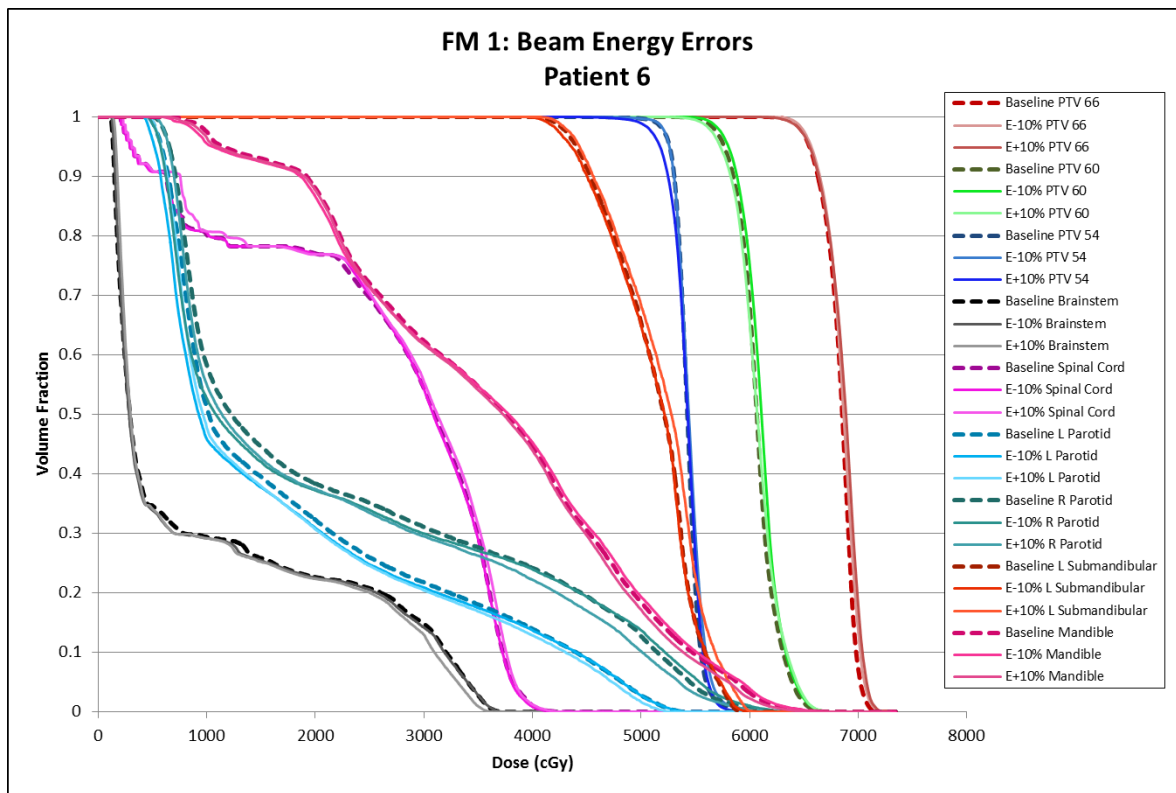


Figure 117: Failure mode 1 DVHs for patient 6.

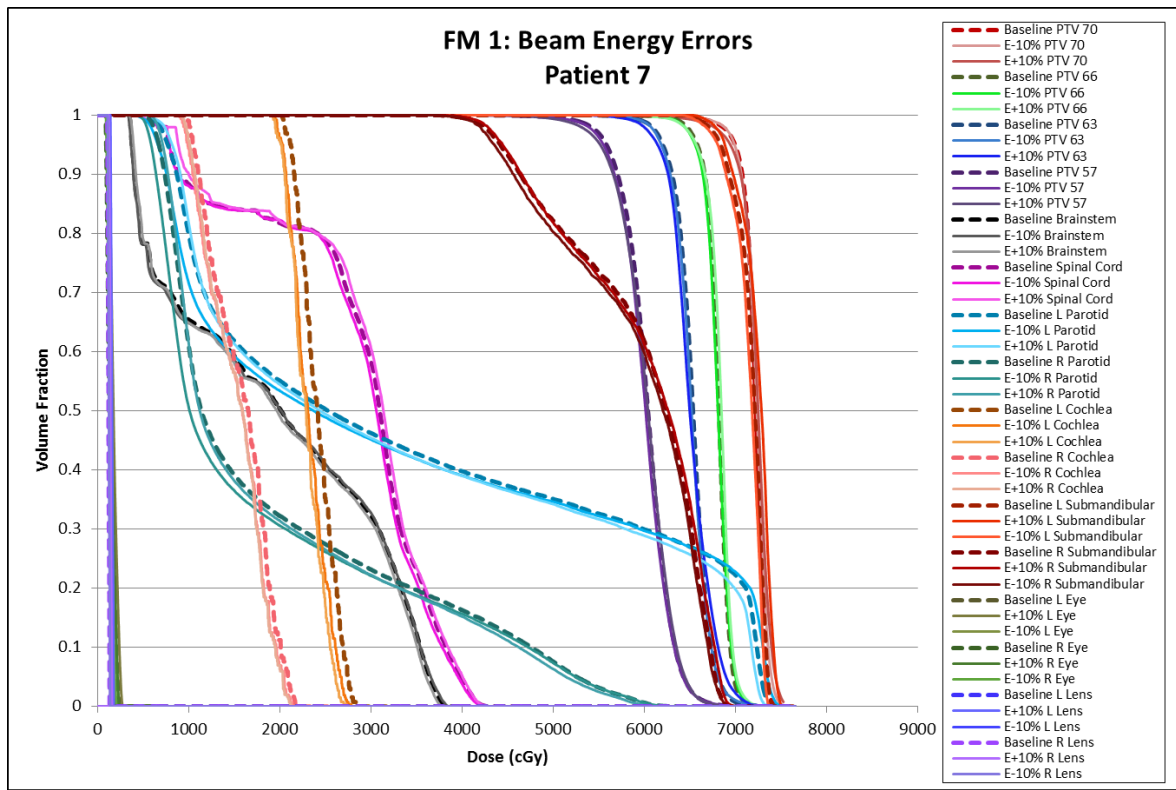


Figure 118: Failure mode 1 DVHs for patient 7.

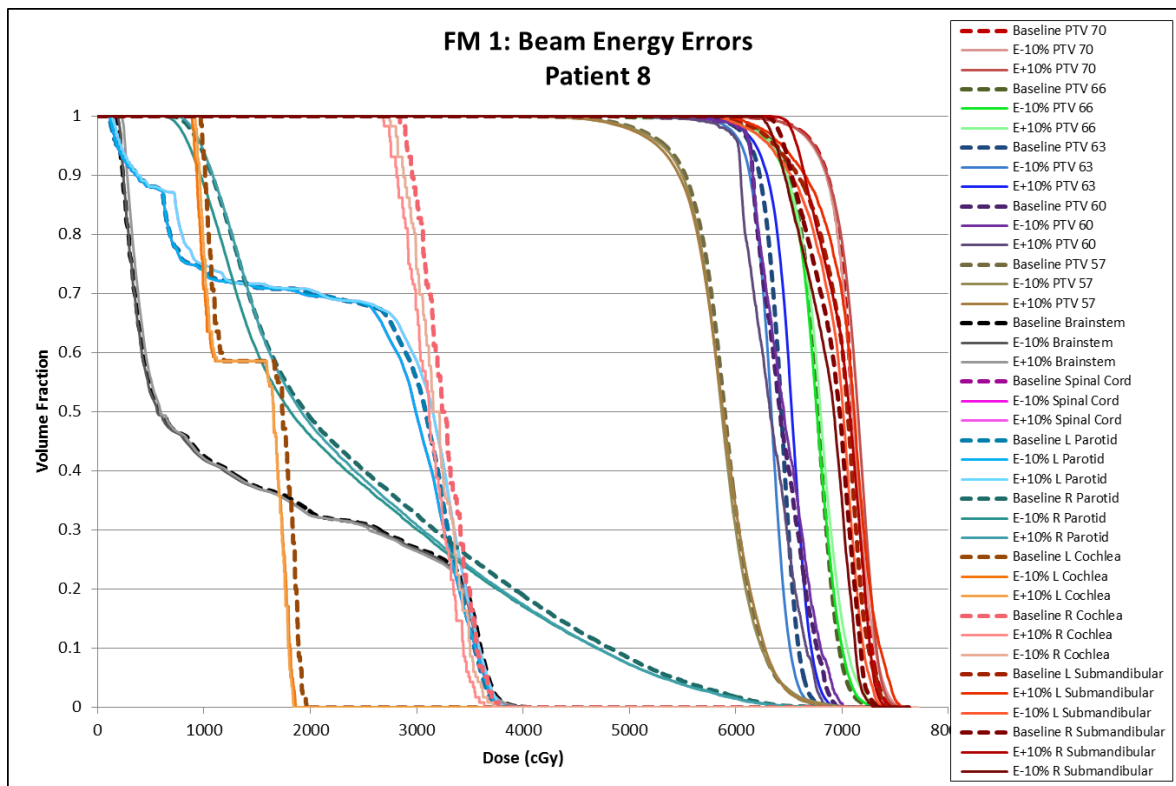


Figure 119: Failure mode 1 DVHs for patient 8.

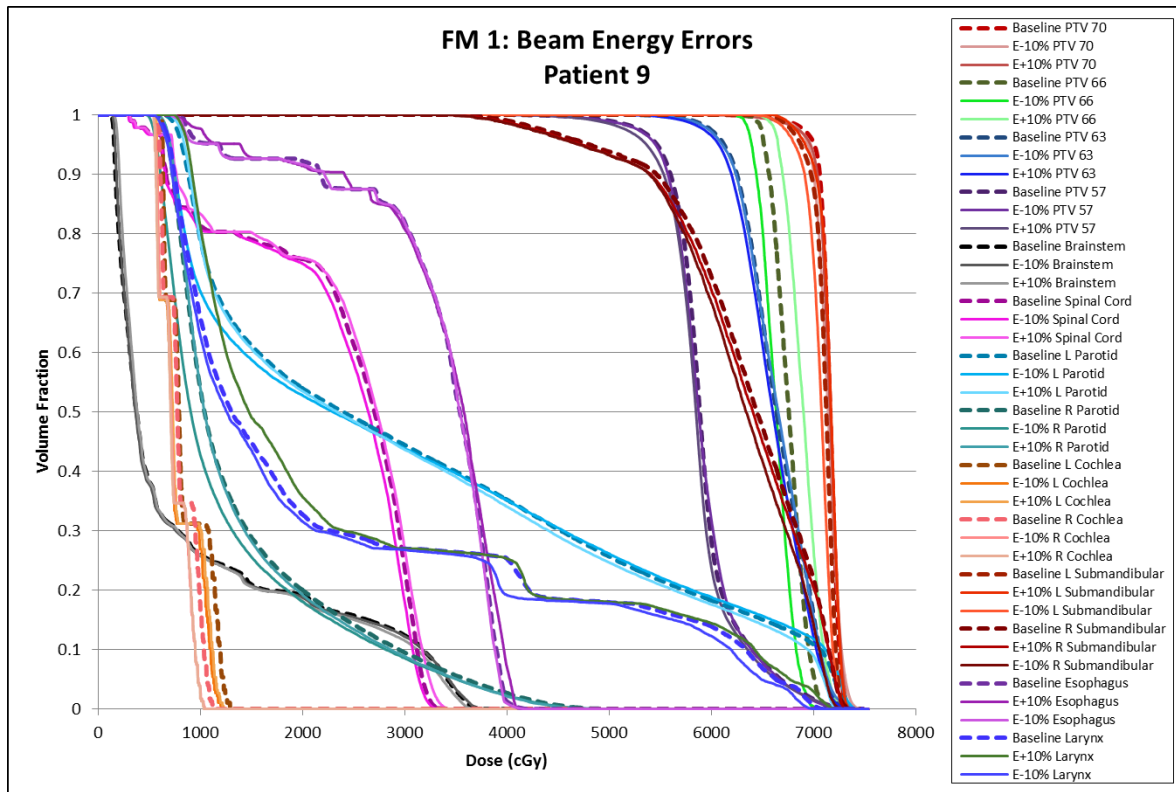


Figure 120: Failure mode 1 DVHs for patient 9.

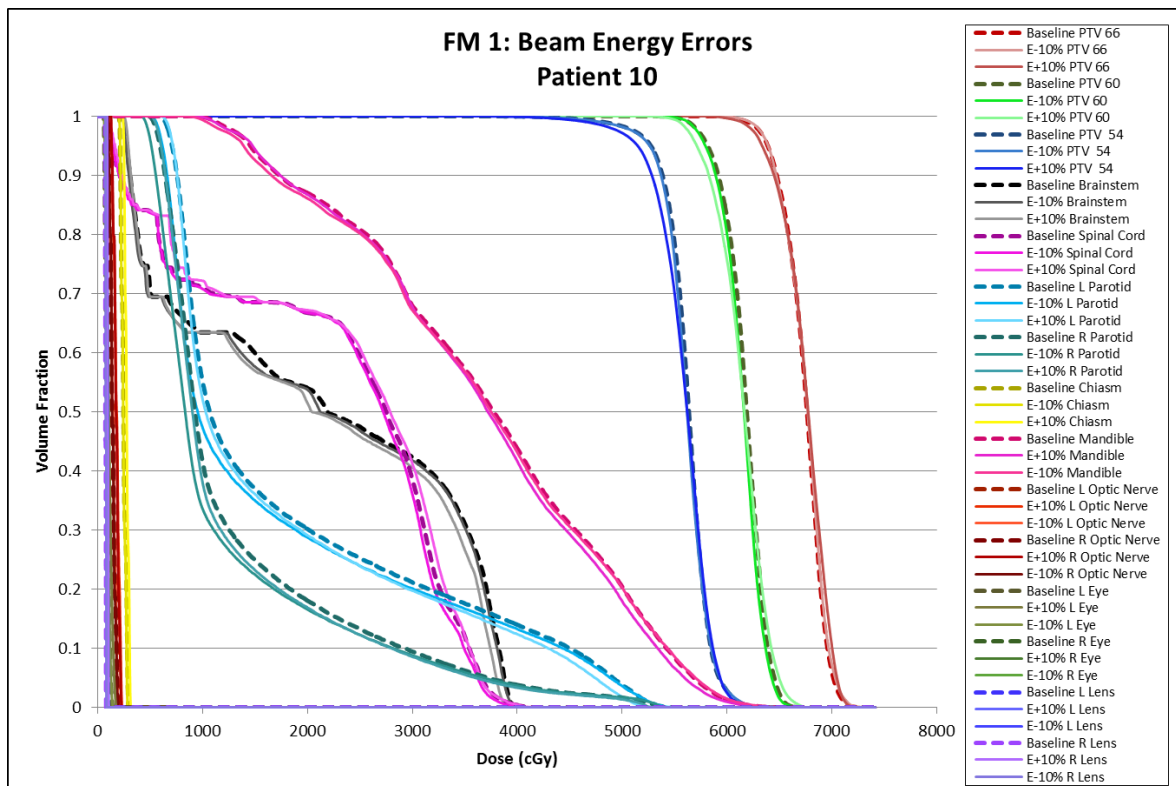


Figure 121: Failure mode 1 DVHs for patient 10.

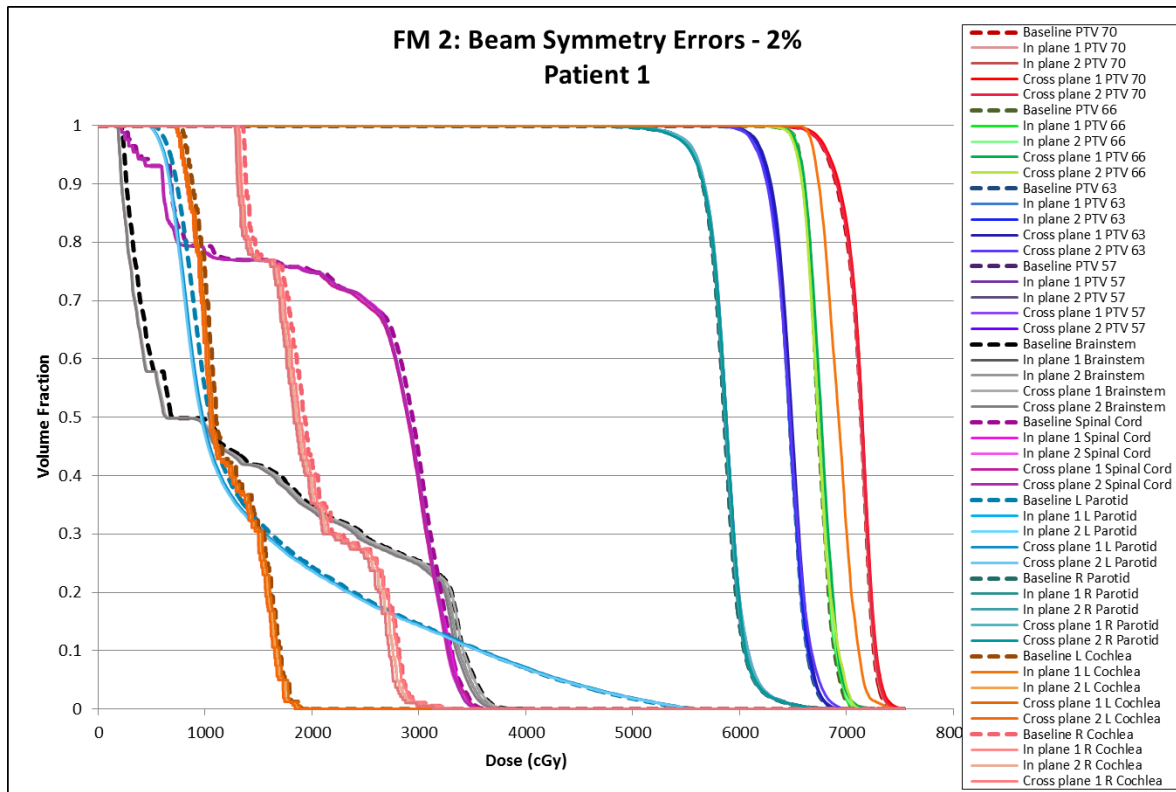


Figure 122: Failure mode 2 (with 2% symmetry errors) DVHs for patient 1.

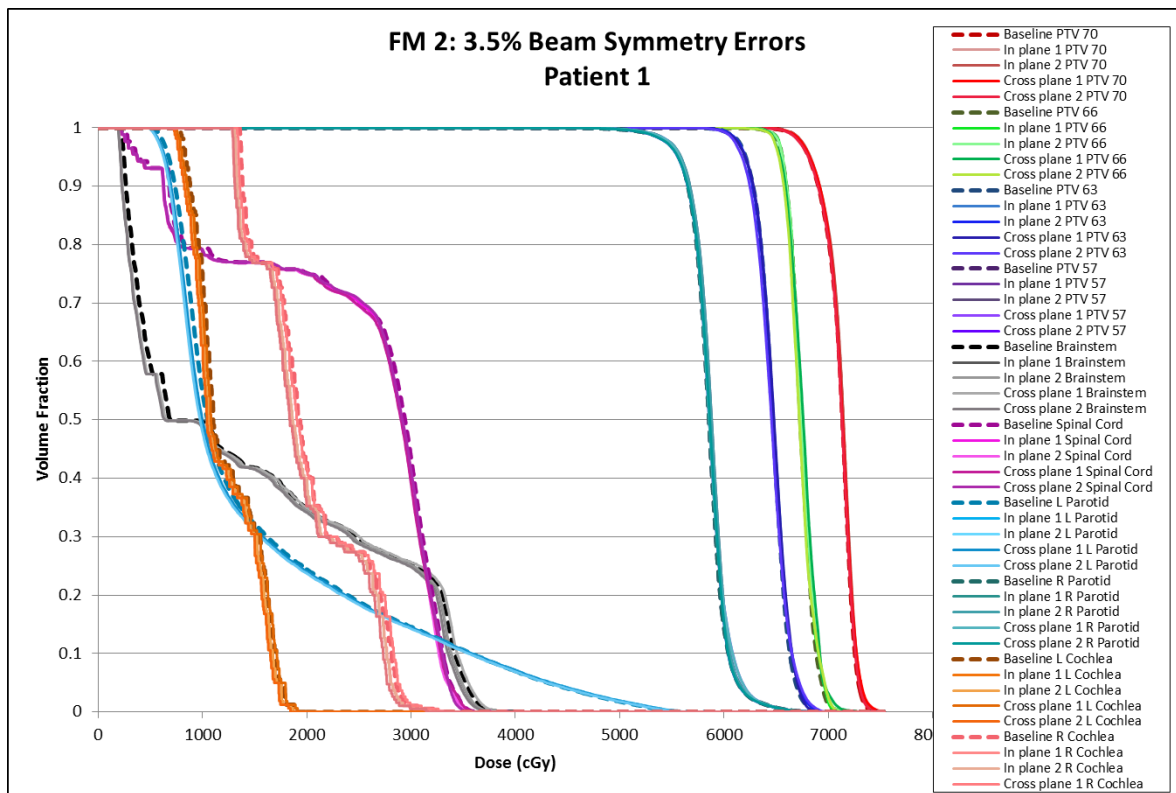


Figure 123: Failure mode 2 (with 3.5% symmetry errors) DVHs for patient 1.

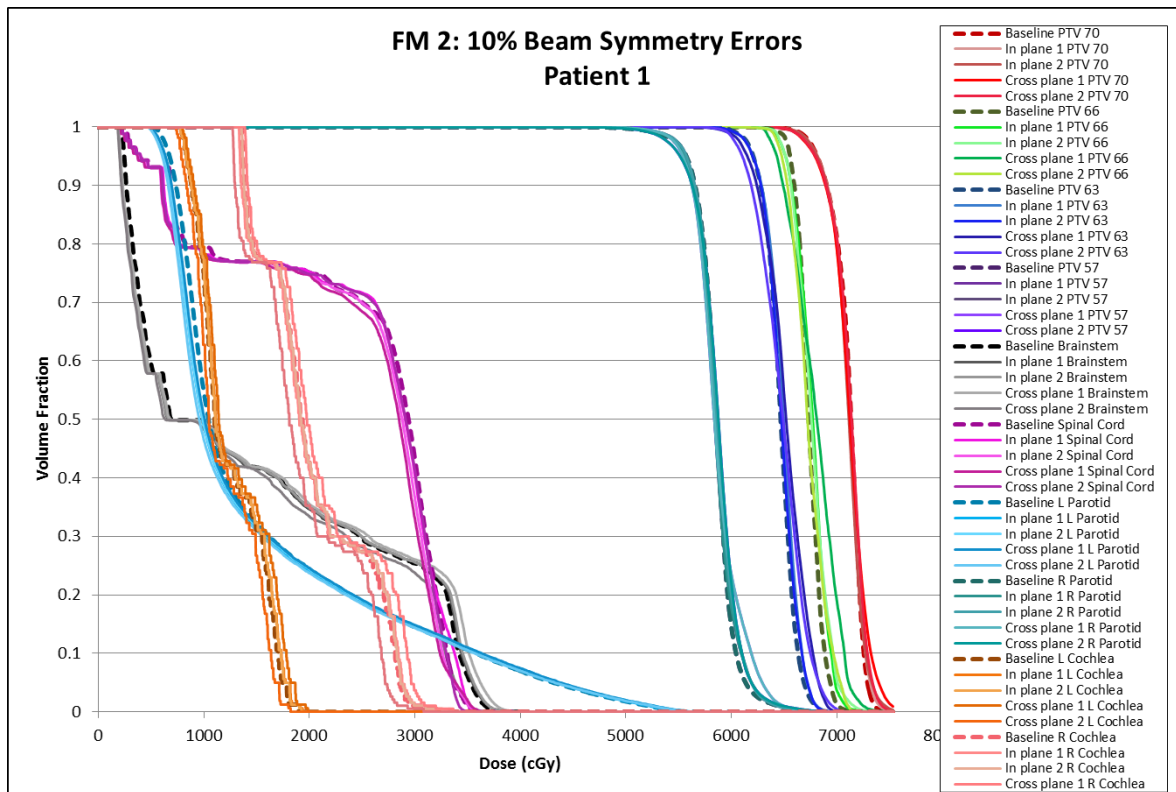


Figure 124: Failure mode 2 (with 10% symmetry errors) DVHs for patient 1.

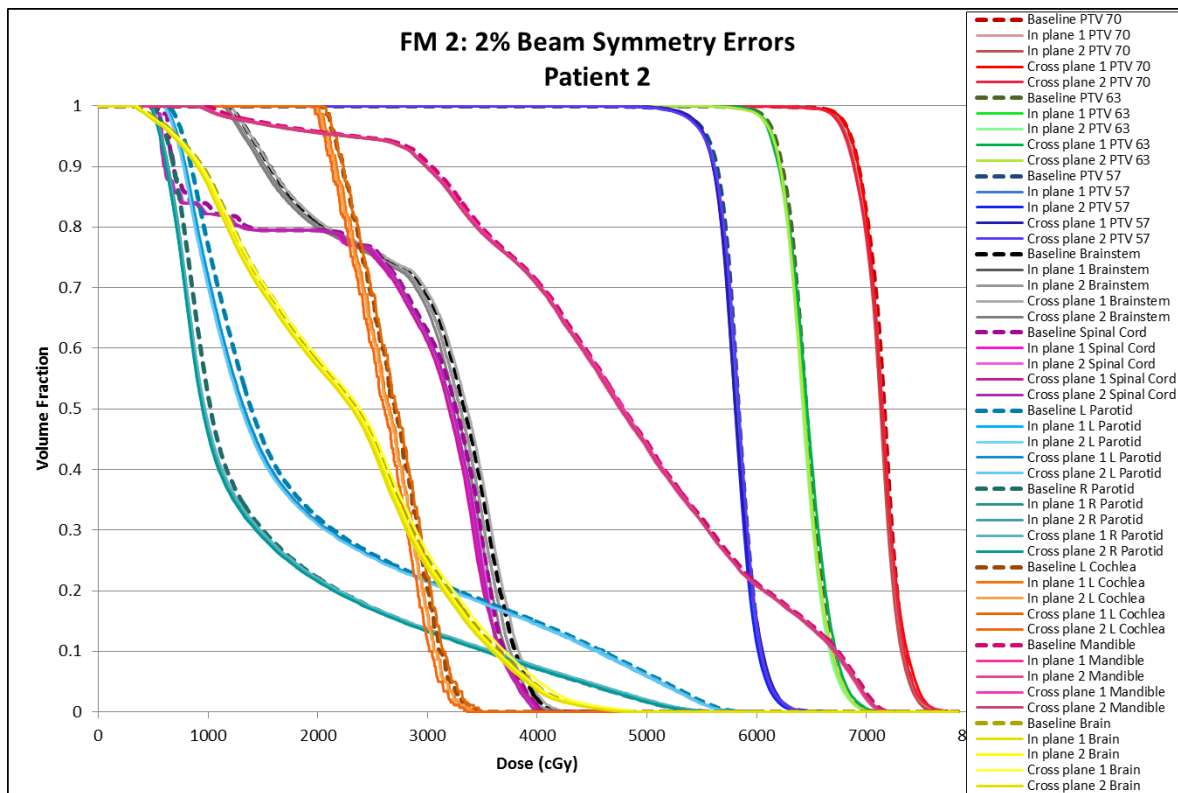


Figure 125: Failure mode 2 (with 2% symmetry errors) DVHs for patient 2.

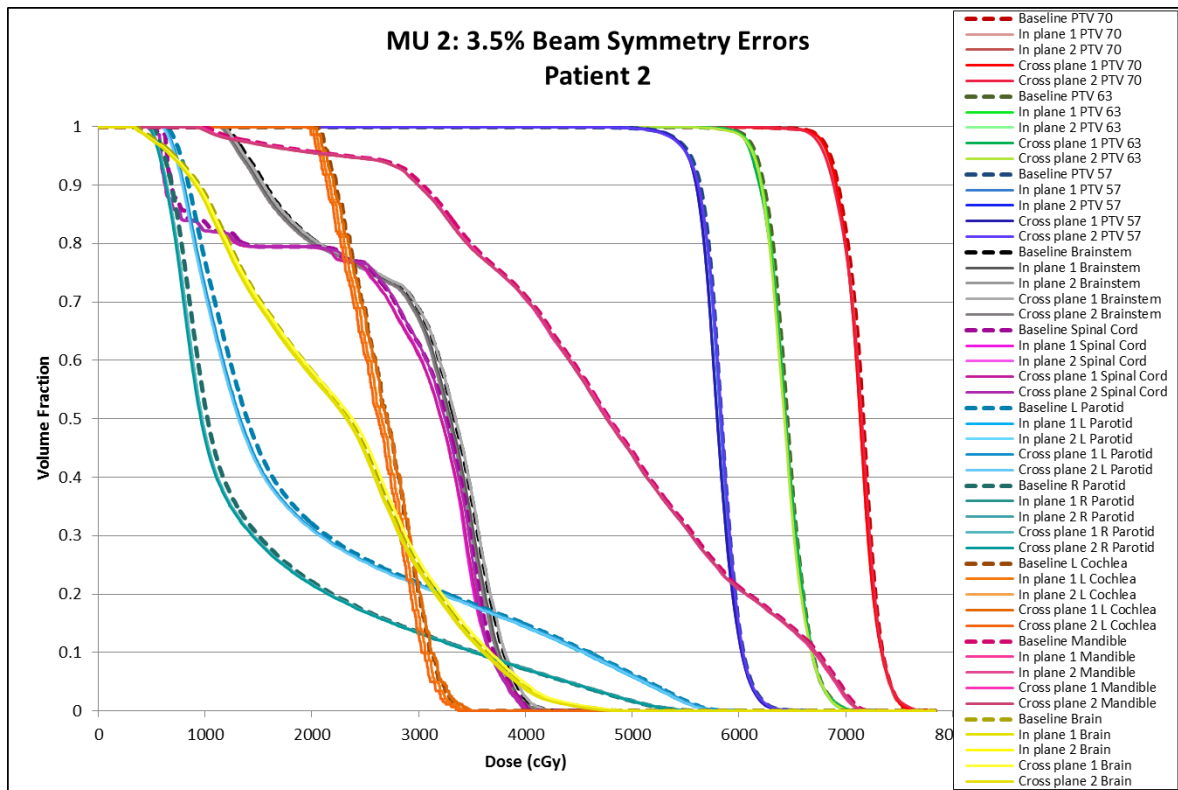


Figure 126: Failure mode 2 (with 3.5% symmetry errors) DVHs for patient 2.

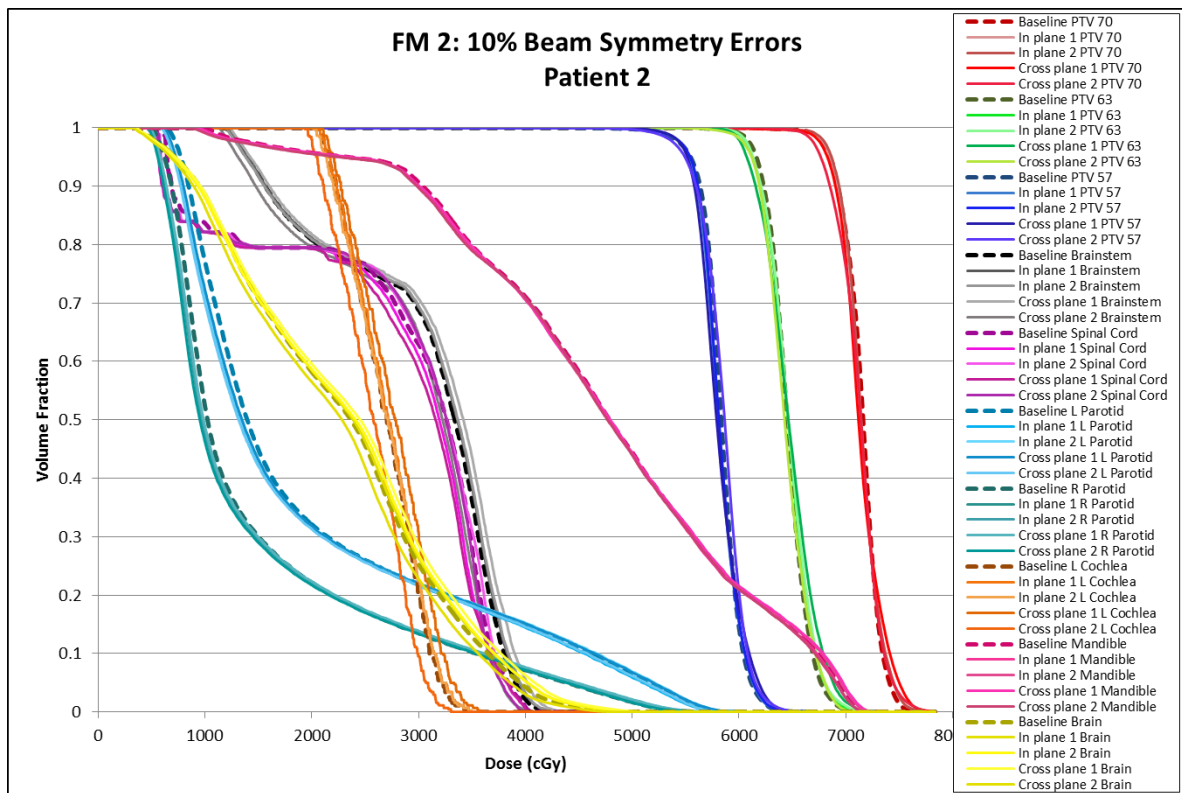


Figure 127: Failure mode 2 (with 10% symmetry errors) DVHs for patient 2.

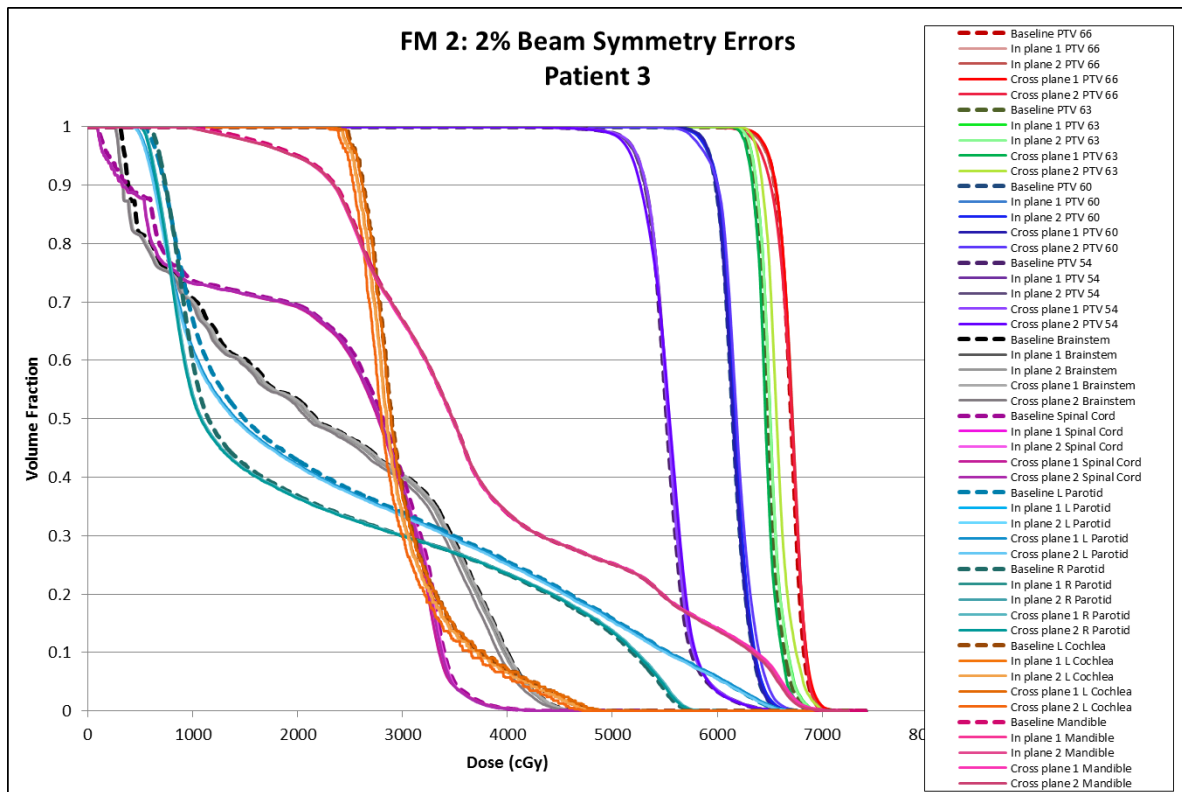


Figure 128: Failure mode 2 (with 2% symmetry errors) DVHs for patient 3.

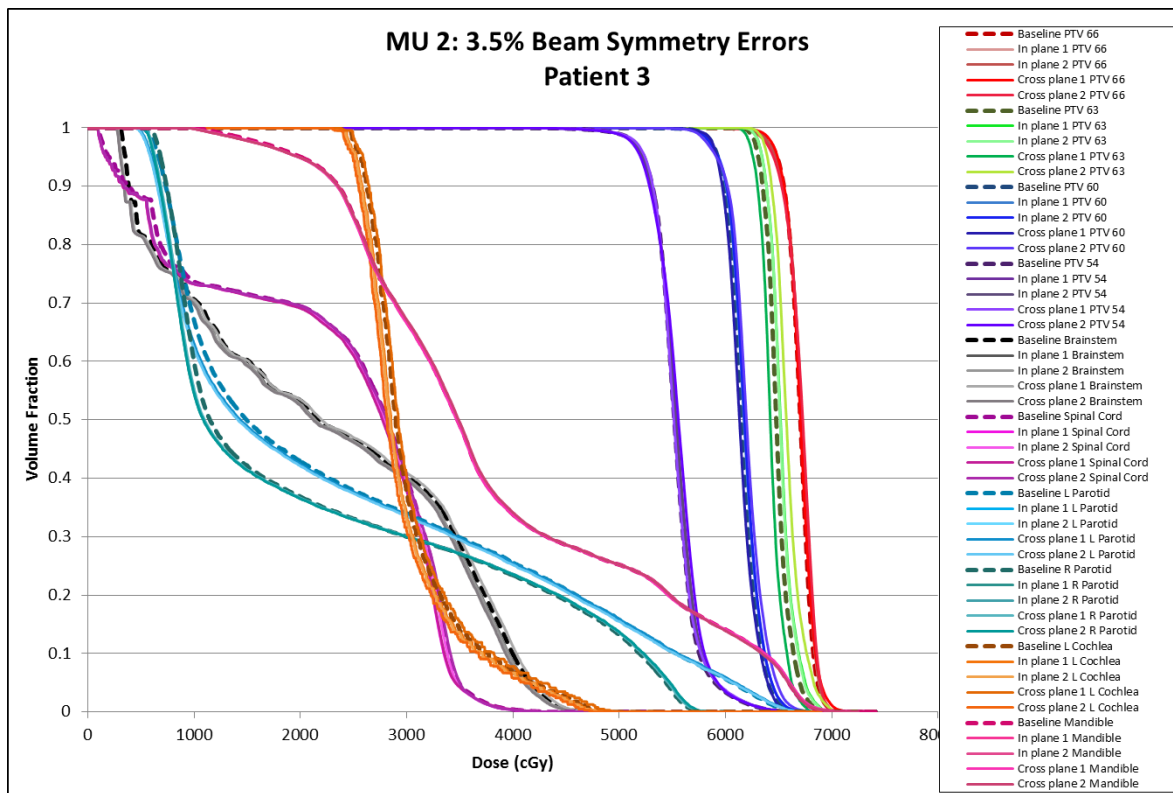


Figure 129: Failure mode 2 (with 3.5% symmetry errors) DVHs for patient 3.

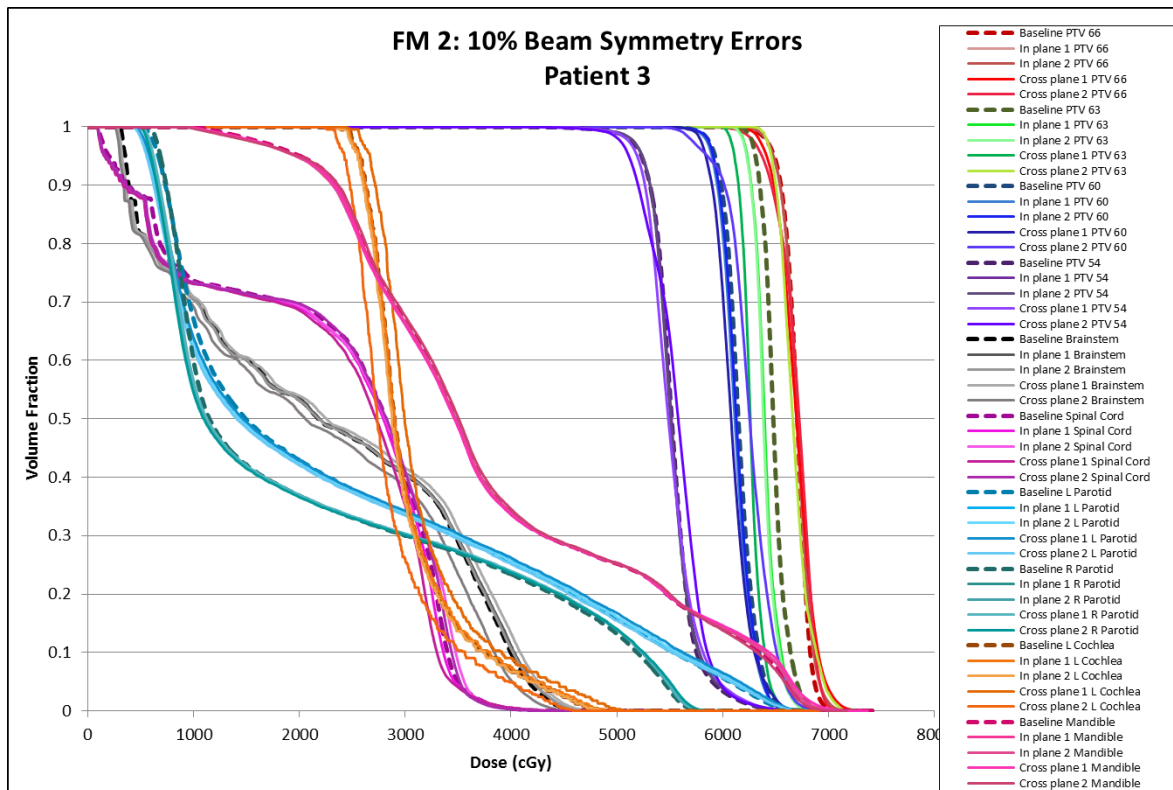


Figure 130: Failure mode 2 (with 10% symmetry errors) DVHs for patient 3.

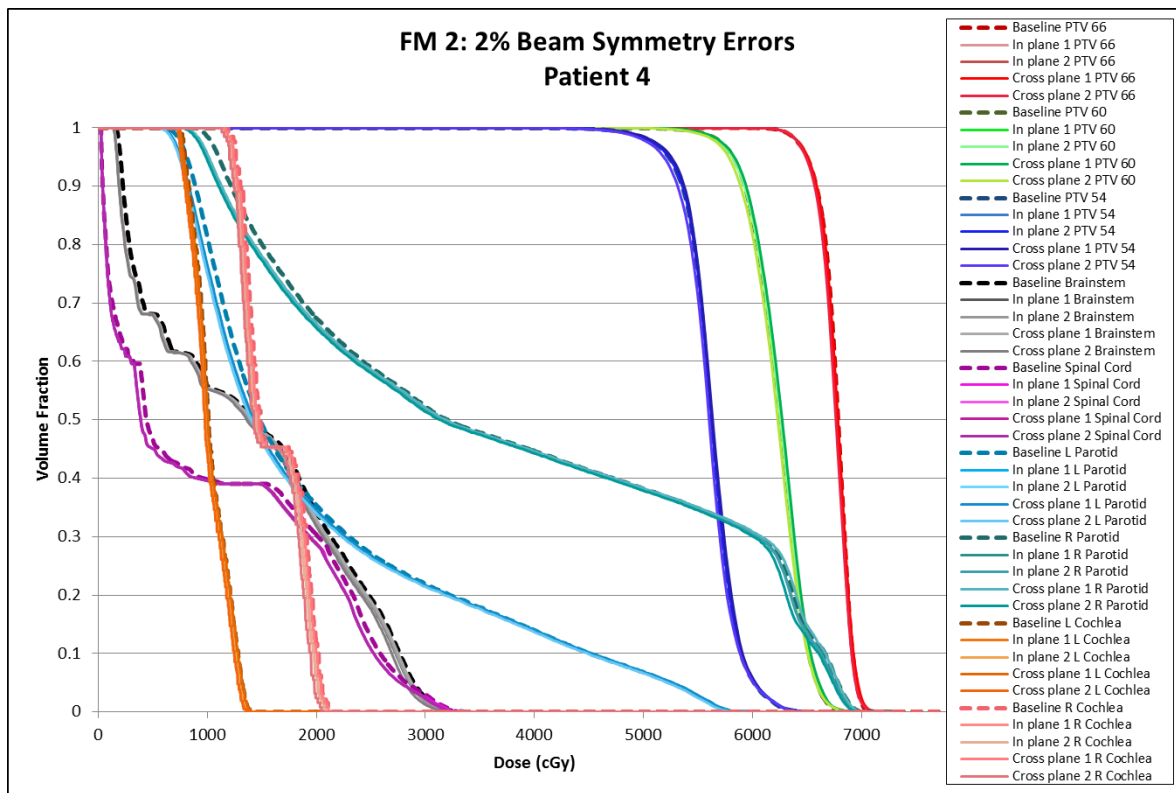


Figure 131: Failure mode 2 (with 2% symmetry errors) DVHs for patient 4.

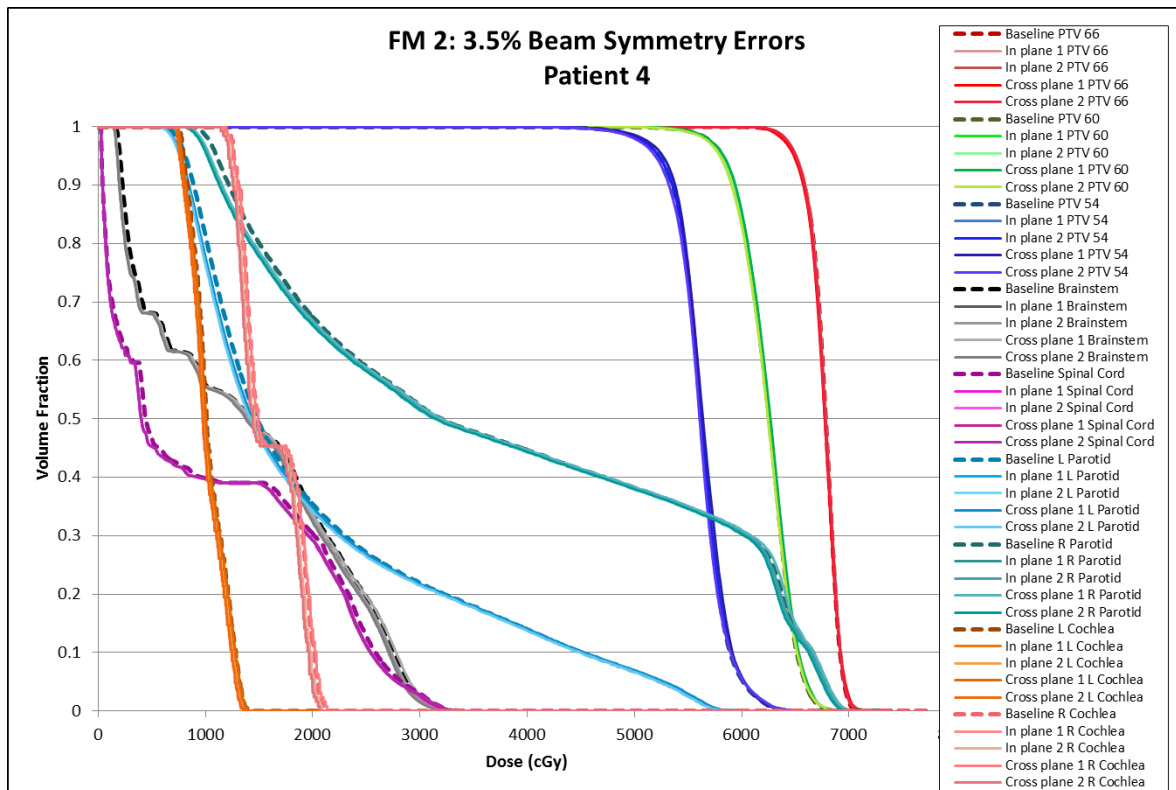


Figure 132: Failure mode 2 (with 3.5% symmetry errors) DVHs for patient 4.

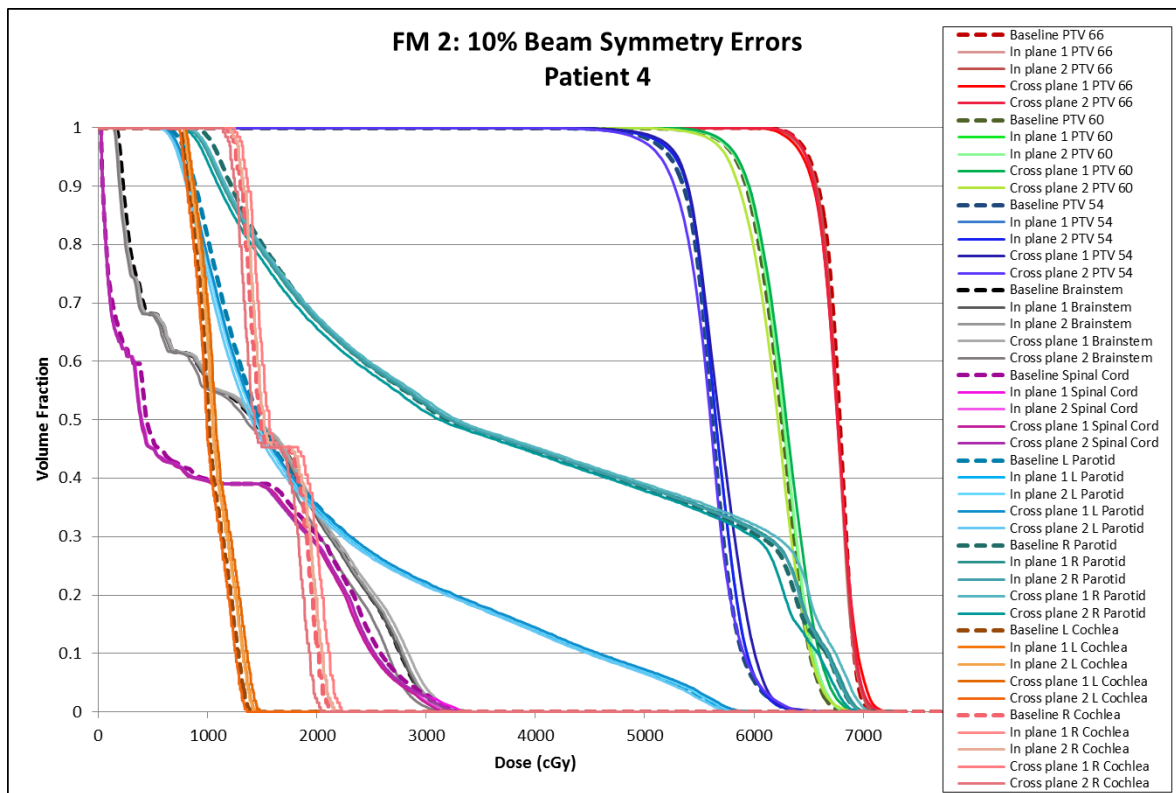


Figure 133: Failure mode 2 (with 10% symmetry errors) DVHs for patient 4.

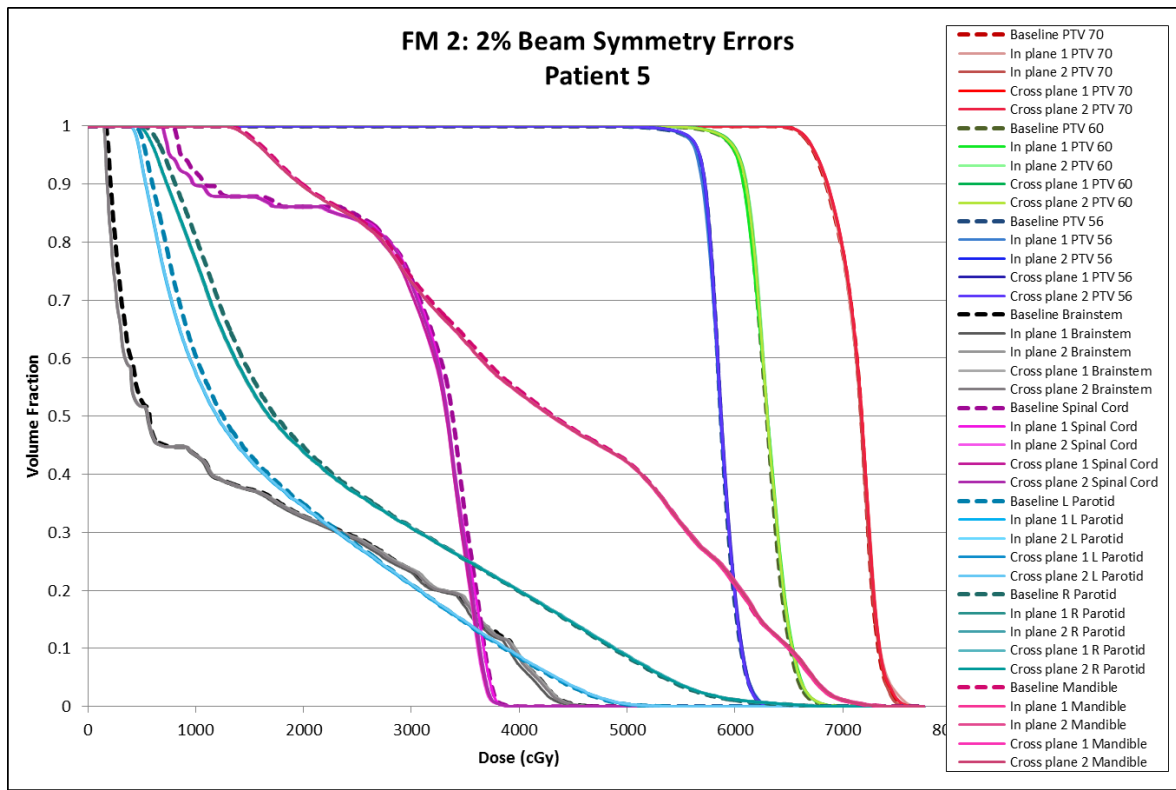


Figure 134: Failure mode 2 (with 2% symmetry errors) DVHs for patient 5.

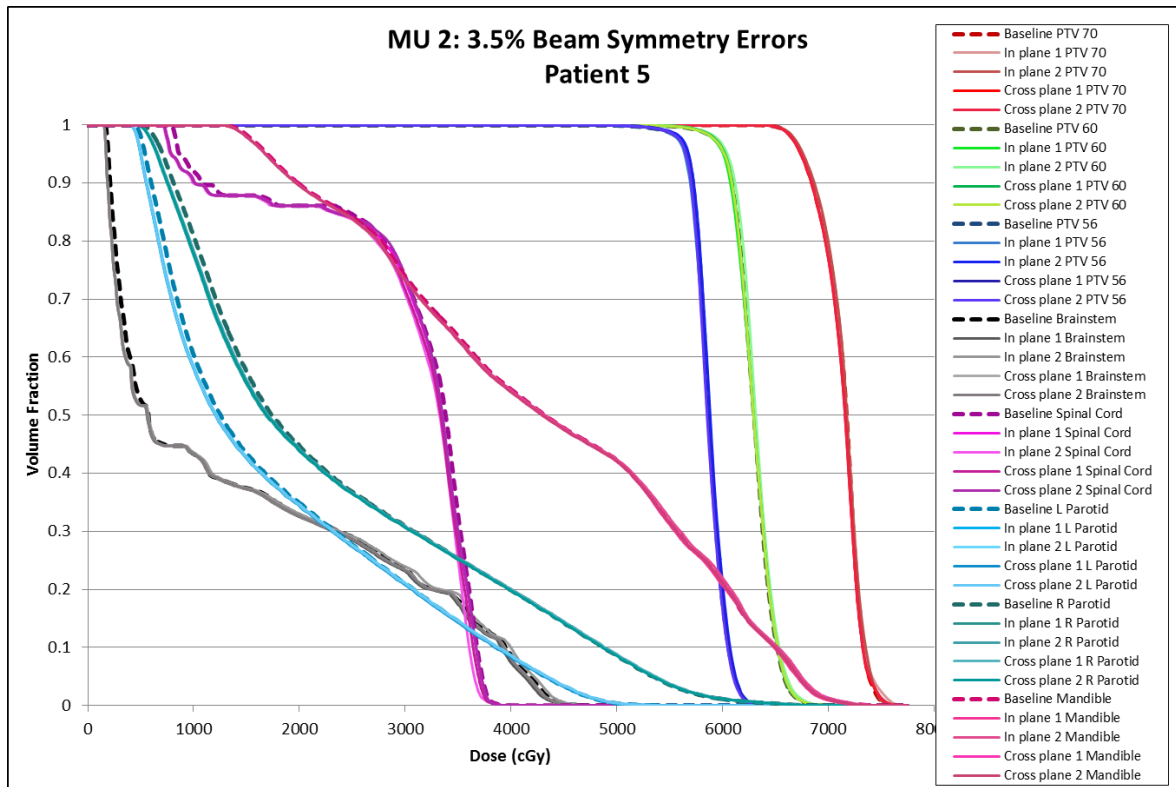


Figure 135: Failure mode 2 (with 3.5% symmetry errors) DVHs for patient 5.

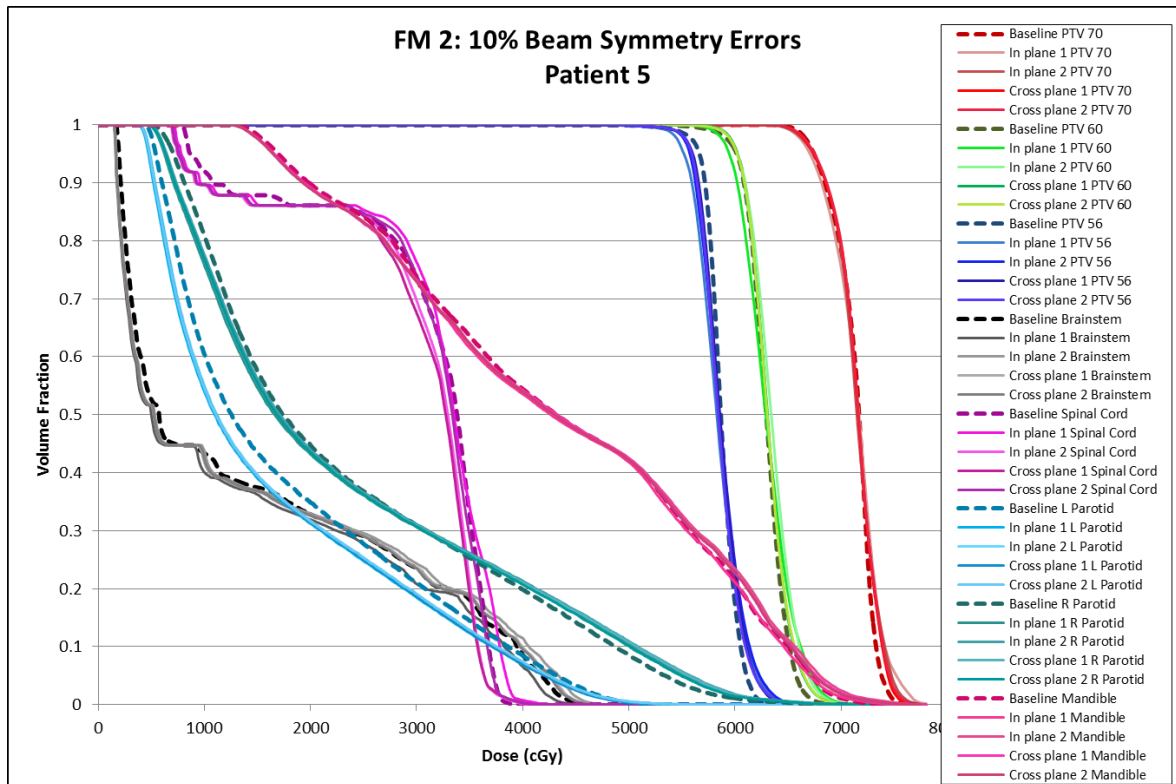


Figure 136: Failure mode 2 (with 10% symmetry errors) DVHs for patient 5.

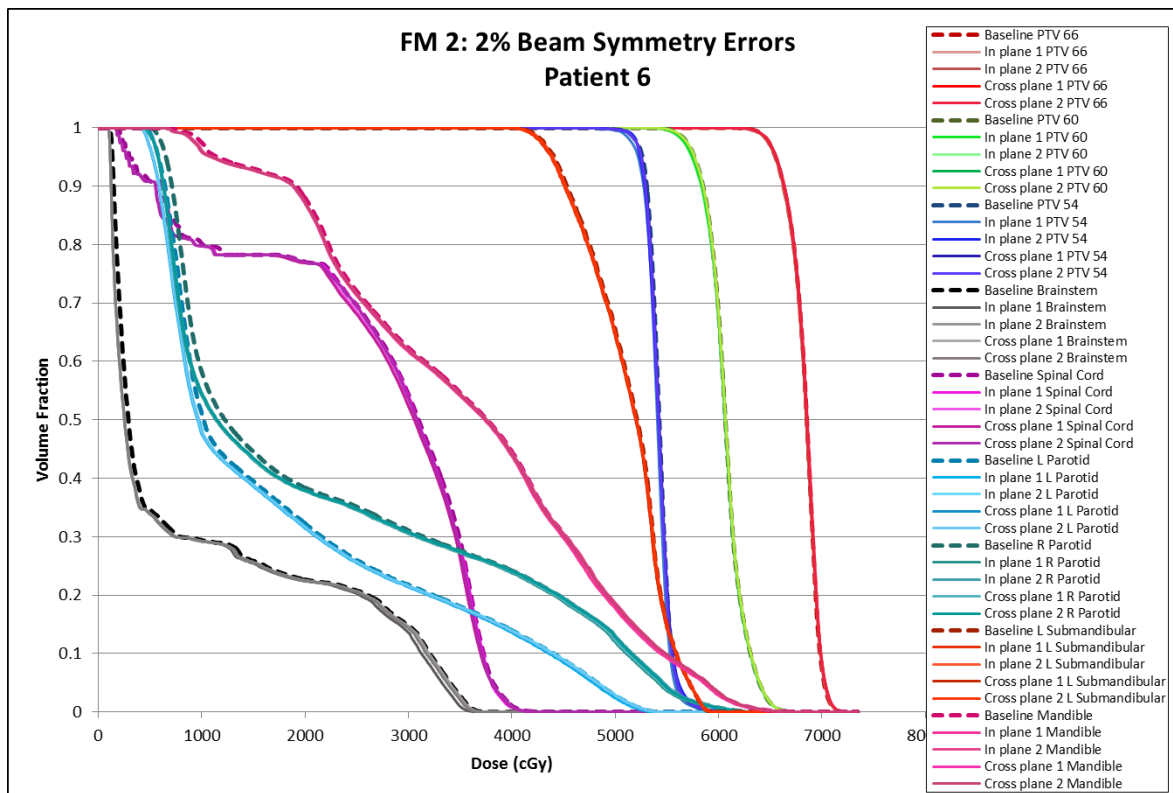


Figure 137: Failure mode 2 (with 2% symmetry errors) DVHs for patient 6.

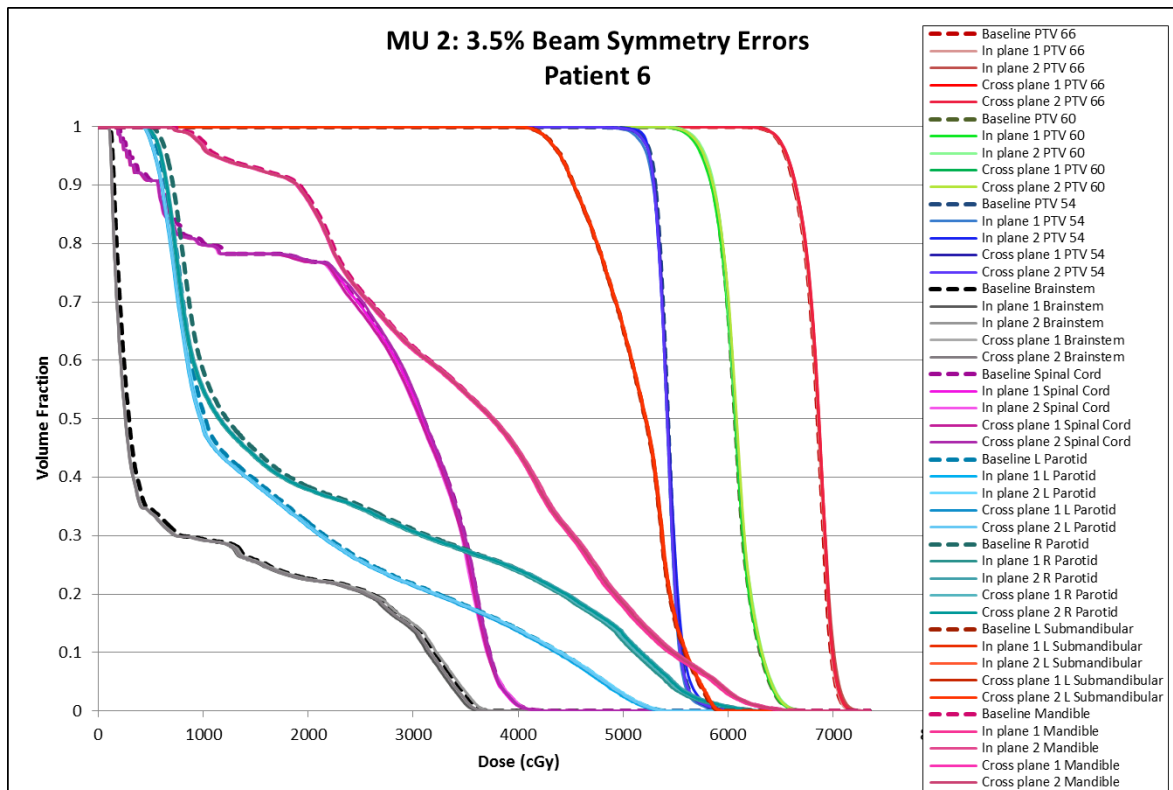


Figure 138: Failure mode 2 (with 3.5% symmetry errors) DVHs for patient 6.

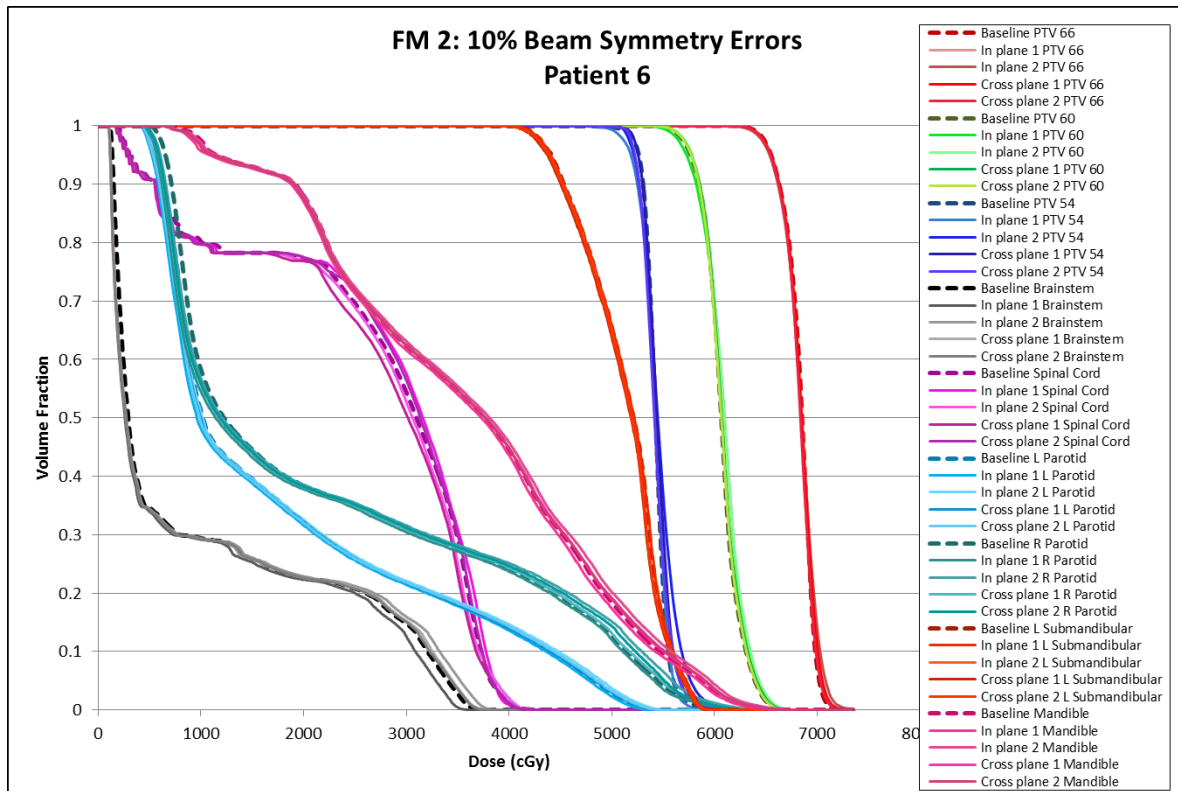


Figure 139: Failure mode 2 (with 10% symmetry errors) DVHs for patient 6.

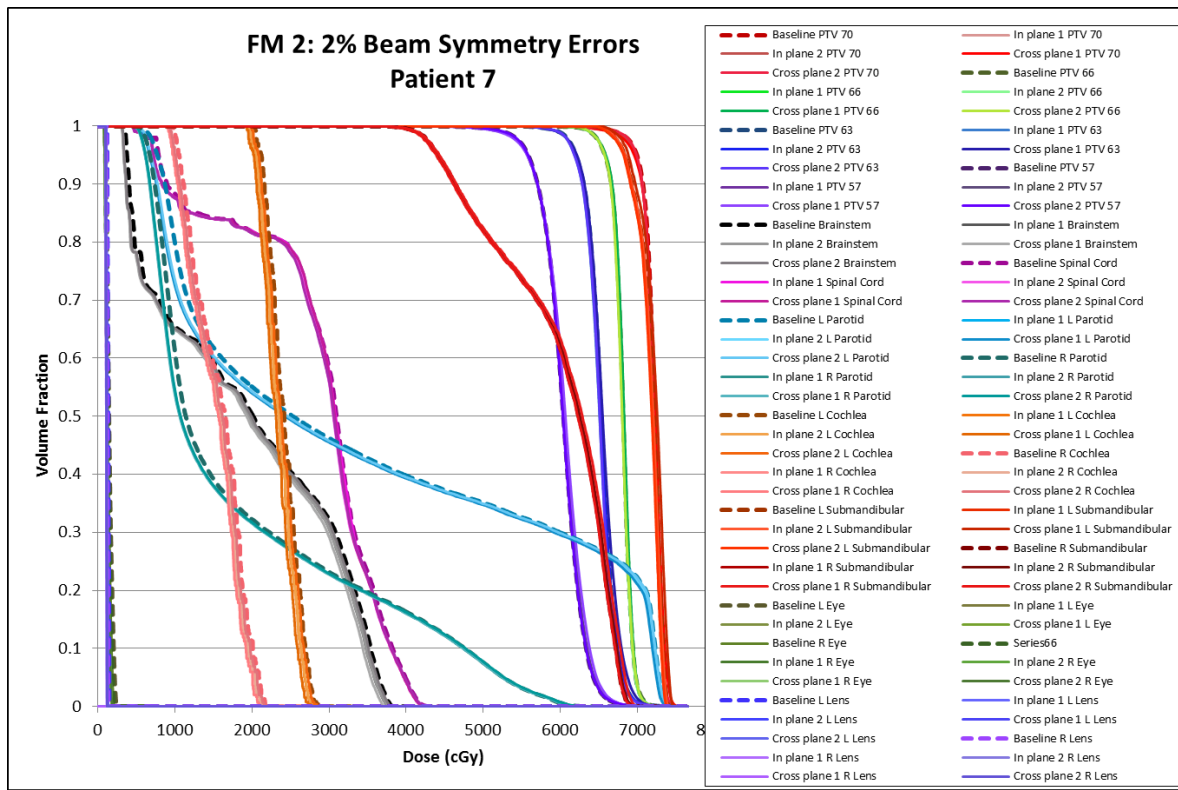


Figure 140: Failure mode 2 (with 2% symmetry errors) DVHs for patient 7.

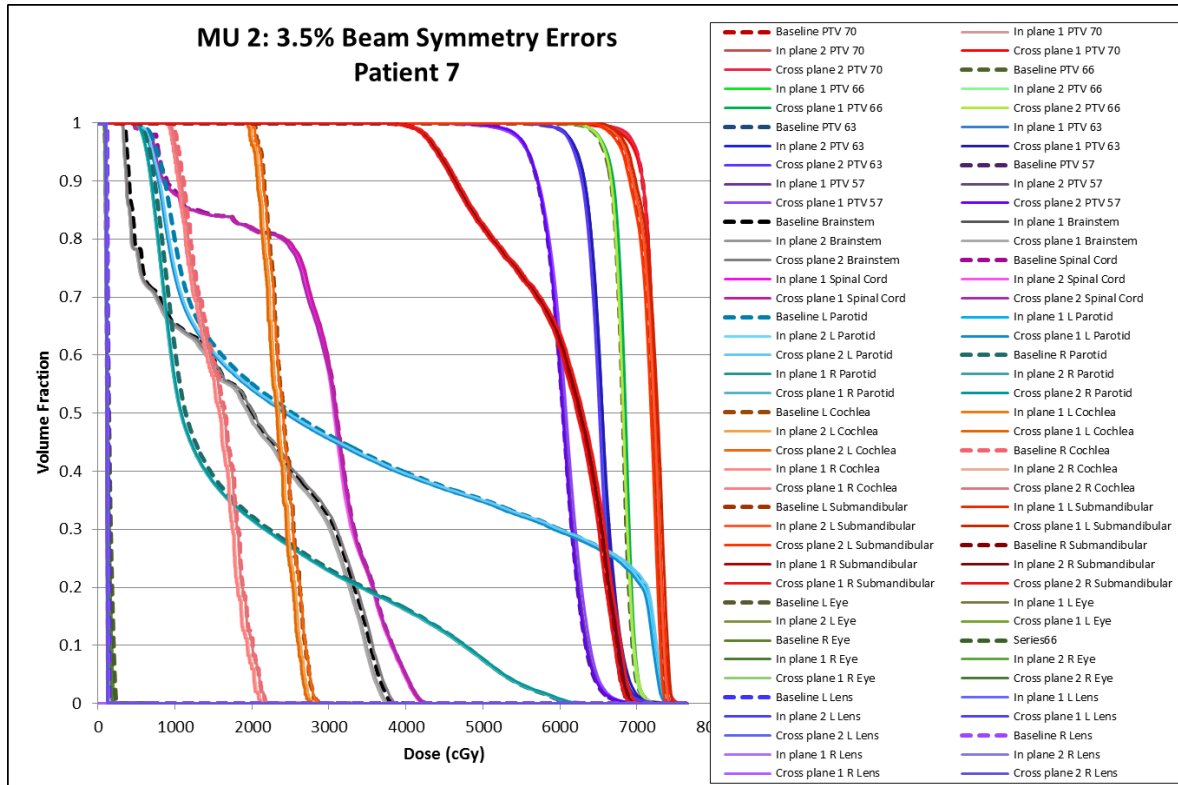


Figure 141: Failure mode 2 (with 3.5% symmetry errors) DVHs for patient 7.

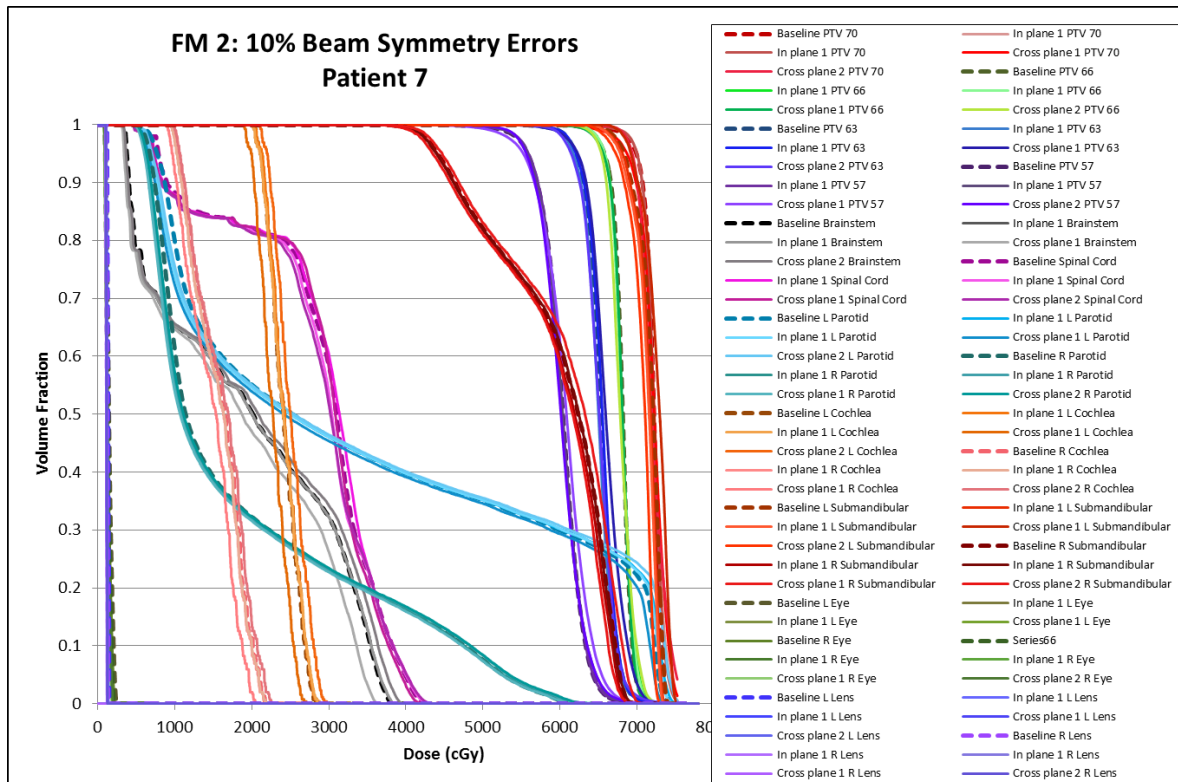


Figure 142: Failure mode 2 (with 10% symmetry errors) DVHs for patient 7.

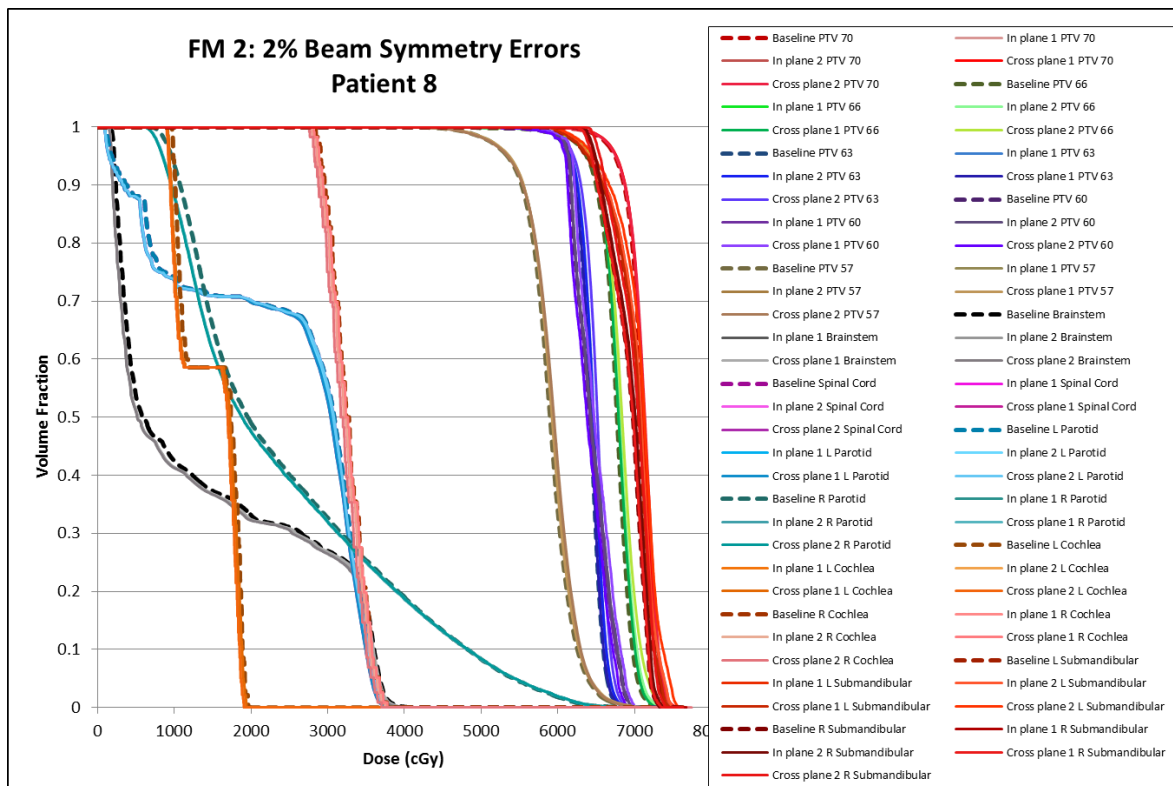


Figure 143: Failure mode 2 (with 2% symmetry errors) DVHs for patient 8.

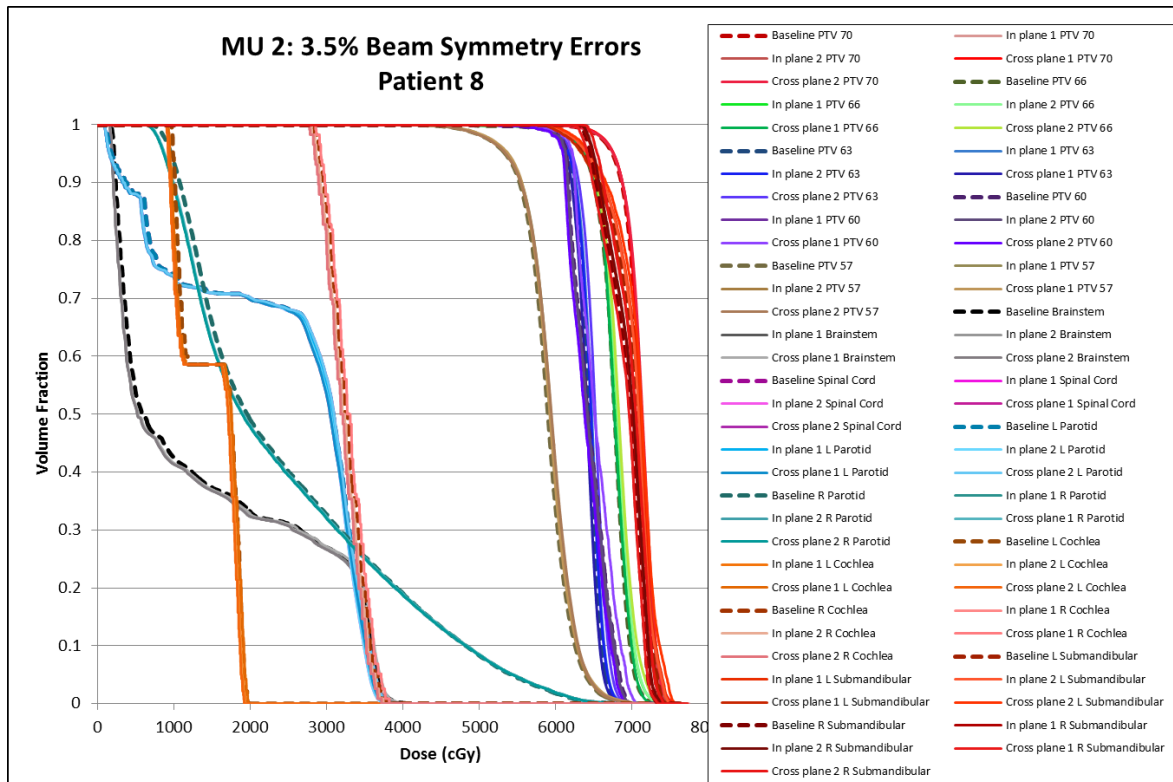


Figure 144: Failure mode 2 (with 3.5% symmetry errors) DVHs for patient 8.

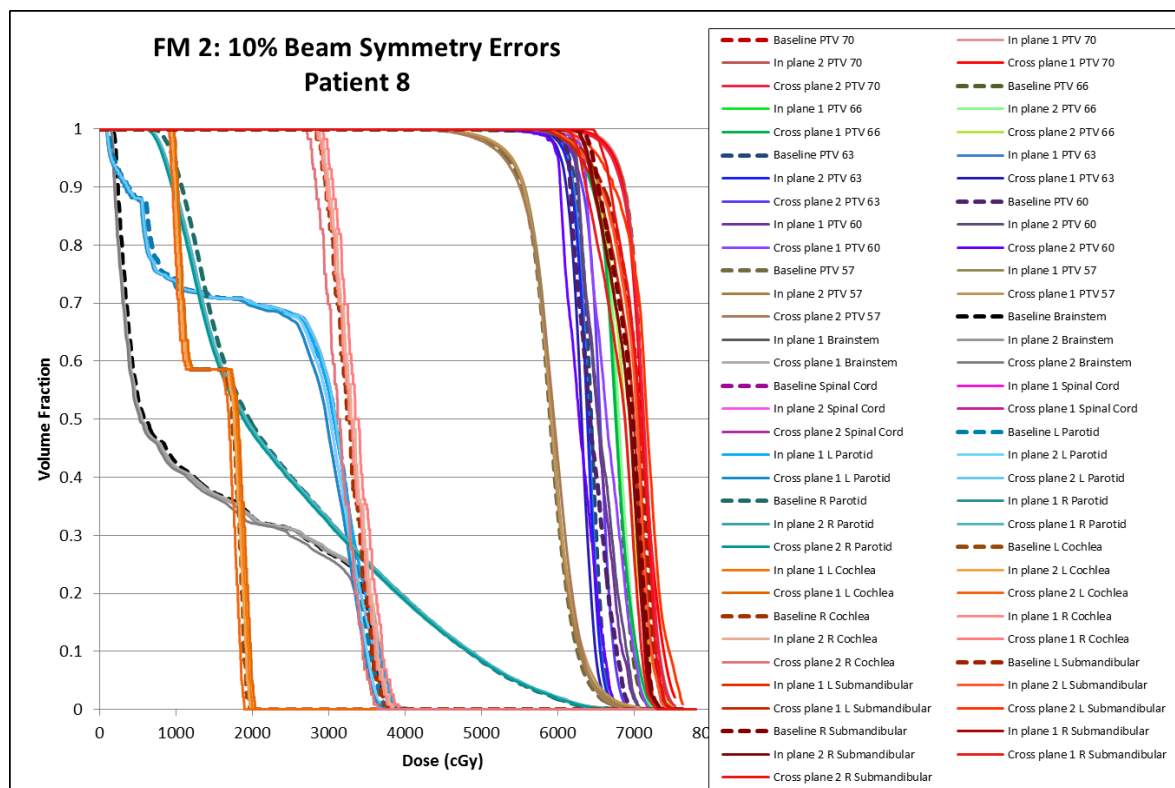


Figure 145: Failure mode 2 (with 10% symmetry errors) DVHs for patient 8.

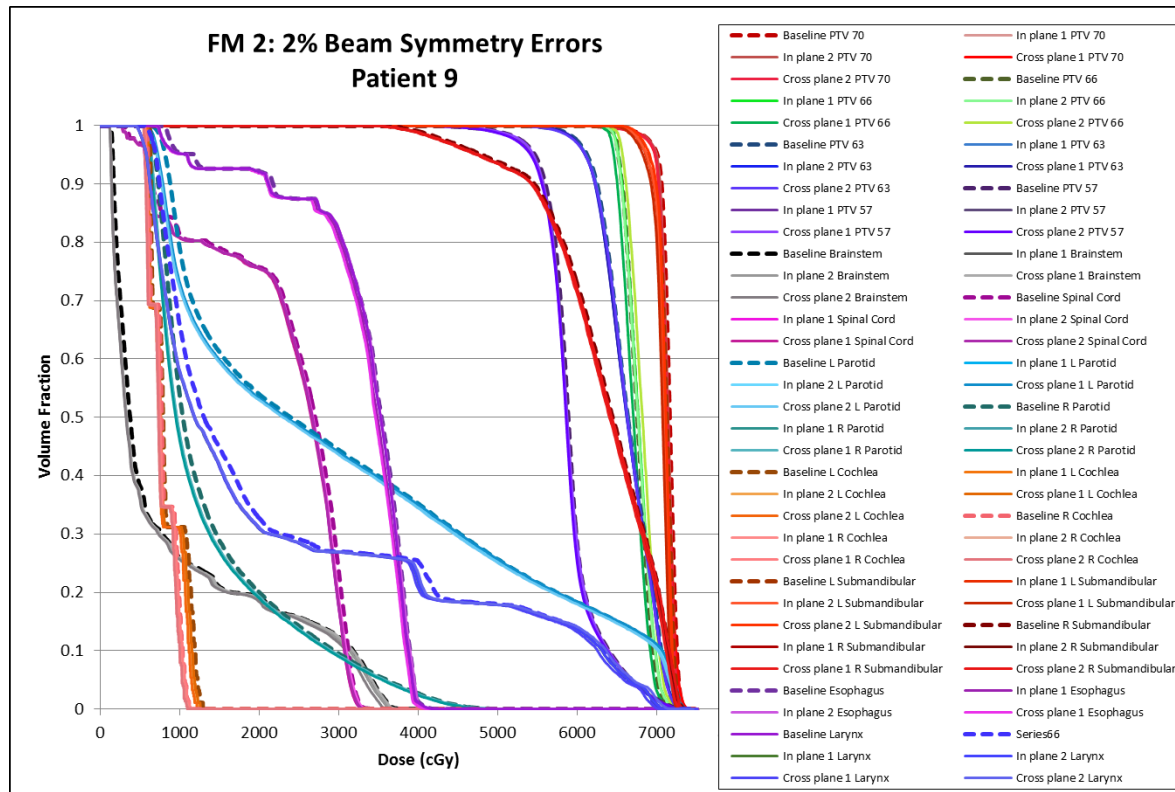


Figure 146: Failure mode 2 (with 2% symmetry errors) DVHs for patient 9.

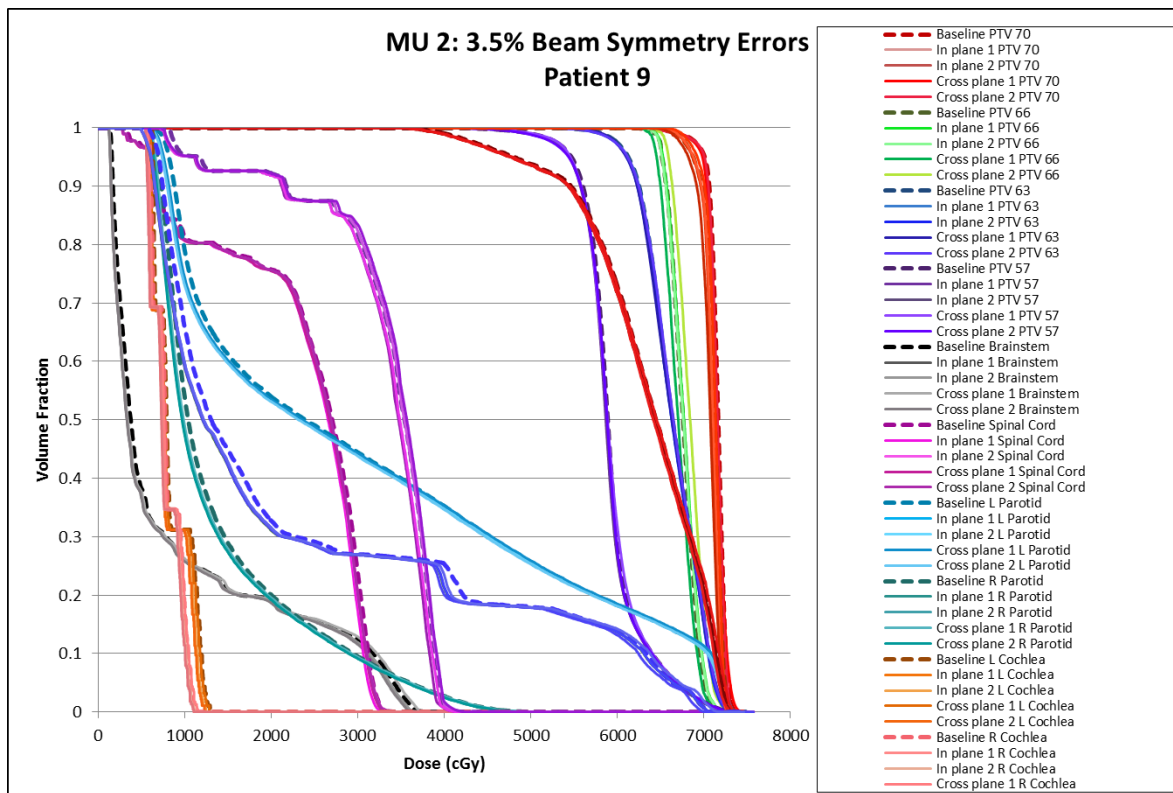


Figure 147: Failure mode 2 (with 3.5% symmetry errors) DVHs for patient 9.

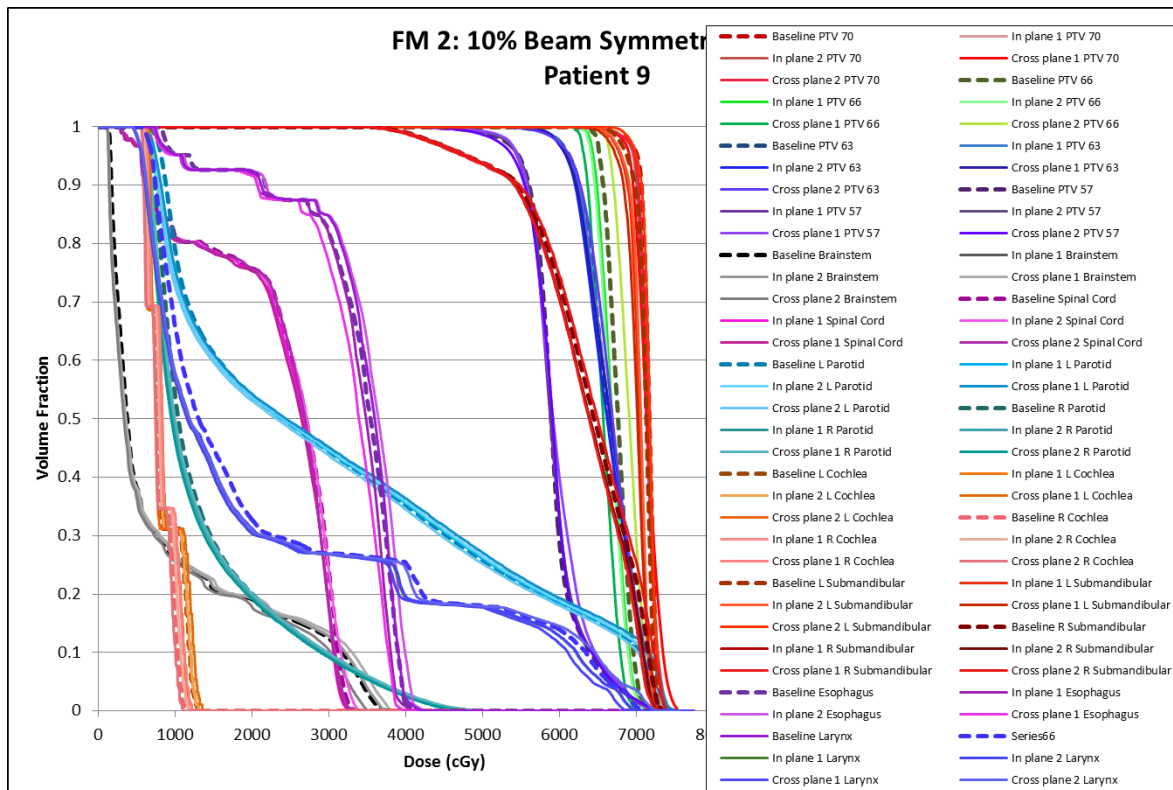


Figure 148: Failure mode 2 (with 10% symmetry errors) DVHs for patient 9.

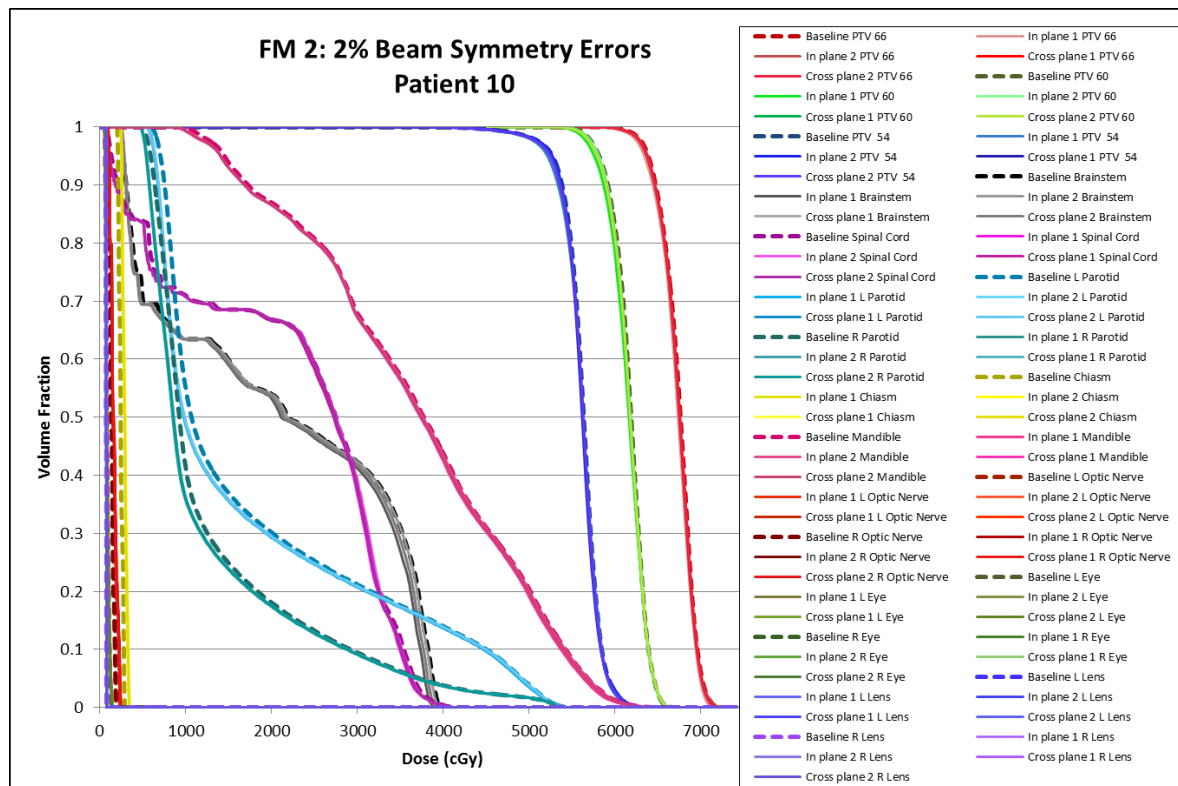


Figure 149: Failure mode 2 (with 2% symmetry errors) DVHs for patient 10.

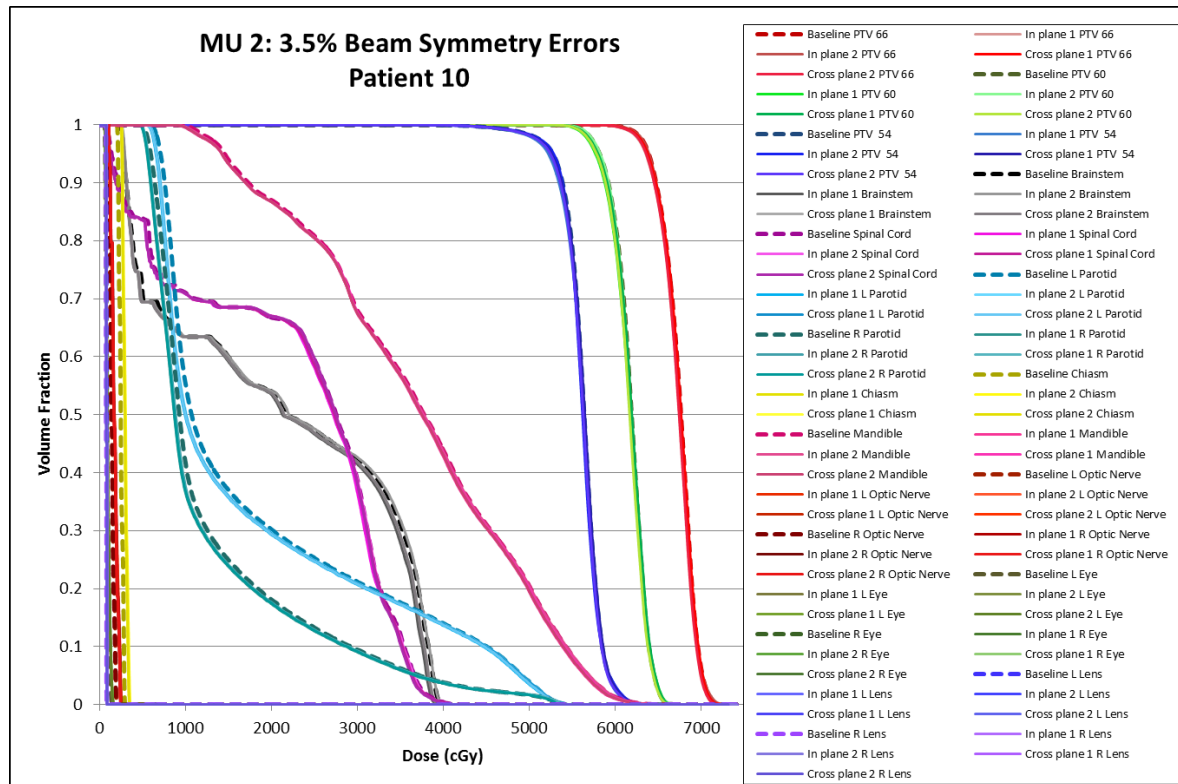


Figure 150: Failure mode 2 (with 3.5% symmetry errors) DVHs for patient 10.

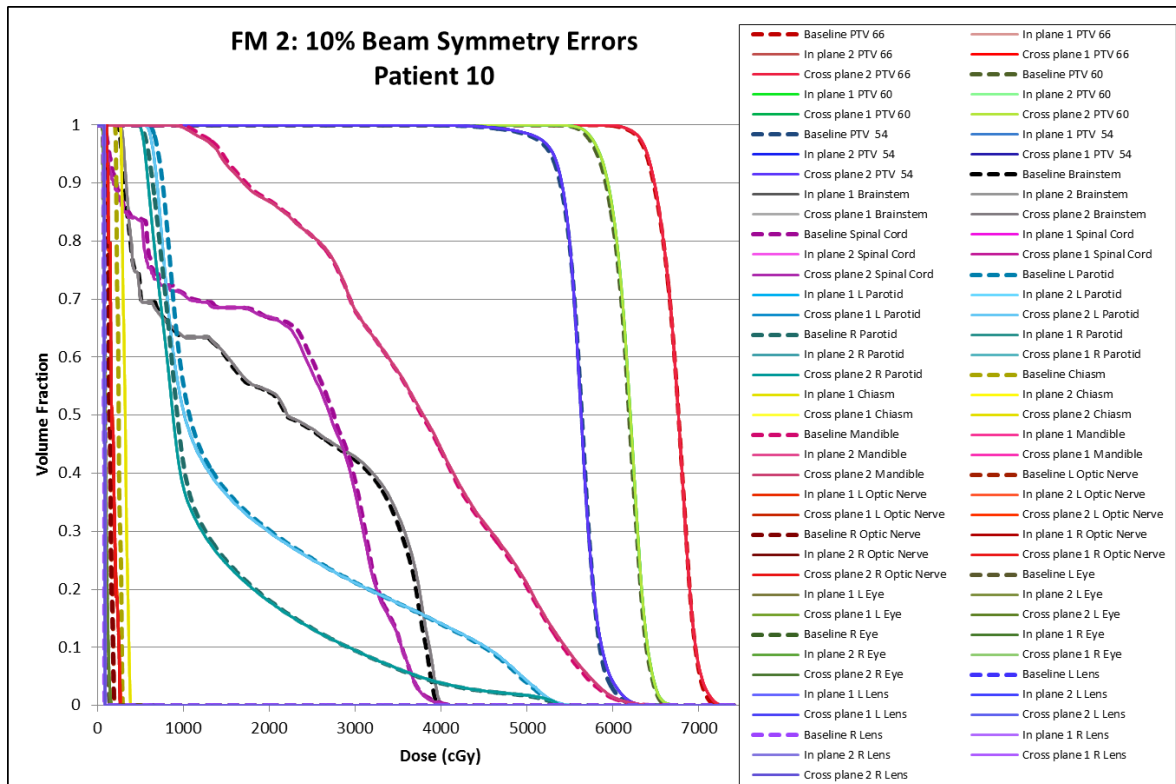


Figure 151: Failure mode 2 (with 10% symmetry errors) DVHs for patient 10.

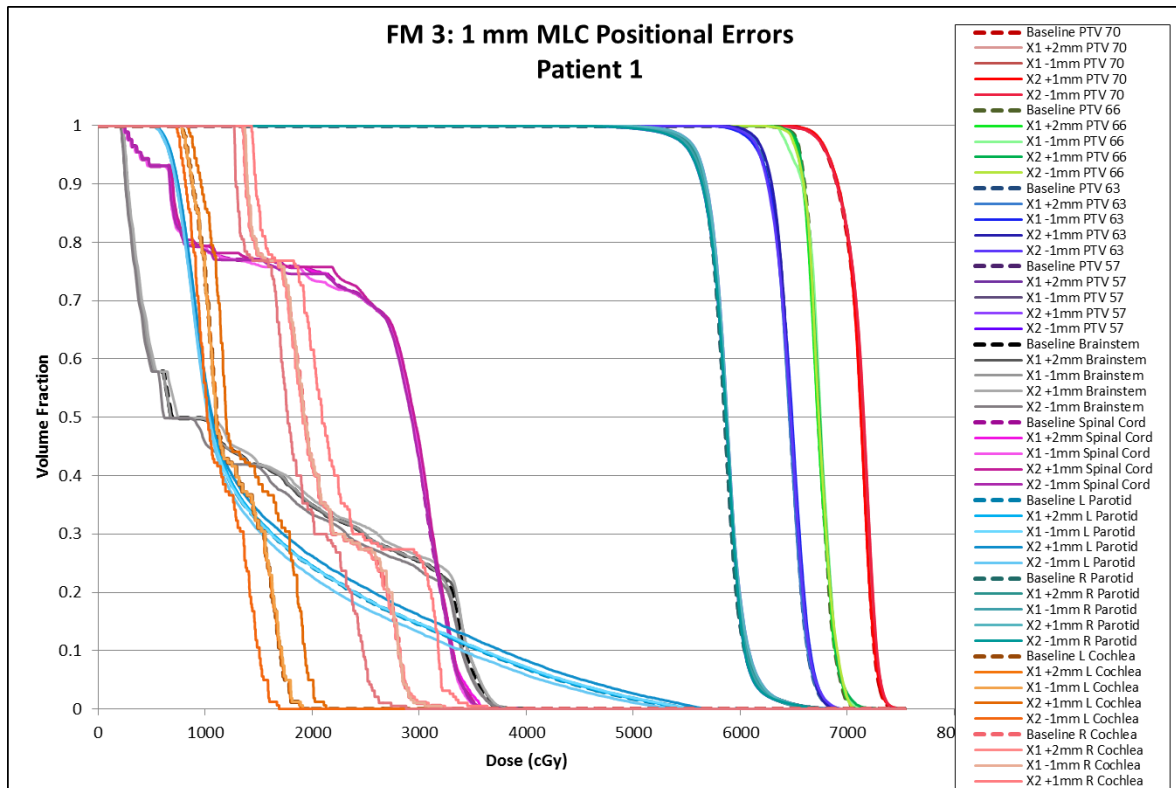


Figure 152: Failure mode 3 (with 1 mm errors) DVHs for patient 1.

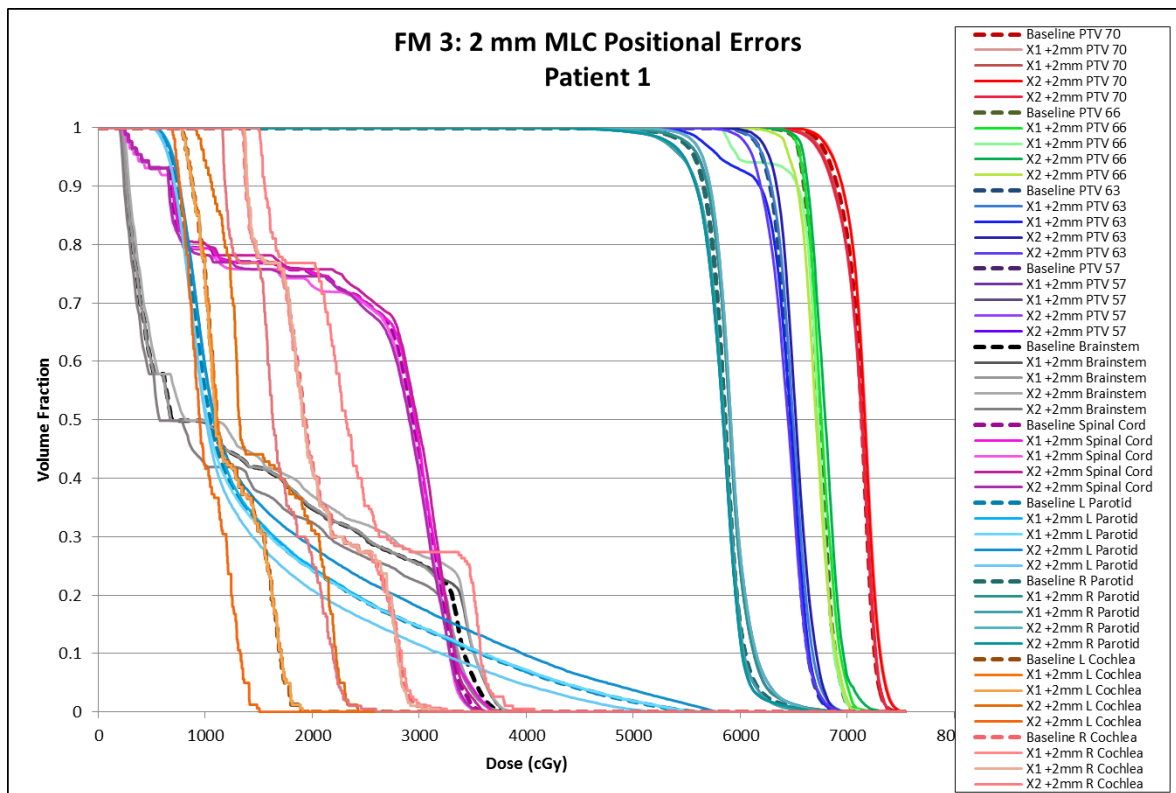


Figure 153: Failure mode 3 (with 2 mm errors) DVHs for patient 1.

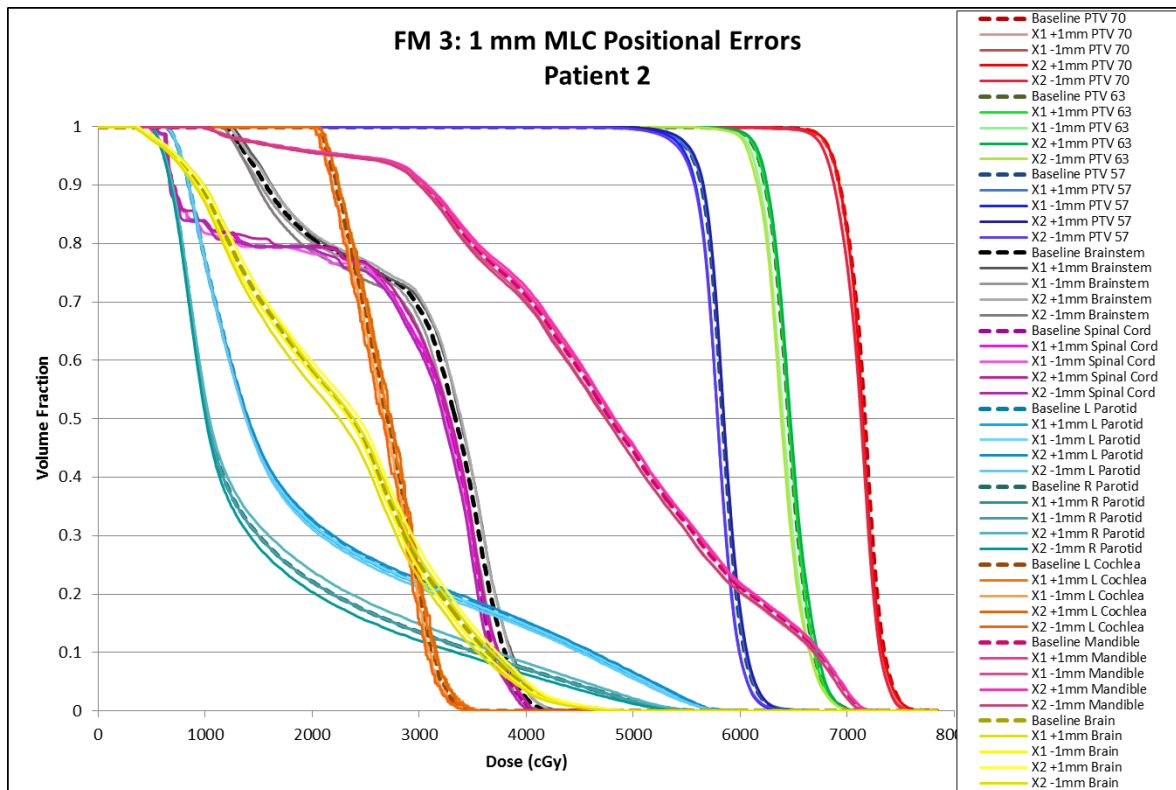


Figure 154: Failure mode 3 (with 1 mm errors) DVHs for patient 2.

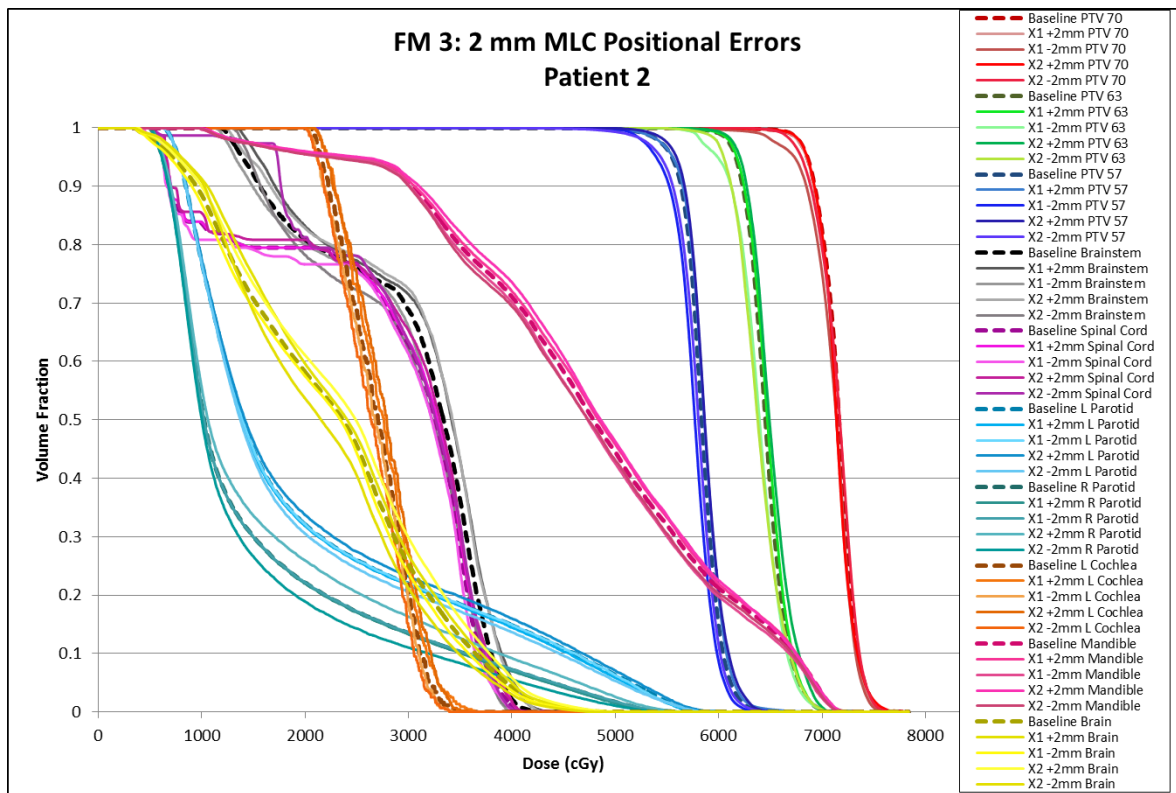


Figure 155: Failure mode 3 (with 2 mm errors) DVHs for patient 2.

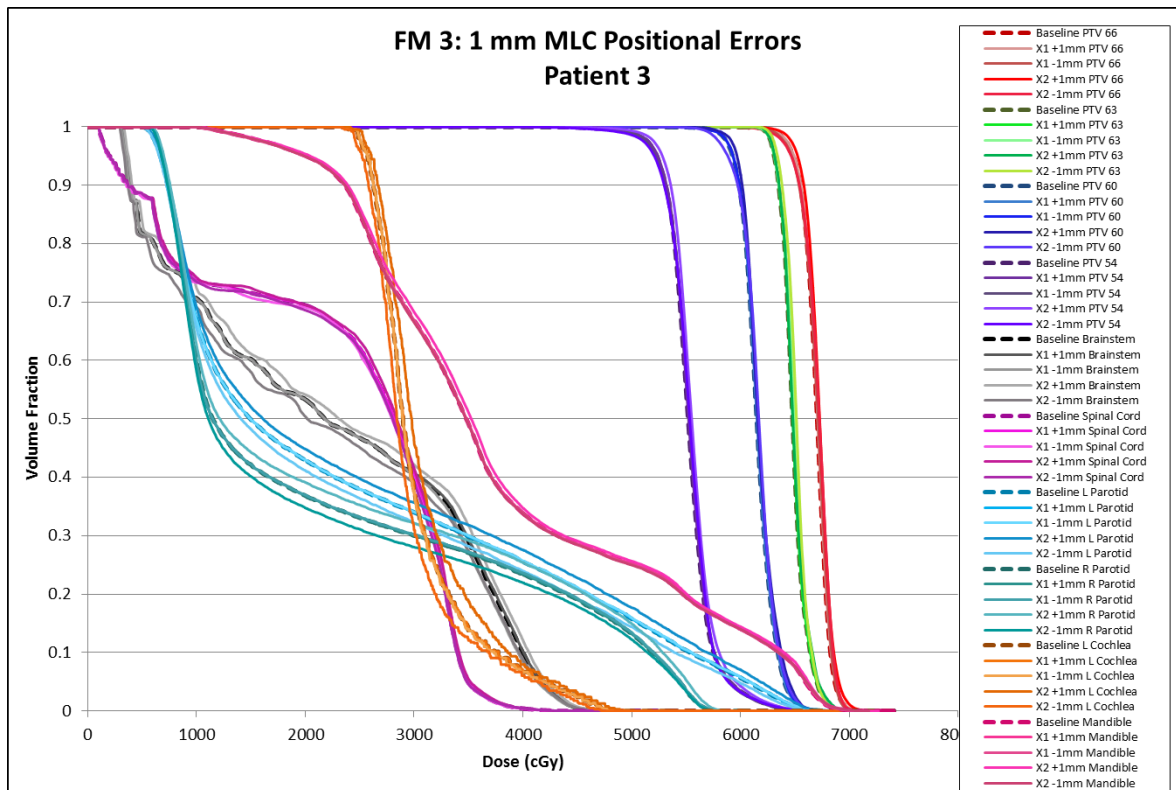


Figure 156: Failure mode 3 (with 1 mm errors) DVHs for patient 3.

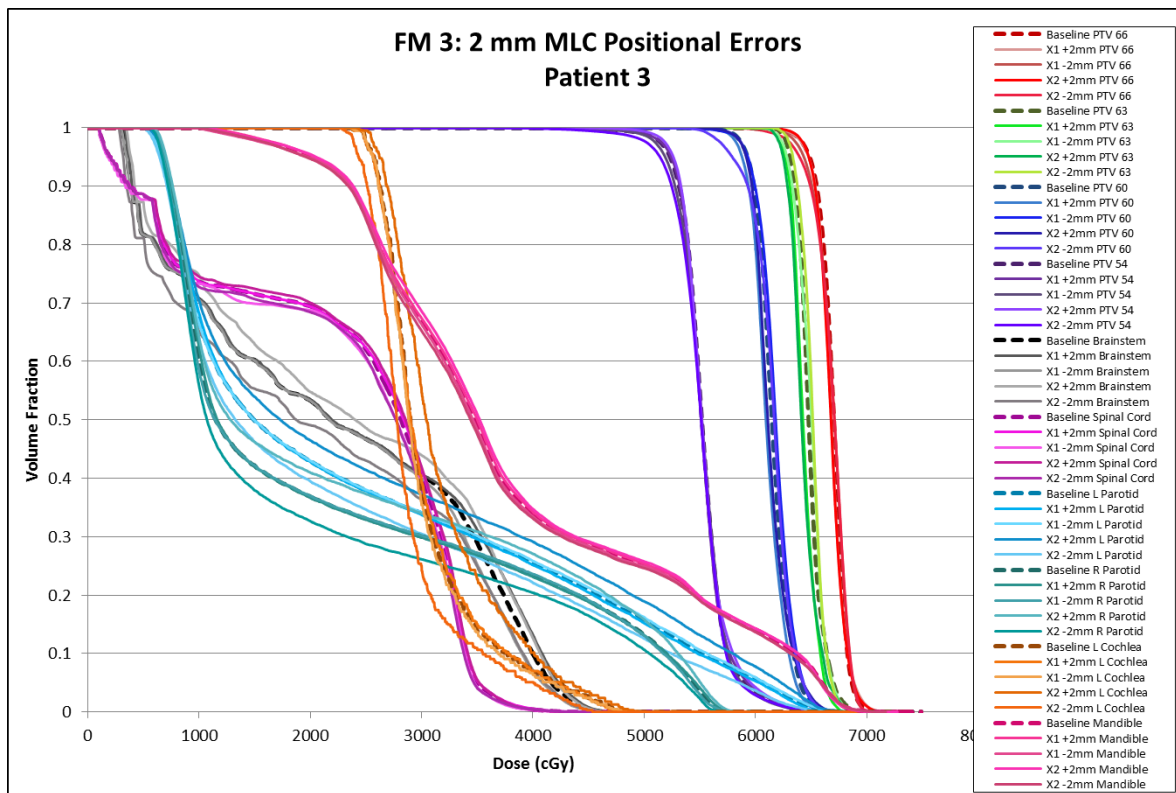


Figure 157: Failure mode 3 (with 2 mm errors) DVHs for patient 3.

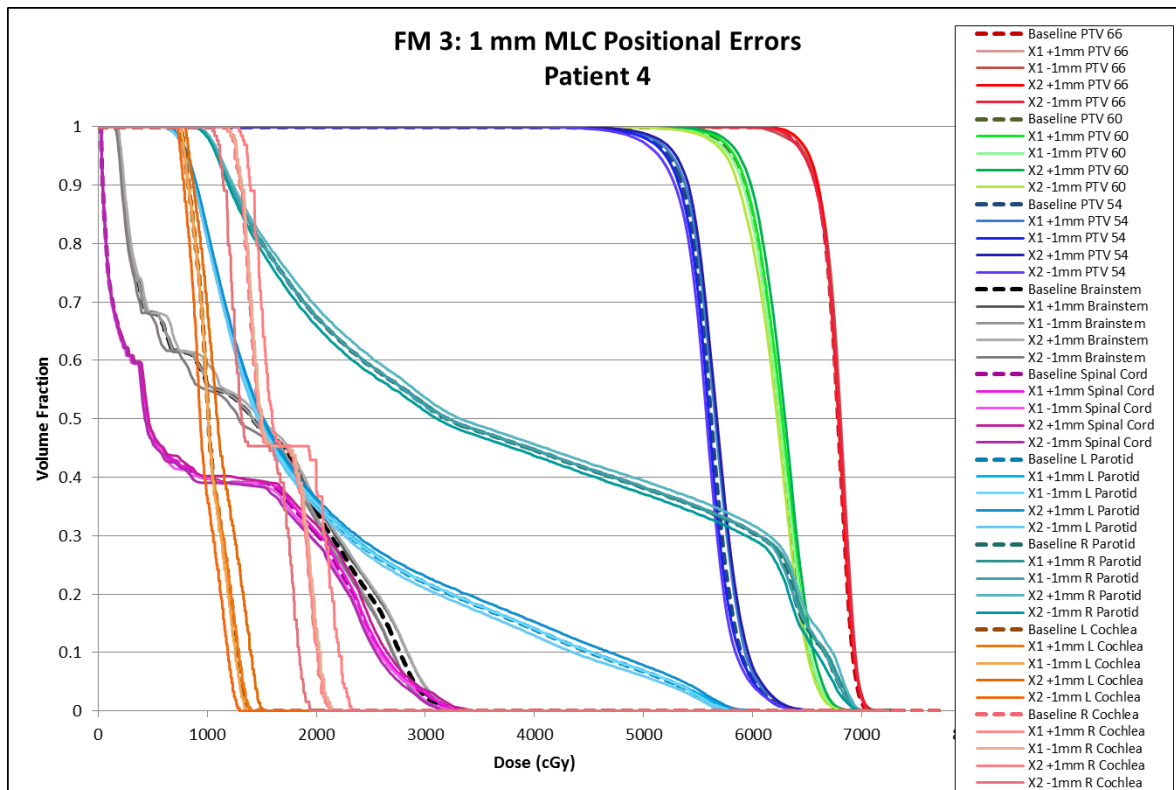


Figure 158: Failure mode 3 (with 1 mm errors) DVHs for patient 4.

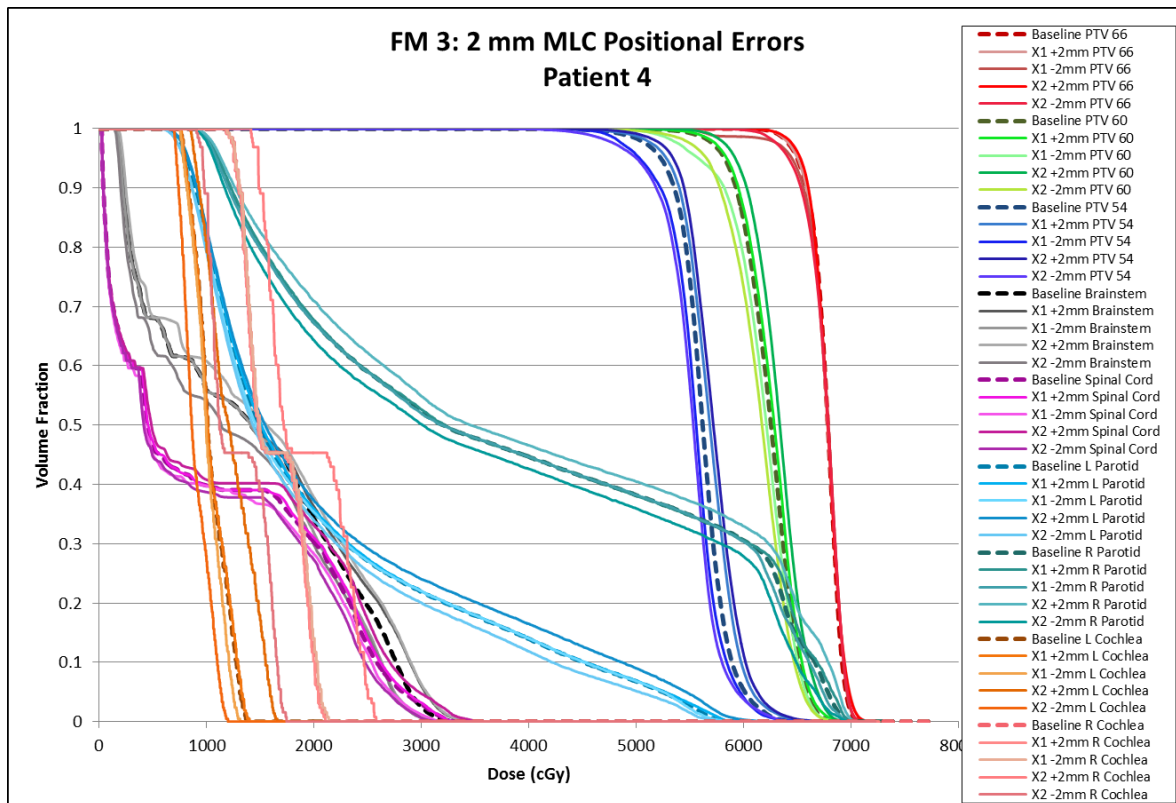


Figure 159: Failure mode 3 (with 2 mm errors) DVHs for patient 4.

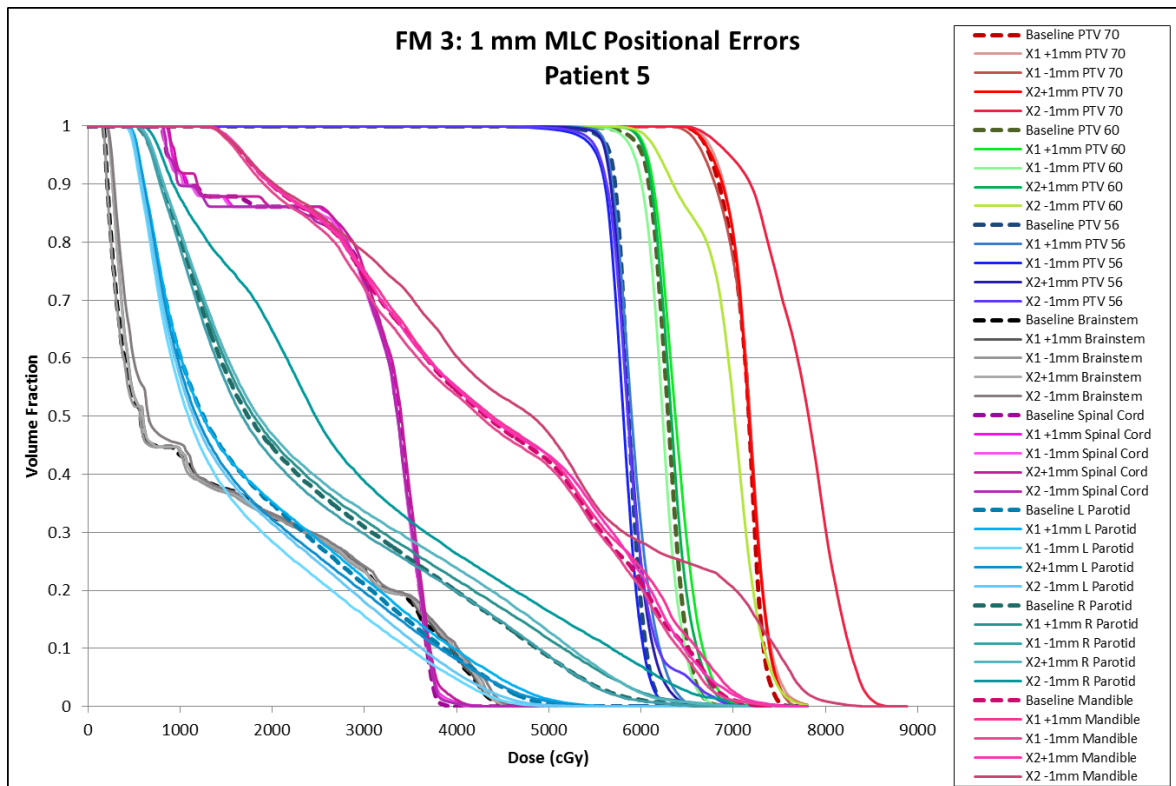


Figure 160: Failure mode 3 (with 1 mm errors) DVHs for patient 5.

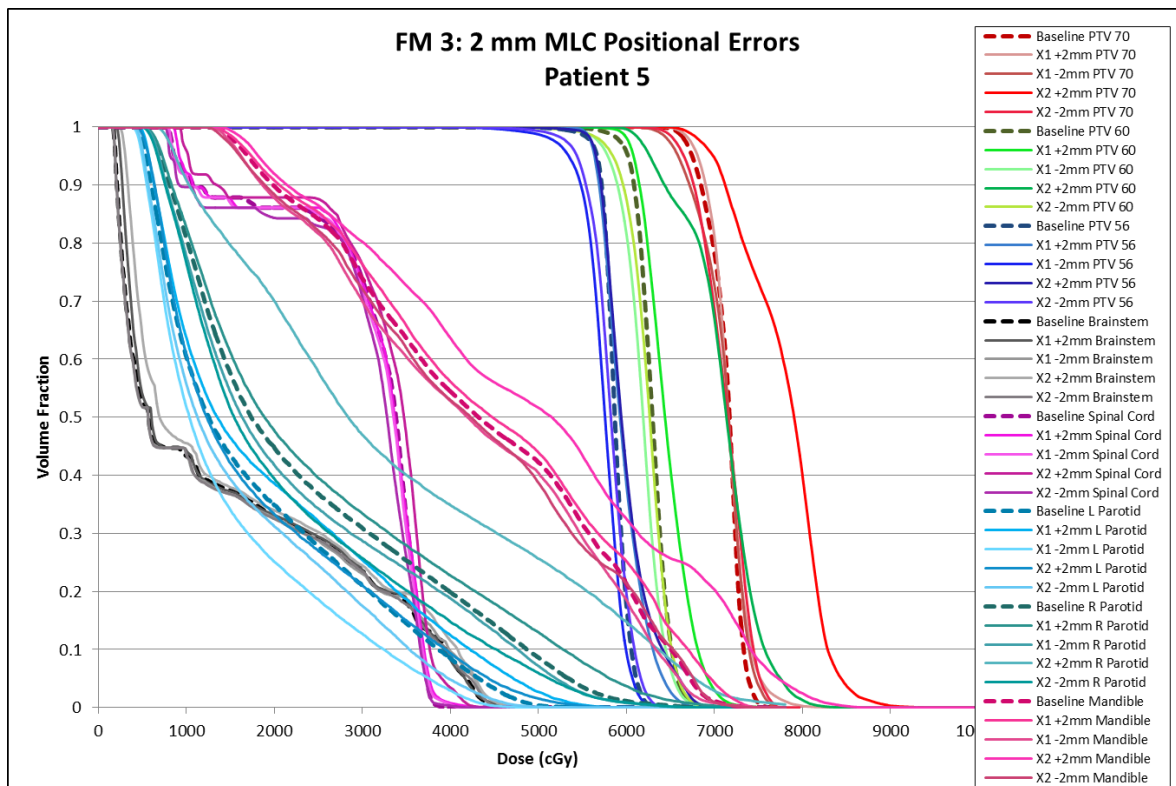


Figure 161: Failure mode 3 (with 2 mm errors) DVHs for patient 5.

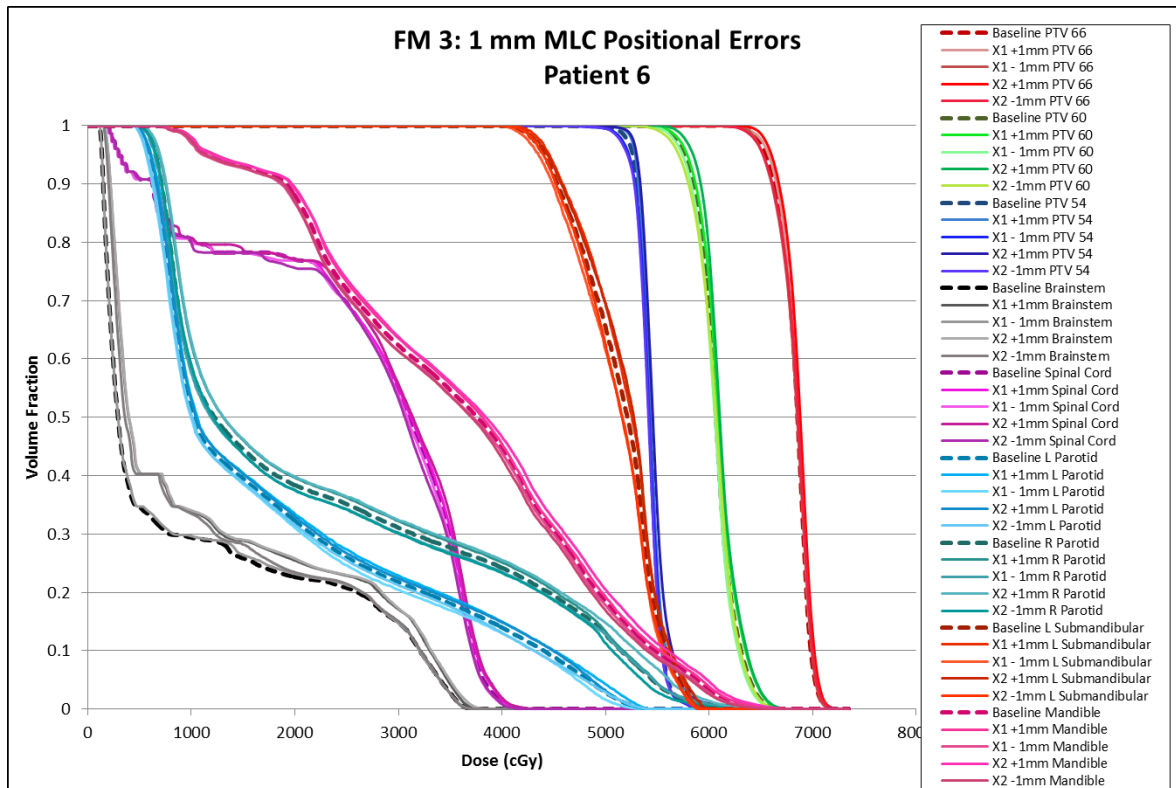


Figure 162: Failure mode 3 (with 1 mm errors) DVHs for patient 6.

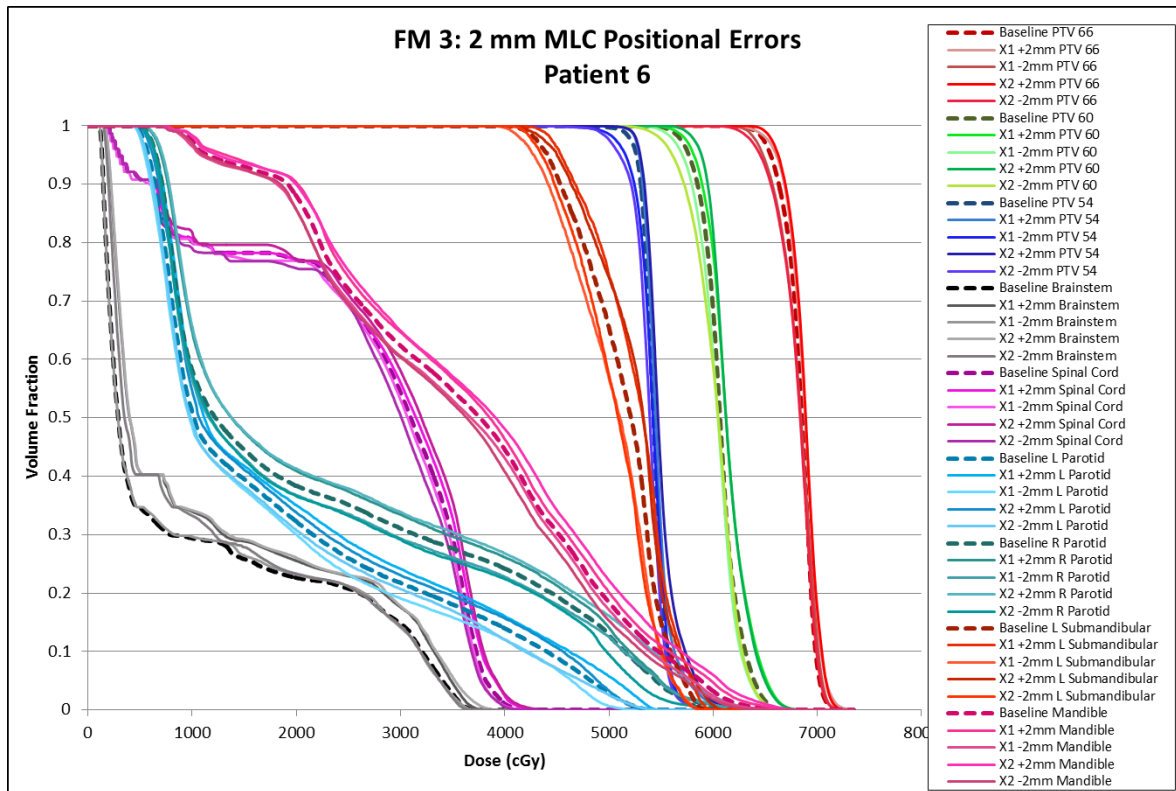


Figure 163: Failure mode 3 (with 2 mm errors) DVHs for patient 6.

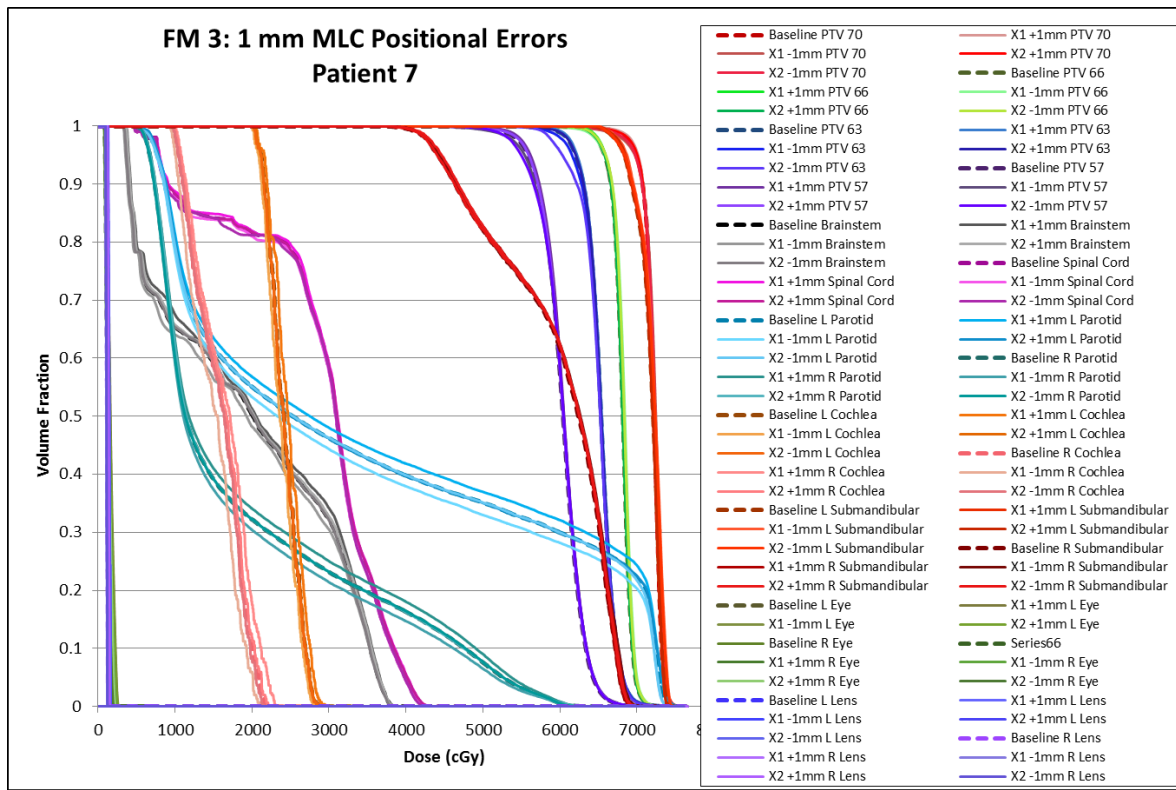


Figure 164: Failure mode 3 (with 1 mm errors) DVHs for patient 7.

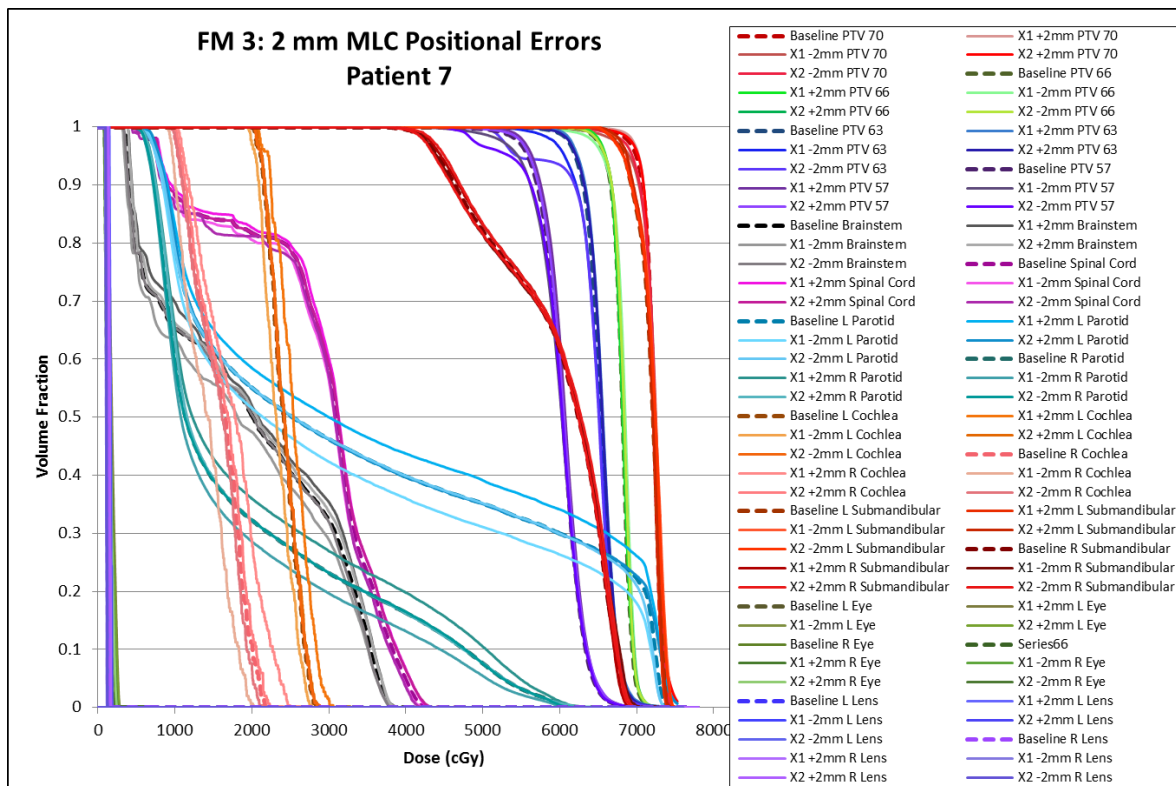


Figure 165: Failure mode 3 (with 2 mm errors) DVHs for patient 7.

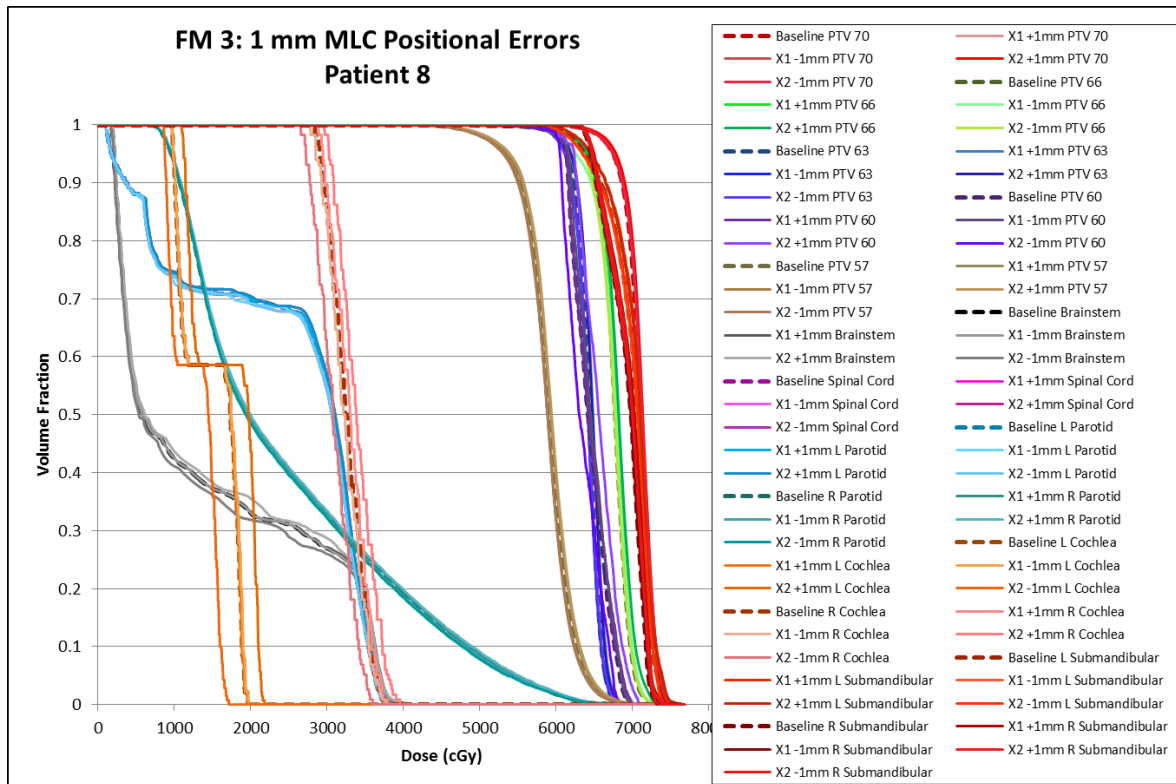


Figure 166: Failure mode 3 (with 1 mm errors) DVHs for patient 8.

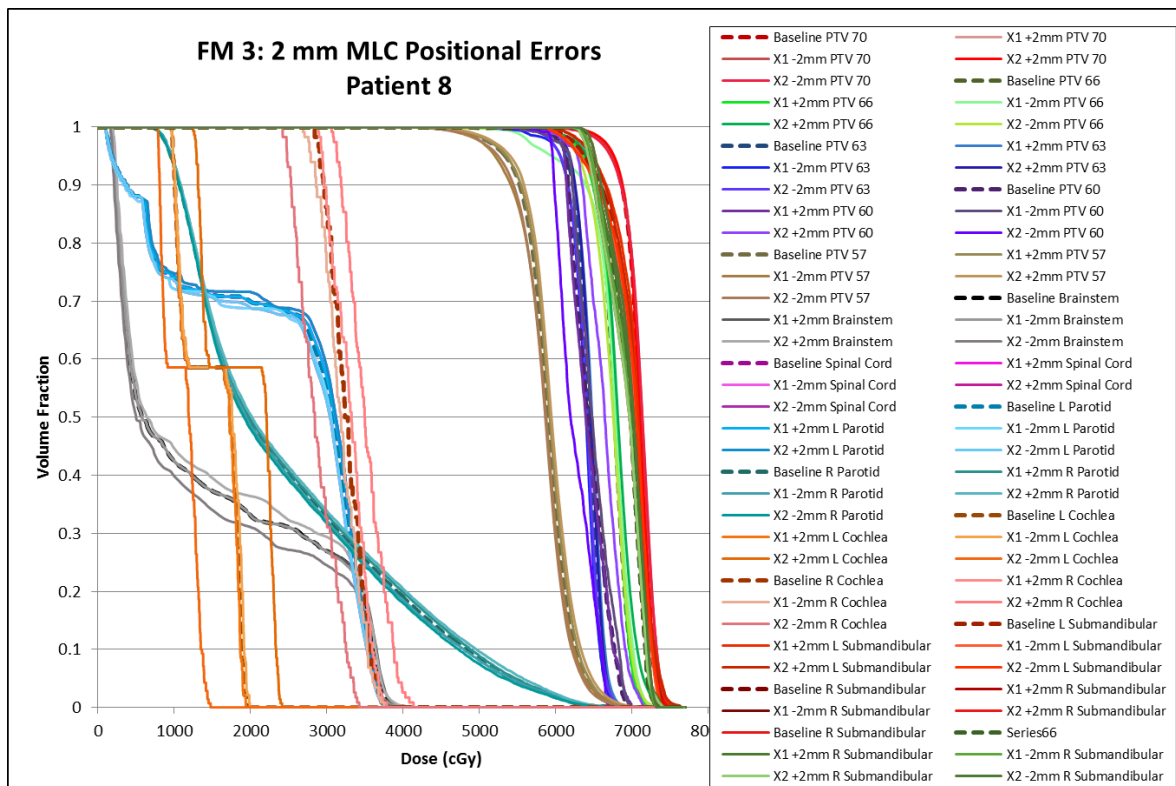


Figure 167: Failure mode 3 (with 2 mm errors) DVHs for patient 8.

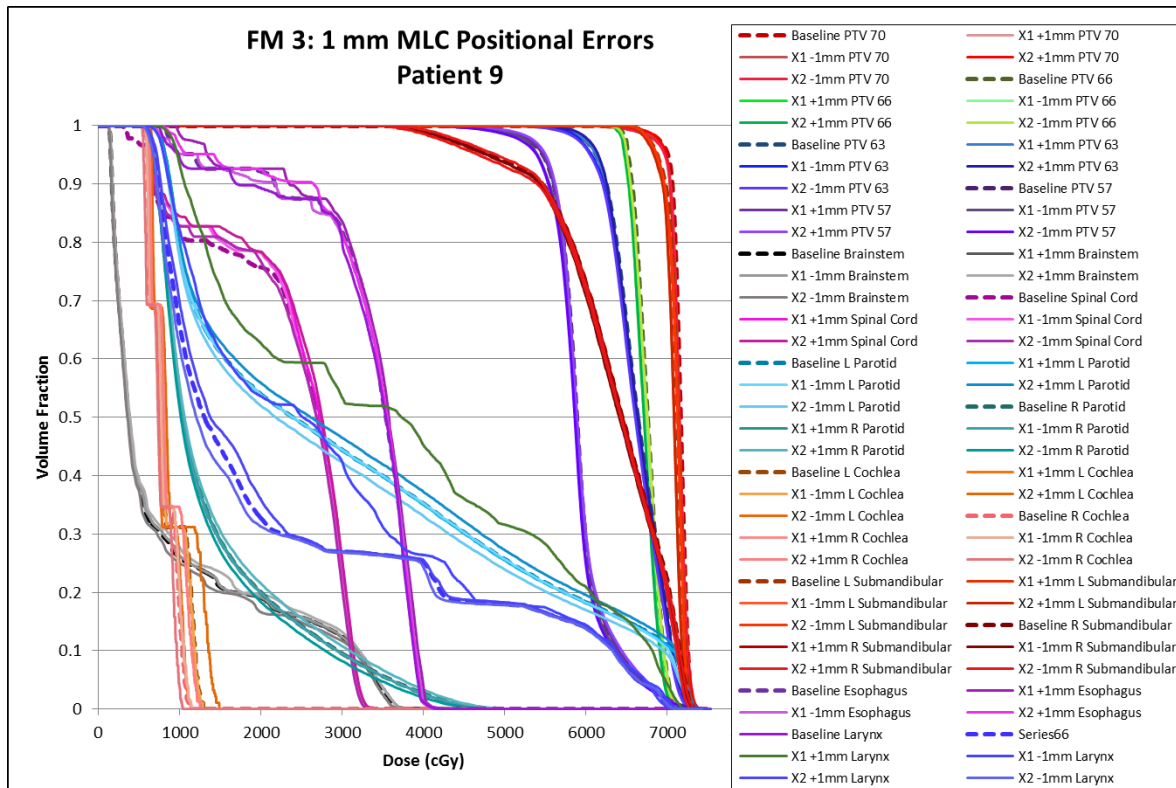


Figure 168: Failure mode 3 (with 1 mm errors) DVHs for patient 9.

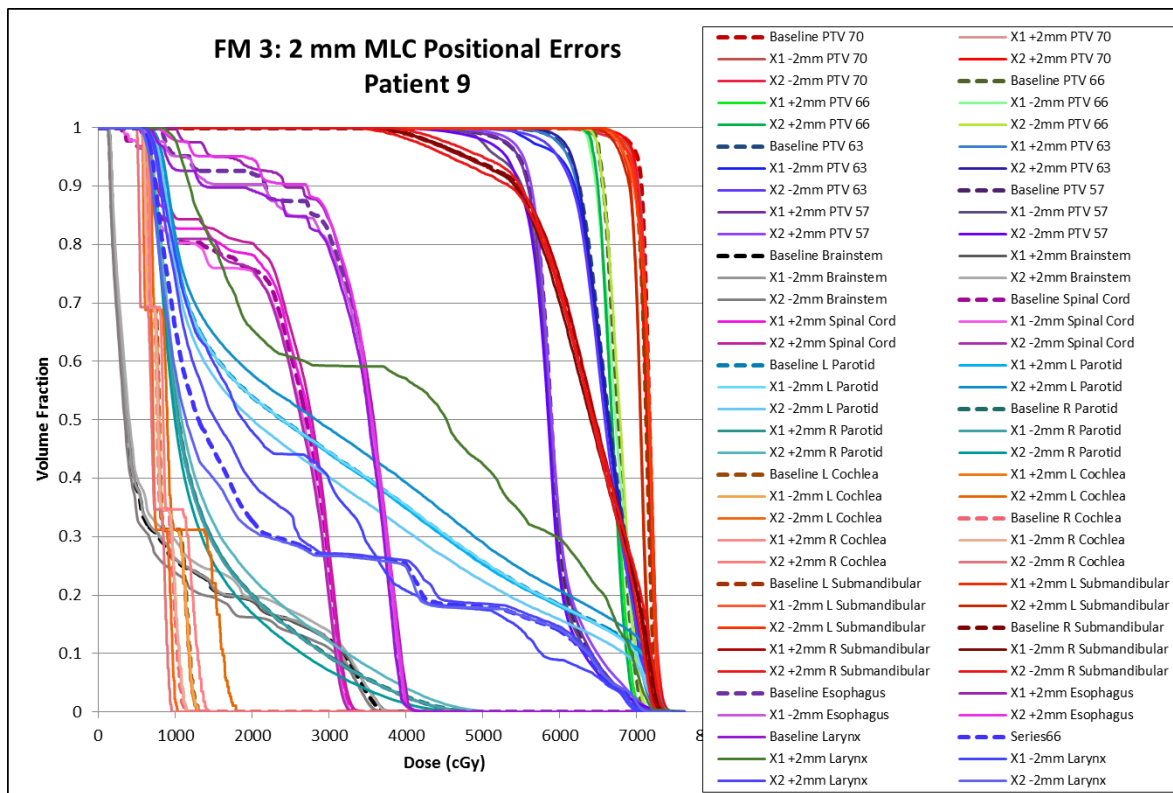


Figure 169: Failure mode 1 (with 2 mm errors) DVHs for patient 9.

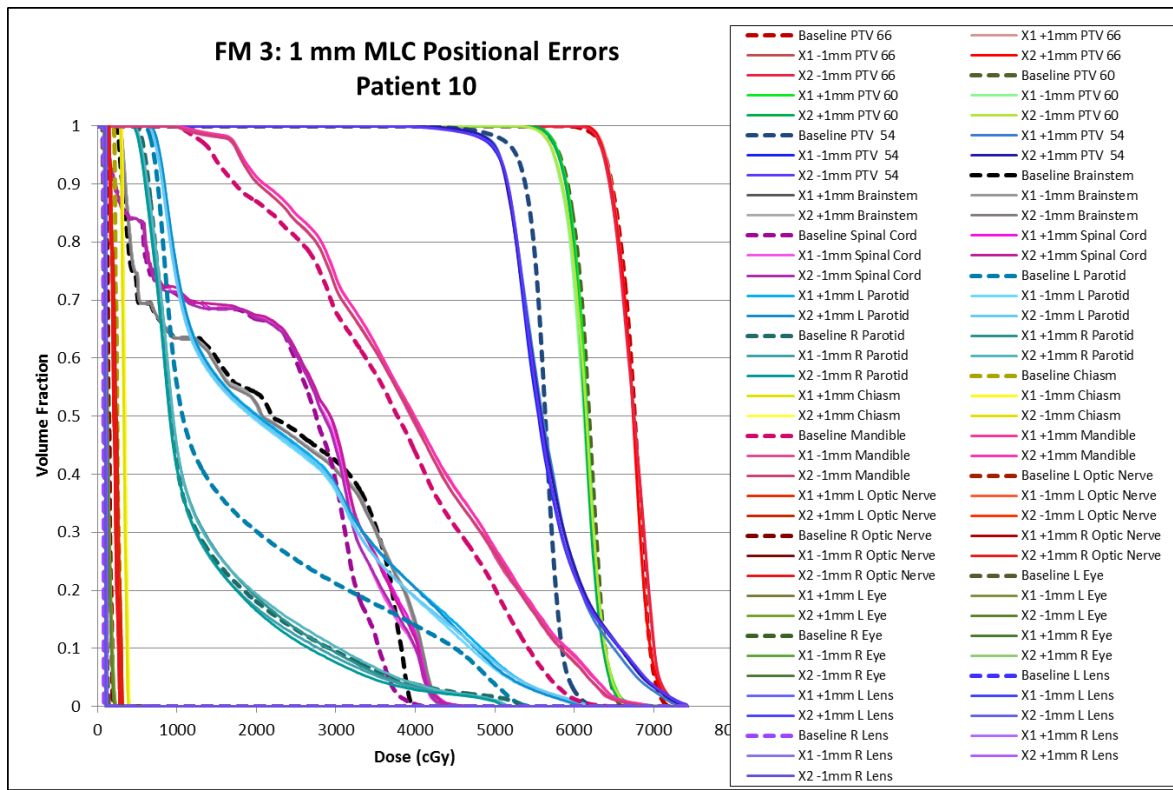


Figure 170: Failure mode 3 (with 1 mm errors) DVHs for patient 10.

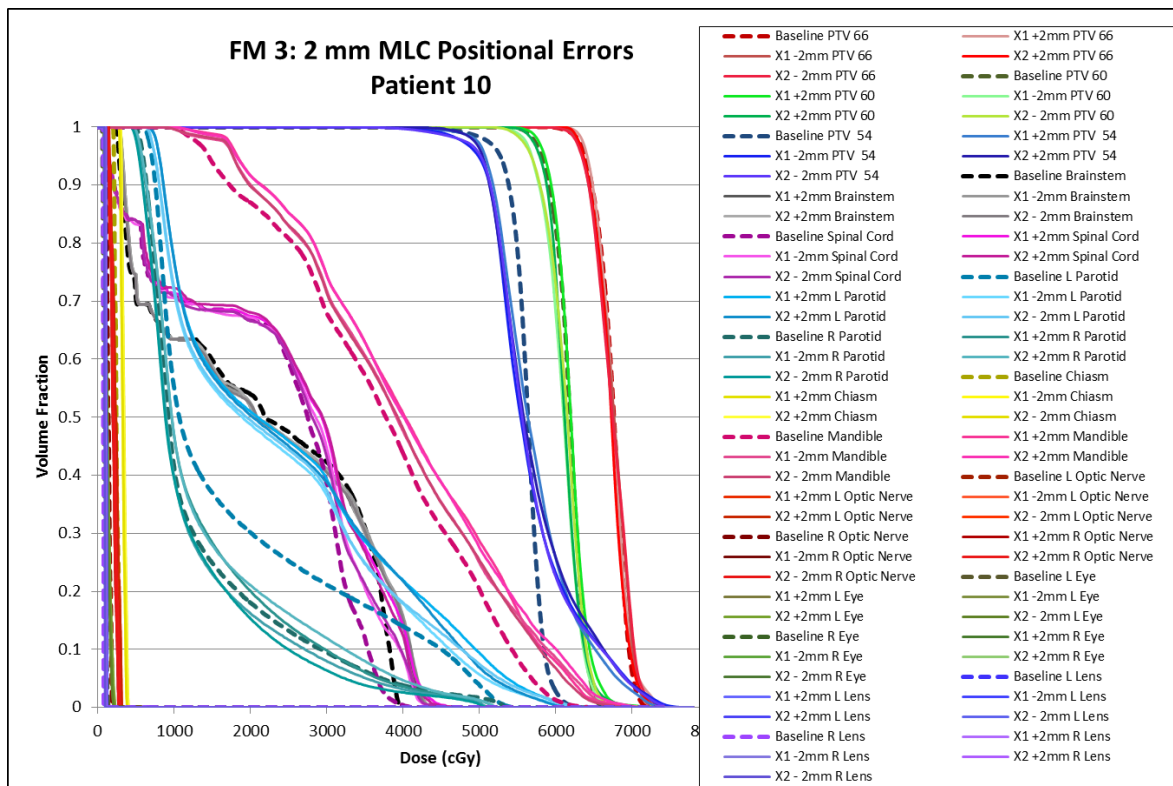


Figure 171: Failure mode 3 (with 2 mm errors) DVHs for patient 10.

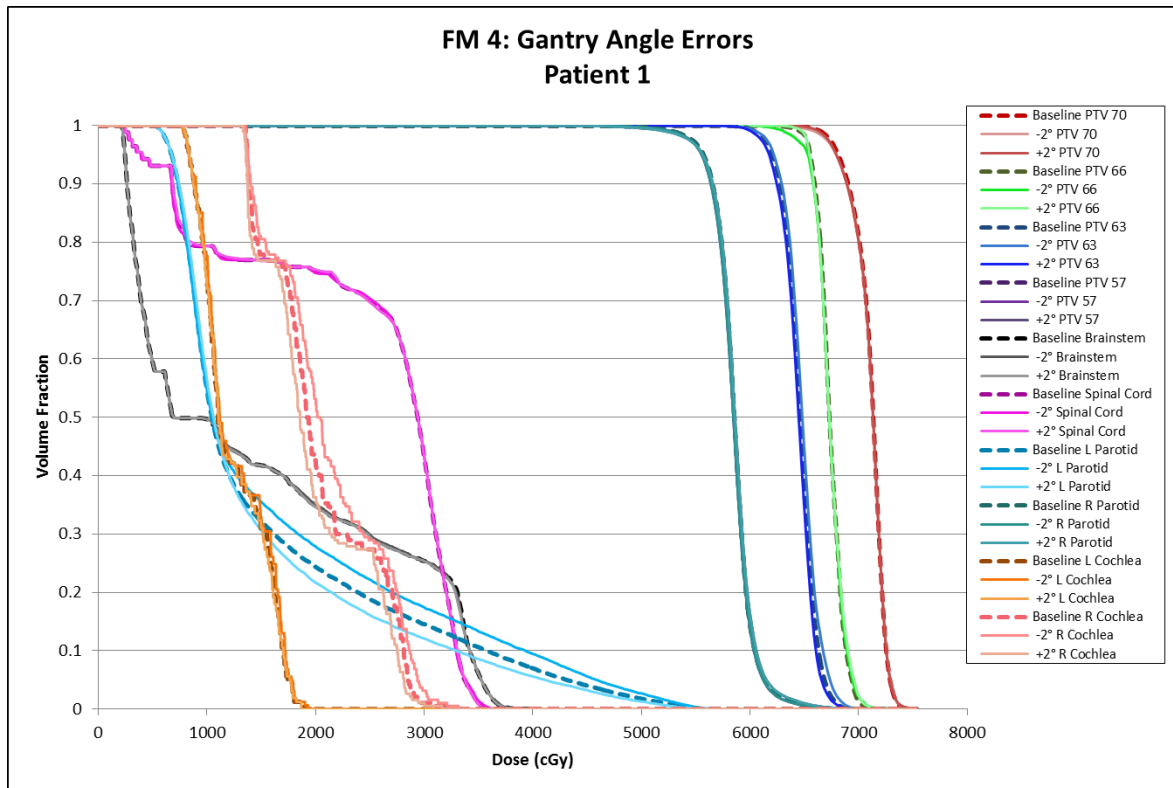


Figure 172: Failure mode 4 DVHs for patient 1.

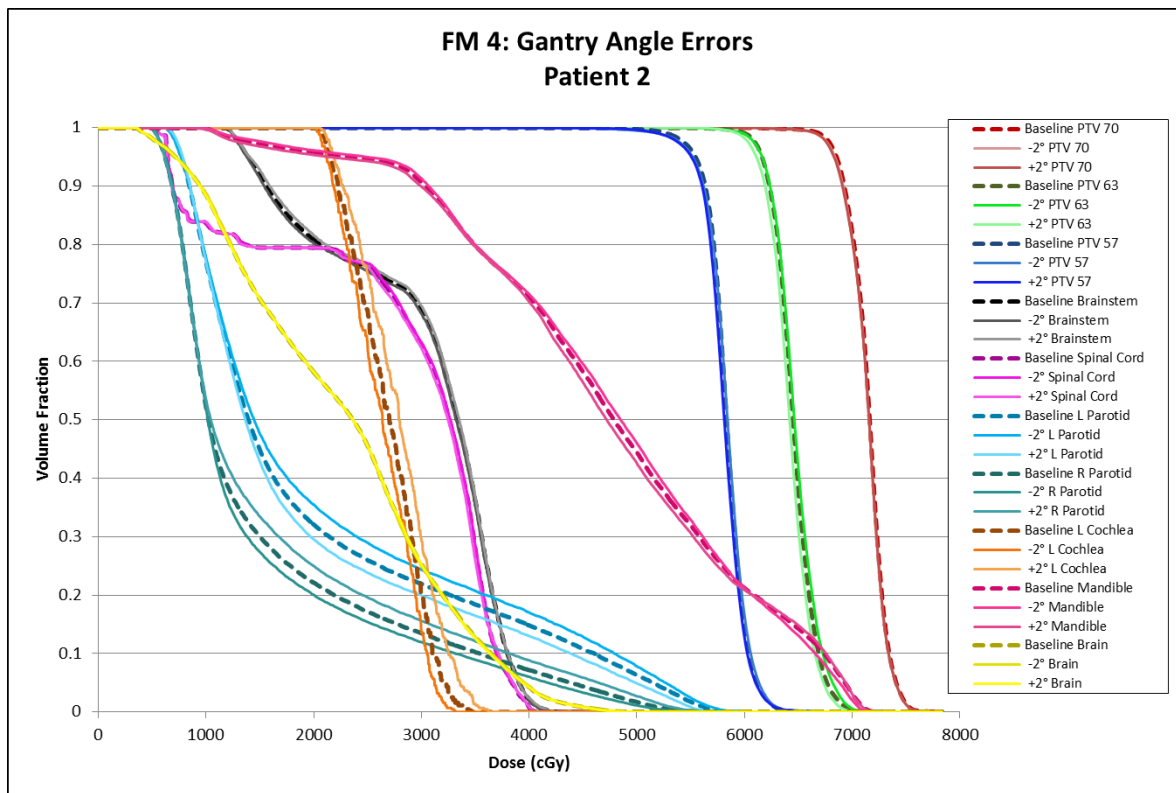


Figure 173: Failure mode 4 DVHs for patient 2.

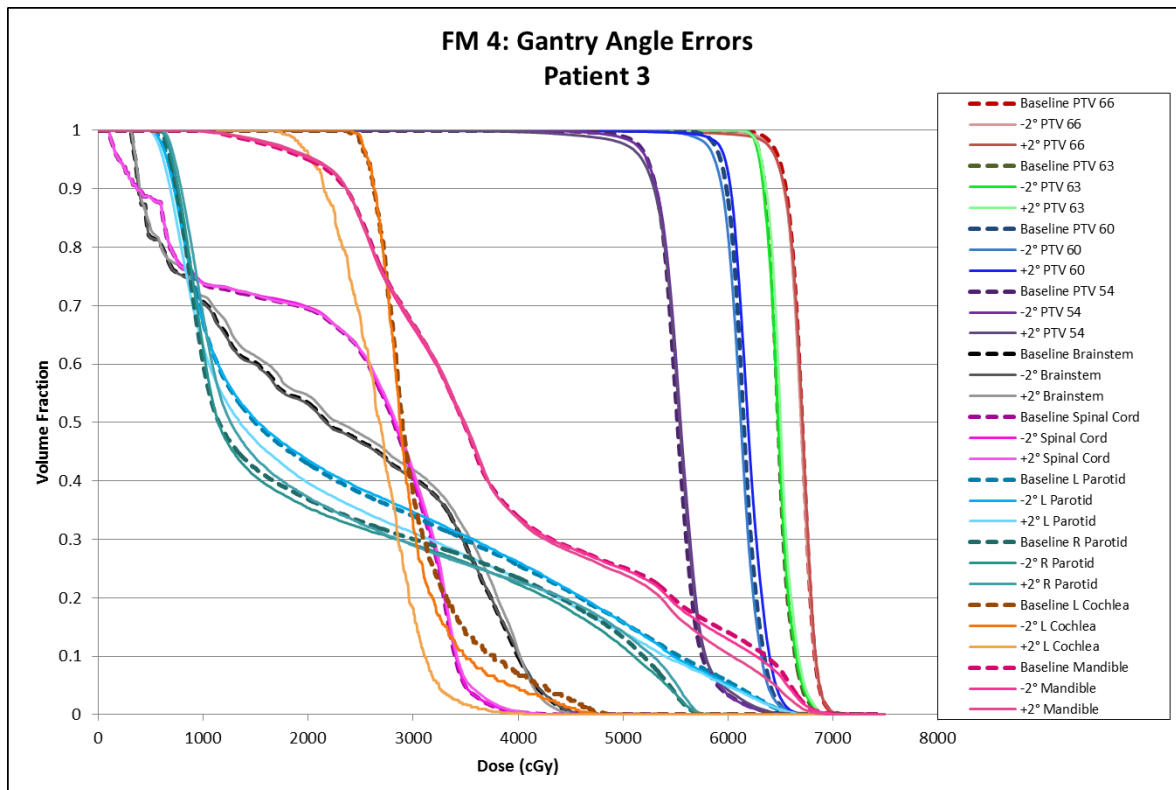


Figure 174: Failure mode 4 DVHs for patient 3.

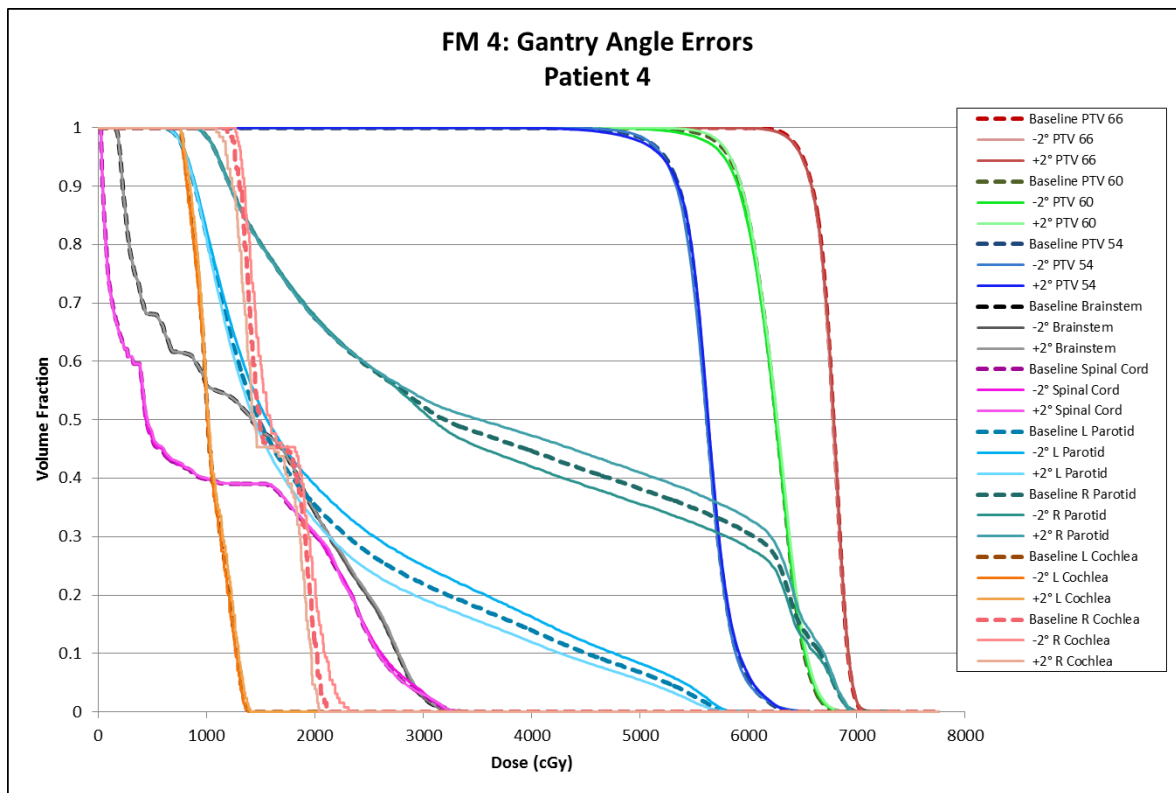


Figure 175: Failure mode 4 DVHs for patient 4.

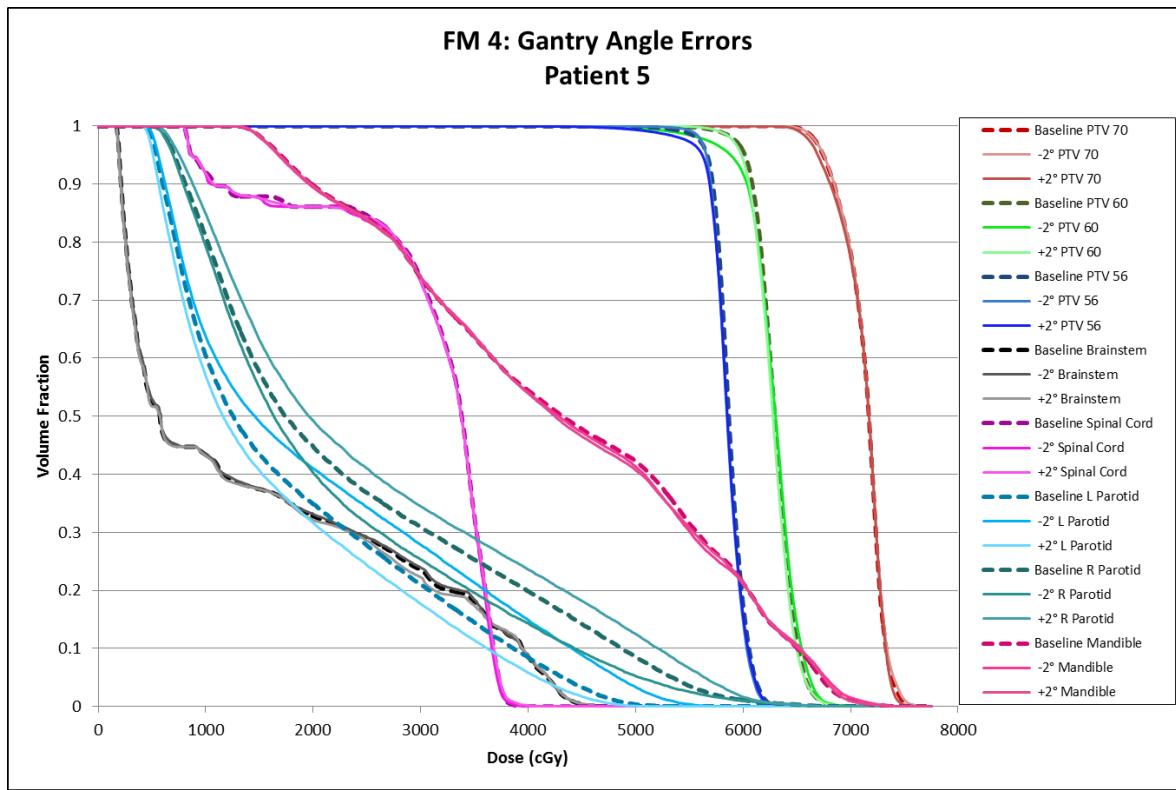


Figure 176: Failure mode 4 DVHs for patient 5.

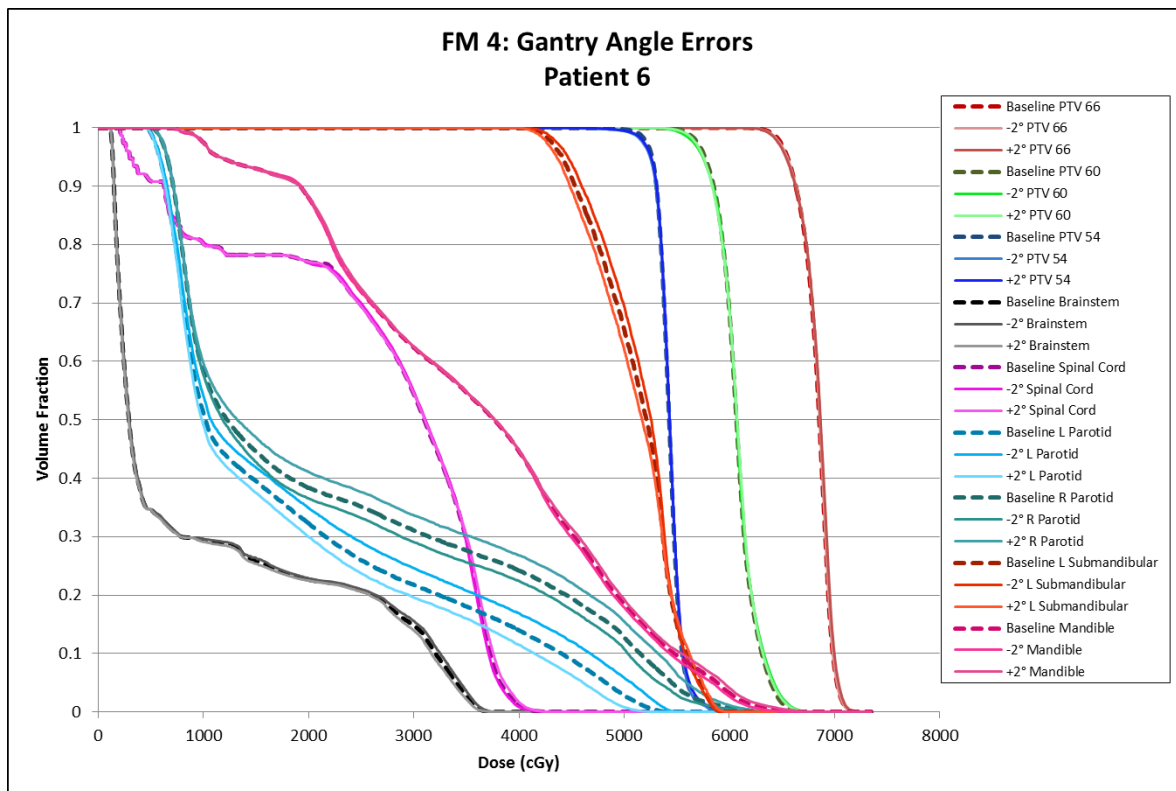


Figure 177: Failure mode 4 DVHs for patient 6.

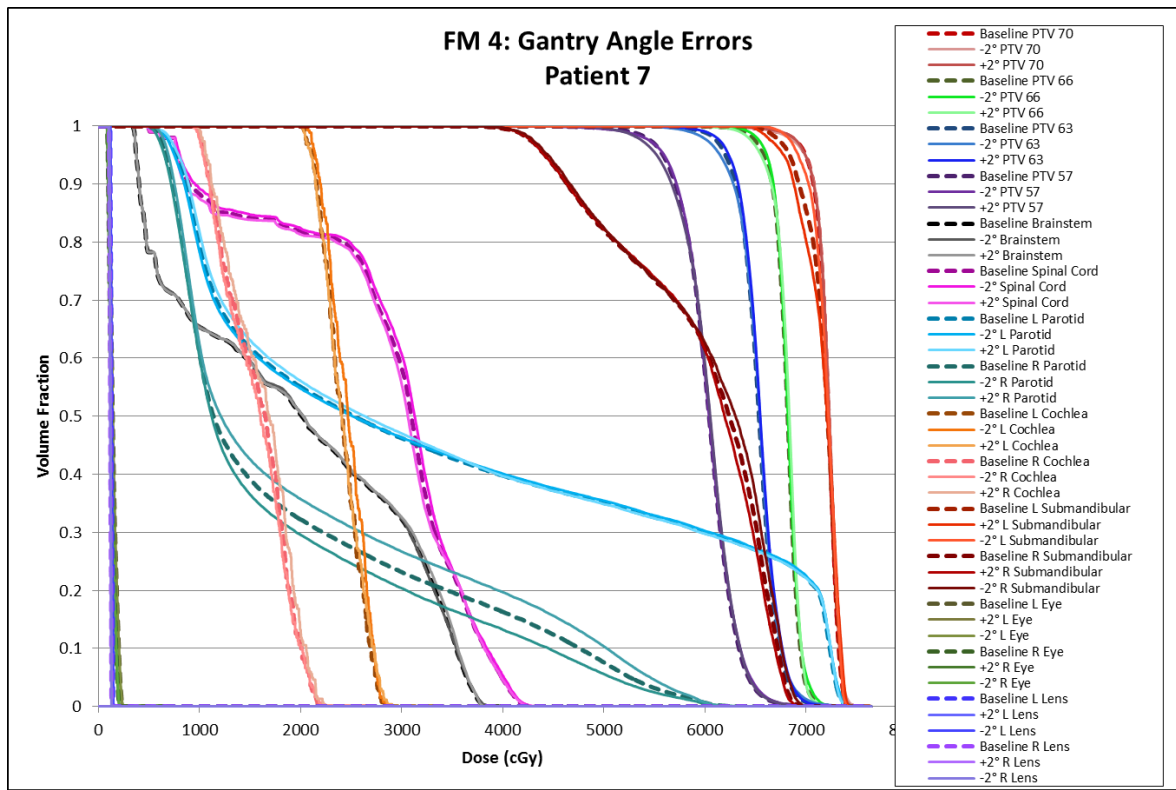


Figure 178: Failure mode 4 DVHs for patient 7.

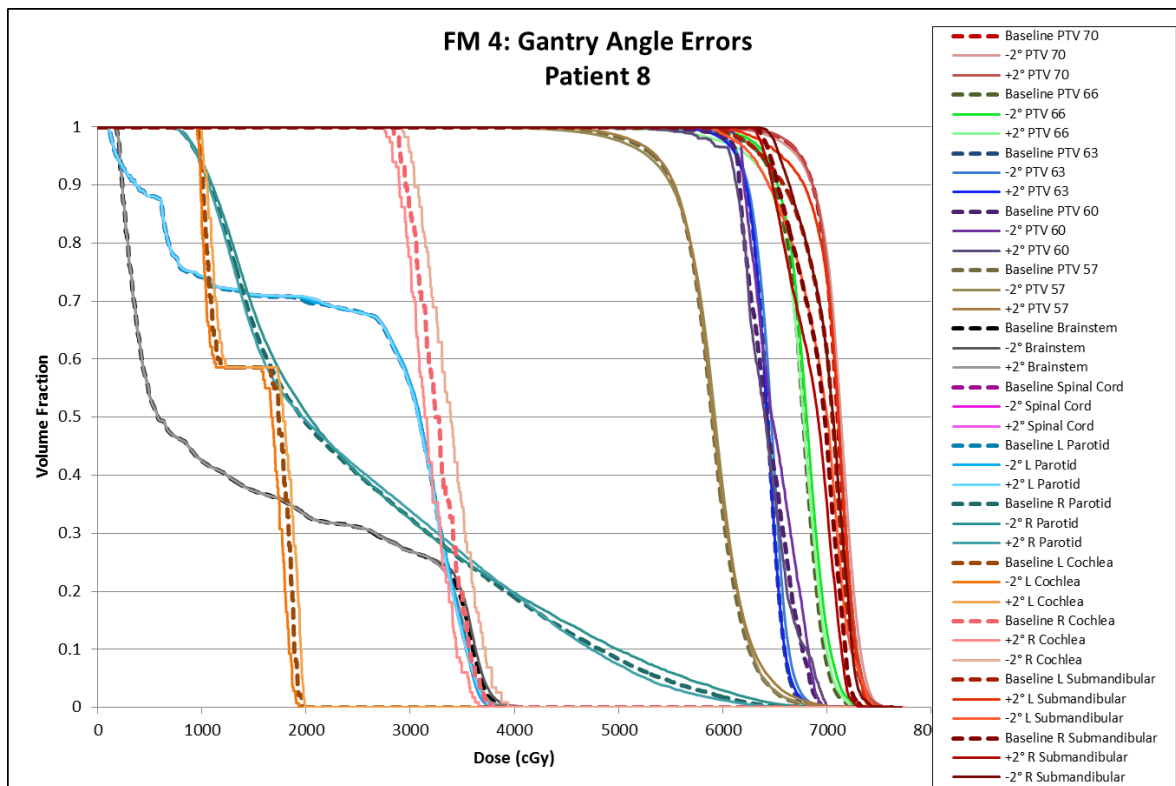


Figure 179: Failure mode 4 DVHs for patient 8.

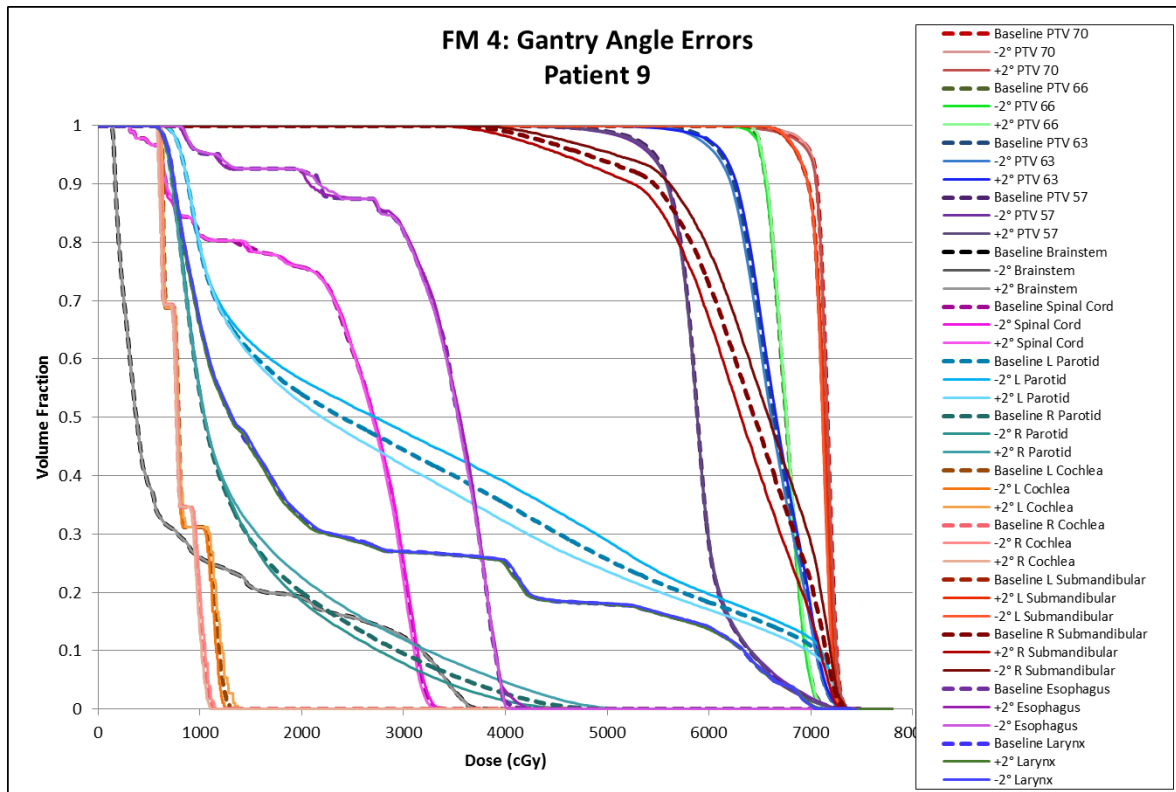


Figure 180: Failure mode 4 DVHs for patient 9.

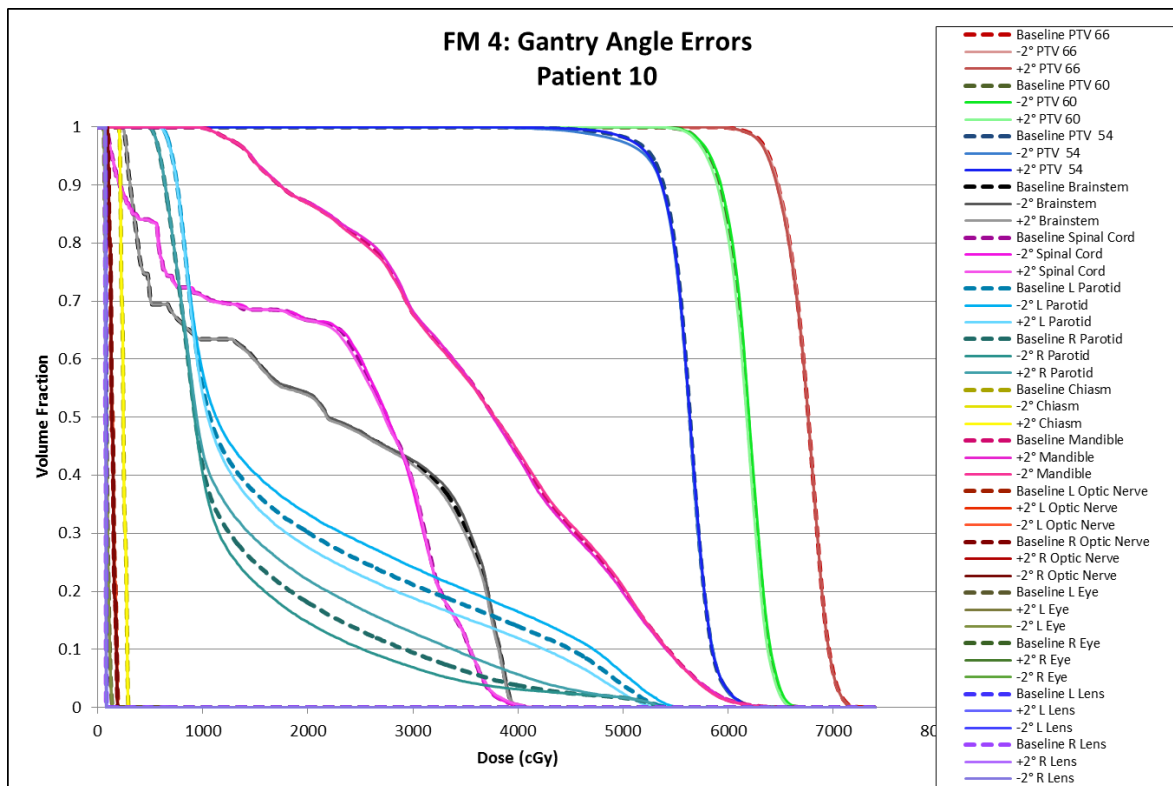


Figure 181: Failure mode 4 DVHs for patient 10.

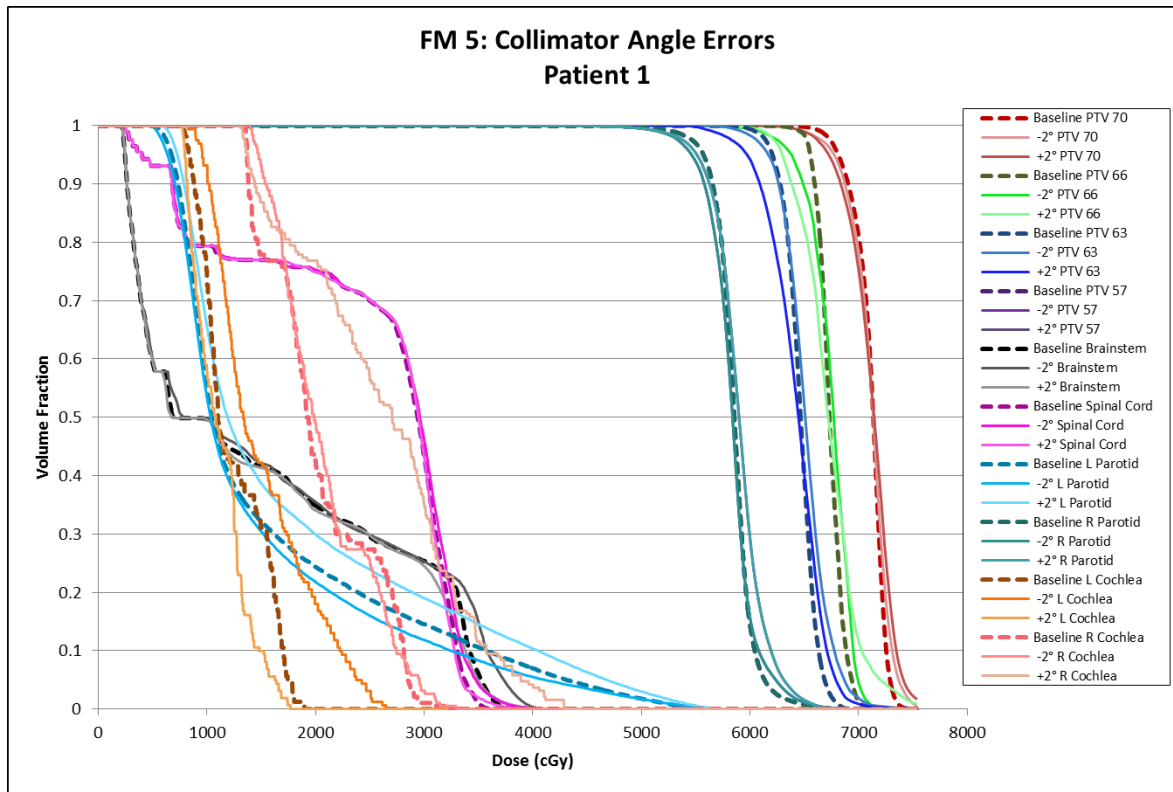


Figure 182: Failure mode 5 DVHs for patient 1.

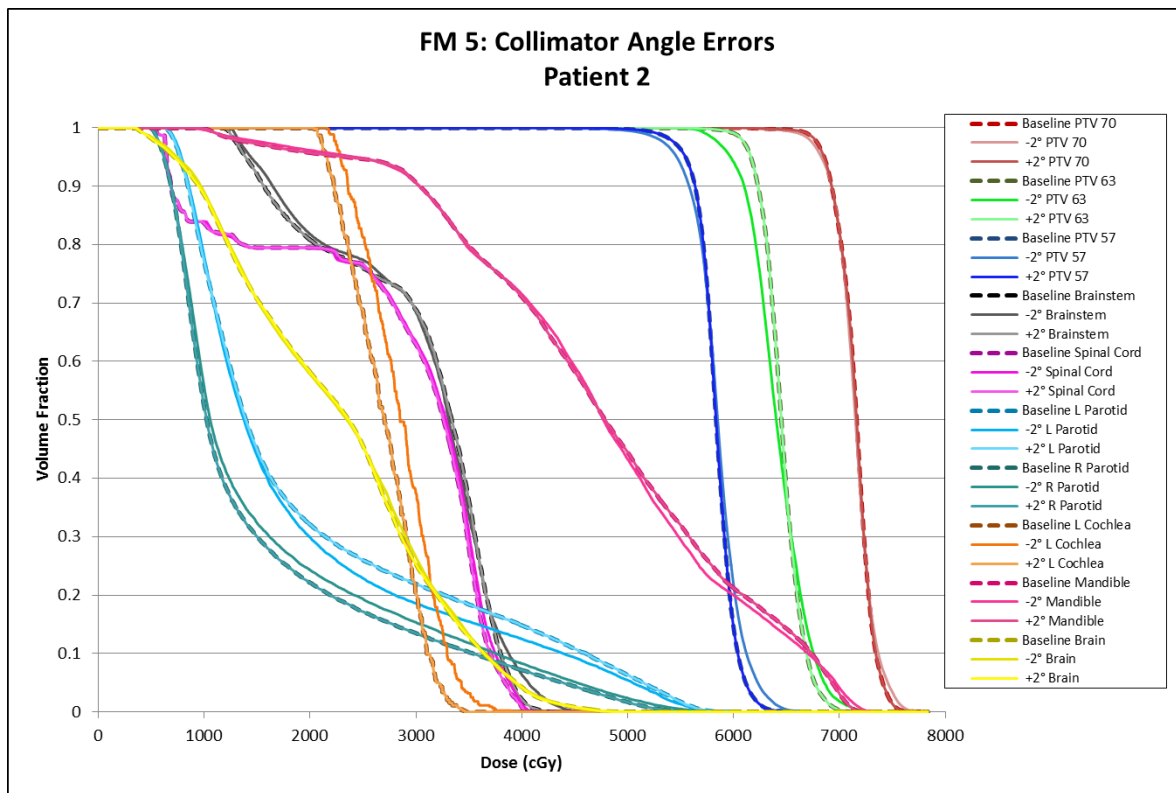


Figure 183: Failure mode 5 DVHs for patient 2.

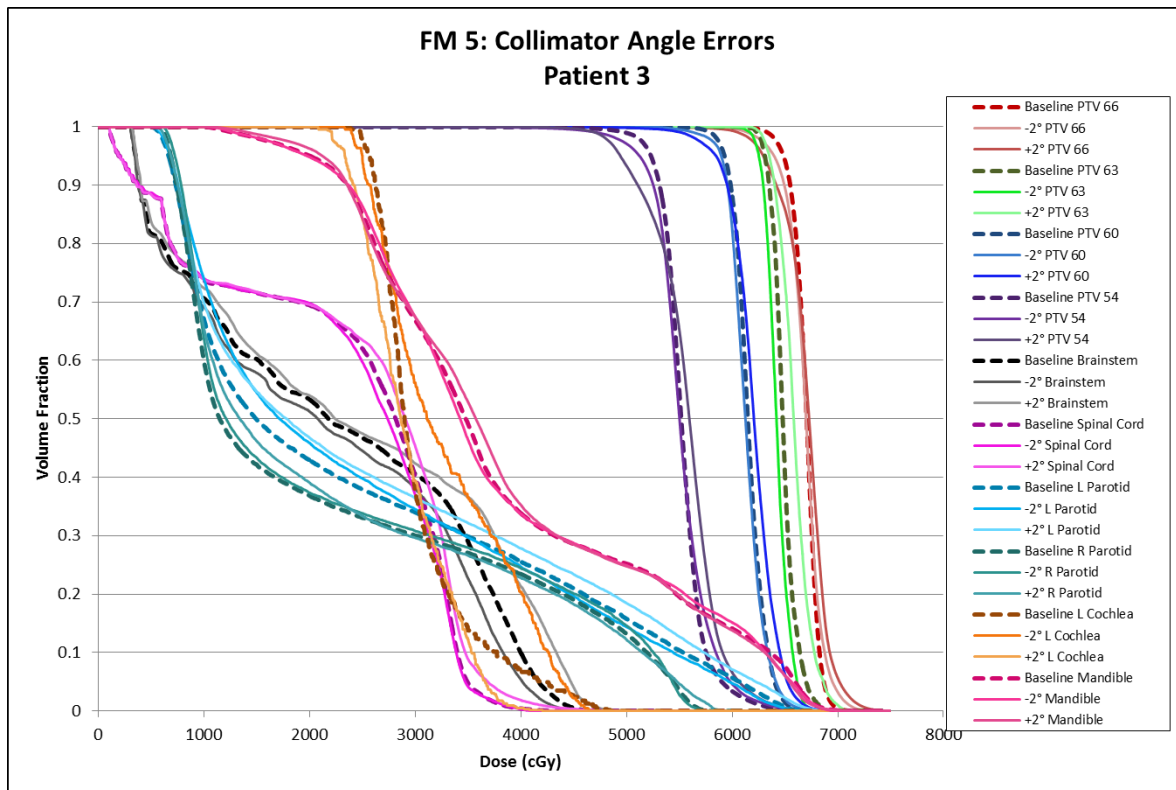


Figure 184: Failure mode 5 DVHs for patient 3.

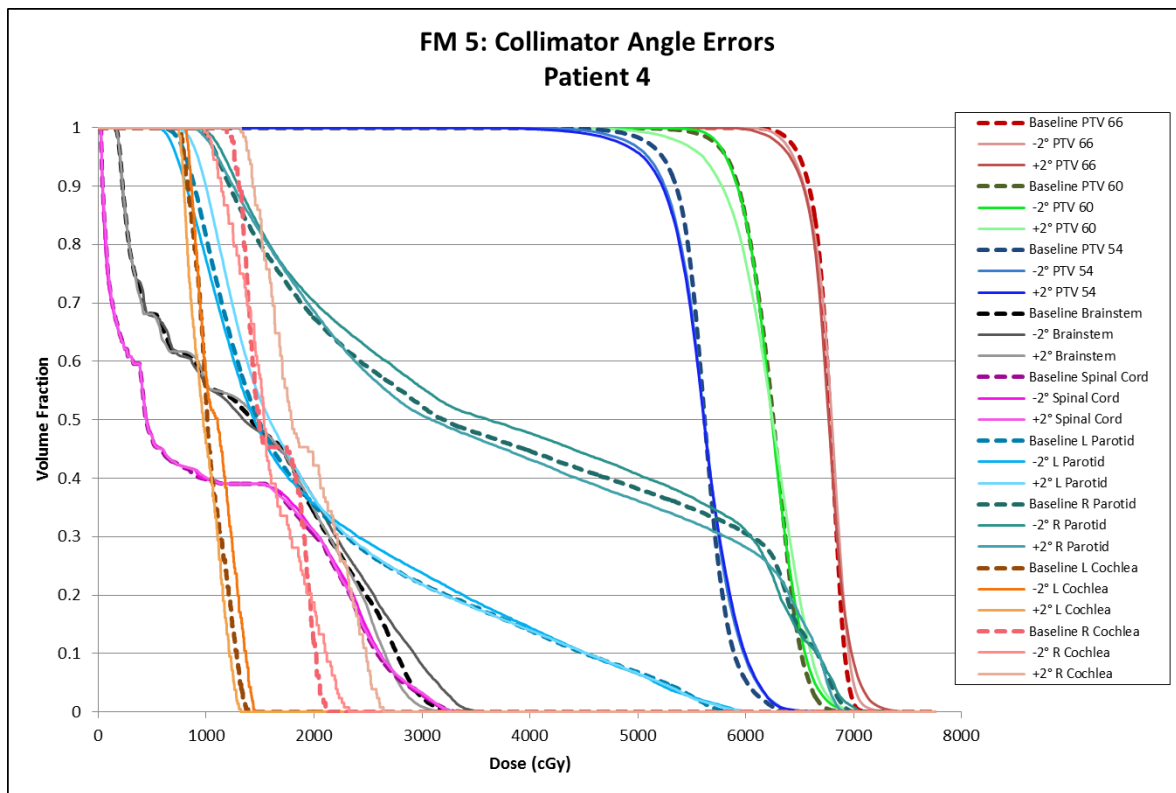


Figure 185: Failure mode 5 DVHs for patient 4.

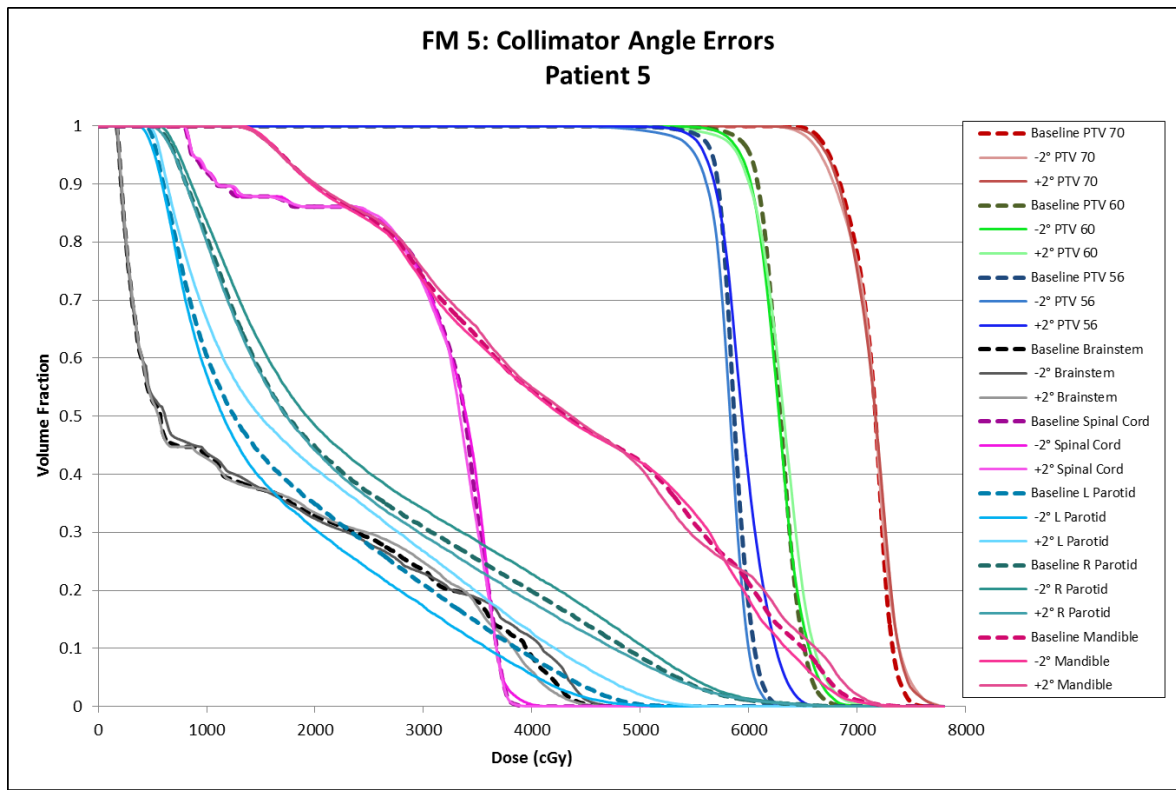


Figure 186: Failure mode 5 DVHs for patient 5.

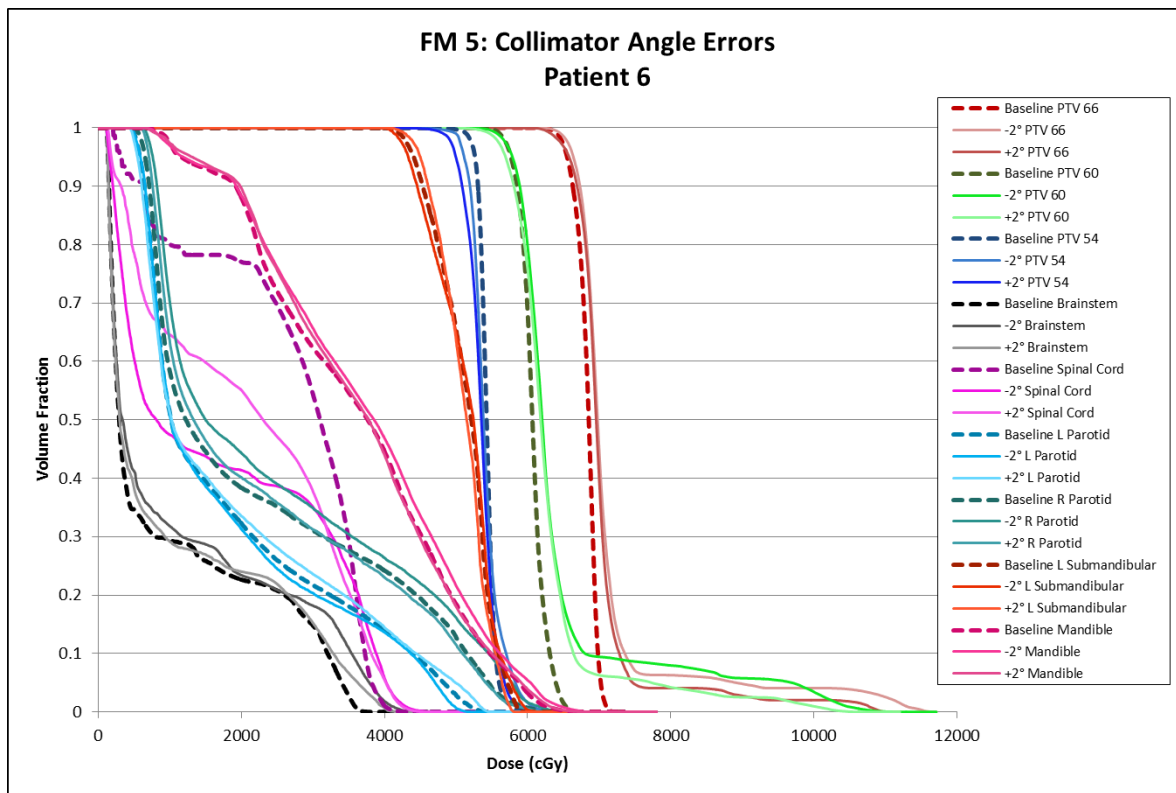


Figure 187: Failure mode 5 DVHs for patient 6.

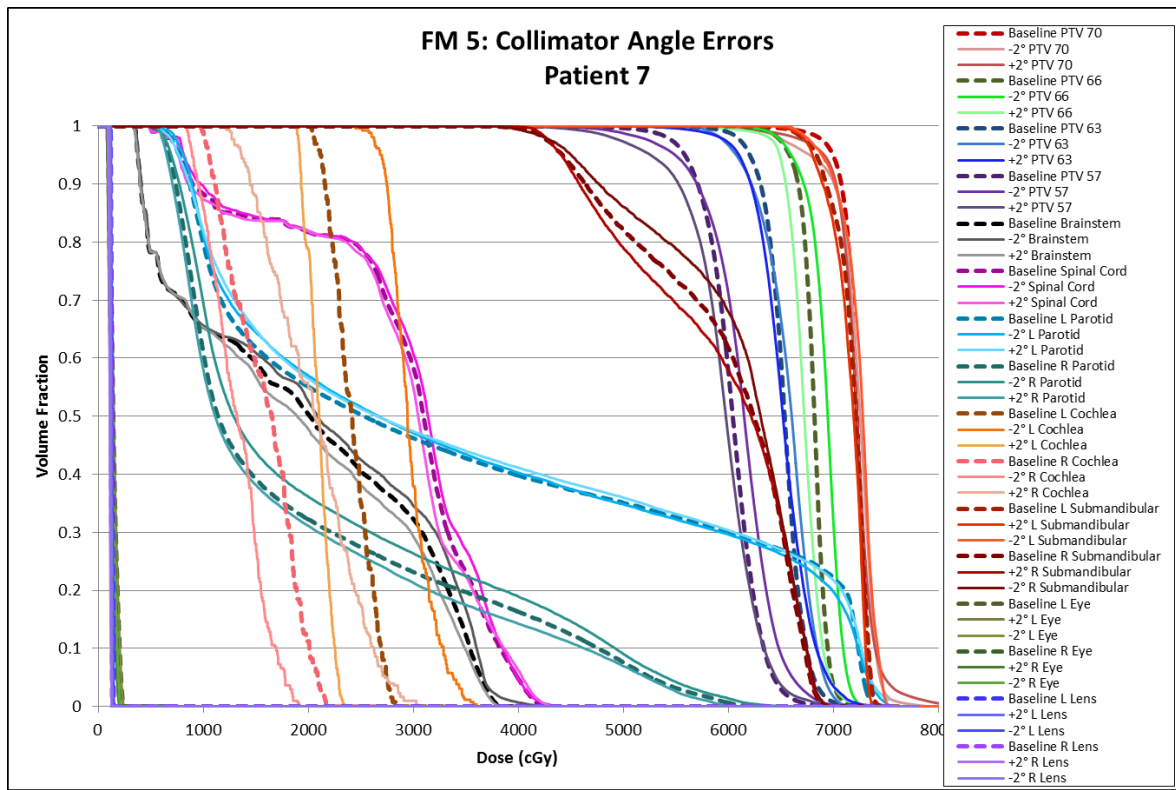


Figure 188: Failure mode 5 DVHs for patient 7.

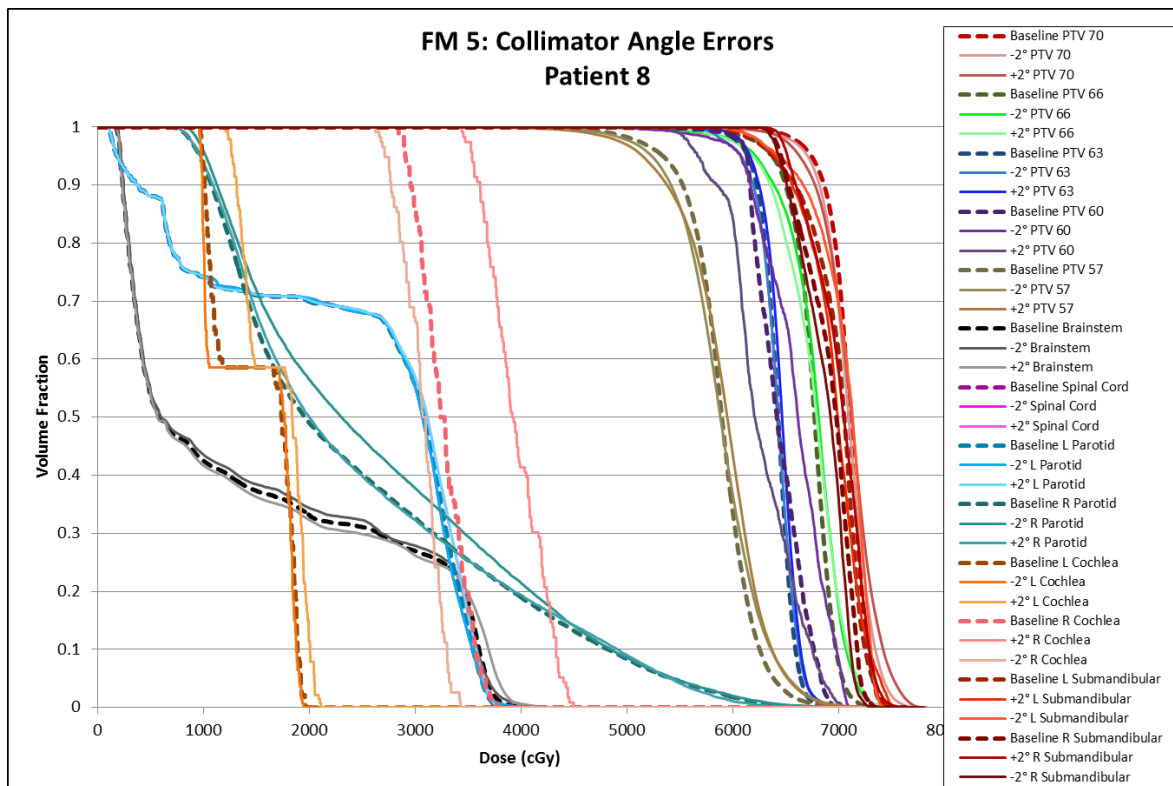


Figure 189: Failure mode 5 DVHs for patient 8.

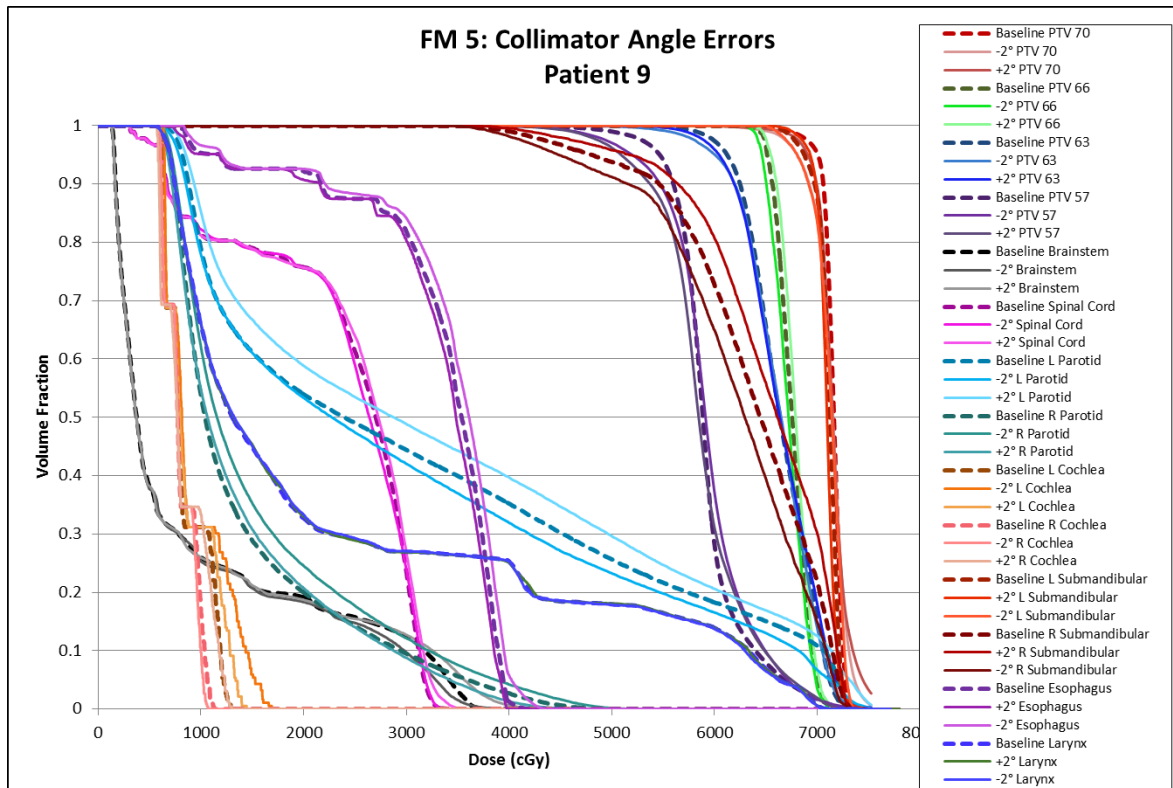


Figure 190: Failure mode 5 DVHs for patient 9.

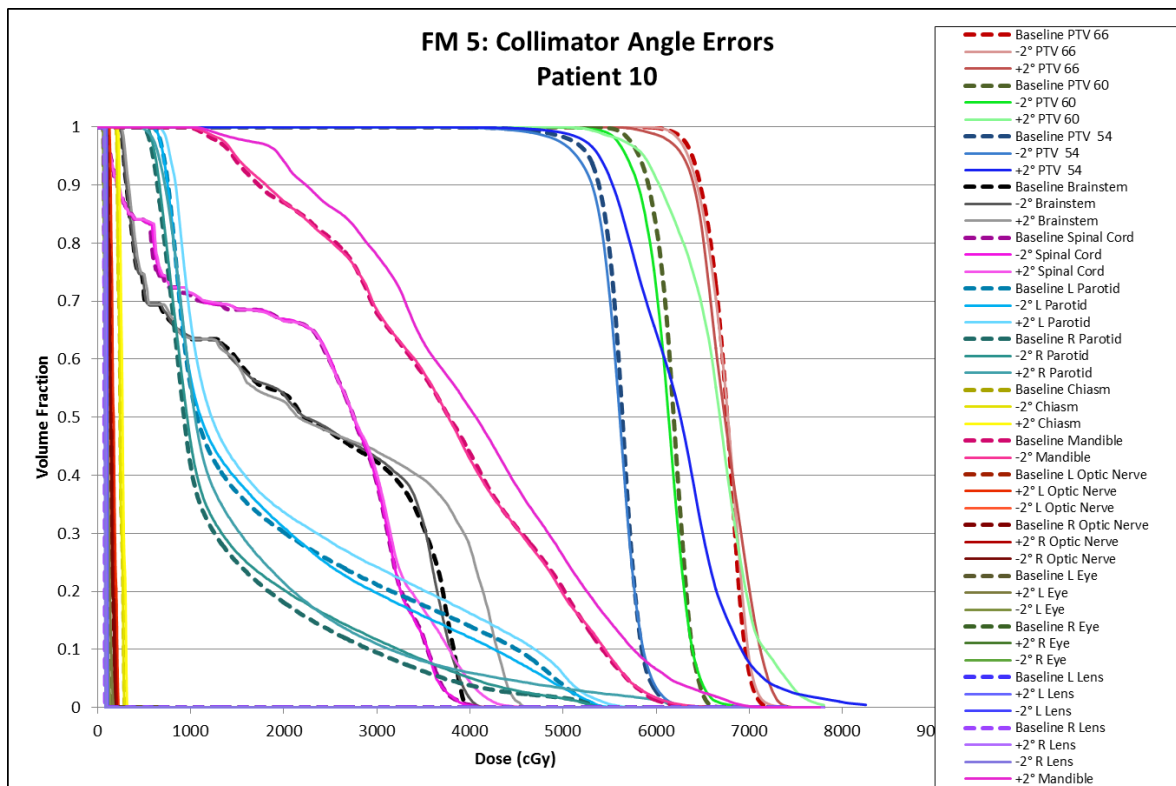


Figure 191: Failure mode 5 DVHs for patient 10.

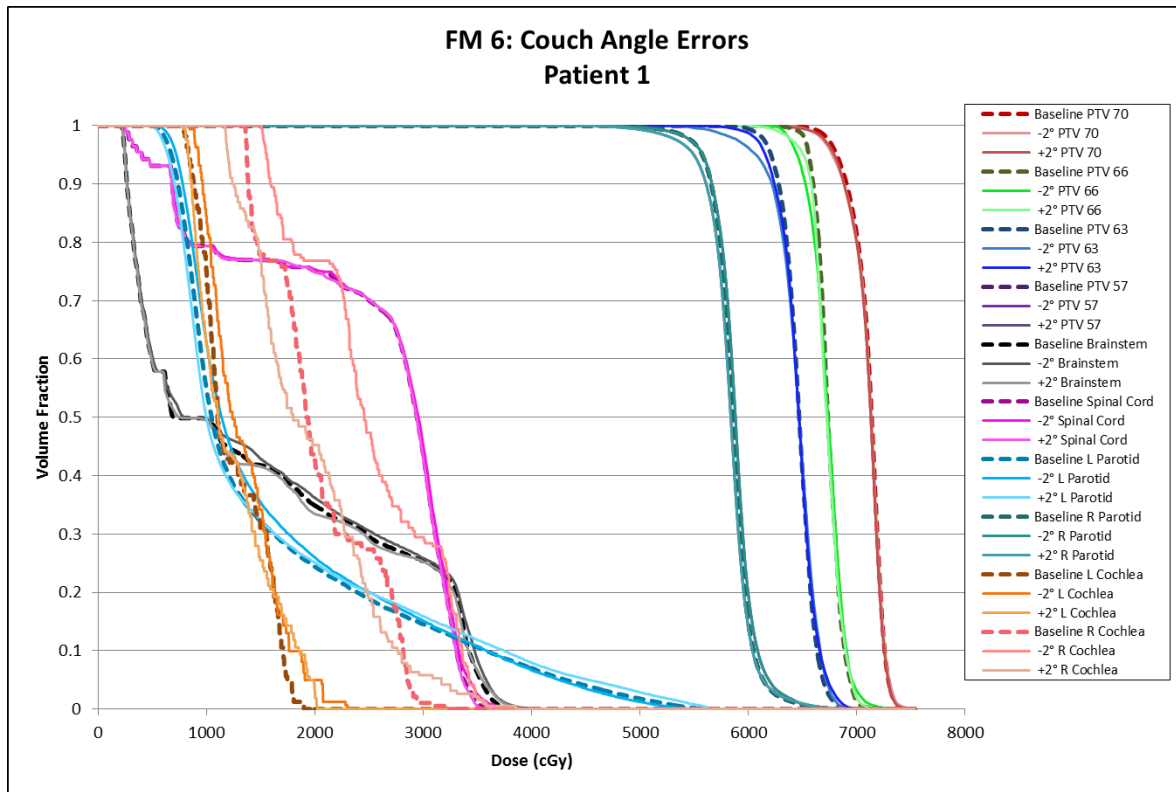


Figure 192: Failure mode 6 DVHs for patient 1.

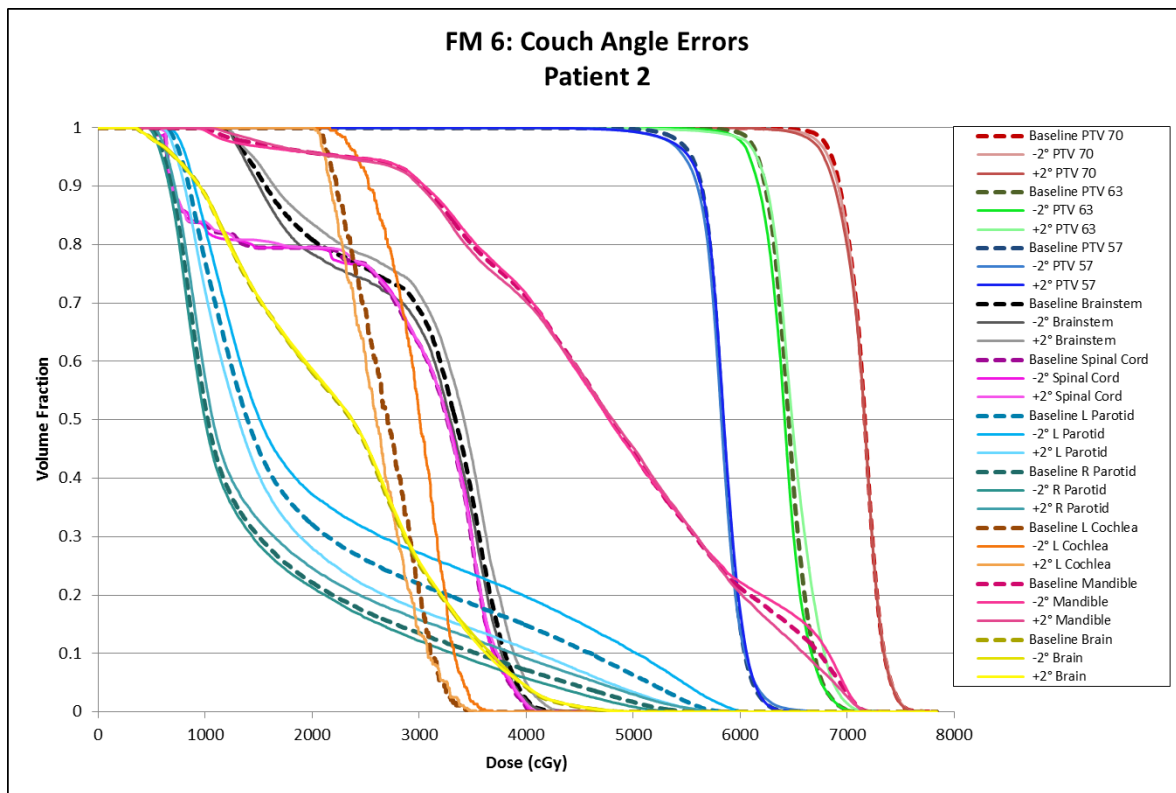


Figure 193: Failure mode 6 DVHs for patient 2.

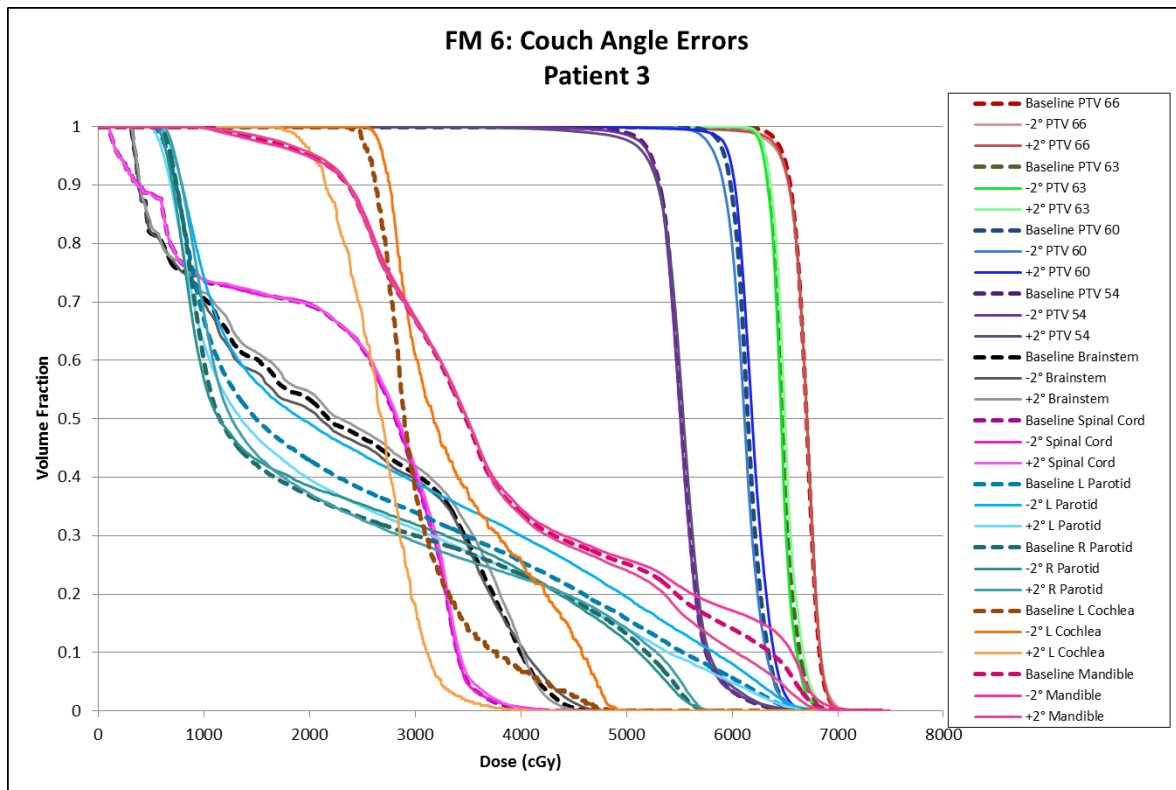


Figure 194: Failure mode 6 DVHs for patient 3.

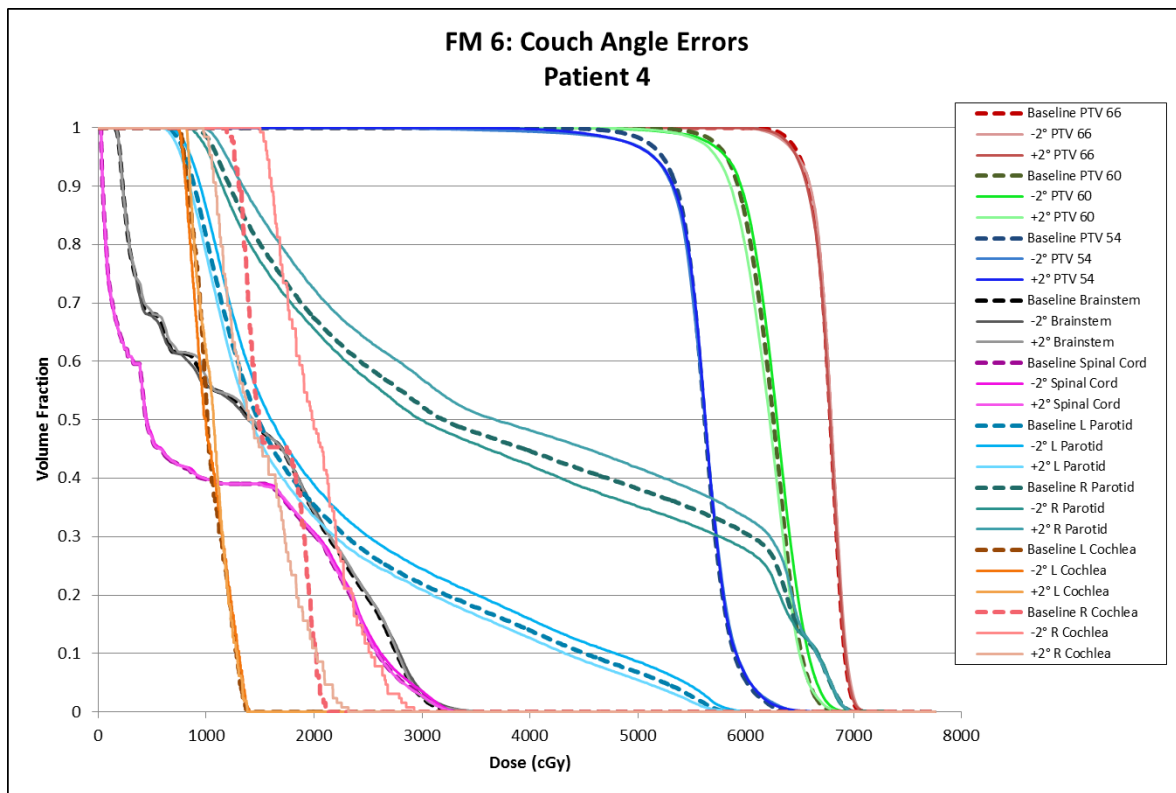


Figure 195: Failure mode 6 DVHs for patient 4.

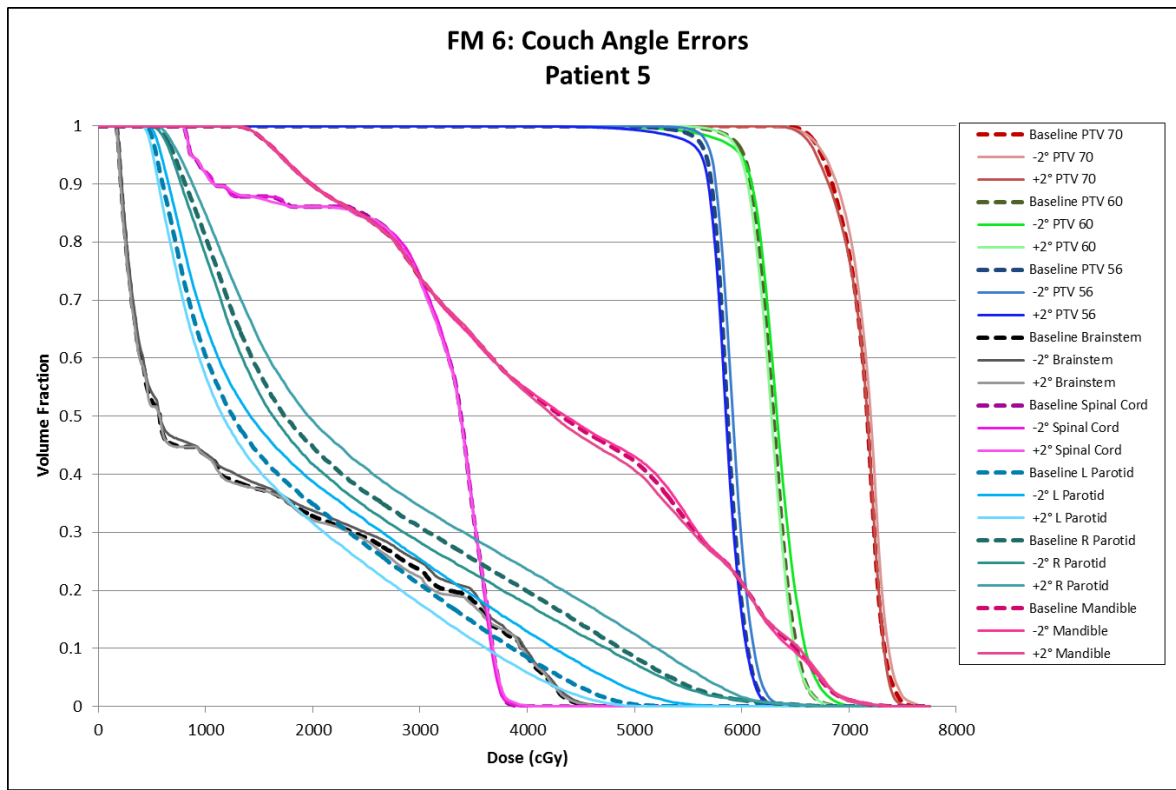


Figure 196: Failure mode 6 DVHs for patient 5.

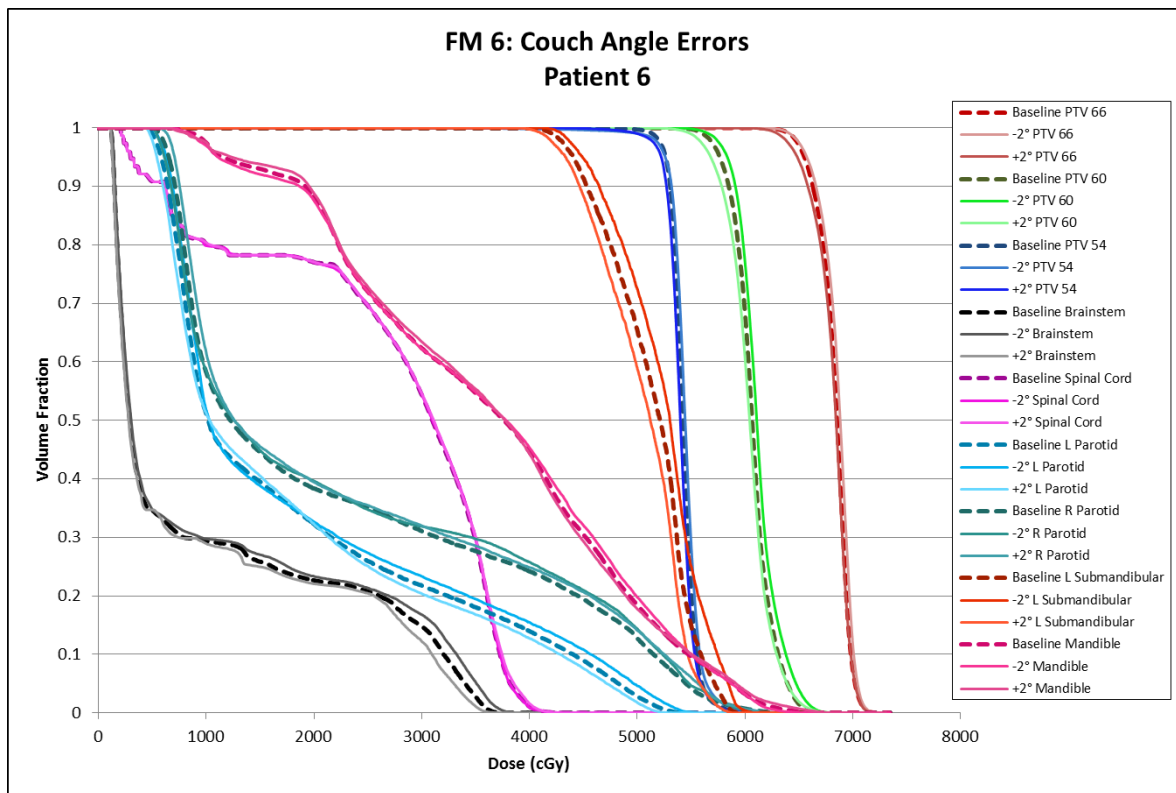


Figure 197: Failure mode 6 DVHs for patient 6.

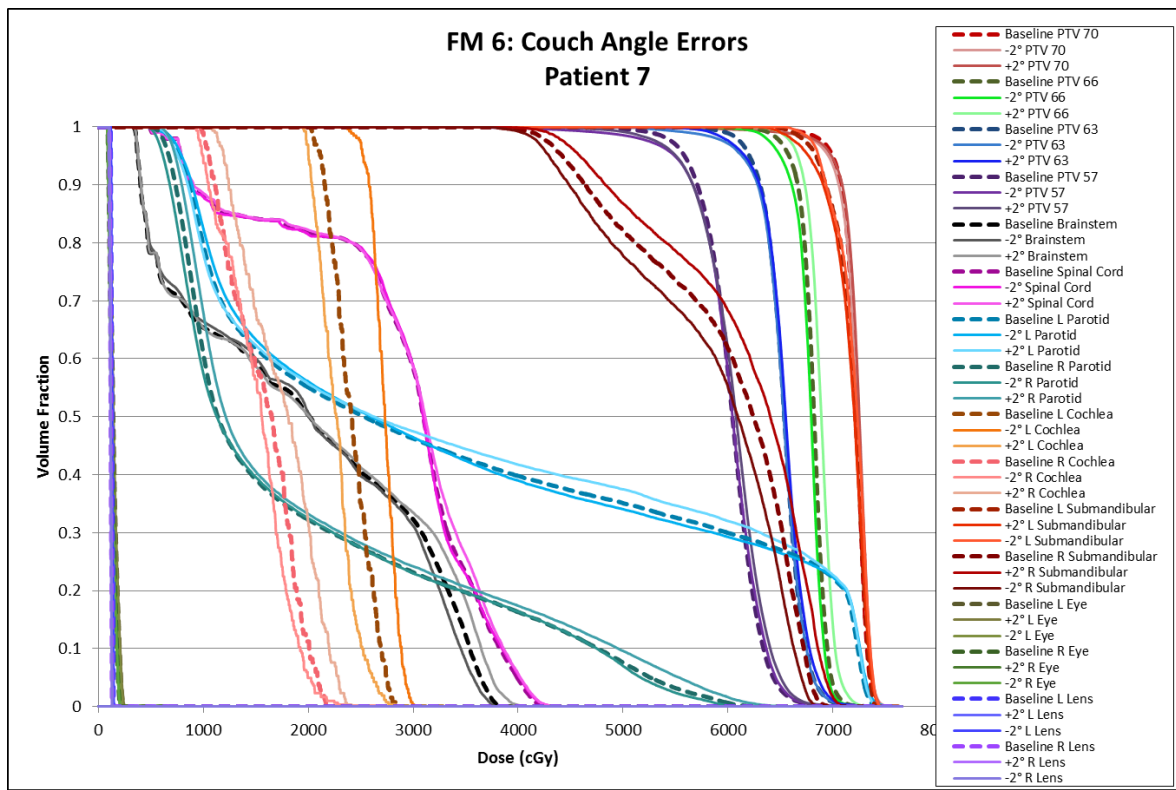


Figure 198: Failure mode 6 DVHs for patient 7.

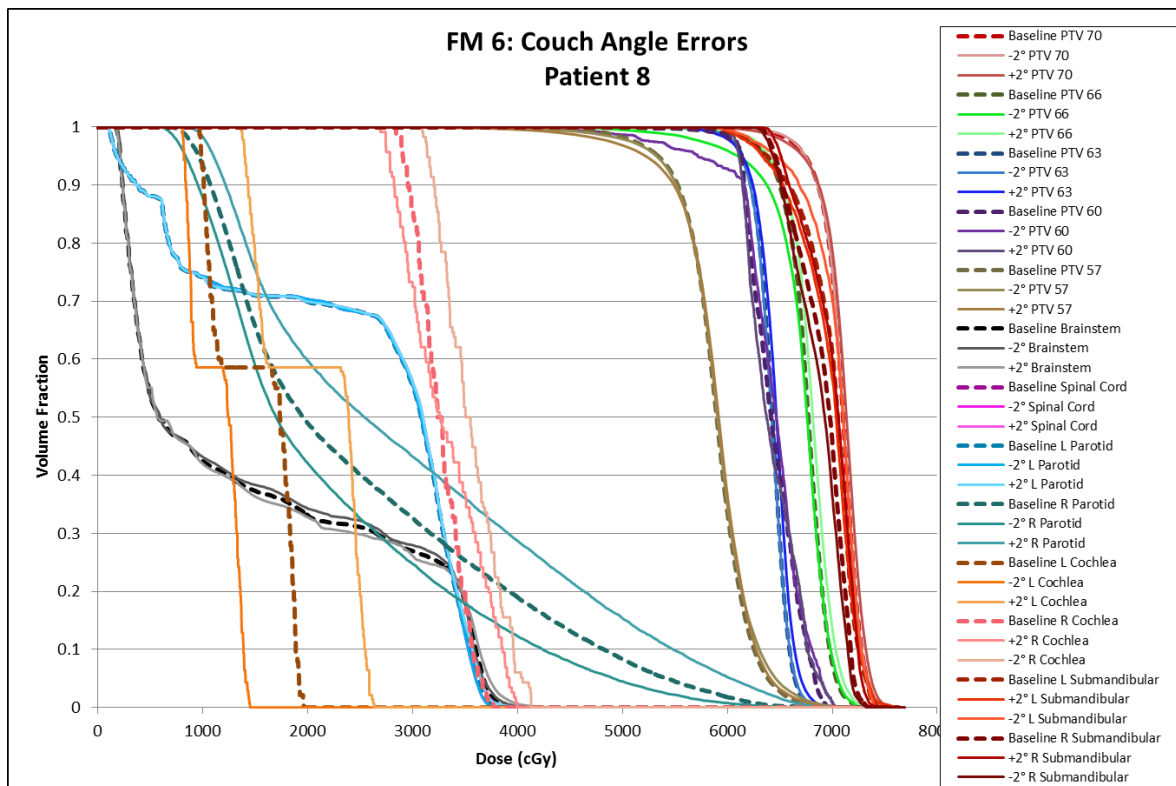


Figure 199: Failure mode 6 DVHs for patient 8.

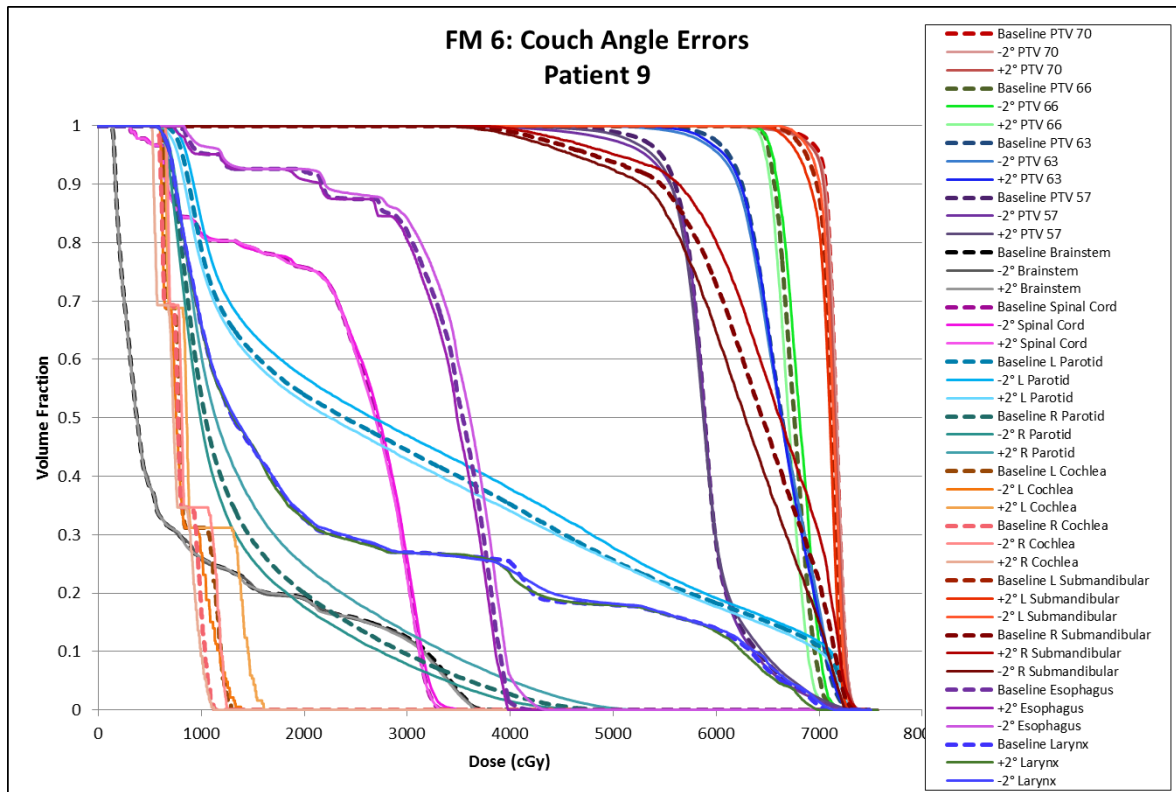


Figure 200: Failure mode 6 DVHs for patient 9.

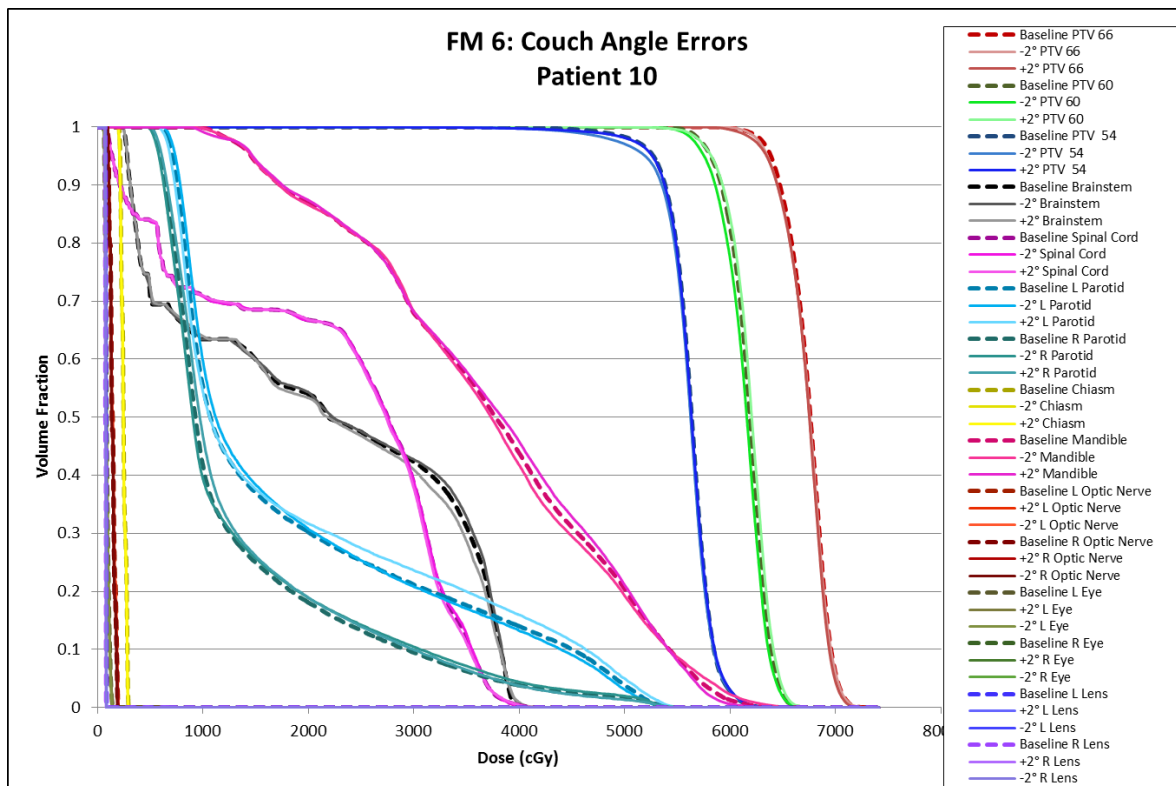


Figure 201: Failure mode 6 DVHs for patient 10.

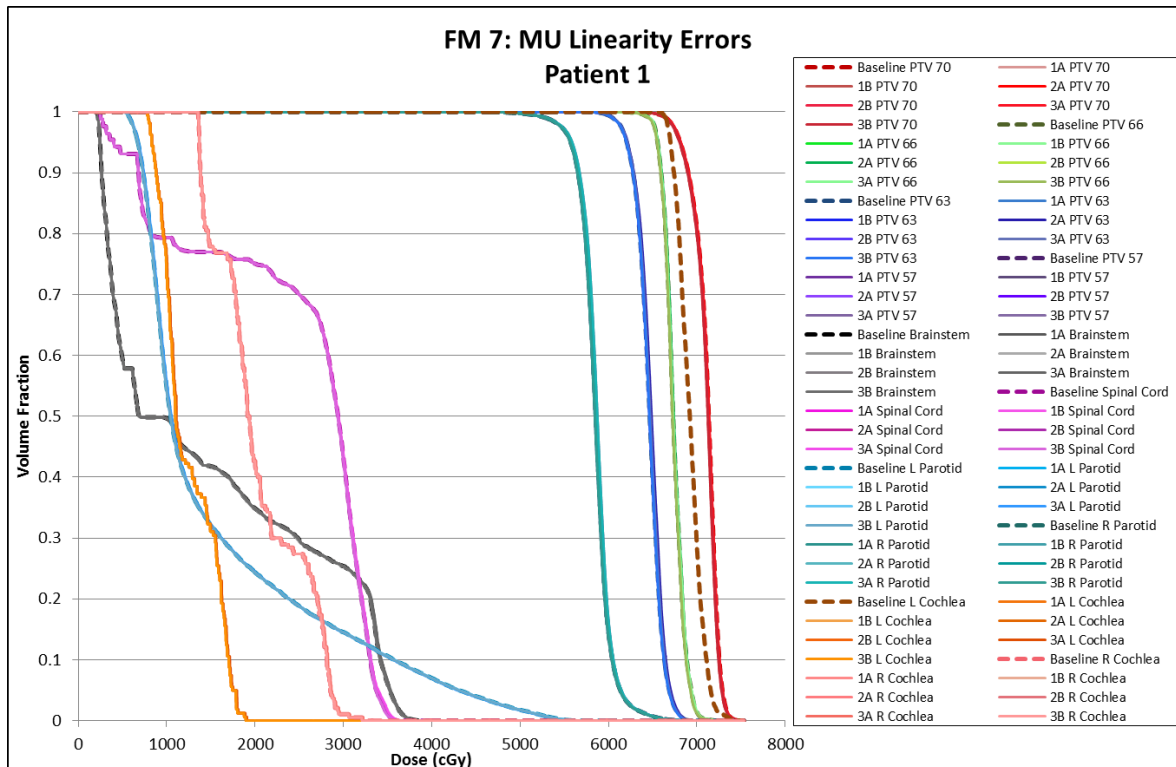


Figure 202: Failure mode 7 DVHs for patient 1.

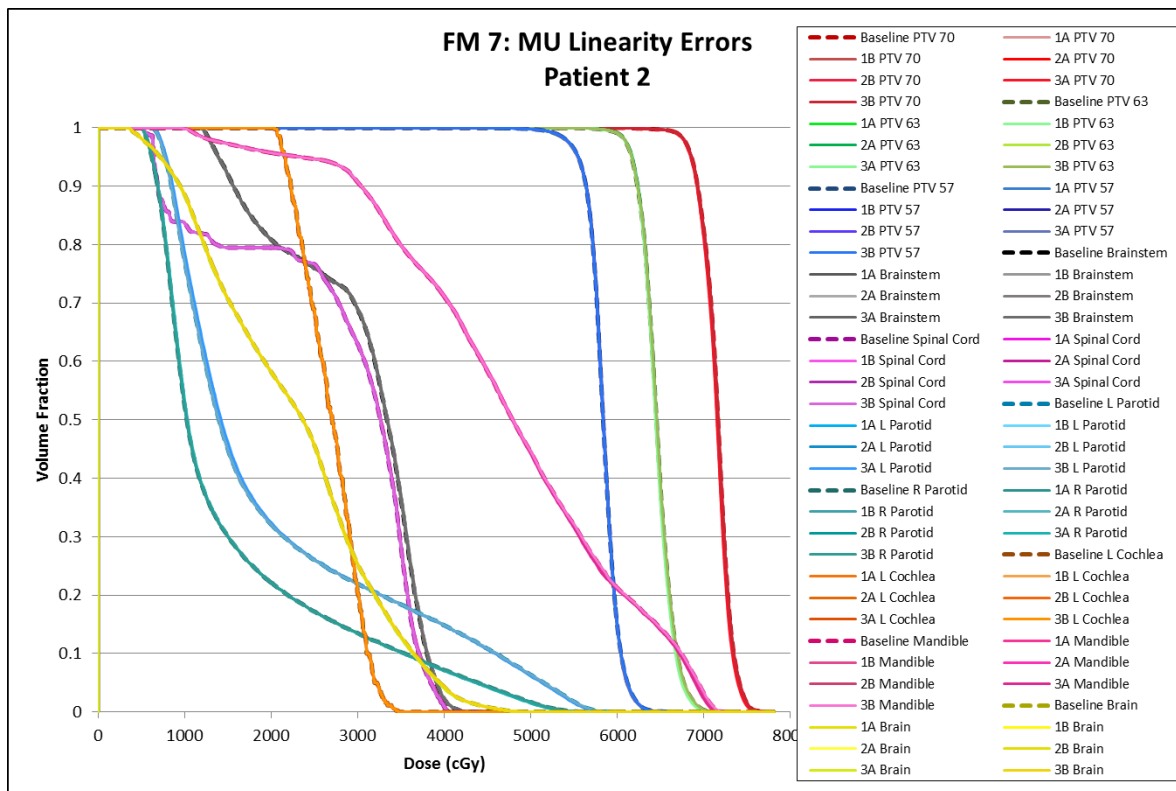


Figure 203: Failure mode 7 DVHs for patient 2.

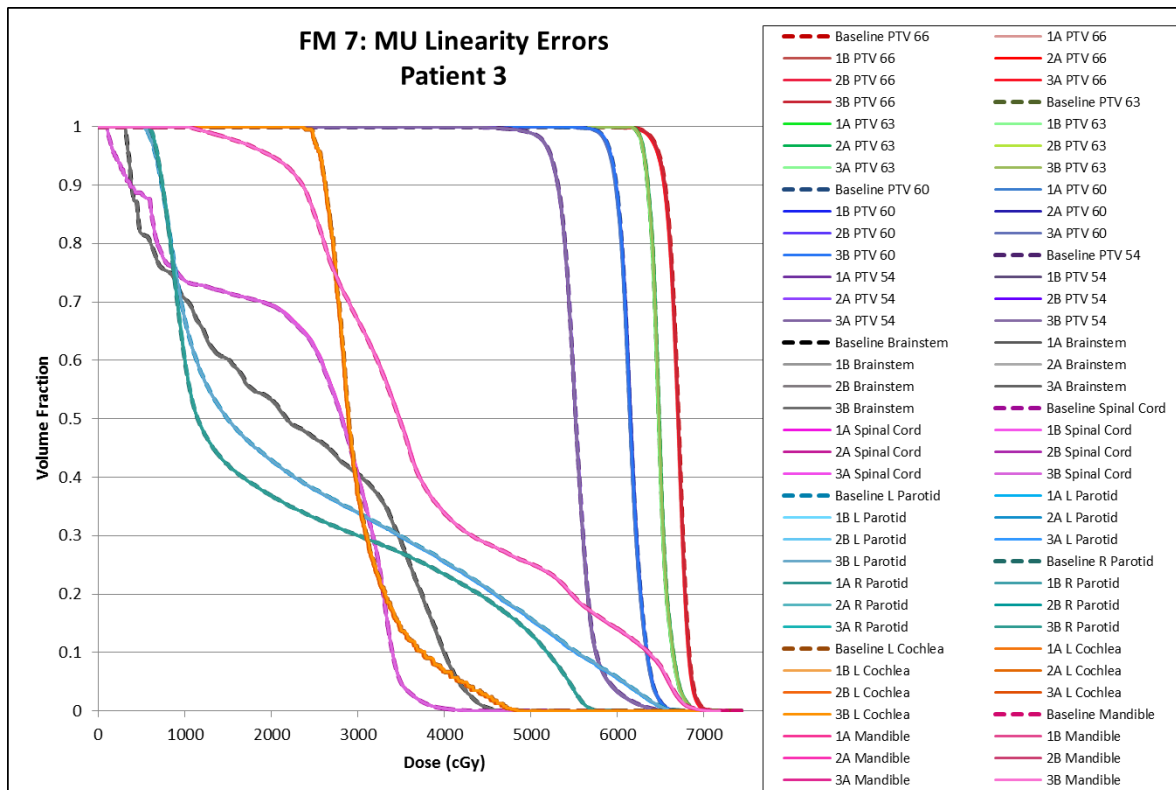


Figure 204: Failure mode 7 DVHs for patient 3.

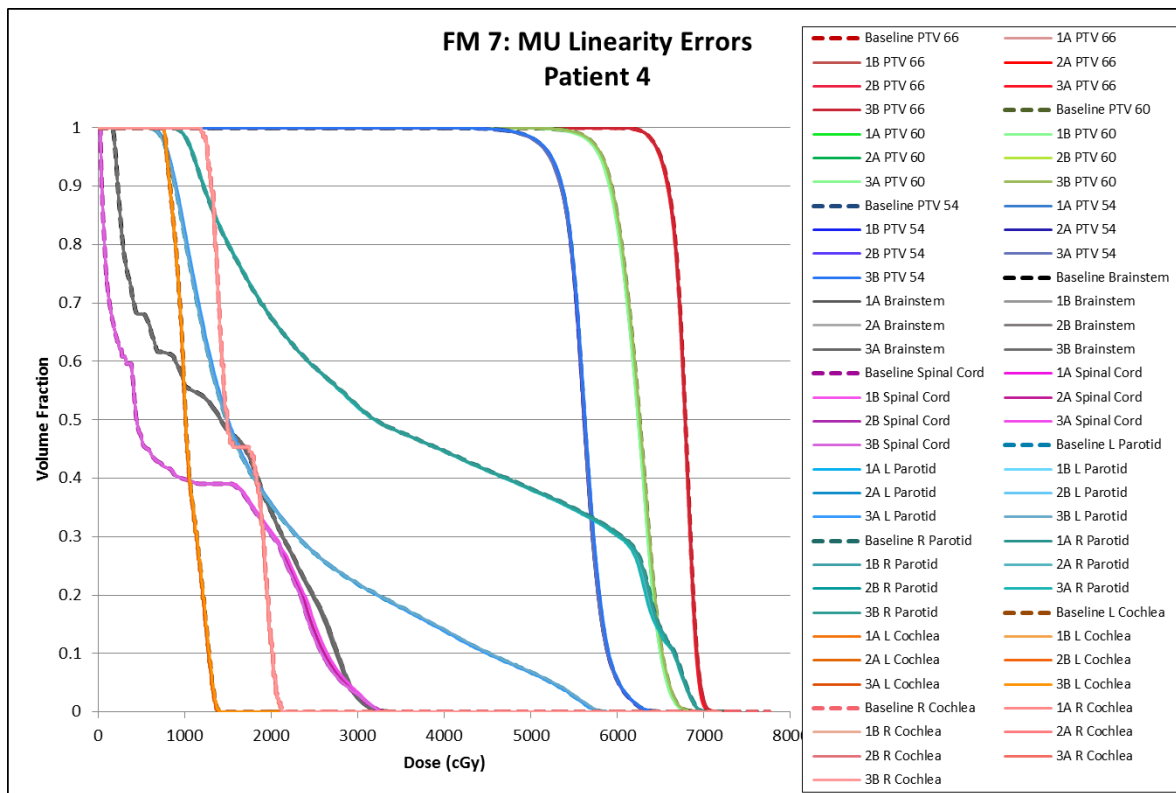


Figure 205: Failure mode 7 DVHs for patient 4.

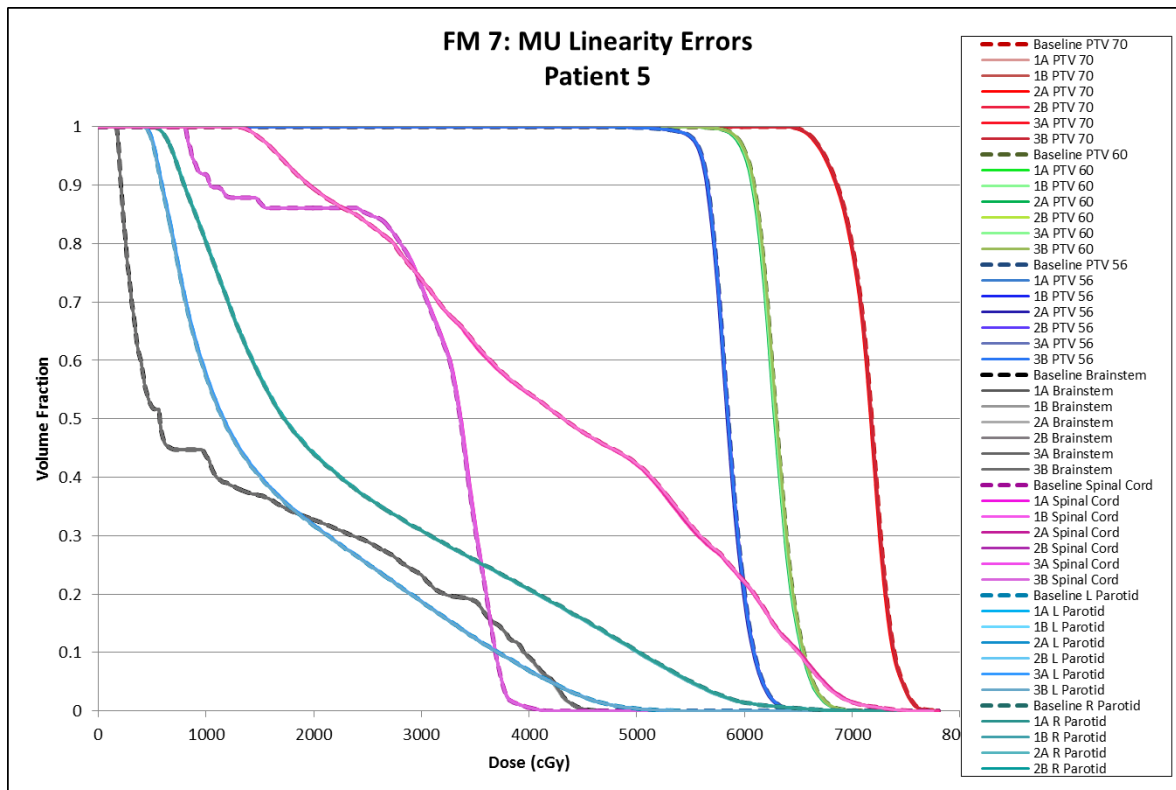


Figure 206: Failure mode 7 DVHs for patient 5.

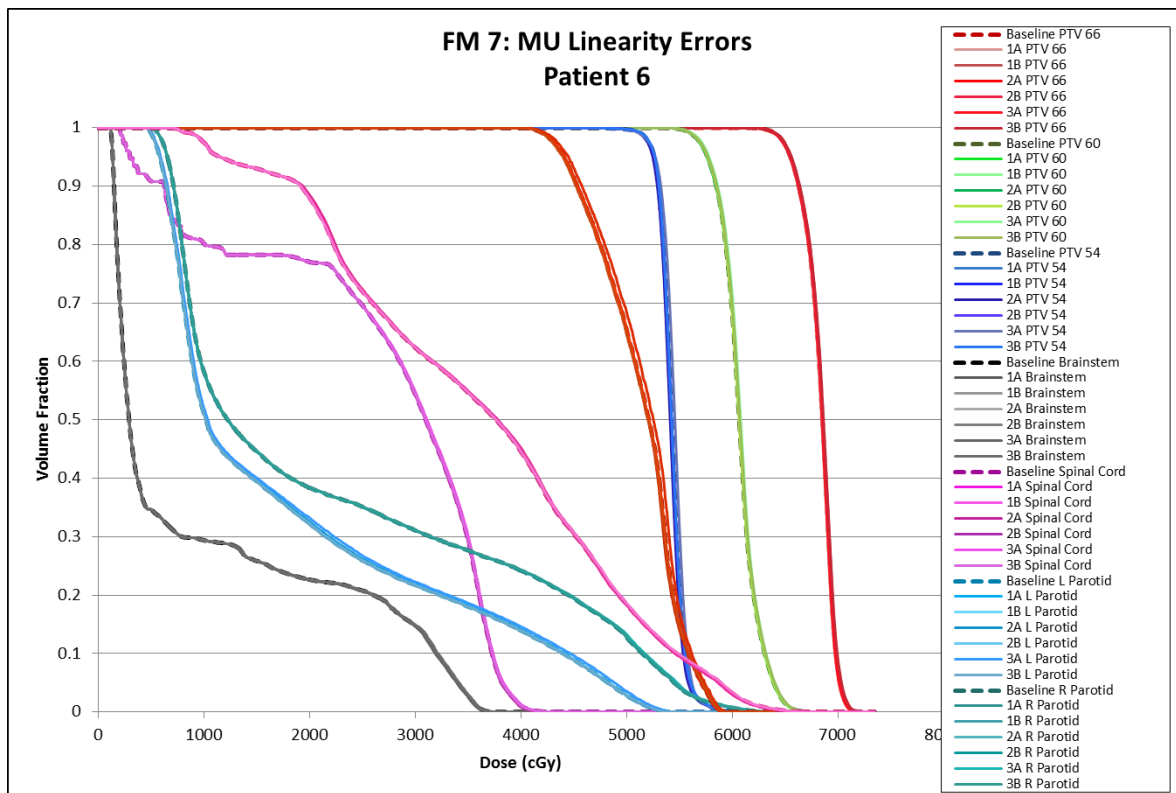


Figure 207: Failure mode 7 DVHs for patient 6.

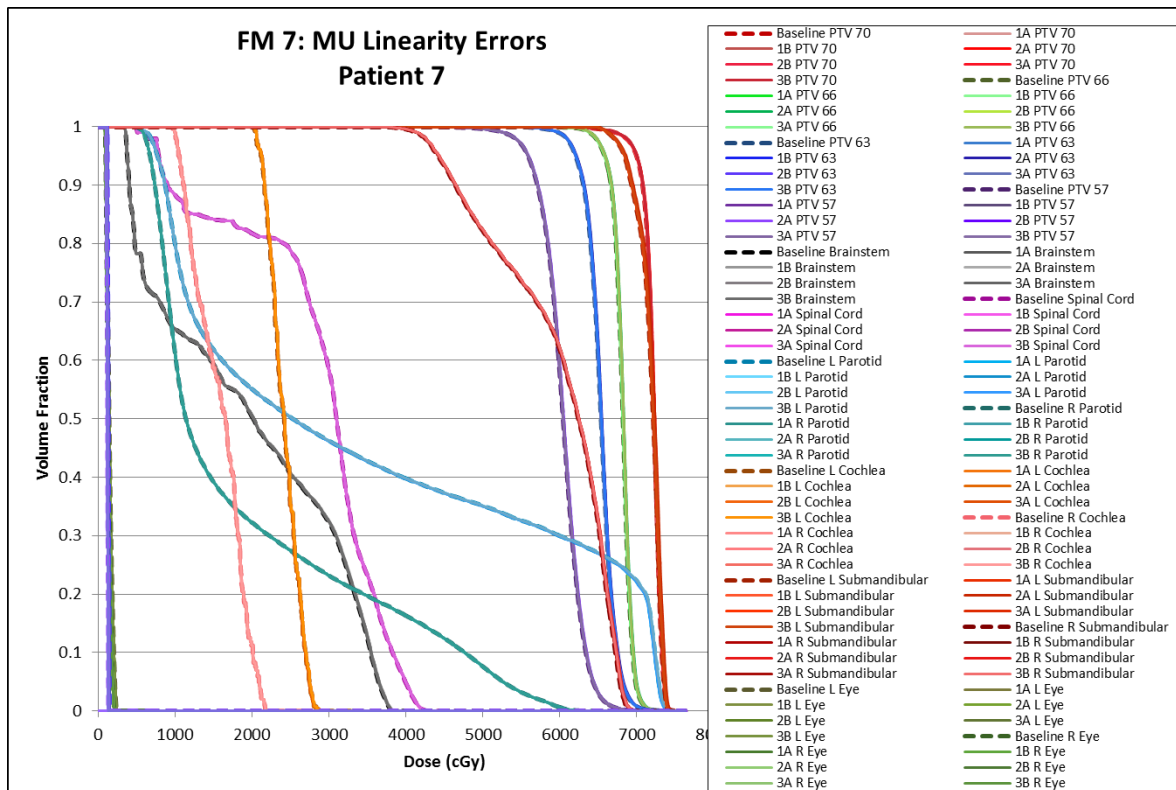


Figure 208: Failure mode 7 DVHs for patient 7.

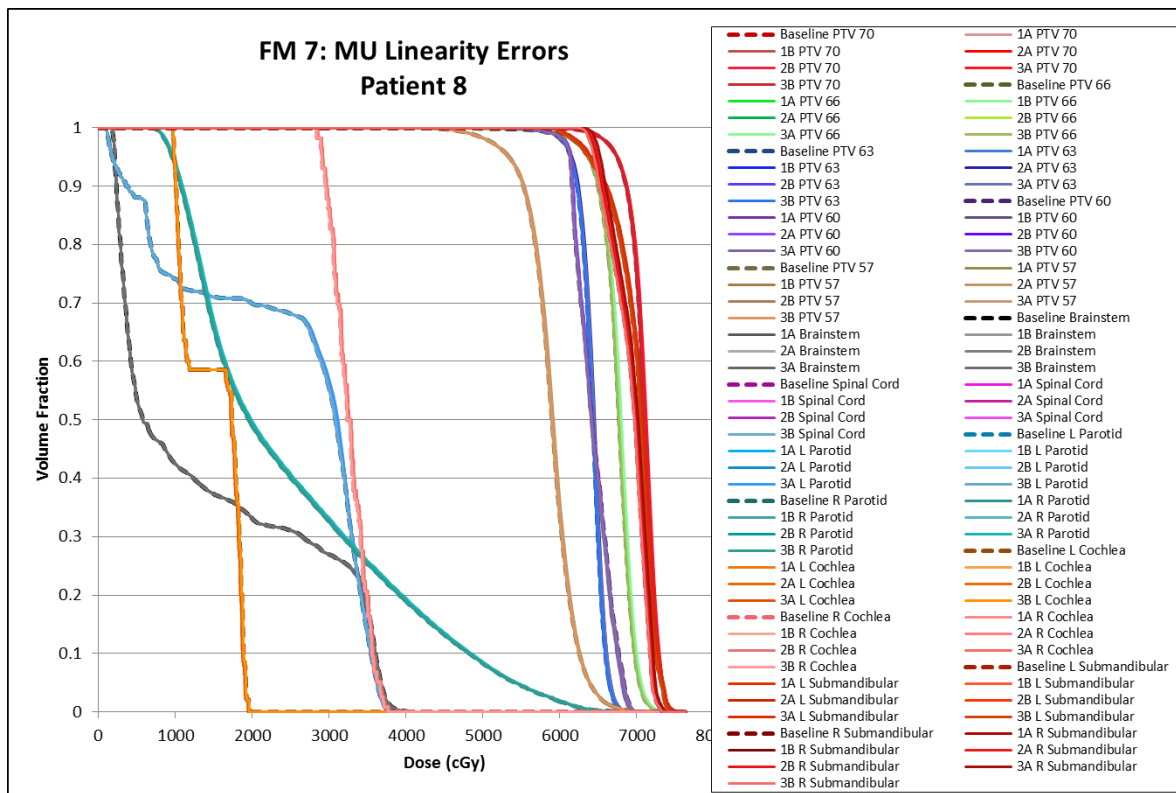


Figure 209: Failure mode 7 DVHs for patient 8.

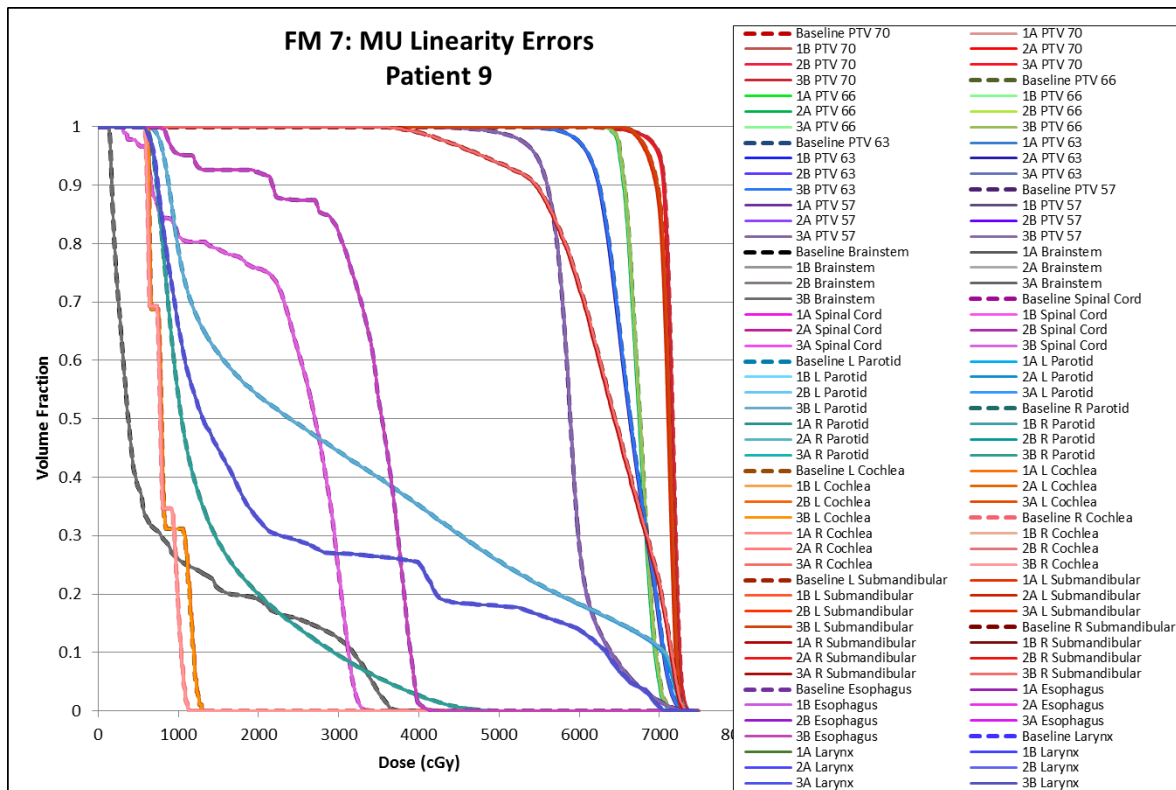


Figure 210: Failure mode 7 DVHs for patient 9.

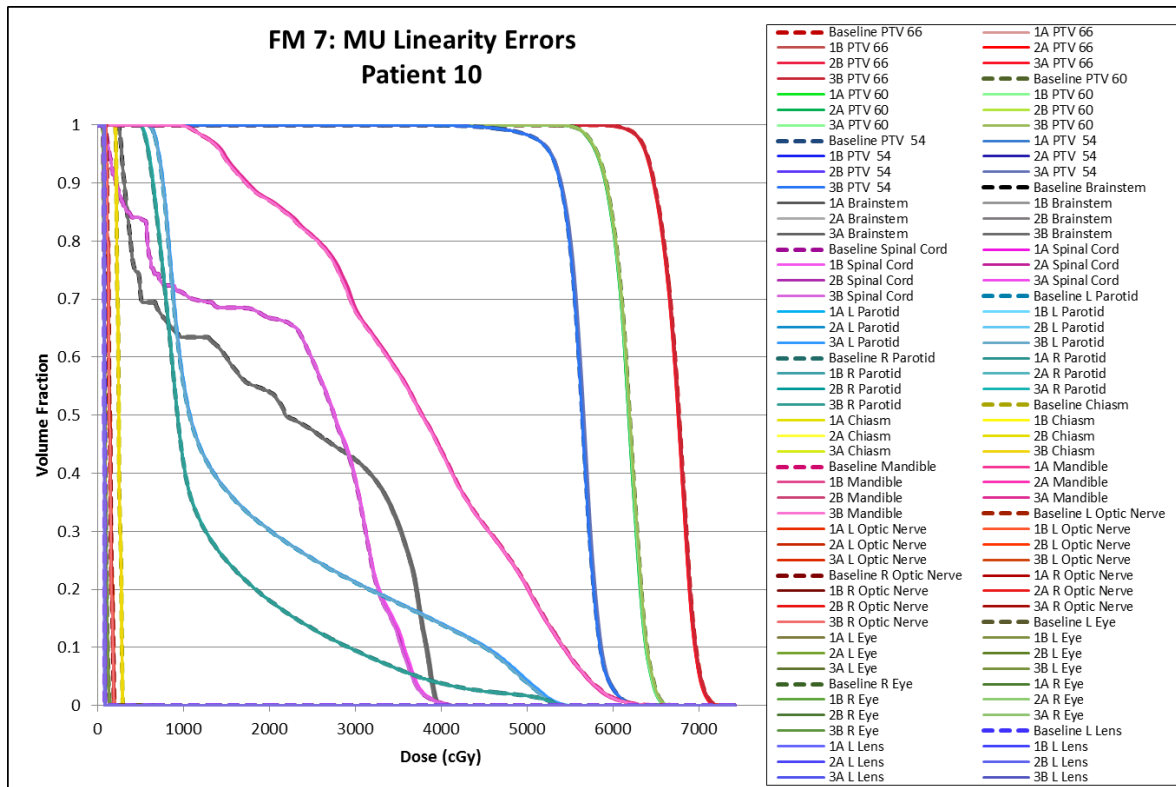


Figure 211: Failure mode 7 DVHs for patient 10.

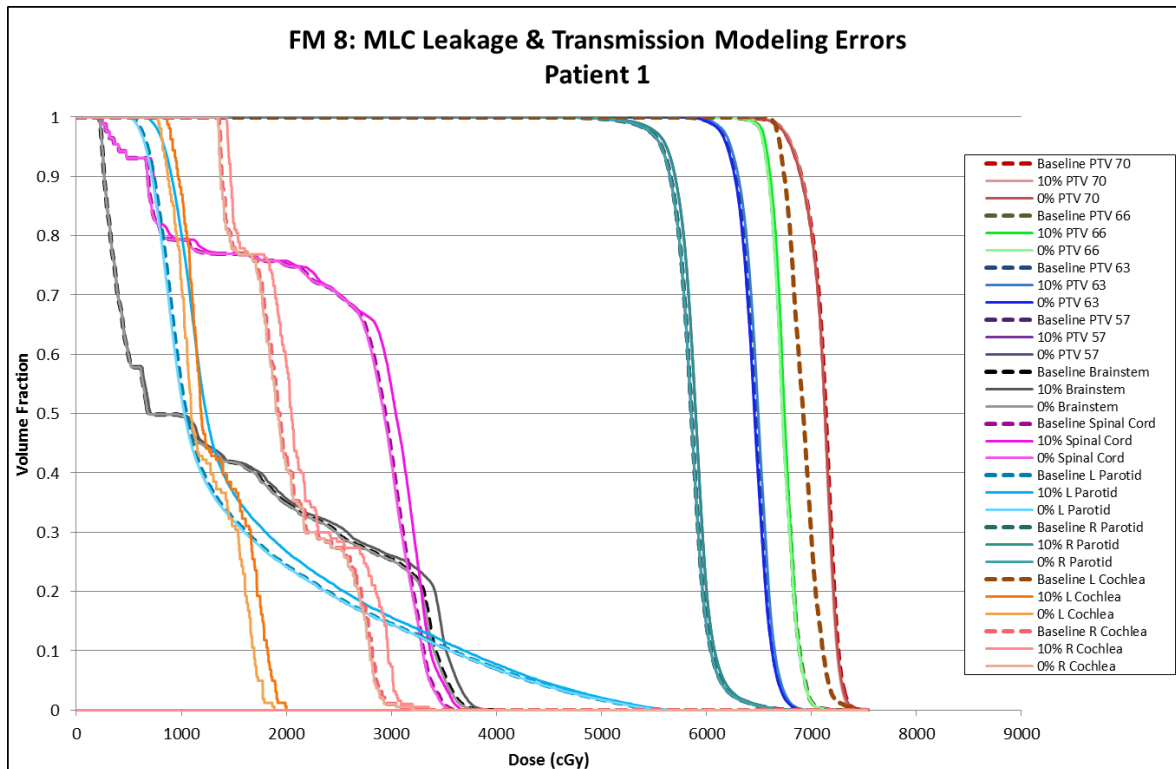


Figure 212: Failure mode 8 DVHs for patient 1.

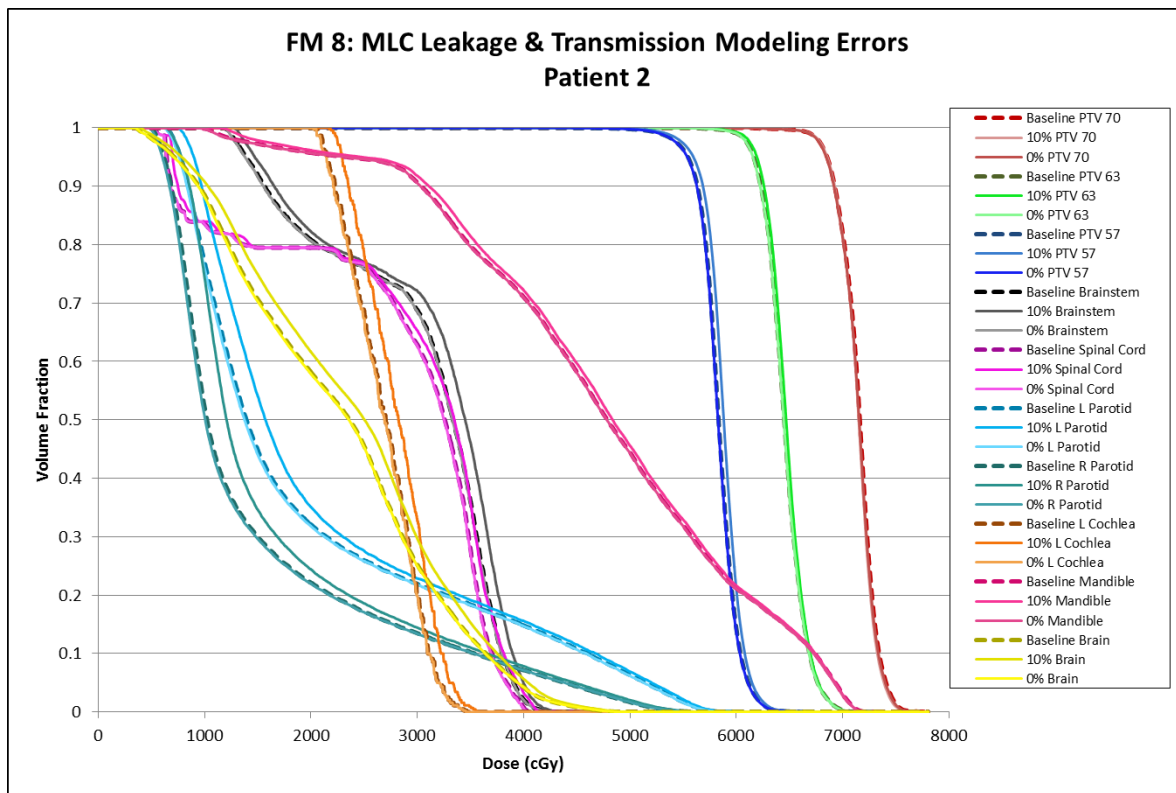


Figure 213: Failure mode 8 DVHs for patient 2.

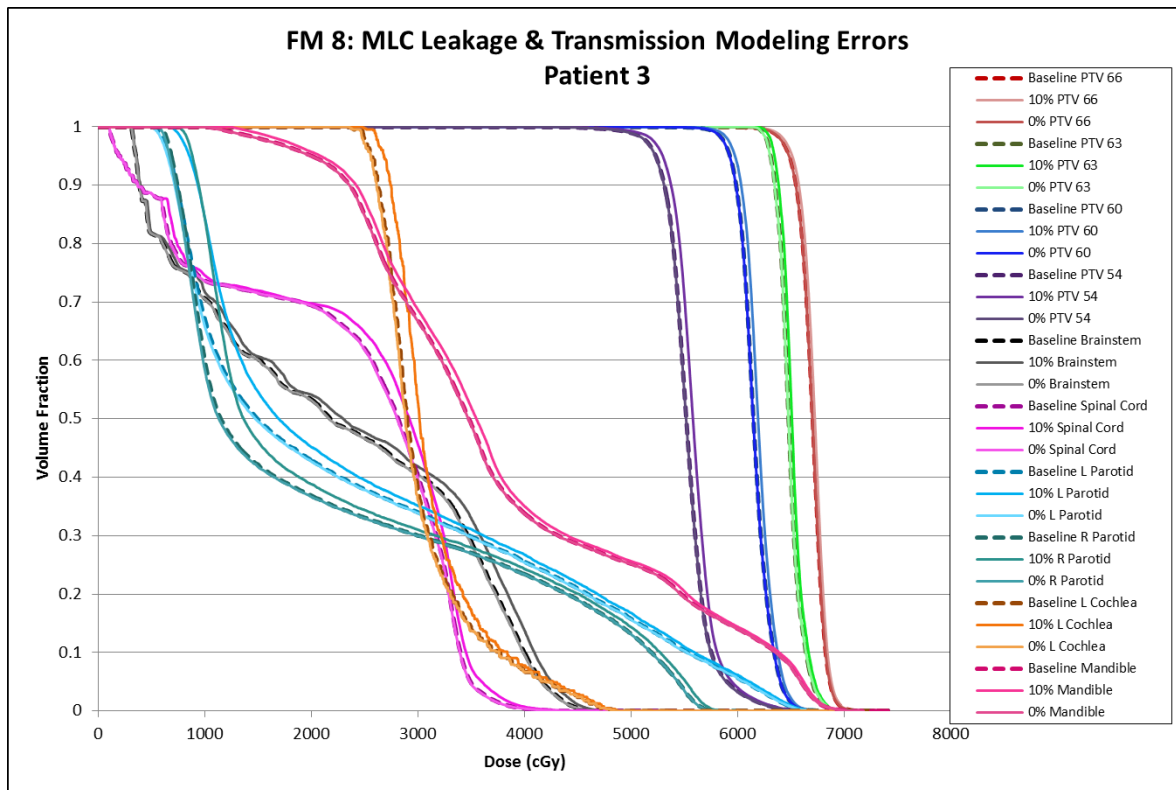


Figure 214: Failure mode 8 DVHs for patient 3.

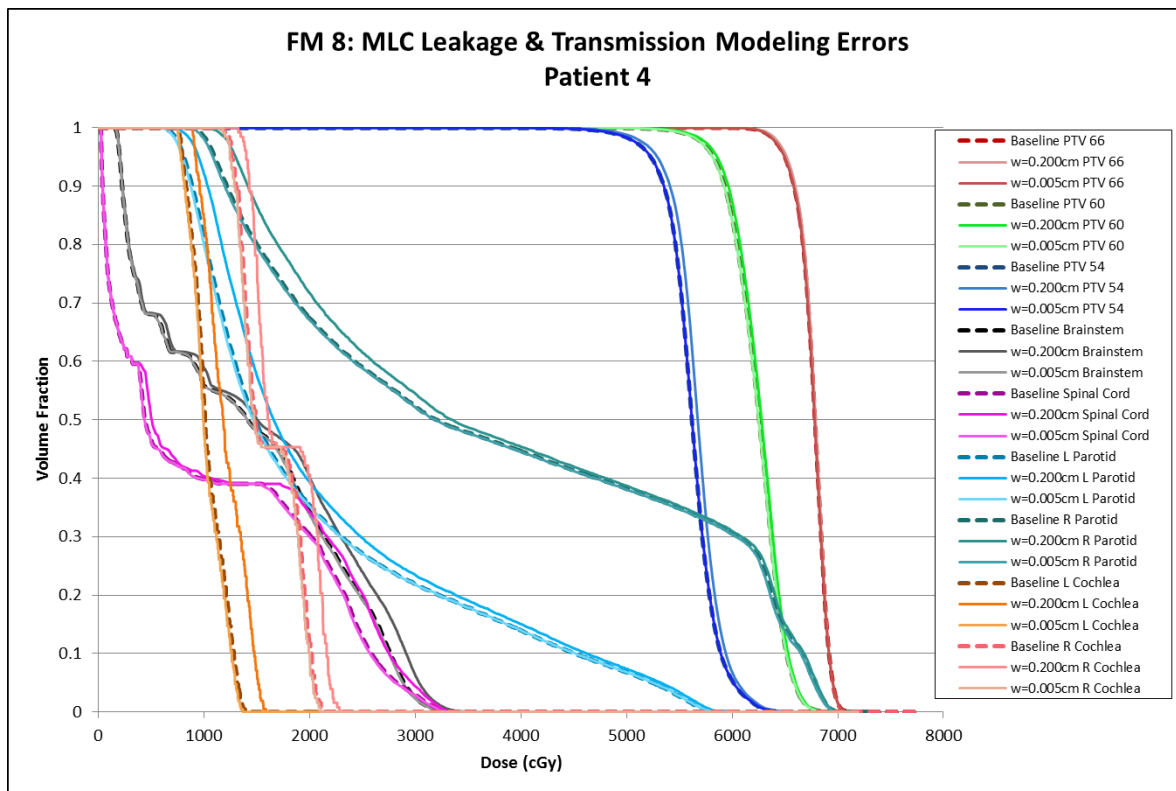


Figure 215: Failure mode 8 DVHs for patient 4.

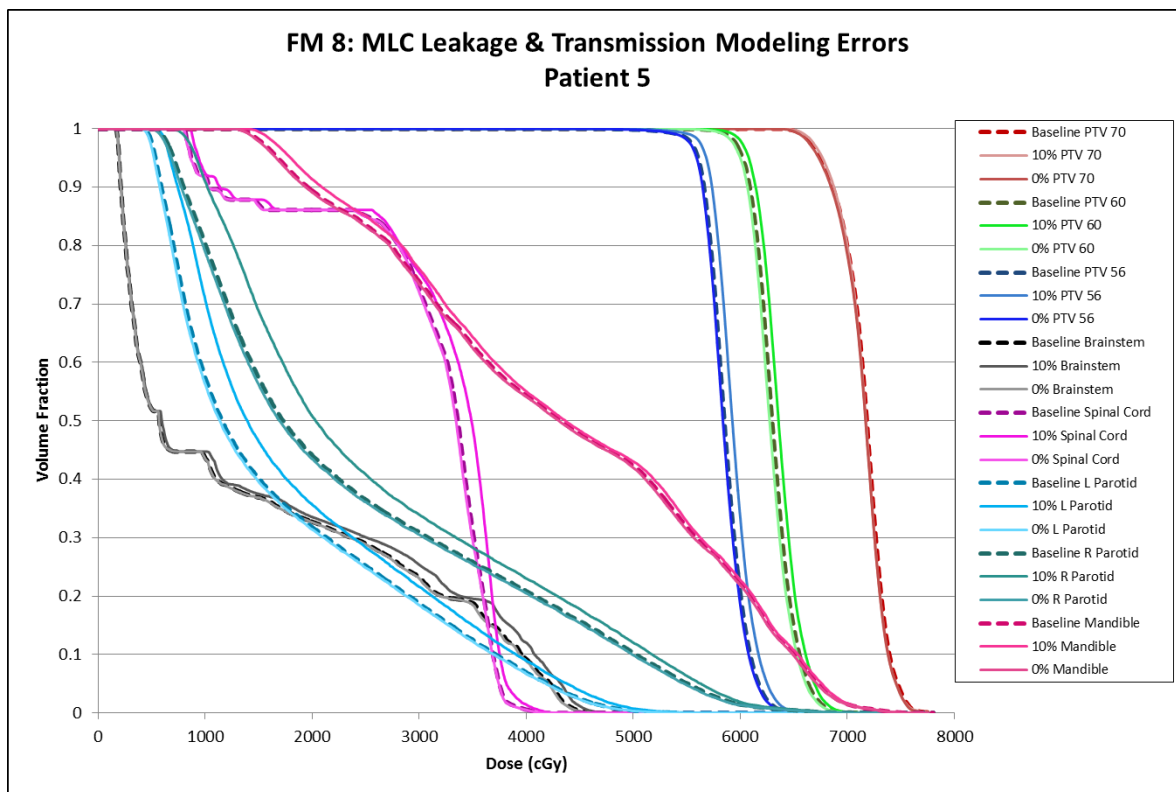


Figure 216: Failure mode 8 DVHs for patient 5.

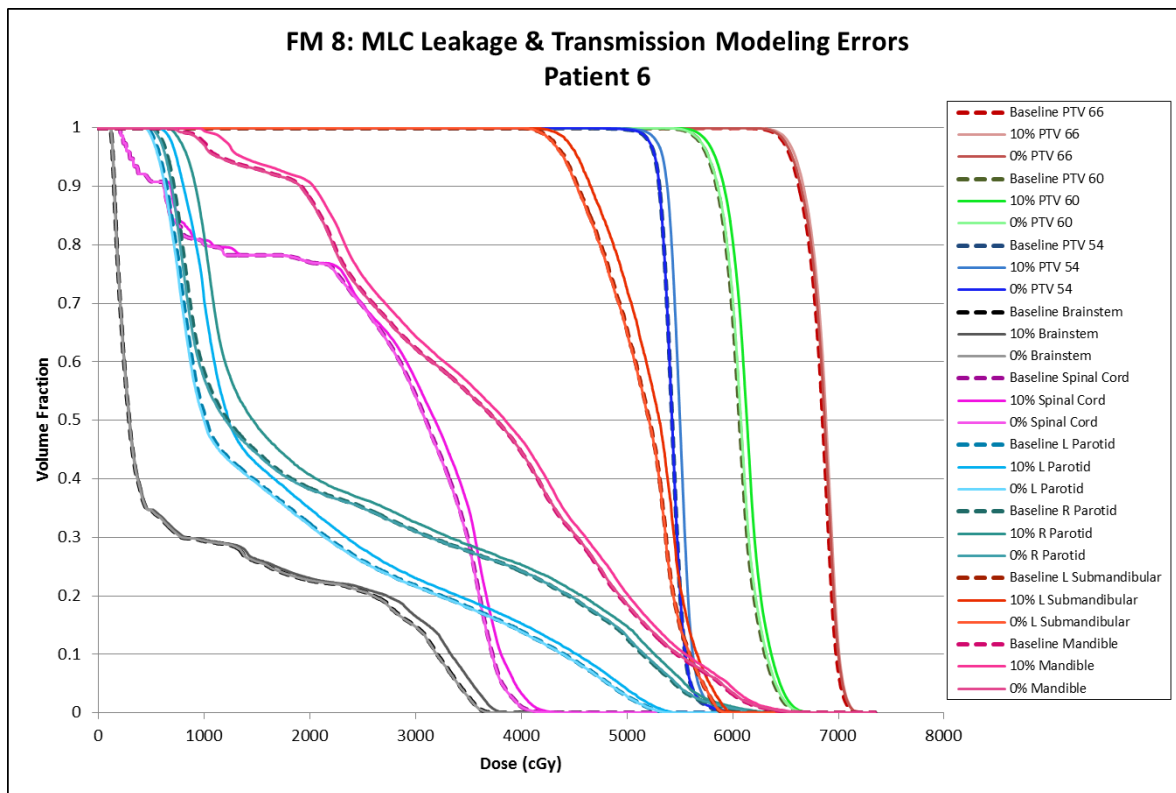


Figure 217: Failure mode 8 DVHs for patient 6.

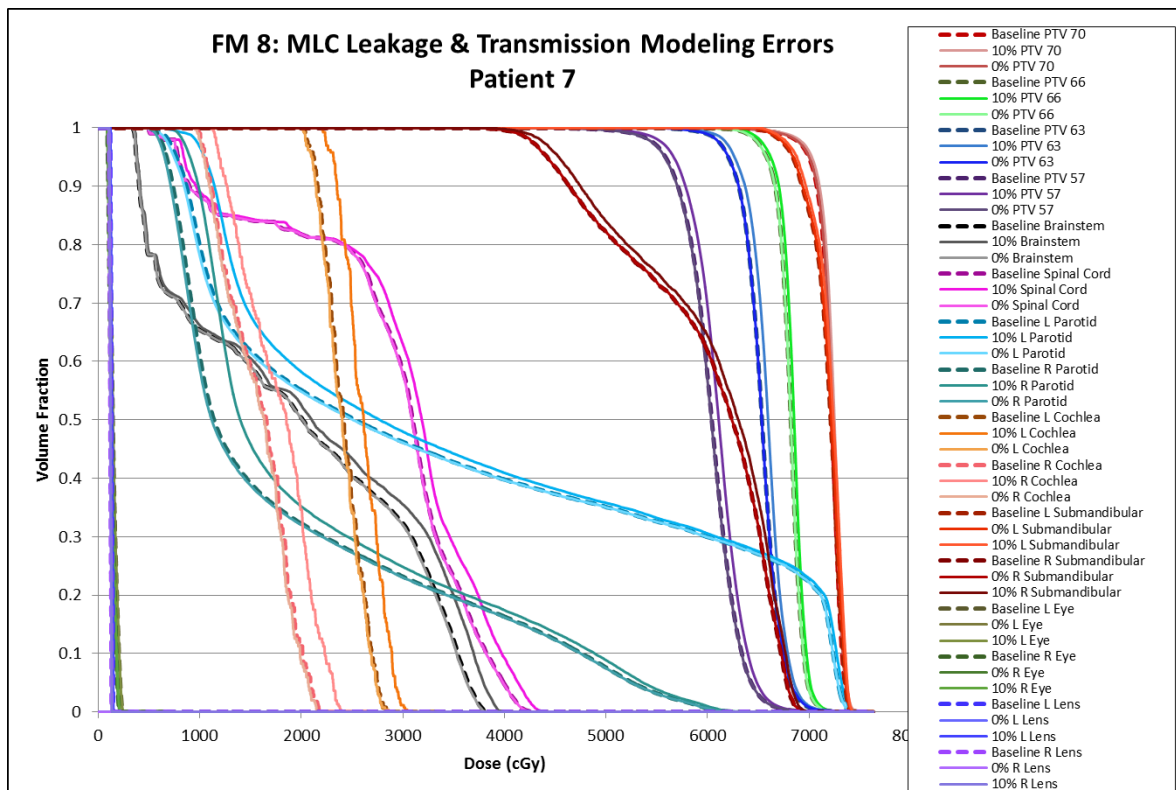


Figure 218: Failure mode 8 DVHs for patient 7.

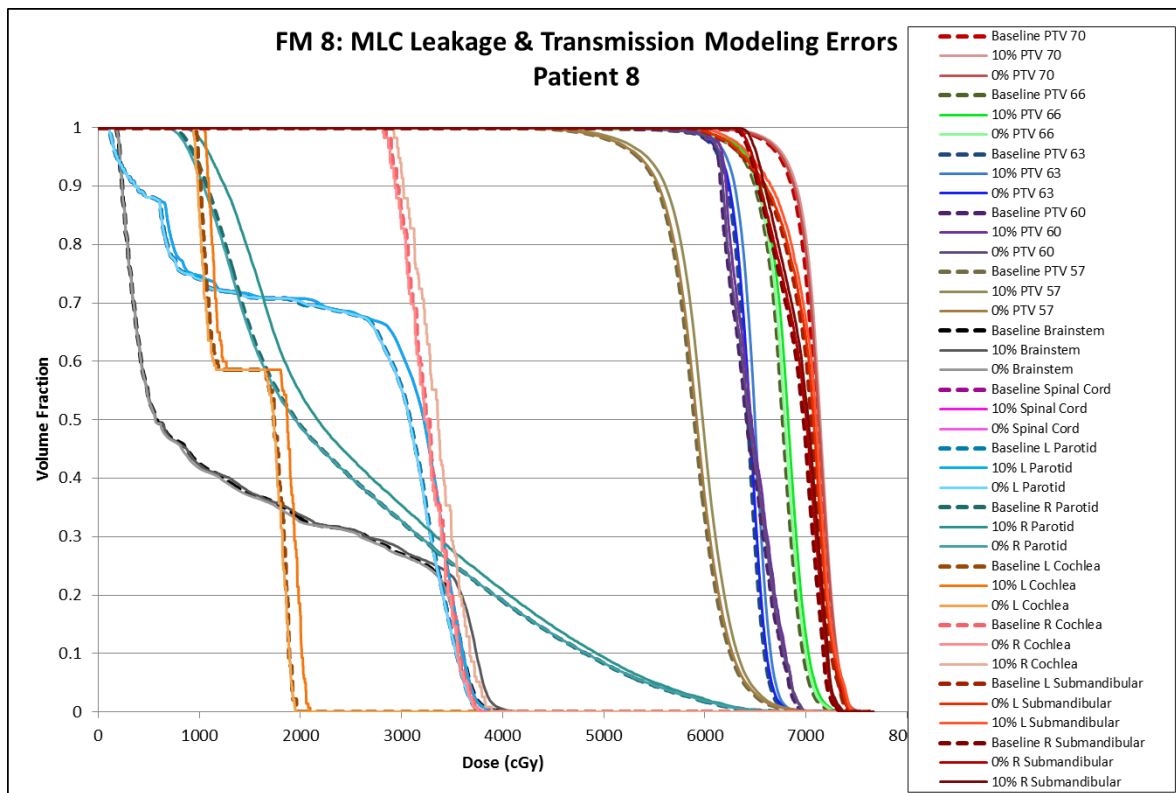


Figure 219: Failure mode 8 DVHs for patient 8.

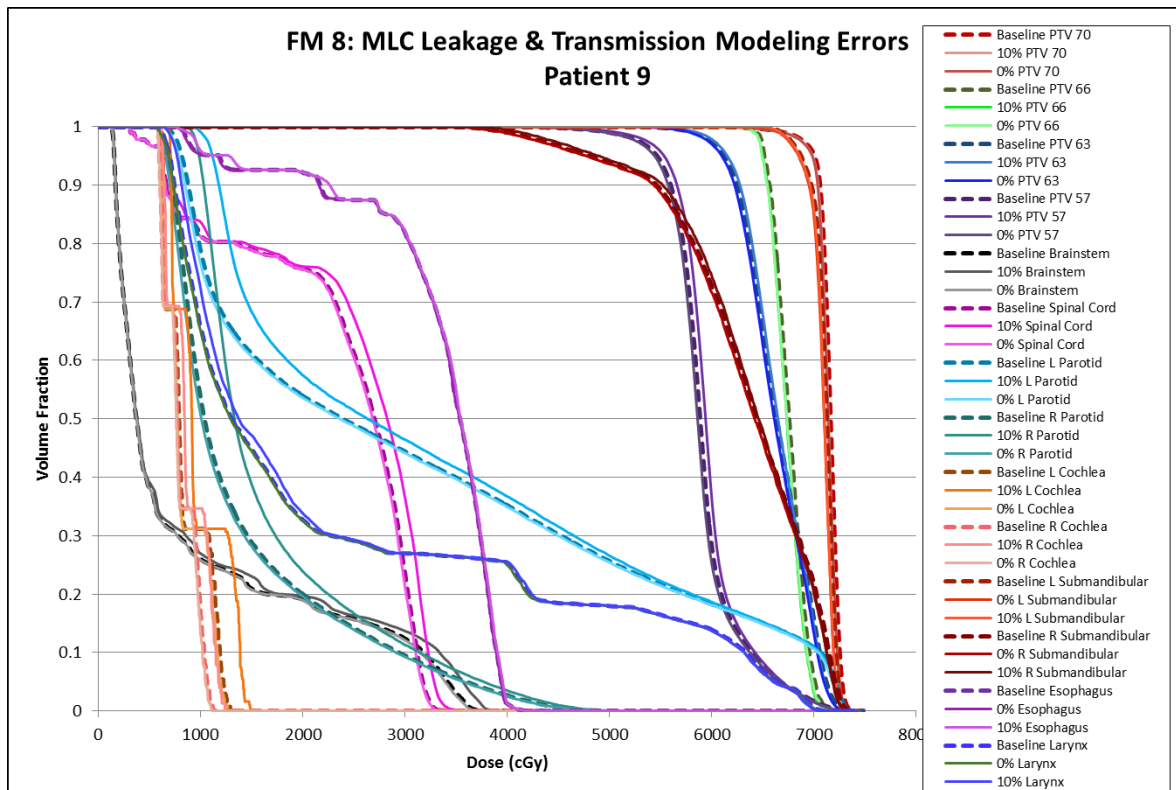


Figure 220: Failure mode 8 DVHs for patient 9.

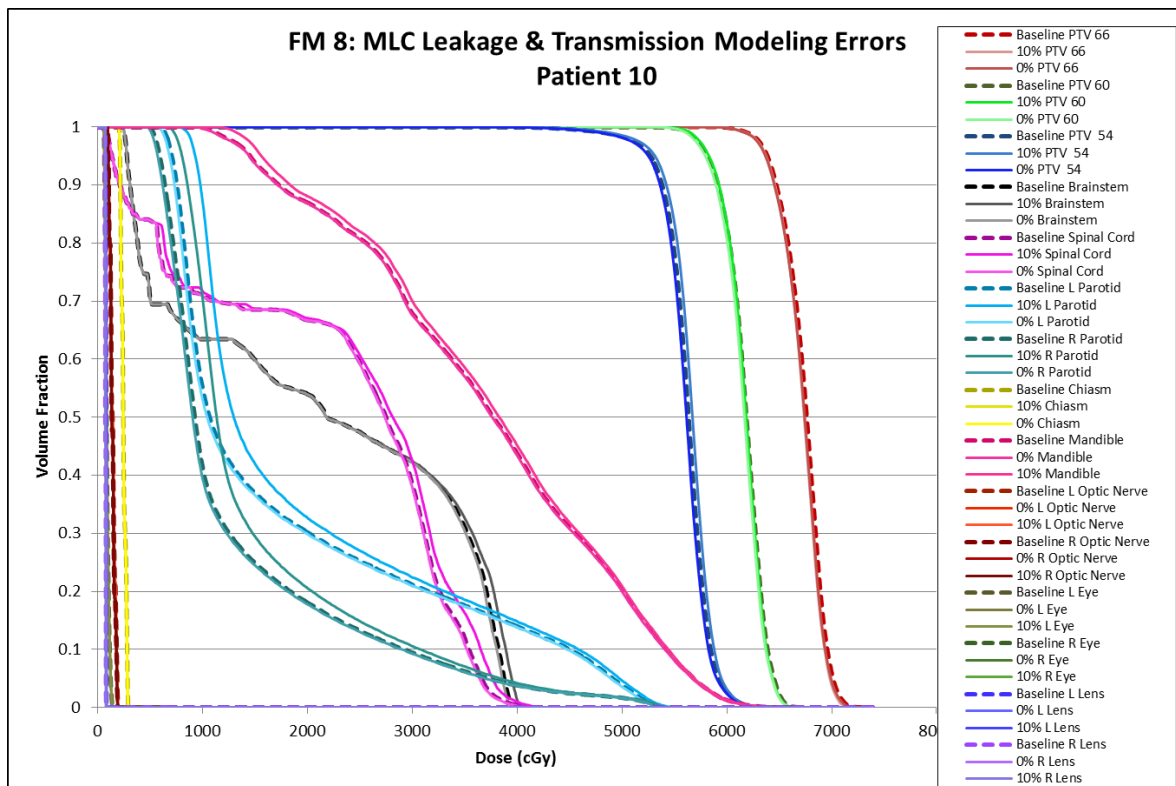


Figure 221: Failure mode 8 DVHs for patient 10.

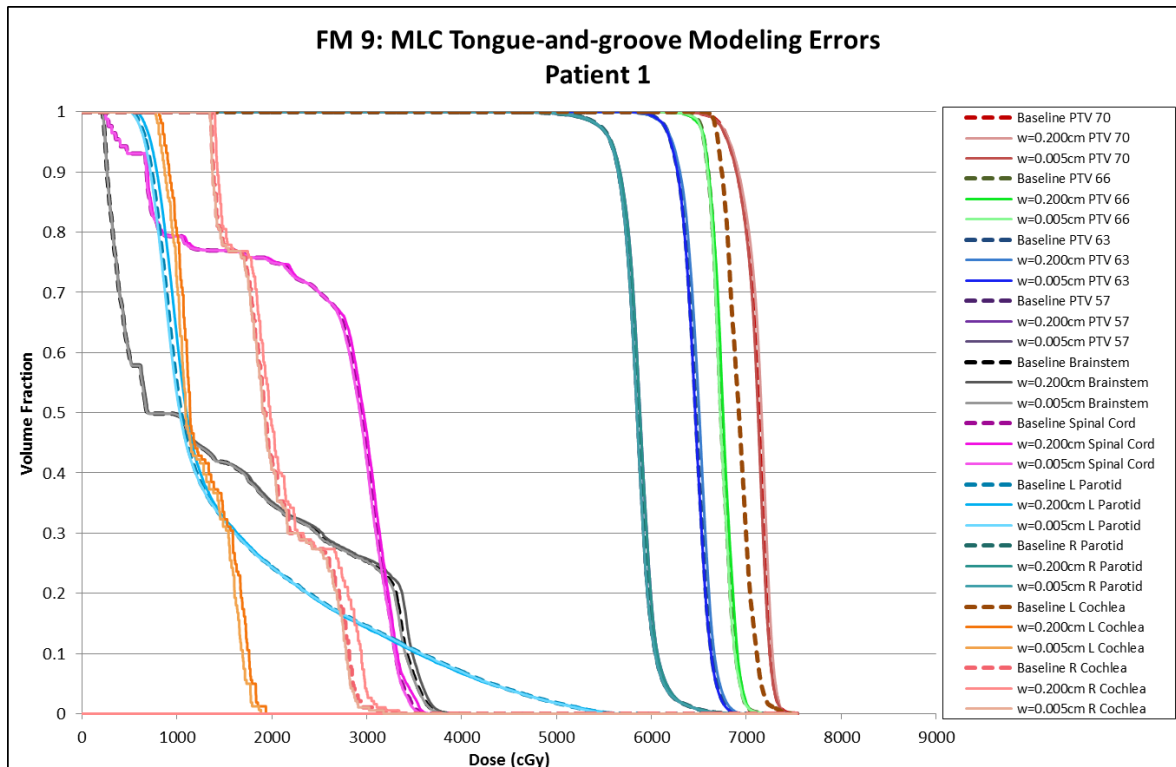


Figure 222: Failure mode 9 DVHs for patient 1.

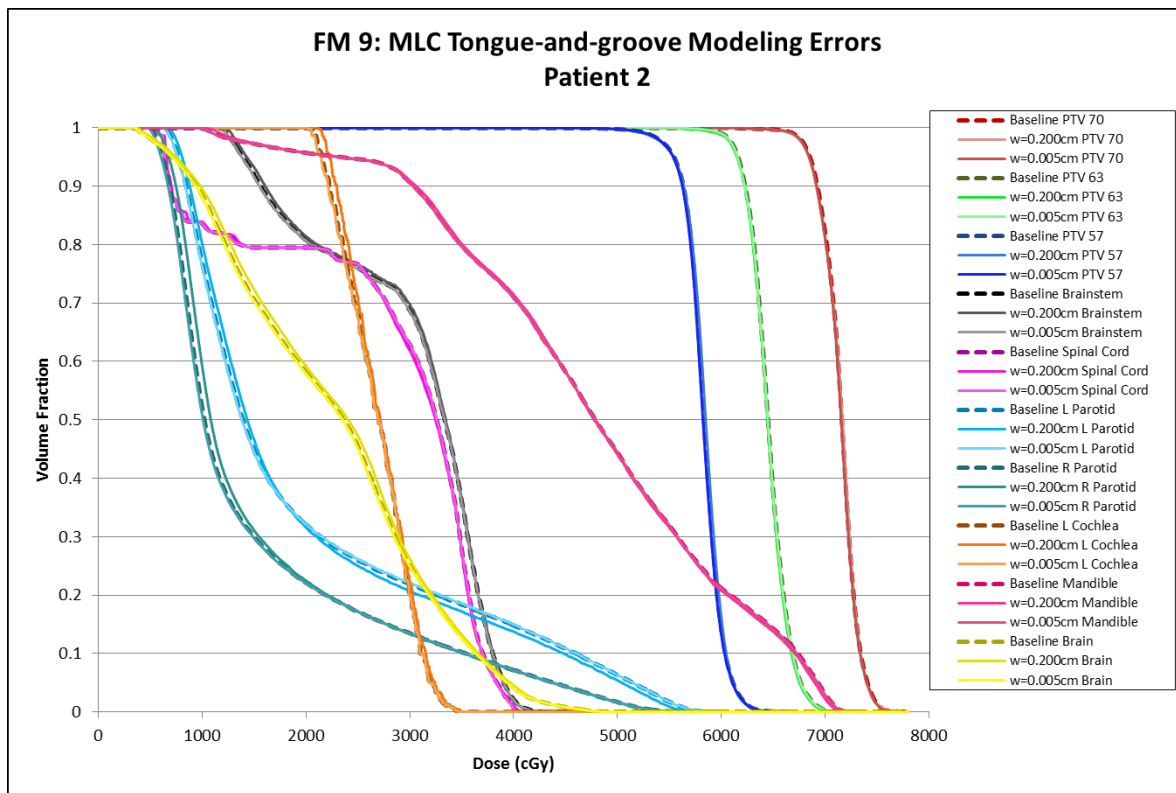


Figure 223: Failure mode 9 DVHs for patient 2.

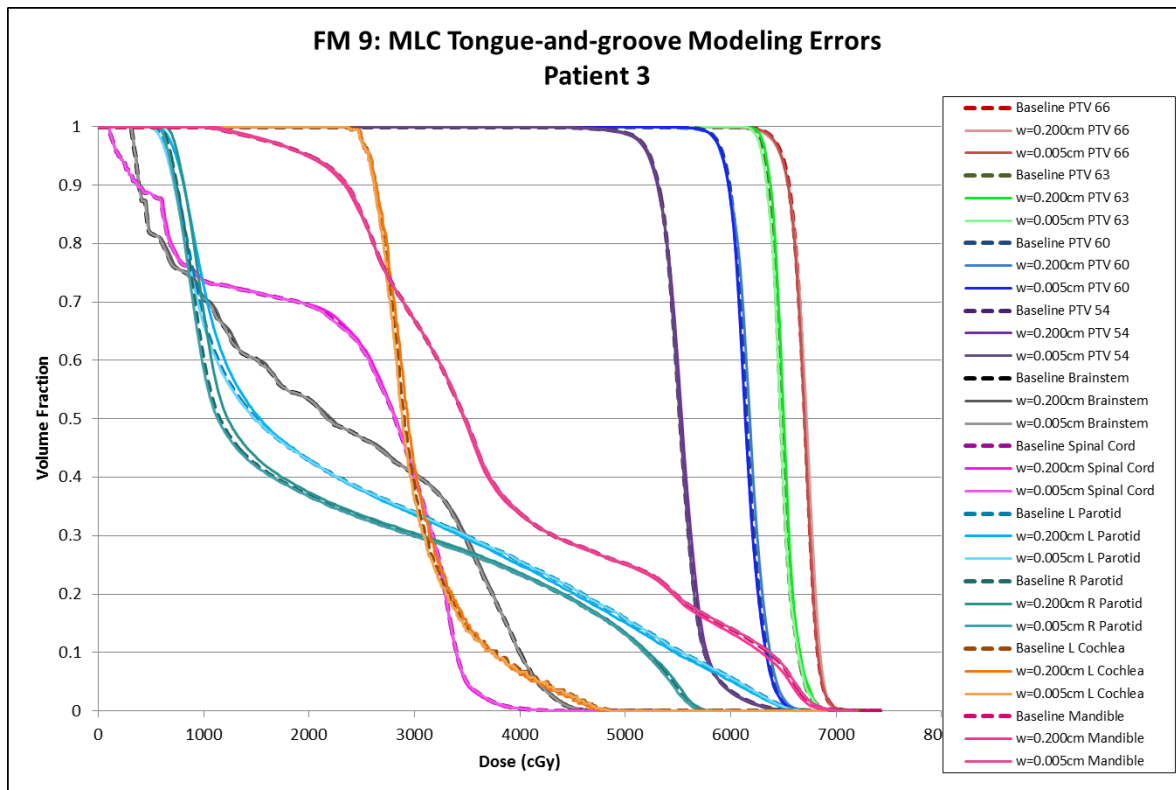


Figure 224: Failure mode 9 DVHs for patient 3.

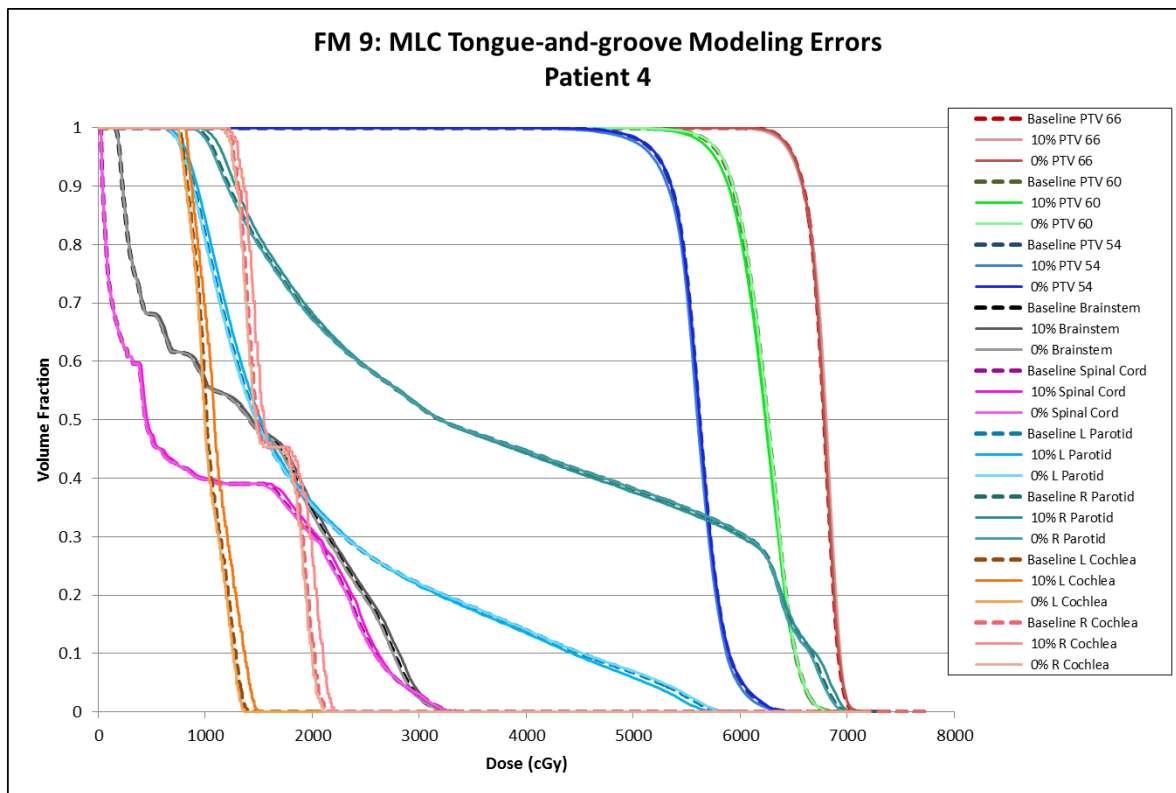


Figure 225: Failure mode 9 DVHs for patient 4.

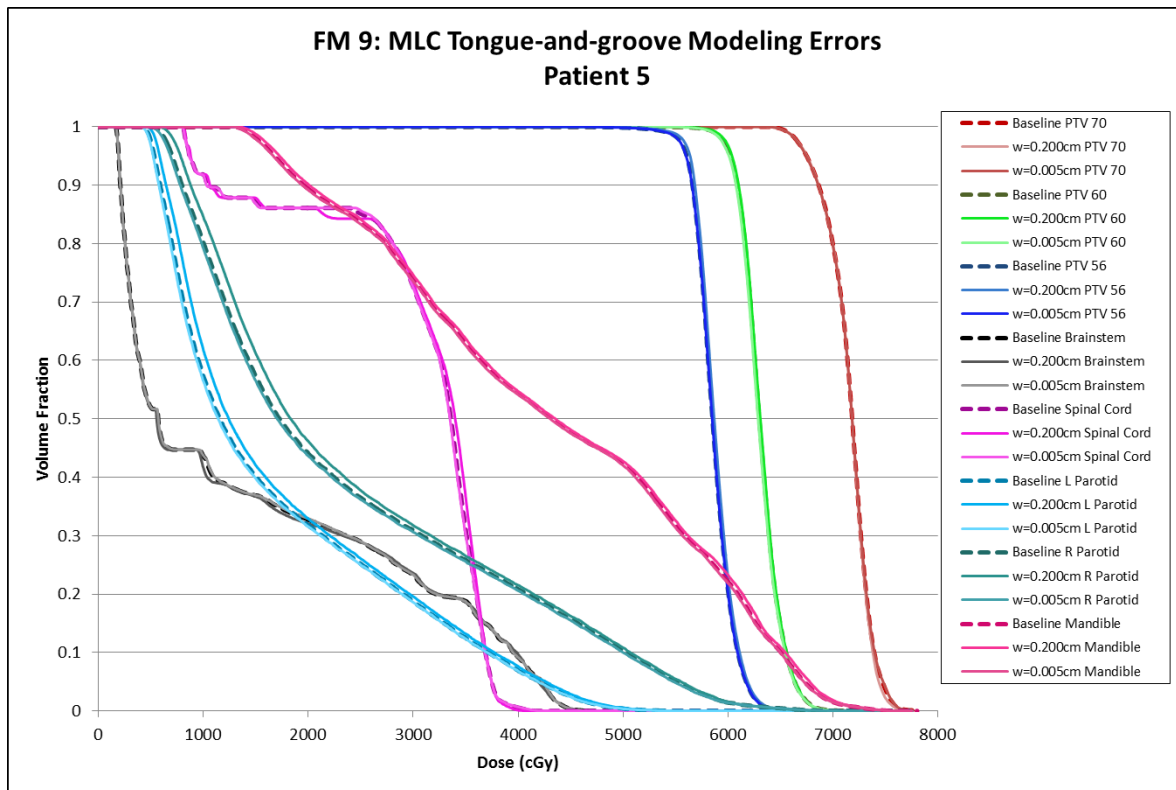


Figure 226: Failure mode 9 DVHs for patient 5.

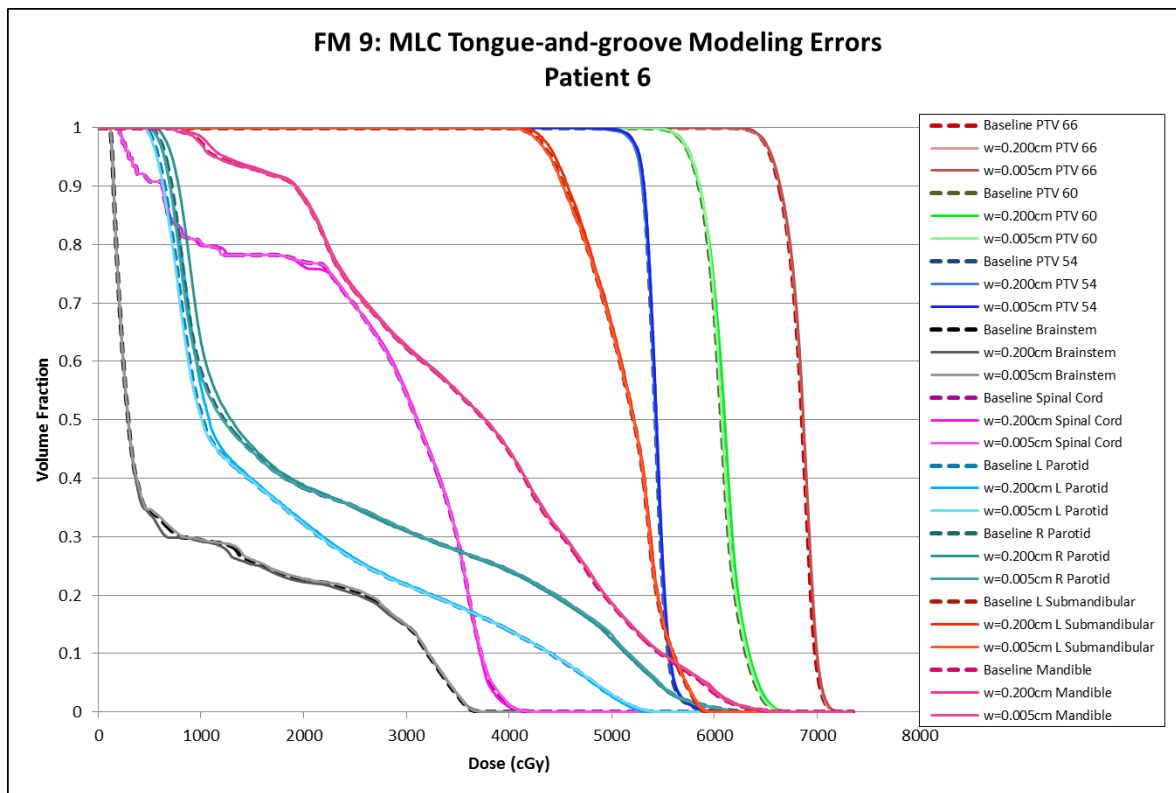


Figure 227: Failure mode 9 DVHs for patient 6.

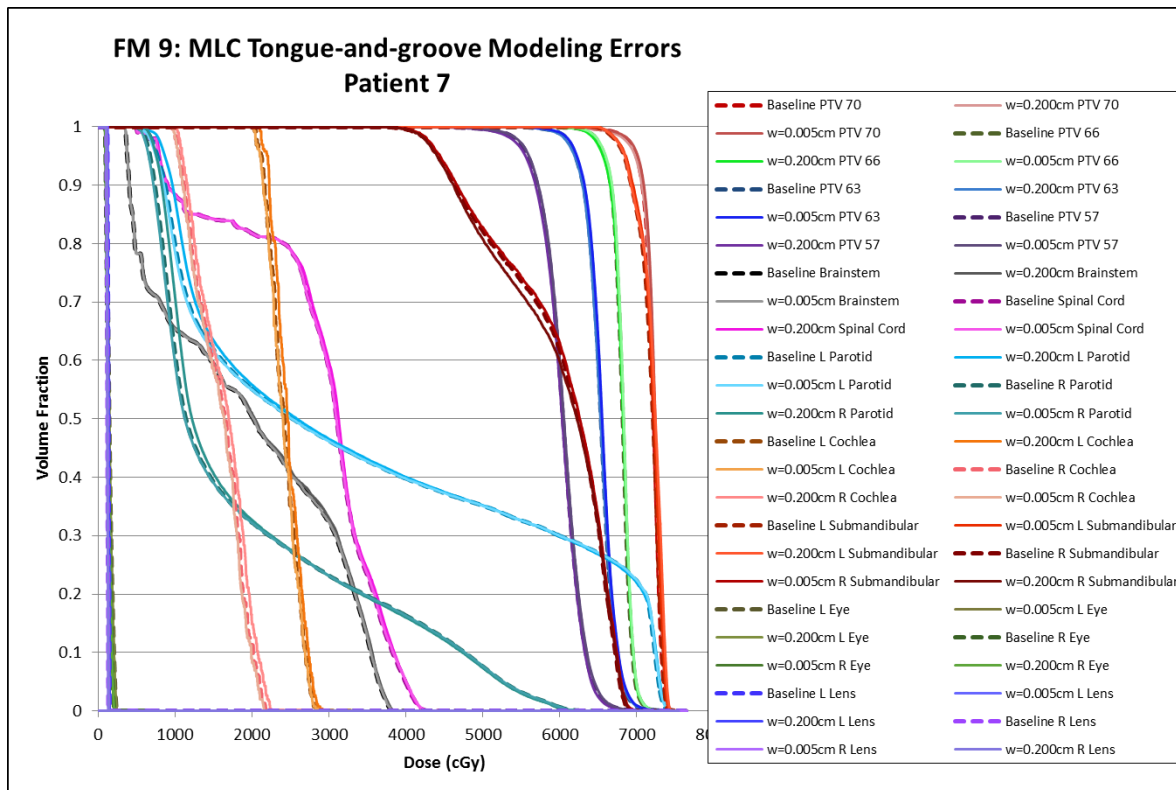


Figure 228: Failure mode 9 DVHs for patient 7.

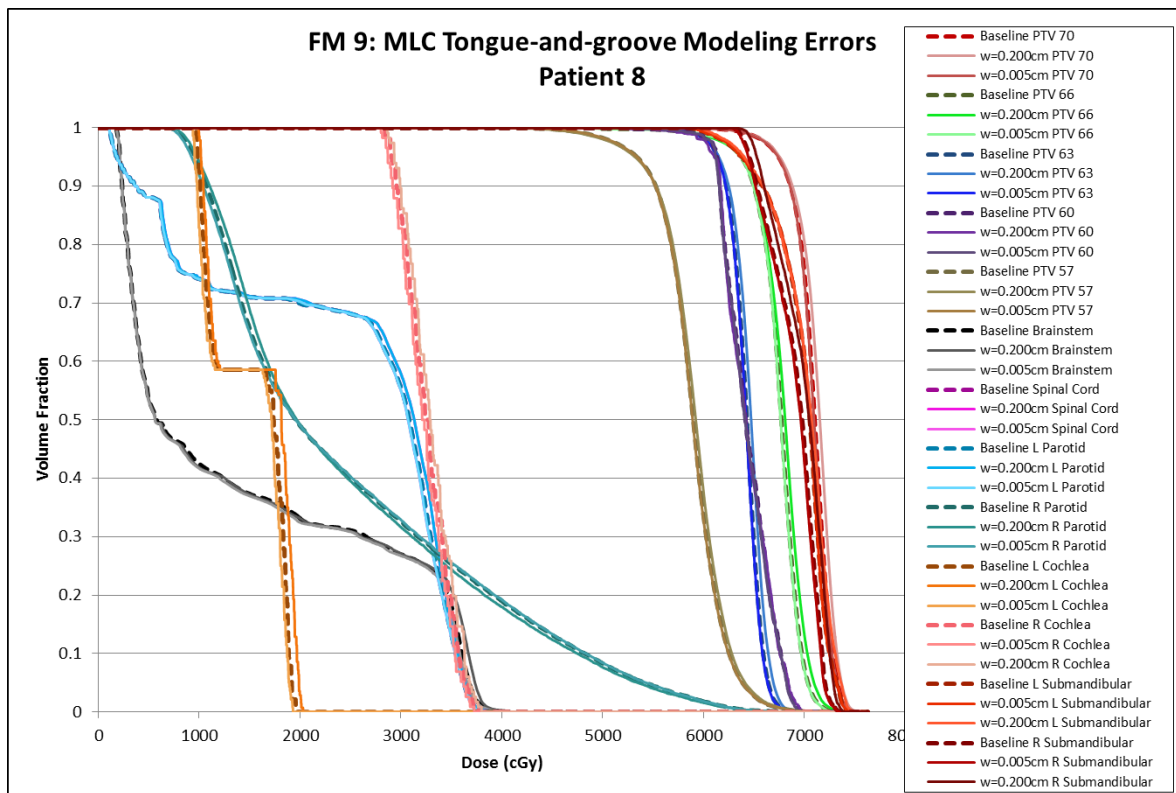


Figure 229: Failure mode 9 DVHs for patient 8.

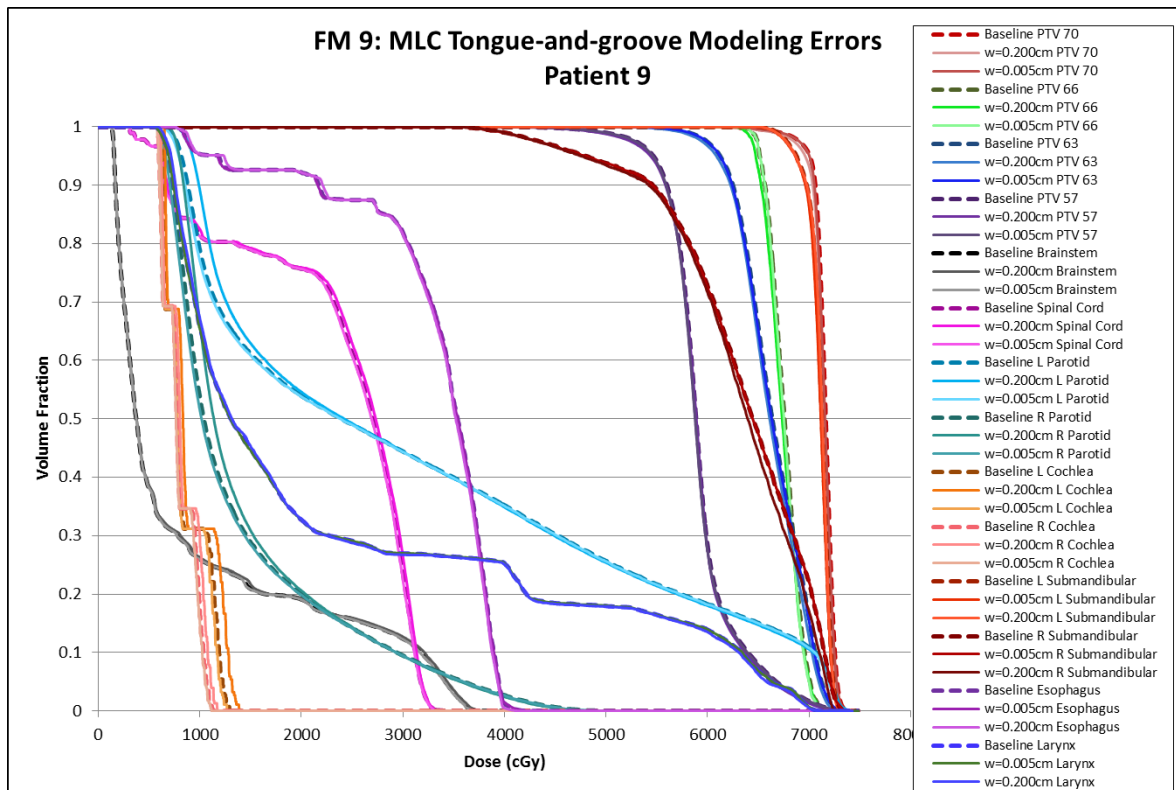


Figure 230: Failure mode 9 DVHs for patient 9.

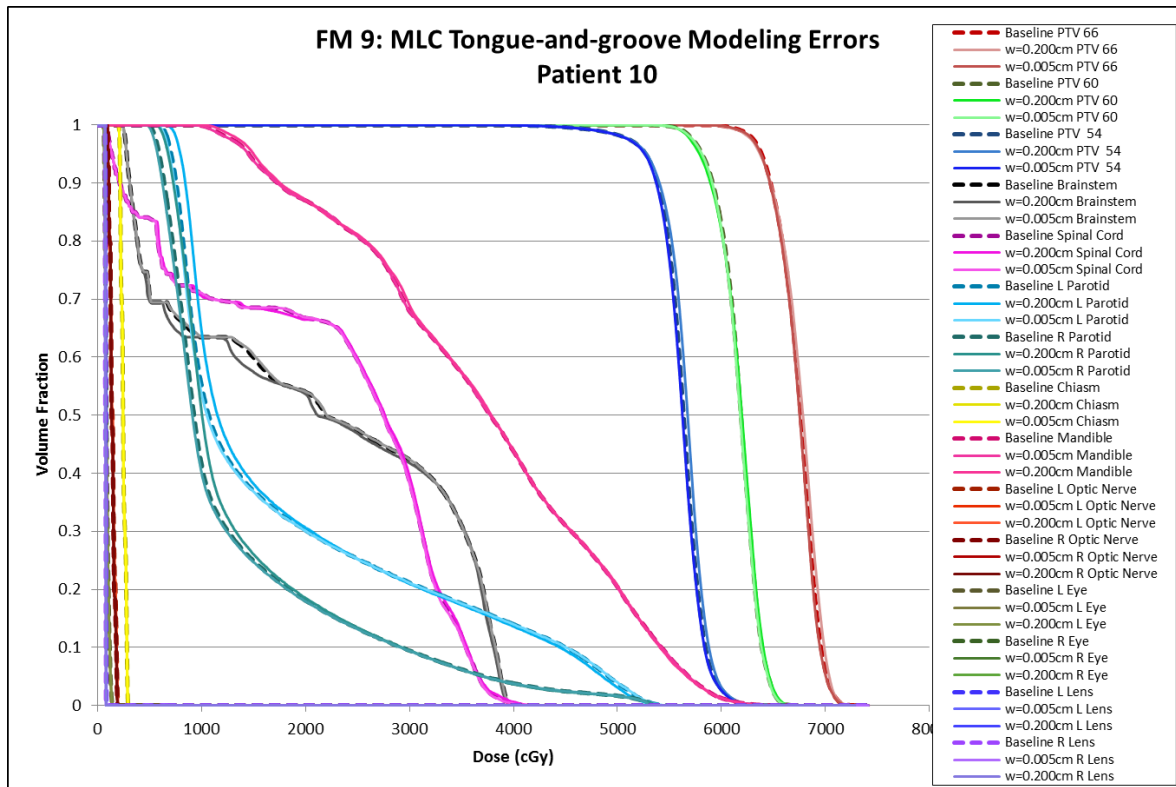


Figure 231: Failure mode 9 DVHs for patient 10.

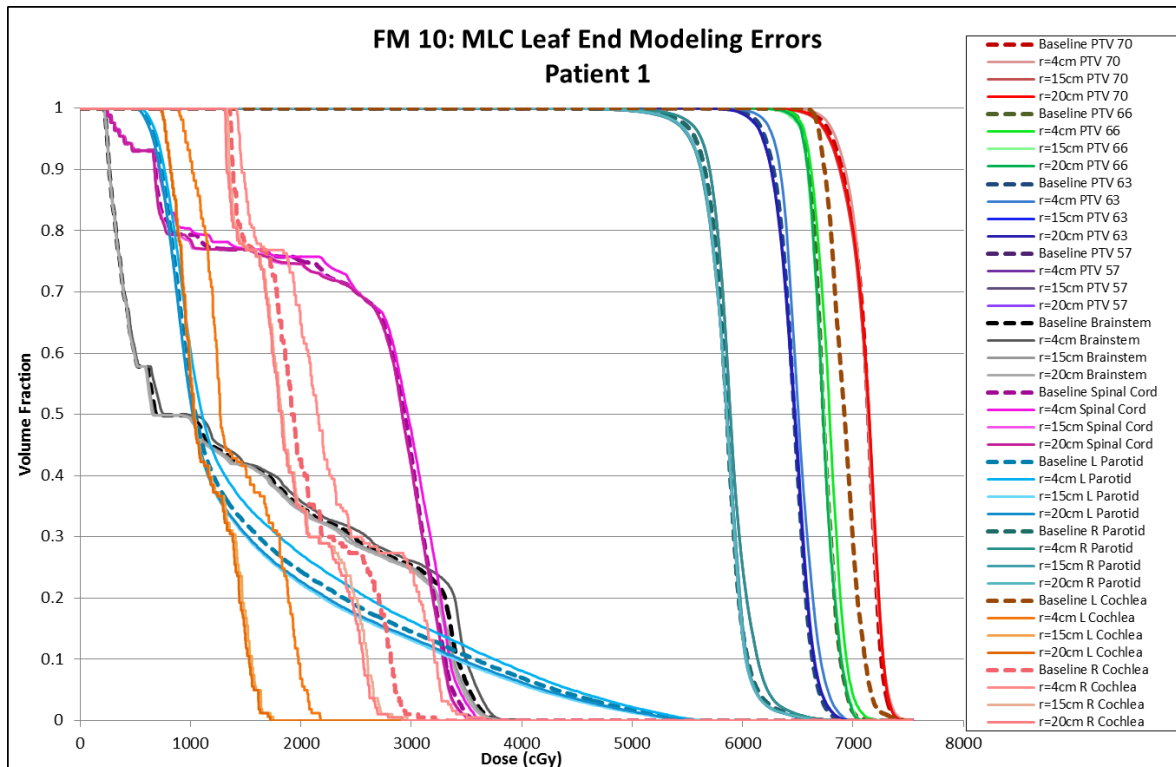


Figure 232: Failure mode 10 DVHs for patient 1.

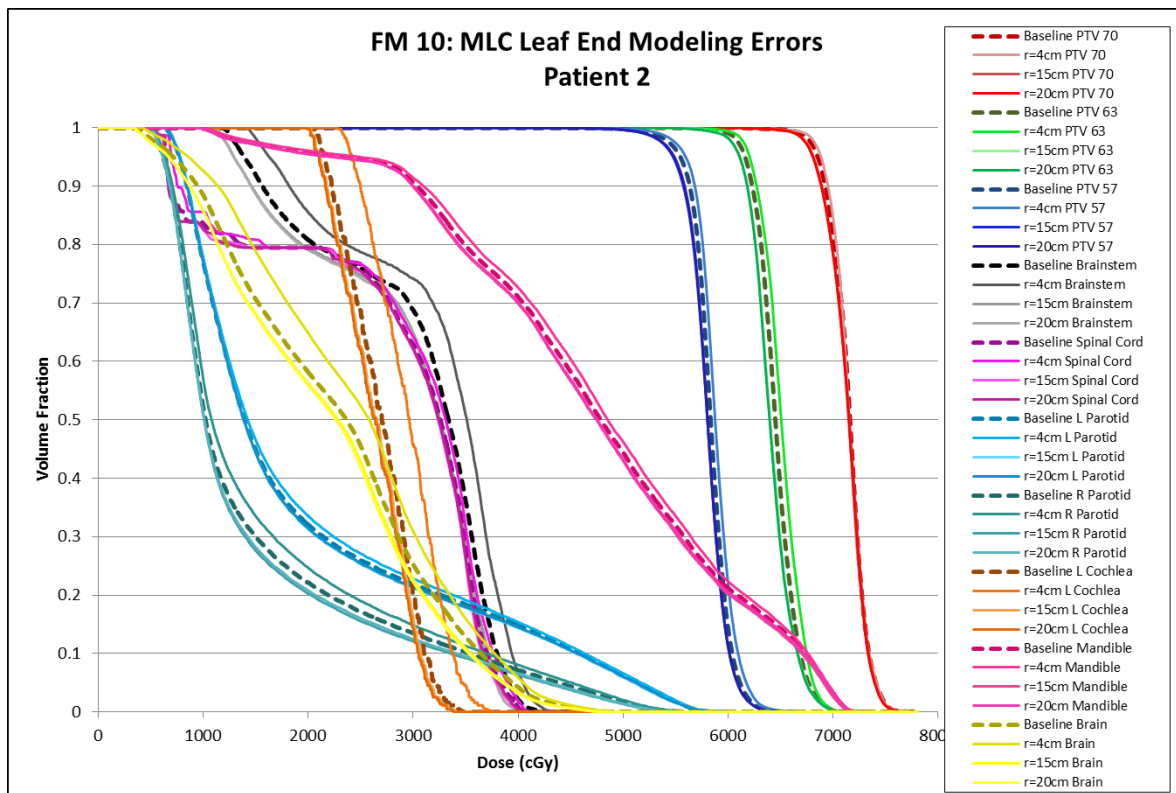


Figure 233: Failure mode 10 DVHs for patient 2.

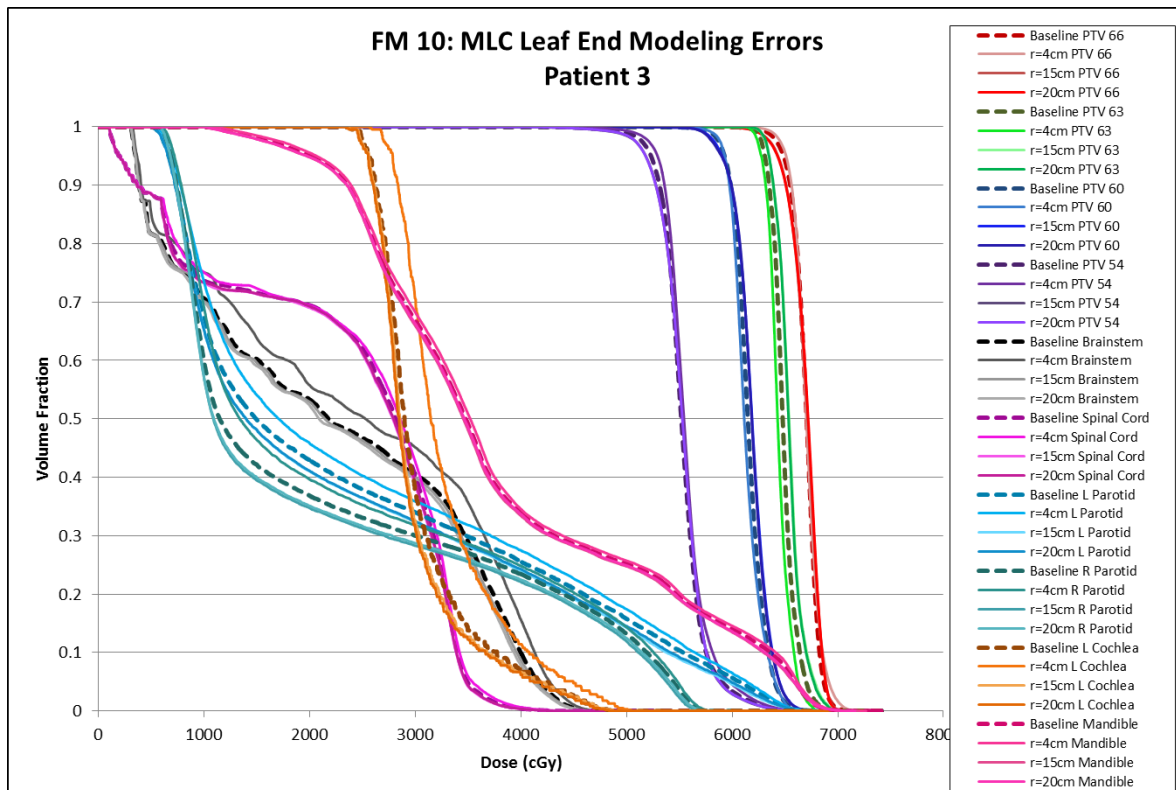


Figure 234: Failure mode 10 DVHs for patient 3.

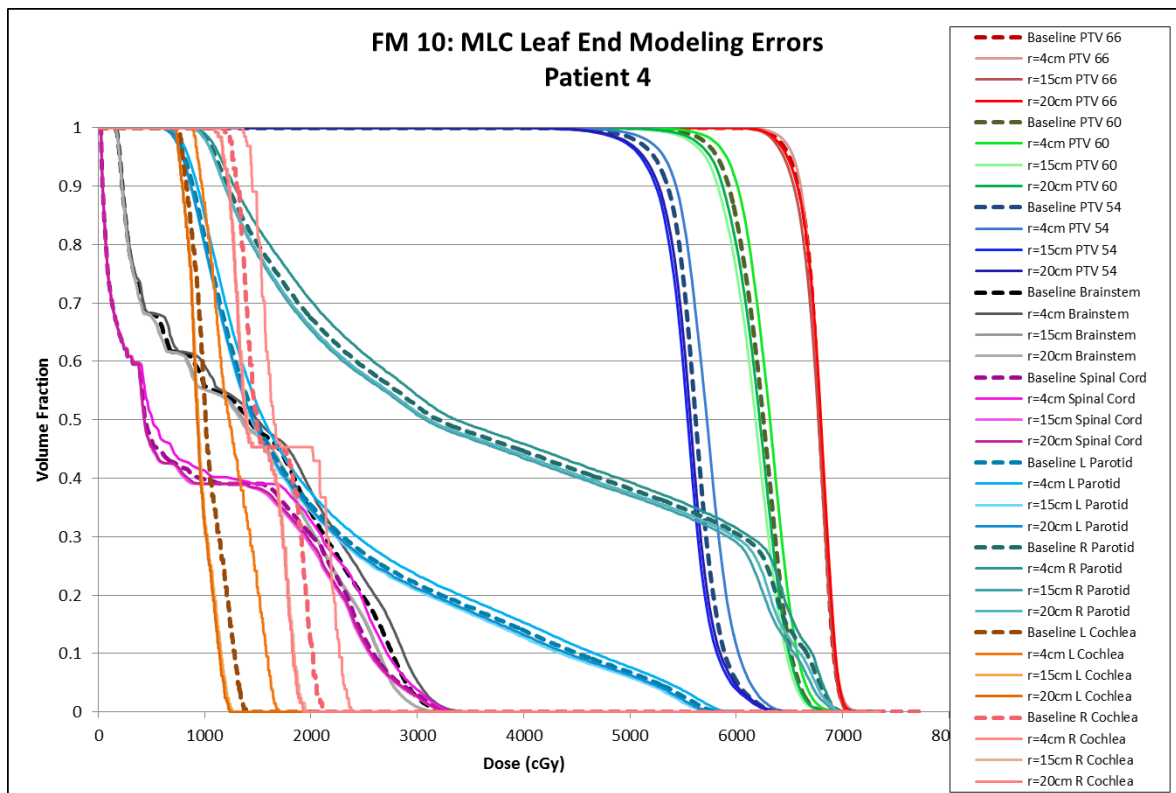


Figure 235: Failure mode 10 DVHs for patient 4.

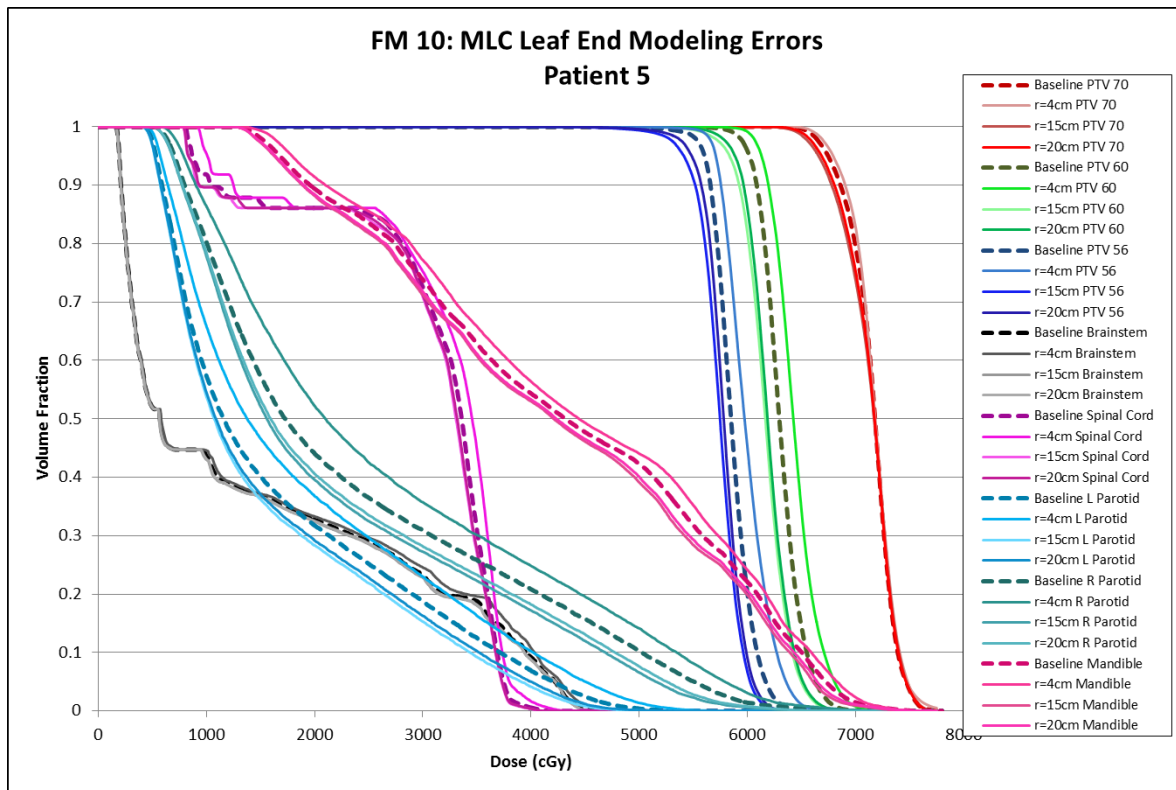


Figure 236: Failure mode 10 DVHs for patient 5.

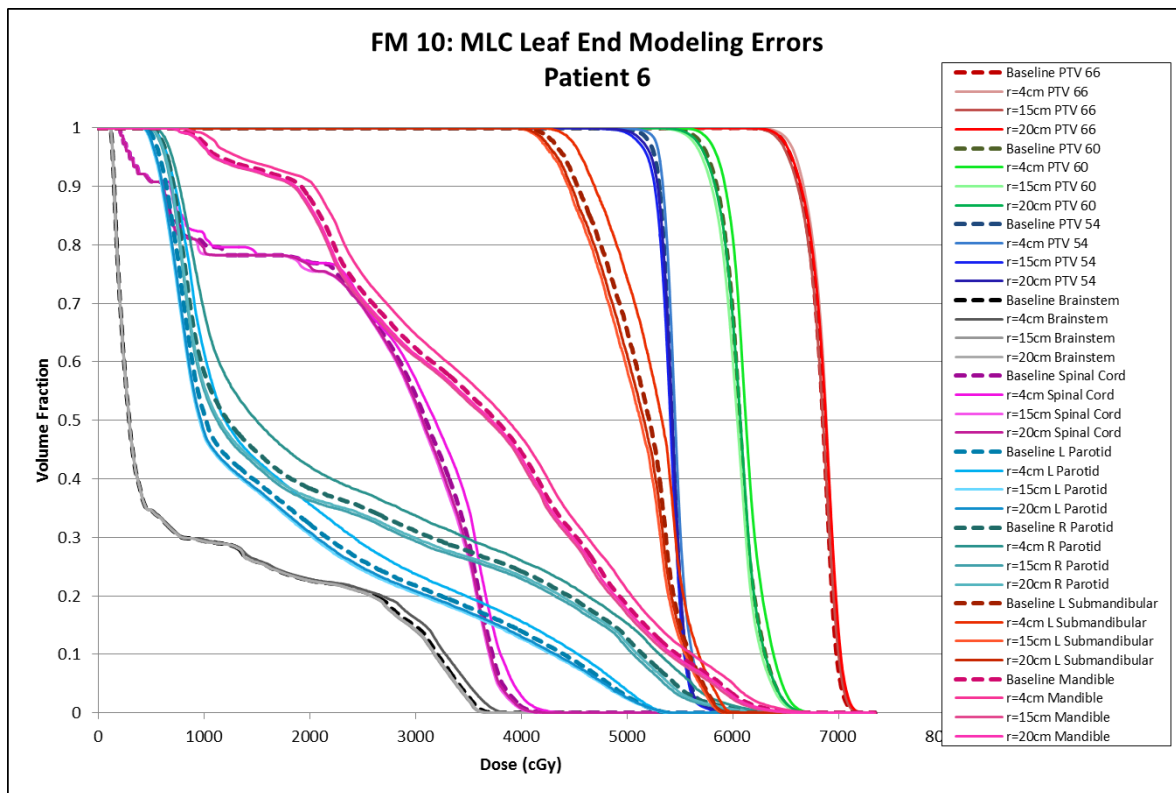


Figure 237: Failure mode 10 DVHs for patient 6.

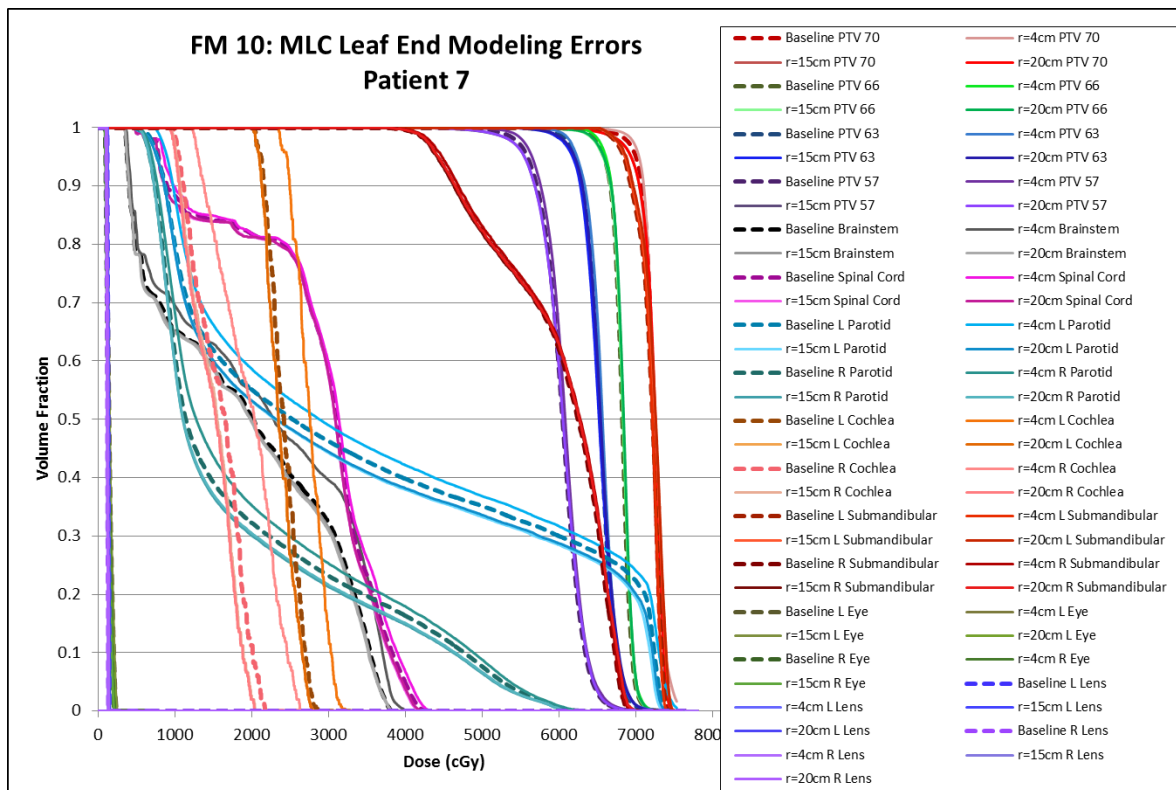


Figure 238: Failure mode 10 DVHs for patient 7.

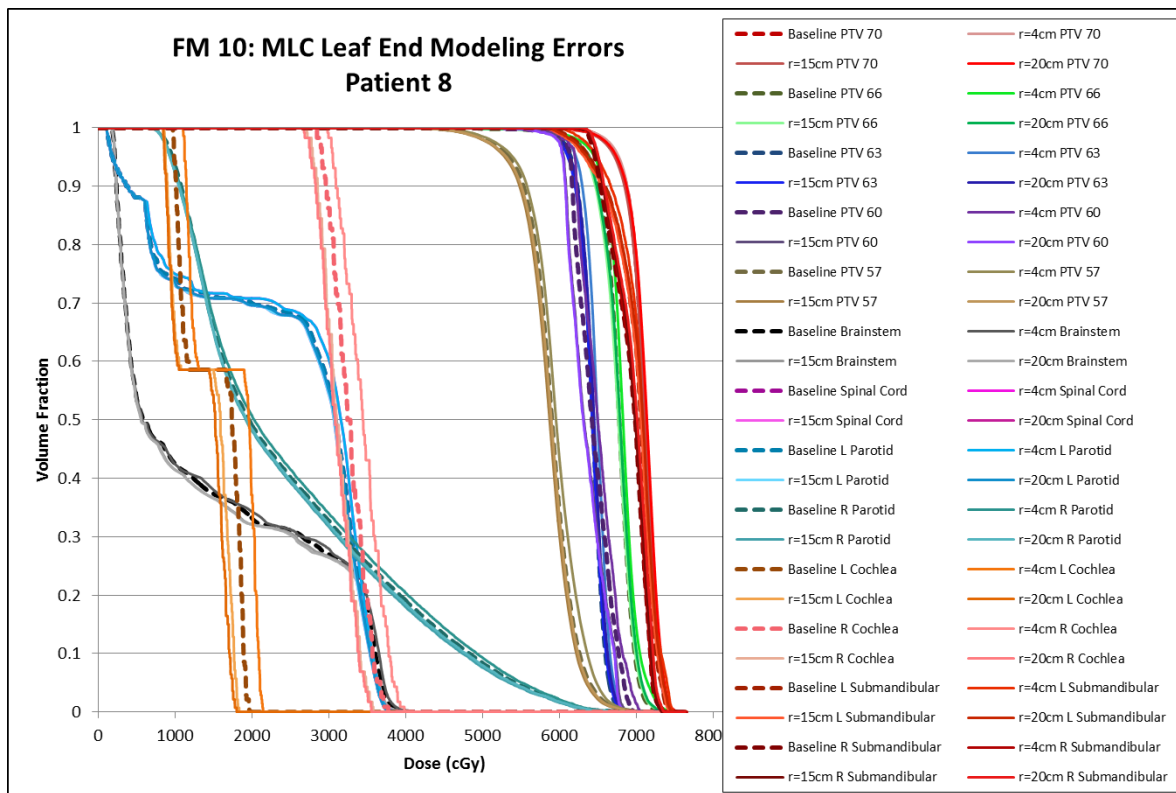


Figure 239: Failure mode 10 DVHs for patient 8.

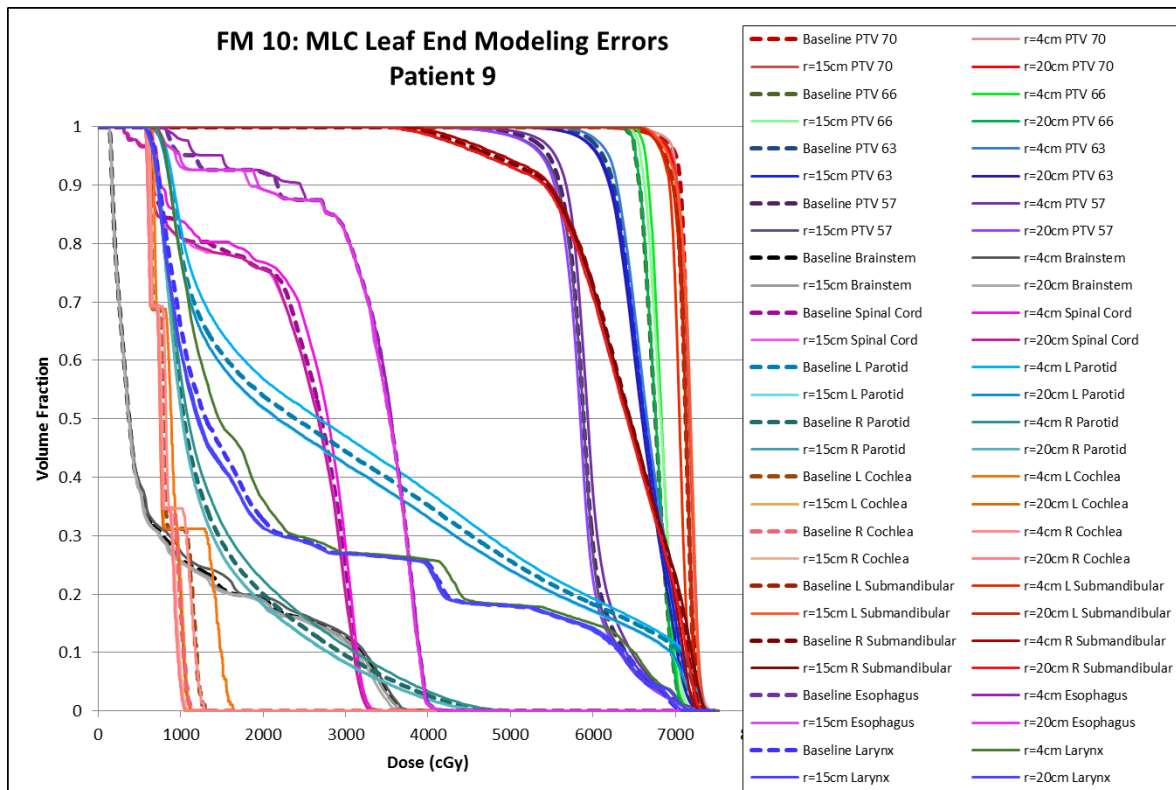


Figure 240: Failure mode 10 DVHs for patient 9.

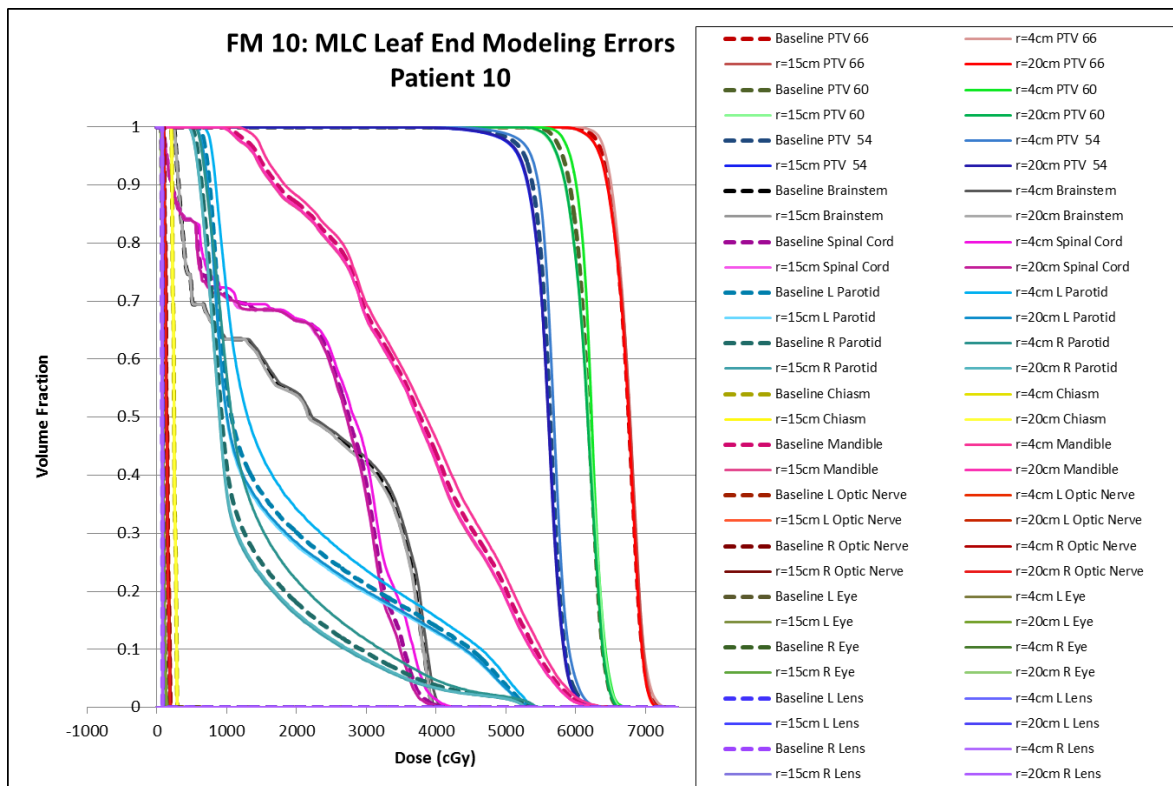


Figure 241: Failure mode 10 DVHs for patient 10.

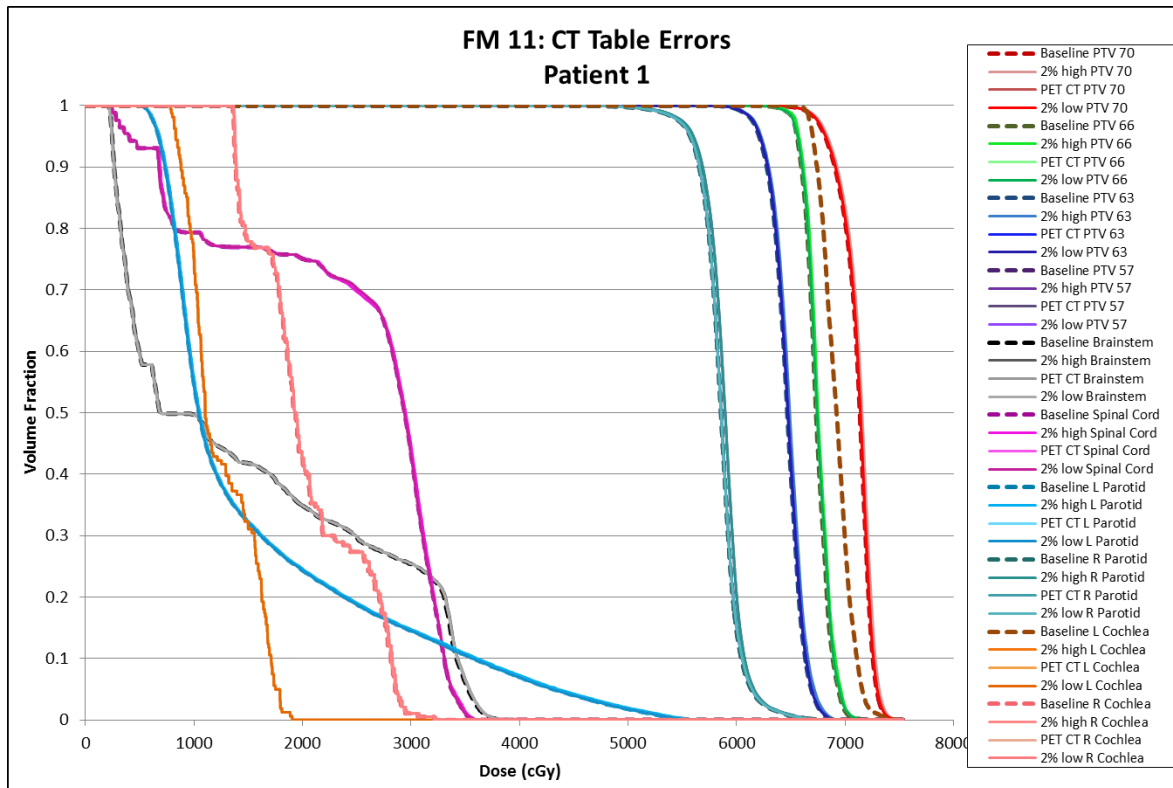


Figure 242: Failure mode 11 DVHs for patient 1.

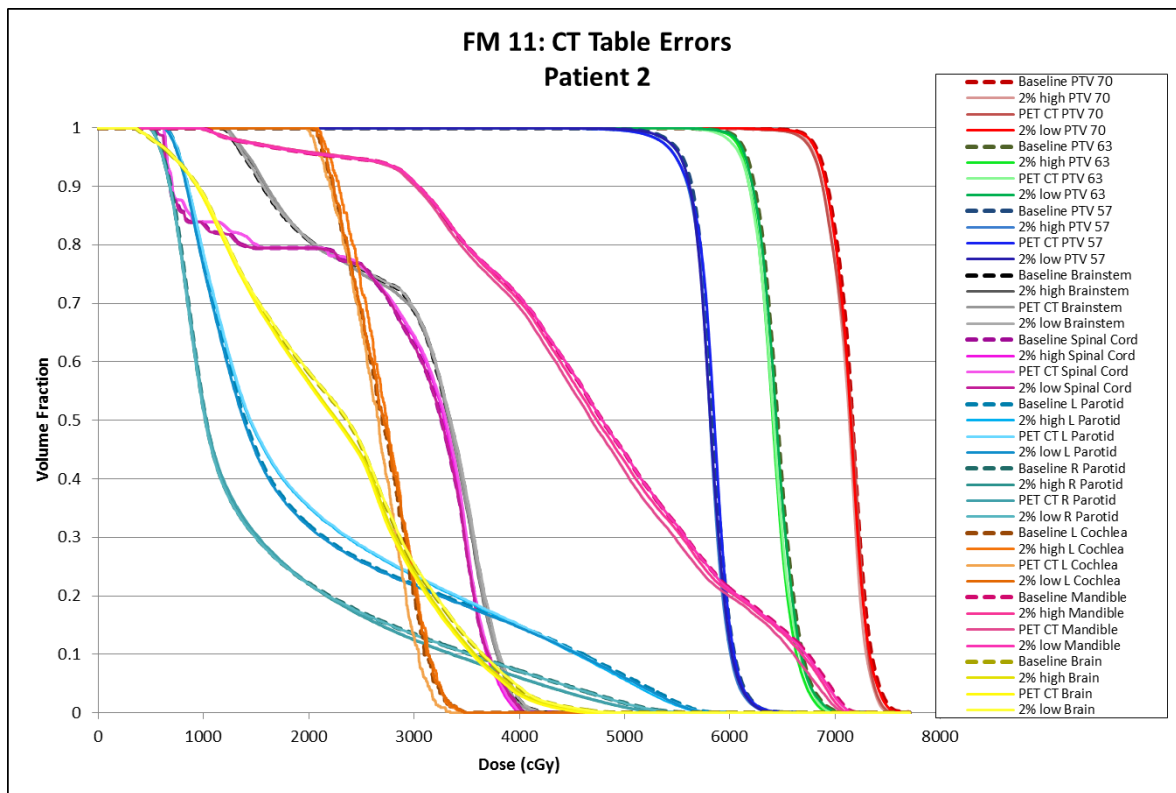


Figure 243: Failure mode 11 DVHs for patient 2.

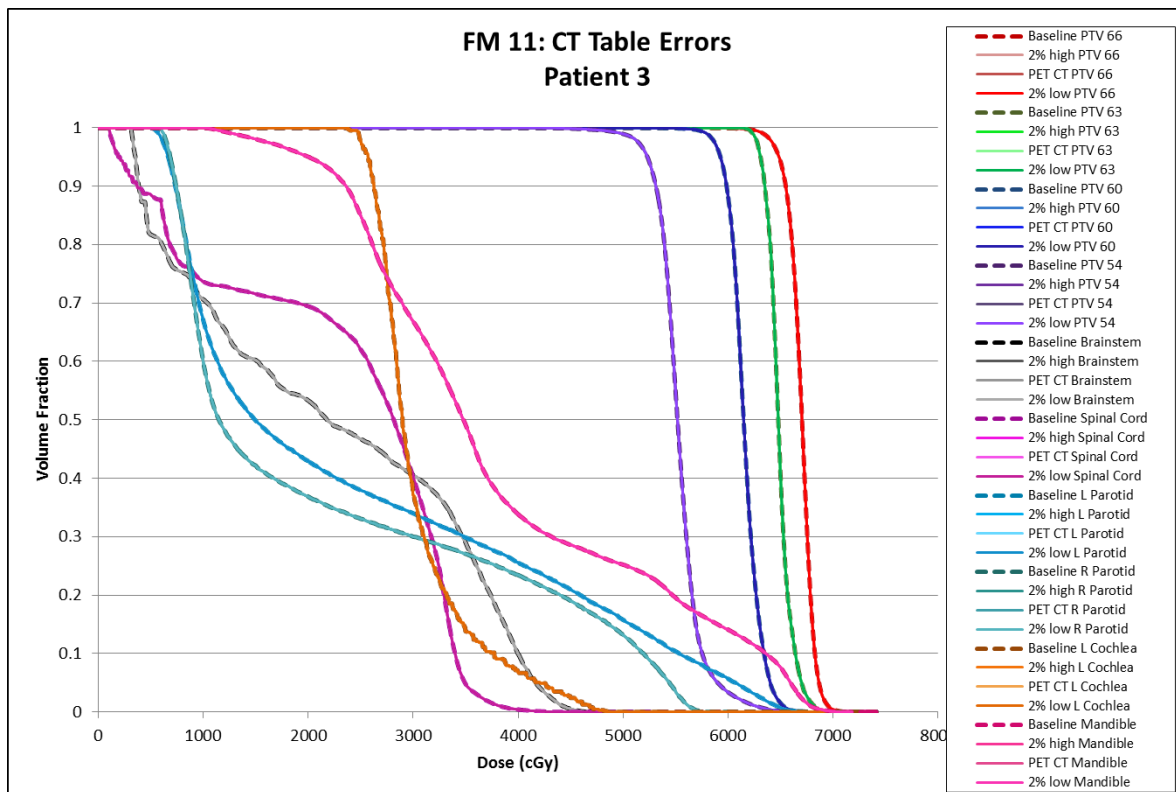


Figure 244: Failure mode 11 DVHs for patient 3.

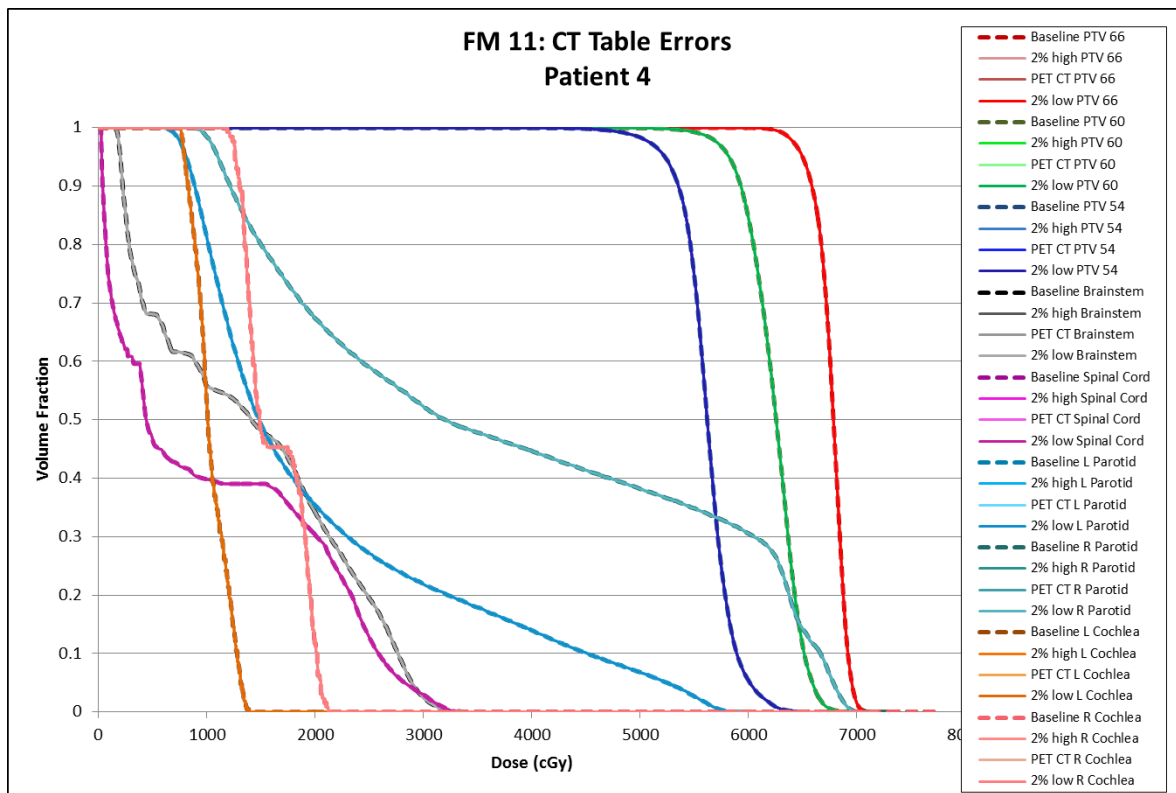


Figure 245: Failure mode 11 DVHs for patient 5.

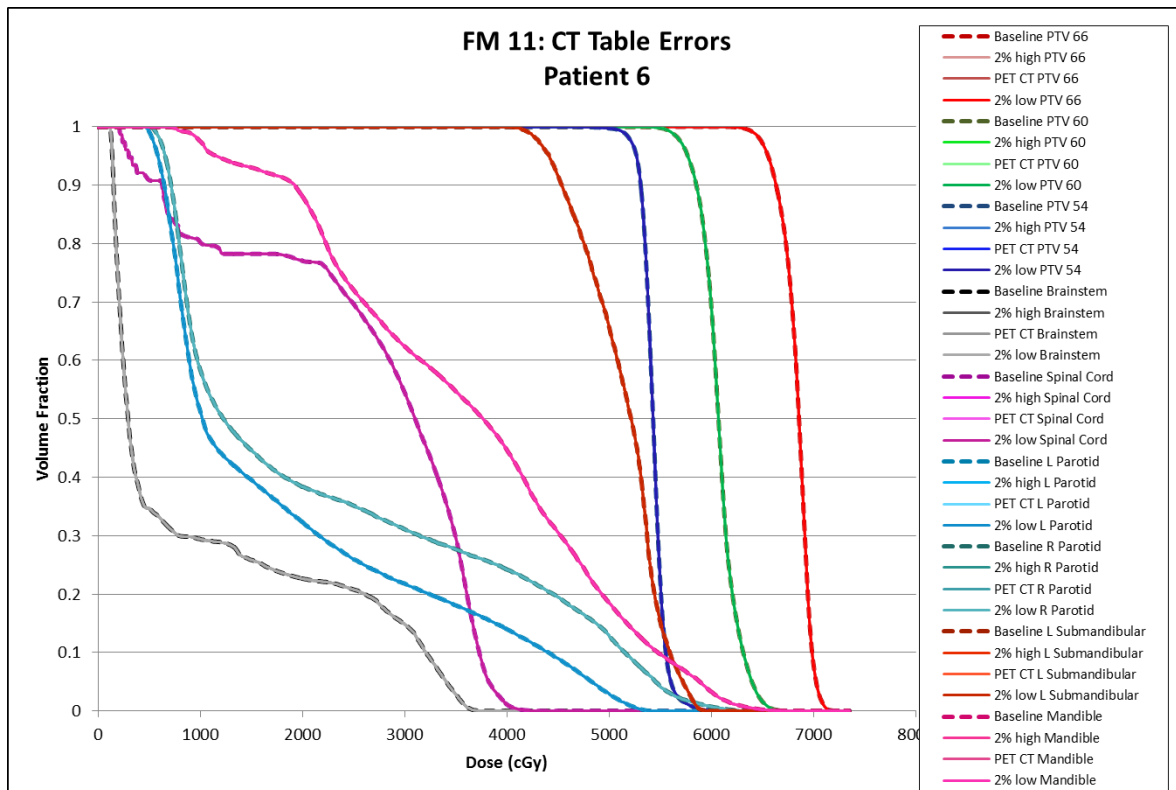


Figure 246: Failure mode 11 DVHs for patient 6.

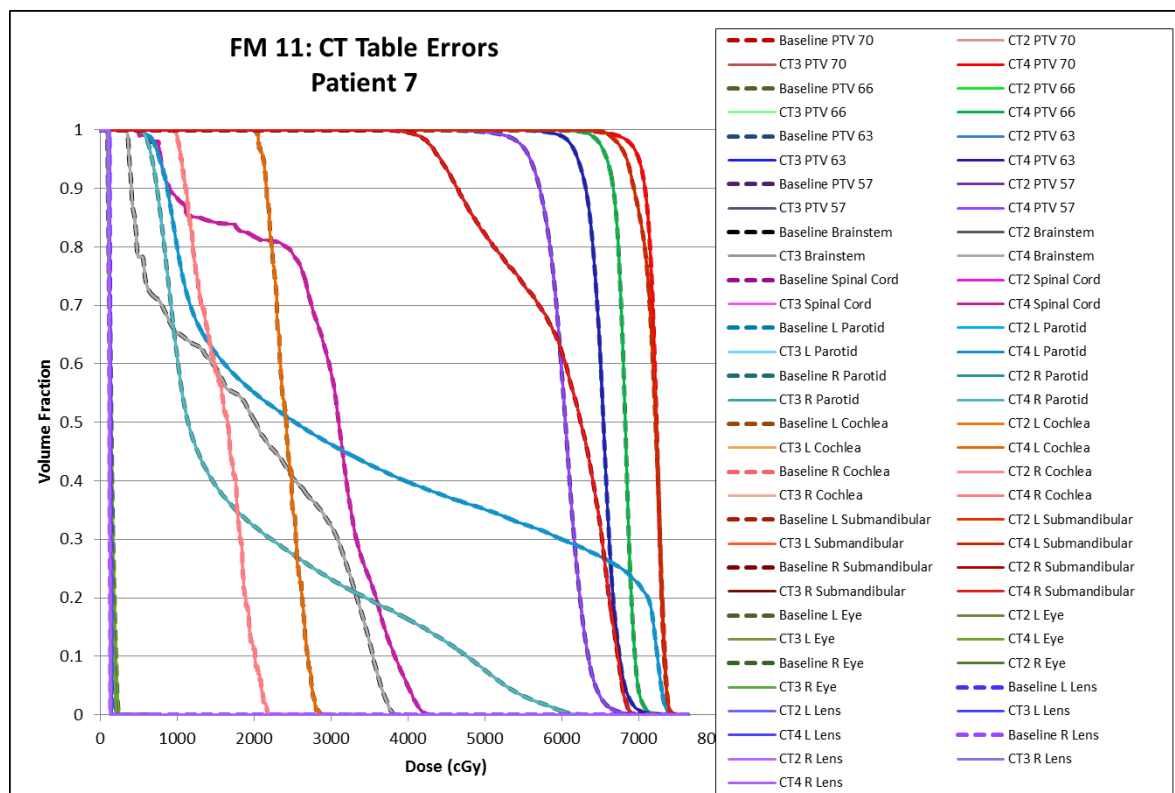


Figure 247: Failure mode 11 DVHs for patient 7.

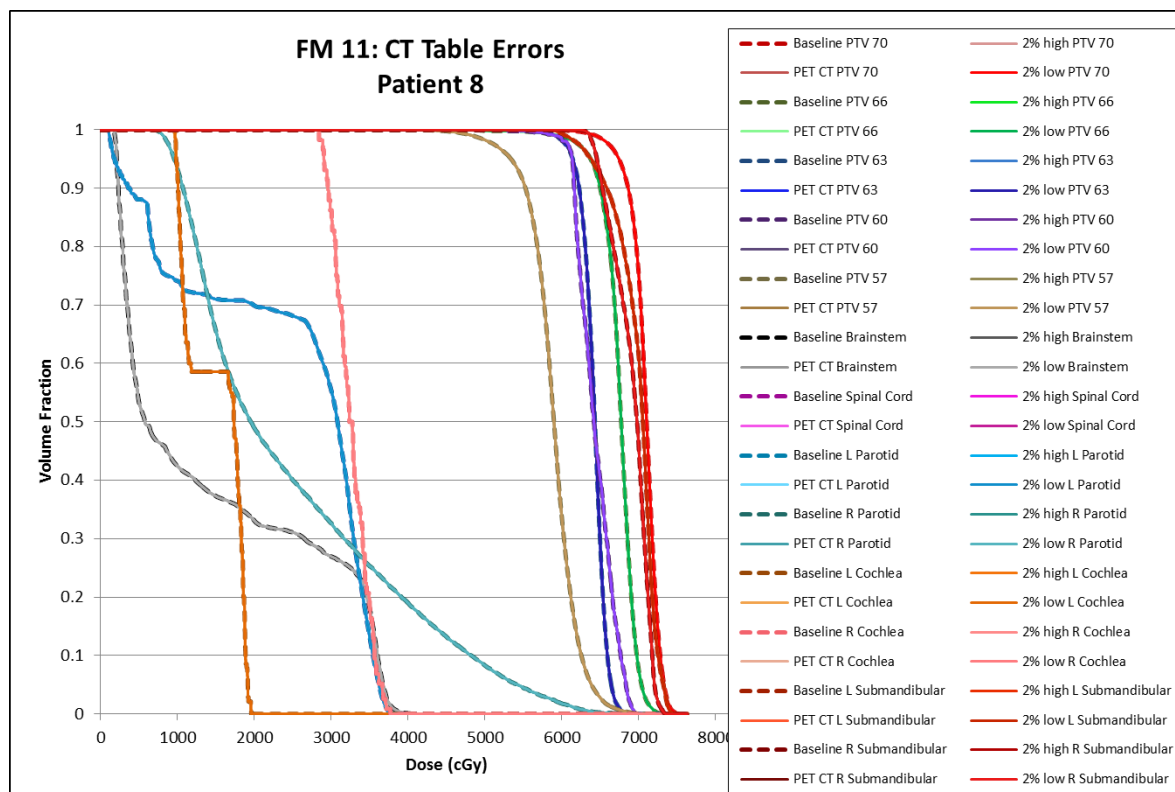


Figure 248: Failure mode 11 DVHs for patient 8.

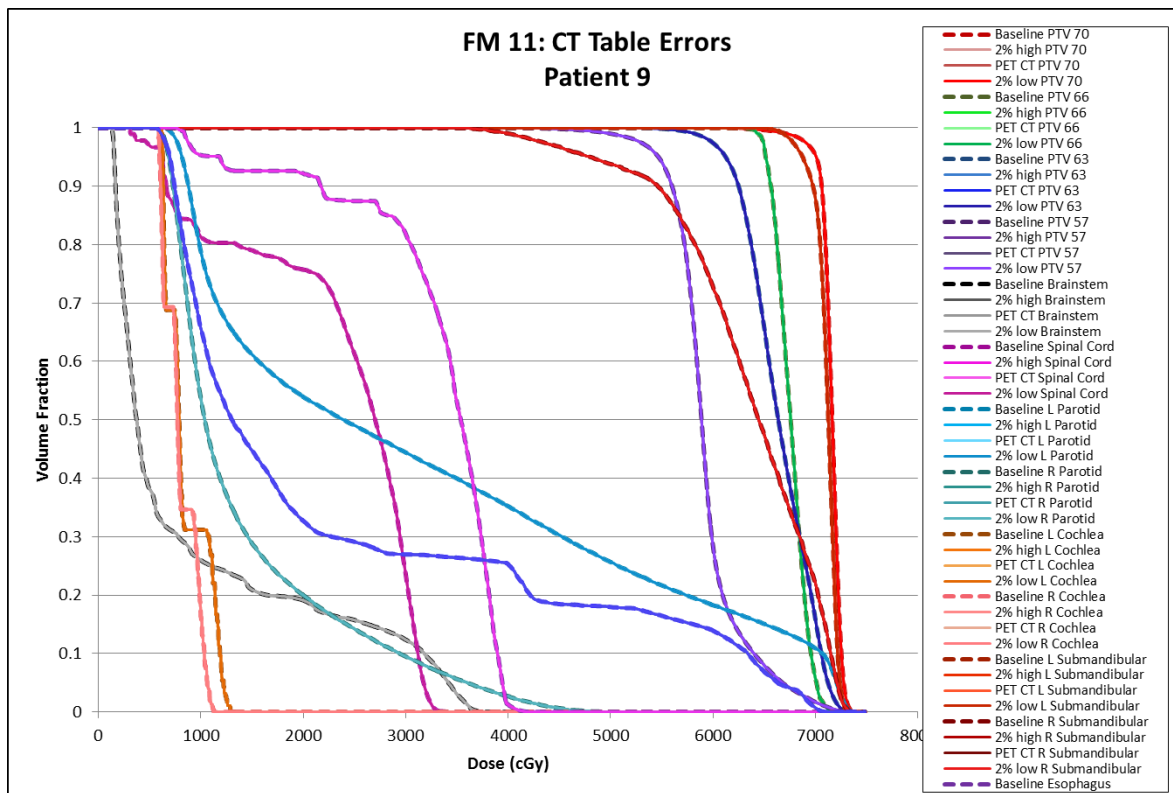


Figure 249: Failure mode 11 DVHs for patient 9.

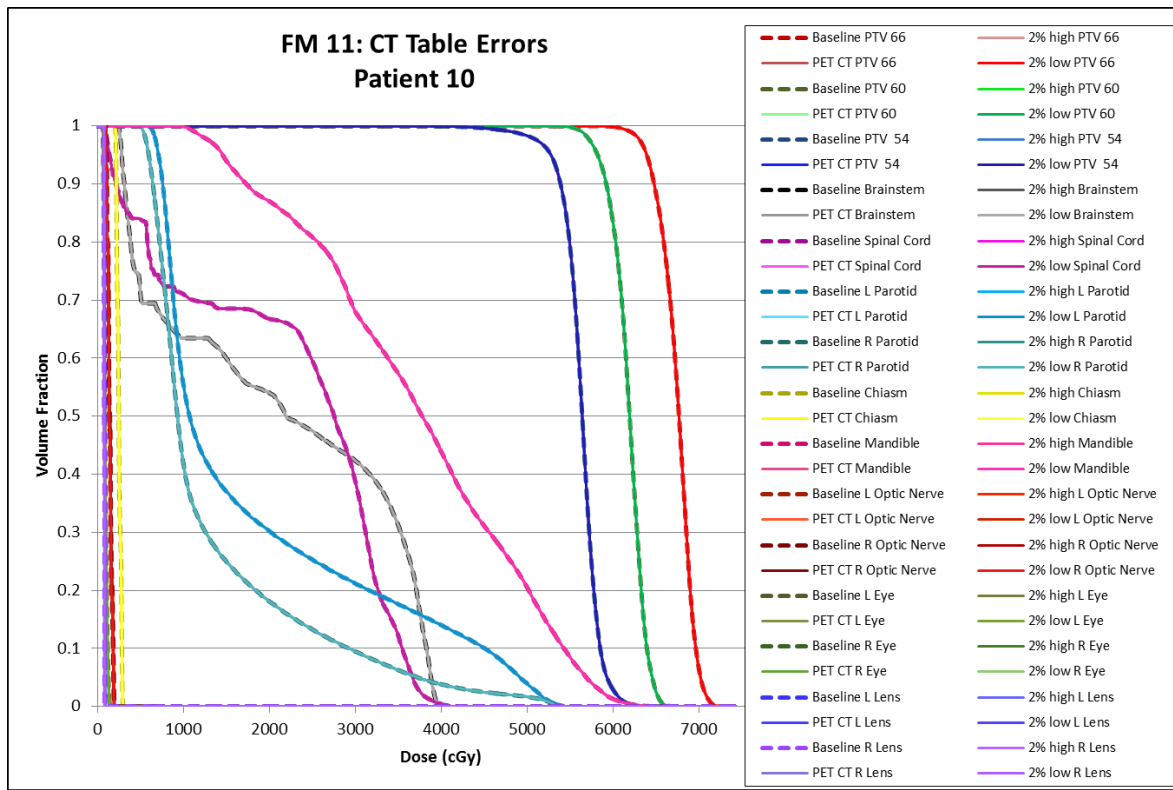


Figure 250: Failure mode 11 DVHs for patient 10.

Bibliography

1. Siegel R, Ma JM, Zou ZH, Jemal A. Cancer Statistics, 2014. *Ca-Cancer J Clin.* Jan 2014;64(1):9-29.
2. RTAnswers. Statistics: About Radition Therapy. 2010;
<http://www.rtanswers.org/statistics/aboutradiationtherapy.aspx>, 2013.
3. Margalit DN, Chen YH, Catalano PJ, Heckman K, Vivenzio T, Nissen K, Wolfsberger LD, Cormack RA, Mauch P, Ng AK. Technological advancements and error rates in radiation therapy delivery. *Int J Radiat Oncol Biol Phys.* Nov 15 2011;81(4):e673-679.
4. Marks LB, Light KL, Hubbs JL, Georgas DL, Jones EL, Wright MC, Willett CG, Yin FF. The impact of advanced technologies on treatment deviations in radiation treatment delivery. *Int J Radiat Oncol Biol Phys.* Dec 1 2007;69(5):1579-1586.
5. Olson AC, Wegner RE, Scicutella C, Heron DE, Greenberger JS, Huq MS, Bednarz G, Flickinger JC. Quality assurance analysis of a large multicenter practice: does increased complexity of intensity-modulated radiotherapy lead to increased error frequency? *Int J Radiat Oncol Biol Phys.* Jan 1 2012;82(1):e77-82.
6. Morganti AG, Deodato F, Zizzari S, Cilla S, Digesu C, Macchia G, Panunzi S, De Gaetano A, Piermattei A, Cellini N, Valentini V. Complexity index (COMIX) and not type of treatment predicts undetected errors in radiotherapy planning and delivery. *Radiother Oncol.* Dec 2008;89(3):320-329.
7. Ford EC, Gaudette R, Myers L, Vanderver B, Engineer L, Zellars R, Song DY, Wong J, Deweese TL. Evaluation of safety in a radiation oncology setting using failure mode and effects analysis. *Int J Radiat Oncol Biol Phys.* Jul 1 2009;74(3):852-858.
8. Kalapurakal JA, Zafirovski A, Smith J, Fisher P, Sathiaseelan V, Barnard C, Rademaker AW, Rave N, Mittal BB. A comprehensive quality assurance program for personnel and procedures in

- radiation oncology: value of voluntary error reporting and checklists. *Int J Radiat Oncol Biol Phys.* Jun 1 2013;86(2):241-248.
9. Huang G, Medlam G, Lee J, Billingsley S, Bissonnette JP, Ringash J, Kane G, Hodgson DC. Error in the delivery of radiation therapy: results of a quality assurance review. *Int J Radiat Oncol Biol Phys.* Apr 1 2005;61(5):1590-1595.
 10. Hunt MA, Pastrana G, Amols HI, Killen A, Alektiar K. The impact of new technologies on radiation oncology events and trends in the past decade: an institutional experience. *Int J Radiat Oncol Biol Phys.* Nov 15 2012;84(4):925-931.
 11. Bissonnette JP, Medlam G. Trend analysis of radiation therapy incidents over seven years. *Radiother Oncol.* Jul 2010;96(1):139-144.
 12. Das P, Johnson J, Hayden SE, Riley BA, Harrelson S, Gillin M, Ibbott G, Buchholz TA. Rate of radiation therapy events in a large academic institution. *Journal of the American College of Radiology : JACR.* Jun 2013;10(6):452-455.
 13. Yeung TK, Bortolotto K, Cosby S, Hoar M, Lederer E. Quality assurance in radiotherapy: evaluation of errors and incidents recorded over a 10 year period. *Radiother Oncol.* Mar 2005;74(3):283-291.
 14. Shafiq J, Barton M, Noble D, Lemer C, Donaldson LJ. An international review of patient safety measures in radiotherapy practice. *Radiotherapy and Oncology.* Jul 2009;92(1):15-21.
 15. Kim JP. Categorizing accident sequences in the external radiotherapy for risk analysis. *Radiat Oncol.* 2013;31(2):88-96.
 16. Terezakis SA, Harris KM, Ford E, Michalski J, DeWeese T, Santanam L, Mutic S, Gay H. An Evaluation of Departmental Radiation Oncology Incident Reports: Anticipating a National Reporting System. *Int J Radiat Oncol.* Mar 15 2013;85(4):919-923.
 17. James JT. A New, Evidence-based Estimate of Patient Harms Associated with Hospital Care. *Journal of Patient Safety.* Sep 2013;9(3):122-128.

18. Herman MG. Guest Editorial: Patient safety and errors in the application of medical radiation: our responsibility. *Journal of Applied Clinical Medical Physics*. 2010;11(2):2-4.
19. Bogdanich W. As Technology Surges, Radiation Safeguards Lag. *The New York Times* 2010.
20. Bogdanich W. A Pinpoint Beam Strays Invisibly, Harming Instead of Healing. *The New York Times* 2010.
21. Bogdanich W. Radiation Errors Reported in Missouri. *The New York Times* 2010.
22. Bogdanich W. Radiation Offers New Cures, and Ways to Do Harm. *The New York Times* 2010.
23. *Determination of absorbed dose in a patient irradiated by beam of x or gamma rays in radiotherapy procedures*. Bethesda, Maryland: International Commission on Radiation Units and Measurements; 1976. ICRU Report No. 24.
24. Thwaites D. Accuracy required and achievable in radiotherapy dosimetry: have modern technology and techniques changed our views? *J Phys Conf Ser*. 2013;444.
25. Molineu A, Hernandez N, Nguyen T, Ibbott G, Followill D. Credentialing results from IMRT irradiations of an anthropomorphic head and neck phantom. *Med Phys*. Feb 2013;40(2):022101.
26. Rath F. Tools for developing a quality management program: proactive tools (process mapping, value stream mapping, fault tree analysis, and failure mode and effects analysis). *Int J Radiat Oncol Biol Phys*. 2008;71(1 Suppl):S187-190.
27. Thomadsen B. Critique of traditional quality assurance paradigm. *Int J Radiat Oncol Biol Phys*. 2008;71(1 Suppl):S166-169.
28. Ishikura S. Quality assurance of radiotherapy in cancer treatment: toward improvement of patient safety and quality of care. *Jpn J Clin Oncol*. Nov 2008;38(11):723-729.
29. Masini L, Donis L, Loi G, Mones E, Molina E, Bolchini C, Krengli M. Application of failure mode and effects analysis to intracranial stereotactic radiation surgery by linear accelerator. *Practical radiation oncology*. 2014;4(6):392-397.

30. Broggi S, Cantone MC, Chiara A, Di Muzio N, Longobardi B, Mangili P, Veronese I. Application of failure mode and effects analysis (FMEA) to pretreatment phases in tomotherapy. *J Appl Clin Med Phys*. 2013;14(5):265-277.
31. Perks JR, Stanic S, Stern RL, Henk B, Nelson MS, Harse RD, Mathai M, Purdy JA, Valicenti RK, Siefkin AD, Chen AM. Failure mode and effect analysis for delivery of lung stereotactic body radiation therapy. *Int J Radiat Oncol Biol Phys*. Jul 15 2012;83(4):1324-1329.
32. Sawant A, Dieterich S, Svatos M, Keall P. Failure mode and effect analysis-based quality assurance for dynamic MLC tracking systems. *Med Phys*. Dec 2010;37(12):6466-6479.
33. Ciocca M, Cantone MC, Veronese I, Cattani F, Pedroli G, Molinelli S, Vitolo V, Orecchia R. Application of failure mode and effects analysis to intraoperative radiation therapy using mobile electron linear accelerators. *Int J Radiat Oncol Biol Phys*. Feb 1 2012;82(2):e305-311.
34. Huq MS, Fraass BA, Dunscombe PB, Gibbons JP, Jr., Ibbott GS, Medin PM, Mundt A, Mutic S, Palta JR, Thomadsen BR, Williamson JF, Yorke ED. A method for evaluating quality assurance needs in radiation therapy. *Int J Radiat Oncol Biol Phys*. 2008;71(1 Suppl):S170-173.
35. Cantone MC, Ciocca M, Dionisi F, Fossati P, Lorentini S, Krengli M, Molinelli S, Orecchia R, Schwarz M, Veronese I, Vitolo V. Application of failure mode and effects analysis to treatment planning in scanned proton beam radiotherapy. *Radiat Oncol*. 2013;8:127.
36. Lopez-Tarjuelo J, Bouche-Babiloni A, Santos-Serra A, Morillo-Macias V, Calvo FA, Kubyshev Y, Ferrer-Albiach C. Failure mode and effect analysis oriented to risk-reduction interventions in intraoperative electron radiation therapy: The specific impact of patient transportation, automation, and treatment planning availability. *Radiother Oncol*. Nov 2014;113(2):283-289.
37. Ford EC, Smith K, Terezakis S, Croog V, Gollamudi S, Gage I, Keck J, DeWeese T, Sibley G. A streamlined failure mode and effects analysis. *Medical Physics*. Jun 2014;41(6).
38. Shebl NA, Franklin BD, Barber N. Is failure mode and effect analysis reliable? *J Patient Saf*. Jun 2009;5(2):86-94.

39. Ashley LaA, G. . Failure Mode and Effects Analysis: An Empirical Comparison of Failure Mode Scoring Procedures. *J Patient Saf.* 2010;6:210-215.
40. Franklin BD, Shebl NA, Barber N. Failure mode and effects analysis: too little for too much? *Bmj Qual Saf.* Jul 2012;21(7):607-611.
41. Shebl NA, Franklin BD, Barber N. Failure mode and effects analysis outputs: are they valid? *BMC Health Serv Res.* 2012;12:150.
42. Hendee WR, Herman MG. Improving patient safety in radiation oncology. *Med Phys.* Jan 2011;38(1):78-82.
43. Sun B, Rangaraj D, Boddu S, Goddu M, Yang D, Palaniswaamy G, Yaddanapudi S, Wooten O, Mutic S. Evaluation of the efficiency and effectiveness of independent dose calculation followed by machine log file analysis against conventional measurement based IMRT QA. *J Appl Clin Med Phys.* 2012;13(5):3837.
44. Molineu A, Followill DS, Balter PA, Hanson WF, Gillin MT, Huq MS, Eisbruch A, Ibbott GS. Design and implementation of an anthropomorphic quality assurance phantom for intensity-modulated radiation therapy for the Radiation Therapy Oncology Group. *International Journal of Radiation Oncology*Biophysics*Physics.* 2005;63(2):577-583.
45. Stamatis DH. *Failure mode and effect analysis : FMEA from theory to execution.* 2nd ed. Milwaukee, Wisc.: ASQ Quality Press; 2003.
46. Dillman D, Smyth, J., and Christian, L. *Internet, Mail, and Mixed-mode Surveys: The Tailored Design Method.* 3rd ed. Hoboken, New Jersey: John Wiley & Sons, Inc.; 2009.
47. McNiven AL, Sharpe MB, Purdie TG. A new metric for assessing IMRT modulation complexity and plan deliverability. *Medical Physics.* 2010;37(2):505-515.
48. Mu G, Ludlum E, Xia P. Impact of MLC leaf position errors on simple and complex IMRT plans for head and neck cancer. *Phys Med Biol.* Jan 7 2008;53(1):77-88.

49. Mohan R, Arnfield M, Tong S, Wu Q, Siebers J. The impact of fluctuations in intensity patterns on the number of monitor units and the quality and accuracy of intensity modulated radiotherapy. *Medical Physics*. 2000;27(6):1226-1237.
50. Kruse JJ. On the insensitivity of single field planar dosimetry to IMRT inaccuracies. *Med Phys*. Jun;37(6):2516-2524.
51. Tonigan JR. *EVALUATION OF INTENSITY MODULATED RADIATION THERAPY (IMRT) DELIVERY ERROR DUE TO IMRT TREATMENT PLAN COMPLEXITY AND IMPROPERLY MATCHED DOSIMETRY DATA* [Thesis]. Houston: Radiation Physics, University of Texas Graduate School of Biomedical Sciences; 2011.
52. Kirby TH, Hanson WF, Johnston DA. Uncertainty analysis of absorbed dose calculations from thermoluminescence dosimeters. *Med Phys*. Nov-Dec 1992;19(6):1427-1433.
53. Niroomand-Rad A, Blackwell CR, Coursey BM, Gall KP, Galvin JM, McLaughlin WL, Meigooni AS, Nath R, Rodgers JE, Soares CG. Radiochromic film dosimetry: recommendations of AAPM Radiation Therapy Committee Task Group 55. American Association of Physicists in Medicine. *Med Phys*. Nov 1998;25(11):2093-2115.
54. Molineu A, Alvarez, P., Kry, S., Follwill, D. SU-E-T-543: Is it feasible to tighten the criteria for IROC's Anthropomorphic Phantoms? *Med Phys*. 2014 2014;41:354.
55. Low DA, Harms WB, Mutic S, Purdy JA. A technique for the quantitative evaluation of dose distributions. *Med Phys*. May 1998;25(5):656-661.
56. Nelms BE, Simon JA. A survey on planar IMRT QA analysis. *J Appl Clin Med Phys*. 2007;8(3):2448.
57. Measurements ICoRUa. *Determination of absorbed dose in a patient irradiated by beams of x or gamma rays in radiotherapy procedures*. Bethesda, MD1976.
58. Papanikolaou N, Battista, J. Boyer, A., Kappas, C., Klein, E., Mackie, T. R., Sharpe, M., Van Dyk, J. Tissue inhomogeneity corrections for megavoltage photon beams. *AAPM Task Group 65*. 2004:1-135.

59. Commission NR. *Code of Federal Regulations, 10 CFR Part 35*. Washington, DC2004.
60. Klein EE, Hanley J, Bayouth J, Yin F-F, Simon W, Dresser S, Serago C, Aguirre F, Ma L, Arjomandy B, Liu C, Sandin C, Holmes T. Task Group 142 report: Quality assurance of medical accelerators. *Medical Physics*. 2009;36(9):4197-4212.
61. Khan FM. *The physics of radiation therapy*. 4 ed. Baltimore, MD: Lippincott Williams & Wilkins, a Wolters Kluwer business; 2010.
62. Gao SaB, P. A comparison of metrics for monitoring changes in energy of flattened and unflattened photon beams on the Varian TrueBeam linear accelerator. *Journal of Applied Clinical Medical Physics*. 2015;Submitted for publication.
63. Gao S, Balter PA, Rose M, Simon WE. Measurement of changes in linear accelerator photon energy through flatness variation using an ion chamber array. *Med Phys*. Apr 2013;40(4):042101.
64. Cheng CW, Tang WL, Das IJ. Beam characteristics of upper and lower physical wedge systems of Varian accelerators. *Phys Med Biol*. Nov 21 2003;48(22):3667-3683.
65. Luo W, Li J, Price RA, Jr., Chen L, Yang J, Fan J, Chen Z, McNeeley S, Xu X, Ma CM. Monte Carlo based IMRT dose verification using MLC log files and R/V outputs. *Med Phys*. Jul 2006;33(7):2557-2564.
66. LoSasso T, Chui CS, Ling CC. Physical and dosimetric aspects of a multileaf collimation system used in the dynamic mode for implementing intensity modulated radiotherapy. *Med Phys*. Oct 1998;25(10):1919-1927.
67. Rangel A, Dunscombe P. Tolerances on MLC leaf position accuracy for IMRT delivery with a dynamic MLC. *Med Phys*. Jul 2009;36(7):3304-3309.
68. Sastre-Padro M, Welleweerd J, Malinen E, Eilertsen K, Olsen DR, van der Heide UA. Consequences of leaf calibration errors on IMRT delivery. *Phys Med Biol*. Feb 21 2007;52(4):1147-1156.
69. Bayouth JE, Wendt D, Morrill SM. MLC quality assurance techniques for IMRT applications. *Med Phys*. May 2003;30(5):743-750.

70. Sasaki M, Tominaga M, Ikushima H, Kishi T, Kawashita T, Hara Y, Fukunaga Y, Kimura M, Shitakubo Y, Takashi S, Oita M. [Impact of multileaf collimator leaf positioning accuracy on intensity modulated radiation therapy]. *Nihon Hoshasen Gijutsu Gakkai zasshi*. 2011;67(5):497-506.
71. Yan G, Liu C, Simon TA, Peng LC, Fox C, Li JG. On the sensitivity of patient-specific IMRT QA to MLC positioning errors. *J Appl Clin Med Phys*. 2009;10(1):2915.
72. Rangel A, Palte G, Dunscombe P. The sensitivity of patient specific IMRT QC to systematic MLC leaf bank offset errors. *Med Phys*. Jul 2010;37(7):3862-3867.
73. Moiseenko V, Lapointe V, James K, Yin L, Liu M, Pawlicki T. Biological consequences of MLC calibration errors in IMRT delivery and QA. *Med Phys*. Apr 2012;39(4):1917-1924.
74. Low DA, Zhu XR, Purdy JA, Soderstrom S. The influence of angular misalignment on fixed-portal intensity modulated radiation therapy. *Med Phys*. Jul 1997;24(7):1123-1139.
75. Xing L, Lin Z, Donaldson SS, Le QT, Tate D, Goffinet DR, Wolden S, Ma L, Boyer AL. Dosimetric effects of patient displacement and collimator and gantry angle misalignment on intensity modulated radiation therapy. *Radiother Oncol*. Jul 2000;56(1):97-108.
76. Li J, Wiersma RD, Stepaniak CJ, Farrey KJ, Al-Hallaq HA. Improvements in dose accuracy delivered with static-MLC IMRT on an integrated linear accelerator control system. *Med Phys*. May 2012;39(5):2456-2462.
77. Reena P, Dayananda S, Pai R, Jamema SV, Gupta T, Deepak D, Rajeev S. Performance characterization of siemens primus linear accelerator under small monitor unit and small segments for the implementation of step-and-shoot intensity-modulated radiotherapy. *Journal of medical physics / Association of Medical Physicists of India*. Oct 2006;31(4):269-274.
78. Kang SK, Cheong KH, Hwang T, Cho BC, Kim SS, Kim KJ, Oh do H, Bae H, Suh TS. Dosimetric characteristics of linear accelerator photon beams with small monitor unit settings. *Med Phys*. Nov 2008;35(11):5172-5178.

79. Grigorov GN, Chow JC, Barnett RB. Dosimetry limitations and a dose correction methodology for step-and-shoot IMRT. *Phys Med Biol*. Feb 7 2006;51(3):637-652.
80. Losasso T. IMRT delivery performance with a varian multileaf collimator. *Int J Radiat Oncol Biol Phys*. 2008;71(1 Suppl):S85-88.
81. Kim JO, Siebers JV, Keall PJ, Arnfield MR, Mohan R. A Monte Carlo study of radiation transport through multileaf collimators. *Med Phys*. Dec 2001;28(12):2497-2506.
82. Huq MS, Das IJ, Steinberg T, Galvin JM. A dosimetric comparison of various multileaf collimators. *Phys Med Biol*. Jun 21 2002;47(12):N159-170.
83. Deng J, Pawlicki T, Chen Y, Li J, Jiang SB, Ma CM. The MLC tongue-and-groove effect on IMRT dose distributions. *Phys Med Biol*. Apr 2001;46(4):1039-1060.
84. Li JS, Lin T, Chen L, Price RA, Jr., Ma CM. Uncertainties in IMRT dosimetry. *Med Phys*. Jun 2010;37(6):2491-2500.
85. Williams MJ, Metcalfe P. Verification of a rounded leaf-end MLC model used in a radiotherapy treatment planning system. *Phys Med Biol*. Feb 21 2006;51(4):N65-78.
86. Hariri S, Shahriari M. Suggesting a new design for multileaf collimator leaves based on Monte Carlo simulation of two commercial systems. *J Appl Clin Med Phys*. 2010;11(3):3101.
87. Constantinou C, Harrington JC, DeWerd LA. An electron density calibration phantom for CT-based treatment planning computers. *Med Phys*. Mar-Apr 1992;19(2):325-327.
88. Kilby W, Sage J, Rabett V. Tolerance levels for quality assurance of electron density values generated from CT in radiotherapy treatment planning. *Phys Med Biol*. May 7 2002;47(9):1485-1492.
89. Cadman P, Bassalow R, Sidhu NP, Ibbott G, Nelson A. Dosimetric considerations for validation of a sequential IMRT process with a commercial treatment planning system. *Phys Med Biol*. Aug 21 2002;47(16):3001-3010.

- 90.** Kutcher GJ, Coia L, Gillin M, Hanson WF, Leibel S, Morton RJ, Palta JR, Purdy JA, Reinstein LE, Svensson GK, Weller M, Wingfield L. Comprehensive QA for radiation oncology: Report of AAPM Radiation Therapy Committee Task Group 40. *Medical Physics*. 1994;21(4):581-618.

Vita

Jacqueline Tonigan Faught was born in Albuquerque, New Mexico on June 7, 1987, the daughter of Diane Moody Tonigan and Richard Eric Tonigan, D.D.S. After completing her work at Eldorado High School, Albuquerque, New Mexico in 2005, she entered the University of New Mexico in Albuquerque, New Mexico. She received the degree of Bachelor of Science with a major in nuclear engineering from the University of New Mexico in May, 2009. In September of 2009 she entered The University of Texas Graduate School of Biomedical Sciences at Houston in Houston, Texas. She received the degree of Master of Science with a major in medical physics from the University of Texas Graduate School of Biomedical Sciences at Houston in August 2011. She immediately continued her education at University of Texas Graduate School of Biomedical Sciences at Houston.